Title

Plant Molecular Pharming Techno-Economic and Virus-Based Nanomaterial Approaches to Limited Resource Recombinant Protein Manufacturing

Author

McNulty, Matthew

Publication Date

2022

Peer reviewed|Thesis/dissertation

Plant Molecular Pharming Techno-Economic and Virus-Based Nanomaterial Approaches to Limited Resource Recombinant Protein Manufacturing

By

MATTHEW JAMES MCNULTY

DISSERTATION

Submitted in partial satisfaction of the requirements for the degree of

DOCTOR OF PHILOSOPHY

in

Chemical Engineering

in the

OFFICE OF GRADUATE STUDIES

of the

UNIVERSITY OF CALIFORNIA

DAVIS

Approved:

_____
Karen A. McDonald, Chair

_____
Somen Nandi

_____
Alison McCormick

Committee in Charge

2022

Abstract

Plants represent a set of richly diverse and genetically tractable sources for high-value natural and recombinant products that can be used to support human health and industry. This work discusses the production of high-value recombinant products in plants, which is formally termed as plant molecular pharming (PMP), through the lens of the manufacturing techno-economics and applies these insights to the experimental development of plant-based pharmaceutical production technology.

PMP must overcome significant challenges as a set of alternative manufacturing platforms. Of primary importance, particular emphasis is required to contextual PMP results in comparison to those of more traditional platforms (e.g., mammalian cell culture, bacterial fermentation) and in terms of economic impact. To encourage the proliferation of such critical context for the field of PMP, we describe a general method for techno-economic analysis of plant-based manufacturing in **Chapter 3**.

We employ this techno-economic method to explore several different opportunities for plant-based manufacturing. In **Chapter 4**, we collaborate with industry partners to simulate the production of antimicrobial proteins in leafy green plants to respond a food safety-driven demand to protect against high-risk pathogens in a cost-sensitive and antibiotic resistance-concerned product landscape. In **Chapter 5**, we simulate scale-up of lab-scale results to evaluate the commercial potential of metabolically-regulated semicontinuous bioreactor production of biopharmaceuticals in transgenic rice cell suspension cultures. In **Chapter 6**, we approach a main barrier facing outdoor field-grown plant-based manufacturing, namely variation in plant quality driving process

variation, by introducing uncertainty quantification to techno-economic simulation of large-market natural and biotechnology products in an outdoor field-grown plant system.

After having evaluated manufacturing in several different established markets and environments for PMP, we use these general insights to consider and introduce the potential of PMP for supporting human health in the upcoming and uniquely resource-limited environments of deep-space exploration in **Chapter 7**. After identifying pharmaceutical purification as a bottleneck in the realization of a robust pharmaceutical foundry for space exploration, we evaluate the current state of terrestrial pharmaceutical purification costs in the space-relevant costing framework of equivalent system mass in **Chapter 8**.

Lessons learned around the constraints of pharmaceutical purification in limited-resource environments, including deep-space exploration and rural terrestrial environments, motivated the experimental development of a plant virus-based immunosorbent nanoparticle (VIN) technology as a simple and bioregenerable reagent for the purification of therapeutic monoclonal antibody and Fc-fusion protein drugs using affinity sedimentation or, when coupled with magnetic particles, affinity magnetic separation in **Chapter 9**.

We then further explore VINs as functional elements within larger system arrangements to exploit novel advantages of the virus-based nanomaterial structure and overcome limitations of the existing methodologies. In **Chapter 10**, we present entrapment and utility of VINs in silica sol-gel matrices by pore confinement, representing a novel system configuration for virus-based nanomaterials (VBNs) in general. In **Chapter 11**, we present a similarly novel process integration of capture, concentration, and diafiltration steps of pharmaceutical purification by circulation of VINs within a tangential flow filtration retentate loop.

Having developed VINs for limited-resource secondary purification, in **Chapter 12** we investigate a novel design for a 3D-printed hand-powered centrifuge that is capable of initial clarification steps of pharmaceutical purification.

Lastly, in **Chapter 13** we conclude and summarize a series of promising yet incomplete research investigations including the purification of VINs with the emerging technology of monolithic chromatography, an exploration of selective pressures to maintain VIN genetic stability over consecutive infection-based production cycles, development of a method for antibody-mediated capture of arbitrary proteins using VINs, important considerations for novel VIN design at the level of the three major structural components, and a novel strategy for the early-stage dynamics of plant cultivation on Mars.

Acknowledgements

"'I can't stop," the shark rasped. 'If I stop, I shall sink and die. That's the way I'm made. I have to keep going always, and even when I get where I'm going, I'll have to keep on. That's living.'"

-Catherynne M. Valente

The doctoral degree has been my target on the horizon for a long time now. The dissertation writing process has served well to punctuate my journey with a period of reflection, and for that I am grateful. I find in myself a tendency or desire to maintain a sense of forward momentum, not unlike the above-quoted fictional shark. But at the conclusion of this incredible and formative experience I can say that I am glad for the opportunity and time to look back, think more deeply on this journey, and give thanks to the many people who have shaped me along the way.

I can't imagine thanking anyone else before taking the time to describe my gratitude to my good friend and lab alumnus Dr. Jasmine Corbin for all that she has done for me and been for me during this education. From showing me around Davis at admitted students' weekend to dozens of email correspondences even prior to my attendance at UC Davis, Jasmine first served as my role model and a real factor in my decision to attend UC Davis. Her abundant generosity, sharp intellect, and steady resolve in and out of the lab quickly earned my deep respect and admiration. As a senior graduate student when I entered, she set the bar high, challenged me to meet it, and was there to support me honestly and vulnerably when I struggled. For that and much more, thank you, Jasmine.

My primary objectives in graduate schools were to develop 1) the scientific skills to conceive of and conduct independent scientific study, 2) the confidence and communication skills to propose and defend those studies, and 3) a network of diverse thinkers on the cutting edge of biotechnology. Dr. Karen McDonald has been more supportive than I could have asked for in helping me towards

all three of these aims. In attempts to not overly belabor my gratitude, I will simply say that I am extremely appreciative to have had a mentor these past years possessed of such a calm collection and mindfulness as Karen; whether in response to my shaky-voiced explanations of my struggles or to my off-handed self-deprecating remarks on my research quality, Karen has shown me an enduring compassion and gentle grounding while still leaving room for me as a researcher (and more importantly, as a human) to encounter and grow from these experiences. I have begun to learn how to let my ego trail behind my science and identify my own vulnerabilities to the sunken cost fallacy from the way that Karen really listens to others, from the most naive undergraduate researcher to the most distinguished professor, and adapts her research in measured response. There are many lessons left unacknowledged here, thank you for the above and the unsaid, Karen.

I would also like to thank Dr. Somen Nandi, co-PI of the lab. If Karen's mentorship has served as the furnace for my growth as a researcher, then surely Somen's has been the bellows. His relentless energy in pursuit of scientific discovery and engineering has picked me up from my lulls in motivation and stoked my passions for research. There is a memory of my time with Somen that encapsulates that feeling – we were both seated at a table overlooking the ocean at the end of the first day of technical conference that I had attended in graduate school, and I remember the air feeling electric with the excitement Somen brought with his vision for the lab and the capability he saw to bring out in me. I came back from that conference invigorated. I count myself lucky to not have just one, but two, faculty mentors in the lab that put their students first. Thank you, Somen.

Dr. Alison McCormick, as an external member of my dissertation committee, has peppered my graduate experience with revitalizing curiosity and introspection. I remember going to meet with Alison on campus and finding her waiting for me at our meeting spot, absorbed in thought and

crouched down inspecting fallen acorns nearby the sidewalk for some side-project or teaching lesson, the specifics of which elude me at this time. It is that playful curiosity, which can be so easily de-prioritize amidst the waterfalls of deliverables and pressures I put on myself, that Alison inspires me to hold onto. Her stories of lessons learned in her career progression and her sense of self in the intention she uses to drive decision-making inspire me to check in with myself separate from the momentum that I have garnered. Thank you, Alison.

Dr. Jonathan Galazka, as my NASA collaborator for over three years of my NASA Space Technology Research Fellowship, has been a brightly positive influence in my education. He always put my education first, even if that meant pulling up an extra desk in his office to teach me molecular biology for a summer. His passion for data democratization that brought me pause and consideration of the impact of the means by which I distribute my own scientific output. Thank you, Jon.

It would not be an exaggeration for me to identify as a fanboy of Dr. Yuri Gleba. He has shown me that a visionary in the field can be kind, compassionate, and creative while still leading with efficiency and impact, that soft and hard are not the only two stances, but that you can be both soft on the people and hard on the merits (popularized as principled negotiation). With only a handful of direct interactions throughout my graduate studies, Yuri has managed to transform my experience as a stalwart role model and generous collaborator. Thank you, Yuri.

My family on the east coast of the country has exuded a welcoming sense of comfort and inspiration, reminding me that love need not be barred by achievement and that we all are found deserving. They are the people in my life through which I find myself understanding how platitude-churning institutions like Hallmark and Homegoods stay afloat. I have come a long way in accepting, and in turn, loving myself over the course of these past five plus years. The space that

my family held for me to shelter in during that process is indescribable and invaluable. I extend this gratitude to the Oliveras family, whom have welcomed me as one of their own with open arms and a contagiously fierce resilience to life's curveballs. And to Ana Skomal – while our paths bifurcate, the time that we have shared together during my graduate experience leaves a lasting and comforting imprint.

I have found a special friend and research colleague in Vince Pane. From hiding our finger paintings on the office wall amidst Dr. Jon Galazka's children's paintings to assembling a graduate student cabal to pitch and lead multi-university research integration efforts, my time with you has always inspired me to be a playful, creative, and self-confident researcher/human.

I would also like to thank Amanda Dang, who has been to me a dear friend and mentor in my journey to identify and explore my relationship with the societal constructs in which we all operate (and which I have often benefited from in my intersectional identities as a researcher and in my other capacities). My lowest lows in graduate school have been in this education, and without Amanda I cannot say that I would have had the composure, humility, and grace to accept and grow from these experiences. I have been repeatedly awed by the force of her presence and the clarity of her articulations of complex ideologies that all researchers should ponder.

I have been very fortunate in the assemblage of friends that I have found and been found by during my doctoral studies. From coffee mornings to pancake nights and so much more in between, my friends in my graduate studies have helped me in ways that are hard to understate and at times may have been just as difficult for them to have seen. An enormously warm thank you to the crew – Noah Felvey, Doug Drakeley, Mike Meloni, Bradley Harris, Christine Smudde, Jose Hernandez, Guilherme de Moura, Can Agca, Michael Bull, Ron Assadi, Andy Lam, Eric Kalosa-Kenyon, Adrian Garcia, Kevin Bradley, and Alex Mendes.

It is difficult to overstate how fortunate I feel to have had so many positive and diverse influences in my life as a doctoral student. It is less than they deserve for the moments we have shared together, but I'd like to take this space to call out by name some of those people that I owe so much to (even if it's just so they know they can collect on it!). This is particularly true for my lab mates, with whom I have spent more time with than anyone else in the world in these past years. In the way that I view this doctoral training as my maturation as a researcher, I view you all as my research family that I have been able to lean on throughout the inevitable growing pains. Scientific puberty, if you can bear with me through this cringe-worthy metaphor, with all the rebellion against the parents, sibling rivalry, and identity crises one may have come to expect.

McDonald-Nandi lab members and visiting scholars of my time: Rupak Goswami, Hiroto Hirano, Pauline Famy, Trent Smith, Marc Tschofen, Zachary Kyser, Kevin Tom, Jesse Delzio, Jacqueline Kelley, Vuthithorn Chinthammit, Min Du, Joshua McMillan, Garrett Barton, Kostyantyn (Stan) Luferov, Stephan Alfaro, Olivia Hart, Anika Varma, Liber McKee, Seongwon (Steve) Jung, Yongao (Mary) Xiong, Sara Sukenik, David Silberstein, Kantharakorn (Korn) Macharoen, Kirolos (Kiro) Kelada, Salem Alkanaimish, Kalimuthu Karuppanan, Kevin Yates, Justin Wong, Brandon Pizarro, Patrick Negulescu, Eric Knapp, Katherine (Katie) Haddad, Imran Khan.

Research collaborators, select course instructors, and mentors: Naomi Hamada, Marjorie Longo, Vince Pane, Bob Waymouth, Aaron Berliner, Jacob Hilzinger, Kelly Wetmore, Adam Arkin, Anthony Abel, Daniel Tusé, Yuri Gleba, Debashis Paul, Abhaya Dandekar, Robert Gilbertson, Diane Ullman, Willam Lucas, Aaron Jacobson, Anton Shvarts, Anatoli Giritch, Jon Galazka, John Hogan, Eliah Overbey, Nancy Lane,

Carroll Cross, Paul Kusuma, Bruce Bugbee, Mathangi (Mattie) Soundararajan, Jennifer Knipe, Hawi Gemeda, Baraquiel Reyna, David Bubenheim.

Chemical Engineering and Designated Emphasis in Biotechnology administrative staff: Susan Lopez, Debbie Snyder, Veronica Stanton, Grace Woods, Alisha Bartolomucci, Megan Heynen, Denneal Jamison-McClung, Judy Kjelstrom, Jacki Balderama.

Equity in Science, Technology, Engineering, Mathematics, and Entrepreneurship outreach members: Hannah Nelson, Alexus Roberts, Isabelle Neylan, Collin Gross, Adrian Perez, Emily Zepeda, Deepshika Gilbile, Erin Doherty, Ayanna Wade, Elena Suglia, Lahari Indraganti, Angel Cobos, April Booth, Christine Smudde.

Hand-powered centrifuge team at Sacramento City College and the UC Davis TEAM lab: William (Bill) Miller, Devoun Stewart, Kevin Yates, Brandon Gregersen, Dylan Estrada, Dylan Beck, Amar Zagdragchaa, Justin Mahley, Kha Ton, Thomas Nakanishi. For providing funding and fruitful discussions, thank UC Davis AvenueE and VIP program leads Subramaniam Muralidharan, Beth Broome, and Erin Silva.

Chemical Engineering and Materials Science and Engineering Graduate Student Organization members: Jose Hernandez, Tanner Finney, Luis Sotelo, Noah Felvey, Christine Smudde, Jared Stimac, Zach Rollins, Grace McClintock, Amanda Dang, Sean Russell, Bradley Harris, Leah Filardi, Jasmine Corbin, David Silberstein, Benji Geveke, Gianmarco Monfared, Jiayu Li, Thomas Nguyen, Fox Thorpe.

I would also like to acknowledge Biorender for some of the figure creation in the works presented. Out of legal obligation, but also personal thanks for the services that they provide.

"Wall Of Shame"

In continuing with my acknowledgements, I would like to make a special point in highlighting the contributions of people in my life that have helped me grow a more comfortable, and at times perhaps even amicable, relationship with failure in the process of emotionally de-coupling sense of worth and achievement or outcome. I have been surrounded by a gentle and nurturing network of people that have committed considerable time and effort.

I was particularly inspired by my friends and colleagues Noah Felvey and Mike Meloni, whose pursuit of quality research led by example. In the process of their research, they established a routine in which the most deformed and broken of their glassware, experimental apparatuses, and else are showcased prominently on a shelf in the lab. This concept of boldly pronouncing failure inspired me bring that forth in my own way. At the end of my second year of graduate training in 2018, I posted up a sheet of paper behind my desk in the lab office and began my own "Wall of Shame," that I titled "Times that Matt ^really really failed."

In dedication to Noah and Mike, I would like to do my best to pass along the opportunity of this lesson in a small way through these acknowledgements. To the reader, if nothing else I hope that enjoy a transcription of my own "Wall of Shame" that I've built my journey through graduate training.

Matt's PhD Wall of Shame

A sampling of particularly notable mistakes, failures, and otherwise shameful events over the course of study

"It is hard to fail, but it is worse never to have tried to succeed… unless you really messed up."
–Matt McNulty, adapting the words of Theodore Roosevelt

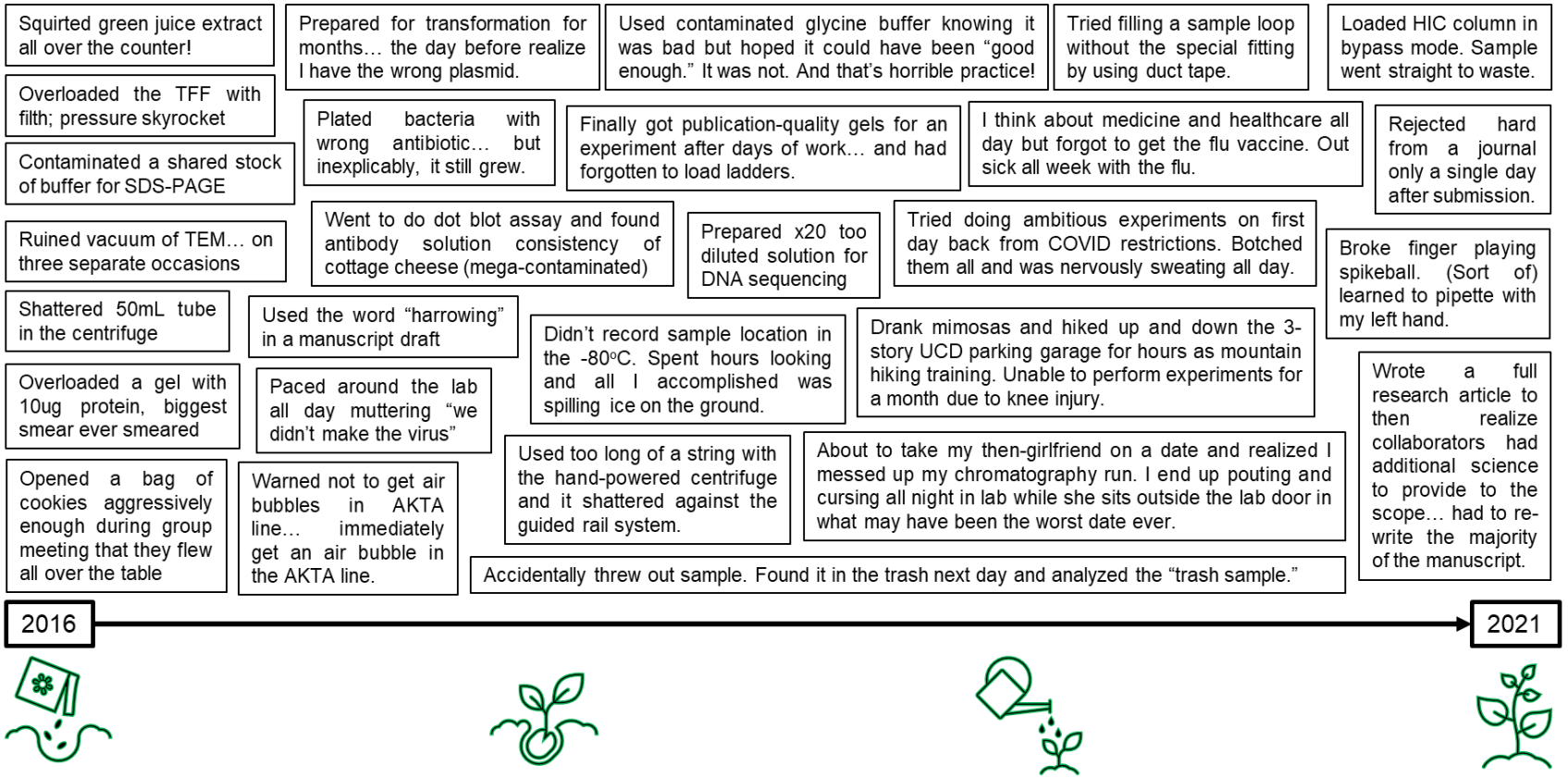

Table of Contents

"Stories have a way of changing faces. They are unruly things, undisciplined, given to delinquency and the throwing of erasers. This is why we must close them up into thick, solid books, so they cannot get out and cause trouble."

-Catherynne M. Valente

Chapter 1. Introduction and Background

"Writing a book is an adventure.
To begin with, it is a toy and an amusement;
then it becomes a mistress,
and then it becomes a master, and then a tyrant.
The last phase is that just as you are about to be reconciled to your servitude,
you kill the monster, and fling him out to the public."

-Winston Churchill

1.1. Motivation: Accessibility and equity in biotechnological innovation

Biotechnology and biomanufacturing can be likened to a modern-day alchemy in the manner that we aim to transmute relatively simple and low-value inputs (e.g., sugar) into staggeringly complex and high-value outputs (e.g., life-changing medical treatments) by channeling through the "awesome power and complexities of nature, every step of the way."[a]

The versatility and power of this platform in human hands is truly amazing – we use it to clear hazardous pollution from our environment through bioremediation[1], power our energy-intensive society through biofuel[2], feed our people with food and agricultural biotechnology[3], improve our healthcare through medical biotechnology[4], and much more.

While the direct process inputs of biotechnology may be simple and low value at times, the infrastructure often required to realize this potential is not. Immense resources have been, and continue to be, poured into the systems of biotechnological innovation required to reap these wide-spanning societal benefits. For example, a recent study on research and development costs to bring a new medicine to market in the United States estimates an average expenditure of ~$1 billion (counting costs of failed trials)[5]. However, the systems of biotechnological innovation are much

[a] https://www.gene.com/stories/modern-day-alchemy

more than just the research and development. They span everything from strategic workforce development (e.g., the 2020 RegeneratOR Workforce Development Initiative[6]), to process development and manufacturing of the product (e.g., constructing a conventional large-scale biopharmaceutical manufacturing facility costs on average $200 – $500 million (in 2014 USD)[7]), to advanced supply chain logistics for product distribution (e.g., the qualitative system dynamics methodology for pharmaceutical supply chains[8]).

This complex infrastructure has been an integral force in shaping the impact of biotechnological innovation, sobering the current outlook and amazement of potential for much of the world. Looking at medical biotechnology, a 2016 study showed that new hepatitis C virus (HCV) medicines have greatly improved treatment efficacy and regimen tolerability, but that their high prices have severely limited access in the process – for 12 of the 30 countries included in the analysis, the price of a course of treatment with the HCV medicine sofosbuvir (not including diagnostic testing or supplementary costs) was equivalent to 1 year or more of the average annual wage of individuals in that country[9]. In agricultural biotechnology, a recent 2020 article provides a direct and somber coloring to the overall geopolitical impact of bioengineered crops, citing that, while there are an estimated 191.7 million hectares around the world using bioengineered crops spanning 526 bioengineered traits and 32 crop types, less than 1% of the total population of the developing world is positively affected by this agricultural biotechnological innovation[10].

Yet even this study, in which the abstract ends with, “those with the greatest need benefit the least from science,” propagates this barrier to access by their decision to publish in the paywalled subscription journal *Molecular Plant*. This is not a statement to lambast these particular authors, although there are open-access journals they could have chosen to publish in (and publicly-available research to support there is largely insignificant differences in scientific impact between

open access and subscription journals[11]), but rather to illustrate that the complexities of access and equity in the infrastructure of biotechnological innovation are wide-spread and with deep roots.

The area of vaccine immunization in medical biotechnology is a particularly interesting slice of biotechnological innovation in which to consider access and equity. To set the stage for this, one should consider the concept of strong/weak link theory. This terminology has been largely popularized by journalist and author Malcolm Gladwell to describe organizational strength – for example in sports, basketball would be defined as a strong link sport because the one or two top players on the team can score points on their own and carry performance (i.e., improving the strongest players is most important), while soccer would be described as a weak link sport in which many players need to touch the ball successively to score a goal (i.e., improving the weakest players is most important). Carrying this into organizational strength of biotechnological innovation, one may argue that while most areas might be viewed by some as operating within a strong link system, vaccine immunization programs are acknowledged to operate in what would be classified as a weak link system. As evidence to this, a 2021 report on the economic case for global COVID-19 vaccinations shows that the cost of not immunizing all countries can be higher for developed countries than the cost of them manufacturing and distributing vaccines globally[12]. However, despite this well-known phenomena there are recent statistics from June 2021 on the current COVID-19 global pandemic facing the world that indicate a vast disparity in COVID-19 vaccination rates (43% in high-income countries, 0.8% in low-income countries)[13]. This outcome underlines the complexities in translating biotechnological innovation into societal impact in a vastly interconnected geopolitical system; equity in biotechnological innovation access is not achieved even when a moral imperative is strongly reinforced with economic best self-interests.

This example of vaccine immunization highlights the need for novel approaches to rolling out biotechnology into society. This need is present in all levels of the translation infrastructure – including workforce development, investment vehicles, intellectual property management, manufacturing, distribution, sales, and regulation. There have been, and continue to be, many initiatives approaching this need from many different angles and with varied success. For an example of mixed-bag success, let us consider that workforce diversity has been consistently shown to result in improved financial returns in biotechnology[14], and thus societal impact, and has been a priority in the United States government for some time. As of now, there has been only slow progress of the United States in areas including ingrained racial prejudice[14–16] and socio-economic inequality[17–19].

In this work, we investigate novel plant-based approaches to biomanufacturing within the biotechnological innovation infrastructure with an emphasis on the potential for enabling societal impact. We perform our investigations at several levels of inquiry – applying both computational approaches to analyze and compare the landscapes of novel biomanufacturing through techno-economic analysis and experimental approaches to developing novel biomanufacturing unit operations.

1.2. An equity-focused landscape of plant molecular pharming

Plant molecular pharming (PMP) is defined as the production of pharmaceuticals and other high-value recombinant products in plants. Plants have been a tool for human health and survival for thousands of years[20], but it is only in recent decades through recombinant DNA technology, starting with the first recombinant protein expressions of antibiotic resistance proteins in 1983[21,22]

and antibodies in 1989[23], that we have realized just how versatile of a tool they can be. Recent reviews cover the potential of PMP and how it has been applied to date[24,25].

However, commercial biomanufacturing of high-value recombinant products has become near synonymous with bacterial fermentation and mammalian cell culture. Recombinant protein expression in bacteria was first reported in 1977[26], and was shortly followed by expression in mammalian cell culture. This decade-plus head start in research and discovery of these culture-based systems over other production platforms like PMP provided them with intensive research-driven increases in productivity, regulatory pathway establishment, and billions of USD in capital infrastructure[27,28].

Thus, it is as an alternative biomanufacturing strategy that PMP has developed, and to a large extent, still operates. Supporters often PMP tout advantages of cost-effectiveness, linear scalability, sustainability, robustness, and inherent safety[29], while critics emphasize productivity limitations rooted in plant cell sizes (due to the presence a dominant vacuolar compartment) and challenges of downstream purification of products from complex plant host constituents[30]. As with any production platform, there are pros and cons that make it more well-suited for certain applications than for others. The diversity of plants, and PMP, is at once a great strength and weakness of the field in the way that the varied potential of different PMP platforms enables opportunities in diverse applications, but which also diffuses scientific progress towards technological maturation and may effectively hinder momentum of any one given platform[31].

There is a general positive commonality amongst the diversity of PMP platforms, however, in the accessibility for developing countries and emerging economies. The advantages of PMP for low to middle income countries is well described[32]. They span multiple levels of the biotechnological innovation infrastructure; the production can be performed in a low-technology manner which also

translates into lower capital costs for facility construction (although the purification would still require advanced technology); the prevalence of basic agricultural skills lightens the burden of workforce development; the linear production scalability simplifies process development and could enable supply of the very large quantities of recombinant product (e.g., medicine) needed in developing countries with a reduced reliance on developed nation supply chains. While not widespread to all PMP products, plant virus-based vaccines and related solutions are also proving to dismantle the need for cold-chain distribution[33], which is traditionally challenging to maintain in developing countries.

Given the aforementioned economic impact of agricultural biotechnology and exclusion of developing countries from that wealth, the advantage of PMP in its synergy with enabling advanced agriculture should not be overlooked. In a recent milestone study, a well-known PMP company, Nomad Bioscience GmbH, which had traditionally focused on producing recombinant products in food and medicine, reported on a new method for transient reprogramming of plants for agronomic performance that bypasses much of the lengthy and resource-intensive process of the typical bioengineering a crop trait in a transgenic line[34]. These results leveraging RNA-based reprogramming can be directly traced back to earlier foundational PMP research by Nomad Bioscience GmbH[35].

Despite the exciting promise of PMP for improving healthcare access and affordability in low- and middle-income countries, uptake of this emerging technology has been slow for a variety of reasons. However, the emergency use of PMP-made medicine (ZMapp) for the 2014 – 2016 Ebola virus outbreak in West Africa served as a pivotal moment in changing the perception of PMP[36]. An Ebola virus outbreak, being historically confined to poor African nations, lacked the profit-incentive for pharmaceutical industries in developed countries to prioritize medication

development (although developed countries did respond with development incentives that yielded a number of primarily developmental phase vaccine and therapeutic candidates[37]). Not only did ZMapp offer aid to these nations in the outbreak (as one of the only available options to treat infected patients[38]), but it illustrated a potential alternative to relying on the support of developed countries, to develop pharmaceutical manufacturing capabilities that are accessible and affordable to low- and middle-income countries.

After a first generation of PMP facilities in the pharmaceutical industry-standard locations of the global North (USA, Europe, Israel, Japan), there are now emerging plans for PMP in developing countries that are seeking to develop pharmaceutical capabilities, including Brazil, Thailand, and South Africa[39]. Brazil is already actively building a PMP facility that is set to open in 2022, while South Africa is building on a 20-year history of PMP research with a government-supported PMP start-up company running a small-scale PMP facility that is also positioning to establish a clear workforce development pipeline, and Thailand has overcome an aversion to genetically-modified crops to declare formal governmental interest in PMP.

Chapter 2. Experimental methods and materials

"Experiment!
Make it your motto day and night
Experiment!
And it will lead you to the light
The apple on the top of the tree
Is never too high to achieve
So take an example from Eve
Experiment!
Be curious
Though interfering friends may frown,
Get furious
At each attempt to hold you down
If this advice you'll only employ
The future can offer you infinite joy
And merriment
Experiment!
And you'll see"

-Cole Porter

2.1. Gene construct

The gene construct for plant virus-based immunosorbent nanoparticle (VIN) expression, pICH25892, was previously described in detail[40]. As shown in Figure 2.1, the VIN gene elements consist of the native turnip vein clearing virus (TVCV) constituents (TVCV RNA-dependent RNA polymerase, movement protein, coat protein, 3' non-translatable region) and immunosorbent protein display constituents inserted as a fusion at the C-terminus of the coat protein (glycine-rich flexible linker $(GGGGS)_3$, D and E antibody-binding domains from *Staphylococcus aureus* protein A with short flanking sequences (amino acids 29 – 161; GenBank accession no. J01786)) are codon-optimized and intron-optimized for expression per the magnICON® strategy for de-bottling production kinetics at the step of formation of active replicons from the primary nuclear

transcript[41]. The pICH25892 expression construct consists of the VIN gene elements led by the *Arabidopsis thaliana* actin 2 (ACT2) promoter and terminated by the *Agrobacterium tumefaciens* nopaline synthase (Nos) terminator within the span of the *A. tumefaciens* T-DNA left border (LB) and right border (RB) sequences. There is also an upstream kanamycin resistance gene, NPTII, controlled by a Nos promoter and Nos terminator.

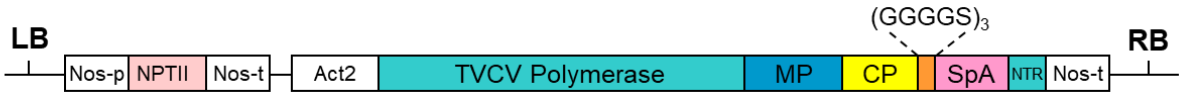

Figure 2.1. *Agrobacterium tumefaciens* T-DNA vector construct for TVCV-based immunosorbent nanoparticle. Act2, actin promoter; MP, movement protein; CP, coat protein; NTR, 3' non-translatable region; Nos-p (-t), nopaline synthase gene promoter (terminator); NPTII, kanamycin resistance gene; SpA, Staphylococcal protein A-based Fc-affinity ligand; LB, left border of T-DNA; RB, right border of T-DNA.

Plasmid amplification of the gene construct pICH25892 was performed using *Escherichia coli* via heat shock transfection. Heat shocked *E. coli* were plated on agar with ampicillin and tetracycline antibiotics. Positive colonies were cultured in suspension and the presence of the VIN gene elements was confirmed via PCR. Freezer stocks were generated as 20% v/v glycerol. Plasmid DNA was recovered from the *E. coli cells* using the QIAprep Spin Miniprep Kit (QIAGEN, Hilden, Germany).

A. tumefaciens EHA105 with the helper plasmid pCH32 was then transfected with gene construct pICH25892 plasmid via electroporation. Transfected *A. tumefaciens* were plated on agar with ampicillin, tetracycline, and kanamycin antibiotics. Positive colonies were cultured in suspension and the presence of the VIN gene elements was confirmed via PCR and Sanger sequencing. Freezer stocks were generated as 20% v/v glycerol.

2.2. Upstream bioprocessing

2.2.1. Plant cultivation

Nicotiana benthamiana plants were cultivated in greenhouse conditions supplemented with electric lighting to maintain a 16-hour light photoperiod. Each plant was grown individually in a 4” square planting pot with bottom drainage holes lightly packed with “Coco mix” soil consisting of three (3) parts coconut coir and one (1) part coarse perlite. The soil was thoroughly drenched with nutrient water (see nutrient water elemental composition in Table 2.1 and concentrated salt solutions in Table 2.2) by hand prior to seeding to strip and replace any residual sodium ions remaining in the coconut coir constituent of the soil – a key consideration given the coconut coir manufacturing which ends with an outdoor sandy beach drying step.

Table 2.1. Elemental composition of the nutrient water solution.

Element	ppm
N	143.455
P	63.707
K	199.343
Ca	125.397
Mg	49.467
S	65.114
Fe	2.759
Cu	0.097
B	0.000
Mn	0.633
Mo	0.055
Zn	0.097

Table 2.2. Composition of the nutrient concentrate solutions, per 10-gallon liquid volume, injected in-line in equal parts for an overall 1:200 into water to generate the nutrient water.

Tank A		Tank B	
Salt	Mass (g)	Salt	Mass (g)
Calcium Nitrate	4740	MKP	2105
Potassium Nitrate	1250	Potassium Nitrate	1250
Iron EDTA	158	Magnesium Sulfate	3816
Zinc EDTA	5.26		
Copper EDTA	5.26		
Manganese EDTA	36.84		
Natrium Molybdate	1.05		

Each plant was watered with nutrient water three (3) times per day for three-minute durations and 2 liter/hour flow rates per watering using an automated system with soil-inserted drippers connected to 4-stack distribution tubing and irrigation line emitters. Approximately 10% differences in water flow were expected between the front and back of the irrigation line (personal communication with greenhouse personnel), although we observed ~15% lower nutrient water dispensing at the front of the irrigation line, defined as being closer to the nutrient feed inlet, as compared to the back (data not shown).

Traditional seeding and hand transplanting methods were initially used, but the majority of plant cultivation in this dissertation was conducted using agar seed suspensions without transplanting. Simple comparator tests were performed and found no discernable disadvantage with the agar seed suspension method. The agar seed suspension was generated by addition of 500 mg agar into 300 mL ddH_2O, followed by microwave heating in 30 second intervals until the agar was fully dissolved, a cooling step to get the agar suspension to room temperature, addition of 200 mg of *N. benthamiana* seeds, and light swirling to mix. The agar seed suspension was then stored at 4 °C

when not in use. Volumes of 1.5 – 3 mL of agar seed suspension were pipetted onto the top of a soil-filled and pre-drenched pot in a diagonal line.

Excess seedlings were plucked from each pot at fourteen (14) days post-seeding to until only a single seedling remained per pot. Generally, the only discrimination on seedling plucking was in regard to location within the pot and seedling size continuity between pots in the same experiment. Plants stalked in a more central location of the pot were preferrable for preventing soil loss during the inversion required for whole-plant vacuum agroinfiltration. Seedling size continuity was generally maintained as best as could be estimated to minimize the impact of differences in mature plant morphology between plants in the same experiment.

Time to flowering differed with the season, but generally was expected after six (6) weeks post-seeding. A minimum of two (2) to three (3) months are required for plants to sufficiently mature for seed collection. Seeds were collected by gentle shaking a plant while holding it above a plastic collection bin and then picking individual seed pods (only the brown and dried seed pods) and storing in a sealed container before sifting to remove seed pod biomass from the seeds at a later time. Multiple rounds of seed collection can be performed for a given plant given sufficient time. Collected seeds were stored dry in a sealed container at 4 °C for up to several years. Germination efficiency was monitored to ensure seeds had maintained integrity throughout storage.

2.2.2. *Agrobacterium tumefaciens* culture

Freezer stocks of *A. tumefaciens* containing viral expression vector pICH25892 were used to inoculate 20 mL of Luria-Bertani (LB) media with selection antibiotics (50 µg/mL rifampicin, 10 µg/mL tetracycline, 50 µg/mL kanamycin) at 1-2% working volume (wv) inoculum for 18 – 24

hours in the dark at 28 °C and 250 RPM. The culture was scaled up to 125 mL LB media with selection antibiotics (1-2% wv inoculum) for an additional 18 – 24 hours of growth.

To collect the cells for agroinfiltration, the *A. tumefaciens* cultures were then centrifuged at 5,000 x g for 10 minutes to pellet the cell biomass and resuspended in infiltration buffer (10 mM MES buffer pH 5.6, 10 mM $MgCl_2$, 150 µM acetosyringone) to obtain a final cell density of OD_{600} = 0.2. The target infiltration buffer volume was dependent on the number of plants to be infiltrated. The cells were first resuspended in a small volume of infiltration buffer to obtain an initial cell density measurement that could be used to calculate the volume of infiltration buffer required to dilute the solution to the target final cell density. The solution of *A. tumefaciens* in infiltration buffer was incubated in the dark for at least one hour prior to use. Silwet-L-77 was added to the infiltration solution at 0.02% v/v and well-mixed with gentle swirling just prior to use.

2.2.3. Vacuum agroinfiltration

Agroinfiltration was performed using whole plant vacuum agroinfiltration. *N. benthamiana* plants were transferred from the glass greenhouse at approximately five weeks post-seeding to the laboratory. A plastic guard with a slot for the plant stalk protrusion was placed over the top of the pot opening to prevent soil loss, and then plants were inverted and submerged into agroinfiltration solution (held in a 1 – 2 L beaker to ensure adequate space for submersion of the plant aerial tissue) in a vacuum chamber. The submerged plants were submitted to 20 inches Hg vacuum pressure for > 30 seconds, upon which the vacuum was released. The plant leaves were visually inspected for complete infiltration, as indicated by a darkening of the leaf. Plants subject to incomplete infiltration were submitted to one additional round of infiltration. The plants were left to dry in ambient conditions before transport into a controlled environment chamber.

2.2.4. Mechanical inoculation with intact viruses

Plant viruses compatible with mechanical transmission, such as those within the tobamovirus genus, were produced via direct mechanical inoculation of intact virions. *N. benthamiana* plants were transferred from the glass greenhouse at approximately five weeks post-seeding to a controlled environment chamber. A total volume of 300 µL of purified virion solution (~0.1 µg/µL) was applied per plant in aliquots of 100 µL to each of three middling leaves[42]. An abrasive powder (Celite) was lightly sprinkled on each leaf and each leaf was gentle rubbed by hand. Excessive pressure during rubbing resulted in detrimental plant leaf damage. The surfaces of the leaves were rinsed with water at 20 minutes post-inoculation to remove excess inoculation reagents.

2.2.5. Plant incubation and leaf harvesting

Post-infiltration and post-infection *N. benthamiana* plants were cultivated in a controlled environment chamber at 60% relative humidity with a 16-hour light/8-hour dark photoperiod, 23 °C/20 °C temperature regime, and a photosynthetic photon flux density of 425 µmol/(m^2·s) derived from a combination of high-pressure sodium, high-pressure metal halide, and incandescent lights for a duration of 6-12 days post-inoculation. Plants were watered once per day with nutrient water (as defined in section 2.2.1) and the pots were kept in trays that held excess water in reservoir and in contact with the potted plants via the bottom drainage holes. Plant leaves were harvested at the petiole and fresh weight was measured prior to storage in a -80 °C freezer.

2.3. Downstream bioprocessing

2.3.1. Polyethylene glycol precipitation-based virion purification

VIN and wild-type tobacco mosaic virus (wt-TMV)-expressing *N. benthamiana* leaf tissue stored at -80 °C was pulverized by hand in the plastic storage bags and then homogenized using either a blender (NutriBullet; NutriBullet, LLC, Pacoima, CA) or liquid nitrogen-assisted mortar and pestle with 0.1 M potassium phosphate pH 7.0 extraction buffer at a 3:1 buffer volume to biomass weight extraction ratio. In the case of the mortar and pestle method, the homogenized leaf powder was mixed with the buffer and nutated for 30 minutes at 4 °C for extraction. All proceeding steps were performed on ice unless otherwise specified. The homogenate was filtered through three layers of cheesecloth (which was squeezed at the end to collect all of the filtrate) and the filtrate was liquid-liquid extracted with 0.25 volumes of chloroform. The chloroform-containing homogenate was briefly hand-mixed and centrifuged at 5,000 x g for 15 minutes at 4 °C. The top aqueous phase was collected with a serological pipette. Precipitation aid, 4% w/v polyethylene glycol (PEG) 6,000 and 1% w/v NaCl, was added to the solution and nutated for 30 – 60 minutes at 4 °C. VINs were then precipitated by centrifugation at 8,000 x g for 15 minutes at 4 °C and resuspended in 0.2 volumes resuspension buffer, 0.01 M potassium phosphate buffer pH 7.0. Insoluble debris post-resuspension was removed by centrifugation at 5,000 x g for 5 minutes at 4 °C.

A variation of this procedure was also developed for improved final purity. The above method was modified as follows: the extraction buffer was changed to 50 mM sodium acetate, 86 mM NaCl pH 5.0, chloroform-based liquid-liquid extraction was removed, a 60 °C heat hold for 5 minutes was added after the PEG precipitation step.

2.3.2. Ultracentrifuge-based tobacco mosaic virus purification

Frozen *N. bethamiana* leaf tissue expressing wt-TMV stored at -80 °C was pulverized by hand in the plastic storage bags and then extracted in a 5:1 w/v extraction ratio with 0.1 M potassium phosphate pH 7.0 and 0.1% v/v beta-mercaptoethanol using a chilled mortar and pestle. All proceeding steps were performed on ice unless otherwise specified. The resulting plant extract was filtered through three-layered cheese cloth (which was squeezed at the end to collect all of the filtrate), mixed with equal parts chloroform and n-butanol up to 1:1 v/v ratio, centrifuged at 8,000 x g and 4 °C for 10 minutes, and the upper aqueous phase layer was collected. The aqueous layer was then precipitated by addition of 4% w/v PEG 8,000 and 1% w/v NaCl, incubation of the mixture for 30-60 minutes at 4 °C, and centrifugation at 8,000 x g and 4 °C for 15 minutes. The pellet was resuspended in 50 mM Tris-HCl pH 7.0 with a glass rod and let to sit at 4 °C for 30 – 60 minutes. The resuspended solution was centrifuged again at 8,000 x g and 4 °C for 10 minutes to clear any remaining insoluble aggregates. The resulting supernatant was then carefully layered on top of 1 mL 15% sucrose cushions per tube and ultracentrifuged at 50,000 RPM and 4 °C for 90 minutes using a 70.1 Ti rotor (Beckman Coulter, Brea, CA, USA). The pellet was resuspended again in 50 mM Tris-HCl pH 7.0 with a glass rod and let to sit at 4 °C overnight for complete resuspension. The resuspended solution was carefully layered on top of a 10 – 40% w/v sucrose gradient, made by carefully capillary pipette layering bottom up with 10%, 20%, 30%, and 40% w/v sucrose solution and confirming layering by visual inspection, and ultracentrifuged at 30,000 RPM and 4 °C for 90 minutes using a SW40 swinging bucket rotor. A 50% sucrose solution was used as a plug to fractionate and collect the wt-TMV containing solution.

2.3.3. Liquid chromatography-based purification of Fc-fusion proteins

Plant-made recombinant parathyroid hormone (amino acids 1 – 34) fragment crystallizable region fusion protein (rPTH-Fc) was purified from *N. benthamiana* leaf tissue frozen at -80 °C. The frozen tissue was pulverized by hand in the plastic storage bags and then homogenized using liquid nitrogen-assisted mortar and pestle. The homogenate powder was mixed at 3:1 v/w extraction ratio with phosphate buffered saline (PBS) pH 7.0 (containing 1 mM EDTA, 2 mM sodium metabisulfite) and nutated at 4 °C for 30 minutes. All proceeding steps were performed on ice unless otherwise specified. The solution was then passed through three-layered cheesecloth (which was squeezed at the end to collect all of the filtrate), centrifuged at 1,800 x g and 4 °C for 30 minutes, and passed through a 0.22 µm dead-end filter to generate a sterile clarified solution, which can be stored at 4 °C for up to 24 hours prior to liquid chromatography processing, but is not recommended to be exposed to freeze-thaw cycles.

The ÄKTA Pure liquid chromatography system was used with a pre-packed HiTrap MabSelect SuRe (Cytiva, Marlborough, MA, USA) 5 mL affinity column for secondary purification of rPTH-Fc. All buffers were 0.22 µm filtered prior to loading into the liquid chromatograph system. All processing steps were performed at a flowrate of 4 mL/min and processing step length was based on in-line measurement stabilization rather than a strict column volume (CV) basis. The system and column were equilibrated with PBS pH 7.0 for 5 – 10 CV and then the clarified solution sample was loaded. The column was then washed with PBS pH 7.0 (~10 CV). Elution was performed using 0.1 M glycine-HCl pH 3.0 for ~3 CV collected as 2 mL fractions. The column was then stripped with 0.1 M NaOH, washed with PBS pH 7.0, and then stored in 20% ethanol at 4 °C. Eluate fractions were pH neutralized by titration with 0.5 M Tris-HCl pH 9.0. Amicon Ultra

centrifugal filter units (catalog #: Z717185, Millipore) were used for buffer exchange into PBS, as needed.

2.4. Fc-protein processing with plant virus-based immunosorbent nanoparticles

2.4.1. Affinity sedimentation-based purification of hIgG

Immunoglobulin G purified from human serum (hIgG) (Sigma-Aldrich, St. Louis, MO) was mixed with a solution of purified VIN diluted to a final working concentration of ~0.1 mg/mL at an approximately 1:1 mass ratio based on total soluble protein assay results and a working volume of 1 mL. The initial VIN and hIgG solution was incubated on ice while nutating for 30 minutes. The incubated solution was centrifuged at 12,000 x g for 10 minutes at 4 °C to precipitate the bound VIN-hIgG complexes. The precipitate was then resuspended in 0.1 M glycine-HCl pH 2.5 elution buffer to promote dissociation of the VIN and hIgG. Precipitation aid, 4% w/v PEG 6,000 and 1% w/v NaCl, was added and the solution and was incubated while nutating on ice for 30-60 minutes. The solution was centrifuged at 8,000 x g for 15 minutes at 4 °C to precipitate the VIN. The precipitated VIN was resuspended in 0.5 volumes of resuspension buffer or PBS pH 7.0 to recover the VIN. The hIgG-containing supernatant was pH neutralized with the addition of 0.1 volumes of 1M Tris-HCl pH 9.0. Additional precipitation aid, up to a working concentration of 14.5% w/v PEG 6000, was added and then followed by 30-60 minutes incubation nutating on ice. The incubated hIgG-containing solution was precipitated via centrifugation at 16,000 x g for 15 minutes at 4 °C and the pellet was resuspended in 1 volume of PBS.

2.4.2. Affinity batch chromatography-based purification of hIgG

Batch chromatographic purification of hIgG was performed with 40 µL VIN-functionalized silica-sol gel beads, synthesized as described in literature[43], individually contained in 2 mL tubes. The gels were equilibrated in a bath of 150 µL PBS pH 7.0 under nutating and 4 °C conditions for a minimum duration of 24 hours and four buffer exchanges. For sample loading, the equilibration buffer was carefully removed via pipette and hIgG-containing liquid samples were added to the gel beads as a bath of 80 µL liquid per gel bead and given 24 hours nutating at 4 °C. The liquid sample was then removed and the gel was washed per the aforementioned equilibration procedure (150 µL PBS pH 7.0, four buffer exchanges, 24 hours nutating at 4 °C). Elution of hIgG was performed by removing the wash bath and adding 80 µL of 0.1 M glycine-HCl pH 2.5 to the gel beads and letting incubate for 4 hours nutating at 4 °C. The low pH eluate bath was collected and pH neutralized with 0.1 volume (8 µL) 0.1 M Tris-HCl pH 9.0.

2.4.3. Affinity filtration-based purification of hIgG

An ÄKTA flux tangential flow filtration system (Cytiva, Marlborough, MA, USA) was used with a Pelicon® XL 1,000 kD and 50 cm^2 filtration area cassette with Ultracel® membrane (MilliporeSigma, Burlington, MA, USA) for all tangential flow filtration (TFF) operations. Normalized water permeability testing was used to confirm TFF membrane cleanliness prior to each use. All buffers were 0.22 µm filtered prior to loading into the TFF system. All processing steps were performed at a feed flow rate of 30-50 mL/min.

The TFF system was equilibrated with PBS pH 7.0 for ~ 30 minutes. A solution of VIN and hIgG at approximately 1:1 mass loading, pre-incubated together at 4 °C for 30 – 60 minutes, was loaded into the TFF feed tank and circulated with the permeate line closed for the equivalent of

approximately five pumped volumes. The permeate line was opened and the solution was concentrated to a total volume of ~20 mL. Batch diafiltration with PBS pH 7.0 was then performed for five (5) diavolumes to clear additional impurities from the retentate loop, which contained the bound VIN-hIgG complexes. The permeate line was closed and five (5) diavolumes of 0.1 M glycine pH 2.45 were added to the storage tank to dissociate the VIN and hIgG. The system was circulated for the equivalent time of approximately five (5) pumped volumes. The permeate line was opened and hIgG-containing permeate was collected in 5 mL fractions. The system was cleaned as follows: the retentate was first drained, PBS pH 7.0 was circulated and drained, 0.1 M NaOH was circulated for 20 minutes with the permeate line open, again for 30 minutes with the permeate line closed, and then again for 20 minutes with the permeate line open. The TFF cassette was stored in this 0.1 M NaOH solution in a sealed container at 4 °C. Eluate fractions were pH neutralized by titration with 0.5 M Tris-HCl pH 9.0. Spin filters were used for buffer exchange into PBS, as needed.

2.5. Biomolecule characterization

2.5.1. Sodium dodecyl sulfide polyacrylamide gel electrophoresis (SDS-PAGE)

Analytical samples were prepared for SDS-PAGE in 40 µL volumes consisting of 28 µL protein sample (diluted as desired using the protein solution buffer or ddH_2O) (70% v/v), 10 µL of 4x Laemmli dye (25% v/v), and 2 µL beta-mercaptoethanol (BME) (5% v/v). BME is omitted for running SDS-PAGE under non-reducing conditions. The aliquots are briefly vortexed and spun down in a mini-centrifuge, heated for 5 minutes at 95 °C, vortexed and spun down again, and let sit to cool.

Precast protein gels, either 4-20% Mini-PROTEAN® TGX Strain-Free ™ Protein Gels, 10 well, 50 µL (Bio-Rad Laboratories, Hercules, CA) or the stain-required equivalent, were loaded into a gel electrophoresis cell (e.g., Mini-PROTEAN® Tetra Vertical Electrophoresis Cell (Bio-Rad Laboratories)) and filled with 1x Tris/glycine/SDS buffer (to the top for the internal chamber, to the demarcation line for the external chamber). Storage buffer was displaced from each precast gel lane using the filled running solution. Prepared samples and protein ladder were loaded into the precast gel lanes. The loaded electrophoresis cell was then run at room temperature for either 35 minutes at 200 V or 19 minutes at 300 V.

Stain-free gels were lightly rinsed with ddH_2O and imaged with the ChemiDoc Imaging System (Bio-Rad Laboratories). The short activation time (45 seconds) was used for gels that were transferred for western blot analysis, while the longer activation time (5 minutes) provided higher sensitivity and was used for gels not being transferred. For gels requiring staining, imaging was accomplished using Coomassie Brilliant Blue-R250 staining solution – gels were first washed in ddH_2O for three cycles of 5 minutes, stained for 1 hour, and then washed in ddH_2O for another three cycles of 5 minutes. Gels were then imaged on a white backdrop using a camera.

2.5.2. Western blot

Gels run for SDS-PAGE (see Section 2.4.1) and deemed to be of value for western blot analysis were then transferred to 0.2 µm nitrocellulose membranes using Trans-Blot Turbo Mini 0.2 µm Nitrocellulose Transfer Packs (Bio-Rad Laboratories) and the Trans-Blot Turbo Transfer System (Bio-Rad Laboratories). The transfers were executed using the pre-programmed “MIXED MW” protocol.

Post-transfer nitrocellulose membranes were blocked with 1% casein in phosphate buffered saline (PBS) solution for 2 hours nutating at room temperature or overnight at 4 °C, washed in PBS with 0.05% v/v Tween-20 (PBST) for three cycles of 5 minutes, probed with a primary antibody (as needed) in 1% casein in PBS for 1 hour at room temperature, washed in PBST for three cycles of 5 minutes, probed with a secondary antibody in 1% casein in PBS for 1 hour at room temperature, washed in PBST for three cycles of 5 minutes, and then developed for 5 minutes using Clarity Western ECL Substrate (Bio-Rad Laboratories) (which are compatible with horseradish peroxidase-conjugated antibodies). Western blots were imaged using the ChemiDoc Imaging System. Antibodies used for western blotting are listed in Table 2.3.

Table 2.3. A list of antibodies used for western blotting. VIN, plant virus-based immunosorbent nanoparticle; CP-FcAL, coat protein fragment crystallizable (Fc) region affinity ligand; rCMG2-Fc, recombinant plant-made capillary morphogenesis protein Fc-fusion; rPTH-Fc, recombinant plant-made parathyroid hormone Fc-fusion; hIgG, human immunoglobulin G; HC, heavy chain; LC, light chain; G-CSF, granulocyte colony stimulating factor; BSA, bovine serum albumin.

Biomolecule of interest	Detection region	Primary antibody (dilution factor)	Secondary antibody (dilution factor)
VIN CP-FcAL	FcAL	Rabbit anti-Protein A IgG (1:25,000)	Goat anti-rabbit IgG-HRP (1:3,000)
rCMG2-Fc, rPTH-Fc, hIgG	HC and LC of IgG	N/A	Goat anti-human IgG-HRP (1:2,500)
G-CSF	G-CSF	Rat anti-G-CSF IgG (1:500)	Goat anti-rat IgG-HRP (1:10,000)
G-CSF	G-CSF	Rabbit anti-G-CSF IgG (1:1,000)	Goat anti-rabbit IgG-HRP (1:3,000)
BSA	BSA	Rabbit anti-BSA IgG (1:3,000)	Goat anti-rabbit IgG-HRP (1:3,000)

2.5.3. Dot blot

The prey protein sample (the sample being tested for binding behavior) was prepared by diluting to 0.5 – 20 µg prey protein per 2 – 10 µL volume. The prey protein sample dilution is only

necessary for "far western" dot blots[44] than the standard dot blot, in that this dilution is used to establish a given molar ratio with the bait protein (the sample with pre-established binding behavior). A 0.2 µm nitrocellulose membrane was prepared by marking a grid formation with either pencil or light physical imprint demarcation (e.g., 2 mL tube cap pressed firmly into the membrane). The prey protein sample aliquots were then expunged onto the membrane and given 30 – 60 minutes to dry.

The prey protein-loaded membranes were blocked with 1% casein in PBS solution for 2 hours nutating at room temperature or overnight at 4 °C and washed in PBST for three cycles of 5 minutes. For "far western" dot blots only, the membrane was first probed with 1 – 10 µg bait protein in 1% casein in PBS for 3 hours at room temperature and washed in PBST for three cycles of 5 minutes. For both the "far western" and standard dot blots, the membrane was then probed with a primary antibody (as needed) in 1% casein in PBS for 1 hour at room temperature, washed in PBST for three cycles of 5 minutes, probed with a secondary antibody in 1% casein in PBS for 1 hour at room temperature, washed in PBST for three cycles of 5 minutes, and then developed for 5 minutes using Clarity Western ECL Substrate (Bio-Rad Laboratories) (which are compatible with horseradish peroxidase-conjugated antibodies). Dot blots were imaged using the ChemiDoc Imaging System. Antibodies used for dot blotting are listed in Table 2.4.

Table 2.4. A list of antibodies used for dot blotting. VIN, plant virus-based immunosorbent nanoparticle; CP-FcAL, coat protein fragment crystallizable (Fc) region affinity ligand; rCMG2-Fc, recombinant plant-made capillary morphogenesis protein Fc-fusion; IgG, immunoglobulin G.

Biomolecule of interest	Detection region	Primary antibody (dilution factor)	Secondary antibody (dilution factor)
VIN CP-FcAL	FcAL	Rabbit anti-Protein A IgG (1:25,000)	Goat anti-rabbit IgG-HRP (1:3,000)

		N/A	Goat anti-rabbit IgG-HRP (1:3,000)
			Goat anti-human IgG-HRP (1:2,500)
			Rat anti-mouse IgG-HRP (1:1,000)
			Rabbit anti-goat IgG-HRP (1:3,000)
			Rat anti-human IgG-HRP (1:250)

2.5.4. Total soluble protein assays

Total soluble protein concentrations were measured using the Bradford assay and Pierce-modified Lowry assay. The latter was used exclusively for the measurement of wild-type tobacco mosaic virus concentration, given that the glassy surface and limited residue exposure was not adequately detected by the Bradford assay.

The Bradford assay was performed in a 96-well plate with each well consisted of 10 µL protein sample (diluted as desired using the protein solution buffer or ddH_2O) and 190 µL 1x Bradford dye. The samples were loaded into technical triplicate and standard curve samples consisting of bovine serum albumin (BSA) at 0 – 0.5 mg/mL were also loaded in technical triplicate to the 96-well plate. The dye loading was performed with a multi-channel pipettor as to minimize differences in dye-exposure time per well. The plate was given > 5 minutes to incubate/develop prior to assay measurement. The incubated plate was then analyzed with the SpectraMax® M4 spectrophotometer (Molecular Devices, San Jose, CA, USA). Absorbance measurements at 590 nm and 450 nm were used to generate outputs of $A_{590\ nm}/A_{450\ nm}$ (see literature supporting the 450 nm normalization for linearization[45]) that were then translated into total soluble protein via the BSA standard curve assessment.

The Pierce-modified Lowry assay is another colorimetric assay performed in 96-well plates like Bradford assay with a working range of 1 – 1.5 mg/mL for total soluble protein content. Accordingly, the standard curve consists of BSA at 0 – 1.5 mg/mL. Each well consisted of 40 µL protein sample (diluted as desired using the protein solution buffer or ddH_2O), 200 µL of Modified Lowry reagent, and 20 µL 1x Folin-Ciocalteu reagent (added with multi-channel pipettor). The loaded plates were mixed on a plate mixer for 30 seconds and then cover and incubated at room temperature for 30 minutes. The incubated plate was then analyzed with the SpectraMax® M4 spectrophotometer (Molecular Devices) at an absorbance of $A_{750\ nm}$ and translated into total soluble protein via the BSA standard curve assessment.

2.5.5. Transmission electron microscopy (TEM)

Virus-containing solutions were TEM imaged using negative stain. Carbon film on 300 mesh copper discs (Ted Pella, Redding, CA, USA) were prepared for increased hydrophilicity by glow discharge at 30 mA for 30 seconds on a glass slide. All manipulations of the copper discs during sample preparation were carried out using anti-capillary reverse (self-closing) tweezers (Ted Pella Inc., Redding, CA, USA) designed to pick up less moisture. 5 µL liquid VIN solution samples were loaded onto the prepared disc, incubated 30 seconds, and then blotted with filter paper. Filter paper was cut into quarters prior to blotting to improve the edge length per filter and generate long stretches of an even edge for blotting. Negative stain was applied in five sequential rounds of 5 µL uranyl sulfate loading, 30 second incubation, and filter paper blotting. TEM was performed using a JEM-1230 transmission electron microscope (JEOL, Peabody, MA, USA).

2.5.6. Amino acid sequence determination

Amino acid sequence determination was performed using a gel band excision sent to the Genome Center Proteomics Core at the University of California, Davis for liquid chromatography tandem mass spectrometry (LC-MS/MS). In brief, the protein sample was loaded at run through Coomassie stain SDS-PAGE (at > 1 µg target protein per sample). Do not use stain-free gels for this application. The gel was lightly stained to determine the band location, a precision scalpel was used to cut the gel band from the bulk gel, and the cut band was stored in a sealed 1.5 µL tube.

The LC-MS/MS analysis data was returned and assessed using the Scaffold 4.0 software (Proteome Software, Portland, OR, USA). Protein thresholds were set to 5.0% false discovery rate (FDR), 0.6% decoy FDR and peptide thresholds were set to 1.0% FDR, 0.06% decoy FDR. Spectrum count and coverage are both important factors in correct identification; spectrum count linearly correlates with abundance and >70% coverage is generally defined as very successful protein analysis. There are multiple reasons why analysis might not pick up identity for all of the peptides (e.g., incomplete protein digestion, peptide may pass through the reverse phase column with salt and not be analyzed).

Chapter 3. Techno-economic Materials and Methods

"You can use an eraser on the drafting table or a sledgehammer on the construction site."

-Frank Lloyd Wright

This chapter is based on the following forthcoming publication:

McNulty M.J., Nandi S., and McDonald K.A. (Accepted). Techno-economic modeling and simulation for plant-based manufacturing of recombinant proteins. *Recombinant Proteins in Plants*.

Abstract

Techno-economic modeling and simulation is a critical step in defining a manufacturing process for evaluation of commercial viability and to focus experimental process research and development efforts. Techno-economic analysis (TEA) is increasingly demanded alongside scientific innovation by both public and private funding agencies to maximize efficiency of resource allocation. It is particularly important for plant-based manufacturing, and other non-traditional recombinant protein production platforms, to explicitly demonstrate the manufacturing potential and to identify critical technical and economic challenges through robust techno-economic analysis. In addition, *in silico* process modeling and TEA of scaled biomanufacturing facilities allows rapid evaluation of the impacts of process and economic changes on capital expenditures (CAPEX, also sometimes referred to as Total Capital Investment), operational expenditures (OPEX, also known as Total Manufacturing Costs or Total Production Costs), cost of goods sold (COGS, also known as Unit Production Costs) and profitability metrics such as net

present value (NPV) and discounted cash flow rate of return (DCROR, also known as internal rate of return or IRR). These models can also be used to assess environmental, health and safety impact of a designed biomanufacturing facility to evaluate its sustainability and environmental-friendliness. Here we describe a general method for performing techno-economic modeling and simulation for and environmental assessment of plant-based manufacturing of recombinant proteins.

3.1. Introduction

Techno-economic analysis (TEA) is the evaluation of a manufacturing process on technical viability, economic viability, and environmental impact. Techno-economic analyses can range from simple back-of-the-envelope calculations completed in several hours to rigorous and highly detailed evaluations performed over the course of months. The cost, accuracy, and scope of the analysis is dictated by the use case of the analysis in the product's life cycle. Table 3.1 details the types of design estimates and Figure 3.1 details where in the product life cycle different types of design estimates are generally executed.

Table 3.1. Types of techno-economic design estimates, a description of their estimate bases, and the probable accuracy range. Adapted from Peters, Timmerhaus, and West (2003)[46].

Level	Type of Design Estimate	Description	Accuracy Range
1	Order-of-magnitude estimate (*ratio estimate*)	Based on similar previous project data	±30%
2	Study estimate (*favored estimate*)	Based on knowledge of major equipment items	±30%
3	Preliminary estimate (*scope estimate*)	Based on sufficient data to permit the estimate to be budgeted	±20%

4	Definitive estimate (*project control estimate*)	Based on almost complete process data	±10%
5	Detailed estimate (*contractor's estimate*)	Based on complete engineering drawings, specification, and site surveys	±5%

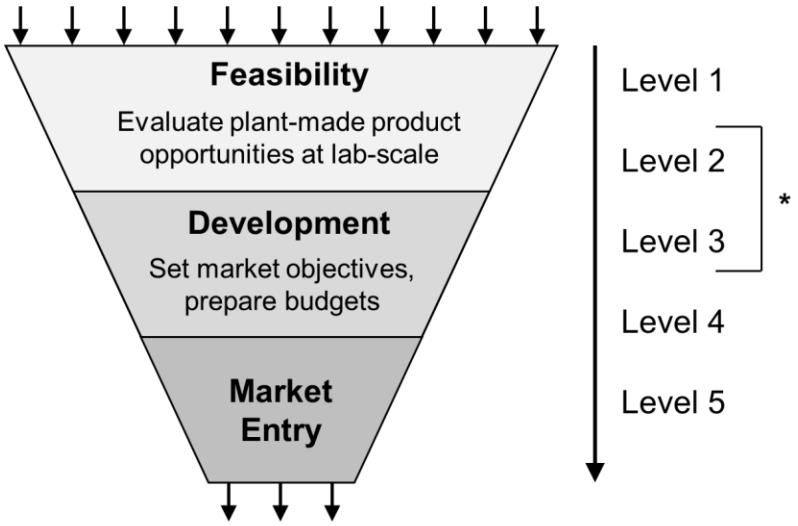

Figure 3.1. A simple illustration of a plant-made product life cycle and an approximation of where in that life cycle a given level techno-economic design estimate is executed. An asterisk (*) indicates the level of design estimates that we have identified as the most pressing need in the plant-made product community, and consequently the target design estimates detailed in this method. Adapted from Petrides, Carmichael, Siletti, and Koulouris (2019)[47].

The most immediate need of the plant-based manufacturing community is to assess, and demonstrate, the commercial potential of lab- or pilot-scale manufacturing process data. Often these analyses are performed prior to extensive process research and development to identify "economic hot spots" and help guide the selection of materials, reagents, and unit procedures and focus experimental and pilot studies. For these reasons and more, the use of techno-economic analyses is well-established for commercialization of chemical, petrochemical, and biofuels

manufacturing. Similarly, techno-economic analyses are credited as a driving force in the commercial success of non-pharmaceutical plant-based manufacturing and are expected to play a similar role in pharmaceutical plant-based manufacturing[48]. Per Figure 3.1, this is typically met by execution of a Level 2 or Level 3 techno-economic design estimate. The focus of this chapter is to detail a techno-economic modeling and simulation method to meet this need with particular focus on plant-made recombinant protein production.

Readers can expect to be able to answer questions such as: does the lab-scale manufacturing process demonstrate potential commercial viability? What is the current process bottleneck? How can research and development efforts be effectively allocated to reach commercial feasibility? How do manufacturing costs vary with facility production level, protein expression level, and/or downstream recovery? Which unit procedures and/or cost items contribute the most to the cost of goods sold (COGS)? Which equipment items contribute the most to the total capital investment (also referred to as capital expenditure (CAPEX))? What are the main contributors to environmental, health, and safety (EHS) impact, and how does the impact compare with alternative production schemes?

3.2. Materials

Techno-economic analyses rely on an often-complex series of mass and energy balances layered with equipment and scheduling constraints, all of which drive economic and profitability calculations. These calculations can be performed manually via spreadsheet or, more commonly, through use of a process simulation tool (PST). A PST is a software with built-in equipment sizing, material and energy balances, operations scheduling, and techno-economic framework and

capabilities. A list of commercially available PSTs commonly used in biomanufacturing is included in Table 3.2; some companies have developed their own in-house tools.

Table 3.2. A list of process simulation tools useful for techno-economic analyses. An asterisk (*) indicates the most common tools used in biomanufacturing, based on the authors' experiences.

Software	Company
Aspen Plus	Aspen Technology, Inc.
BioSolve*	Biopharm Services Limited
CHEMCAD	Chemstations, Inc.
SuperPro Designer®*	Intelligen, Inc.

The techno-economic model and simulation method detailed in this chapter is based on the use of SuperPro Designer. A free trial version of SuperPro Designer (http://www.intelligen.com/demo.html) can be used to view and manipulate existing techno-economic models. The full paid version of SuperPro Designer is required to execute the complete method detailed in this chapter. Lite and Intermediate editions are also available at reduced cost and may be present a viable solution for modeling a restricted number of process steps.

3.2.1. Technical Considerations of SuperPro Designer

SuperPro Designer is a powerful PST with over 140 unit procedures/operations typically used in biomanufacturing, drag-and-drop construction of process flow diagrams, built-in capabilities for mass and energy balances, equipment sizing and cost models, scheduling and more, supported by an extensive suite of charts and reports on facility performance and economics and a chemical component and mixture database for some commonly used chemicals. This greatly enhances and simplifies the techno-economic analysis as compared to manual spreadsheet methodology.

However, the software structure in turn imposes constraints, some of which are important to note for readers new to techno-economic analysis and SuperPro Designer. Key considerations and limitations include:

- Limited thermophysical property database for biochemical systems making vapor-liquid and liquid-liquid equilibrium calculations more challenging.
- Mass balances are used. Other units of accounting (e.g. activity units, cell number/density, viral genome copies) must be converted to an equivalent mass.
- Facility scheduling capabilities are limited, with advanced functions segmented into Intelligen's complimentary software product, SchedulePro. Without this complimentary software, SuperPro Designer scheduling limitations include that only a single-product facility can be designed, every batch must be identical, every year of operation during the facility lifetime is assumed to be the same (although production level as a percentage of the maximum capacity can be modified each year), and scheduling resets at the end of every year (e.g. partial batches extending past year end do not complete in the following year, and are not counted in costs or production level, instead the recipe scheduling begins anew)

3.2.2. Plant-Based Manufacturing Limitations with SuperPro Designer

Upstream unit procedures for plant-based manufacturing, from the various methods of plant cultivation (e.g. indoor hydroponic, greenhouse, outdoor field) to plant-specific transfection strategies (e.g. agroinfiltration) to plant harvesting, are not included in SuperPro Designer's built-

in unit procedures/operations. However, users can adapt the “Generic Box” unit procedures that SuperPro Designer provides to implement these operations.

It is worth noting that SuperPro Designer does allow for integration with other software (e.g. Microsoft Excel, Matlab) through the Component Object Model (COM) library, a feature which provides the information for accessing SuperPro Designer variable-related values. This feature is recommended for advanced users and can be used to plug-in existing model behavior generated in a different software to augment the kinetic modeling options available in SuperPro Designer for a specific unit procedure (e.g., plant cultivation performance dependence on daily temperature and humidity levels).

The authors have found that local agricultural extension hubs that deal with agricultural production and economics can serve as valuable resources in populating the plant-specific unit procedure and equipment information. Other useful resources include published literature on agricultural economics and direct contact with regional farms, vertical agriculture companies, and agricultural businesses.

Realistic input data for plant-specific unit procedures are critically important for the analysis. A significant shortcoming in the techno-economics of plant-based manufacturing is the lack of publicly available standard databases for plant-specific unit procedures. Development of such databases would immensely benefit the plant-based manufacturing research community to assess lab- or pilot-scale results and translate them into commercial feasibility.

3.2.3. Techno-Economic and Plant-Based Manufacturing Resources

Plant-based manufacturing is a relatively nascent yet growing area, arguably on the cusp of realizing more mainstream commercial successes. There are currently about ten commercial plant-based production facilities worldwide. Research in plant-based manufacturing to date has spanned a diverse set of production platforms, ranging in production hosts from leafy greens to grain seeds to hairy roots, and in cultivation strategies from transient indoor hydroponics to transgenic outdoor field growth. However, despite this breadth in methodology, there is only a limited number of TEAs, which cover a few of the many plant-based manufacturing methodologies. This book chapter aims to provide a more holistic perspective on developing plant-based manufacturing TEAs to address this gap.

The published plant-based manufacturing TEAs, as shown in Table 3.3, represent an indispensable resource for readers new to TEA. Much of the information built into the models described in the publication can be accessed and leveraged for future analyses. In fact, in several cases the models themselves are available for download, viewing, and direct manipulation for readers interested in exploring them further.

Additional publications that are recommended to the reader include those related to reporting by commercial-scale plant-based manufacturing companies. This currently includes work published by iBio in 2015[49], Protalix in 2015[50], Medicago in 2010[51], and Ventria in 2005[52].

Table 3.3. A list of recently published plant-based manufacturing techno-economic analyses spanning multiple industries, target molecules, expression systems, degree of product purity required, and facility production level. BChE, Butyrylcholinesterase; mAb, monoclonal antibody; HRP, horseradish peroxidase enzyme; human lactoferrin.

Industry	Target Molecule	Expression System	Production (kg/year)	Source
Pharmaceutical	BChE	Transgenic suspension culture	25	Corbin et al., 2020[53]
Food Safety	Antimicrobial protein	Transgenic whole plant	500	McNulty et al., 2019[54]
Pharmaceutical	Griffithsin	Transient whole plant	20	Alam et al., 2018[55]
Pharmaceutical	mAb	Transient whole plant	300	Nandi et al., 2016[56]
Reagent	HRP	Transient whole plant	5	Walwyn et al., 2015[57]
Pharmaceutical	BChE	Transient whole plant	25	Tusé et al., 2014[58]
Biofuel	Cellulase enzyme	Transgenic whole plant	3 x 10^6	
Pharmaceutical	hLF	Transgenic plant seed	600	Nandi et al. 2005[52]

3.3. Method

The following method is designed to guide the reader through the process of translating lab- and/or pilot-scale data into a biomanufacturing facility techno-economic model via project scoping, *in silico* scale-up, and performance exploration with sensitivity and scenario analysis. Figure 3.2 displays a high-level graphical representation of the complete method workflow.

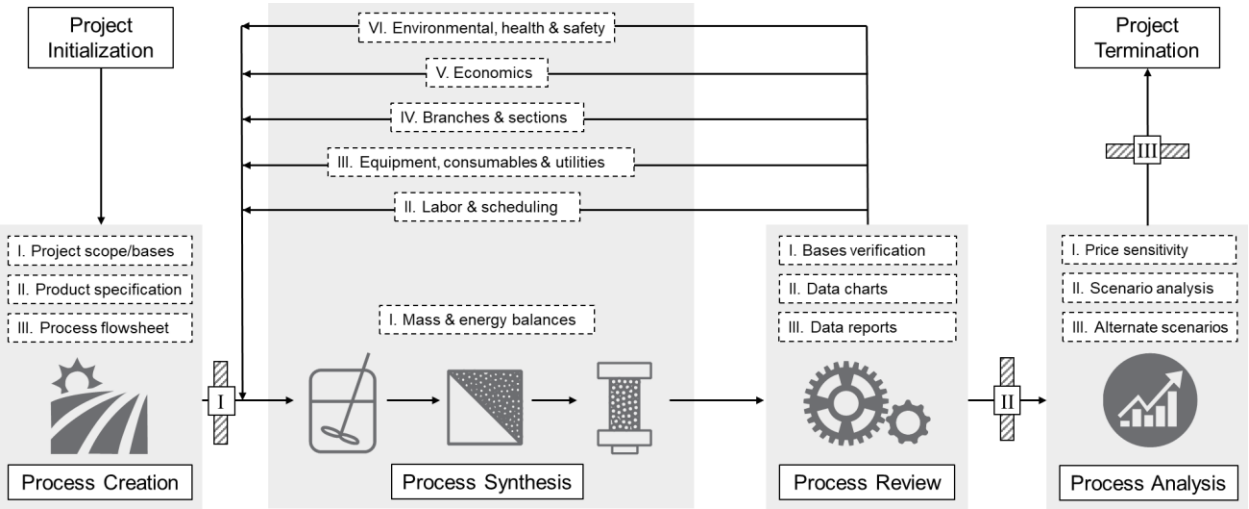

Figure 3.2. Graphical representation techno-economic simulation and modeling workflow presented in the method detailed in this chapter. The hashed line rectangle represents a recommended Stage Gate, an important step in project management in which the project progress is reviewed and approved by key stakeholders.

3.3.1. Process Creation

In the following section the reader will be defining high-level project targets, managing project expectations, and getting key stakeholder buy-in.

1. Define project scope. This includes defining the project scope, deliverables, timeline, and key stakeholders (this may involve project management, funding agency point-of-contact, a board of advisors, business strategists, and research collaborators, to name a few).

2. Define the facility design premises. This includes the regulatory framework within which the product is expected to be governed (see Note 1), the mode of operation (batch, semicontinuous, or continuous), the general manufacturing strategy and facility (greenfield – new construction on undeveloped land, contract manufacturing organization (CMO), and/or expansion of an existing facility), expression system/plant host, the anticipated annual operating factor (hours per year of operating time), the facility location (see Note 2), the production demand (see Note 3), and facility lifetime (see Note 4).

3. Define the product specifications. This includes the required product purity and quality specifications, the desired final product stream composition, and the value of by-products.

4. Develop a process block diagram with select critical process parameter and key performance indicator ranges defined (see Note 5), as shown in Figure 3.3.

5. Develop a more detailed process flowsheet with specific raw materials, consumables, and specific unit procedures appropriate to the manufacturing production scale (see Note 6).

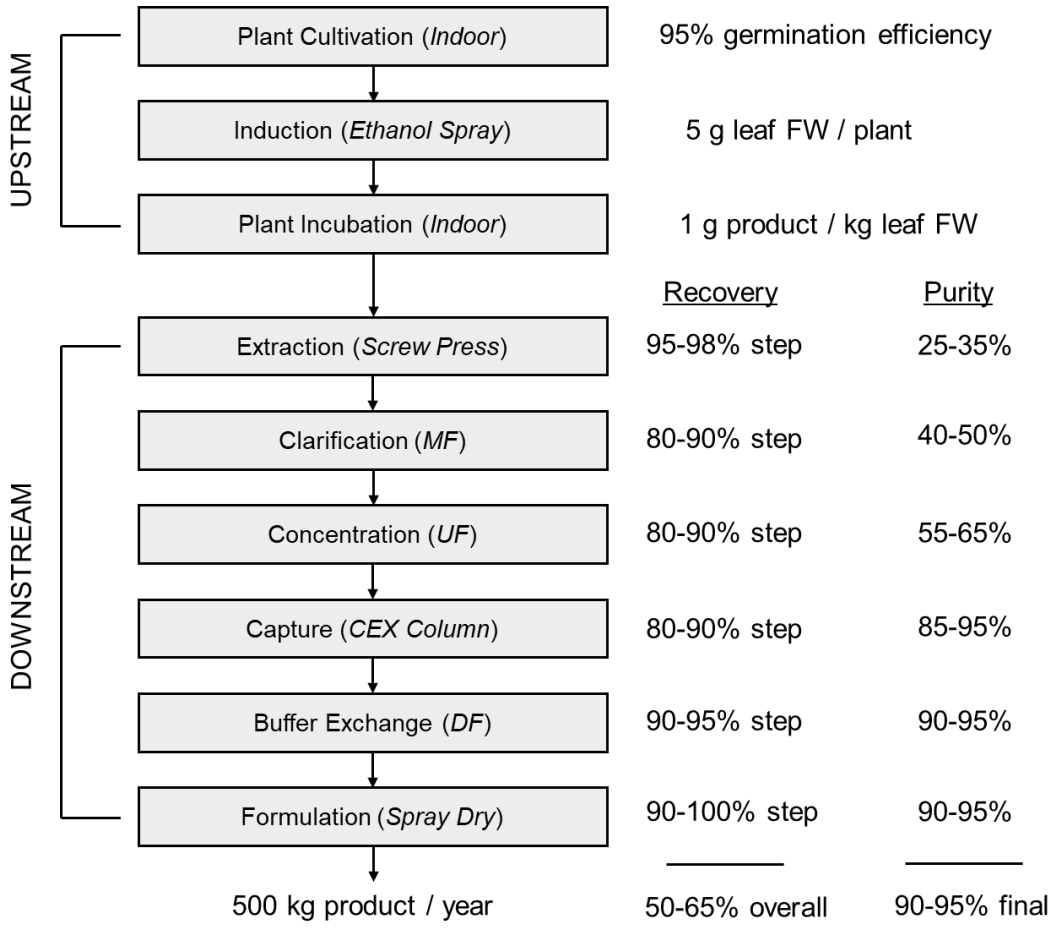

Figure 3.3. An example block flow process diagram with defined general process schematic and facility performance parameters, such as expression level, downstream recovery, final product purity, and annual production capacity. This example is loosely based on the commercial manufacturing process simulated in our recently published techno-economic analysis of antimicrobial protein production in whole plants for food safety applications. FW, fresh weight; MF, microfiltration; UF, ultrafiltration; CEX, cation exchange; DF, diafiltration.

3.3.1.1. Stop Gate I

Here the reader will be assembling a process creation report and communicating with key stakeholders for a Stop Gate before proceeding to process synthesis. This step is critical for setting

project expectations. Precise contents and format of the report and/or presentation will depend on the specific project and agreement with key stakeholders. Below are generally recommended steps.

1. Confirm engagement of key stakeholders and come to an agreement on preferred communication format and frequency.
2. Detail a preliminary project scope based on current knowledge, being as specific as possible to identify any mismatched expectations early on. Include questions on ill-defined and/or unknown aspects of the project scope, prepared in such a way to actively engage the key stakeholders.
3. Detail project roles and responsibilities linked to precise deliverables that are mapped to a project timeline.

3.3.2. Process Synthesis

In the following section the reader will be developing the "base case" techno-economic model, iteratively building layers of mass & energy balances (Section 3.3.2.1), labor & scheduling (Section 3.3.2.2), equipment, consumables & utilities (Section 3.3.2.3), branches & sections (Section 3.3.2.4), economics (Section 3.2.5), and environmental, health, and safety impact (Section 3.3.2.6), followed by developing a report and initiating review with key stakeholders at Stop Gate II (Section 3.3.2.7).

3.3.2.1. Mass & energy balances

Here the reader will be developing the first layer of the model, the mass & energy balances, and consequently the layout of unit procedures and stream connections in the visual design environment (VDE). The first step in process simulation is generally to select either batch or continuous mode of operation and annual operating time available per year. This method focuses on detailing process modeling and simulation for a facility run in batch mode operation, which is currently most commonly used in plant-made recombinant protein production processes. For reference, see the recent work of Pleitt et al. 2019 for an example of techno-economic evaluation of continuous downstream biomanufacturing[59].

The reader will be walked through how to register pure components and stock mixtures (solutions commonly used throughout the process such as buffers, cleaning agents, etc.). This is followed by populating the process flowsheet with unit procedures, a sequence of actions performed in single equipment item, defining each of those actions, which are referred to as operations, connecting the populated unit procedures with stream lines to indicate flow directionality, and populating both the operations and input streams with registered components and stock mixtures.

Process review recommended during mass & energy balance development is primarily to assess stream contents at each at step of the process flow. Two tools to assist in this review: a) the unit procedure activity overview window (*VDE > Unit Procedure > Procedure Activity Overview*) for a table showing the status of the contents at the start of every operation, and b) enable view of information tags on process streams (*VDE > Stream > Style > Edit Style > Display Also > Info Tag checkbox > Info Tag*) for a simple view of stream contents including temperature, pressure, and total mass/volumetric flow.

1. Begin process simulation and modeling on SuperPro Designer. Figure 3.4 introduces the SuperPro Designer user interface and highlights key terminology referenced in the remainder of the method.

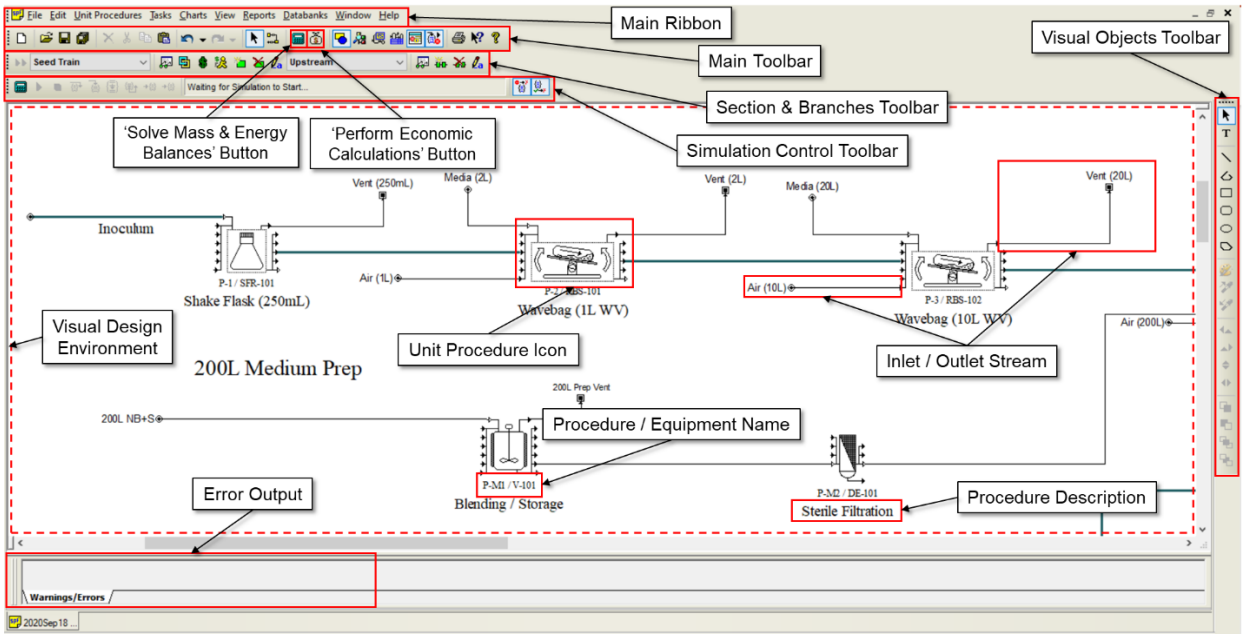

Figure 3.4. The SuperPro Designer® user interface annotated with key terms used throughout the methodology detailed in this chapter. The primary user interface includes a series of toolbars and the visual design environment (VDE). A portion of our recently published techno-economic analysis on semicontinuous bioreactor production of biopharmaceuticals in transgenic rice cell suspension cultures (Corbin et al., 2020)[53] is used for this illustration.

2. Check the Pure Components and Stock Mixtures databanks (*Main Ribbon* > *Databanks* > *Pure Components OR Stock Mixtures*) for required processing stream constituents, including both raw material inputs and reaction products (see Note 7).

3. Register the required Pure Components and Stock Mixtures (*Main Ribbon* > *Tasks* > *Pure Components OR Stock Mixtures* > *Register/Edit, View Properties*) from existing databanks or by adding a new item not previously stored in a databank with any processing stream

constituents that are missing from the existing set by registering new items (see Notes 8, 9).

4. Drop-in the first (high upstream) unit procedure defined in the detailed process flow block diagram (Section 3.1, Step 3) to the VDE (*Main Ribbon > Unit Procedures*). Use "Connect Mode" (*Main Toolbar > Connect Mode*) to add stream connection lines to the unit procedure input/output ports on the VDE to define the number, and relationship of, stream inputs/outputs (see Note 10).

5. Initialize the first unit procedure by defining the input/output streams with registered ingredients (*VDE > Stream > Registered Ingredients > Add Ingredient*), setting total flowrates (*VDE > Stream > Total Flowrates*) and ingredient mass composition (*VDE > Stream > Composition*), and populating the unit procedure with an operation sequence (*VDE > Unit Procedure > Add / Remove Operations*). Only operations compatible with the given unit procedure are available to be added to the sequence list.

6. Initialize each operation in the sequence in turn (*VDE > Unit Procedure > Operation Data > Select Operation > Oper. Cond's*). Operation-specific conditions required to perform the mass balances are required at minimum (e.g., for the "Transfer In" operation, the inlet stream must be defined; for the "Stoichiometric Reaction" operation, the reaction sequence must be defined).

7. Use SuperPro Designer's "Solve mass & energy balances" button (*Main Toolbar > Solve ME Balances*) to confirm that the unit procedure has been properly initialized. Any relevant warnings and/or errors associated with the mass & energy balances as they are defined will population in the Error Output window below the VDE.

8. Repeat steps 3 – 7 for each unit procedure defined in the detailed process flow block diagram (Section 3.1, Step 3) until the entire process flow diagram has been described in the VDE (see Note 11).
9. Define the main product stream and flow basis for which all material and economic reports are referenced by (*Main Ribbon* > *Tasks* > *Stream Classification* > *Main Product/Revenue*).
10. Add relevant cleaning operations to unit procedures (see Note 12).

3.3.2.2. Labor & scheduling

Here the reader will be defining the labor and scheduling of the model. The reader will be provided with information on how to define process scheduling constraints, which inform the number of times that the full process flow sheet (also referred to as a recipe) is executed per year, followed by how to define the manufacturing operator positions (termed labor types) executing the recipe. Then the operations are populated with specific labor types and labor rates. Lastly, the duration of, and coordination between Operations is defined to determine scheduling and ultimately the total duration of the recipe.

Process review recommended during labor & scheduling development is to assess scheduling connections between different unit procedures and operations within each procedure, and operators required to meet labor demands. Two tools to assist in this review: a) the Operations Gantt Chart (*Main Toolbar* > *Charts* > *Gantt Charts* > *Equipment GC*) to confirm scheduling connections, and b) the Labor Demand chart (*Main Toolbar* > *Charts* > *Labor*) to assess the number of operators required at any given time.

1. Define the high-level process scheduling constraints (e.g., number of batches per year, annual operating time) in the Recipe Scheduling Information window (*Main Ribbon > Tasks > Recipe Scheduling Information*) (see Note 13).

2. Check the Labor databank (*Main Ribbon > Databanks > Labor Types*) and populate with any labor types that are missing from the existing set by registering any new items (see Note 14). Labor types that are currently used in the existing process can be viewed alongside their annual demand, for reference (*Main Ribbon > Tasks > Other Resources > Labor*).

3. Designate the labor type and labor rate associated with each operation in each unit procedure (*VDE > Unit Procedure > Operation Data > Select Operation > Labor, etc. > Labor*) (see Note 15).

4. Set the duration of each operation, given by the setup time and process time, in each unit procedure (*VDE > Unit Procedure > Operation Data > Select Operation > Oper.Cond's > Duration*) (see Note 16).

5. Set the scheduling of each operation in each unit procedure (*VDE > Unit Procedure > Operation Data > Scheduling*) (see Note 17).

3.3.2.3. Equipment, consumables & utilities

Here the reader will be defining the equipment items that house the unit procedures, as well as the specific consumables and utilities used with the equipment during execution of the unit procedure. It is recommended that the equipment items be first defined using "Design Mode", wherein the

equipment size is calculated by SuperPro Designer to be able to meet the throughput requirements of the unit procedure operations and to process the full stream volume.

The reader will be walked through how to assign equipment items to unit procedures. This is followed by defining and populating the equipment with consumables, items used by equipment resources for a limited duration (e.g., use hours, recipe cycles) before they must be disposed of and replaced, and then defining and populating the operations with utilities, useful resources required for equipment operation (e.g., power, heat transfer agents).

Process review recommended during equipment, consumables & utilities development includes checking equipment-related scheduling and facility power demands. Three tools to assist in this review: a) the Equipment Occupancy chart (*Main Ribbon > Charts > Equipment Occupancy*), b) the Equipment Gantt Chart (*Main Ribbon > Charts > Gantt Charts > Equipment GC*), and c) the Power Demand chart (*Main Ribbon > Charts > Power*).

1. Designate the equipment associated with each unit procedure, and the respective equipment attributes (e.g., material of construction, sizing dimensions, number of units) (*VDE > Unit Procedure > Equipment Data > Equipment*). By default, SuperPro Designer assigns each unit procedure to a distinct equipment sized according to the mass & energy balance calculations using “Design Mode” (see Notes 18, 19, 20).

2. Check the Consumables databanks (*Main Ribbon > Databanks > Consumables*) and populate with any processing consumables that are missing from the existing set by registering any new items. Consumables that are currently used in the existing process can be viewed alongside their annual demand, for reference (*Main Ribbon > Tasks > Other Resources > Consumables*).

3. Set the consumable type and replacement frequency for each unit procedure (*VDE > Unit Procedure > Equipment Data > Consumables*) (see Note 21).

4. Check the Power Types databank (*Main Ribbon > Databanks > Power Types*) and populate with any power types that are missing from the existing set by register any new items (see Note 22). Power types that are currently used in the existing process can be viewed alongside their annual demand, for reference (*Main Ribbon > Tasks > Other Resources > Power*).

5. Check the Heat Transfer Agents databank (*Main Ribbon > Databanks > Heat Transfer Agents*) and populate with any heat transfer agent types that are missing from the existing set by registering any new items. Heat transfer agent types that are current used in the existing process can be viewed alongside their annual demand, for reference (*Main Ribbon > Tasks > Other Resources > Heat Transfer Agents*).

6. Set the power and heat transfer agent types and rate for each operation within each unit procedure (*VDE > Unit Procedure > Operation Data > Select Operation > Labor, etc. > Auxiliary Utilities*).

3.3.2.4. Branches & sections

Here the reader will be defining sections, a grouped set of unit procedures, and branches, a grouped set of sections, to enable future information gathering specifically on these groupings. For many bioprocesses it is useful to at least have an upstream and downstream differentiation (either by branches, if additional granulation/grouping is desired, or sections) since these process areas might

have different regulatory requirements that could impact things like QA/QC and labor costs. This is particularly relevant in some plant-based manufacturing processes.

Process review recommended during branches & sections development is simply to verify that proper unit procedure allocations have been made to branches and sections. Two tools to assist in this verification include: a) the Edit Branch button (*Section & Branches Toolbar > Edit Branch*), and b) the Materials & Streams report (*Main Ribbon > Reports > Materials & Streams*).

1. Define process branches, as needed (*Sections & Branches Toolbar > New Branch*).
2. Define process sections, as desired, either directly within the active process branch (*Sections & Branches Toolbar > New Section*). The section sequence within in a specific process branch can be modified to reflect the desired process flow (*Sections & Branches Toolbar > Edit Branch > Section Sequence*).
3. Add unit procedures into the relevant process branches sections (*with a Unit Procedure highlighted in the VDE… Sections & Branches Toolbar > Add to Section*).

3.3.2.5. Economics

Here the reader will be defining the cost structure for the techno-economic model developed so far. Figure 3.5 displays an example cash flow diagram to illustrate the key economic stages of a project lifetime that should be considered when developing the cost structure in this method.

The reader will be walked through how to define project time valuation (e.g. year of analysis, construction period, project lifetime), project financing (e.g. debt incurred and loan period), operating capacity for each year (i.e. ability to set gradual facility production ramp-up), and the

manufacturing cost, as defined by the costs associated with operation, namely the facility operating expenditure (OPEX) ($/year), referred to as Total Annual Operating Cost in SuperPro Designer, constituents (materials, facility-dependent costs, labor-dependent costs, laboratory/QC/QA, consumables, utilities, waste treatment/disposal, transportation, miscellaneous, and other), by the costs associated with capital assets and their fixed capital costs, namely capital expenditure (CAPEX) ($), referred to as Total Capital Investment in SuperPro Designer, including direct fixed capital (comprised of direct costs that typically includes costs for listed and unlisted purchased equipment, equipment installation, piping, instrumentation, insulation, electrical facilities, buildings, yard improvement, auxiliary facilities and indirect costs that typically includes engineering, construction, contractors fee and contingency), working capital, start-up and validation, up-front research & development, up-front royalties.

In most cases of Stage 2 and Stage 3 design estimates, manufacturing costs will be sufficient economic information to assess feasibility. The OPEX normalized by production level, known as cost of goods sold (COGS), and also termed as Unit Production Cost in SuperPro Designer, is often used for decision-making. However, there are instances in which profitability can provide essential information on economic viable at this stage of design estimate. Profitability calculations will be detailed in which a product selling price is defined to determine total revenue, and from there to subtract OPEX (including depreciation) and income taxes, to determine the net profit after taxes. Annual cash flows are defined as the net profit after taxes plus depreciation minus any capital expenditures; annual cash flows are used to determine profitability metrics. Common profitability metrics are Return on Investment (ROI) (%), a simple metric of investment efficiency that returns annual growth rate, Discounted Flow Rate of Return (DCFROR) (also referred to as Internal Rate of Return (IRR)) (%), a more complex and time-valued metric of investment

efficiency for the annual return, and Payback Time (years), the time required for the facility to reach the break-even point when positive cash flows offset the initial negative cash flows associated with capital expenditures.

Readers should refer to the works of Peters, Timmerhaus, and West (2003)[46] and Turton, Shaewitz, Bhattacharyya, and Whiting (2018)[60] for more detail in estimation of capital cost and scaling, estimation of manufacturing costs, generation of cash flow diagrams, and profitability analyses including the time value of money.

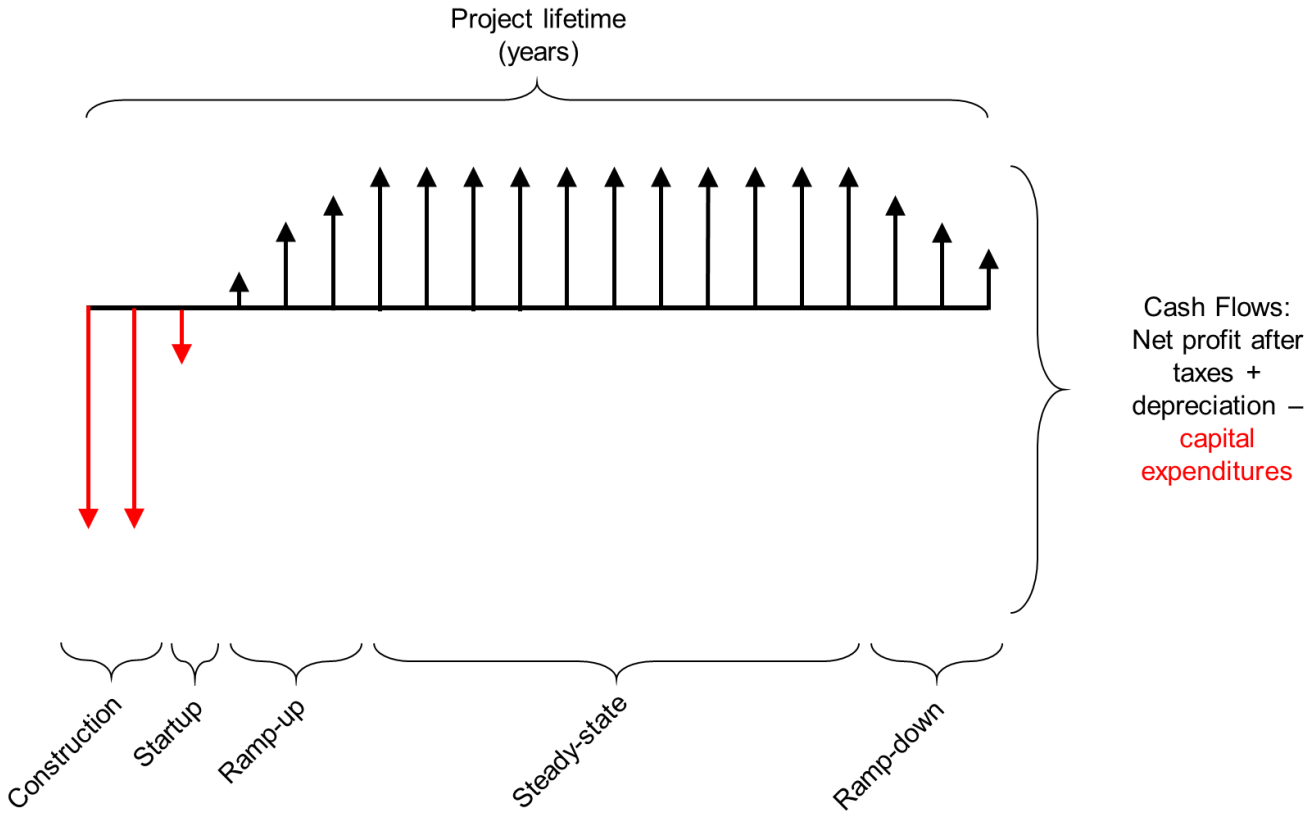

Figure 3.5. An example cash flow diagram for a plant-based manufacturing facility that illustrates the key stages of the project lifetime. The cash flow arrows are not drawn to a particular scale.

Process review recommended during the economics development includes checking correctness and completeness of economic allocations through multiple lenses (e.g., asking questions such as, what is the ratio of upstream to downstream costs, and what are the top economic determinants). Three tools to assist in this review include: a) the Economic Evaluation report (*Main Ribbon > Reports > Economic Evaluation*), b) the Cash Flow Analysis report (*Main Ribbon > Reports > Cash Flow Analysis*), and c) the Itemized Cost report (*Main Ribbon > Reports > Itemized Cost*). The report outputs can be customized (*Main Ribbon > Reports > Report Options*) and entirely custom reports can be defined (*Main Ribbon > Reports > Custom Excel Report*).

Note: numbered steps labeled with an asterisk (*) indicate those related to profitability calculations which are not necessary for manufacturing cost calculations.

1. Define the project time valuation, including year of analysis, construction period, start-up period, project lifetime, inflation rate, and Net Present Value (NPV) interest/discount rate of return (*Main Ribbon > Edit > Process Options > Economic Evaluation Parameters > Time Valuation*) (see Note 23)*.

2. Define the project financing, including the amount of debt incurred, associated loan characteristics, and method for calculation of depreciation (*Main Ribbon > Edit > Process Options > Economic Evaluation Parameters > Time Valuation*) (see Note 24)*.

3. Define project operating capacity for each year within the project lifetime, including a product failure to account for manufacturing not meeting specifications and needing to be scrapped (*Main Ribbon > Edit > Process Options > Economic Evaluation Parameters > Production Level*)*.

4. Define remaining project economic evaluation parameters, including income taxes, advertising and selling expenses, and royalty expenses (*Main Ribbon > Edit > Process Options > Economic Evaluation Parameters > Misc*)*.

5. Define the purchasing price, selling price, and waste treatment or disposal costs for all registered pure component and stock mixtures (*Main Ribbon > Tasks > Pure Components OR Stock Mixtures > Register, Edit/View Properties > View/Edit the Selected Component OR Mixture Properties > Economics*) and for all output streams (*Main Ribbon > Tasks > Stream Classification*) (see Note 25).

6. Define equipment purchasing price and adjustments (e.g. installation cost, maintenance costs) for each equipment item (*VDE > Unit Procedure > Equipment Data > Purchase Cost OR Adjustments*). By default, SuperPro Designer will initialize these values with built-in cost models and adjustments.

7. Define the purchasing price and disposal cost for all registered consumables (*Main Ribbon > Tasks > Other Resources > Consumables > View/Edit Properties > Properties > Cost Data*).

8. Define the purchasing price for all registered power types (*Main Ribbon > Tasks > Other Resources > Heat Transfer Agents > View/Edit Properties > Properties > Price*).

9. Define the purchasing price for all registered heat transfer agents (*Main Ribbon > Tasks > Other Resources > Power Types > View/Edit Properties > Properties > Agent Cost*).

10. Define the cost rate for all register labor types (*Main Ribbon > Tasks > Other Resources > Labor Types > View/Edit Properties > Properties > Cost Data*). The cost rate can be defined either by a Detailed Estimate (including a basic rate plus factors like benefits and

supervision) or by Lumped Estimate. Additionally, define the Labor Time Estimation, the fraction of work time devoted to process-related activity (see Note 26).

11. Define the operating cost adjustments for all process sections (*with a section selected from the Sections & Branches Toolbar drop-down menu… Sections & Branches Toolbar > Section Operating Cost Adjustments*). This includes estimations of facility-dependent costs (e.g. maintenance, depreciation, insurance), lab/quality control/quality assurance costs (as a fraction of the section's labor costs), and miscellaneous expenses (e.g. research and development, validation) (see Note 27).

12. Define the capital cost adjustments for all process sections (*with a section selected from the Section & Branches Toolbar drop-down menu… Sections & Branches Toolbar > Section Capital Cost Adjustments*). This includes estimations of direct fixed capital costs (e.g. cost contributions of direct costs like piping, instrumentation, and indirect costs like engineering and construction), cost allocation factors, and miscellaneous costs (e.g. working capital, upfront research and development, startup and validation costs) (see Note 28).

13. Define stream classifications for each of the output streams (*Main Ribbon > Tasks > Stream Classification*). Set the disposal cost for waste streams and the selling price of revenue streams (see Note 29).

14. Use SuperPro Designer's "Perform economic calculations" button (*Main Toolbar > Perform Economic Calculations*) to update the economic calculations with the newly populated values. Any relevant warnings and/or errors associated with the economic values as they are defined will population in the Error Output window below the VDE.

15. View manufacturing cost metrics (COGS, OPEX, CAPEX) and profitability metrics (ROI, IRR after tax, Payback Time) through the Executive Summary (*Main Ribbon* > *View* > *Executive Summary*) or by generating Economic Evaluation and/or Cash Flow Analysis reports, as referred to in the aforementioned process review tools (see Note 30).

3.3.2.6. Environmental impact

Here the reader will be using the techno-economic model mass balance data to identify environmental, health, and safety "hotspots" that could suggest benefits in changes in raw materials, or incorporation of processes to reduce stream flows or detoxification prior to disposal, and to quantify the amount of water, raw materials, and consumables required to produce a kg of product. In addition, these metrics can be used to compare different biomanufacturing facility designs from a "green engineering" perspective.

The reader will be walked through two complimentary methods – an Environmental, Health, and Safety (EHS) assessment and a Process Mass Intensity (PMI) assessment. The EHS assessment detailed here is based on the semiquantitative short-cut method described by Biwer and Heinzle (2004)[61] that provides EHS metrics for process inputs and outputs that incorporates the degree of hazardousness of a particular component and the amount of that component used in the process. A diagram overview of the method is shown in Figure 3.6. Examples demonstrating how this analysis is performed for a variety of bioprocesses are presented in Heinzle et al. (2007)[62].

The PMI metric is a simpler tool, originally implemented for small molecule bioproduction by the Green Chemistry Institute Pharmaceutical Roundtable, that has recently been used in the

biomanufacturing industry to quantify the mass (kg) of materials (water, raw materials, consumables) used to produce a kg of product (active pharmaceutical ingredient or API)[63].

Here we describe the steps to implement these analyses and benchmarks that can be used for comparison. It is important to note that these analyses are not explicitly supported by SuperPro Designer, and as such, the steps are intended to be completed on a spreadsheet supported by SuperPro Designer-generated data.

1. Set up a table or spreadsheet containing the mass flowrates for all registered pure components in the techno-economic model. This information can be easily accessed through the Materials & Streams Report (*Main Ribbon > Reports > Materials & Streams*) (see Note 31).

2. Separate registered pure component mass flowrates into input and output flowrates.

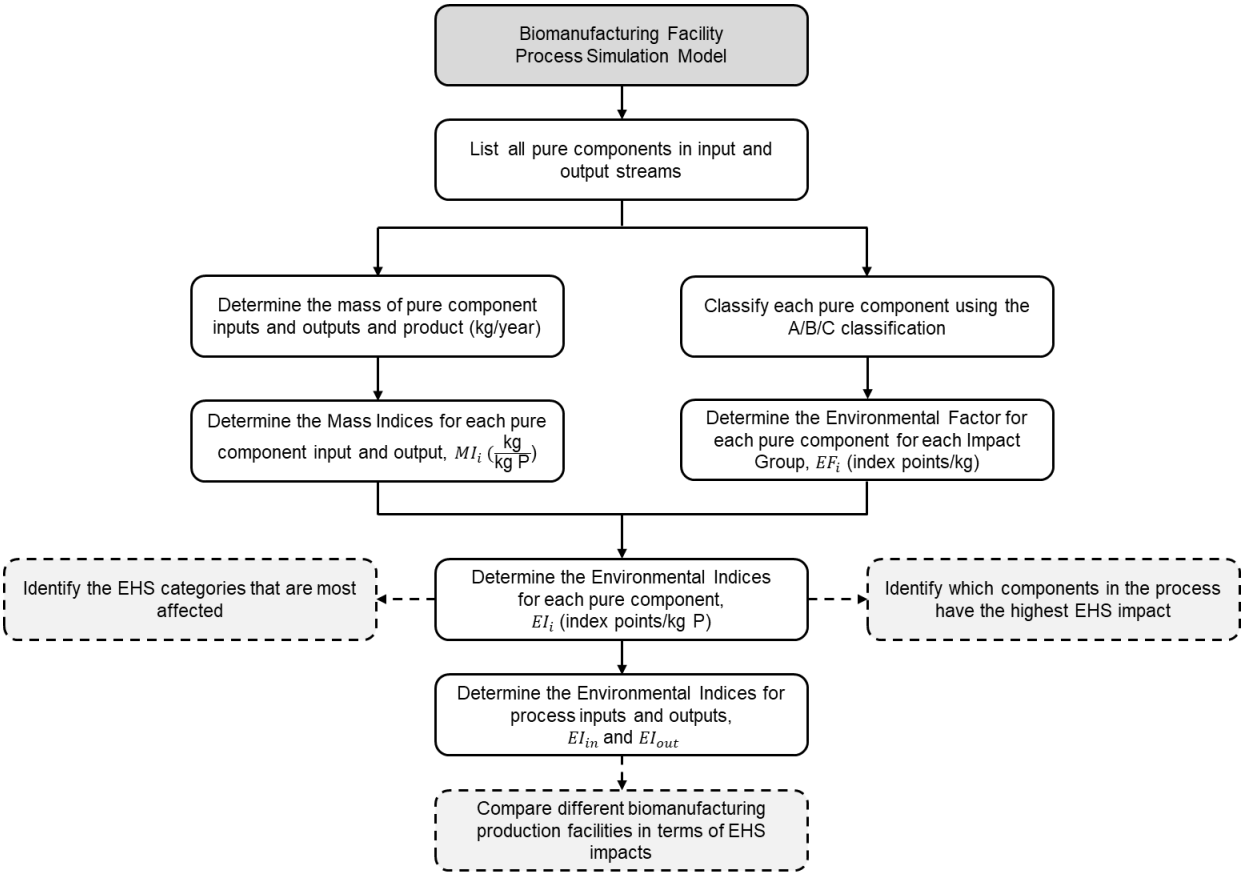

Figure 3.6. Diagram showing the steps in the Environmental, Health, and Safety assessment for biomanufacturing facilities. Analysis steps (solid line white fill) leading to EHS metric use cases (dotted line grey fill) illustrate different ways in which the EHS metrics can be used. Adapted from Biwer and Heinzle (2004)[61].

3.3.2.6.1. Environmental, Health and Safety Assessment

Here the reader is walked through the EHS assessment using the Biwer and Heinzle (2004) method. There are fourteen EHS impact categories, some of which are combined into six EHS impact groups as shown in Figure 3.7. Four of the impact groups are important and/or relevant for process input components (Resources, Grey Input, Component Risk, and Organisms) and four impact groups are relevant for process output components (Component Risk, Organisms, Air, Water/Soil).

Suppose N_{in} is the number of different components in input streams and N_{out} is the number of components in output streams.

1. Determine the Mass index for each pure component i, MI_i, where

$$MI_i \left(\frac{\text{kg } i}{\text{kg MP}}\right) = \frac{\text{mass of component } i \text{ (kg)}}{\text{mass of main product (kg MP)}},$$

where $i = 1, \ldots N_{in}$ for inputs and $i = 1, \ldots N_{out}$ for outputs

and enter these values in the spreadsheet for each pure component input or output (see Note 32).

2. Classify the hazardousness of each pure component in each of the fourteen EHS impact categories with ranking of an A, B, or C, where A corresponds to the most hazardous/toxic/environmentally unfriendly/least sustainable classification and C corresponds to the least hazardous/nontoxic/environmentally benign/sustainable classification with B as an intermediate classification (see Note 33). Enter the A/B/C classification for each input component and each output component into the spreadsheet for each of the fourteen EHS impact categories.

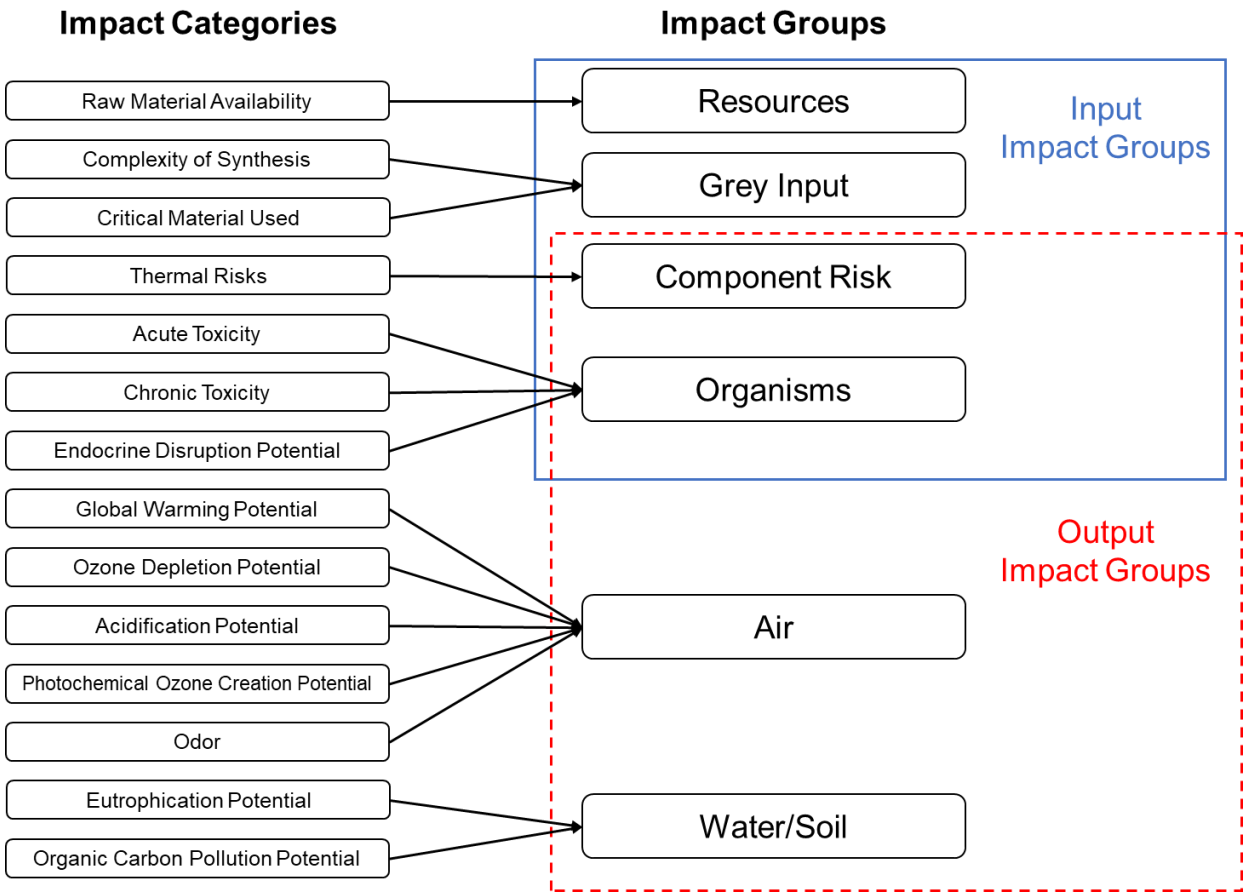

Figure 3.7. Diagram showing the Environmental, Health, and Safety impact categories for biomanufacturing facilities and how each impact category maps onto the EHS impact groups, which are defined by either input impact (boxed in solid blue line) or output impact (boxed in dotted red line). Categorization are according to the Biwer and Heinzle (2004) method[61].

3. Determine the A/B/C classification for the four EHS impact groups, using the "worst case" classification from the EHS impact categories in cases where multiple EHS impact categories are combined in an EHS impact group. For example, if component i is classified as a B in acute toxicity, A for chronic toxicity and B for endocrine disruption potential, that component would be classified as an A for the organism impact group. Enter the A/B/C classification for the four EHS impact groups for both the input and output components in the spreadsheet.

4. For each of the input and output components i, assign a numerical value to A, B, and C. Biwer and Heinzle suggest two methods for this depending on whether the arithmetic or multiplicative weighting is used[61]. For method illustration, we will use the arithmetic weighting formula in which A=1, B=0.3 and C=0 in subsequent steps.

5. For each of the input and output components i, determine the Environment Factor, EF_i, by using a formula to convert A/B/C classifications defined with numerical values into an overall Environmental Factor using either the arithmetic or multiplicative weighting[61]. For method illustration, we define EF_i as the average numerical value of the classifications over the four relevant EHS impact groups. For example, if an output component i had an A for component risk, a B for organisms, C for air and A for water/soil, the EF_i would calculated as

$$EF_i = \frac{1 + 0.3 + 0 + 1}{4} = 0.575$$

With this approach EF values will range from 0 to 1, with 0 being the best case and 1 being the worst case. Enter the EF values for each input and each output component into the spreadsheet.

6. For each input component and each output component i determine the Environment Index, $EI_i = EF_i \times MI_i$, and enter it into the spreadsheet. The higher the numerical value is, the more deleterious (from either an environmental, health or safety standpoint) that component is in the process indicating that it may be worthwhile to consider an alternative compound or try to reduce the amounts used/produced in the process.

7. The overall Environmental Index of the inputs EI_{in} can be determined by summing EI_i over all N_{in} and the overall Environmental Index of the outputs EI_{out} can be determined by summing EI_i over all N_{out}. These values can be "benchmarked" by comparing to the best case (0) and the worst case ($\sum_{i=1}^{N_{in} \text{ or } N_{out}} MI_i$) (Note 34).

3.3.2.6.2. Process Mass Index (PMI)

The PMI is a measure of how much "material" is required/consumed to make a kg of product, so it is similar to $\sum_{i=1}^{N_{in}} MI_i$ but also includes the mass of consumables. This is particularly helpful in comparing water use between different types of manufacturing facilities since potable water is becoming a more precious resource. The facility PMI can be calculation from the following equation:

$$PMI \text{ (kg/kg product)} = PMI_{Water} \text{ (kg/kg product)} +$$
$$PMI_{Raw\ Materials} \text{ (kg/kg product)} + PMI_{Consumables} \text{(kg/kg product)}$$

1. Determine the PMI_{Water} for the process from the table or spreadsheet of pure component mass flowrates. Assuming that process water (PR), purified water (PW) and water for injection (WFI) are made on-site from municipal water though reverse osmosis and distillation process with efficiencies typically found in the biopharmaceutical industry, the PMI_{Water} can be determined from the following formula where M_P(kg) is the mass of product produced per year.

$$PMI_{water} = \frac{\left(W_{municipal}(\text{kg}) + 1.25W_{PR}(\text{kg}) + 1.25W_{PW}(\text{kg}) + 1.41W_{WFI}\ (\text{kg})\right)}{M_P(\text{kg})}$$

2. Determine the PMI for raw materials. In this analysis since water is considered separately, the $PMI_{Raw\ Materials}$ can be determined from the process input components as described in Section 3.2.6.1 but excluding water as a component.

$$PMI_{Raw\ Materials} = \sum_{i=1}^{N_{in}} MI_i(\text{kg/kg product})$$

3. Record the demand for each registered consumable (e.g., bioreactor bag, media bag, chromatography resin, filter and membrane, including primary packing material) in a table or spreadsheet. This information can be easily accessed from an Economic Evaluation report or registered Consumables view window (*Main Ribbon > Tasks > Other Resources > Consumables*).

4. Record the mass (in kg) for each registered consumable i, C_i, in a table or spreadsheet (see Note 35).

5. In some cases, the consumable material can be used multiple times (e.g., chromatography resins, some filters). To take this into consideration (see Note 36), the consumable utilization factor U_f is defined as

$$U_f = \frac{\text{Number of cycles the material is used per batch}}{\text{Number of cycles the material can be used before replacement}}$$

6. Determine $PMI_{Consumables}$ from the demand and mass of consumables used annually in the process using the following equation

$$PMI_{Consumables} = \frac{\left(U_f C_{bag} + U_f C_{resin} + U_f C_{filter} + U_f C_{membrane}\right)}{M_P}$$

7. Calculate the sum of the PMI values for water, raw materials and consumables to get the PMI for the facility (see Note 37).

3.3.2.7. Stop Gate II

Here the reader will be assembling a status report and communicating with key stakeholders for a Stop Gate before proceeding to process analysis. Precise scope and format of the report and/or presentation will depend on the initial project scope and agreement with key stakeholders. Below are generally recommended steps to assembling a robust status report to convey the completed base case techno-economic model and simulation.

1. Detail a review of the initial, or most recent, project scope including the specific agreed upon deliverables and timeline.
2. Detail a review of the techno-economic methodology, including the specific process simulation tool employed for analysis as well as a compilation of the various types of information sources (e.g., lab-scale data, pilot-scale data, literature results, similar existing facilities) used as the basis for techno-economic parameters.
3. Detail the key project assumptions built into the model and simulation, including the previously agreed upon bases for process design, production specifications, and process flowsheet with critical process parameter and key performance indicator ranges, as well as the bases for OPEX and CAPEX (and profitability) economic calculations (e.g., maintenance costs, utility types, depreciation method, pricing for select cost items).

4. Detail the technical manufacturing results of the model and simulation. This may include a progression of processing metrics (e.g., product mass, concentration, purity, and recovery) and their status at each unit procedure.

5. Detail the economic results of the model and simulation. This may include a snapshot summary of key economic metrics (e.g., COGS, OPEX, CAPEX, ROI, IRR after tax) and more detailed breakdowns of those metrics by process section (e.g., harvest, concentration, capture) or cost item category (e.g., raw material, consumables, labor-dependent).

6. Review the remaining work to meet the project scope, including the specific deliverables, timelines, a proposed path, and any questions. Be prepared to iterate on the base case model and simulation based on key stakeholder feedback. This may require several iterations before there is agreement amongst all key stakeholders to proceed to the next step of the project scope.

3.3.3. Process Analysis

In the following section the reader will be manipulating the base case techno-economic model developed in process synthesis (Section 3.3.2) to gain insight into the manufacturing design space and inform design and/or research and development directions. This will be performed in this method by evaluating price sensitivity (Section 3.3.3.1), scenario analysis (Section 3.3.3.2), and alternate scenarios (Section 3.3.3.3), followed by developing a report and initiating review with key stakeholders at the final Stop Gate III (Section 3.3.3.4).

3.3.3.1. Price sensitivity

Here the reader will be performing univariate price sensitivity analyses. For two classes of price parameters, purchase price and product selling price, the reader will be introduced to possible methods of identifying how to select parameters for sensitivity analysis, and then be led through a process of executing a sensitivity analysis. In this analysis, only the cost structure of the facility model is modified.

1. Assemble a list of purchase price parameters for sensitivity analysis using criteria of cost contribution, uncertainty in parameter value, and expected change in parameter value. The relative weighting of these criteria and the list size is based on individual project scope. The Economic Evaluation or Itemized Cost reports provide a list of cost item factor contributions that can be used to form cost contribution rankings.

2. Define the extent of variation to be tested for each parameter in the purchase price sensitivity analysis, usually structured plus/minus a percentage of the base case value.

3. Update the purchase price values in SuperPro Designer, followed by running the "Perform economic calculations" button to update the economics, which can then be recorded on a spreadsheet for graphical interpretation. This is recommended for CAPEX purchase price sensitivity. Alternatively, the facility simulation economics can be manually updated with the adjustment of the OPEX purchase price parameter value, as these costs do not factor into additional downstream calculations.

4. Define a set of product selling prices. This can be set up as exploratory, based on intervals of percentage change from the base case value, or this can be derived from calculations on market analysis (e.g., testing market entry strategies).

5. Update the product selling price in SuperPro Designer, and relevant profitability metrics of choice (e.g., ROI, IRR after tax) can be pulled from the updated economic calculations and recorded on a spreadsheet for graphical interpretation.

3.3.3.2. Scenario analysis

Here the reader will be performing univariate process parameter scenario analysis. It is often beneficial to elucidate the techno-economic impact of varying high-level facility performance parameters including key performance indicators (e.g., expression level/titer), critical quality attributes (e.g., product purity), and market parameters (e.g., yearly production level). These insights can be crucial for allocating research & development resources, general decision-making, and defining business strategy. In this analysis, the technical performance, facility design modifications, and cost structure of the model are modified.

1. Assemble a list of process parameters for scenario analysis, and extent of variation, based on project scope, complimentary analyses, and/or additional key stakeholder feedback.

2. Generate a clone of the base case model for each process parameter value to be tested in SuperPro Designer. The model will change significantly in this analysis and it is important to isolate these changes from the base case model.

3. Update the model with the process parameter setpoint selected. This update will result in a cascade of process performance changes.

4. Modify the model to negate off-target impact of the process parameter variation. Usually a series of modifications are needed to accomplish this. Some of these changes can be automatically calculated by SuperPro Designer (e.g., equipment in Design Mode will re-

size accordingly to the new stream composition and volume/mass basis), while other aspects will require manual intervention (e.g., variation in expression level will subsequently result in changes to production level and product purity, which will have to be adjusted for).

5. Generate reports for each model and compile desired technical/economic outputs on a spreadsheet for graphical interpretation.

3.3.3.3. Alternate scenarios

Here the reader will be performing comparative alternate scenario analysis. Alternate scenarios can range from evaluating a single new unit procedure all the way to evaluating an entirely new upstream section or, in some cases, complete process flowsheets. It may be valuable to chart out the preferred manufacturing among several similar options (e.g., cultivation of plants using a greenhouse or a controlled environmental facility). Additionally, it may also be valuable to generate comparisons of drastically different manufacturing options (e.g., plant cell suspension culture or whole plant transient expression).

1. Follow the steps detailed in process creation (Section 3.1) as closely as is needed for the alternate scenario and the extent of process flowsheet modification.

2. Follow the steps detailed in section process synthesis (Section 3.2) as needed. Either revise the existing facility model(s) or start with a new model.

3. Generate reports for the new model(s) and compile desired technical/economic outputs alongside the base case model outputs on a spreadsheet for graphical interpretation.

3.3.3.4. Stop Gate III

Here the reader will be assembling a project summary report and communicating with key stakeholders for a final Stop Gate before concluding project work. This report and/or presentation is often viewed as the primary project deliverable, and as such, should be given commensurate attention. Precise scope and format of the report and/or presentation will depend on the initial project scope and agreement with key stakeholders. Below are generally recommended steps to assembling a robust status report to convey the completed techno-economic analysis.

1. Begin by updating and compiling information communicated in the previous two Stop Gates, namely the project scope and base case model.
2. Generate a single-page executive summary with key findings from the analysis, usually including a note on economic viability for scaling up to pilot- or commercial-scale, to serve as a reference for key stakeholders.
3. Generate an extended length report and/or presentation with detailed findings of the base case model and process analysis, as framed by the project scope. Include figures that convey key takeaways for use by key stakeholders in external communications after the project has concluded.

3.4. Notes

3.4.1. Process Creation

1. Regulatory framework will constrain the manufacturing process to meeting proper standards for design, monitoring, and control. For example, manufacturing of biopharmaceutical proteins

intended for commercial use in the United States must follow current Good Manufacturing Practices (cGMP).

2. The facility location is an important techno-economic consideration and will influence factors such as raw materials and utility availability and pricing, labor supply, taxation, and environmental and legal restrictions.

3. Forecasts of production demand are most commonly based on market analyses. It is important to consider that production demand may change over time (e.g., dynamic market penetration forecasts).

4. Facility lifetime is only an important design premise if one intends to perform a profitability analysis as a part of their techno-economic method. This is not needed if the economic insights sought are scoped at manufacturing costs (OPEX, CAPEX, COGS).

5. Critical quality attributes and key performance indicators may not yet be defined at the time of the techno-economic analysis. Therefore, valuable parameters to include at this stage may be loosely defined using working process knowledge. For the typical plant-based manufacturing process, parameters such as expression level, downstream recovery, and product purity are generally recognized as important parameters for which key stakeholder agreement should be established early in the project.

6. When building a techno-economic model from lab-scale data, it is recommended that a notable amount of time is devoted to considering commercial-scale equivalent unit operations (e.g., while liquid nitrogen-assisted homogenization and extraction may have been used at the lab scale, one might consider employing a screw press at commercial scale simulation).

3.4.2. Process Synthesis

7. User-populated databanks can be transferred between projects. This can save considerable start-up time if one is building their analysis starting from another techno-economic model.

8. One shortcut to registering the pure components and stock mixtures is to initialize the new registration using a source for default property values (e.g., registering “transgenic rice cell” can be initialized with biomass default property values). It is also important to note that the economics and pollutant categories will be visited later in the method.

9. It is important to consider the different types/qualities of water, ranging from potable water for process cooling to water-for-injection (WFI) for the last chromatography step and bulk drug substance formulation.

10. The stream inlet/outlet arrows of some unit procedure icons are designed to handle specific stream types (e.g., tank vent stream). For detailed information on the restrictions of a given unit procedure icon stream inlets/outlets, navigate to the “Help” menu in the Main Ribbon and search for that unit procedure by name.

11. The authors have found that this iterative method of process synthesis in SuperPro Designer’s visual design environment results in a streamlined and hassle-free troubleshooting process. Alternatively, SuperPro Designer does possess a “Simulation Control” toolbar with a set of functions to enable process breakpoints and partial simulations for a more classical programming approach to troubleshooting.

12. Cleaning operations for plant-based manufacturing at commercial scale generally include Steam-in-Place and/or Clean-in-Place. Cleaning heuristics that the authors have found to be

relevant and useful for development of cleaning operations can be found in the works of Chisti, 1999[64], Bremer and Brent, 2010[65], and Davies et al., 2015[66].

13. It is important to consider the operating schedule of the facility when defining the annual operating time; is the facility operating according to 24 hours/7 days per week, 24/5, 8/5, 8/7? SuperPro Designer is primarily suited for 24/7 manufacturing. As mentioned earlier, SchedulePro can be used to augment the native scheduling capabilities, which includes simulation of different facility operating schedules like 8 hours per 5 days per week.

14. Default labor types do not necessarily accurately reflect the upstream operators of whole plant-based manufacturing, whom have been historically less expensive given the lower complexity of plant growth operations. The target product and facility location may also influence labor type pay rates.

15. The labor rate can be strongly influenced by the product industry and regulations. For example, cGMP operation often requires one operator to perform the commercial manufacturing task while another is dedicating to observing, verifying, and signing off as a witness for critical operations such as preparing/adding media and/or buffers, equipment sterilization, etc. The labor amount needs to reflect additional expenditures of this nature.

16. Process time can either be set by the user, calculated based on a mass or volume flowrate (for some operations), or set as matched to the duration of another operation by defining a Master-Slave Relationship. In this last case, one should consider if the labor of the Slave operation should be accounted for or negated. In some situations (e.g., Tank 1 transfer out is a slave to Tank 2 transfer in), it may be appropriate to negate the labor of the Slave operation when the labor for both operations is adequately reflected in the Master operation.

17. Scheduling the connections of operations is one place that a new practitioner of techno-economic analysis may struggle. It is important to consider the scheduling bottleneck. Scheduling may also need to be re-considered after equipment allocations are completed in Section 3.2.3.

18. A single piece of equipment can be assigned to multiple unit procedures; there does not have to be a one-to-one mapping. Equipment is assigned to the unit procedure in the 'Selection' sub-window of the 'Equipment' tab.

19. Equipment can be defined in either Design or Rating Mode. In Design Mode, equipment is sized according to SuperPro Designer calculations. In Rating Mode, the equipment size is user-defined and fixed, and the throughput/scheduling is determined.

20. The number of equipment units can be increased to split the processing between multiple identical equipment units. Additionally, "Stagger Mode" can be enabled, which generates identical sets of equipment units, only one set of which is for any given batch. This is an effective strategy to de-bottleneck the manufacturing scheduling when the equipment in question is identified as a bottleneck.

21. The default SuperPro Designer Consumables database is a very useful tool. However, the default property values for use cycles have not been developed based on plant-based manufacturing data. One may find that the use cycles are significantly higher or lower than evidenced in supporting plant-based manufacturing data.

22. Power types and their subsequent pricing structures are geographically dependent and should be defined with the facility location in mind. It is important to consider fees and/or discounts

associated with certain thresholds of power demand, which are generally embedded in power consumption calculations.

23. The user is required to specify an NPV interest/discount rate of return. Typically, 7% is the value used here unless key stakeholders provide a specific value.

24. Depreciation can be applied to the total depreciable capital investments using common methods such as straight line, declining balance, and sum of the years digit methods, along with specification of the depreciation period and the salvage value. Depreciation is specified in the 'Time Valuation' tab, but section- and equipment-specific depreciation calculations are controlled through the 'Section Operating Cost Adjustments' window.

25. Values defined for output streams can be selected to override the base component and/or stock mixture economic property value in the techno-economic simulation by checking the box 'Is Cost/Price Set by User.'

26. The often-lower complexity of upstream whole plant-based manufacturing, as referenced in Note 15 (labor), also generally results in a higher labor time estimation, as less time is needed for paperwork in simpler operations.

27. Generally, the operating cost adjustments for downstream processes are significantly higher than for upstream processes. This is mainly attributed to the higher labor, lab/QA/QC, ongoing validation, and maintenance costs as the stream progresses closer to the final product.

28. In general, the capital cost adjustments for upstream whole plant-based manufacturing are lower than those of traditional bioreactor-based processes. This can be attributed to several factors, including lower capital complexity for plant cultivation and reduced startup and validation costs due to the linear scalability of whole plants. Within whole plant systems, the

heuristics for capital cost adjustments are that indoor agriculture > greenhouse > open field cultivation.

29. The selling price of the product can be difficult to determine at this stage of development, largely depending on the extent of market analysis and business model development. If the reader does not have quality information at hand to estimate a selling price, the authors recommend that the reader focus on the cost of goods sold, termed Unit Production Cost in SuperPro Designer, rather than the profitability based on the selling price. Later in the method, price sensitivity analysis represents a valuable tool for exploring viable selling price options, as desired.

30. Positive cash flows following production startup are of course a necessary but not sufficient requirement for profitability.

31. Components involved in internal streams (those connecting one unit procedure to another unit procedure), utilities, and/or consumables are not included in this analysis.

32. The Materials & Streams Report provides pure component mass flowrates on an annual (kg/year), batch (kg/batch), and main product (kg/kg MP) basis. The main product basis can be used directly here.

33. This classification, although, somewhat arbitrary is based on information about the component often found in Material Data Safety Sheets or U.S. National Fire Protection Agency (NFPA) rating (see Table 1 in Biwer and Heinzle, 2004).

34. Because there is an overall mass balance for the entire process, the summation of mass over all input components is equal to the summation of mass over all output components.

35. The mass of consumables is not a property field in SuperPro Designer. Mass data must be manually identified and compiled.

36. The consumables demand listed in SuperPro Designer accounts for use cycles by default. This manual calculation is not required for demand data obtained from SuperPro Designer.

37. For comparison Budzinski et al. (2019)[63] presents the average PMI values for fourteen commercial biomanufacturing production runs for monoclonal antibody production using mammalian cell culture (although it should be noted that cleaning solutions were not included in the analysis): $PMI_{water} =$ 7,711 kg/kg P, $PMI_{Raw\ Materials} =$ 551 kg/kg P, $PMI_{Consumables} =$ 65 kg/kg P, giving a total PMI of 8,327 kg/kg P.

Chapter 4. Techno-economic analysis of a plant-based platform for manufacturing antimicrobial proteins for food safety

"Food safety involves everybody in the food chain."

-Mike Johanns

This chapter is based on the following publication:

McNulty, M.J., Gleba, Y., Tusé, D., Hahn-Löbmann, S., Giritch, A., Nandi, S., and McDonald, K.A. (2020). Techno-economic analysis of a plant-based platform for manufacturing antimicrobial proteins for food safety. *Biotechnol. Prog.* 36. doi:10.1002/btpr.2896

Abstract

Continuous reports of foodborne illnesses worldwide and the prevalence of antibiotic-resistant bacteria mandate novel interventions to assure the safety of our food. Treatment of a variety of foods with bacteriophage-derived lysins and bacteriocin-class antimicrobial proteins has been shown to protect against high-risk pathogens at multiple intervention points along the food supply chain. The most significant barrier to the adoption of antimicrobial proteins as a food safety intervention by the food industry is the high production cost using current fermentation-based approaches. Recently, plants have been shown to produce antimicrobial proteins with accumulation as high as 5 g/kg fresh weight and with demonstrated activity against major foodborne pathogens. To investigate potential economic advantages and scalability of this novel platform, we evaluated a highly efficient transgenic plant-based production process. A detailed

process simulation model was developed to help identify economic “hot spots” for research and development focus including process operating parameters, unit operations, consumables, and/or raw materials that have the most significant impact on production costs. Our analyses indicate that the unit production cost of antimicrobial proteins in plants at commercial scale for three scenarios is $3.00 – 6.88/g which can support a competitive selling price to traditional food safety treatments.

4.1. Introduction

The World Health Organization estimates 600 million cases of foodborne illness worldwide in 2010, of which 420,000 resulted in death[67]. Food safety is an alarming global challenge for human health. Food supply chains are increasingly geographically diverse, requiring coordination between multiple governments and food industry stakeholders[68]. In the United States, surveys estimate 9.4 million cases of foodborne illness, 55,961 hospitalizations, and 1,351 deaths each year[69]. A single foodborne illness outbreak can have significant economic impact, estimated to cost a restaurant between $4,000 and $2.6 million U.S. dollars (USD)[70]. Such statistics underscore the fact that foodborne illnesses not only place a significant burden on the United States healthcare system at $14 billion annual cost of illness[71], but also on key stakeholders in the food industry and our economy in general.

Current food sanitizing practices aimed at minimizing such outbreaks predominantly involve thermal inactivation or treatment of food with organic acids, salts, or ultraviolet (UV) irradiation. These treatments are largely effective yet may still present foodborne disease vulnerability in key processing steps for many products. For example, recent literature highlights the challenge of the 'viable but nonculturable' (VBNC) state of microorganisms in these food sanitizing treatments[72]. One or more of the current food sanitizing treatments have been shown to induce a VBNC state from which reversion to a culturable state is possible for major foodborne disease-associated microorganisms such as *Escherichia coli*[73], *Salmonella enteritidis*[74], *Listeria monocytogenes*[75], and *Shigella flexneri*[76].

Biotic approaches to food sanitization have high potential as supplementary treatments to de-risk the supply chain by employing efficacious and orthogonal protection against high-risk pathogens. Food safety applications of bacteriophages (viruses capable of killing bacteria), endolysins

(antibacterial proteins derived from bacteriophages), and bacteriocins (antimicrobial proteins produced by bacteria for ecological dominance), have already been approved for commercial use in the United States. For example, Intralytix Inc. offers a suite of FDA-approved bacteriophage-based antibacterial food safety products (ListShield™, EcoShield™, SalmoFresh™, and ShigaShield™). Human exposure to large numbers of bacteriophage and bacteriocin is likely in a typical diet as well as from commensal microflora in the gastrointestinal tract. Therefore, there is a strong and intuitive case for acceptance of certain bacteriophage- and bacteriocin-derived antimicrobial treatments for food safety applications[77]. In fact, various preparations of bacteriophages, such as the *Salmonella*-specific bacteriophage cocktail SalmoFresh™[78], endolysins[79,80], and bacteriocins, such as colicins[81,82] and nisins[83], have already been granted Generally Recognized as Safe (GRAS) status as food antimicrobials by the US Food and Drug Administration (FDA). It is anticipated that similar antimicrobial preparations will be granted GRAS status by FDA in the future, as the popularity of these technologies grows and additional regulatory notices are filed.

The costs of standard food sanitizing treatments are as low as $0.01 – 0.10/kg food[84]. In the cost-constrained markets of food additives and processing aids, these new biotic approaches to food sanitation will need to be accessible at the low selling prices that the food industry is accustomed to, or gain market entrance as a luxury good on the basis of their differentiating features, including worker safety in the preparation and handling of the products, environmentally friendly disposal, non-impact on the organoleptic properties of food, and no or minimal food matrix alteration[85]. Strategies to meet low cost of use can be broadly classified as either pertaining to molecular engineering of the treatment agent or manufacturing science and technology. Substantial research has been done to employ genetic engineering to alter the action of native antimicrobial proteins[86].

For example, the modular structure of the bacteriophage class of enzymes known as endolysins provides a perfect "Lego® block"-like molecular engineering platform to swap the N-terminal catalytic domain or the C-terminal binding domain to create novel hybrid moieties[87].

While molecular engineering approaches possess substantial potential for human therapeutics, changes to the native structure of antimicrobial proteins for food safety applications bar them from taking advantage of the expedited GRAS marketing allowance pathway. For antimicrobials that are novel, or altered, and hence not "generally recognized" as safe, the alternative marketing approval route (food additive petition) requires a full preclinical safety data package, which is a costly and time-consuming process that creates a significant barrier to entry for new food safety interventions, given the above-mentioned current pricing structures, regulations, and public perception. Consequently, biotic food safety approaches are more amenable to cost containment through manufacturing science and technology.

The cost sensitivity of the food industry is the most significant barrier to the adoption of new food sanitizing treatments, such as antimicrobial protein (AMP) preparations. Plant-based platforms have the potential for producing market-relevant volumes of AMPs at competitive costs, because they do not require expensive bioreactors and culture media. In recent studies we have shown that plants such as *Nicotiana benthamiana*, spinach, and leafy beets are an attractive and scalable production platform for production of AMPs, including antibacterial colicins, salmocins, and bacteriophage endolysins. We have previously reported expression levels as high as 3 g/kg plant fresh weight (FW)[77,80,81,88–90]. In this study, we address cost sensitivity with a comprehensive techno-economic analysis of plant-based production of AMP for food safety applications. We used laboratory-scale results and working process knowledge from pilot and commercial processes to develop a process simulation model using SuperPro Designer® to assess the commercial viability

of the production platform and to identify economic "hotspots" to help guide future research and development.

A selection of recently published studies on the techno-economics of *N. benthamiana* plant-based production of a variety of recombinant proteins are summarized in Table 4.1[55–58]. To our knowledge, this study is the first techno-economic analysis of a plant-based production platform for AMPs as food safety additives.

Table 4.1. A selection of recently published techno-economic analyses of *Nicotiana benthamiana* plant-based production models for molecular farming. CAPEX, capital expenditures; COGS, cost of goods sold; U/D, ratio of upstream to downstream costs; HRP, horseradish peroxidase; mAb, monoclonal antibody; BChE, butyrylcholinesterase.

Parameter	Unit	Tusé et al. 2014		Walwyn et al. 2015	Nandi et al. 2016	Alam et al. 2018
		(1)	(2)			
Industry	--	Pharma	Biofuel	Reagent	Pharma	Pharma
Molecule	--	BChE	Cellulase Enzyme	Horseradish Peroxidase Enzyme	Monoclonal Antibody	Antiviral Protein
Expression System	--	Transient; Agroinfiltration	Transgenic; Inducible	Transient; Agroinfiltration	Transient; Agroinfiltration	Transient; Viral Vector
Production	kg/year	25	3×10^6	5	300	20
Expression	g/kg FW	0.5	4	0.24	1	0.52
Recovery	%	20	--	54	65	70
Purity	%	>95	--	250 kU/g	>95	>99
CAPEX	$ million	92.4 (U/D 3:7)	11.5 (U/D 10:0)	--	122 (U/D 4:6)	--

COGS	$/g	1180 (U/D 3:7)	6.9×10^{-3} (U/D 10:0)	1279 (U/D 2:8)	90 - 121 (U/D 4:6)	105.80 (U/D 6:4)

4.2. Materials & Methods

4.2.1. Process Simulation

The plant-based AMP production and purification process was modeled using SuperPro Designer® Version 10 (Intelligen, Inc., Scotch Plains, New Jersey, USA; http://www.intelligen.com), a computer modeling tool capable of sizing equipment, performing material and energy balances, developing flowsheets, scheduling operations and debottlenecking. SuperPro Designer® built-in unit models include a suite of manufacturing unit operations (>140) that can be configured to represent a manufacturing process flow diagram for the biotechnology, pharmaceutical, and food industries. The software uses these process flows and unit operations to then generate process and economic reports, including annual operating expenditures (OPEX) and capital expenditures (CAPEX). All currency is listed in USD.

The manufacturing process flow (e.g., unit operations, materials, process parameters) was developed using working process knowledge, unpublished lab-, pilot- and commercial-scale data, and data published in the literature. Built-in SuperPro Designer® equipment design models were used for equipment sizing.

4.2.2. Host Selection

Nicotiana benthamiana is used as the plant host organism in the base case scenario. *N. benthamiana* is used extensively for indoor plant molecular farming applications based on its rapid growth, genetic tractability, susceptibility to agrobacterium transformation, and high expression levels of recombinant proteins[91–93]. The species is used in the commercial-scale production of therapeutics and vaccines by companies such as Kentucky BioProcessing Inc. (Owensboro, Kentucky, USA)[94], Medicago Inc. (Québec, Quebec, Canada)[51], and iBio CMO (Bryan, Texas, USA)[49].

The modeled facility is designed to accommodate a previously reported process using transgenic *N. benthamiana* featuring a double-inducible viral vector, developed by Icon Genetics GmbH (Halle/Saale, Germany). Published results demonstrate minimal background expression of recombinant protein until the induction of deconstructed viral RNA replicons from stable DNA proreplicons is triggered by 1-20% (v/v) ethanol applied as a spray on the leaves and/or a drenching of the roots, to achieve expression levels as high as 4.3 g/kg plant FW[95]. While the more common *Agrobacterium*-mediated transient expression production platform enables rapid production of recombinant target molecules[96], this transgenic system obviates the need for additional expenses associated with *Agrobacterium tumefaciens* preparation, vacuum infiltration, and agrobacterium-introduced endotoxin removal[97].

4.2.3. Facility Design

The simulated manufacturing facility is composed of two separate process models/flowsheets: (1) the upstream processing models the plant growth, ethanol-induction, and product generation, which feeds into (2) the downstream processing model for purification of the product from the

process and product impurities to meet food processing aid specification. Quality Assurance (QA), Quality Control (QC), and laboratory costs associated with good agricultural and collection practices (GACP) for upstream processing and FDA food industry current good manufacturing practice (cGMP) for downstream processing are included in the design. Equipment, materials of construction and prices are also modeled on food cGMP standards[98]. The location of commercial-scale plant molecular farming operations of Kentucky BioProcessing Inc. (Owensboro, Kentucky, USA) was selected as the basis for location-dependent costs. Location-dependent costs (e.g., electricity and municipal water) are based on values obtained from publicly available Owensboro, Kentucky municipal pricing charts (https://omu.org/).The simulated manufacturing facility is assumed to be a greenfield single-product biomanufacturing facility that is operational 24 hours per day and 7 days per week with an annual operating time of 90%, or 329 days per year.

Independent market analyses project a reasonable base case facility production level of 500 kg AMP per year for food safety applications of interest (unpublished data). To meet this demand, the proposed facility employs three-layer vertically stacked indoor plant cultivation stages designed for hydroponic host plant growth in a soilless substrate to support the plant and its roots. The cultivation stages are equipped with a light-emitting diode (LED) lighting system and a recirculating ebb and flow hydroponic water supply. The cultivation stage plant growth is divided into a series of trays that advance unidirectionally across the plant cultivation room towards automated plant harvesters and further downstream processing. Automated belts convey harvested plant tissue to the double-stack disintegrator and further downstream processing.

A compilation of facility and process parameter inputs is presented in Supplementary Information Tables S4.1 – S4.6 or in the base case model itself, which is publicly available at http://mcdonald-nandi.ech.ucdavis.edu/tools/techno-economics/.

4.2.4. Upstream Processing

The upstream processing model flowsheet is graphically depicted in Figure 4.1. Transgenic *N. benthamiana* seeds consumed in upstream processing are generated in-house from validated Working Seed Banks, which were in turn generated from validated Master Seed Banks. The seed bank release testing includes germination efficiency >95%, confirmation of growth kinetics, and viral testing. Capital expenditures (CAPEX) related to seed generation are excluded, but associated seed production costs are included in the estimate of $9.50/g seed (1 gram of seed is approximated as 9,500 seeds).

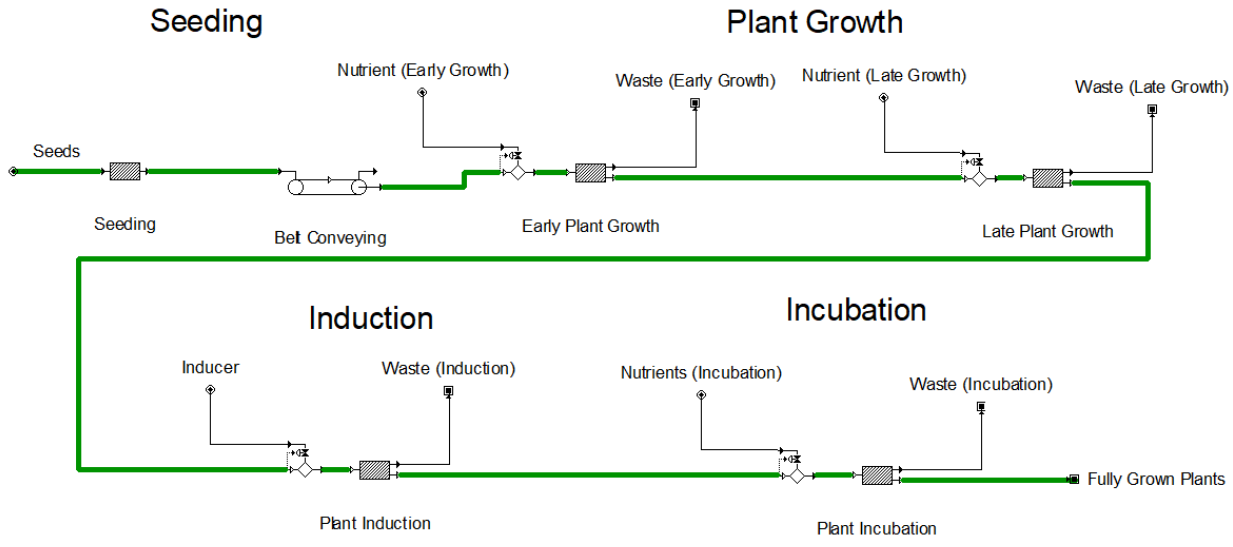

Figure 4.1. Upstream process flowsheet for the *Nicotiana benthamiana* base case scenario and *Spinacia oleracea* alternative scenario in the SuperPro Designer® model.

The seeds are set in soilless plant substrate at a density of 94 *N. benthamiana* seeds per 30 x 50 cm tray. The seedlings are cultivated hydroponically during the plant growth phase to reach manufacturing maturity by 35 days. Nutrient solution for plant growth is recirculated with minimal waste and routinely monitored and adjusted for consistent quality based on pH and conductivity. At manufacturing maturity, the plants are transferred to an induction space, complete with a separate hydroponic reservoir, curtains for temporary enclosure, and double rail spray booms. Recombinant expression of AMP is induced over the course of one hour via root drenching and aerial tissue spraying with a combined 0.01 liter of 4% (v/v) ethanol per kg FW plant tissue. The plants are then moved to the incubation phase. Post-induction plants are expressing recombinant AMP, and so the nutrient solution is circulated via a separate feed tank and hydroponic reservoir. The nutrient solution in the incubation phase may contain trace levels of ethanol which may prematurely initiate AMP production and impair plant growth kinetics. AMP accumulates in the *N. benthamiana* tissue over the course of 6 days. The nutrient solution in the incubation phase is not recirculated between batches, but sent to biowaste instead, amounting to an overall 23% plant uptake of the nutrient solution. The spent nutrient solution in the incubation phase is treated as biowaste to address trace amounts of the viral expression vector that may be present in solution.

4.2.5. Downstream Processing

The downstream processing model flowsheet is graphically depicted in Figure 4.2. Downstream processing begins with plant harvest. This starts with automated harvester collection of aerial *N.*

benthamiana plant tissue. The spent soilless plant substrate is sent to waste along with the remaining *N. benthamiana* root matrix. The disposal costs for this step are considered negligible and are not explicitly calculated in the model. There are several routes possible for disposal of plant growth substrate such as composting on site, using it for mulch on facility landscape, collection by farmers for spreading on agricultural land, and, as a last resort, sending it to a landfill. It may be possible, and more cost effective, to sterilize and reuse the growth media but this was not considered in the model. The harvested trays are cleaned in an automated washer with 0.1 liters of water per tray. The harvested plant tissue is conveyed via automated belts to extraction, which starts with a double-stack disintegrator to reduce plant biomass particle size. The disintegrated tissue is then sent to a screw press with an extraction ratio of 0.5 (v/w) extraction buffer:plant FW for acidic extraction. The extraction buffer and conditions for efficient *N. benthamiana* extraction have been reported[99]. All buffer compositions can be viewed in Supplementary Information, Table S4.5. A plant-made AMP purification protocol uses similar acidic extraction to remove *N. benthamiana* host proteins[77].

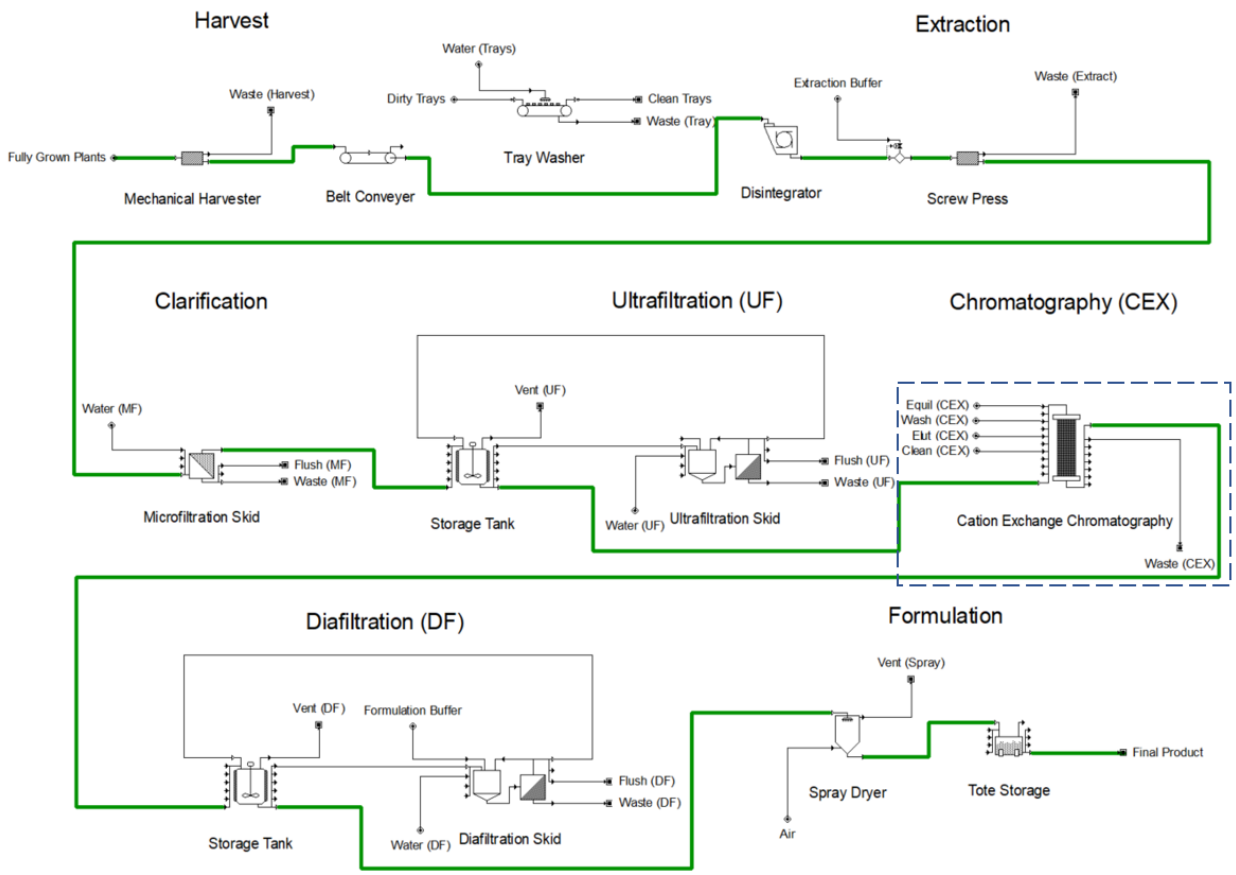

Figure 4.2. Downstream process flowsheet for the *Nicotiana benthamiana* base case scenario and *Spinacia oleracea* alternative scenario in the SuperPro Designer® model. The chromatography step, outlined in dotted blue, is only in the *N. benthamiana* base case model.

The plant extract is clarified using tangential flow microfiltration. The clarified stream is then ultrafiltered with additional tangential flow filtration using a 10 kDa molecular weight cutoff to a concentration factor of 20.

The AMP in the retentate stream is then purified with cation exchange column chromatography in a bind-and-elute mode of operation. The AMP is eluted isocratically in elution buffer (50mM sodium di-hydro phosphate, 1 M NaCl). The purified stream is subjected to one final tangential flow filtration procedure for buffer exchange into phosphate-buffered saline (PBS) with a

diafiltration factor of 3 (i.e., volume of diafiltrate buffer/volume of solution). The purified formulation is spray dried and filled in 1 L plastic bags to obtain the final bulk AMP.

All downstream processing water in direct contact with the product stream is reverse osmosis (RO) water. All equipment from extraction to formulation are sanitized post-processing with a clean-in-place (CIP) procedure consisting of a pre-rinse with municipal water, caustic wash with 0.5 M NaOH, post-rinse with municipal water, acid wash with 0.5% (w/w) HNO_3, and a final rinse with RO water. Storage tanks are additionally sanitized pre-processing with steam-in-place (SIP).

4.2.6. Scenario Analysis

Base case scenario outputs were used to identify parameters with significant impact on process economics. We focused the scenario analysis on two different classes of parameters: facility performance parameters and resource purchase costs. Facility performance parameters are defined as inputs which directly impact the physical outputs of the model. Typical biotechnology facility performance parameters include host organism expression level, unit operation recovery, and yearly production level. We chose to investigate expression level and yearly production level. To analyze the impact of facility performance parameters, we set a parameter range based on working process knowledge and then developed a model (corresponding to a redesigned facility) derived from the base case scenario for each parameter increment within the range. Facility performance parameter changes result in a cascade of changes to the model inputs and outputs; each model is adapted to the resulting stream composition and throughput of the given parameter value while maintaining the constraints of the fixed base case scenario process inputs.

Resource purchase costs are defined as inputs which directly control the economic impact of resource utilization for outputs of the model. For the purpose of this analysis, purchase price parameters are contained to cost items within OPEX.

4.2.7. Alternative Scenarios

Alternative facility design scenarios were developed as comparative models to more broadly explore the context of the base case scenario process economics. The alternative scenario models were designed in alignment with base case scenario inputs unless otherwise noted; each alternative scenario was chosen to isolate the impact of a key facility design assumption.

The first scenario investigates an alternative transgenic leafy plant host organism, spinach (*Spinacia oleracea*) cultivar Industra, for the base case scenario indoor growth and ethanol-inducible expression. Some colicins have been successfully expressed in *S. oleracea* (spinach) plants, however the expression levels were approximately 10-times lower than in *Nicotiana benthamiana* so additional research is needed to increase production levels[77,80,88]. Several salmocins and lysins can be expressed at high levels in spinach, comparable to expression levels in *N. benthamiana* [17,20]. The primary distinction in this alternative plant host organism is the lack of nicotine, the major alkaloid in *Nicotiana* species. In the base case scenario, significant downstream processing emphasis is placed upon nicotine removal. The upstream and downstream processing model flowsheets are graphically depicted in Figure 4.1 and Figure 4.2. A complete list of changes to the base case scenario inputs can be viewed in Supplementary Information, Table S4.4.

The second scenario investigates outdoor field-grown transgenic ethanol-inducible *Nicotiana tabacum* as an alternative to an indoor plant growth facility. Large Scale Biology Corporation previously investigated *N. tabacum* outdoor field-grown production of recombinant proteins and personnel involved in that work recommended pursuit of this agronomic approach, with special consideration of field condition variability on product consistency[100]. *N. tabacum* is used instead of *N. benthamiana* for its increased resilience to agricultural pathogens and weather fluctuation[100]. The upstream processing model is adapted from a techno-economic analysis of plant-made cellulase produced in the field[58]. The upstream and downstream processing model flowsheets are graphically depicted in Supplementary Information, Figure S4.1 and Figure S4.2. A complete list of changes to the base case scenario assumptions can be viewed in Supplementary Information, Table S4.6.

4.3. Results

4.3.1. Facility Operation of Base Case

The base case manufacturing facility scenario produces 500 kg of AMP per year at 92% purity including a 42% loss in extraction, downstream processing and formulation. This yearly production is achieved in 91 manufacturing batches, each with a 42.3-day duration, which process 1.22 million plants (or 1.22 x 10^6 plants) per batch with an expression level of 1 g AMP per kg plant FW for a yearly total of 111 million plants processed. The facility plant inventory is 14.7 million plants, divided into 12 concurrent batches of plant growth. Initialization of batches is staggered by 3.42 days. The AMP is produced and recovered through a series of manufacturing steps: plant growth, ethanol induction, incubation, harvest, extraction, clarification, concentration, chromatographic purification, buffer exchange, and formulation. The upstream processing recipe

(seeding, plant growth, induction, incubation) cycle time is 41.4 days and has been designed as the production bottleneck; the downstream processing recipe cycle time is 0.91 days and is thus executed well within the allowable stagger time between plant harvest cycles.

4.3.1.1. Upstream Processing

To meet the yearly production demand of 500 kg AMP, upstream processing must produce 867 kg AMP to offset the 42% downstream processing loss. Each upstream processing batch yields 9,520 kg *N. benthamiana* plant FW containing 9.52 kg AMP, which represents 10% of the total soluble protein (TSP)[77]. This results in 866,000 kg *N. benthamiana* plant FW processed over the course of the 91 annual batches, grown in 111,000 units of soilless plant substrate with 1.30 million liters of plant nutrient. Of the annual plant nutrient volume, 436,000 liters are sent to waste while the remainder is utilized during plant growth. A total of 7,410 liters of 4% (v/v) ethanol are consumed annually for induction.

4.3.1.2. Downstream Processing

Manufacturing batches continue directly from upstream to downstream processing; batches are not pooled, and thus 91 downstream processing batches are executed annually. Each batch begins with the upstream production of 9,520 kg *N. benthamiana* plant FW and 9.52 kg AMP. Screw press extraction results in a stream mass flow of 11,200 kg per batch (0.61% host impurities, 0.08% AMP). After microfiltration (membrane area, 26 m^2) and ultrafiltration (membrane area, 26 m^2) the stream is considerably reduced to 476 kg per batch (0.83% host impurities, 1.41% AMP). The product stream is eluted from the cation exchange chromatography (resin volume, 283 L) at 236

kg per batch (0.22% host impurities, 2.48% AMP). The product stream is then diafiltered for a buffer exchanged product stream of 230 kg per batch (0.21% host impurities, 2.38% AMP). The final spray dry formulation results in 9.06 kg formulated product per batch (5.32% host impurities, 60.64% AMP).

4.3.2. Economic Analysis of Base Case

The base case manufacturing facility requires $50.1 million CAPEX and $3.44 million/year OPEX. The AMPs cost of goods sold (COGS) is calculated to be $6.88/gram. Figure 4.3 shows an economic assessment of upstream and downstream processing. Upstream processing represents 58% of overall operating expenditures (OPEX), and downstream processing makes up the remaining 42% of operating costs. Of the $2.01 million/year upstream OPEX, the seeding operation (mainly due to the cost of the consumable soilless plant substrate) represents the majority (79%) of the cost. Chromatography (38%) and ultrafiltration/diafiltration (UF/DF) operations (35%) represent the majority of downstream processing OPEX of $1.43 million/year. The downstream CAPEX accounts for 62% of the overall CAPEX with the clarification and UF/DF filtration units representing the largest portion (49%) of the downstream capital investment costs.

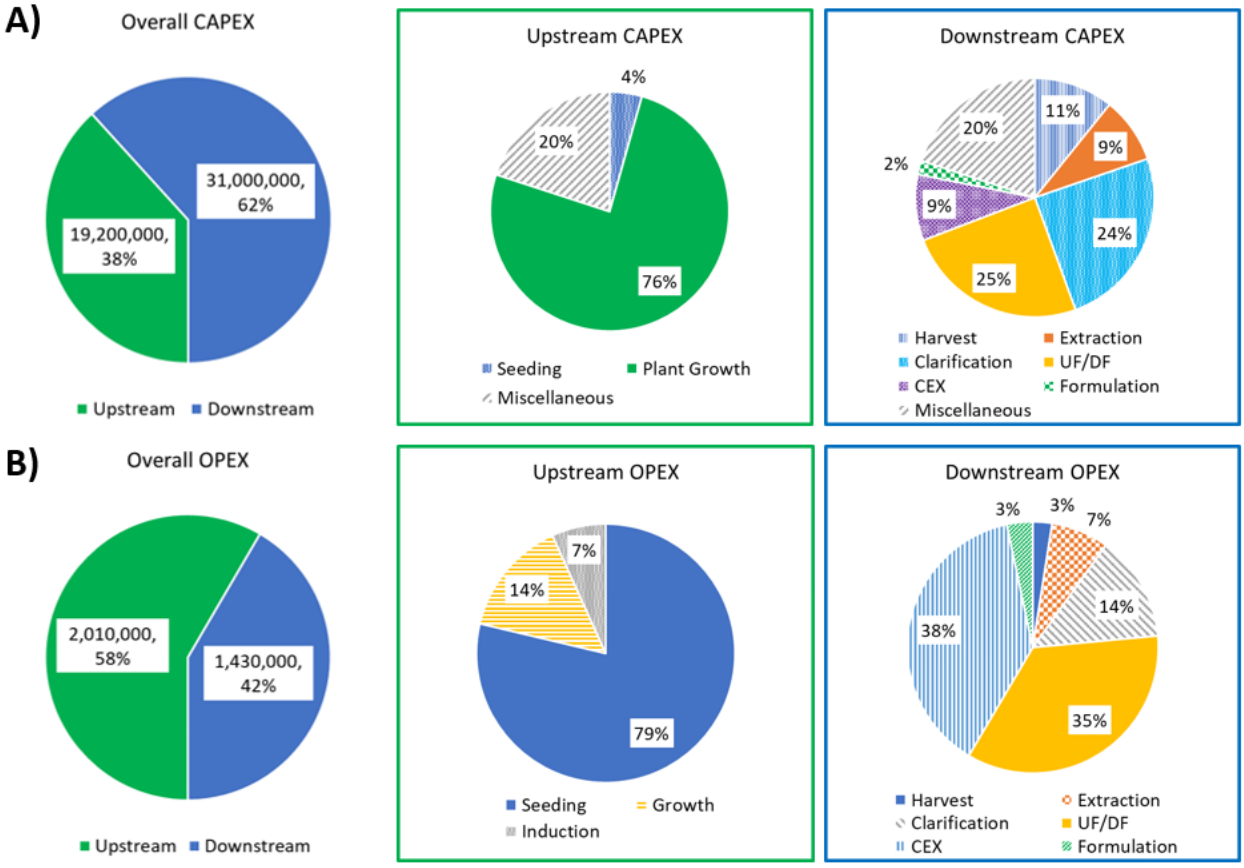

Figure 4.3. Economic assessment of upstream and downstream processing (A) operating expenditures (OPEX), and (B) capital expenditures (CAPEX) for the *Nicotiana benthamiana* base case scenario. CEX, cation exchange chromatography; UF/DF, ultrafiltration/diafiltration.

4.3.3. Purchase Price Sensitivity Analysis

The annual operating costs are heavily weighted by a small number of process inputs; the top ten cost factors collectively represent 90% of the annual operating cost. Figure 4.4 shows the top ten cost factors and the impact of largest contributor percentage variation (±10, 20, 30%) on the AMP COGS. At 1.3 cents per plant, the soilless plant substrate alone accounts for 41% of the OPEX; ±30% variation in soilless plant substrate corresponds to ±12% overall COGS. Variation of ±30% in the tenth largest contributor, the chromatography elution buffer, results in ±0.41% change in

overall COGS. As expected, variation in the larger contributors to annual operating cost result in larger changes in COGS.

A)

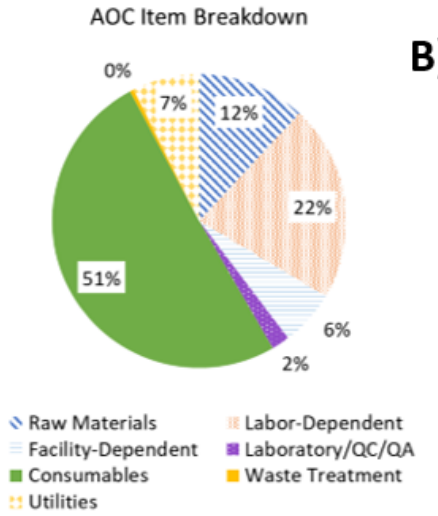

B)

#	Cost Category	Factor	% AOC
1	Consumables	Soilless Plant Substrate	41
2	Labor-Dependent	Downstream Operator	19
3	Consumables	Chromatography Resin	9.2
4	Utilities	Local Power	7.3
5	Raw Materials	Plant Seed	3.4
6	Labor-Dependent	Upstream Operator	3.3
7	Raw Materials	Plant Nutrient	1.9
8	Raw Materials	Extraction Buffer	1.8
9	Raw Materials	NaOH (CIP)	1.6
10	Raw Materials	Elution Buffer	1.4
TOTAL			90.

C)

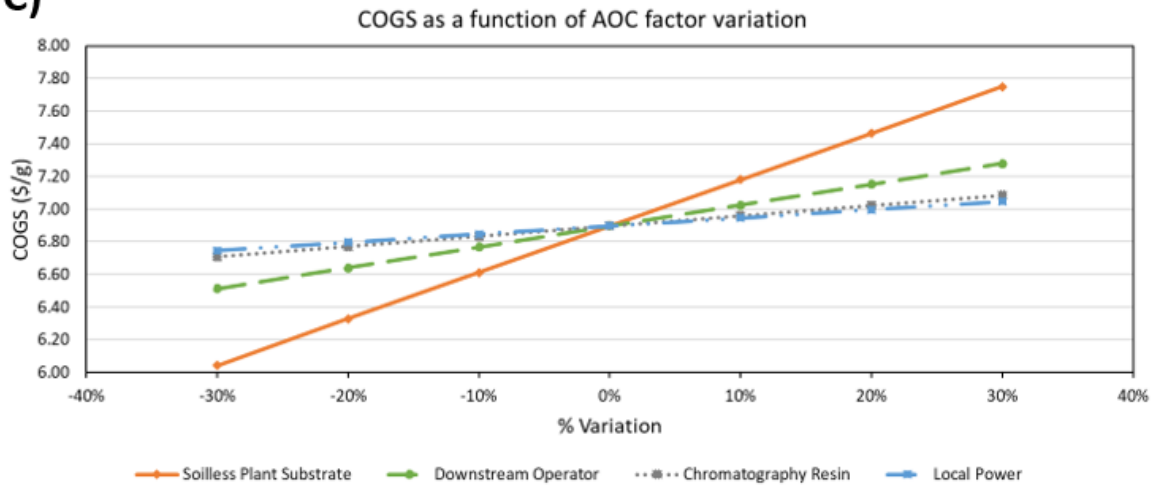

Figure 4.4. For the *Nicotiana benthamiana* base case scenario (A) Annual operating cost (AOC) breakdown of the base case scenario based on cost category. (B) Top individual factors, and the respective cost category, contributing to the AOC of the base case scenario. (C) Cost of goods sold (COGS) as a function of the price of the top individual factors contributing to the AOC.

4.3.4. Expression Level and Production Capacity Analysis

To evaluate the impact of AMP expression level and facility AMP production level, we developed models for a 500 kg AMP/year production level with different AMP expression levels ranging from 0.5 to 5 g AMP/kg FW (Figure 4.5A and 4.5B), and for an expression level of 1 g AMP/kg FW over a range of AMP production levels from 100 kg AMP/year to 1000 kg AMP/year (Figure 4.5C and 4.5D). Note that in all cases the unit operations were resized to meet the design requirements. COGS decreases with diminishing returns as a function of expression level, as can be seen in Figure 4.5. To illustrate this point, consider that an increase of expression level from 0.5 to 1 g/kg FW results in $4.43/g decrease in COGS, while an increase from 4 to 5 g/kg FW results in $0.22/g decrease in COGS. These changes are equivalent to 39% and 6% reductions, respectively. Also note that at low expression levels the upstream operating costs contribute more to the COGS whereas at high expression levels downstream operating costs contribute more to the COGS. This is reasonable since the number of plants per batch will increase as expression level decreases, requiring more soilless growth media, seeds and nutrients. CAPEX follows a similar trend with expression level, however the downstream process is the main contributor to CAPEX except for very low expression levels (less than 0.5 g/kg FW). The majority of COGS and CAPEX variation with expression level is attributable to upstream processing, with downstream process costs remaining fairly consistent over the range of expression levels considered.

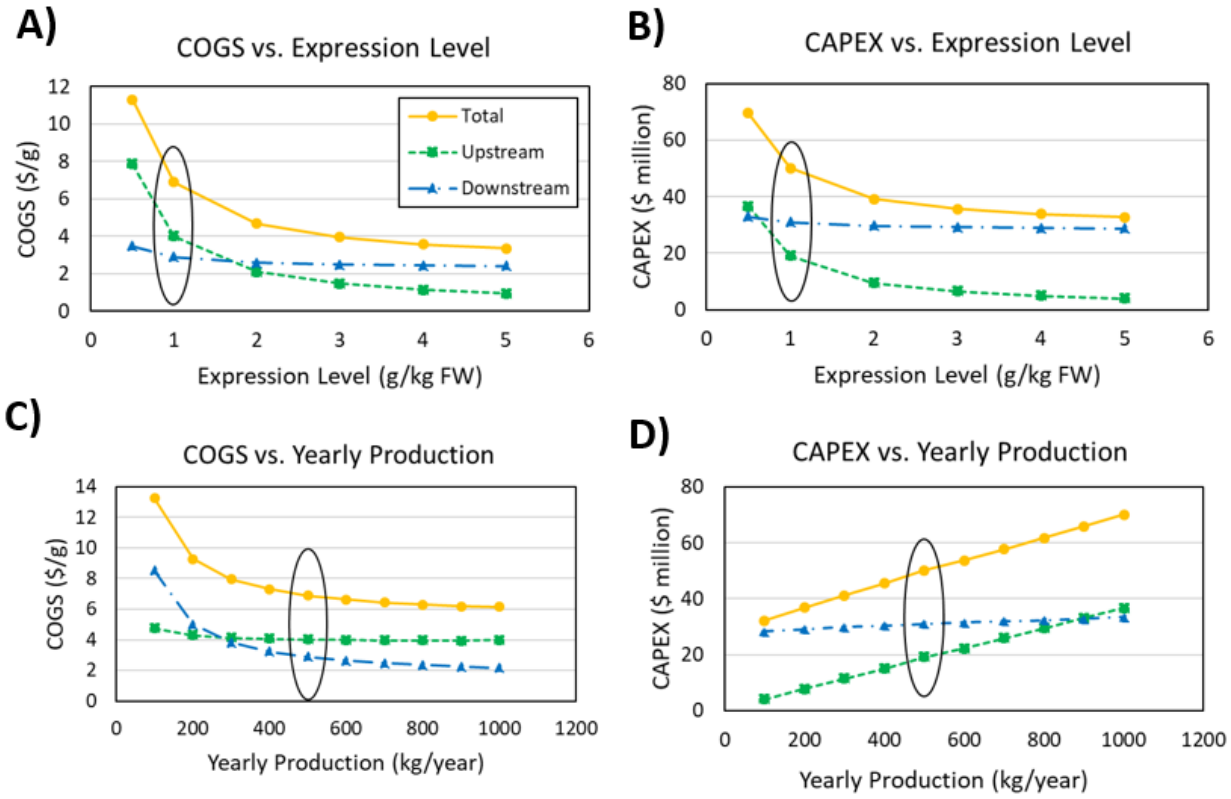

Figure 4.5. For the *Nicotiana benthamiana* scenario, analysis of expression level variation on (A) cost of goods sold (COGS), (B) capital expenditures (CAPEX), and of yearly production variation on (C) COGS, (D) CAPEX. Yearly production is fixed at the base case 500 kg AMP/year for expression level variation analyses (A, B). Expression level is fixed at the base case value of 1 g AMP/kg FW for yearly production variation analyses (C, D). Total, upstream, and downstream contributions of COGS and CAPEX are displayed. The base case scenario values are circled in black. FW, fresh weight.

COGS also decreases with diminishing returns as a function of yearly production capacity. Downstream processing is the main contributor to COGS at low production levels while upstream processing is the main contributor at high production levels; at 100 kg/year, downstream processing represents 64% ($8.51/g) of the COGS, while at 1,000 kg/year the contribution is reduced to 35% ($2.15/g) of the COGS. Within the given parameter range for expression level and production capacity, COGS shows a higher sensitivity to expression level.

Figure 4.6 shows *N. benthamiana* FW per batch as a function of expression level and yearly production demand. As expected, biomass requirements are reduced at higher expression levels and lower yearly production demand. Variation in expression level has a higher impact on biomass requirements for higher yearly production demands. At all yearly production levels, significant diminishing returns for increases to expression level are evident within the selected range expression level.

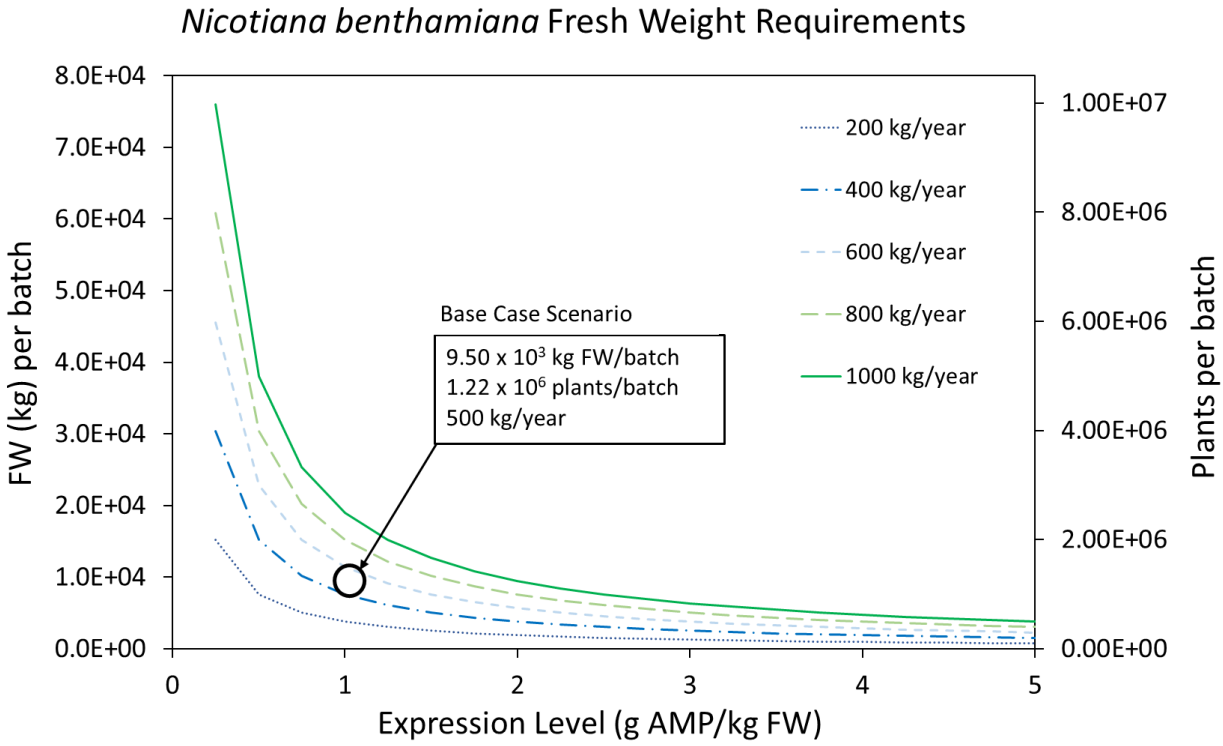

Figure 4.6. *Nicotiana benthamiana* plant fresh weight (FW) as a function of expression level and yearly production of antimicrobial product (AMP). The base case scenario of 1 g AMP/kg FW expression and 500 kg yearly production requires 9.50 x 10^3 kg FW, which translates into 1.22 x 10^6 plants, per batch.

4.3.5. Alternative Scenario Analysis

The nicotine-free *S. oleracea* scenario produces 500 kg AMP/year at 1 g AMP/kg FW with 66% product recovery and 63% purity formulation (Supplementary Information, Table S4.4). Manufacturing batches require ~10% fewer plants than the base case at 1.08 million *S. oleracea* plants/batch, and a correspondingly lower plant inventory of 11.1 million plants. The upstream processing duration remains consistent with the base case, while the downstream processing time is reduced to 0.67 days after removal of the nicotine clearance chromatography step of the base case scenario. The *S. oleracea* manufacturing facility requires $46.5 million CAPEX and $2.50 million/year OPEX. In this scenario, AMP are manufactured at a COGS of $4.92/gram.

The field-grown *N. tabacum* scenario produces 500 kg AMP/year at 1 g AMP/kg FW with 58% product recovery and 92% purity formulation (Supplementary Information, Table S4.6). There are 63 manufacturing batches yearly of 13,900 *N. tabacum* plants per batch within the late March to late October growing season of the US Midwest/South. The lower number of plants is due to the much larger size of field grown *N. tabacum* plants compared with indoor grown *N. benthamiana* plants. The total inventory during steady state operation is 619,000 plants. The upstream processing duration is 88.4 days, and the larger batches increase the downstream processing time to 1.08 days per batch. The *N. tabacum* manufacturing facility, including dedicated outdoor field equipment for transgenic handling, requires $27.5 million CAPEX and $1.51 million/year OPEX. We have neglected labor costs associated with overseeing environmental release of transgenic material, the United States Department of Agriculture (USDA) Biotechnology Regulatory Services (BRS) regulatory application, and routine USDA Animal and Plant Health Inspection Service (APHIS) inspections. In this scenario, AMP are manufactured at a COGS of $3.00/gram.

A comparison of the capital investment, production costs and AMP COGS for the *N. benthamiana* base case, nicotine-free *S. oleracea*, and field-grown *N. tabacum* scenarios is shown in Table 4.2.

Table 4.2. A comparison of capital expenditures (CAPEX), operating expenditures (OPEX), and cost of goods sold (COGS) for the three different studied plant-based antimicrobial product (AMP) production scenarios.

Parameter	Unit	Section	*Nicotiana benthamiana* Indoor Growth (Base Case)	*Spinacia oleracea* Indoor Growth	*Nicotiana tabacum* Field-Grown
CAPEX	$ million	Upstream	19.1	19.1	1.30
		Downstream	31.0	27.4	26.2
		Total	50.1	46.5	27.5
OPEX	$ million/ year	Upstream	2.01	1.79	0.280
		Downstream	1.43	0.711	1.23
		Total	3.44	2.50	1.51
COGS	$/ g AMP	Upstream	4.02	3.52	0.555
		Downstream	2.86	1.40	2.45
		Total	6.88	4.92	3.00

4.4. Discussion

4.4.1. Facility Operation of Base Case Scenario

A greenfield single-product biomanufacturing facility was chosen to reflect the current whole plant protein biomanufacturing environment in the United States. There is significant, yet limited, existing manufacturing capacity, most of which is positioned for pharmaceutical-grade production. For smaller annual production demands (<300 kg product/year), a single- or multi-product contract

manufacturing organization (CMO) model would also be viable. These trends are also reflected globally.

The yearly production was determined to meet the demand of a projected market share anticipated for a product of this nature (unpublished data). The number of yearly batches was determined to fully utilize upstream plant growth capacity while leaving idle time for downstream equipment which is likely to require more maintenance. Future work could include an optimization of the plant inventory size, and thus batch size, to maximize the discounted cash flow rate of return over the project lifetime. The optimization will need to identify a balance in the fluctuation of equipment-associated CAPEX and labor- and utility-associated OPEX for both the upstream and downstream.

The low purity requirements of the AMP at 92% is associated with the selection of plant-based production and is a distinct advantage over traditional production platforms for food safety applications. Leafy plant extracts are safe for consumption, and routinely consumed as a staple of human diet; when the impurities of the host organism are Generally Recognized as Safe (GRAS) for consumption, there is considerably lower burden on downstream processing. The major focus is redirected from product application safety to product stability and functionality in the presence of the host impurities. Depending on the application rate and consumer consumption, we expect that formulations of 50-95% purity could be employed. Therefore, this analysis represents an upper bound for the anticipated production costs.

N. benthamiana has been developed as an efficient recombinant protein expression platform. Except for nicotine and traces of anabasine, the *N. benthamiana* leaf constituents are considered safe for human consumption. Therefore, the processing and quality control are centered on host alkaloid reduction. Processing with a single cation exchange column can provide log reduction in

nicotine level in the product stream to <10 ng nicotine/mg total soluble protein (TSP) in the formulated product. Based on this reduction, the maximum daily intake of nicotine from the use of colicin as a food safety AMP would be much lower than is encounter in everyday consumption of *Solanaceae* plants like peppers, tomatoes, or potatoes[81].

4.4.1.1. Upstream Processing

Vertical farming is just beginning to receive commercial interest as an agricultural solution for year-round, locally grown produce free of pesticides. As the vertical farming industry continues to gain traction, technological advances and process intensification will arise that substantially reduce manufacturing costs for both vertical farming of agricultural crops and plant molecular farming. For example, efficient capture and recirculation of water lost to transpiration (up to 99% water absorbed by roots) will greatly reduce water requirements Continued development of light emitting diode (LED) systems is expected to further improve growth rates, which should help reduce CAPEX, utility costs, and plant growth cycle time.

Based on this current techno-economic analysis, advances in plant substrate processing strategies have particularly high potential for economic gain. Soilless plant substrate represents 41% of the overall OPEX in the *N. benthamiana* base case scenario. A single re-use of the soilless plant substrate prior to disposal would lower the overall OPEX by ~21% in the reduction of consumables cost. Re-use of the plant substrate can be achieved by either regrowth of harvested plants or a second round of seeding to generate new plants. In the former situation, manufacturing cost reductions would also include those associated with seeding and tray cleaning operations.

4.4.1.2. Downstream Processing

Future model optimization could be explored to investigate the impact of lot pooling on COGS. However, lab data should be performed in tandem to support the choice of lot pooling in the manufacturing scheme and the storage conditions. It is well known that proteases present in the leafy plant extract can degrade protein molecules of interest[101]. Proteases present in the leafy plant extract should be removed or inactivated to reduce proteolytic cleavage and maintain product recovery in the case of a hold step prior to lot pooling.

4.4.2. Economic Analysis of Base Case

Techno-economic analysis provides critical information at all stages of a project's lifetime. Efficiency of internal research and development in biotechnology companies has suffered in recent years[102]. Techno-economic analysis is a useful tool for improving this efficiency through identification of key economic-influencing parameters and insights into the commercialization potential of the proposed technology. This preliminary analysis provides early indicators of success potential and reduces risk of investment for key stakeholders. Furthermore, scenario analysis can guide research and development prioritization to maximize return on investment. In the base case model of this study, a change in expression level from 0.5 to 1 g AMP/kg FW resulted in 20-fold greater COGS savings than from 4 to 5 g AMP/kg FW. This knowledge makes it clear that there is a significant economic incentive to improve expression levels, but only up to a point. Refinement of the analysis with pilot-scale data further strengthens the analysis and provides perspective to inform future scale-up work. At the stage of commercial production, techno-economic analyses can provide essential insights in areas such as scheduling, vendor contracts, continuous improvement, and process intensification.

4.4.3. Purchase Price Sensitivity Analysis

Analysis of these individual factor sensitivities provide a preliminary framework for understanding expected bounds of manufacturing costs. It can also serve as a prioritization tool for vendor selection when considering larger, multi-material contracts, as well as with research and development efforts.

This analysis could be strengthened to include a forecasting capacity in future work by integrating market analyses to weight each level of factor variation with a likelihood based on predictive market data. From this information, one could establish an anticipated range of COGS based on key cost factors to holistically define uncertainty and risk.

4.4.4. Yearly Production Demand & Expression Level Analysis

Within the given parameter range for expression level and yearly production volume, COGS is more strongly impacted by expression level. This behavior is specific to the defined parameter ranges, which were selected based on anticipated needs and expectations. In this study, we assumed that raw material and consumable resource purchase costs per unit are independent of yearly amount purchased. As yearly production increases, economies of scale dictates that the material unit price will decrease. This becomes a more important consideration when evaluating COGS over a wide yearly production range.

Figure 4.5 shows similar behaviors for changes in total COGS with expression level and yearly production. However, there is a dissimilar behavior in the upstream versus downstream contributions to COGS over the parameter range. Varying expression level largely influences the

upstream processing COGS, while varying yearly production largely influences the downstream processing COGS. The low downstream COGS sensitivity to expression level is mainly attributed to two items. The main reason is that the costly downstream operations (e.g., chromatography) are economically dependent on AMP quantity rather than stream composition. Additionally, we chose to conservatively fix AMP recovery in the downstream regardless of expression level. The low upstream COGS sensitivity to yearly production is due to the approximately linear scalability of the production platform. This is a main advantage of plant-based production that makes the scale-up from lab to commercial-scale considerably simpler and faster than traditional bioreactor-based production platforms[24]. As yearly production changes, the upstream processing scales in an approximately linear fashion for a given processing strategy. However, one could anticipate that scaling to even higher yearly production could enable higher efficiency upstream processing strategies and thus improve the scaling dynamics of upstream economic contributions.

4.4.5. Alternative Scenario Analysis

The nicotine-free *S. oleracea* scenario provides insight into the manufacturing costs associated with nicotine clearance. There are minor differences in plant growth and harvest operations, but the majority of upstream COGS reduction is due to higher product recovery and thus lower biomass requirements for a given yearly production level. Higher product recovery is attributed to removal of the nicotine clearance chromatography step present in the *N. benthamiana* base case scenario, as illustrated in Figure 4.2. The smaller batch size and simpler downstream processing as compared to the *N. benthamiana* base case scenario result in a 26% reduction in the downstream cycle time and 37% reduction in downstream labor costs, yielding a COGS of $4.92/g AMP.

The field-grown *N. tabacum* scenario results in the lowest COGS of $3.00/g AMP, providing reasonable justification to pursue this manufacturing process. However, our assumptions do not account for potential upstream difficulties associated with product expression consistency, greenhouse growth and transplantation of seedlings (direct field seeding is assumed) or crop loss due to adverse weather events throughout the growing season, nor do they account for the downstream difficulties associated with removal of the more viscous *N. tabacum* host leaf impurities. Future work to experimentally support key assumptions of field growth could add higher confidence and value to this alternative scenario. Additionally, the current growth strategy is based on tobacco production as a commodity good; there may be a different growth strategy that is optimal for recombinant protein production (e.g., increased planting density with reduced time to harvest and higher number of batches per year). It is worth noting that this manufacturing process is expected to scale especially well. In our model, we assume that dedicated personnel and upstream equipment are required for transgenic handling. At an annual production level of 500 kg AMP this results in 17% upstream equipment utilization. This means that as the yearly production demand increases, we expect marginal increases to upstream CAPEX and OPEX. As such, we expect upstream-related COGS to reduce dramatically with increases in yearly production demand.

4.4.6. Cost of Use

Biotic food sanitizers can be used in a variety of applications to augment traditional food sanitizing treatments against specific high-risk pathogens. Given the differences in food safety practices among food products, it can be difficult to measure cost of use as a single value. Instead, we focused our discussion on cost of use calculations with application rates representative of AMP use – colicins for control of *E. coli* on red meats. We choose to investigate this example at several

points along beef processing: animal washing, post-slaughter carcass cleaning, and meat product protection. We anticipate an application rate of 2-10 parts per million (ppm) AMP in water for animal and carcass wash or 2-10 mg AMP per kg meat product. It should be pointed out that, according to the recently published paper of Hahn-Löbmann et al. 2019, application rates of salmocins, *Salmonella* -derived bacteriocins, could be up to 10 times lower because of higher potency of salmocins[103].

Figure 4.7 shows cost of use estimates for select techno-economic scenarios modeled in this study compared to relevant standard sanitizing treatments. Cost of use assumptions and a sample calculation of those performed to generate the cost of use estimates can be viewed in Supplementary Information, Table S4.7 and Calculation S4.1, respectively. In all three points of intervention, AMP application cost ranges are below or overlapping those of standard treatments. Additional information is needed on application rates and spray volume used in animal washing to reduce AMP cost of use range and increase confidence in cost comparison to standard treatments. On the other hand, AMP cost of use ranges for treatment of meat product overlap significantly with standard interventions, indicating comparable costs. Lastly, AMP cost of use ranges for post-slaughter carcass cleaning suggest that the use of AMP at this beef processing juncture has the potential to be substantially lower in cost than standard treatments.

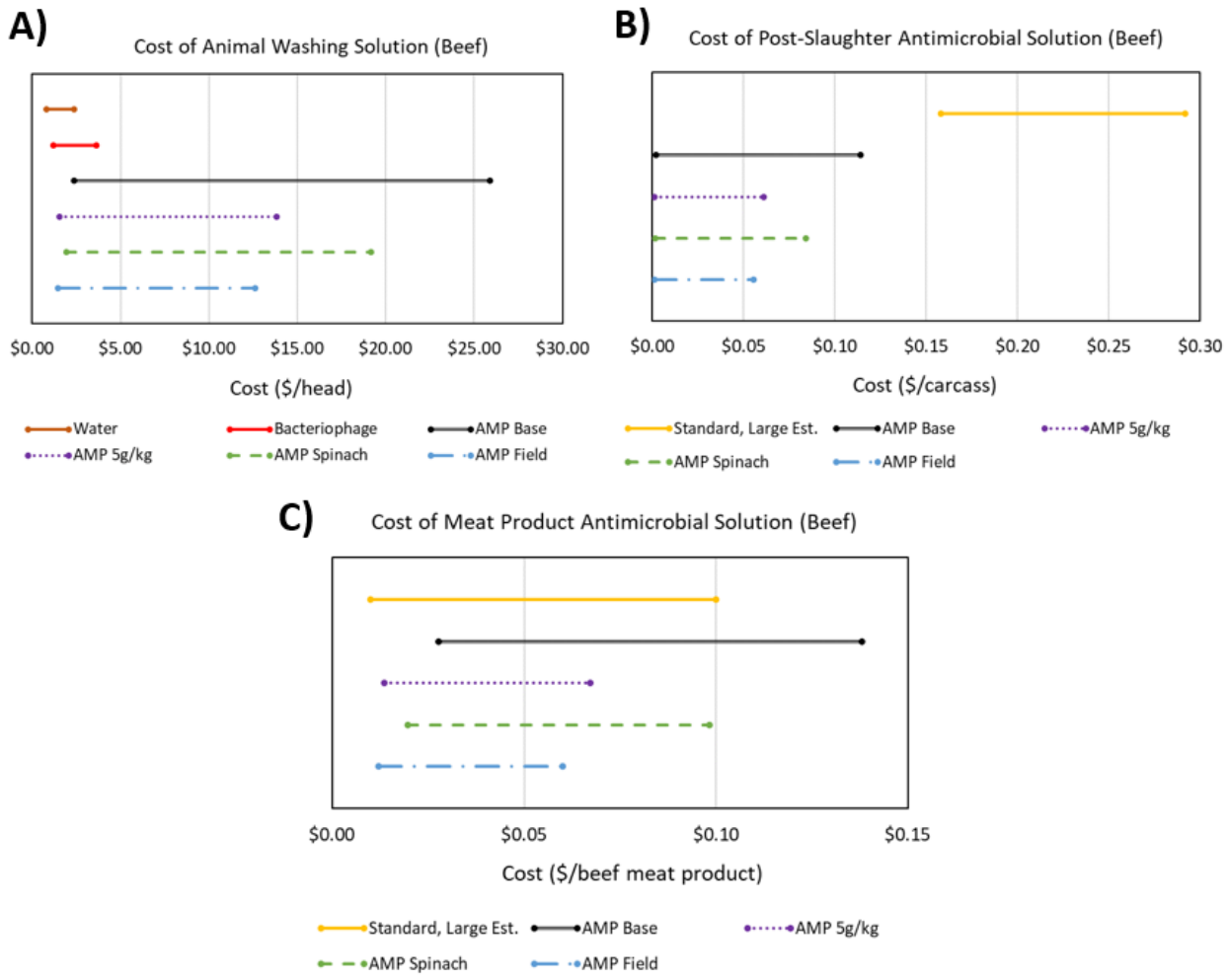

Figure 4.7. Cost of use estimates for antimicrobial protein (AMP) on beef based on expected application rates for (A) animal washing, (B) post-slaughter carcass spray, and (C) meat products. Values are compared to relevant product pricing and across multiple manufacturing production strategies: the base case *Nicotiana benthamiana*, the highest expected expression *N. benthamiana* (5 g AMP/kg Fresh Weight), the nicotine-free *Spinacia oleracea*, and the field-grown *Nicotiana tabacum* scenarios.

4.5. Conclusions

Current food safety practices, although largely effective, result in foodborne illnesses that impose a $14 billion annual burden on the US healthcare system. As the looming prevalence of anti-biotic

resistance grows, so will the impact of foodborne illnesses. The need for protection against foodborne pathogens is only increasing.

Reports as far back as twenty years ago acknowledge that areas of the food industry like the meat sector will need to absorb additional costs to improve food safety levels[104]. We investigated bacteriophage-derived lysins and bacteria-derived AMPs to explore the capacity of this class of biotic sanitizers to improve food safety levels in the cost-sensitive food industry. While previous studies illustrate the efficacy of AMPs, in this study, we performed a techno-economic analysis of plant-based production of AMPs to better understand the commercialization potential of products produced using this platform. Our analysis predicts a $6.88/g AMP COGS for the base case scenario, $4.92/g for the nicotine-free *S. oleracea* scenario, and $3.00/g for the field-grown *N. tabacum* scenario. We also evaluated the sensitivity of the base case COGS to changes in purchase price, expression level, and yearly production. In doing so, we identified economic "hot spots," which include the large contribution of the soilless plant substrate (41.2% of annual operating costs; Figure 4.4B) and downstream labor dependent costs (18.5%). Cost of use analysis indicates that AMPs are projected to de-risk foodborne disease in beef processing as supplemental sanitizing treatments at only minor economic perturbation across several key processing junctures. It is expected that other food processing operations would yield similar benefit.

This techno-economic analysis of plant-based production of AMPs is focused on manufacturing costs and the implications for application costs. In developing this model and analysis, we have identified several areas of importance for future analysis, for example consideration of avoided costs associated with the prevention of food disease and illness. An example of a major avoided cost is that associated with food recall, which includes impact to brand image and loss of sales. A cost-benefit model that includes these avoided costs may provide more complete insights into

AMPs as a food sanitizing treatment. In addition, there are social, cultural and behavioral factors that can impact food safety that are not considered in this economic analysis.

In our analysis, we describe plant-based production of AMPs as a food processing aid. A direct evaluation of traditional manufacturing platforms, such as mammalian cell suspension culture and bacterial fermentation, as alternative scenarios would be a valuable future contribution. To our knowledge, there are no existing direct comparisons of whole plant, microbial fermentation, and mammalian cell culture platforms in the literature. Future work to compare AMP manufacturing in different locations would also add insight into the geographical and national sensitivity of AMP manufacturing process costs.

We compare three host plant batch production models in our analysis, all with different manufacturing processes. A valuable future analysis would be to additionally compare alternative operational modes for a single host plant. Continuous manufacturing is a nascent biotechnology process intensification trend that describes processing of a target molecule from raw materials to final product without any hold steps, in a continuous flow process. This contrasts with the more traditional batch manufacturing investigated in this analysis, in which discrete batches are processed at time intervals. It is generally accepted that continuous manufacturing reduces facility footprint, buffer usage, and equipment sizing as compared to batch manufacturing. To date, there are no publications of continuous manufacturing using plant-based production. We anticipate that plant-based production is a favorable platform for continuous manufacturing, which can reduce CAPEX costs through the replacement of large steel vessels with small disposable containers; whole plant production does not require disposable containers, as the plant itself functions as the bioreactor. A techno-economic analysis comparing these two manufacturing modes will provide additional insight into the economics of plant-based production.

4.6. Supplementary information

4.6.1. Supplementary figures

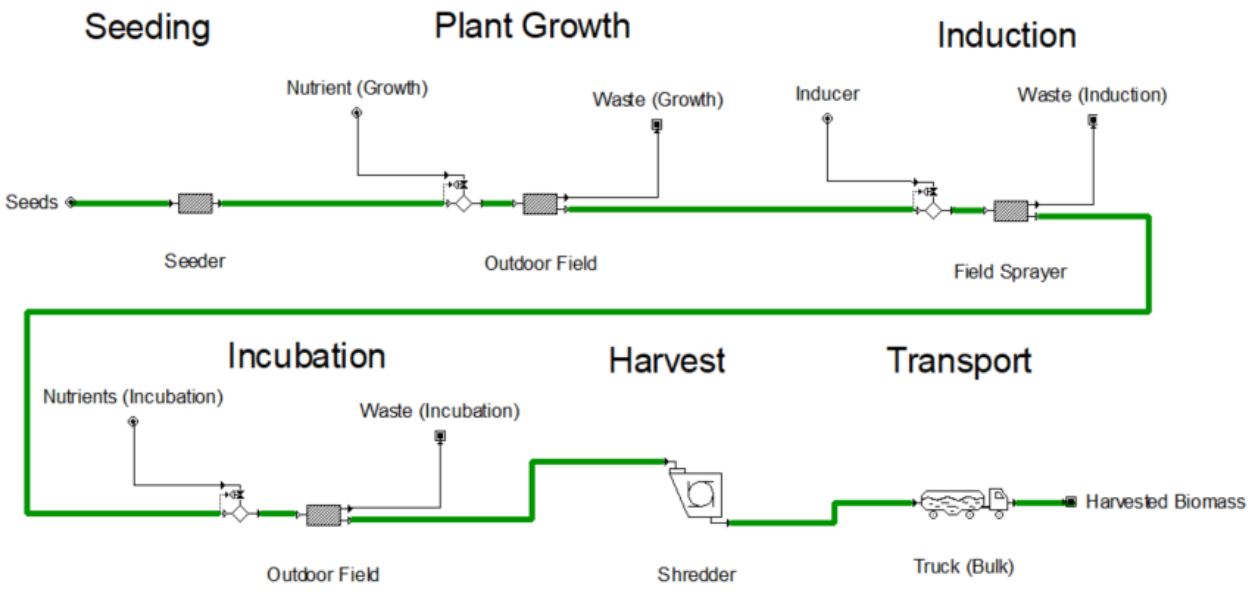

Figure S4.1. Visual representation of the *Nicotiana tabacum* alternative scenario upstream processing SuperPro Designer® model.

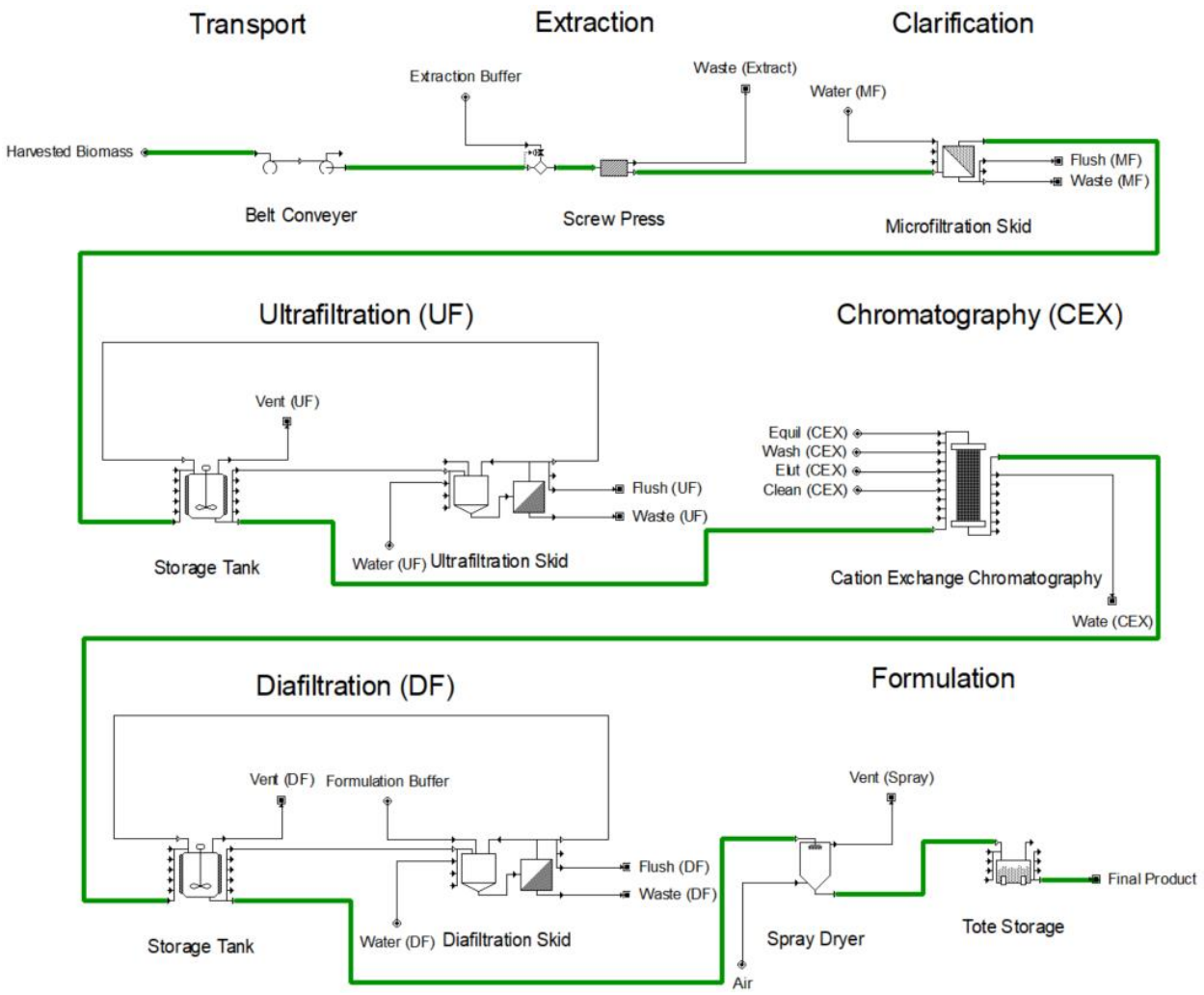

Figure S4.2. Visual representation of the *Nicotiana tabacum* alternative scenario downstream processing SuperPro Designer® model.

4.6.2. Supplementary tables

Table S4.1. Facility design assumptions for the base case scenario model. Values are based on working process, in general. Expression level is based on Werner et al. 2011.

Input Parameter	Value
Yearly Production Demand	Per year: 500 kg antimicrobial product Per batch: 9.50 kg antimicrobial product
Germination Efficiency	95%
Expression Level	1 g antimicrobial product/kg biomass FW; 10% total soluble protein
Downstream Recovery	97% Screw Press 85% Microfiltration 85% Ultrafiltration 87% Chromatography 94% Diafiltration 100% Spray Dry 58% TOTAL
Product Purity	92%

Table S4.2. Model operating expenditure input purchase prices and quantity used for the base case scenario model. Values are based on working process, in general. Local power and water values were obtained from Owensboro, Kentucky municipal services.

Input Parameter	Purchase Price Per Year	Quantity Per Year
Upstream Operator	$159,000 Total Labor Cost = $46/hr 95% Time Utilization	3,450 labor hours
Downstream Operator	$507,000 Total Labor Cost = $81/hr 60% Time Utilization	6,300 labor hours
Local Power	$244,000 Rate = $0.0548/kW-h	4,450,000 kW-h
Local Water	$1,000 Rate = $0.809/MT	1,180,000 L
Steam	$1,070 Rate = $12/MT	89.0 MT
Chilled Water	$381 Rate = $0.4/MT	952 MT
Plant Seed	$117,000 Rate = $9.5/g	12,400 g (1 gram = 9500 seed)
Soilless Plant Substrate	$1,420,000 Rate = $12.8/1000 plants	111,000 items
Nutrient Solution	$65,000 Rate = $0.05/L	1,300,000 L
Ethanol, 3% (w/w)	$172 Rate = $0.02/L	7,400 L
Extraction Buffer	$64,000 Rate = $0.16/L	407,000 L

Equilibration Buffer	$32,000 Rate = $0.15/L	204,000 L
Wash Buffer	$5,000 Rate = $0.04/L	127,000 L
Elution Buffer	$47,000 Rate = $0.35/L	128,000 L
Cleaning Buffer	$11,000 Rate = $0.14/L	77,000 L
Formulation Buffer	$4,000 Rate = $0.07/L	63,000 L
HNO_3, 0.5% (w/w)	$1,000 Rate = $2.61/MT	400 MT
NaOH (0.5 M)	$54,000 Rate = $0.14/L	382,000 L
Plastic Bag (1 L)	$240 Rate = $0.20/unit	1,200 units

Table S4.3. Operating expenditure and capital expenditure bases for the base case scenario model. Values are based on working process, in general.

Input Parameter	Value
Facility-Dependent Costs	Basis: maintenance cost Neglected: depreciation, insurance, local taxes, factory expense
Maintenance Cost	Basis: % equipment purchase cost (section dependent)
Laboratory / Quality Assurance / Quality Control	Basis: % total labor cost (section dependent)
Labor Cost	Basis: total labor cost (TLC) = basic labor rate x (1 + benefits(0.4) + supervision(0.2) + supplies(0.1) + administration(0.6))
Labor Types	Upstream Operator • Basic rate = $20.00/hr; TLC = $46.00/hr • Time Utilization = 95% Downstream Operator • Basic rate = $35.00/hr; TLC = $81.00/hr • Time utilization = 60%
Direct Fixed Capital (DFC)	Basis: 1.2 x listed purchase equipment cost (20% for unlisted equipment) + section-dependent factor (see below) Upstream + 3.0 x listed purchase equipment cost (direct and indirect costs, e.g. piping, instrumentation) Downstream + 6.0 x listed purchase equipment cost (direct and indirect costs, e.g. piping, instrumentation)

Working Capital (WC)	Basis: 30 days raw materials, labor, utilities, waste treatment
Startup Costs	Basis: % DFC (section dependent) Neglected: upfront research and development, upfront royalties, land purchase cost
Income Tax	Basis: 40%
Project Financing	Basis: 0% debt; no loans for DFC or WC

Table S4.4. *Nicotiana benthamiana* base case and *Spinacia oleracea* alternative scenario assumptions for cultivation inputs. Facility design parameters that are different between the two scenarios are also highlighted. All input values are based off working process knowledge.

Parameter		Value		Units
		Nicotiana benthamiana Indoor Growth (Base Case)	*Spinacia oleracea* Indoor Growth	
Facility Design	AMP Recovery	58	66	%
	AMP Purity	92	63	%
Plant Cultivation	Growth facility cost	500	500	$/m^2
	Growth space utilization	70	70	%
	Growth space layers	3	3	layers
	Seed mass	1.05E-04	1.05E-04	g/seed
	Seed mass per batch	1.36E+02	1.20E+02	g seed/batch
	Plants per batch	1.22E+06	1.08E+06	plants/batch
	Plant density	6.24E+02	6.00E+02	plant/m^2
	Tray area	1.50E-01	1.73E-01	m^2/tray
	Plants per tray	9.40E+01	1.04E+02	plant/tray
	Trays per batch	1.30E+04	1.04E+04	trays/batch
	Plant growth rate	1.89E-04	1.86E-04	kg/day/plant
	Leaf biomass, harvest	4.29E-03	3.85E-03	leaf kg/plant
	Aerial biomass, harvest	7.77E-03	7.74E-03	aerial kg/plant
	AMP per plant, harvest	7.77E-06	7.74E-06	kg AMP/plant
	Plant inventory	1.25E+07	1.11E+07	plants/facility

Table S4.5. Buffer composition and usage for the base case scenario downstream processing model. Values are based on working process, in general. Extraction buffer composition is based on Azzoni et al. 2002.

Buffer	Constituents	Quantity
Extraction buffer (pH 4.0)	200 mM glycine 200 mM sodium acetate 200 mM sodium phosphate 200 mM sodium bicarbonate 200 mM sodium chloride	Location: screw press 4,510 L/batch
Equilibration buffer (pH 4.0)	Same composition as extraction buffer	Location: chromatography 2,260 L/batch
Wash buffer (pH 4.0)	50 mM sodium chloride 2.5 mM sodium di-hydro phosphate	Location: chromatography 1,410 L/batch
Elution buffer (pH 7.8)	1 M sodium chloride 50 mM sodium di-hydro phosphate	Location: chromatography 1,410 L/batch
Cleaning buffer (pH 13.5)	0.5 M NaOH	Location: chromatography 848 L/batch
Formulation buffer (pH 7.4)	Phosphate-buffered saline (PBS) 137 mM sodium chloride 2.7 mM potassium chloride 10 mM sodium hydro phosphate 1.8 mM potassium di-hydro phosphate	Location: diafiltration 690 L/batch

Table S4.6. Field-grown *Nicotiana tabacum* alternative scenario unique inputs from the base case scenario. All input values are based off Tusé et al. 2014 and working process knowledge. AMP, antimicrobial product.

Parameter		Value	Units
Facility Design	Yearly batches	63	batches/year
	Growing season	214	days/year
	AMP purity	92	%
		Basis: 1.2 x listed purchase equipment cost (20% for unlisted equipment) + section-dependent factor (see below) Upstream + 1.0 x listed purchase equipment cost (direct and indirect costs, e.g. piping, instrumentation) Downstream + 6.0 x listed purchase equipment cost (direct and indirect costs, e.g. piping, instrumentation)	
Plant Cultivation	Irrigation equipment	0.247	$\$/m^2$
	Irrigation operation	0.099	$\$/m^2$/year
	Tobacco production	0.334	$\$/m^2$/year
	Plant density	1.30E+01	plant/m^2
	Aerial biomass, harvest	1.00E+00	aerial kg/plant
	Plant growth rate	1.12E-02	kg/day/plant
	Plant growth time	82	days
	AMP per plant, harvest	1.00E-03	kg AMP/plant
	Plants per batch	1.39E+04	plants/batch
	Seed mass per batch	1.54E+00	g seed/batch
	Plant inventory	6.19E+05	plants/field
	Land turnaround time	3	days
	Field utilization	95	%

Table S4.7. Assumptions for AMP cost of use estimations in beef processing, based on information provided by the USDA (Noyes et al. 2015). Meat product antimicrobial costs are based on working process knowledge and unpublished market analyses.

Parameter		Value			Units
		Low	Midpoint	High	
Large Establishment Antimicrobial Costs (Post-Slaughter)	Organic Acids	0.158	0.175	0.193	$/head
	Peracetic Acid	0.239	0.265	0.292	$/head
Water Use (Post-Slaughter)		0.05	0.40	0.75	L/head
Bacteriophage Cost (Animal Wash Only)		1.22	2.42	3.64	$/head
Water Use (Animal Wash)		57	114	170	L/head
Large Establishment Antimicrobial Costs (Meat Product)	Undisclosed treatment	0.01	0.05	0.10	$/kg meat

Calculation S4.1. Cost of use estimates for select techno-economic scenarios

Costs of relevant sanitizing applications for animal washing and post-slaughter carcass cleaning are based on 2015 values prepared by the United States Department of Agriculture (USDA)[84], while reference application pricings for red meat products are based on unpublished market analysis. Carcass size is based on previously reported values[105]. Liquid volume required to wet a carcass volume with AMP solution (15 – 45 gallons/head) is based on working process knowledge and values in literature[106]. The AMP COGS is expected to represent 50% of the selling price.

Example Cost of Animal Washing Solution calculation for the AMP base case using the lower bound AMP concentration (2 ppm) and lower bound water use (15 gallons/head) for the animal wash point of intervention:

$$Production\ cost\ of\ AMP\left(\frac{\$6.88}{g\ AMP}\right) \times selling\ price\ conversion\ (2)$$

$$\times\ AMP\ working\ concentration\ \left(\frac{0.002\ g\ AMP}{L\ water}\right)$$

$$\times application\ rate\ \left(\frac{56.8\ L\ water}{head}\right)$$

$$+\ \ purchase\ price\ of\ water\ \left(\frac{\$0.014}{L\ water}\right) \times\ application\ rate\ \left(\frac{56.8\ L\ water}{head}\right)$$

$$=\ AMP\ sanitizing\ treatment\ cost\ (\frac{\$2.36}{head})$$

Chapter 5. Techno-economic analysis of semicontinuous bioreactor production of biopharmaceuticals in transgenic rice cell suspension cultures

"An ounce of prevention is worth a pound of cure."

-Benjamin Franklin

This chapter is based on the following publication:

Corbin, J.M. and **McNulty, M.J.** (co-first author), Macharoen, K., McDonald, K.A., and Nandi, S. (2020). Technoeconomic analysis of semicontinuous bioreactor production of biopharmaceuticals in transgenic rice cell suspension cultures. *Biotechnol. Bioeng.* 117, bit.27475. doi:10.1002/bit.27475

Abstract

Biopharmaceutical protein production using transgenic plant cell bioreactor processes offers advantages over microbial and mammalian cell culture platforms in its ability to produce complex biologics with simple chemically-defined media and reduced biosafety concerns. A disadvantage of plant cells from a traditional batch bioprocessing perspective is their slow growth rate which has motivated us to develop semicontinuous and/or perfusion processes. Although the economic benefits of plant cell culture bioprocesses are often mentioned in the literature, to our knowledge no rigorous techno-economic models or analyses have been published. Here we present techno-

economic models in SuperPro Designer® for the large-scale production of recombinant butyrylcholinesterase (BChE), a prophylactic/therapeutic bioscavenger against organophosphate nerve agent poisoning, in inducible transgenic rice cell suspension cultures. The base facility designed to produce 25 kg BChE per year utilizing two-stage semicontinuous bioreactor operation manufactures a single 400 mg dose of BChE for $263. Semicontinuous operation scenarios result in 4-11% reduction over traditional two-stage batch operation scenarios. In addition to providing a simulation tool that will be useful to the plant-made pharmaceutical community, the model also provides a computational framework that can be used for other semicontinuous or batch bioreactor-based processes.

5.1. Introduction

Growing global demand and public spotlight on the biopharmaceutical industry is driving increased importance on production costs. This spotlight also exacerbates the importance of viral contamination control [107]. These external pressures position the industry to consider alternatives to microbial fermentation and mammalian cell culture production systems.

Plant cell suspension cultures have demonstrated promise as an alternative production system. Plant cells are higher eukaryotes, able to produce a wide array of complex protein products through a versatile set of expression and processing techniques[108,109]. Plant cell cultures are relatively inexpensive to operate due to their simple, often chemically-defined culture medium free from animal-derived components[110]. They have been used at the commercial manufacturing scale for production of multiple drug products, including the secondary metabolite paclitaxel[111] and the recombinant human enzyme glucocerebrosidase produced by Protalix Biotherapeutics[112]. Currently, Protalix is the only company with an FDA approved recombinant biologic produced in plant cell suspension culture[50], and they have several more products in clinical development[113,114]. Protalix's process, which has paved the way for regulatory approval of this technology, serves as an excellent guide for design of future plant cell culture processes.

We have recently demonstrated the utility of plant cell culture technology for production of a challenging recombinant human therapeutic, the human enzyme butyrylcholinesterase (BChE). BChE is a large and heavily glycosylated tetrameric protein that functions as a bioscavenger agent to provide protection against organophosphorus compounds that have been used in chemical warfare and also used as agricultural pesticides. The previously reported cell culture system is able to produce BChE in a metabolically-regulated transgenic rice culture (referred to as rice recombinant BChE or rrBChE) over multiple cycles in a stirred tank bioreactor[115] and can operate

semicontinuously for >6 months with no decrease in the rrBChE production (unpublished data). Using a combination of scalable, commonly used operations including tangential flow filtration and column chromatography, rrBChE can be purified to >95% with a 41% overall process recovery at laboratory scale. Furthermore, rrBChE has shown comparable structure, activity, and *in vitro* organophosphate inhibition efficacy to native human BChE (hBChE)[116]. These factors indicate that manufacturing-scale implementation of this technology could lead to effective and affordable production of this important drug.

Despite the promise of plant cell cultures for biopharmaceutical production and their demonstrated efficacy and ease of use by Protalix, manufacturing scale use of these cultures has been limited. Due to the high cost of entry into the pharmaceutical manufacturing business, novel processes are often viewed as too risky for development. To mitigate risk associated with adoption of a new process, risk severity and probability must both be considered.

Techno-economic analysis is one method to reduce economic uncertainty of manufacturing costs and gauge risks. It can also be helpful to assess process operation strategies and predict theoretical costs to identify process and economic parameters with the highest impact on manufacturing costs. This can be done using "back-of-the-envelope" calculations, spreadsheets, computer modeling, and simulation tools such as SuperPro Designer®[117].

Several traditional biopharmaceutical manufacturing processes have been studied using SuperPro Designer® and other process simulation tools, including tissue plasminogen activator[118,119] and monoclonal antibody[120] production in transgenic mammalian cells. Other studies have focused on whole plant-based biopharmaceutical processes, including lactoferrin[52] and lysozyme production in transgenic rice[121], and transient expression of monoclonal antibody[56,122], recombinant BChE[58], antimicrobial proteins [54], and Griffithsin[55] in *Nicotiana benthamiana* plants. These studies suggest

that plant-based protein expression can produce high quality recombinant proteins with a substantial cost savings, though the magnitude of this savings depends on the specific molecule, as well as the production and processing system.

However, to our knowledge, no such analyses have been performed for a plant cell culture-based biomanufacturing process. In this work, we present a techno-economic model, simulation, and analysis of a large-scale version of the process our group has developed for semicontinuous production of rrBChE in rice cell suspension culture. Our design inputs draw from laboratory-scale process data we have generated and demonstrate the potential cost savings that can be obtained by implementing this process for production of a challenging human biopharmaceutical. The base case facility is designed to produce 25kg of purified rrBChE/year at >95% purity as bulk drug substance with single-use bioreactors used in the seed train and stainless steel bioreactors used for production. The rrBChE was assumed to be cell-associated, extracted from the rice biomass, and purified using tangential flow filtration and chromatographic operations. An additional goal of this model development is to create a tool that can be easily modified, adapted, and broadly applicable to similar processes. To the best of our knowledge, this work represents the first techno-economic analysis reported for production of recombinant protein in plant cell culture and the first facility simulation model for semicontinuous bioreactor operation over long time frames (~6 months). We believe this analysis can be considered as a general model, and the simulation tool can be used for widespread evaluation of semicontinuously-operated cell culture platforms for production of moderate-volume biopharmaceutical products.

5.2. Materials and Methods

5.2.1. Target Selection

The target product, BChE, was selected based on the suitability of plant cell culture operation for small to moderate drug indications, such as chemical or biological defense stockpiles and rare disease treatment. The target production level for rrBChE is 25 kg per year. With a single dose at 400 mg, this corresponds to production of 62,500 doses of rrBChE annually. The production level was estimated on the basis of stockpile generation and emergency deployment. Many orphan diseases would require similarly small production capabilities, such as alpha-1-antitrypsin deficiency, which affects approximately 100,000 people in the US[123], or amyotrophic lateral sclerosis (ALS), commonly known as Lou Gehrig's disease, which affects approximately 30,000 people in the US[124].

The large-scale biomanufacturing facility designs are based on laboratory-scale data. However, process design inputs assume modest improvements in culture performance and downstream recovery based on anticipated process optimization work to be done as part of scale up to pilot and commercial manufacturing.

5.2.2. Process Assumptions

Upstream process performance was assumed to improve from a previous report of laboratory-scale operation[115] in two major categories, cell doubling time (4 to 3 days) and cell-associated rrBChE expression (20-25 to 200 mg rrBChE/kg fresh weight (FW) rice cell). Table 5.1 displays recently obtained values at the laboratory-scale along with the projected values at manufacturing scale to

be used for this process model. A detailed justification of the projected upstream and downstream values can be found in Supplementary Information.

Table 5.1. A summary of production costs for scenarios within this study. CMO, contract manufacturing organization; COGS, cost of goods sold; OPEX, operating expenditures; CAPEX, capital expenditures.

Case	Adjustments	COGS ($/400 mg rrBChE)	OPEX ($ million/year)	% Upstream (OPEX)	CAPEX ($ million)	% Upstream (CAPEX)†
Base Case Two-Stage Semicontinuous, CMO	+20% CMO Fee	263	16.2	21	--	--
Two-Stage Batch, CMO	+20% CMO Fee	274	17.5	53	--	--
Single-Stage Batch, CMO	+20% CMO Fee	266	17.0	52	--	--
Two-Stage Semicontinuous, New Facility	With Depreciation	573	35.3	62	168	86
	Without Depreciation	389	23.9	50		
Two-Stage Batch, New Facility	With Depreciation	644	41.1	77	151	88
	Without Depreciation	428	27.3	70		
Single-Stage Batch, New Facility	With Depreciation	607	38.7	75	140	87
	Without Depreciation	406	25.9	69		

†excluding contributions of unlisted equipment (designated as 20% total equipment)

The downstream processing scheme consists of each of the major steps described in the previous report of laboratory-scale downstream process development[116]. Current laboratory-scale and projected modeling values of rrBChE recovery are shown in Table 5.2.

Table 5.2. Upstream design parameters, current and projected. FW, fresh weight; rrBChE, rice recombinant butyrylcholinesterase; TSP, total soluble protein.

Category	Parameters	Current Laboratory Scale Values	Base Case Model Values	Units
Cell Growth	Dry/Fresh Weight	0.1	0.1	--
	Scale-up Step	varying	10	% WV
	Inoculation Density	7	10	g FW/L
	Transfer Density	70	100	g FW/L
	Doubling Time	4	3	days
	Step Duration	13	10	days
rrBChE Expression	Expression Level	60	200	mg BChE/kg FW
	Expression Period	4	3	days
	Concentration	1	3	% TSP

Clean-in-Place (CIP) assumptions were developed using working process knowledge and literature[65,125,126]. Details of the procedures used in the modeling can be found in Table S5.1 of Supplementary Information.

5.2.3. Process Simulation and Economics

All process modeling was performed in SuperPro Designer® version 10 build 7 (Intelligen, Inc.), and additional calculations were performed in Microsoft Excel. The process models are publicly available at http://mcdonald-nandi.ech.ucdavis.edu/tools/techno-economics/. A free trial version of SuperPro Designer® (http://www.intelligen.com/demo.html) can be used to view the model. Process simulation operating expenditure (OPEX) and capital expenditure (CAPEX) assumptions such as startup costs, labor pay rates, and utility rates are based on current Good Manufacturing Practices (cGMP) operation and are listed in Table S5.2 of Supplementary Information.

5.3. Results

5.3.1. Base Case Processing

The upstream processing model is shown in Figure 5.1. It contains five seed train stages prior to the full-scale production bioreactor. Each seed train step represents a ten-fold increase in working volume over the previous step and is operated in batch mode. The culture is inoculated at 10 g FW per liter (L), then allowed a 10 day growth phase to reach 100 g FW/L. The entire culture is then transferred to the next stage of the seed train to inoculate at 10 g FW/L. At the 20,000 L production bioreactor stage, the culture begins operating semicontinuously in alternating phases of growth and rrBChE expression as shown in Figure 5.2 for the two-stage semicontinuous operation. The transgenic rice cell culture controls rrBChE expression with an inducible promoter (rice alpha amylase 3D or RAmy3D promoter) that is triggered by sugar starvation. A more in-depth explanation of the two-stage semicontinuous operation is included in the Supplementary Information.

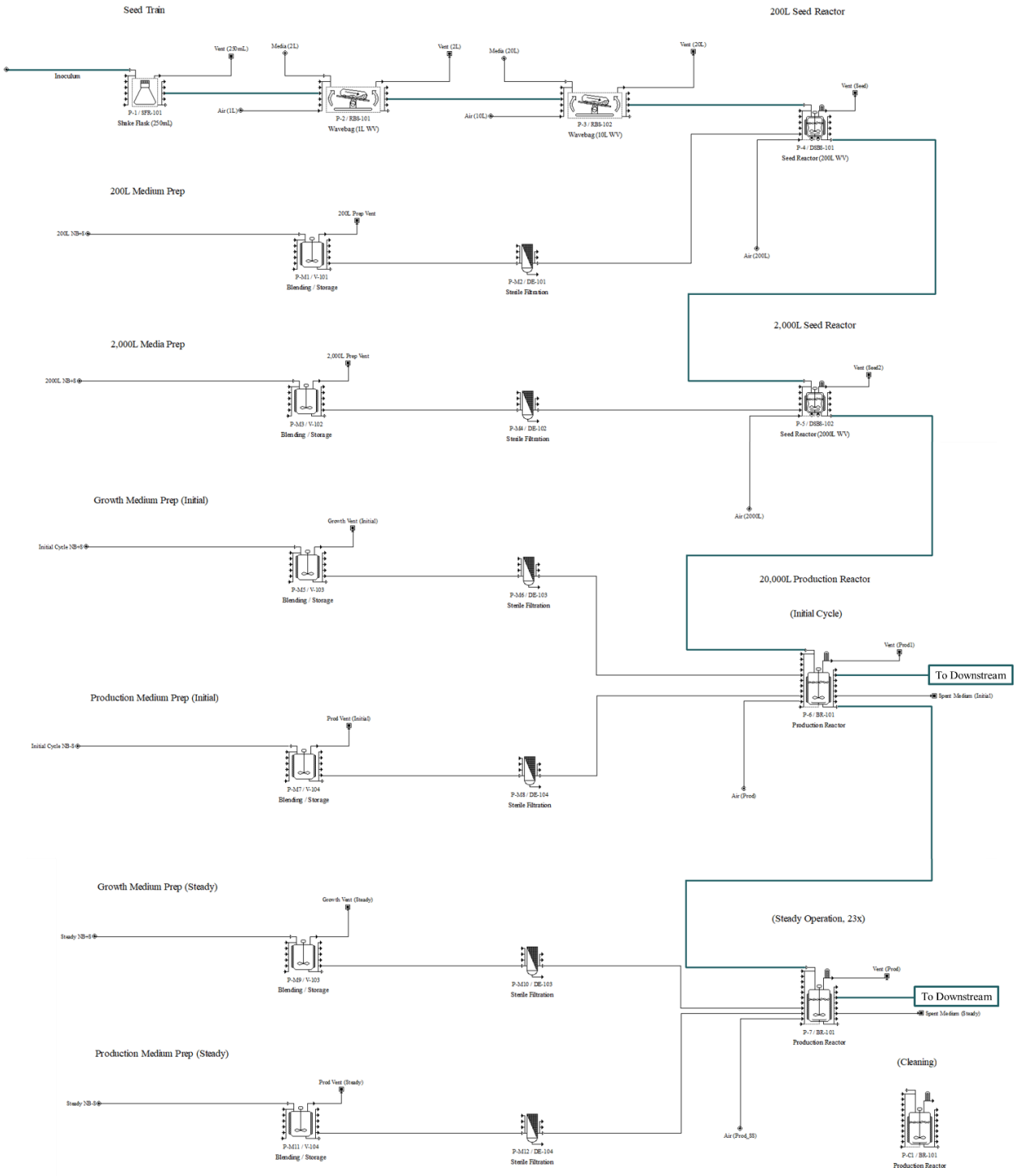

Figure 5.1. Upstream process flowsheet for the two-stage semicontinuous operation base case scenario in the SuperPro Designer® model.

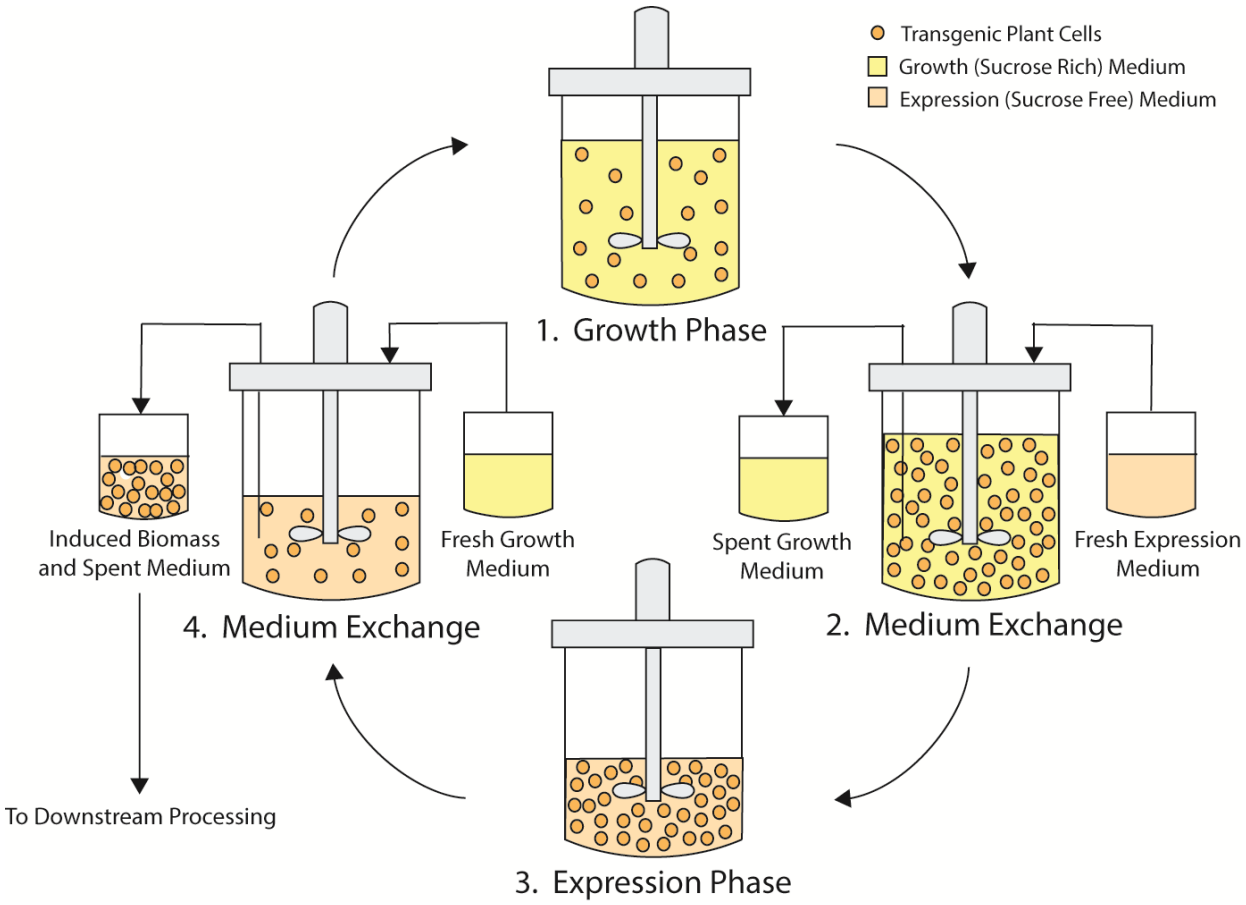

Figure 5.2. Two-stage semicontinuous operation of transgenic rice cell culture with the RAmy3D expression system.

The downstream process flowsheet is shown in Figure 5.3. The harvested material from the upstream process is composed of rice cell biomass containing 200 mg rrBChE/kg FW and spent expression medium. The medium is separated from the biomass using a decanter, where 95% of the spent medium is removed. The biomass is then mixed in a 1:3 (w/v) ratio with extraction buffer and homogenized in a bead mill. After extraction, the resulting supernatant is clarified using a disk-stack centrifuge followed by two dead-end filtration steps (0.45 µm then 0.2 µm pore size). The clarified extract is concentrated 10-fold before diafiltration with 4 equivalent volumes of

buffer in a tangential flow filtration operation and is then passed through a 0.2 μm dead-end filter before the first of two chromatography steps.

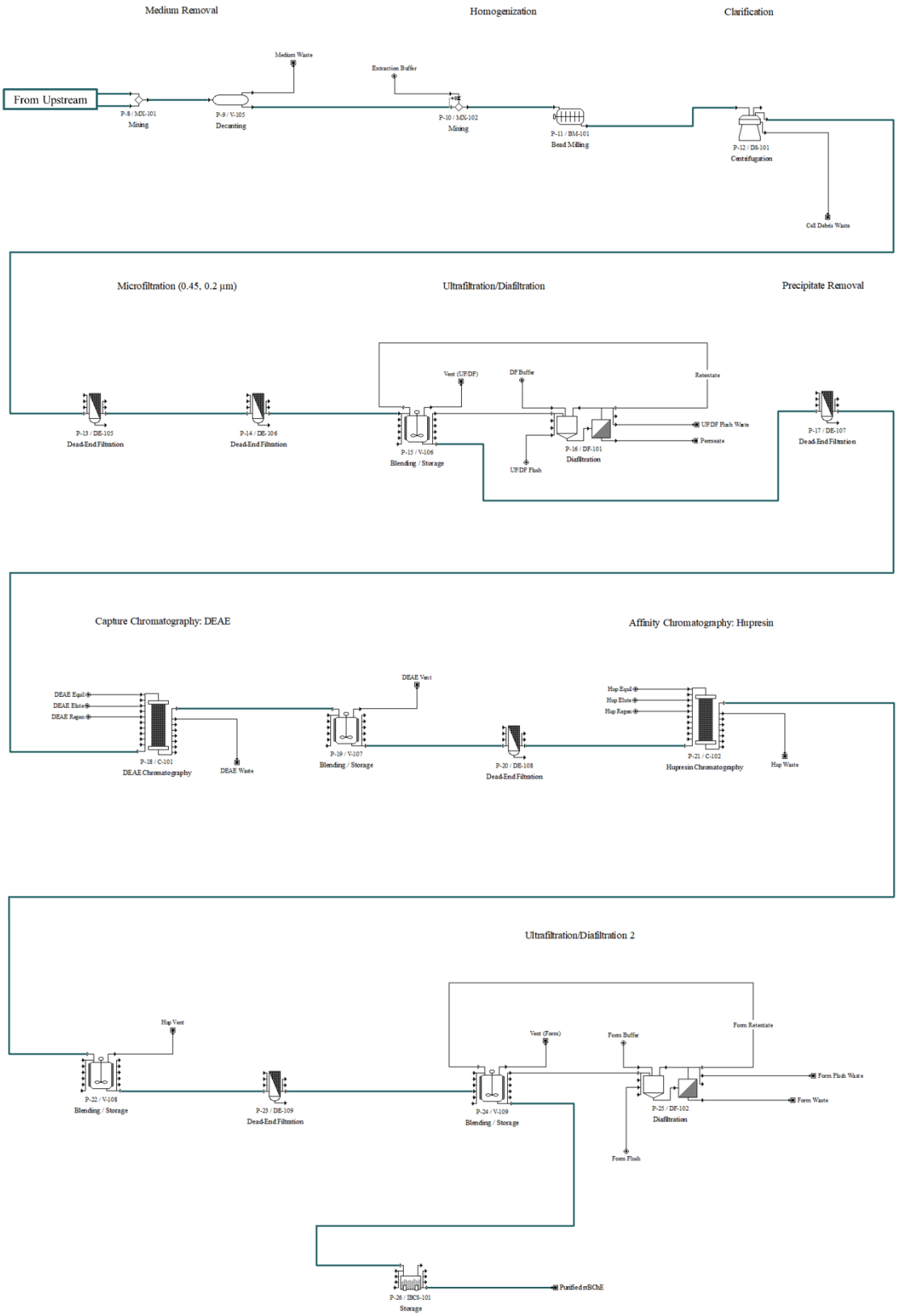

Figure 5.3. Downstream process flowsheet for the two-stage semicontinuous operation base case scenario in the SuperPro Designer® model.

An anion exchange resin is first used as a capture chromatography step before being polished using an affinity resin developed specifically for BChE (Hupresin, CHEMFORASE, Rouen, France). The linear flow rate for all chromatography steps for both resin types is 300 cm/hr and they are operated in bind-and-elute mode with the same buffer compositions (20 mM sodium phosphate buffer at pH 7.4) as previously described[116]. Each chromatography operation is paired with a holding tank for pooling of elution fractions, which are passed through a 0.2 μm filter before the following unit operation. The pooled, eluted fractions from Hupresin are sent to a final ultrafiltration/diafiltration (UF/DF) operation, where they are concentrated 20-fold, diafiltered into phosphate buffer, and aliquoted in 1 L single-use bioprocess bags stored in totes (plastic storage bins). The overall rrBChE downstream process recovery, from homogenization through storage, is 57%.

This process was modeled as a single recipe, which involves one seed train, 24 harvest cycles from the production bioreactor, and 24 downstream process cycles. The production bioreactor produces 0.2 kg rrBChE per harvest cycle and 4.8kg rrBChE per entire recipe. After downstream processing, 0.1 kg rrBChE per harvest and 2.7 kg rrBChE per entire recipe are recovered at 99.7% purity. To reach the target production of 25 kg pure rrBChE per year, 9 recipes are executed to completion.

5.3.2. Base Case Process Economics

In the base case simulation, we assume the described process will be performed in a contract manufacturing facility (CMO) rather than a new facility to be used exclusively for this process. This can be economically favorable for low to moderate volume drug products, especially those

with intermittent demand requirements that can be stockpiled such as BChE. Therefore, all facility-dependent costs, such as equipment maintenance, insurance, local taxes, factory expense, and depreciation, are excluded from determination of the drug price, and an extra 20% is added to the operating costs to account for a fee charged by the CMO.

A summary of production costs for base case process scenarios is shown in Table 5.3. Given the stated base case design parameters, a single batch produces 2.7 kg of pure rrBChE for total OPEX of $1.5 million, which corresponds to a unit production cost of $656/g or $263 per 400 mg dose. Upstream processing comprises 21% of the OPEX, while downstream processing costs comprise the remaining 79%.

Table 5.3. Downstream design parameters, actual and projected. rrBChE, rice recombinant butyrylcholinesterase; UF/DF, ultrafiltration/diafiltration.

	Current Laboratory Scale Values			**Base Case Model Values**		
Step	Equipment	rrBChE Recovery (Step)	rrBChE Recovery (Overall)	Equipment	rrBChE Recovery (Step)	rrBChE Recovery (Overall)
Medium Removal	Buchner Funnel	--	--	Decanter	100%	100%
Cell Disruption	Tissue Homogenizer	--	--	Bead Mill	100%	100%
	Centrifuge	100%	100%	Centrifuge	94%	94%
Microfiltration	0.45 µm	--	--	0.45 µm	99%	93%
	0.2 µm	--	--	0.2 µm	99%	92%
UF/DF	TFF	95%	95%	TFF	96%	88%
DEAE	0.22 µm	--	--	0.22 µm	100%	88%
	Column	75%	70%	Column	80%	70%
Hupresin	Column	60%	42%	Column	85%	60%

UF/DF 2	TFF	--	--	TFF	95%	57%

5.3.3. Base Case Scenario Analysis

We evaluated the impact of process parameter variation on the model facility production costs, univariately investigating 1) rrBChE expression level in rice biomass, 2) the proportion of culture harvested per cycle of semicontinuous operation, and 3) the dynamic binding capacity of the Hupresin in the affinity chromatography procedure. The facility model was re-designed (e.g., resized) for each parameter variation scenario to maintain the same production level and final product consistency with the base case, while all other parameters were fixed for the analysis. The ranges of the process parameter variation tested in the analyses were determined using working process knowledge. The results of the scenario analyses are shown in Figure 5.4.

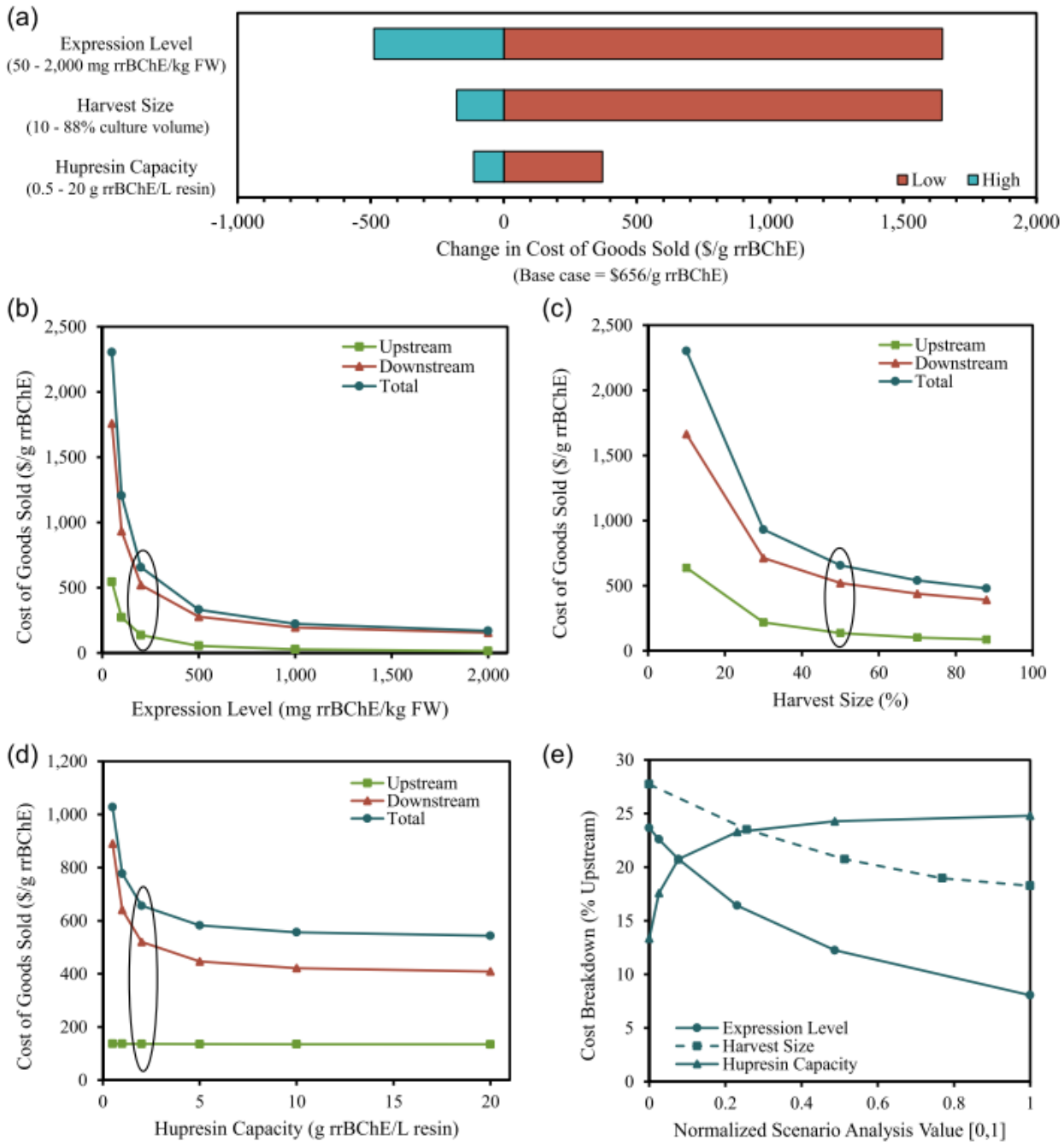

Figure 5.4. Results of the base case scenario analysis. (a) Tornado chart displaying sensitivity of rrBChE cost of goods sold (COGS) to variation in the tested process parameters over the selected analysis range. Individual scenario analyses of (b) expression level, (c) harvest size, and (d) Hupresin capacity variation on rrBChE COGS. (e) Variation in COGS breakdown in the three scenario analyses. The simulated facility is re-sized for each scenario analysis result to maintain base case production level and concentration in product formulation. Values corresponding to the base case are circled in black. FW, fresh weight.

Cost of goods sold (COGS) is most sensitive to expression level variation within the selected parameter ranges, as shown in Figure 5.4. In each of the analyses there is a clear display of COGS decreasing monotonically with increasing parameter value with diminishing returns. As an illustrative example, the COGS decreases by 46% ($549/g rrBChE reduction) when increasing expression from 100 to 200 mg rrBChE/kg FW, but a larger increase from 200 to 500 mg rrBChE/kg FW is required for a comparable 49% reduction in COGS from that point (at $325/g rrBChE reduction).

5.3.4. Alternate Case 1: New Facility

To build on the model of our base case, which utilizes CMO production, we have also modeled the case in which a new facility constructed ground-up on an empty lot of land (referred to as a "greenfield" facility) is exclusively devoted to the production of rrBChE using the two-stage semicontinuous operating strategy. To do so, our models are adapted to consider CAPEX associated with purchasing and maintaining the required equipment and facilities. We calculated that the most cost-effective facility would have four complete sets of seed train equipment, four production bioreactors, and one set of downstream processing equipment (data not shown). The equipment and fixed capital costs are all scaled accordingly, along with all the facility-dependent OPEX contributions.

With these modifications, the cost of a 400 mg dose of rrBChE produced in a new facility is $573 when depreciation is included, and $389 when it is omitted, with CAPEX of $168 million (Table 5.3). The inclusion of facility-dependent costs increases the relative costs of the upstream

processing from 21% in the CMO case to 62% with depreciation, which is expected as four full sets of upstream processing equipment are paired with one set of downstream processing equipment.

5.3.5. Alternate Case 2: Batch Operation

To evaluate the impact of the semicontinuous processing strategy on the rrBChE COGS, we adapted the semicontinuous operation models to examine the process costs associated with the equivalent facility operated in a traditional two-stage batch mode. Here, each production bioreactor operation results in a single cycle of growth, expression, and harvest before CIP, steam-in-place (SIP), and introduction of a fresh inoculum. Five sets of seed train and production bioreactors are required to maintain base case production capacity. Each harvest produces 0.2 kg of pure rrBChE, as the entire 20,000 L culture is collected at the time of harvest. To minimize the size of the decanter, 80% of the spent medium is removed in the bioreactor via gravity sedimentation, and the remaining 15% is removed by the decanter to match the overall 95% medium removal in the semicontinuously-operated base case. Otherwise, the performance of all other downstream steps remains unchanged.

COGS and CAPEX of the two-stage batch operation cases are listed in Table 5.3. Most notably, OPEX contributions are more heavily weighted by the upstream (52%), as compared to the base case. A comparison of the two-stage semicontinuous and two-stage batch mode operation OPEX contributions is shown in Figure 5.5 and a comparison of CAPEX contributions is shown in Figure 5.6.

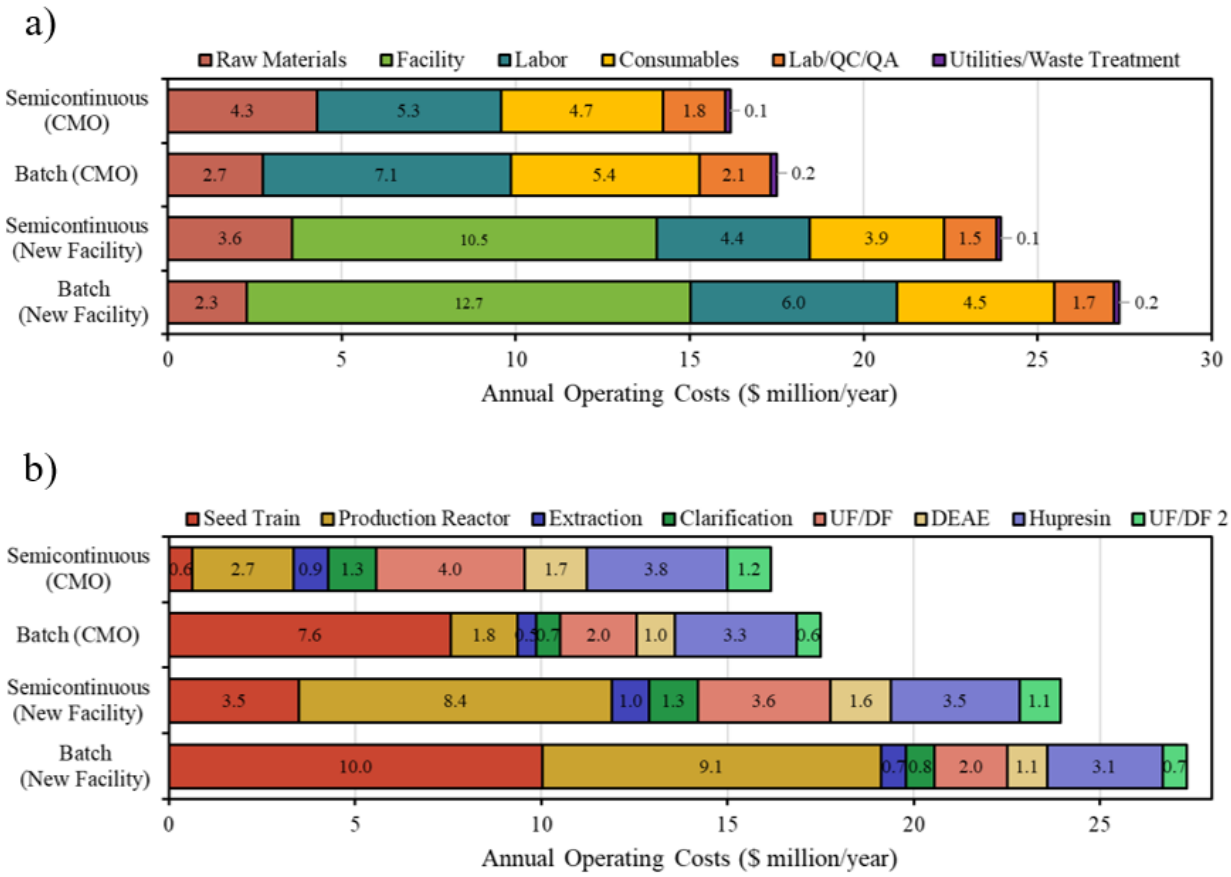

Figure 5.5. Annual operating expenditures for production of rrBChE in two-stage semicontinuous and two-stage batch mode operation using a contract manufacturing organization and with a greenfield single-product facility broken down by (a) cost items, and (b) manufacturing section. Depreciation costs are not included in the annual operating costs for the new facility scenarios.

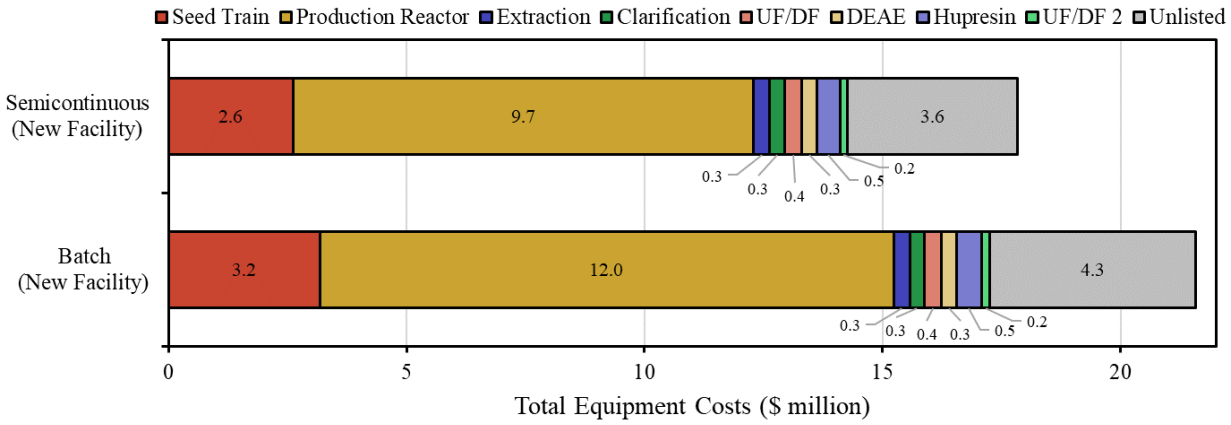

Figure 5.6. Total equipment costs for a greenfield single-product facility producing rrBChE in two-stage semicontinuous and two-stage batch mode operation broken down by manufacturing section.

5.3.6. Alternate Case 3: Single-Stage Batch Operation (Simple Induction)

The expression phase is initiated by sugar starvation, which is achieved using gravity sedimentation-assisted medium exchange. A simple induction method would be to let the sugar deplete naturally – to tune the culture sugar concentration such that the time to depletion is set to coincide with desired final cell concentration. This is referred to as single-stage induction since a medium exchange operation is not required. Preliminary data suggest that this method has the potential to yield comparable growth and expression kinetics, but that the culture is slow to recover in semicontinuous operation (unpublished data). The batch mode operation models were adapted to the simple induction procedure by eliminating the medium exchange operation from sucrose-rich growth medium to sucrose-free medium and reducing sucrose concentration in the production bioreactor growth media by one-half of the base case growth medium.

COGS and CAPEX of the single-stage batch cases are listed in Table 5.3. These results correspond to a 3-6% reduction in COGS over the two-stage batch mode operation.

To better understand the economic impact of the two-stage (medium exchange) and single-stage (simple) induction methods, we performed a sensitivity analysis of the COGS to the cost of culture medium. The culture medium used in this study is inexpensive ($0.10/L growth medium; $0.09/L growth medium (half-sucrose); $0.11/L production medium). The costs, while calculated based on bulk price estimates of the raw material components, are comparable to a previously published analysis on cost-optimized plant cell culture media[110]. Other sources of culture medium for eukaryotic cell culture in batch mode operation cite $5-10/L[127–129].

The results of the analysis for a new facility including depreciation costs are shown in Figure 5.7. COGS increases linearly with culture medium cost in the two-stage and single-stage scenarios but at different rates proportional to culture medium requirements. There is a 6% reduction in COGS using single-stage batch operation when media costs are neglected, which increases to a 23% reduction in COGS at a scenario of $10/L culture medium.

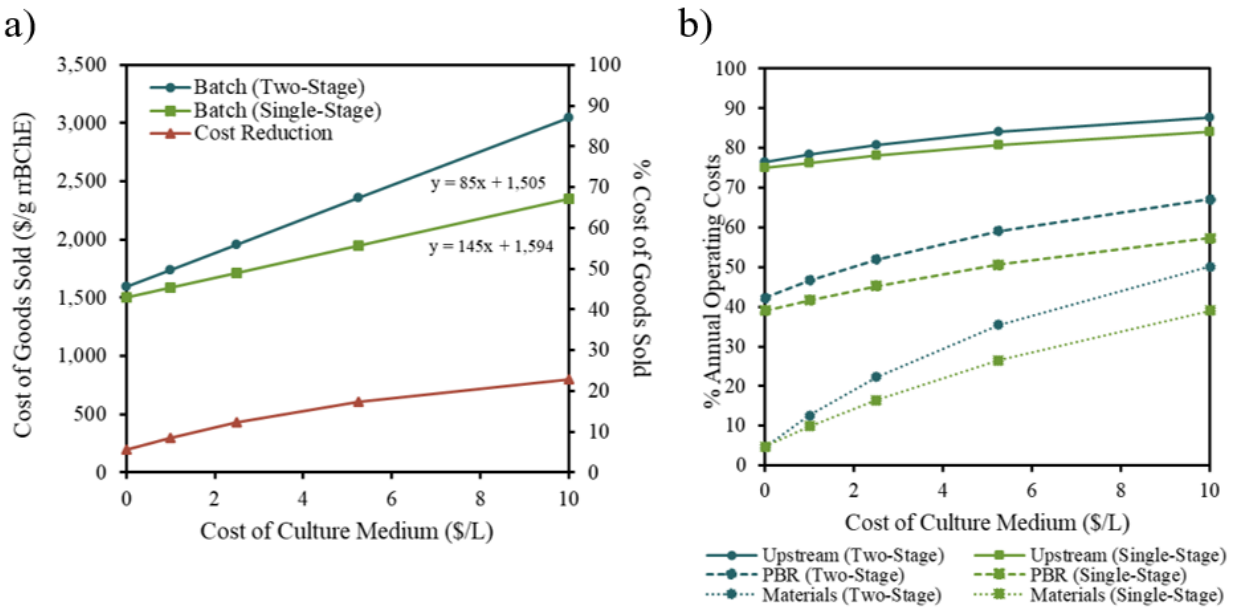

Figure 5.7. (a) Sensitivity analysis of rrBChE cost of goods sold to the cost of culture media for batch mode operation using two-stage (medium exchange) and single-stage (simple) induction strategies for new greenfield single-product facility design including depreciation costs. (b) The variation in operating cost contributions as a function of culture medium cost. The base case scenario price is at $0.10/L. PBR, production bioreactor.

5.4. Discussion

The techno-economic process simulation in this work demonstrates the potential cost-savings for production of a moderate volume drug substance in a two-stage semicontinuously-operated plant cell suspension culture. It also illustrates viability of batch-mode operation of plant cell suspension

culture for commercial manufacturing and highlights significant differences in facility design between these two modes of operation. This simulation uses recombinant BChE as a model product, which has long been a challenging and costly molecule to produce but could represent any complex biologic molecule needed at moderate production levels (10's of kg per year).

In this analysis, two-stage semicontinuous operation yields 4% lower COGS than two-stage batch operation in the CMO scenario, 11% lower in the new facility scenario, and 9% lower in the new facility scenario excluding depreciation costs. Based on the product of interest and the stability of the product in the cell culture environment (e.g., resistance to protease degradation, pH denaturation), semicontinuous operation may provide significant benefits over batch operation which are not captured in this model since the product was assumed to be cell-associated.

We found that semicontinuous operation may be particularly favorable for facilities with high upstream costs; the economic benefits of semicontinuous operation realized in these models are in the 31- 63% lower upstream operating costs. As compared to two-stage batch operation, there are 100 fewer executions of the seed train per year. The higher starting biomass density in the "steady state" semicontinuous growth phase results in production reactor cycles every 6 days as opposed to every 13 days in batch. However, raw material costs are 58% higher than in two-stage batch operation. Media requirements are 97% volumetrically higher in semicontinuous operation wherein a full 20,000 L of each growth and expression media are consumed for a return on only 10,000 L of culture harvested in each cycle. Interestingly, the CIP costs of semicontinuous operation are 70% higher than the batch case despite 100 fewer executions of production bioreactor cleaning. This is due to the lower harvest size of semicontinuous (10,000 L) compared to batch (20,000 L) resulting in twice as many annual downstream processing batches.

We demonstrate that a simple induction strategy to let the sugar in the media naturally deplete could provide additional benefits to batch operation, reducing COGS to within 1% of that of two-stage semicontinuous operation. However, there is appreciable uncertainty as to whether the assumptions of comparable growth and expression kinetics between the medium exchange and simple induction strategies are appropriate. Simple induction is a promising avenue for research and development to improve manufacturing of rrBChE, or other recombinant products under the control of the RAmy3D promoter, particularly in case gravity sedimentation and medium exchange in large-scale conventional bioreactors may be difficult to implement. The benefit of simple induction with the Ramy3D promoter would also be expected to increase substantially with the cost of culture media.

The semicontinuous process modeled here has some similarities and differences to the one used by Protalix for production of their product Elelyso®, an orphan drug used for treatment of Gaucher's disease. Elelyso® is produced intracellularly in carrot root cell culture and uses a semicontinuous process[130]. Thus, Protalix's process provides an additional reference point to justify the feasibility of the process described in this model. Another major hurdle overcome by Protalix was initial establishment of the regulatory pathway for plant-made recombinant human biologics. The mammalian viral contamination-related shutdown of a competing mammalian cell culture production facility, along with the competing product's market exclusivity at the time, served to accelerate regulatory evaluation of Protalix's product and establish a more trusting and favorable view of plant-made pharmaceuticals[131].

Despite this, a few hurdles remain for mainstream adoption of plant cell culture technologies. Pharmaceutical manufacturing processes require stably preserved cell-banking to supply a well-defined starting material and prevent genetic drift in the culture. Cryopreservation techniques have

been established for plant cell cultures[132,133], but there is no protocol that can be universally applied to all species[134]. There is also an ongoing literature debate as to the potential immunogenicity of plant glycan structures. While some studies indicate a potential for an immune response to plant glycans on human therapeutics[135], several other studies of actual *in vivo* administration indicate that this does not occur in practice[136,137]. However, the difficulty in proving that something does not occur will likely continue to challenge regulatory approval and mainstream acceptance of this technology.

For BChE specifically, this study provides manufacturing models which demonstrate a substantial improvement over current production technology in terms of product safety, reliability, and cost. To date, no form of BChE has been approved for therapeutic use in humans. Recombinant hBChE produced in transgenic goats (Protexia®, product by PharmAthene, now Altimmune) reached Phase I clinical trials (ClinicalTrials.gov Identifier: NCT00744146), and results indicated that it was well-tolerated[138]. However, the project was discontinued after project funding expired in 2010 and the production facilities were sold[139]. No production cost analysis was reported. Aside from Protexia®, the most well-developed technology for BChE production involves purification of hBChE from human blood plasma. This product, too, has passed Phase I clinical trials (ClinicalTrials.gov Identifier: NCT00333528). Though many technical aspects of pilot scale purification of hBChE have been documented[140], to our knowledge, no cost analyses have been publicly reported for this process either. However, in February of 2012, the Defense Advanced Research Projects Agency (DARPA 2012) released a call for research proposals titled "Butyrylcholinesterase Expression in Plants." In this document, DARPA cites a BChE dose size of 400 mg and estimates a cost per dose of hBChE as ~$10,000[141], though no references are given for this value. In addition to the extremely high cost of plasma-derived hBChE, availability is

extremely limited: the entire theoretically available blood supply in the US could only produce 1 to 2 kg of pure hBChE, or 2,500 to 5,000 doses, per year[142]. Therefore, cost-effective production of recombinant BChE has been a long-standing goal. Our models suggest that plant cell suspension culture manufacturing has the potential to reduce the COGS to less than 3% of the 2012 DARPA manufacturing estimate.

To that end, we have not only studied rrBChE production in rice cell culture, but have also evaluated production of recombinant BChE using transient expression in *N. benthamiana* plants through agroinfiltration[143], and published a techno-economic analysis of this system[58]. In this work, a single dose of recombinant BChE is estimated to cost $234 when produced in an existing facility and $474 when a new facility is constructed. Overall, these values are lower than, but comparable to, our findings for rrBChE production in rice cell. However, the two models differ in several important ways. Tusé et al. (2014) assume an expression level of 500 mg BChE/kg FW of plant tissue, which is significantly higher projection than what is assumed in the rice cell culture model. The Tusé et al. (2014) model assumes a low downstream recovery of 20%, which is supported by literature surrounding purification of BChE from *N. benthamiana* whole plant systems[144]. Much of the BChE loss occurs in the initial recovery steps; assumptions regarding the costs and binding capacities of the chromatography steps are comparable to this model.

While these two plant-based systems appear to give similar product costs, the choice of expression host depends on other factors, in addition to cost. Transient expression avoids the long lead times associated with development of a transgenic line, which can be essential in rapid response applications. However, transgenic bioreactor-based systems benefit from increased process controllability, reproducibility, and compatibility with existing infrastructure and regulatory guidelines. For BChE and similar targets, a combination of both these strategies may prove

beneficial in meeting global defense needs for both stockpiling and rapid response situations. For other products, such as orphan drugs to treat rare disease, cell culture systems may be preferred for the regulatory process familiarity.

5.5. Supplementary information

5.5.1. Upstream Process Assumptions

The initial and final culture densities were increased slightly, while the culture doubling time decreased from 4 days to 3. This corresponds to a reduction in the duration of each seed train step from 13 to 10 days. It is assumed that the cell density remains constant during the expression phase. The most significant projected change is the cell-associated rrBChE expression level, which is modeled as 200 mg rrBChE/kg FW. This value is roughly 10-fold higher than in our initial reports for this culture, which showed an expression level of 20-25 mg/kg. However, in the time since publication, continued development in culture handling techniques have led to a typical expression level of 60-100 mg/kg at laboratory scale (unpublished data). We could easily expect the expression level to rise even further by developing the cell line and culture conditions using previously demonstrated techniques[145–147]. This increase in rrBChE expression would result in an increase in the initial relative purity (ratio of rrBChE to total protein in the extract) at the start of downstream processing from 1% to 3%. While this increase would likely impact the performance of many downstream processing techniques, notably the chromatography steps, the exact nature of this impact is difficult to predict. Therefore, we also project a slight increase in rrBChE recovery from many of our downstream processes.

5.5.2. Downstream Process Assumptions

These downstream processing operations were selected specifically to match readily available biomanufacturing equipment that do not require custom design to accommodate this process. Altogether, modest improvements in the recovery of downstream operations and assumptions

regarding scale-specific operations increase overall process recovery from 42% at laboratory-scale to 58% in our manufacturing-scale model.

Many of the unit operations required at manufacturing-scale cannot be reliably modeled at laboratory-scale due to extreme changes in the required equipment and operating modes at each scale. As there is no reference for rrBChE recovery for these operations, reasonable estimations were used. The diethylaminoethyl cellulose (DEAE) chromatography step, which at laboratory-scale has given 75% recovery of rrBChE, is modelled as 80%. The binding capacity of DEAE-Sepharose is 110 mg/mL as quoted by GE Healthcare. The Hupresin affinity recovery is projected to increase from 60% to 85%. Such a substantial increase is anticipated as the manufacturer, CHEMFORASE, is relatively new and is actively working to improve the resin's performance. Though substantial improvements are expected as the resin is developed, the binding capacity of Hupresin for the base case is modelled as the current, empirically-determined binding capacity of 2 mg/mL. Since Hupresin is not currently produced at manufacturing-scale, we have based the cost on Protein A resin, with a ~25% increase for custom manufacturing, giving a resin cost of $10,000/L. Another challenge of working with Hupresin is that elution from the resin currently requires tetramethylammonium (TMA) salts (bromide, chloride, etc.), which are classified as acute toxins. Thus, another major assumption of this model is that an alternative elution method can be established that removes the need for these hazardous materials, which not only create additional risk to users of the final product, but also significantly increase waste handling and disposal costs. For the purpose of this model, 500 mM TMA is used for elution as a placeholder, but there are no additional hazardous material handling costs included.

5.5.3. Semicontinuous Operation using the Ramy3D Promoter

Semicontinuous operation begins with a growth phase wherein the culture density is increased from 10 to 100 g FW/L in sucrose-rich growth medium over a period of 10 days. The presence of sucrose represses the promoter, and the cells are free to grow without the metabolic burden of recombinant protein production. After reaching the final culture density, the biomass is allowed to settle (via gravity sedimentation) for 2 hours before spent medium is removed. An equal volume of fresh sucrose-free expression medium is then introduced into the culture, which is incubated for 3 days during the expression phase. The absence of sucrose both activates the RAmy3D promoter and thus expression of rrBChE and minimizes cell growth. This shifts the cells' metabolic resources away from growth and toward protein expression. rrBChE accumulates cell-associated over the course of the expression phase. At the end of the 3 day expression phase, half (10,000 L) of the well-mixed culture (cells and medium) is harvested and sent to downstream processing. The spent medium is drained from the bioreactor while the remaining cells are retained. Fresh growth medium is then provided to the retained biomass, which is given 3 days to regrow from 50 to 100 g FW/L. Beginning with this next cycle, the culture alternates between 3 days of growth and 3 days of expression for 6 months before the bioreactor is shut down for cleaning, sterilization, and re-inoculation from the seed train. In addition to these phase durations is the time required for gravity sedimentation and medium exchanges. Any potential lag in growth rate, which our laboratory scale data suggests is minimal, is included in the empirical growth phase duration[115].

5.5.4. Supplementary tables

Table S5.1. Clean-in-place procedures used in the process simulation models. LPM, liter per minute per meter circumference; RO, reverse osmosis; WFI, water-for-injection.

Category	Step	Material	Flow Rate	Time (minutes)	Temperature (°C)
Cylindrical Tanks	Pre-Rinse	RO water	38‡/25§ LPM	5	25
	Caustic	NaOH (0.5M)		20	75
	Mid-Rinse	RO water		5	25
	Acid	H_3PO_4 (5% w/w)		5	60
	Post-Rinse	RO water		5	25
	End-Rinse	WFI†		5	25
Tangential Flow Filtration	Pre-Rinse	RO water	30 L/m^2 filter	3	25
	Caustic	NaOH (0.5M)	450 L/m^2 filter	45	45
	Post-Rinse	RO water	40 L/m^2 filter	4	25
	End-Rinse	WFI†	15 L/m^2 filter	1.5	25

†use WFI post-Hupresin chromatography; otherwise use RO water
‡for production bioreactor cleaning
§for all other cylindrical tank cleaning

Table S5.2. Process simulation operating expenditures (OPEX) and capital expenditures (CAPEX) assumptions. Parameters. UF/DF, ultrafiltration/diafiltration.

Expense Type	Parameter	Value
OPEX	Labor Cost	Basis: total labor cost (TLC) = basic labor rate x (1 + benefits(0.4) + supervision(0.2) + supplies(0.1) + administration(0.6))
	Labor Types	Upstream Operator • Basic rate = $20/hour; TLC = $46/hour • Time utilization = 100% Downstream Operator • Basic rate = $35/hour; TLC = $81/hour • Time utilization = 60%
	Laboratory / Quality Assurance / Quality Control	Basis: % total labor cost (25-40%) • Prior to UF/DF: 25% • UF/DF onwards: 40%
	Utility	Basis: $0.1/kW-h
	Facility-Dependent Costs	Basis: maintenance, depreciation, insurance, local taxes, factory expense
	Maintenance Cost	Basis: % equipment purchase cost (section dependent)
CAPEX	Unlisted Equipment	Basis 20% of the total equipment costs are devoted to overlooked equipment and accessories (e.g. integrity testing equipment) that are not explicitly included in the model
	Direct Fixed Capital (DFC)	Basis: 1.2 x listed equipment purchase cost (20% for unlisted equipment) + direct cost factors* (piping, instrumentation, insulation, electrical facilities, buildings, yard improvement, auxiliary facilities) + indirect cost factors* (engineering, construction) + other cost factors* (contractor's fee, contingency) *Note: see model for associated calculations
	Working Capital (WC)	Basis: 30 days raw materials, labor, utilities, waste treatment
	Startup Costs	Basis: % DFC (section dependent) Neglected: upfront research and development, upfront royalties, land purchase cost

Chapter 6. Introducing uncertainty quantification to techno-economic models of manufacturing field-grown plant-made products

"Uncertainty is the only certainty there is, and knowing how to live with insecurity is the only security."

-John Allen Paulos

This chapter is based on the following publications:

McNulty M.J. and Kelada K., Nandi S., and McDonald K.A. (2021) Introducing uncertainty quantification to manufacturing field-grown plant-made products. *Food Bioprod. Process.* 128: 153-165. doi:10.1016/j.fbp.2021.04.013

McNulty M.J. and Kelada K., Nandi S., and McDonald K.A. (2021) Techno-economic process modelling and Monte Carlo simulation data of uncertainty quantification in field-grown plant-based manufacturing. *Data Br*. 2021;38:107317. doi:10.1016/J.DIB.2021.107317

Abstract

There is a growing demand for large-market natural and biotechnological products driven by shifting consumer preferences in food and calls for decentralized vaccine and medication production capabilities. The current paradigm of bioreactor-based biomanufacturing faces difficulties of scalability and a high entry barrier of capital intensity and workforce specialization.

Field-grown plant-based manufacturing, as an inexpensive and readily scalable platform, is a promising strategy to meet this call. Despite some successes in field-grown bioproducts manufacturing, concerns including process variability, have largely stymied adoption. Here we report on the development of techno-economic modeling coupled with Monte Carlo simulation as an effective tool to quantify, and mitigate, the impact of variation in field-grown plant-based manufacturing on profitability-related (internal rate of return, cost of goods) and process performance (product purity, annual throughput) forecast variables. In the base case, we observe 80.8% certainty of meeting all forecast variable specifications, defined generically to represent those of a high-volume food-grade commodity product. We observe an internal rate of return (with a selling price of $2,275/kg bioproduct) as low as 10.7% and as high as 47.9% across facility scenarios. We also demonstrate optimization under uncertainty in a facility retrofitting to find a profitability-optimal chromatography column diameter of 1.2 m.

6.1. Introduction

Recent times have brought to the forefront of attention the need for large and reliable source of medication and other biologically-derived products. In these times, world leaders are more concerned than ever with the global biotechnology manufacturing capability. Current manufacturing strategies often depend on bioreactors that require complex equipment infrastructure, large time and capital investments to construct them, and a highly trained specialized workforce to operate them. The ability of this current biotechnology manufacturing paradigm to scale to meet projected global needs across the breath of medical, agricultural, and industrial products is yet unproven. Biotechnology, as a set of emerging industries within which is contained high-profit margin of production, has been traditionally averse to manufacturing platform risks for established product categories such as biopharmaceuticals. This in turn generates vulnerabilities as one considers projections of demand for biologically-derived products, such as biopolymers[148], plant-based protein[149] and oils[150], natural sugar alternatives[151], and biopharmaceuticals[152], increasing several orders of magnitude while sometimes also demanding several orders of magnitude shorter product cycle time. In a recent perspective, we highlighted these vulnerabilities and proposed one solution of how to tackle both the immediate need to address COVID-19 diagnostic reagent shortages and crop surpluses using plant molecular farming[153].

Plant molecular farming, the production of high-value natural or recombinant products in plants, has been heralded as an accessible platform for expanding manufacturing globalization with lower infrastructure costs and workforce specialization than traditional bioreactor-based systems[154]. Stainless steel bioreactors with advanced control systems for a suite of online process variables are replaced by plants, within which a portion of the control systems are absorbed by the natural supracellular regulation systems.

The most advanced efforts in commercialization of molecular farming currently utilize advanced infrastructure, controlled environment facilities containing artificial lighting, controlled atmospheric composition and flow rate, and hydroponic systems to produce recombinant products with demands of 10's to 1,000's of kilograms per year[49]. However, even the complexity and cost of indoor plant cultivation may be prohibitive to broaching larger market products and generally meeting a growing global need across different biotechnological product classes.

Molecular farming of recombinant products in an outdoor agricultural field setting has been an alluring and aspirational target for as long as molecular farming has been an area of research. Despite some early successes with companies like Large Scale Biology Corporation[100], and continued successes of companies like Ventria Biosciences[52,155,156], molecular farming of recombinant products in an outdoor agricultural field setting has faced setbacks including regulatory backlash from Prodigene's pharmaceutical crop mishandling[157] and from mixed public perception, in part as it is lumped with genetically modified food crops[158]. It is prudent to note that the regulation of transgenic crops outdoors has matured significantly, as exemplified by the clear language in the U.S. Department of Agriculture (USDA) Animal and Plant Health Inspection Service Biotechnology Regulatory Services and comfort of the agency to drop requirements for annual USDA permit renewal in some cases where the transgenic lines are declared safe after years of evaluation. Recent publications on molecular farming in an outdoor agricultural field setting highlight the significance of the pitfalls, but also detail a path forward into commercial success driven by the low cost, production scale, and accessibility[32,153,159].

Perhaps the largest blocker to development of outdoor molecular farming is the crop variation, both intra- and inter-batch, that arises from exposure to natural soil and climate variation and is perceived as a concern for consistency of product critical quality attributes[160]. If concerns of

product consistency are alleviated, it is likely that there will be a subsequent need to also address the intertwined concern of crop yield fluctuation[161].

In manufacturing products, such as commodity goods, for which ensuring consistent supply can be critical, the evaluation of risks associated with meeting target throughput and variation in product cost of manufacturing should be evaluated and communicated to stakeholders to complement the decision-making process when assessing the feasibility of processes under uncertainty and strategic planning.

All biomanufacturing introduces a degree of variation in the production. There is a myriad of external factors that can influence production rate and product quality. For example, consider that in biopharmaceutical production, where the product attributes are highly controlled to ensure efficacy and safety to the patient, there are some raw material changes (e.g., source of certain culture media components) can be made by the vendor without the biopharmaceutical manufacturer being notified. Manufacturers and regulators understand the potential variation, and the product is validated with process and product ranges to accommodate this uncertainty. Outdoor plant molecular farming is no different in this respect, but there are concerns that the magnitude or unpredictability of variation is greater than can be absorbed by either downstream processing or a given threshold of an attribute within the quality target product profile. However, to our knowledge, there has not been in-depth evaluation of crop variation that quantifies and propagates the impact to key performance metrics such as cost of goods sold, facility throughput, and product critical quality attributes (e.g., product purity).

Earlier studies have established the concept of uncertainty quantification using techno-economic models to capture production variation of biomanufacturing processes. These investigations have focused primarily on biofuel[162,163] and biopharmaceutical[164,165] production systems with

limitations of coarse techno-economic models and/or limited uncertainty quantification analyses. Notably rigorous, the uncertainty analysis of penicillin V production using fermentation processes includes a detailed model and robust inclusion of uncertainty parameters[166]. However, this report does lack scenario analysis and optimization under uncertainty, both of which are important methodology considerations for plant molecular farming-based manufacturing.

Kelada and coauthors recently published the first techno-economic analysis of plant molecular farming to manufacture a target commodity product at a rate of 50,000 kg per year[167]. In this analysis, the authors simulate a larger production-scale facility than has been commercially realized to date to provide perspective on the feasibility and benefits of plant molecular farming for large demand products. The findings indicate that outdoor field cultivation is one manufacturing strategy to reduce costs compared with the traditional indoor cultivation to meet the price points of commodity and industrial products. In the work by Kelada and in all other molecular farming techno-economic studies to date, a fixed and constant production rate is assumed in designing and sizing the facility.

Other molecular farming techno-economic studies have explored technical and economic viability of primarily indoor production of monoclonal antibodies[56], antiviral proteins[55], biodefense agents[58], and antimicrobial proteins[159], although the latter two studies did compare indoor growth to outdoor field growth scenarios but at much smaller production scales.

Here we present an introductory investigation into uncertainty quantification in outdoor field-grown plant-made products. We use Monte Carlo-based simulation to augment a techno-economic model of an ultra-large-scale manufacturing facility producing 50 MT per year of 98% pure commodity product. The primary objective of this work is to present a foundational tool for

quantifying uncertainty to reduce stakeholder concerns and to optimize outdoor field-grown plant molecular farming facilities.

6.2. Materials and Methods

6.2.1. Process simulation

This work builds on our recently published techno-economic model of ultra-large-scale field-grown production of the recombinant sweetener, thaumatin II, in ethanol-inducible transgenic *Nicotiana tabacum* using a process simulation tool, SuperPro Designer® version 10 build 7 (Intelligen, Inc.), and Microsoft Excel-based calculations. The published model, as well as the modified model used for this work, is publicly available at http://mcdonald-nandi.ech.ucdavis.edu/tools/techno-economics/. A free trial version of SuperPro Designer (http://www.intelligen.com/demo.html) can be used to view the model and run the simulation. The previously published model has been generalized for the production of high-value recombinant proteins, the upstream and downstream processing process flowsheets have been merged, and the process scheduling is defined by rated throughput of the equipment when applicable (Figure 6.1). The generalized model can be readily adapted for production of natural protein products by omission of the tractor spraying procedure, which serves as the induction of ethanol-inducible transgenic production.

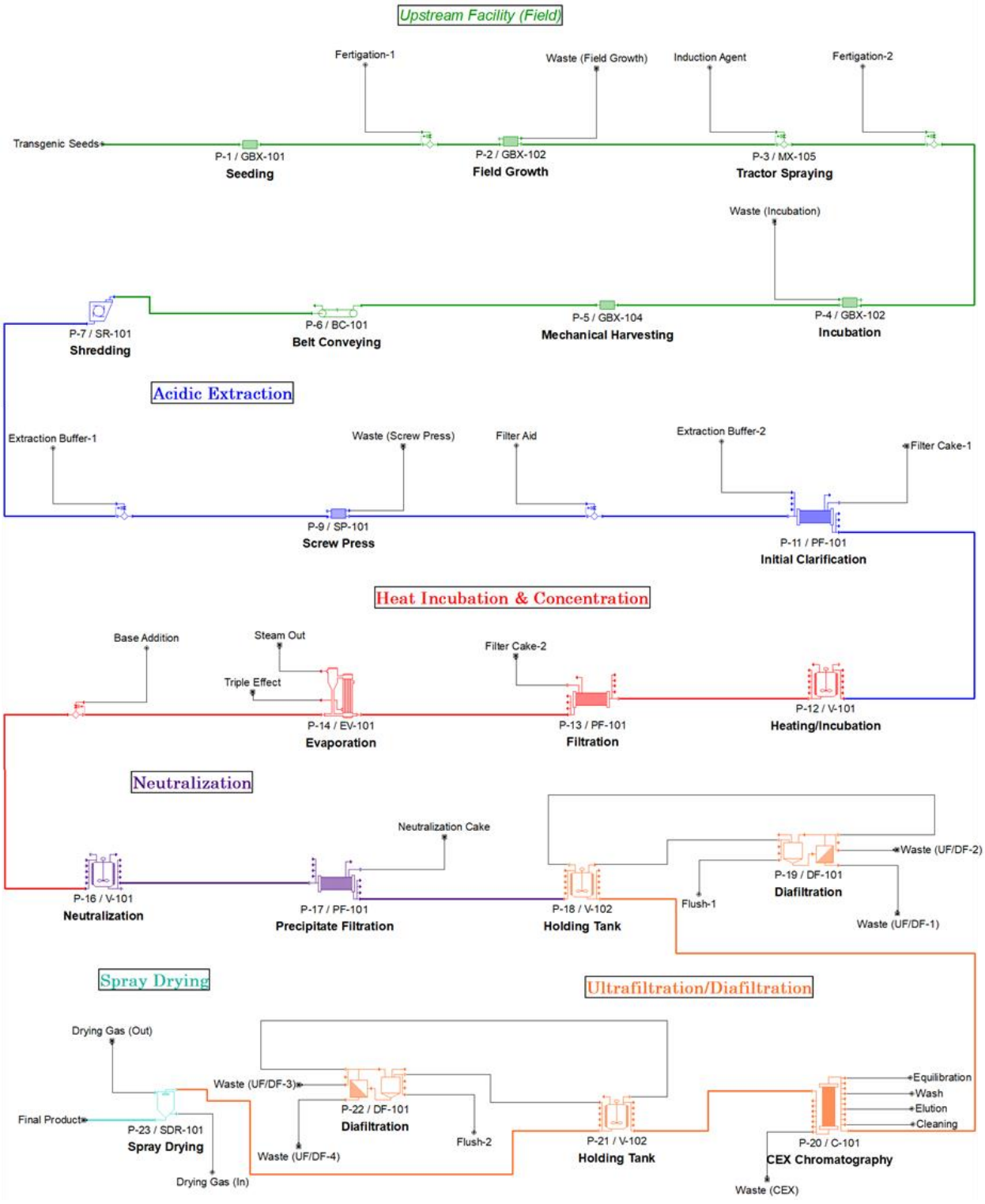

Figure 6.1. Process flowsheet for the field-grown production of recombinant proteins in *Nicotiana tabacum* in the SuperPro Designer® model. Process flowsheet has been adapted from the work of Kelada et al. 2021 [167].

Our previous work did not include profitability analysis. For this analysis, we selected three selling prices of $1,138/kg, $2,275/kg (base case), and $4,225/kg based the cost of goods sold of our previously reported base case techno-economic model ($591/kg, without depreciation)[167] and on previously reported average of gross margins from 1994 to 2005 for an aggregate of companies qualified as generic pharmaceuticals (48%), brand-name pharmaceuticals (74%), and biotechnology (86%)[168]. Lower gross margins, as are typical for other relevant sectors (agriculture (11%); food processing (26%); specialty chemicals (31%)), were also considered but not included within scope (retrieved from New York University's Stern School of Business; http://pages.stern.nyu.edu/~adamodar/New_Home_Page/datafile/margin.html; data compiled from Bloomberg, Morningstar, Capital IQ and Compustat). The selling prices selected for analysis in this study are further supported by profitability analysis in Kelada et al. 2021[167] which reports that recombinantly produced sweetener product selling prices of $3,000/kg - $4,500/kg, depending on the achievable reduction in sugar at a sugar cost of $0.30/kg, were shown to be potentially cost saving for use in sweetened soft drinks.

6.2.2. Uncertainty quantification

We combine Monte Carlo-based stochastic simulation analysis using Oracle® Crystal Ball with deterministic techno-economic process simulation in SuperPro Designer. We have written custom Visual Basic for Applications (VBA) scripts in Microsoft Excel to interact with SuperPro Designer using SuperPro Designer's built-in Component Object Module library, which is expressly designed for this purpose. The Crystal Ball plug-in to Microsoft Excel generates stochastic input parameter values based on a pre-determined probability distribution and the VBA script then sets

the SuperPro Designer facility model performance accordingly and records the results of selected forecast variables (e.g., cost of goods sold, annual throughput).

The facility model equipment is sized for maximal equipment utilization according to the static average base case values. As such, equipment throughput and capacity are exceeded for input parameter values that result in higher stream volume or product mass than the base case model. In these instances, SuperPro Designer triggers a warning or error notification, but regardless still sends the full process stream (including any capacity exceeding that of the equipment) to the next unit operation by default. We implemented a simple Microsoft Excel-based algorithm to correct the facility model in these cases. For exceeded stream volume capacity, biomass from field growth yield, which dictates stream volume, is reduced from the stochastically determined value to a value corresponding to the "effective" field growth yield, defined as the maximal yield that the facility can process based on equipment capacity. Physically, this is designed to be representative of plowing excess biomass back into the fields for soil enrichment. For exceeded product mass capacity, as only chromatography performance is assumed to be sensitive to this value, it is assumed that there will be negligible impact to chromatography binding capacity and that excess will be diverted to the flow-through, resulting in a reduction of the stochastically determined cation exchange chromatography (CEX) recovery of product value to a value corresponding to the "effective" CEX recovery of product, defined as the maximal recovery that the resin binding capacity can accommodate.

One known disadvantage of Monte Carlo-based simulation is the high trial number needed to closely approximate the distributions. We chose to run each uncertainty analysis for 20,000 trials. Profitability-related forecast variables include 20,000 trials for each plot, while process-related variables include 60,000 trials (combined 20,000 trials for each of the three selling prices analyzed

for profitability-related forecasts). Each trial returns the facility forecast variables values calculated for a full facility lifetime of 25 years. For process performance forecast variables, each trial can also be interpreted on a batch-basis, while profitability forecast variables would need to be calculated differently for a batch-basis interpretation, rather than facility lifetime, of trial results. We were able to run each set of 20,000 trials of combined stochastic-deterministic evaluation on a personal computing machine on the order of several hours running time.

6.2.3. Input parameter uncertainty

We selected a set of input parameters for uncertainty analysis (Table 6.1). Input parameters were screened and selected on the basis of known uncertainty, techno-economic impact, and relevance to outdoor field growth. Supporting information for determination of the input parameter probability distributions, and graphical depictions of these distributions, are included in Supplementary Information. Probability distributions are defined such that the mean is equal to the static value assigned in the base case model.

Table 6.1. Input parameters selected for uncertainty quantification and the defined probability distributions. FW, fresh weight; P&F, plate and frame; UF/DF, ultrafiltration/diafiltration.

Variable	Procedure	Base Case Value	Distribution	Variation [Range]
Field growth yield (% maximal*/100) *132 g FW/plant	P-2	0.76	scaled beta	alpha = 2.57, beta = 4.80 [0.63, 1.0]
Field growth time (days)	P-2	34.83	triangular	likeliest = 34.83, ± 5% likeliest [33.09, 36.57]
Expression level (g product/kg FW)	P-4	1.5	logistic	mean = 1.5, scale = 0.08 [0.95. 2.05]
Harvesting time (hours)	P-5	8	scaled beta	alpha = 1, beta = 8 [4, 40]

P&F filtration removal (% product lost)	P-11	5.15	normal	mean = 5.15, SD = 0.52 [3.55, 6.75]
P&F filtration removal (% impurities removed)	P-11	5.15	normal	mean = 5.15, SD = 0.52 [3.55, 6.75]
P&F filtration flux ($L/m^2 \cdot h$)	P-11	180	triangular	likeliest = 180, ± 20% likeliest [144, 216]
P&F filtration removal (% product lost)	P-13	5.43	normal	mean = 5.43, SD = 0.54 [3.75, 7.11]
P&F filtration removal (% impurities removed)	P-13	95.0	normal	mean = 95.0, SD = 0.54 [93.32, 96.68]
P&F filtration flux ($L/m^2 \cdot h$)	P-13	200	triangular	likeliest = 200, ± 20% likeliest [160, 240]
P&F filtration removal of product (% product lost)	P-17	1.72	normal	mean = 1.72, SD = 0.17 [1.08, 2.26]
P&F filtration removal of impurities (% impurities removed)	P-17	1.72	normal	mean = 1.72, SD = 0.17 [1.08, 2.26]
P&F filtration flux ($L/m^2 \cdot h$)	P-17	30	triangular	likeliest = 30, ± 20% likeliest [24, 36]
UF/DF filtration flux ($L/m^2 \cdot h$)	P-19	30	triangular	likeliest = 30, ± 20% likeliest [24, 36]
CEX recovery (% product recovered)	P-20	88.5	triangular	± 10% base case [80, 97]
CEX recovery (% impurities recovered)	P-20	5.0	triangular	± 10% base case [4.5, 5.5]
UF/DF filtration flux ($L/m^2 \cdot h$)	P-22	40	triangular	likeliest = 40, ± 20% likeliest [32, 48]

6.2.4. Input parameter correlations

Input parameter values are by default generated independent of each other using random selection from the given probability distribution. However, parameter-parameter interactions and correlations are to be expected during manufacturing. We consider several parameter correlations in the uncertainty quantification analysis by defining Pearson correlation coefficients in Crystal Ball to establish a degree of linear relationship between two variables (Table 6.2). The Pearson correlation coefficients used in the model are primarily based on the reported findings in Knödler

and colleagues[169]. We also assume on the basis of working process knowledge that there is a moderate positive correlation (r = 0.7) between product loss and impurities removal in the plate and frame filtration procedure P-11.

Table 6.2. Pearson correlation coefficients

	Field growth yield (P-2)	Field growth time (P-2)	Expression level (P-4)	P&F removal of product (P-11)	P&F removal of impurities (P-11)	CEX recovery of product (P-20)
Field growth yield (P-2)	--	r = 0.8842		r = -0.6321		
Field growth time (P-2)	r = 0.8842	--				
Expression level (P-4)			--			r = 0.6042
P&F removal of product (P-11)		r = -0.6321		--	r = 0.7	r = 0.9432
P&F removal of impurities (P-11)				r = 0.7	--	
CEX recovery of product (P-20)			r = 0.6042	r = 0.9432		--

6.2.5. Forecast variable selection

We selected a set of forecast variables to capture the value in uncertainty quantification as a tool to identify parameters that are likely to impact the bottom line and to optimize field-grown plant-made product facilities. Table 6.3 provides a list of all forecast variables measured in the uncertainty quantification analysis. The cost of goods sold (COGS) forecast variable is calculated with depreciation included.

Table 6.3. The selected forecast variables, a brief justification of their inclusion/significance, and hypothesized desired output ranges are included for the sake of illustrating richness of analysis capabilities.

Forecast Variable	Justification	Desired Output
Internal rate of return, after tax (% discount rate)	Represents a measure of the project profitability based on future cash flows in present dollar value, while taking in consideration the initial investment, operating costs, revenues, and taxes.	≥ 30%
Cost of goods sold ($/kg product)	Represents the production cost and serves as a key determinant of profitability.	≤ $850/kg product
Annual throughput (kg product/year)	Represents the product supply and can inform supply chain management and market penetration strategies.	≥ 4.0×10^4 kg/year ≤ 6.5×10^4 kg/year
Product purity (% purity)	Represents the product quality and can inform manufacturing strategies to ensure standards for the product critical quality attributes are met.	≥ 97.5%

6.2.6. Facility model analyses

Sensitivity analysis is generated by Crystal Ball for each forecast variable using simulation run data. A rank correlation coefficient is calculated between every forecast and assumption. Percent contribution to variance is calculated from the rank correlation coefficient. Correlation among the input parameters was not included while considering the Monte Carlo-based simulations runs for sensitivity analysis.

The influence of equipment capacity on forecast variable outputs is investigated in facility oversizing analysis. The equipment of the base case facility model is sized to maximize equipment utilization for the nominal static average input parameters. Here we investigate the impact of oversizing equipment (base case = 0% oversize) to reduce or eliminate probability of process

stream waste for above average throughput trials on techno-economics. A facility model with 100% oversizing is defined as a scenario with equipment sized to process the maximum stream volume possible within the selected input parameter ranges. Simulations were performed at 0% (base case), 25%, 50%, 75%, and 100% oversizing. The following equipment were re-sized for this analysis: heat tank (V-101), evaporator (EV-101), tangential flow filtration hold tank (V-102), CEX column (C-101). Details of the re-sizing are included in Supplementary Information. All other equipment were capable of processing the maximum stream volume without re-sizing using a rated throughput.

The optimization of the CEX column size under input uncertainty is investigated as an optimization scenario. The base case scenario CEX column size, which was calculated using static average values, is used as the optimization starting point. We fixed the bed height and allow the CEX resin volume to vary with bed diameter for CEX size optimization. Oracle Crystal Ball's OptQuest tool was used to determine the CEX diameter that maximizes the mean value IRR of simulations of 20,000 trials in the range of 0.7 – 1.7 m diameter (base case = 1.2 m) discretized in 0.01 m increments.

6.3. Results

6.3.1. Uncertainty quantification

Individual forecast variable uncertainty quantification is shown by histogram, cumulative probability distribution, and top input parameter contributions to variance in Figure 6.2. Expression level (P-4), field growth yield (P-2), field growth time (P-2), P&F removal of product (P-13), and CEX recovery of product (P-20) have been generally identified as top contributors to

variance for the selected set of forecast variables analyzed. Additional information on the forecast variable outputs, including graphical assessment of normality and a list of contributions to variance for all input parameters, is included in Supplementary Information.

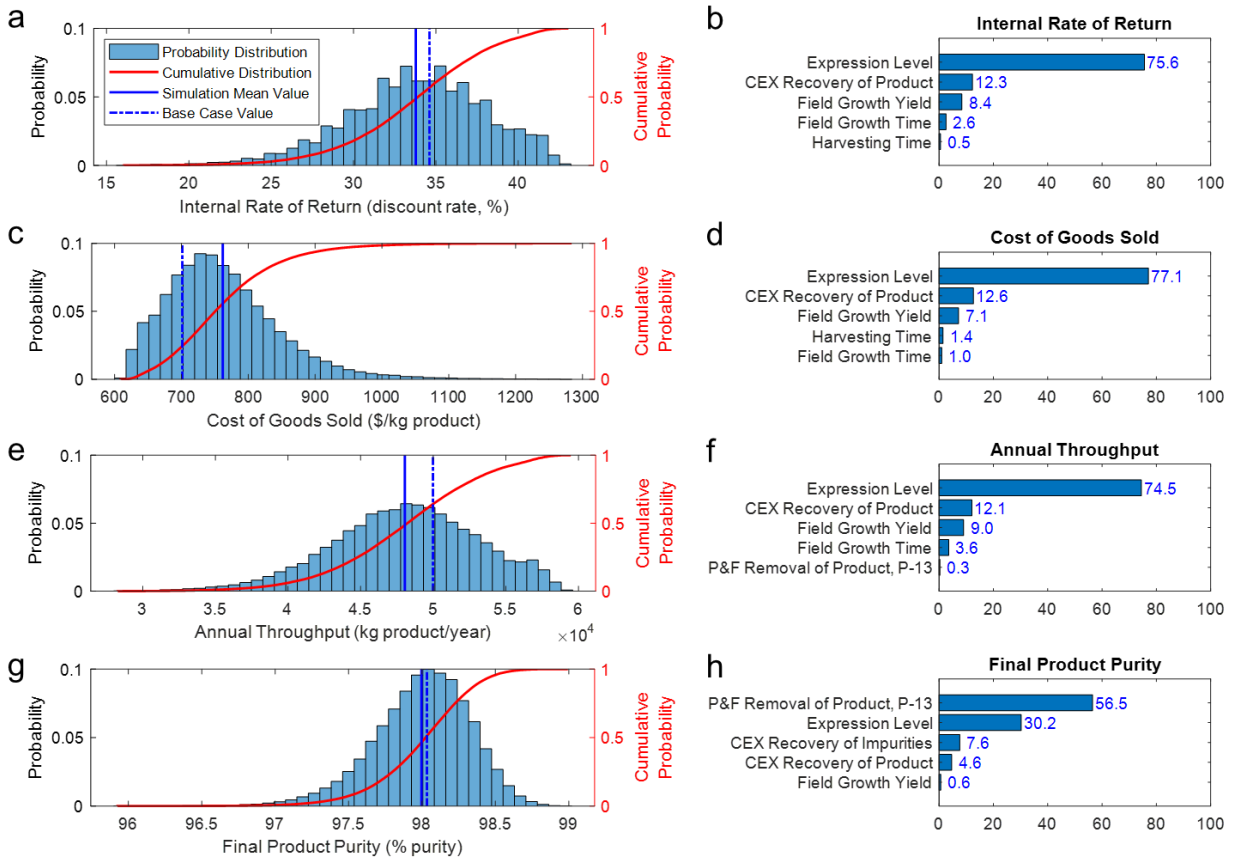

Figure 6.2. Probability distributions and top five assumption contributions to forecast variance for internal rate of return (a, b), cost of goods sold (c, d), annual throughput (e, f), and product purity (g, h).

Relationships between the forecast variables are shown in Figure 6.3, highlighting the interplay between the process performance and profitability forecast variables. As can be generally expected, high Annual Throughput and low COGS are associated with high internal rate of return (IRR). The density plots (Figure 6.3, e-h) show a negative skewness for all three process performance forecast variables. Based on the desired forecast target ranges listed in Table 6.3, we

project the manufacturing, as given by the model simulation, meeting desired COGS output specifications with 86.5% certainty (17,299/20,000 trials), annual throughput with 93.7% certainty (18,747/20,000 trials), product purity with 92.6% certainty (18,529/20,000 trials), IRR with 82.5% certainty (16,490/20,000 trials), and meeting all four output specifications with 80.8% certainty (16,161/20,000 trials).

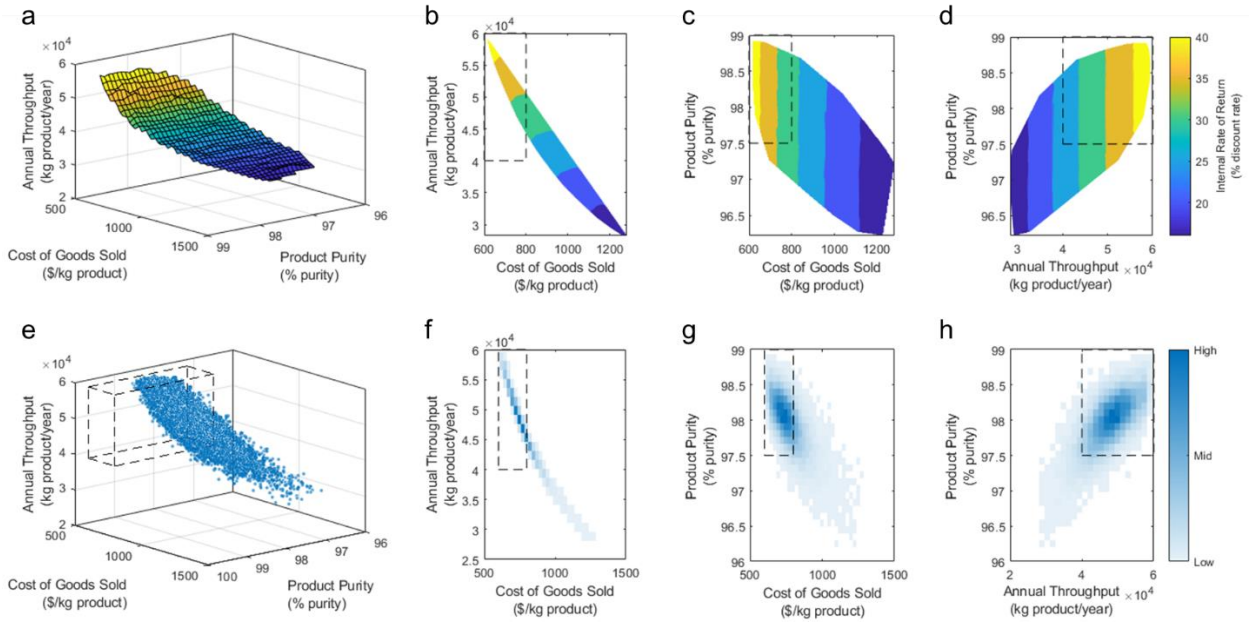

Figure 6.3. Relationship between the forecast parameter outputs as a function of internal rate of return and data density. Contour plots display overall and pairwise relationships (a – d). A 3D-scatter plot displays the overall relationship (e) and binned scattered plots display pairwise relationships (f – h).

6.3.2. Facility oversizing

An effective assumption constrained by equipment capacity is observed at lower extents of facility oversizing for field growth yield and CEX recovery of product, as shown in Figure 6.4. There is a pronounced difference between the effective field growth yield and the governing field growth yield probability distributions under the 0% and 25% equipment oversize scenarios, the differences being statistically significant from all other equipment oversize scenarios. The hypotheses being

tested here are about the equality of the means of the two probability distributions, and the tests used are the standard two-sample t-tests with two-sided alternatives, at level of significance $\alpha = 0.05$. Means of these two probability distributions under 50%, 75%, and 100% oversizing scenarios were not statistically different. Subsequent statistical evaluation of the probability distributions of these scenarios illustrated that the 50% scenario output is not borne of an equal distribution to that of the 75% and 100% oversizing scenarios (tests for equality of pairs of probability distributions are performed using the two-sample Kolmogorov-Smirnov test, at significance level $\alpha = 0.05$). The difference between the mean effective CEX recovery of product for the 0% oversizing scenario and all other scenarios is statistically significant. Means, and more generally, the distributions, under the 25%, 50%, 75%, and 100% oversizing scenarios were not statistically different. Additional details of the two-sample statistical analyses are included in Supplementary Information.

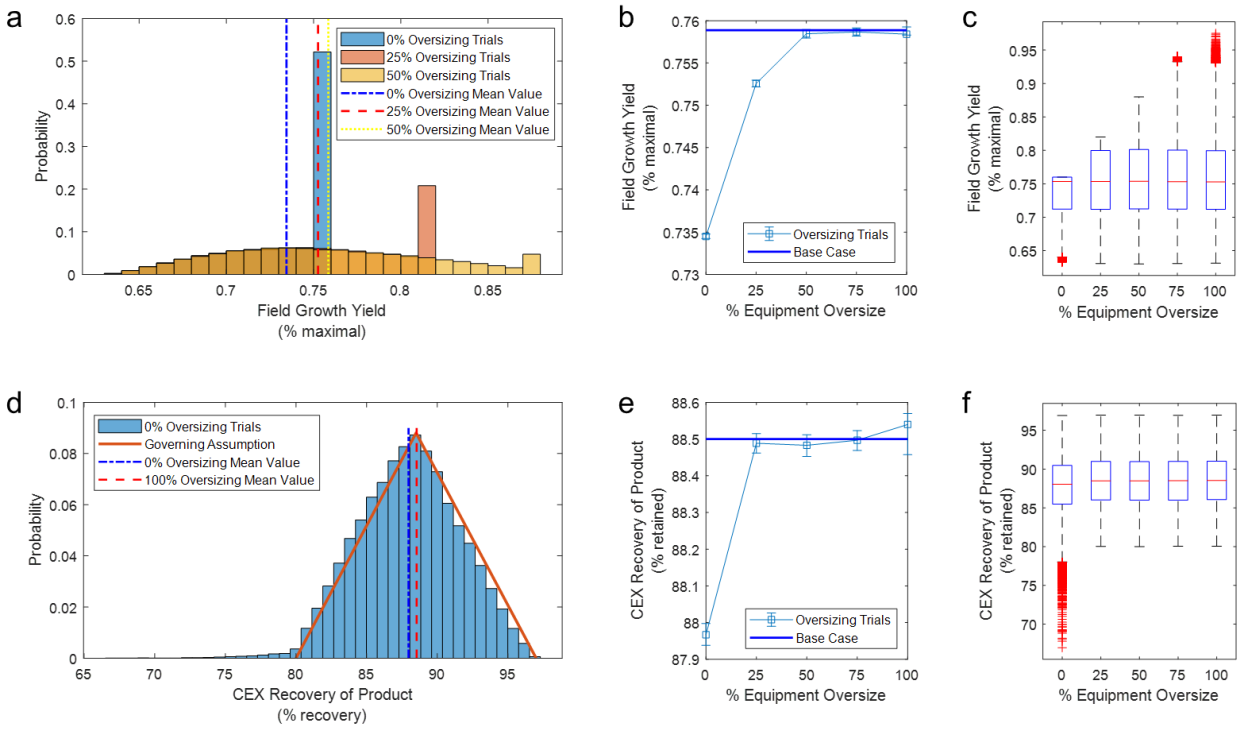

Figure 6.4. Impact on input variables due to extent of equipment oversizing is displayed using histograms, scatter plots of the mean simulation values, and box plots for field growth yield (a, b, c) and CEX recovery of product (d, e, f). Error bars represent the 95% confidence interval of the mean.

Individual forecast variable uncertainty quantification is shown across the equipment oversize scenarios by histogram and scatter plots of the mean values in Figure 6.5. The profitability of the facility model, as given by IRR, is inversely related to extent of equipment oversizing. The mean IRR values for the different scenarios are significantly different. We postulate that this can be largely explained by the monotonically increasing mean value of COGS (the mean COGS value for each scenario is also statistically distinct). The mean value of annual throughput also increases with extent of equipment oversizing up until 50% oversizing, whereupon additional oversizing does not contribute a statistically significant difference in the mean (or distribution) of throughput. For perspective on the relative cost of increased throughput for these scenarios, consider that the mean value of the 100% equipment oversizing scenario results in 3.85% greater annual throughput and 21.4% greater COGS than the 0% scenario values. In contrast, product purity is more comparable across scenarios; only in the 0% oversizing scenario, the mean and the distribution of purity are statistically distinct from those in the other scenarios.

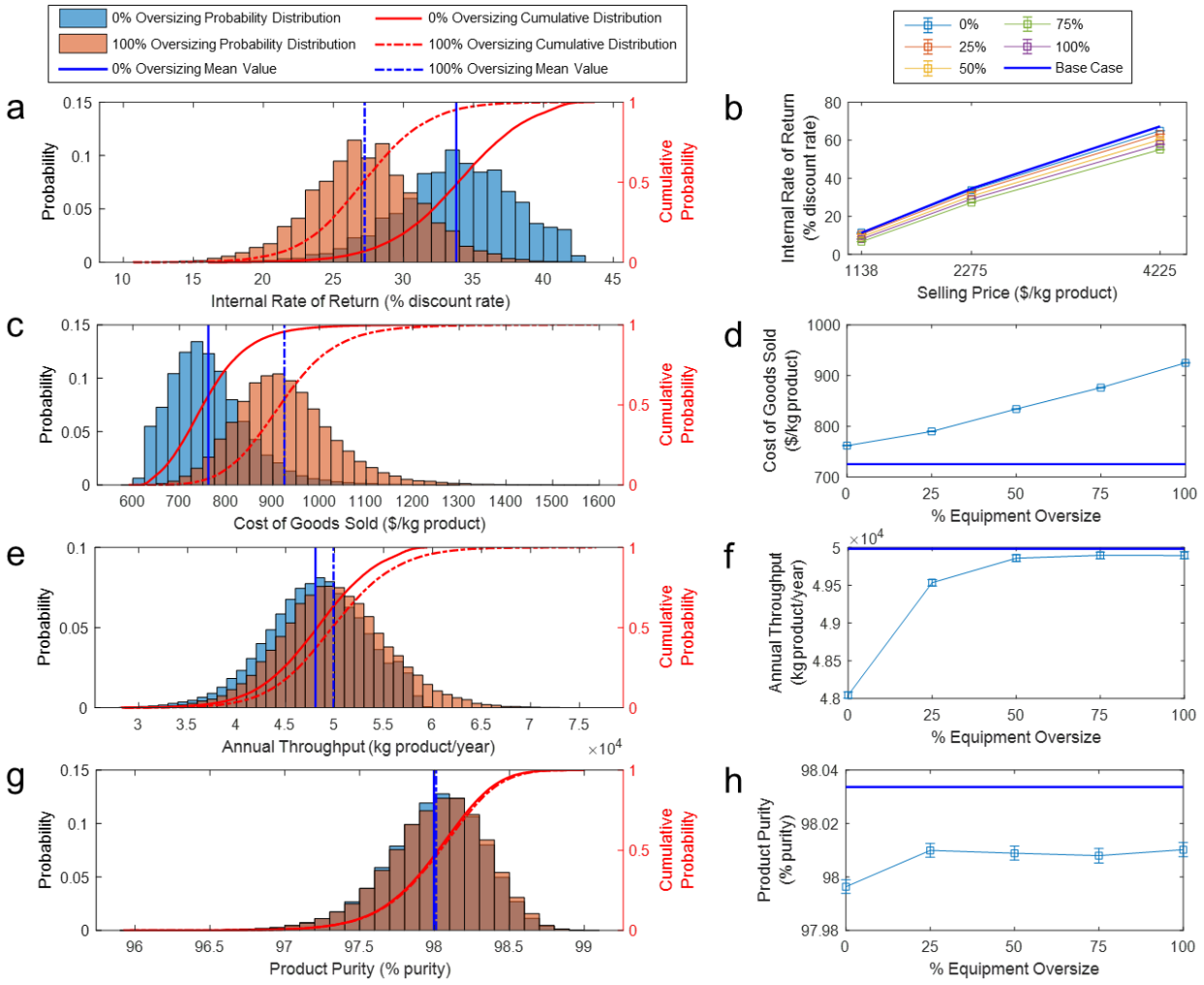

Figure 6.5. Impact on forecast variables due to extent of equipment oversizing is displayed using histograms and scatter plots of the mean simulation values for internal rate of return after tax (a, b), annual throughput (c, d), cost of goods sold (e, f), and product purity (g, h). Error bars represent the 95% confidence interval of the mean.

A comparison of cost breakdowns for the equipment oversizing scenarios is shown in Figure 6.6. Consumables are the most sensitive cost items to the extent of equipment oversizing, increasing the relative contribution to operating expenditures (OPEX) by ~20% from the 0% to 100% oversizing scenario. The UF/DF process section is the most sensitive to extent of equipment oversizing, increasing relative contribution to OPEX by ~15% from the 0% to 100% oversizing scenario. This is primarily due to the contribution of the CEX procedure. The ratio of upstream-

to-downstream OPEX generally decreases with extent of equipment oversizing, while the capital intensity, the ratio of OPEX to capital expenditures (CAPEX), generally increases. This is consistent with the generally accepted notion that downstream processing is higher capital intensity than upstream processing.

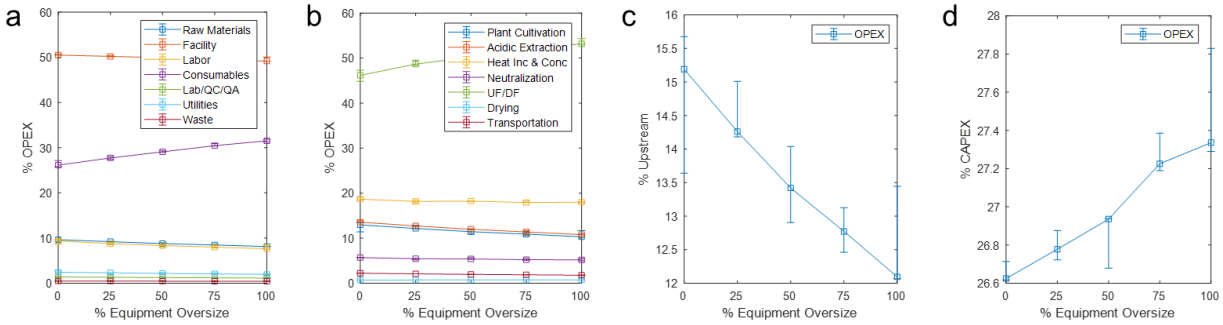

Figure 6.6. A comparison of cost breakdowns and equipment oversizing of the facility for the mean simulation values shown by (a) cost item, (b) process section, (c) total upstream contribution, and (d) the ratio between operating and capital expenditures. Data points represent the cost breakdowns of the simulation trials with the mean internal rate of return, while error bars represent those of the minimum and maximum internal rate of return. QC, quality control; QA, quality assurance; UF/DF, ultrafiltration/diafiltration; OPEX, operating expenditures; CAPEX, capital expenditures.

6.3.3. Optimization scenario: chromatography retrofit

Here, we demonstrate how the process simulation model representing an existing facility can be used to aid in a retrofitting process. We suppose that the facility, represented by the base case scenario (0% oversizing), is fixed and fully constructed except for the CEX chromatography step, which is anticipated to be added to the floor as the facility manufacturing switches to a new target protein product. In this case, the process simulation model can be used to optimize the sizing of the CEX chromatography step in the context of the otherwise existing facility.

The results of the CEX optimization are show in Figure 6.7. The optimal value was determined to be a diameter of 1.2 m, which is consistent with the value in the base case scenario.

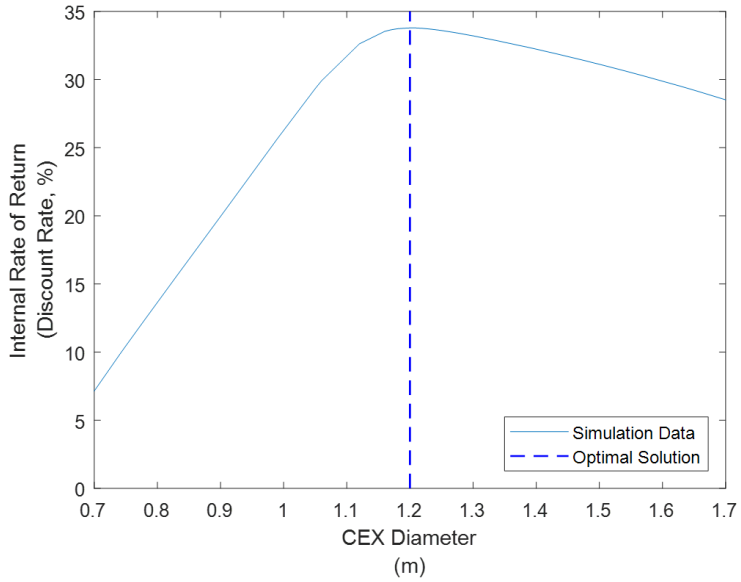

Figure 6.7. Uncertainty-based optimization of cation exchange chromatography sizing in the 0% oversize scenario set to maximize the mean internal rate of return given the assumed input parameter probability distributions. The mean internal rate of return is calculated using 20,000 simulation trials at each diameter value tested. Diameter range of 0.7 – 1.7 m is discretized in 0.01 m increments.

6.4. Discussion

The uncertainty quantification analysis of techno-economic process simulation in this work presents a range of potential technical and business insights that can be gained for production of natural and recombinant products in biotechnology manufacturing. In this work, we have specifically focused on field-grown plant molecular farming as a high-priority target to benefit from the quantification and management of uncertainty in driving commercial manufacturing. Field-grown molecular farming is a critical manufacturing platform for key commercial products including artemisinin for malaria treatment[170], vinca alkaloids for multiple health indications including diabetes and cancer[171], and stevia as a food sweetener[172], and provides distinct advantages in the future of biotechnological integration in a range of global markets. Addressing

the uncertainty associated with plant-based production is one promising strategy to approach supply stabilization and to develop compelling plant-based manufacturing schemes.

6.4.1. Positioning plant molecular farming with outdoor field cultivation

A recent paper on scaling-up plant molecular farming does an excellent job in summarizing blockers and opportunities in the industry from the perspective of key stakeholders working on the Pharma-Factory project (https://pharmafactory.org) and the Newcotiana project (https://newcotiana.org)[173]. Plant molecular farming has faced a slower technological maturation compared to traditional biotechnology manufacturing platforms. This has been attributed to a variety of factors – from being constrained to existing regulatory frameworks that are not amenable to assessing plant-based product manufacturing[174,175], to a lack of landscape-level pressures like policy driving sustainable manufacturing[176], to being locked out of the market from past ventures whose failures are independent of the technology potential/value[157], to a lack of public acceptance of genetically modified crops[177]. Plant molecular farming has responded to these factors by focusing on reducing public concerns, seeking niche-innovation, and establishing legitimacy through positive discourse. The industry is working to reduce public concern of contamination using non-food status crops (e.g., *Nicotiana benthamiana*)[178,179], manufacturing in indoor controlled environment facilities, and employing non-germline editing transient expression platforms[49,94,180]. Niche-innovations with plant molecular farming to aid technological development outside of the normal market pressures focuses on spaces including orphan diseases, emergency treatments, and inexpensive vaccines[157]. And finally, legitimation of plant molecular farming clusters around comparisons to traditional biotechnology manufacturing platforms that emphasize the safety advantages, low cost, sustainability or scalability[160,181,182] and the

opportunities for low- and middle-income countries with minimal existing pharmaceutical production capacity and expertise[39,183].

These strategies have served well to move plant molecular farming towards technological maturation[48]. However, the direction of plant molecular farming technological development borne of these strategies can appear to be at cross-purpose with itself. For example, the response to public concerns emphasizes indoor cultivation and transient expression platforms, while legitimation-facing strategies emphasize low cost, simple scalability, and accessibility, all of which may be better suited to outdoor field cultivation and transgenic expression platforms. Additionally, consider that while niche-innovation in plant molecular farming has usually targeted small to moderate market size products to break into the commercial space, there are new and promising food and industrial markets well-suited to plant molecular farming with considerably larger market sizes and considerably smaller gross margins that would be greatly benefited by outdoor field cultivation; in fact, perhaps the most alluring feature of plant molecular farming is its potential to manufacture high-value protein products at a larger scale than is feasible with traditional culture-based systems[184].

In recent years, the plant molecular farming community has renewed investigation of glass greenhouse cultivation as an in-between manufacturing platform that provides adequate containment and control with minimal cost and infrastructure complexity[169,185]. However, the complexity of greenhouse cultivation may still prohibit the pursuit of ultra-large-scale manufacturing for commodity goods that demand lean manufacturing costs. In our perspective, it is critical to re-visit outdoor field cultivation as a platform to enable plant molecular farming to re-position for larger food, industrial, and pharmaceutical markets.

6.4.2. Quantifying uncertainty in facility performance

Here it is important to re-iterate that the probability distributions selected are not based on commercial-scale data and are primarily based on working process knowledge, however the uncertainty framework developed, coupled with detailed process modelling, can be generally applied to assess commercial risks of plant molecular farming. Thus, the results are not necessarily representative of an existing or prospective outdoor field-based facility, but may instead be leveraged in development, improvement, or monitoring of such projects.

Our investigation of uncertainty in IRR shows that, given the selected probability distribution assumptions, this facility (in the 0% oversize scenario) is calculated to produce a mean IRR (selling price: $2,275/kg) of 33.8%, a 6.63% decrease from the static average base case of 36.2%. Expression level was found to be the major contributor (75.6%) to IRR variance. The 100% oversize scenario decreased the mean IRR by 24.9% to 27.2% due to the imbalance of the more greatly increased capital investment costs and lesser increase in revenue at the selling prices, and thus profit margins, established in this analysis. Additionally, the distribution is increasingly platykurtic (i.e., flat-shaped, or thinner tailed) with extent of oversizing and inversely so with the selling price.

The simulation resulted in a mean throughput of 48,046 kg product/year, a 3.88% decrease from the static average base case of 49,983 kg product/year. Annual throughput spans from 58.8% capacity (28,248 kg product/year) up to 124% capacity (59,467 kg product/year) of the mean. Expression level was found to be the major contributor (75.6%) to annual throughput variance. The 100% oversize scenario increased the mean throughput by 3.85% (49,893 kg product/year) to match the base case static average. This intuitive shift is a result of the 0% oversizing scenario

resulting in over-capacity stream volumes that are accounted for in the 100% oversizing scenario, thus restoring the effective mean value to that of the governing distribution mean.

The simulated facility is projected to produce the main product (including depreciation) at a mean COGS of $762/kg, an 8.7% increase from the static average base case of $701/kg. COGS spans as low as 79.8% ($608/kg) and as high as 169% ($1,284/kg) of the mean value. Expression level was also the major contributor (77.1%) to variance in this case. The 100% oversize scenario results in an increased mean COGS by 21.4% ($925/kg). The quantification of uncertainty in COGS is critical for understanding which product markets are economically accessible for a given facility. Conversely, this provides information that can be used to inform the target product selling price.

The simulated facility product purity mean value is equal to the base case static average of 98.0%. The product purity ranges from 97.9% lower (95.9%) to 102% higher (99.0%) purity than the mean value. The plate and frame filtration product loss was the most significant contributor (at 56.5%) to product purity variance. The 100% oversizing scenario resulted in a mean value equal to the 0% oversizing scenario mean. The quantification of uncertainty in product purity obtained in this study shows that there is considerable variation in extent of purity, which may or may not be problematic for a specific product, which is also largely dependent on the impurities profile (e.g., variation in native allergen or microbial toxin levels would present a larger obstacle). Realistically, annual product purity variation is not particularly useful for designing a facility. This process performance metric, which in preparation for an actual facility construction would be split into its meaningful constituents, would be better suited to analysis at a level of batch-to-batch variation.

6.4.3. Batch-to-batch uncertainty in facility performance

The analysis thus far has focused on uncertainty in the annual average values for input assumptions. This is representative of a project planning or preliminary engineering estimate, classified as level 2 or level 3 in some systems[47], where design errors are expected to be in the range of ±20-30%. When the product development and commercialization life cycle is sufficiently advanced, there is greater value in detailed engineering estimates (classified as a level 4 design estimate). At that juncture, it is probable that the expected facility performance is better characterized, with more preliminary data available, and that batch-to-batch variance may more appropriately describe the questions around uncertainty. In these situations, we can treat each process performance simulation trial result as a single batch output, rather than an annual average value. It is important to note that the probability distributions for batch-level and annual average-level descriptions will most likely be designed using different sets of assumptions.

For the sake of illustration in comparing annual- to batch-level uncertainty in this analysis, we perform a brief exercise in describing batch-level uncertainty, assuming that the input assumptions previously defined for annual-level uncertainty are instead describing batch-level uncertainty. To understand the annual facility behavior given batch-level uncertainty, we randomly group trial outputs into sets whose size corresponds to the affordable number of batches per year, which is calculated based on scheduling. Performing such a calculation, the range of uncertainty in process performance metric outputs is much more controlled, as would be expected; for the 0% oversizing scenario the annual throughput uncertainty spans 93.8 – 98.3% of the base case static average capacity, COGS uncertainty spans 106.0 – 111.3% of the base case static average cost, and product purity uncertainty spans 99.9 – 100.1% of the base case static average level.

Future analysis of batch-to-batch variance and uncertainty has the potential to play an instrumental role in aiding development of processing strategies to that take in to account noisy quality attributes of the processing input material (i.e., field-grown crop) and translate that into a product meeting well-defined quality attributes. This is of particular importance for outdoor molecular farming, for which the input material noise may be expected to be more variable than other production platforms. One particularly valuable aspect of batch-to-batch variance research would be to include scenario analyses of lot pooling considerations of the facility.

6.4.4. Managing uncertainty in facility performance

In this work we considered management of uncertainty by investigating the impact of equipment oversizing on select process performance metrics. It is clear that the 0% oversizing scenario is the most profitable, based on the IRR results. In large part, this can be attributed to the shape of the field growth yield probability distribution used. The positive skewness dictates that the oversizing captured a smaller fraction of the field growth yield integral for a given increment above 0% oversizing (i.e., smaller throughput return for a given capital investment). For this particular model, there was no statistically significant increase in throughput past 50% oversizing; the additional 75% and 100% oversizing scenarios contributed additional costs without a significant return on throughput. However, it is important to point out that facility design is a complex process. In reality, the target industry and business strategy of the company may dictate a design based on transient market penetration strategies, anticipated scaling, and/or other opportunities, to name a few considerations.

The other aspect of this work aimed to manage uncertainty in facility performance is the optimization of CEX chromatography column sizing in a facility retrofitting exercise. What we

found in this example is that equipment utilization, which was by default maximized in the base case column size, was the economic driver in this scenario. Maximization of equipment utilization is a well-established heuristic in a facility design for manufacturing with relatively small perturbations in demand. In other facility simulations and input assumptions (including the balance between product selling price and capital investments), the optimal column sizing may have instead reflected those different balances in facility dynamics with a larger size, in the case of valuable products and positively skewed throughput distributions, or smaller size, in the inverse situations.

Valuable future works to investigate the impact, and mitigation, of uncertainty in forecast variables include exploring commonly employed manufacturing strategies that tend to absorb localized fluctuations. In outdoor field cultivation this includes consideration of multi-plot or multi-site production and plant tissue silaging[186]. Multi-site manufacturing considerations would involve an optimization of the balance of production scales between multiple facilities based on transient performance probability distributions. It will also be valuable to augment uncertainty quantification of plant molecular farming manufacturing with more granulized and transient scheduling information to understand the impact to supply chain logistics and solutions to overcome them (e.g., propagating the impact of manufacturing shutdown periods and lot failure).

Perhaps most relevant to the advancement of outdoor field cultivation for plant molecular farming would be to consider upcoming and future manufacturing strategies to reduce variation. Technological advances in areas such as seed coating[187], precision agriculture[188], and robotic agricultural systems[189] are all positioned on the horizon to drastically reduce variation and improve yield of outdoor field cultivation. It will be critical for the plant molecular farming community to leverage these innovations.

From the perspective of downstream processing, consideration of lot pooling – the combination/pooling of multiple batches into a larger lot size, often implemented to reduce quality control costs or improve supply chain logistics[190] – and the impact on output variation is an important area of investigation.

In summary, this work has aimed to provide the plant molecular farming community with contextual motivation and a framework and toolkit to further explore outdoor field cultivation through the lens of uncertainty quantification and management in manufacturing process simulation to drive future experimentation and inform business decisions. This was presented in the form of a deterministic SuperPro Designer-based techno-economic facility model integrated with a stochastic Monte Carlo-based simulation to propagate the impact of noisy manufacturing inputs through to forecast variable outputs. Scenario analysis and optimization aspects provide direct examples of how this toolkit can be used in decision making.

6.5. Supplementary Information

6.5.1. Assessment of Assumption Distributions

Assumption distributions were primarily determined by working process knowledge supported by reports in literature. We used our working process knowledge to select probability distributions reflective of plant-made pharmaceutical production that one might observe at lab- and/or pilot-scale production. The probability distributions are not based on any existing commercial facility capability.

Expression level variations were performed by changing the mass coefficients of "Thaumatin" and "Biomass week 6" in P-18's RXNSEP-1, while keeping their sum constant. The probability distribution profile was obtained from Werner et al. (2011)[95] supplementary section. The data were normalized so that the mean is 1.50 g/kg (base case expression level) and was best fit by a logistic distribution. A triangular distribution was used to represent the uncertainty with field growth time before induction in P-16. Mechanical harvesting (P-21/GBX-104) time variability was represented by a beta distribution with minimum and maximum values based off an assumed 1-10 km/hr harvester speed. UF/DF filtrate flux was assumed to vary by ±25% from the base case value according to a triangular distribution[191]. Cation exchange chromatography (CEX) losses were assumed to vary according to a uniform distribution with minimum and maximum values ±10% their mean (base case)[165]. Harvesting time, plate & flame removal, and field growth time distributions were based on assumptions determined using working process knowledge not directly supported by reported values in public literature.

The field growth yield probability distribution was derived from an analysis of previously published literature. The following subsections 6.5.1.1 – 6.5.1.3 detail the development of the field growth yield assumption distribution.

6.5.1.1. Model for tobacco dry weight estimation as a function of temperature

Experimental data of tobacco dry weight were extracted from Figure 1 (A-E) in [192] using an open source software DataTheif (B. Tummers, DataThief III. 2006 https://datathief.org/). The data was collected by measuring the dry weight of plants at different intervals during their growth; the high and low temperatures were kept constant for 9 and 15 hours, respectively. A weighted average of these temperatures was used in the model calculations (i.e., 9/24*high + 15/24*low). Plants were rotated between different growth chambers where high and temperatures were kept constant, however, different in each chamber, resulting in 10 different sets of experimental data. To construct the model, all 10 sets of data were fit to equations S6.2 and S6.3 by using an initial guess for the equation parameters (A,k,S,H) from [193] and calculating the root mean squared error (RMSE) - (equation S6.3). A built-in Microsoft-Excel solver was then used to find the model parameters that would minimize the RMSE between model predictions and experimental data.

$$W_i = W_0 + (W_0 \cdot r(T) \cdot \Delta t\ ) \qquad \text{(equation S6.1)}$$

Where W_i – tobacco dry weight at day "i" post-transplant (g/plant), W_0 – initial dry weight at day "i-Δt"(g/plant), r(T) temperature- dependent growth rate in g/(plant day), Δt – time between W_0 and W_i in days.

$$r(T) = \frac{A\ T\ \exp\left(\frac{-k}{T}\right)}{1\ + \exp\left(S - \frac{H}{T}\right)} \qquad \text{(equation S6.2)}$$

A,k,S,H – model parameters, T – temperature (K).

There is an optimum temperature for tobacco growth below which the growth rate follows the Arrhenius law. Above this optimum temperature, the rate declines due to the inactivation of enzymes and the denaturation of plant proteins. Therefore, the complex function (equation S6.2) was chosen to model the growth rate response to temperature[193].

$$RMSE = \sqrt{\frac{1}{N}\sum(y_i - o_i)^2} \qquad \text{(equation S6.3)}$$

Where y_i is model prediction, o_i is experimental data, and N is the total number of predictions/observations.

All data points – experimental on x-axis and model predictions on y-axis– were plotted on the same graph (Figure S6.1), in addition to a 1:1 line to show model deviation from experimental data. The R^2 value was calculated using equation S6.4

$$R^2 = 1 - \frac{\sum(y_i - o_i)^2}{\sum\left(o_i - o_{avg}\right)^2} \qquad \text{(equation S6.4)}$$

Where y_i – model prediction, o_i – observation, and o_{avg} – average of all observations.

Model parameters that result in a minimized RMSE value of 9.839 are shown in Table S6.1. The model was validated using a different set of experimental data (obtained from Figure 2 in [192]. The two sets of data were plotted on the same graph (Figure S6.2) with the calculated R^2 value. Figure

S6.3 shows the growth rate "r(T)" values for a range of temperature. It confirms previously reported optimal growth range (18.5 - 28.5 °C)[169] which corresponds to 291.5 - 301.5 K.

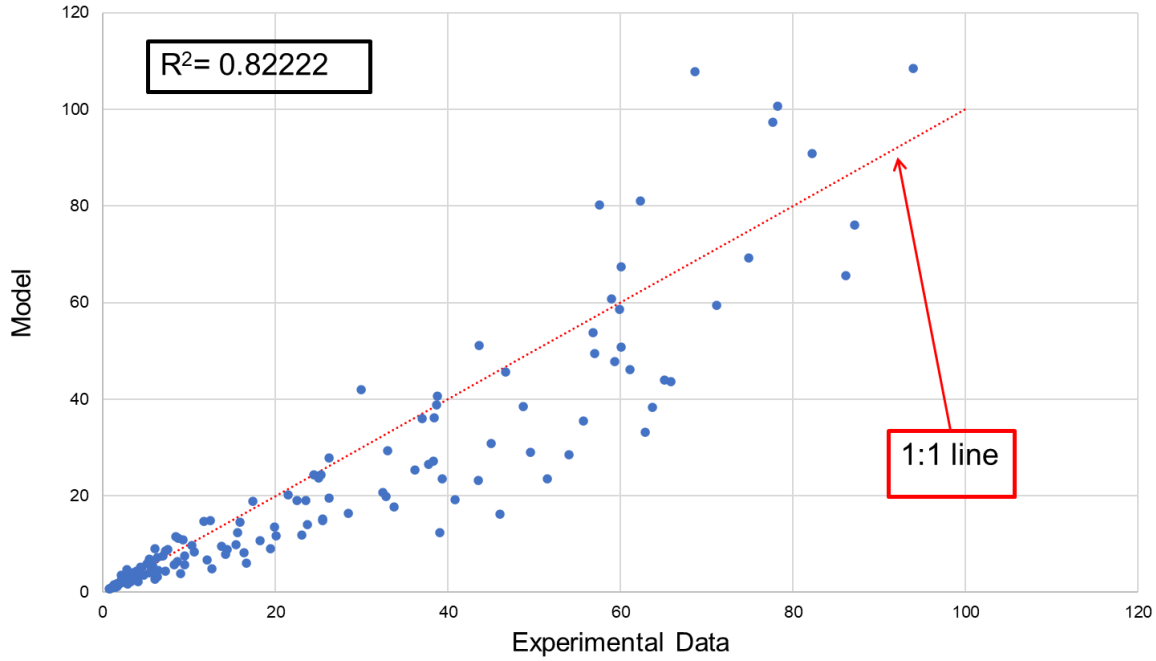

Figure S6.1. Regression plot of model vs experimental data points, showing calculated R^2 value.

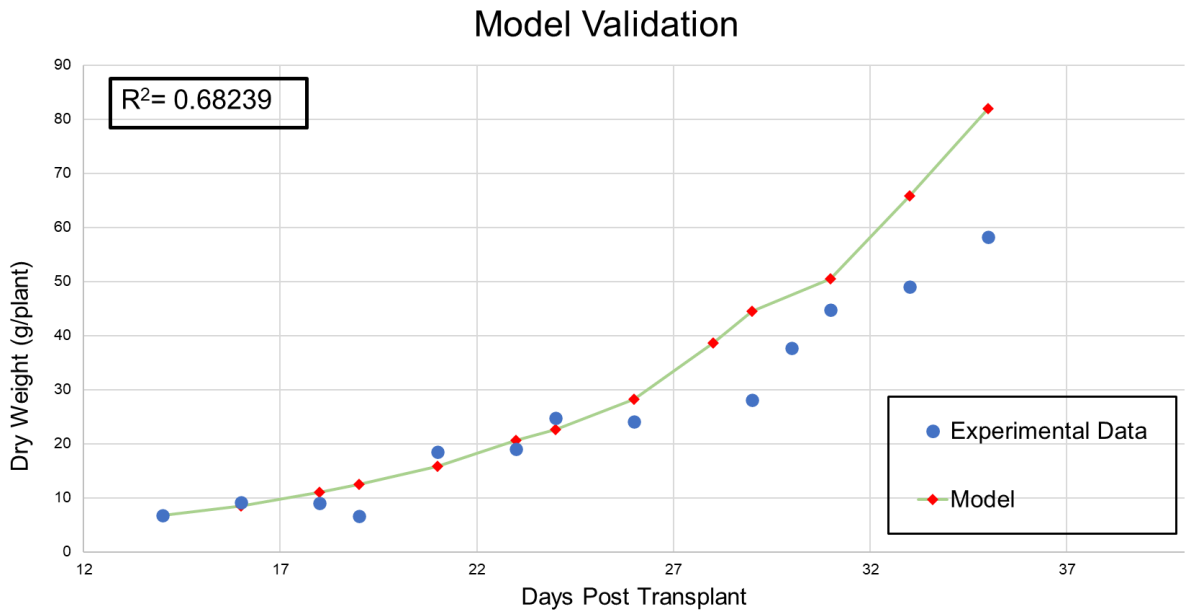

Figure S6.2. Model validation results using data in Figure 2 in Wann et al. (1984)[192].

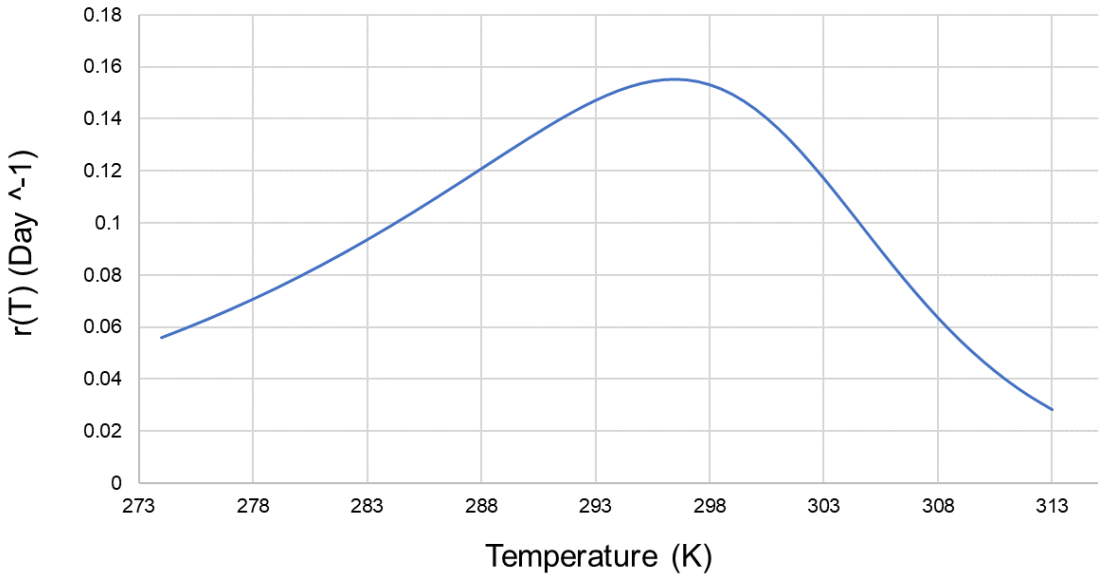

Figure S6.3. Growth rate as a function of temperature based on fitted model parameters.

Table S6.1. Model parameters obtained by minimizing the root mean squared error (RMSE).

A (day^{-1} K^{-1})	S	k (K)	H (K)
924.6	75.43	4,199	22,780

6.5.1.2. Tobacco yield estimation and monthly variations

The previous model was used to predict tobacco dry weight per plant as a function of temperature. Hourly temperature (60 cm above ground level) data in Homestead, Florida was obtained from the Florida automated weather network (FAWN) database for three consecutive years (2017-2019). The model predicts tobacco dry weight at day 27 after emergence of seedlings (assuming a constant initial dry weight of 0.5g/plant seedling), starting at the first hour of the first day of every month and ending on the 23rd hour of the 27th day of the same month. Assuming that germination occurs over the course of 15 days, the model predicts the dry weight yield at day 42 post seeding.

Figure S6.4 shows the model results for each year at the end of 27th day of each month. The average of the monthly yield over 3 years is also displayed as a solid green line, indicating a slight drop in yield during the month of July, most likely due to the consistently elevated temperature. The average dry weight yield was 21.28 ± 2.37 g/plant. This 11% standard deviation from the mean reflect a low variation in temperature ranges due to seasonal changes in Homestead, Florida. However, this model can be further improved by incorporating other weather factors such as photon flux, ambient CO_2 concentration, plant nutrients availability, wind, and humidity. Germination efficiency as a function of these variables should also be considered to produce a more robust model.

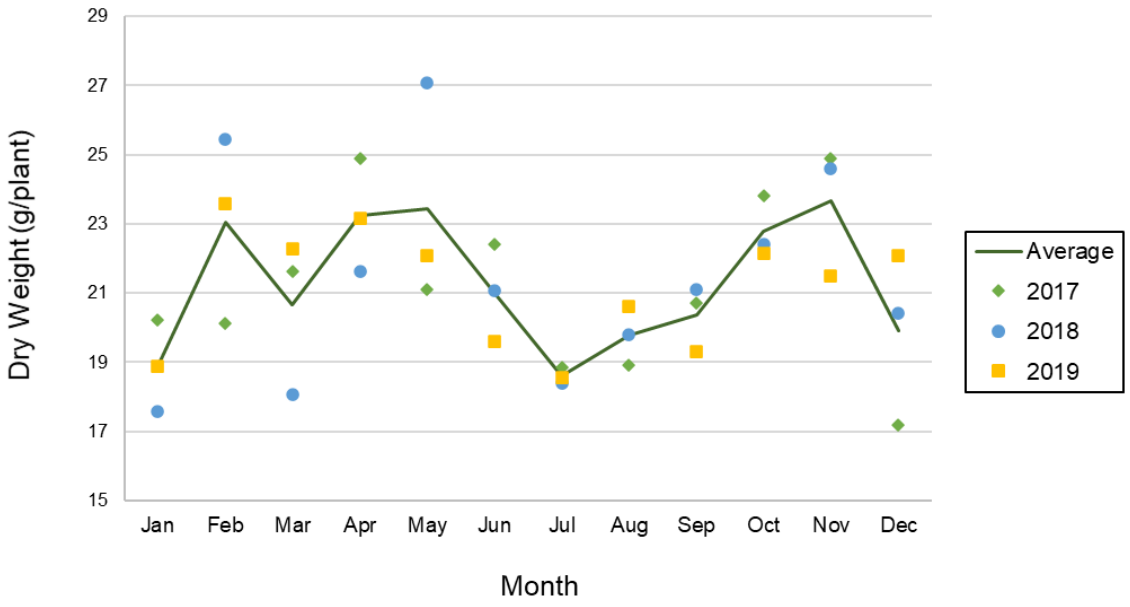

Figure S6.4. Tobacco dry weight prediction based on historical Homestead, FL weather data from three consecutive years.

6.5.1.3. Probability distribution justification

The data generated from the dry weight yield prediction model (n=36) was used to obtain biomass conversion distribution, assuming a linear relationship between fresh weight and dry weight. The yield prediction model results were normalized by its maximum value and were best fit by a beta probability distribution (alpha = 2.57, beta = 4.80, minimum = 0.63, maximum = 1). The mean of this distribution was calculated to be 0.76 (base case).

6.5.2. Assumption Distributions & Trial Data (Histograms)

The following are figures for each of the input parameter uncertainties detailing simulation trial data as a histogram, the mean value of the trial data as a vertical blue line, and the governing distribution data as a red line plot. Simulation trial data for the 100% oversize scenario with 60,000 total trials (combined from 20,000 trials for each of the three selling prices analyzed) are used to for each of these sample histograms.

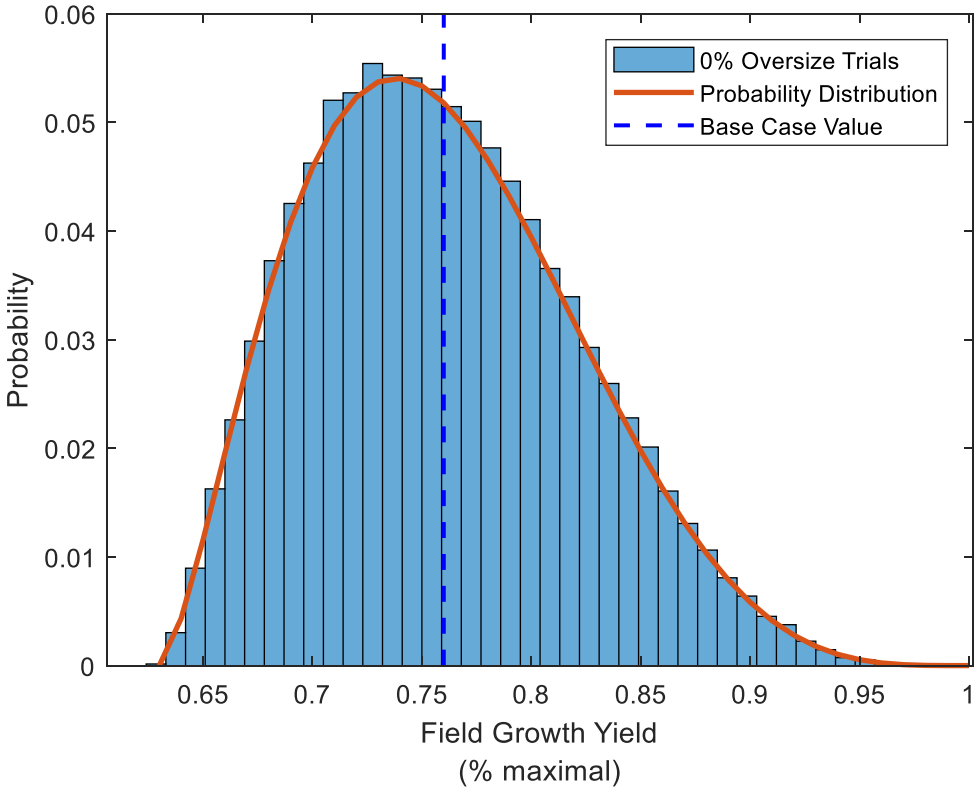

Figure S6.5. Field growth yield from P-2

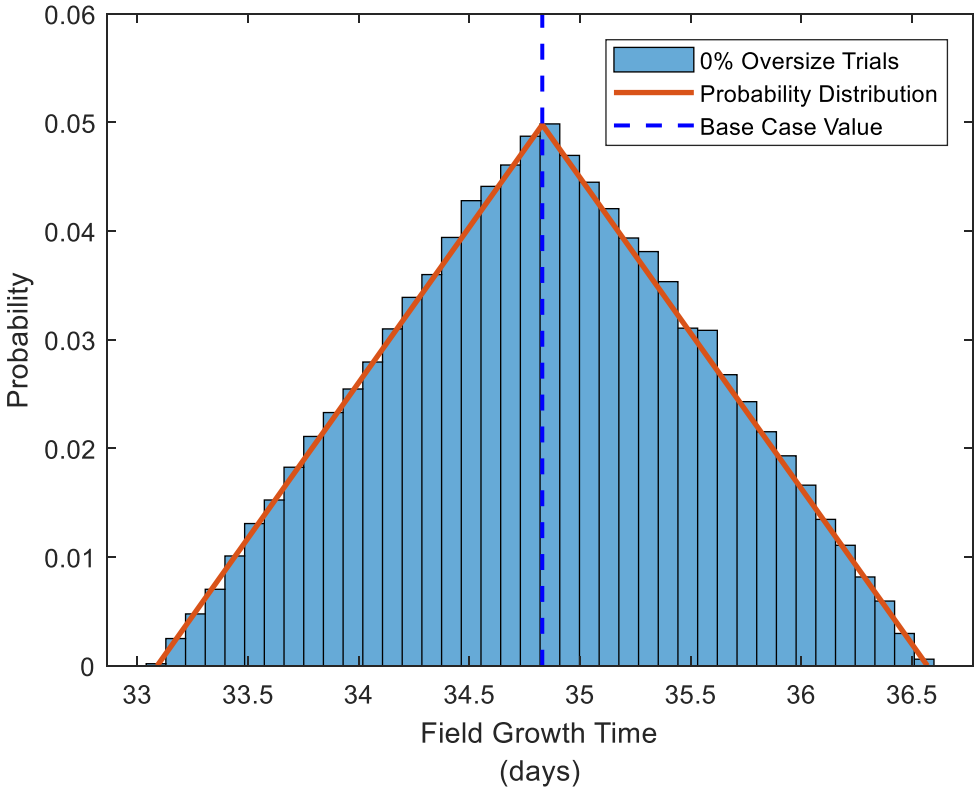

Figure S6.6. Field growth time in P-2

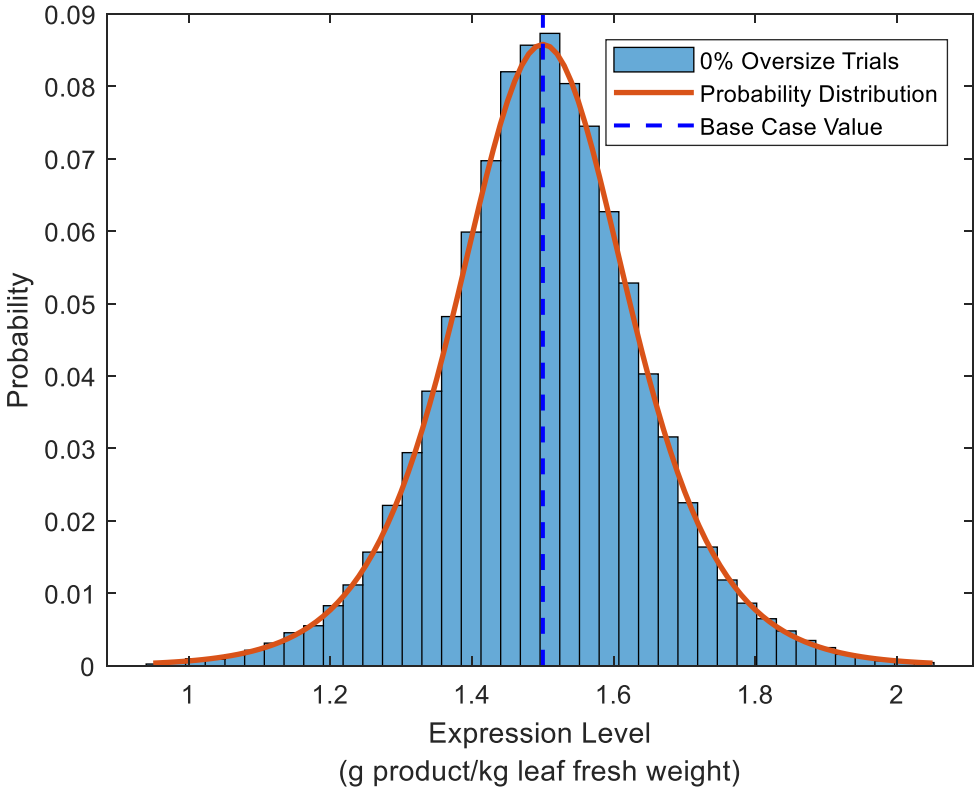

Figure S6.7. Expression level in P-4

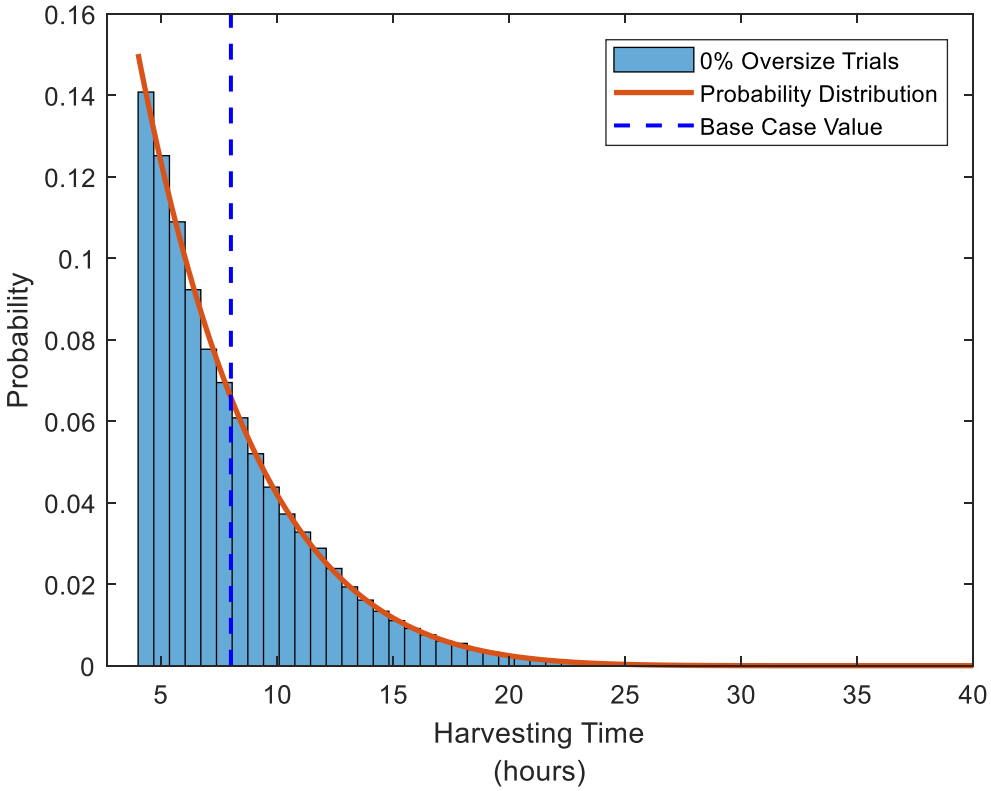

Figure S6.8. Harvesting time in P-4

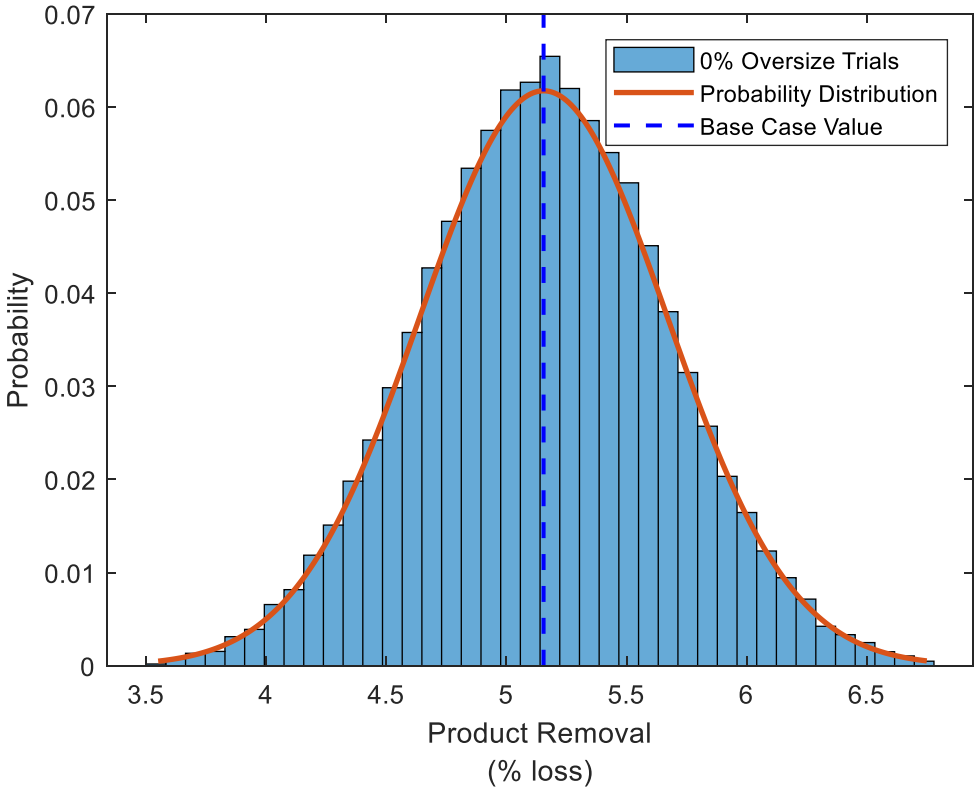

Figure S6.9. Product lost, plate and frame filtration in P-11

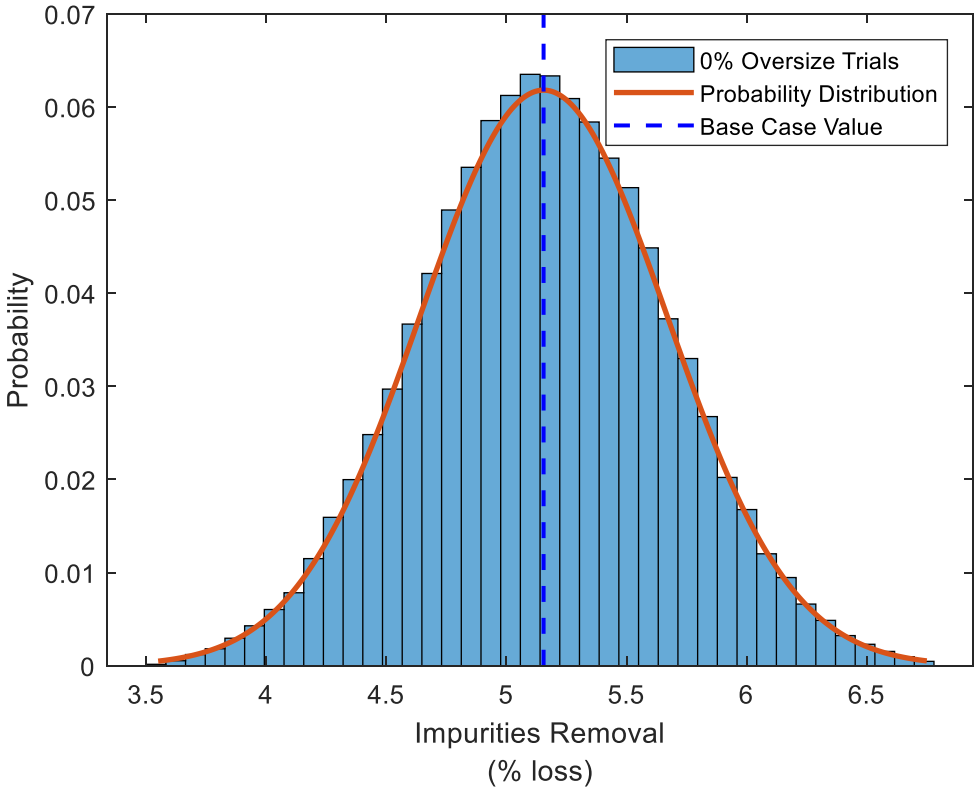

Figure S6.10. Impurities removed, plate and frame filtration in P-11

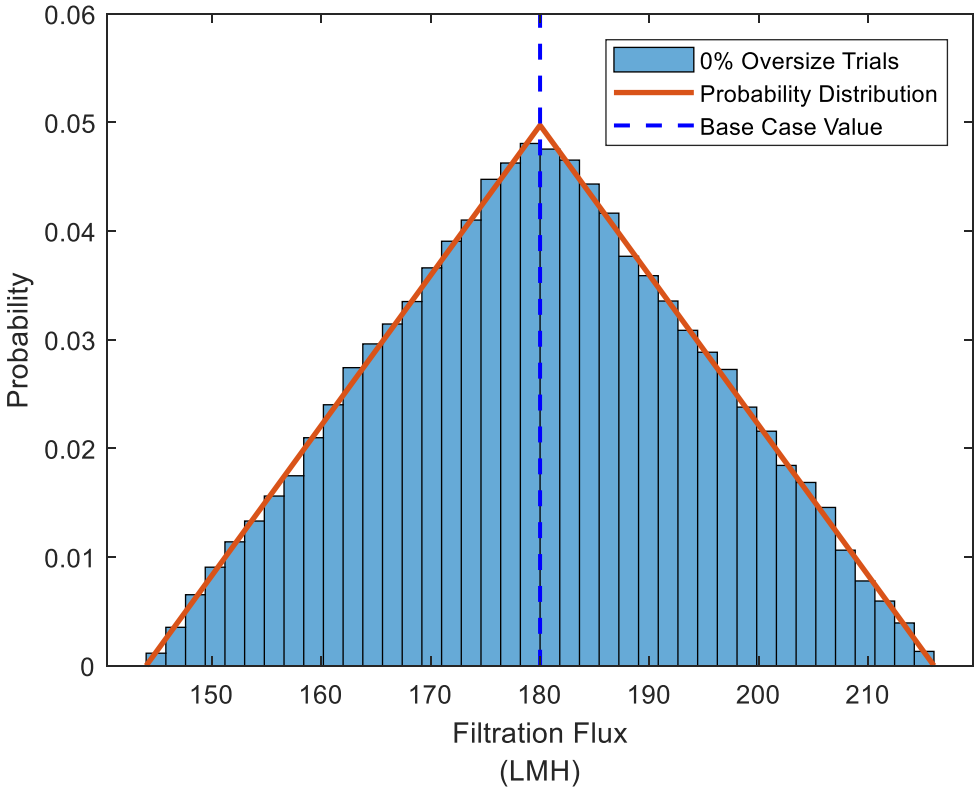

Figure S6.11. Filtration flux, plate and frame filtration in P-11

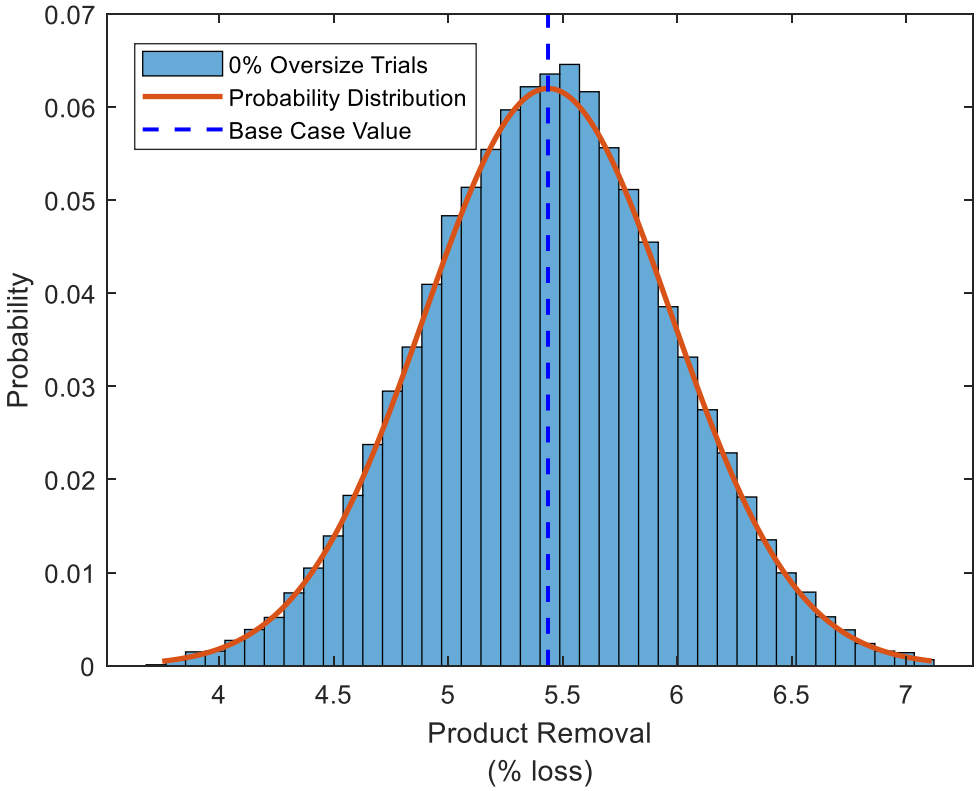

Figure S6.12. Product loss, plate and frame filtration in P-13

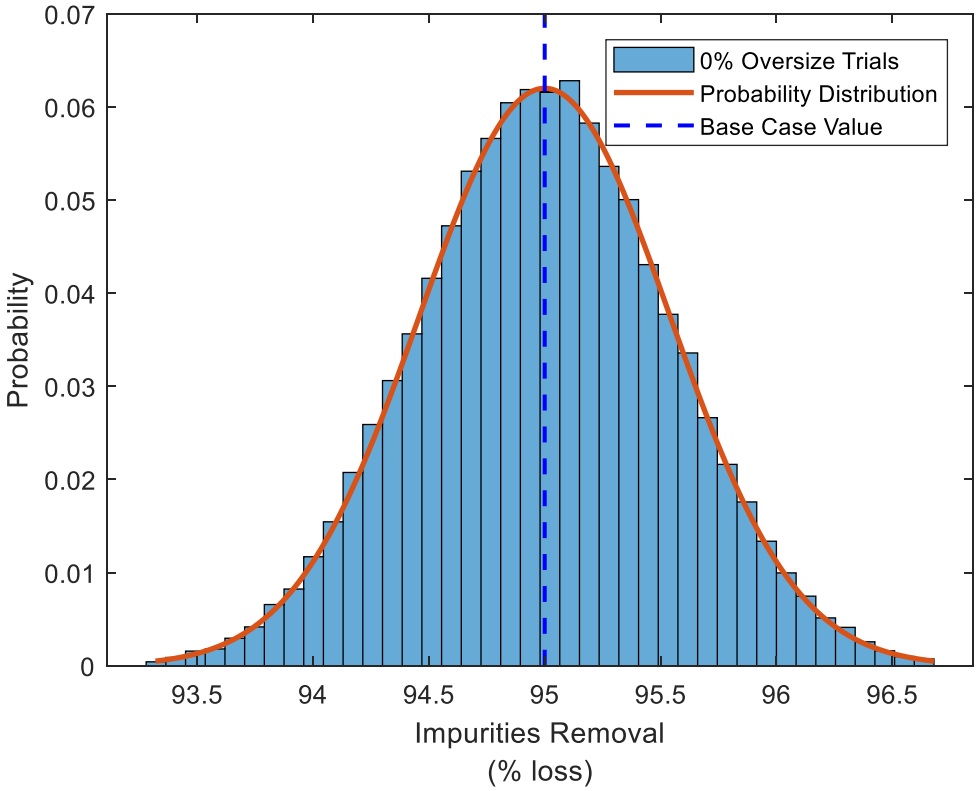

Figure S6.13. Impurities removal, plate and frame filtration in P-13

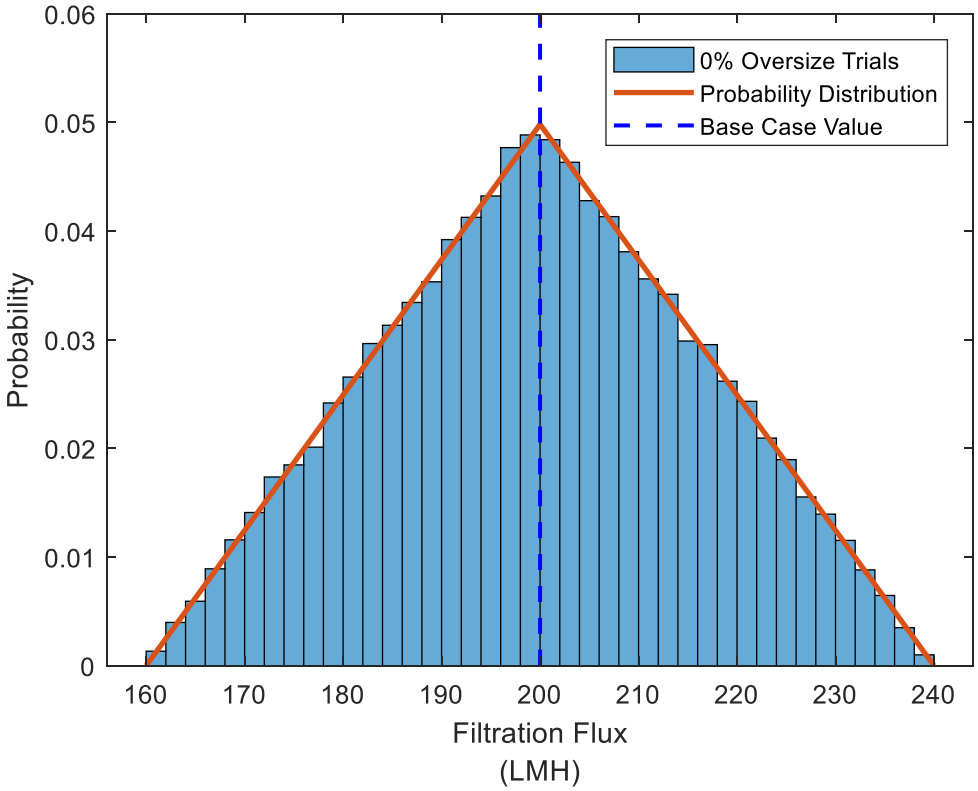

Figure S6.14. Filtration flux, plate and frame filtration in P-13

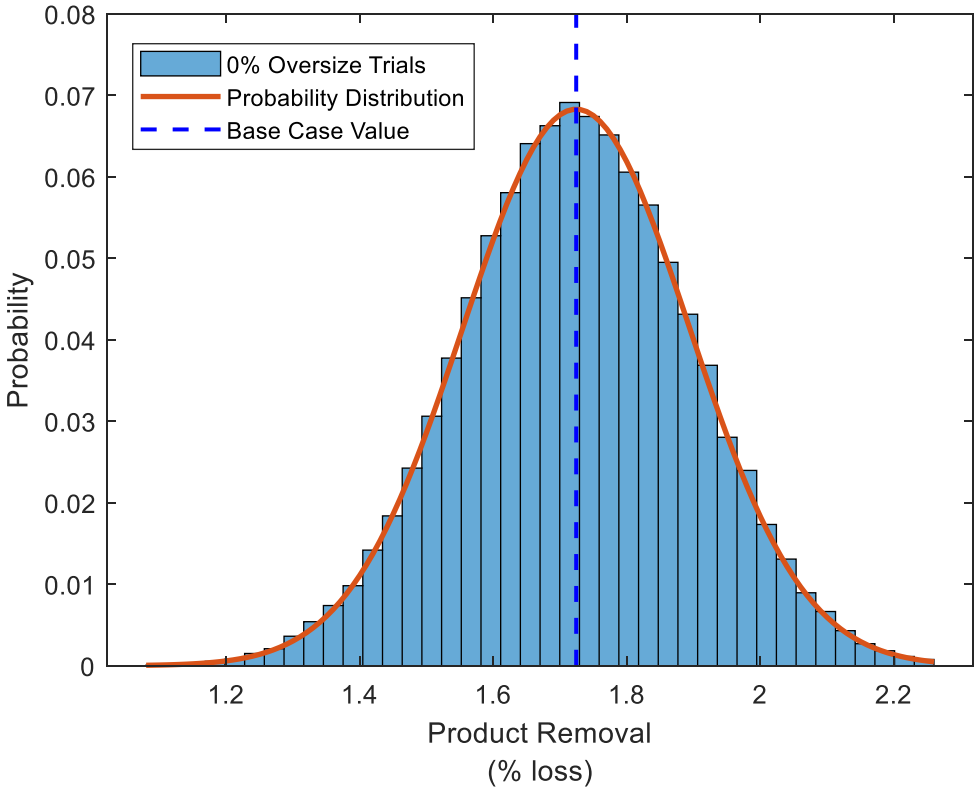

Figure S6.15. Product lost, plate and frame filtration in P-17

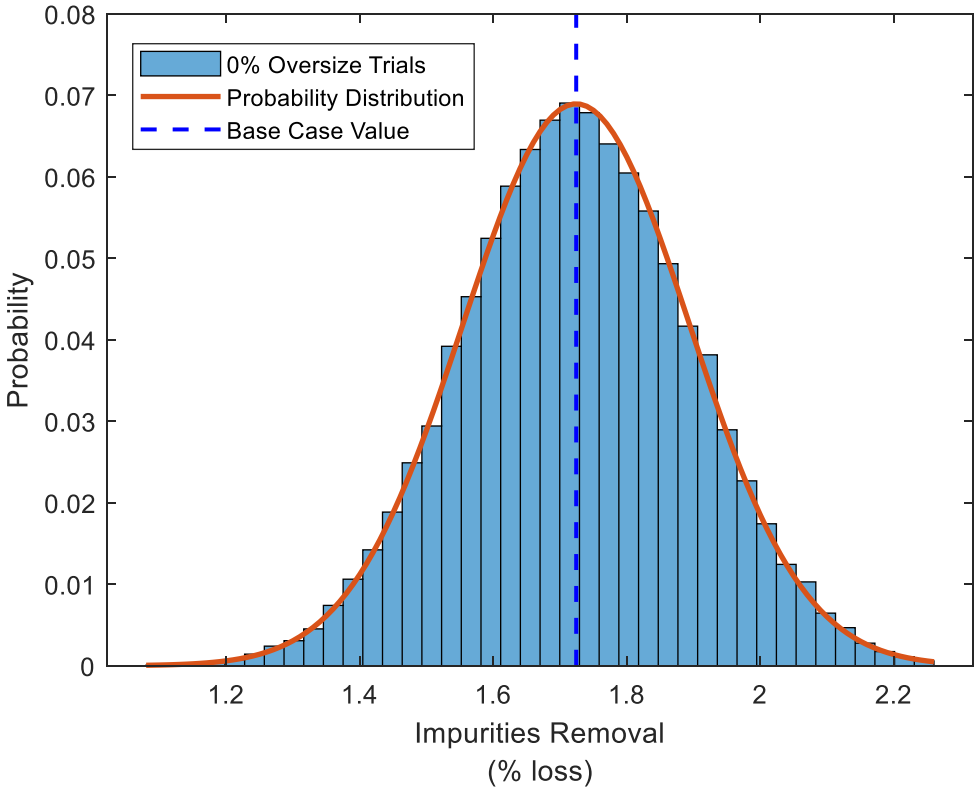

Figure S6.16. Impurities removal, plate and frame filtration in P-17

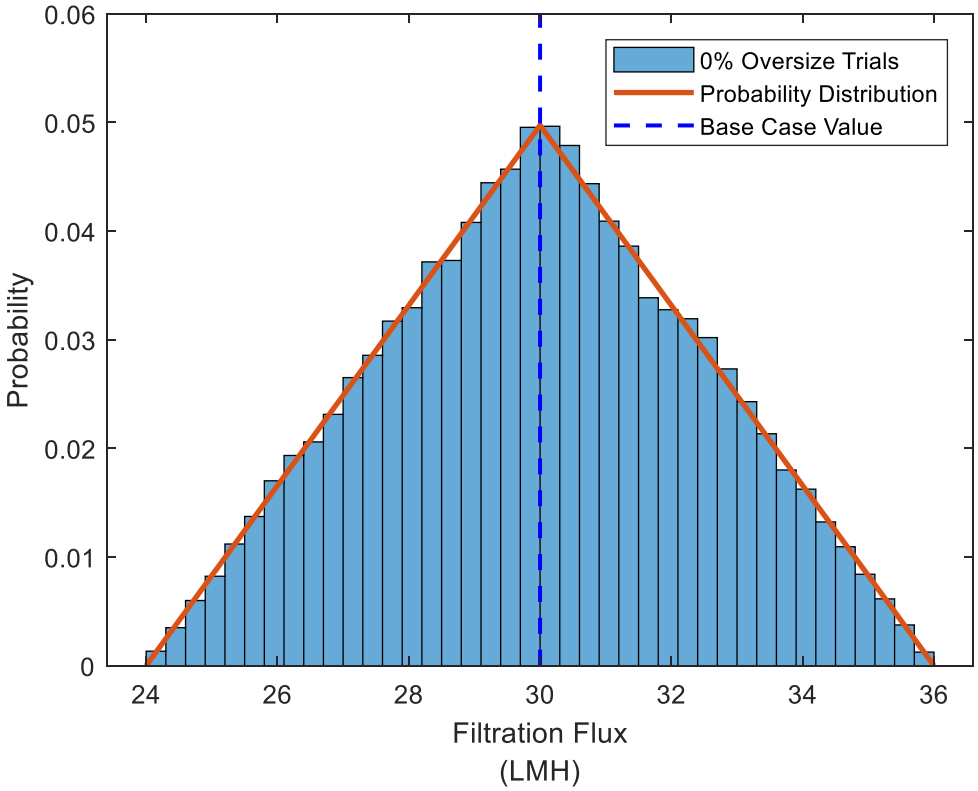

Figure S6.17. Filtration flux, plate and frame filtration in P-17

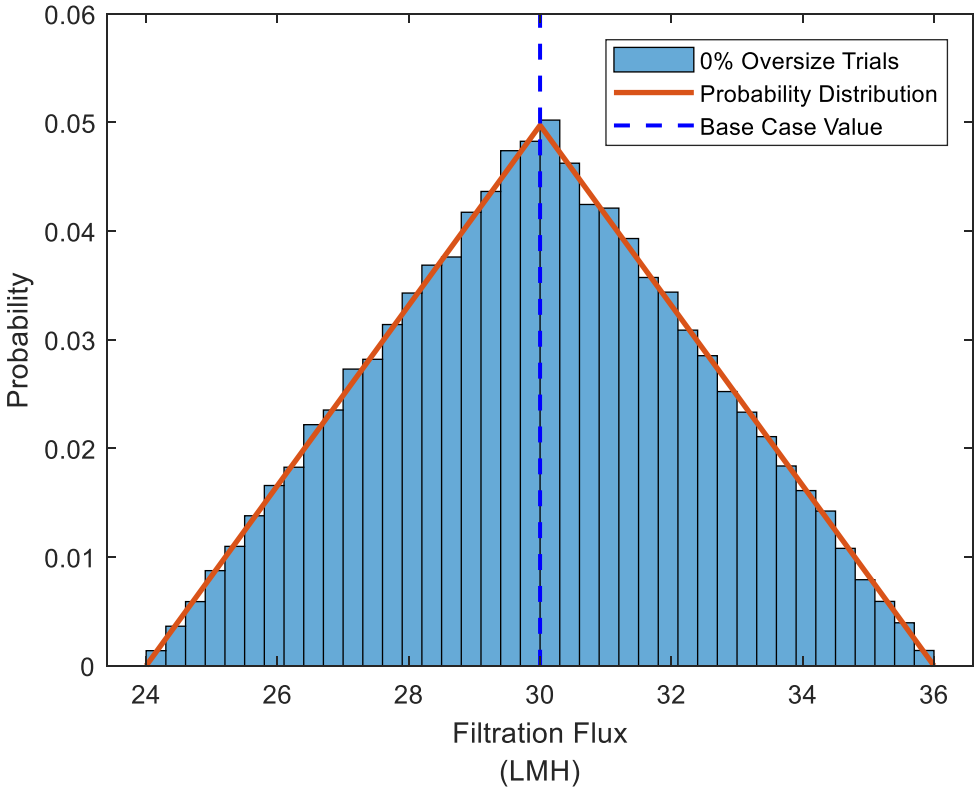

Figure S6.18. Filtration flux, ultrafiltration/diafiltration in P-19

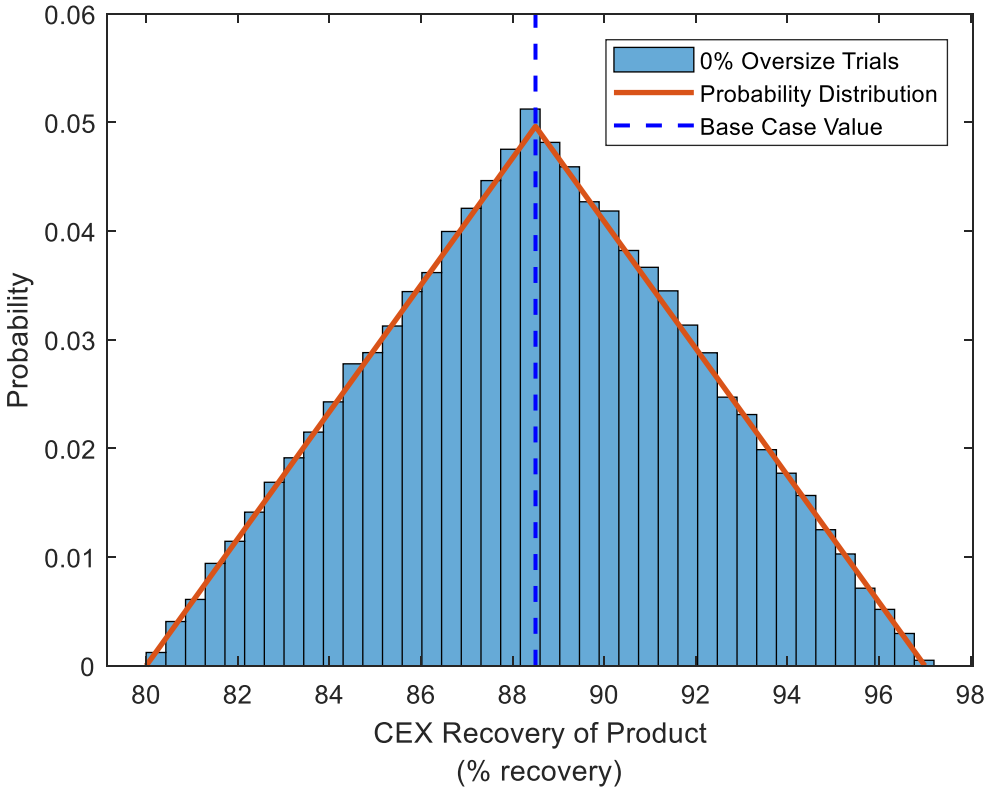

Figure S6.19. Product recovery, cation exchange chromatography in P-20

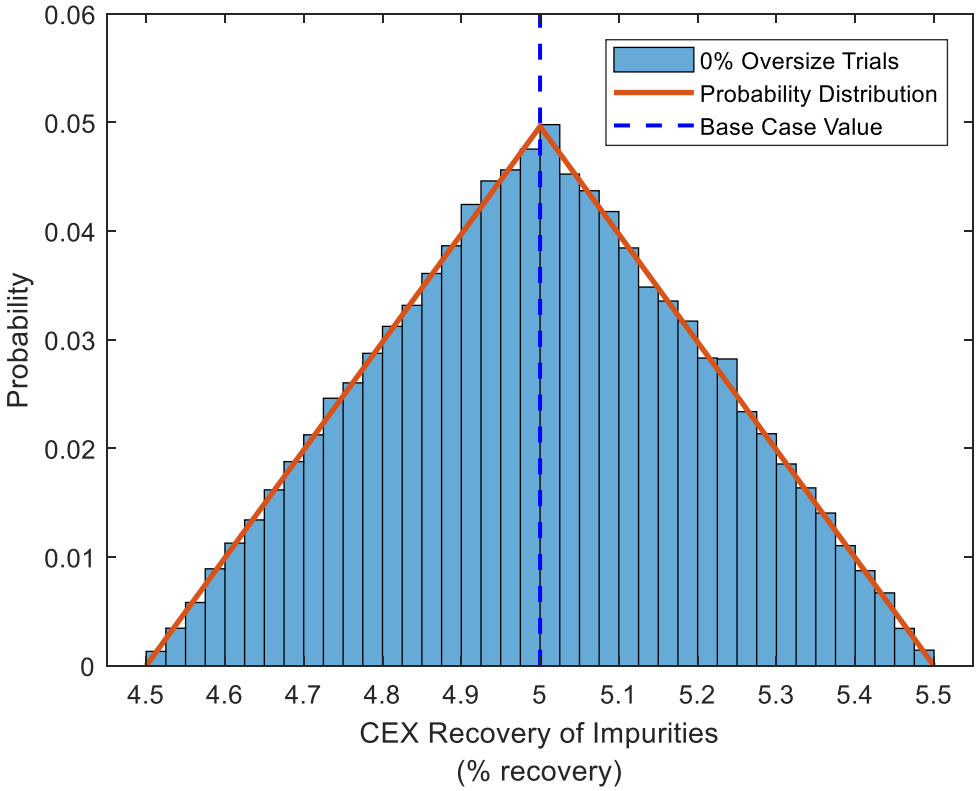

Figure S6.20. Impurities recovery, cation exchange chromatography in P-20

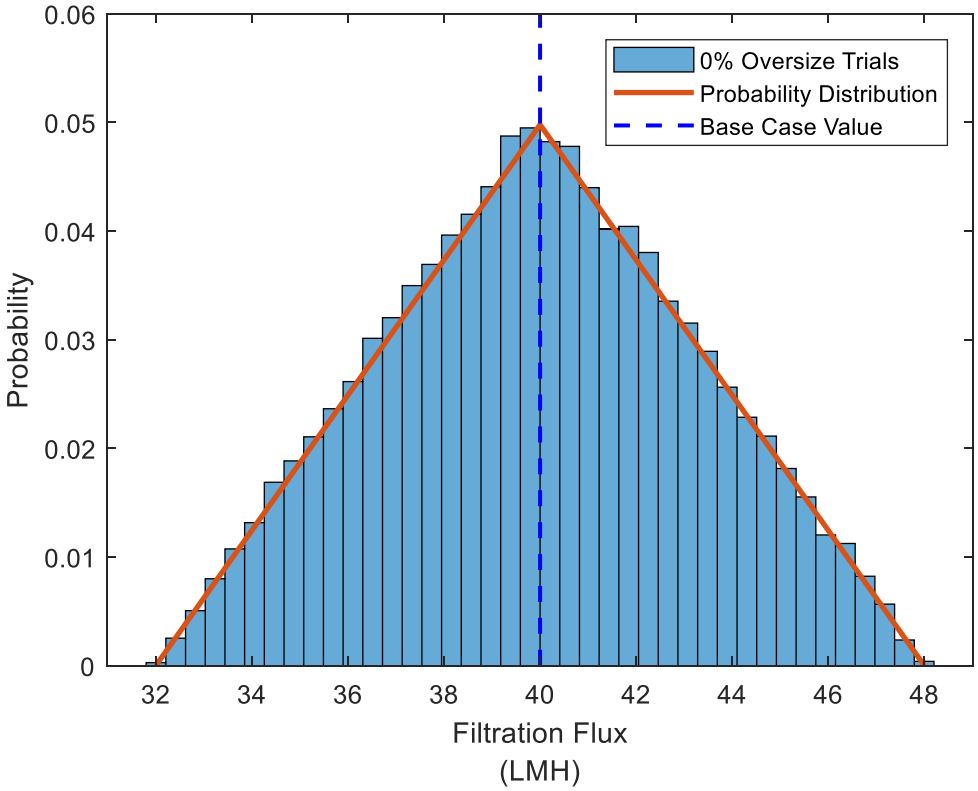

Figure S6.21. Filtration flux, ultrafiltration/diafiltration in P-22

6.5.3. Forecast Univariate Sensitivity (Tornado Plots)

The following is a series of tornado plots displaying univariate sensitivity of the forecast variables in the 0% oversize scenario from the base case value to the 1st and 99th percentile values of the input parameter assumptions. A monotonic relationship between input parameters and forecast variables was confirmed by testing eight input parameter values evenly disbursed across the assumption range. The exception to this is the assumption for Field Growth Yield, which did not maintain a monotonic relationship when the biomass generated exceeded the capacity of the processing equipment; a monotonic relationship is re-established in the 100% oversize scenario in which case there is no Field Growth Yield that results in biomass generated above capacity.

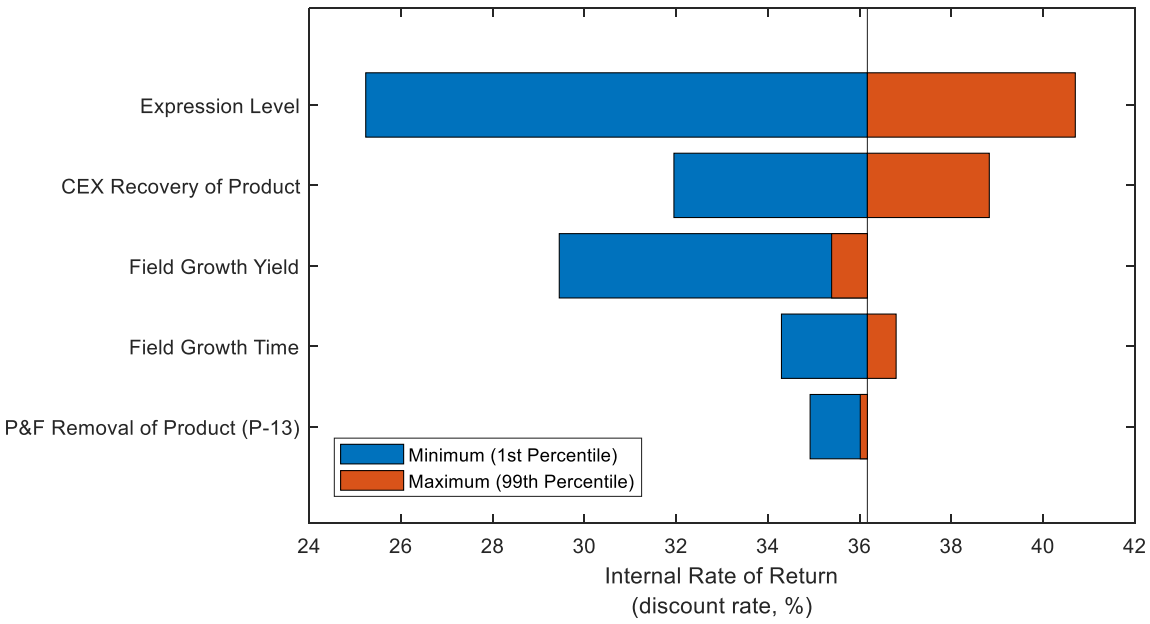

Figure S6.22. Internal rate of return, after tax

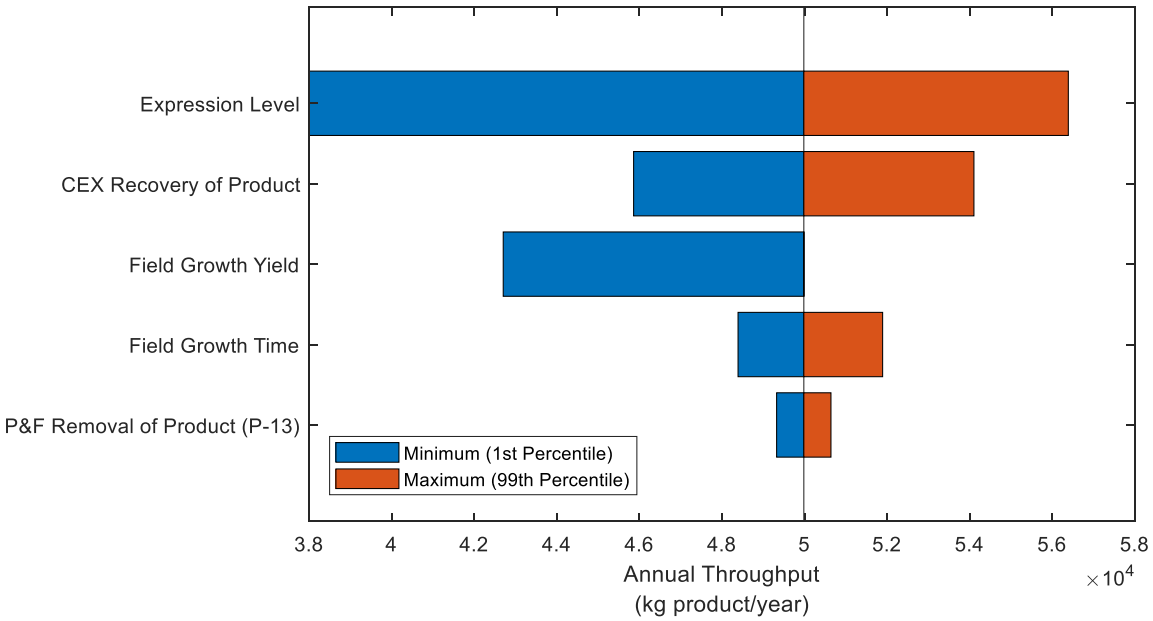

Figure S6.23. Annual throughput

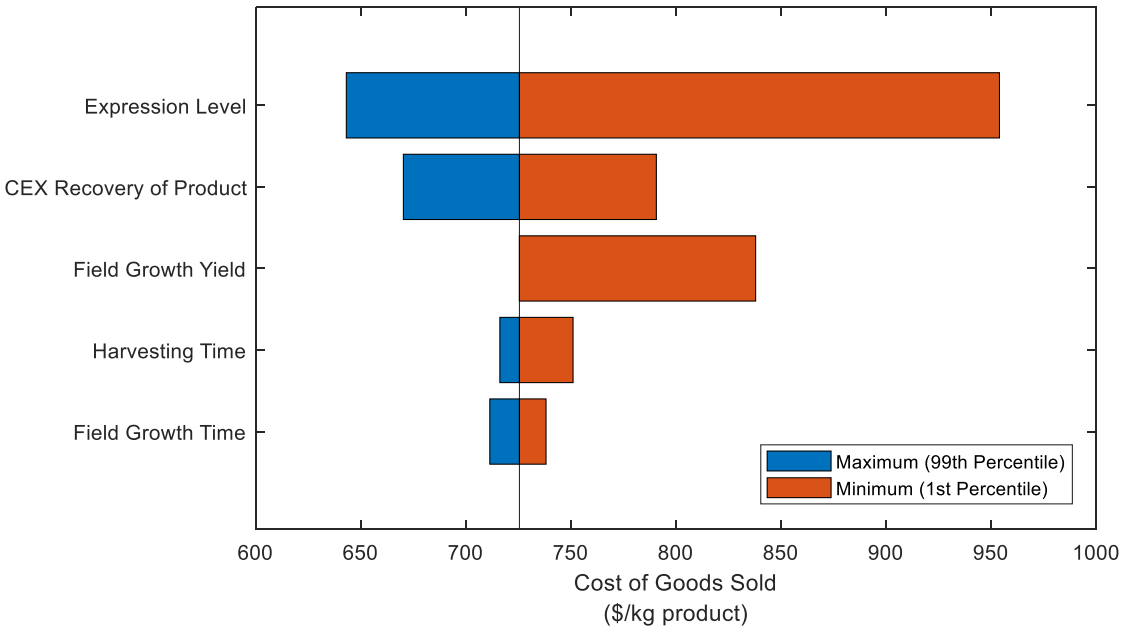

Figure S6.24. Cost of goods sold

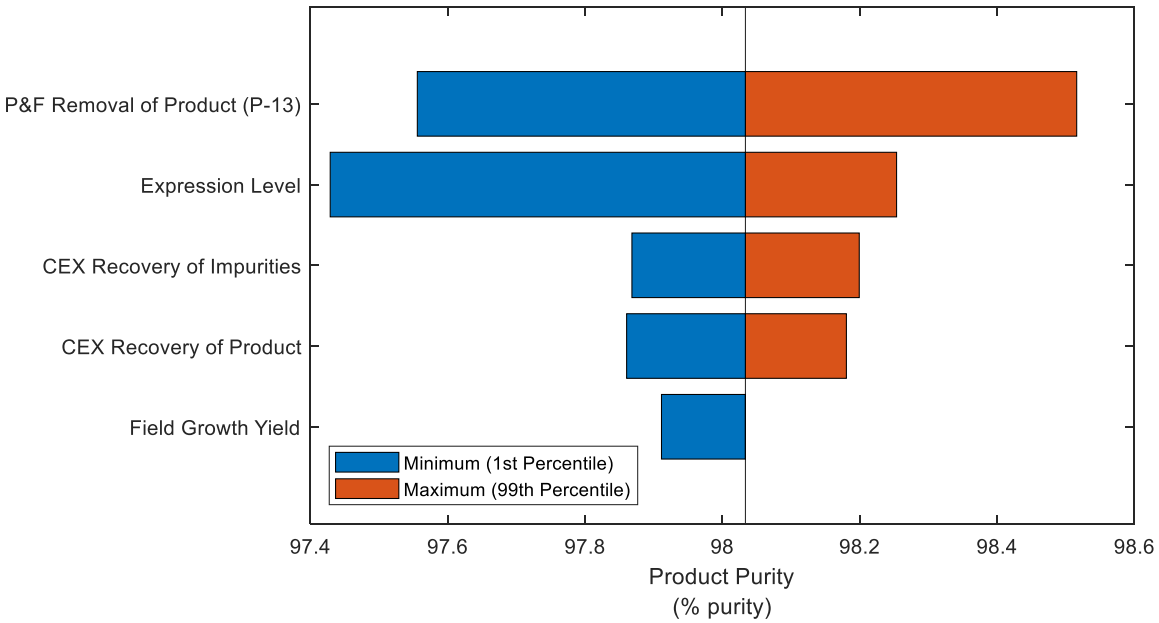

Figure S6.25. Product purity

6.5.4. Forecast Contributions to Variance

The following is a series of tables containing the forecast sensitivity to each of the input assumptions for the 0% oversize scenario as given by the contributions to variance and rank correlations. Forecast sensitivity is generated from a simulation (20,000 trials) of the 0% oversize scenario at the $2,275 selling price with assumption correlations excluded.

Table S6.2. Internal rate of return, after tax

Sensitivity: Internal Rate of Return, After Tax		
Assumptions	Contribution to Variance	Rank Correlation
Expression Level, P-4	7.71E-01	-7.98E-01
CEX Recovery of Product, P-20	1.26E-01	-3.23E-01
Field Growth Yield, P-2	7.15E-02	-2.43E-01
Harvesting Time, P-5	1.43E-02	1.09E-01
Field Growth Time, P-2	9.95E-03	9.06E-02
P&F Removal of Product, P-13	3.69E-03	5.52E-02
P&F Removal of Product, P-11	1.62E-03	3.66E-02
P&F Removal of Product, P-17	8.49E-04	2.65E-02
UF/DF Filtration Flux, P-19	4.57E-04	-1.94E-02
P&F Removal of Impurities, P-13	1.60E-04	-1.15E-02
P&F Removal of Impurities, P-11	1.53E-04	1.12E-02
P&F Removal of Impurities, P-17	1.35E-04	1.05E-02
UF/DF Filtration Flux, P-22	5.00E-05	-6.43E-03
P&F Filtration Flux, P-17	4.98E-05	-6.42E-03
P&F Filtration Flux, P-11	4.78E-05	-6.29E-03
CEX Recovery of Impurities, P-20	2.26E-05	4.32E-03
P&F Filtration Flux, P-13	7.64E-07	7.94E-04

Table S6.3. Annual throughput

Sensitivity: Annual Throughput		
Assumptions	Contribution to Variance	Rank Correlation
Expression Level, P-4	7.45E-01	7.82E-01
CEX Recovery of Product, P-20	1.21E-01	3.15E-01
Field Growth Yield, P-2	9.00E-02	2.72E-01
Field Growth Time, P-2	3.58E-02	-1.71E-01
P&F Removal of Product, P-13	3.35E-03	-5.25E-02
Harvesting Time, P-5	2.26E-03	-4.30E-02
P&F Removal of Product, P-11	1.50E-03	-3.51E-02
P&F Removal of Product, P-17	7.52E-04	-2.48E-02
P&F Removal of Impurities, P-11	1.56E-04	-1.13E-02
P&F Removal of Impurities, P-13	1.55E-04	1.13E-02
P&F Removal of Impurities, P-17	1.32E-04	-1.04E-02
UF/DF Filtration Flux, P-22	4.18E-05	5.85E-03
P&F Filtration Flux, P-17	2.74E-05	4.74E-03
CEX Recovery of Impurities, P-20	1.94E-05	-3.99E-03
P&F Filtration Flux, P-13	1.02E-05	-2.90E-03
P&F Filtration Flux, P-11	8.21E-06	2.60E-03
UF/DF Filtration Flux, P-19	7.56E-07	-7.88E-04

Table S6.4. Cost of goods sold

Sensitivity: Cost of Goods Sold		
Assumptions	Contribution to Variance	Rank Correlation
Expression Level, P-4	7.71E-01	-7.98E-01
CEX Recovery of Product, P-20	1.26E-01	-3.23E-01
Field Growth Yield, P-2	7.15E-02	-2.43E-01
Harvesting Time, P-5	1.43E-02	1.09E-01
Field Growth Time, P-2	9.95E-03	9.06E-02
P&F Removal of Product, P-13	3.69E-03	5.52E-02
P&F Removal of Product, P-11	1.62E-03	3.66E-02
P&F Removal of Product, P-17	8.49E-04	2.65E-02
UF/DF Filtration Flux, P-19	4.57E-04	-1.94E-02
P&F Removal of Impurities, P-13	1.60E-04	-1.15E-02
P&F Removal of Impurities, P-11	1.53E-04	1.12E-02
P&F Removal of Impurities, P-17	1.35E-04	1.05E-02
UF/DF Filtration Flux, P-22	5.00E-05	-6.43E-03
P&F Filtration Flux, P-17	4.98E-05	-6.42E-03
P&F Filtration Flux, P-11	4.78E-05	-6.29E-03
CEX Recovery of Impurities, P-20	2.26E-05	4.32E-03
P&F Filtration Flux, P-13	7.64E-07	7.94E-04

Table S6.5. Product purity

Sensitivity: Product Purity		
Assumptions	Contribution to Variance	Rank Correlation
P&F Removal of Impurities, P-13	5.65E-01	7.16E-01
Expression Level, P-4	3.02E-01	5.23E-01
CEX Recovery of Impurities, P-20	7.64E-02	-2.63E-01
CEX Recovery of Product, P-20	4.62E-02	2.05E-01
Field Growth Yield, P-2	6.23E-03	-7.52E-02
P&F Removal of Product, P-13	1.41E-03	-3.58E-02
P&F Removal of Impurities, P-11	8.71E-04	2.81E-02
P&F Removal of Product, P-17	5.78E-04	-2.29E-02
P&F Removal of Product, P-11	5.13E-04	-2.16E-02
Harvesting Time, P-5	2.69E-04	-1.56E-02
P&F Filtration Flux, P-13	1.14E-05	3.22E-03
UF/DF Filtration Flux, P-19	1.12E-05	-3.18E-03
P&F Filtration Flux, P-11	3.40E-06	1.76E-03
Field Growth Time, P-2	2.38E-06	1.47E-03
P&F Removal of Impurities, P-17	1.20E-06	1.04E-03
P&F Filtration Flux, P-17	6.97E-07	7.95E-04
UF/DF Filtration Flux, P-22	3.21E-07	-5.39E-04

6.5.5. Equipment Oversizing Specifications

The following is a tabular description of the equipment capacity values for each of the facility oversizing models (0, 25, 50, 75, 100%). The equipment capacity values for each oversizing increment were calculated by taking the difference in equipment capacity between the 0% and 100% oversizing scenario and adding incremental capacity to the prescribed % oversizing.

Table S6.6. Equipment capacity values used in the facility oversizing scenarios.

Equipment Description		Heat Tank (V-101)	Evaporator (EV-101)	Hold Tank (V-102)	CEX Column (C-101)
Units of Measurement		m^3	m^2 transfer area	L	L resin
0%	Unit Capacity	71	265	77,864	520
	# Units	9	1	1	5
	Total Capacity	641	265	77,854	2,601
25%	Unit Capacity	77	286	41,989	523
	# Units	9	1	2	6
	Total Capacity	692	286	83,978	3,136
50%	Unit Capacity	74	306	45,051	524
	# Units	10	1	2	7
	Total Capacity	742	306	90,102	3,670
75%	Unit Capacity	79	327	48,113	526
	# Units	10	1	2	8
	Total Capacity	793	327	96,226	4,205
100%	Unit Capacity	77	348	51,175	527
	# Units	11	1	2	9
	Total Capacity	843	348	102,350	4,740

6.5.6. Forecast Variable Normality (Box Plots, Q-Q Plots)

The following is a series of box plots and quantile-quantile (Q-Q) plots comparing forecast variable distribution to a normal distribution. Box plots are displaying the median as the center mark, 25^{th} and 75^{th} percentiles as the box limits, +/- 2.7 σ as whisker limits, and outliers marked with red plus symbols. For Q-Q plots, normally distributed forecast variable data will lie approximately on a straight line. Profitability-related forecast variables include 20,000 trials for each plot, while process-related forecast variables include 60,000 trials (combined from 20,000 trials for each of the three selling prices analyzed).

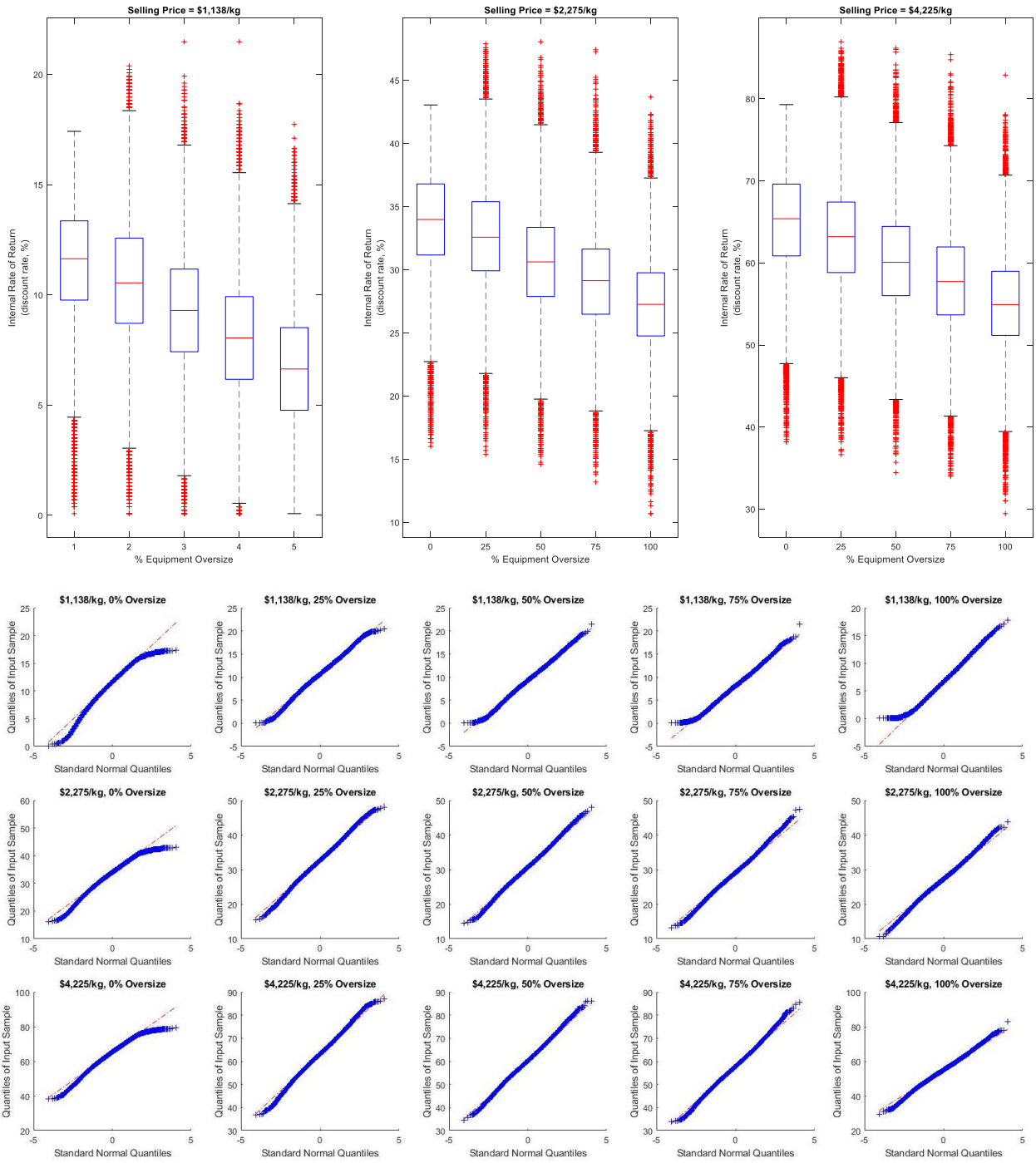

Figure S6.26. Box plots (top) and Q-Q plots (bottom) for internal rate of return, after tax

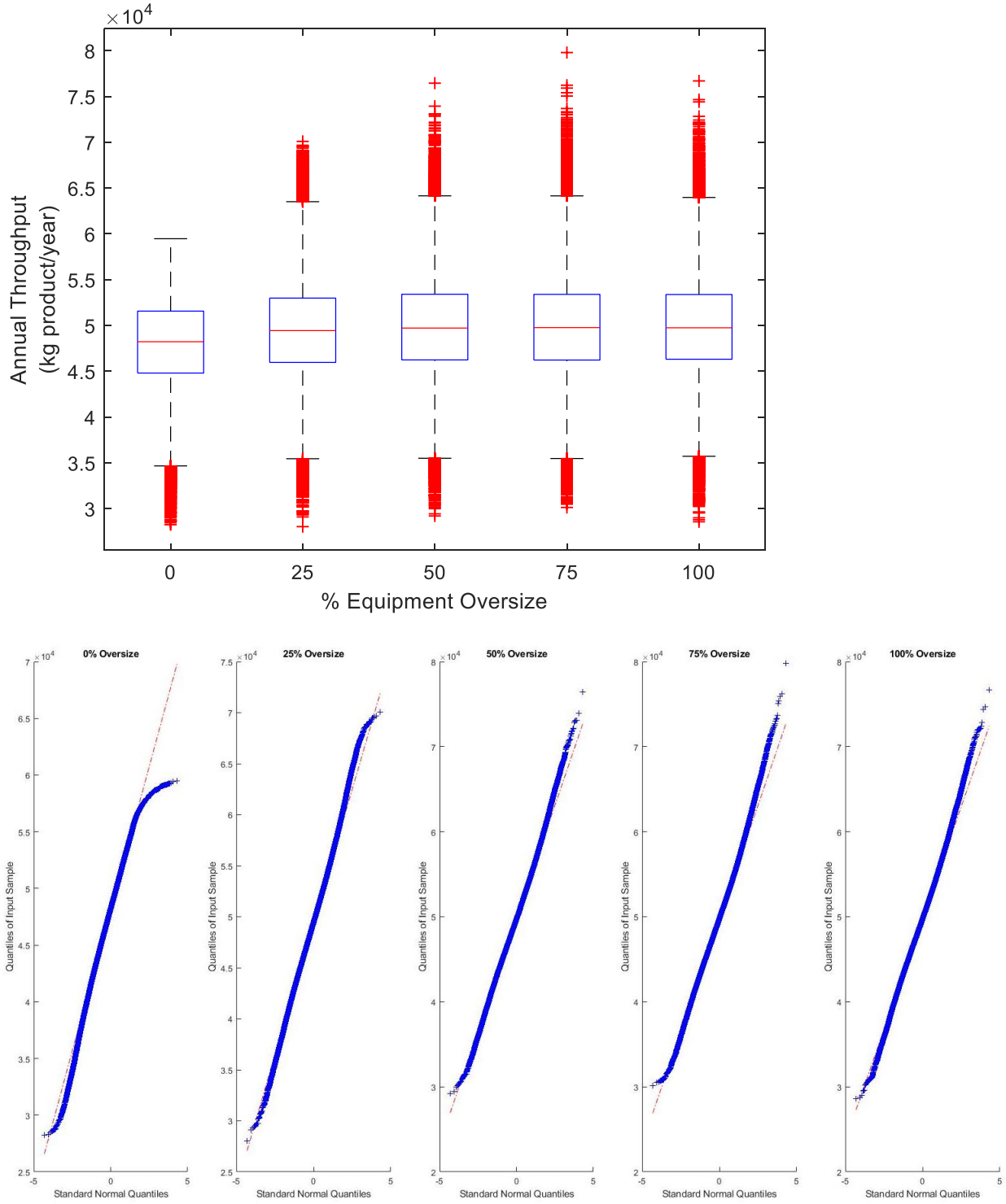

Figure S6.27. Box plots (top) and Q-Q plots (bottom) for annual throughput

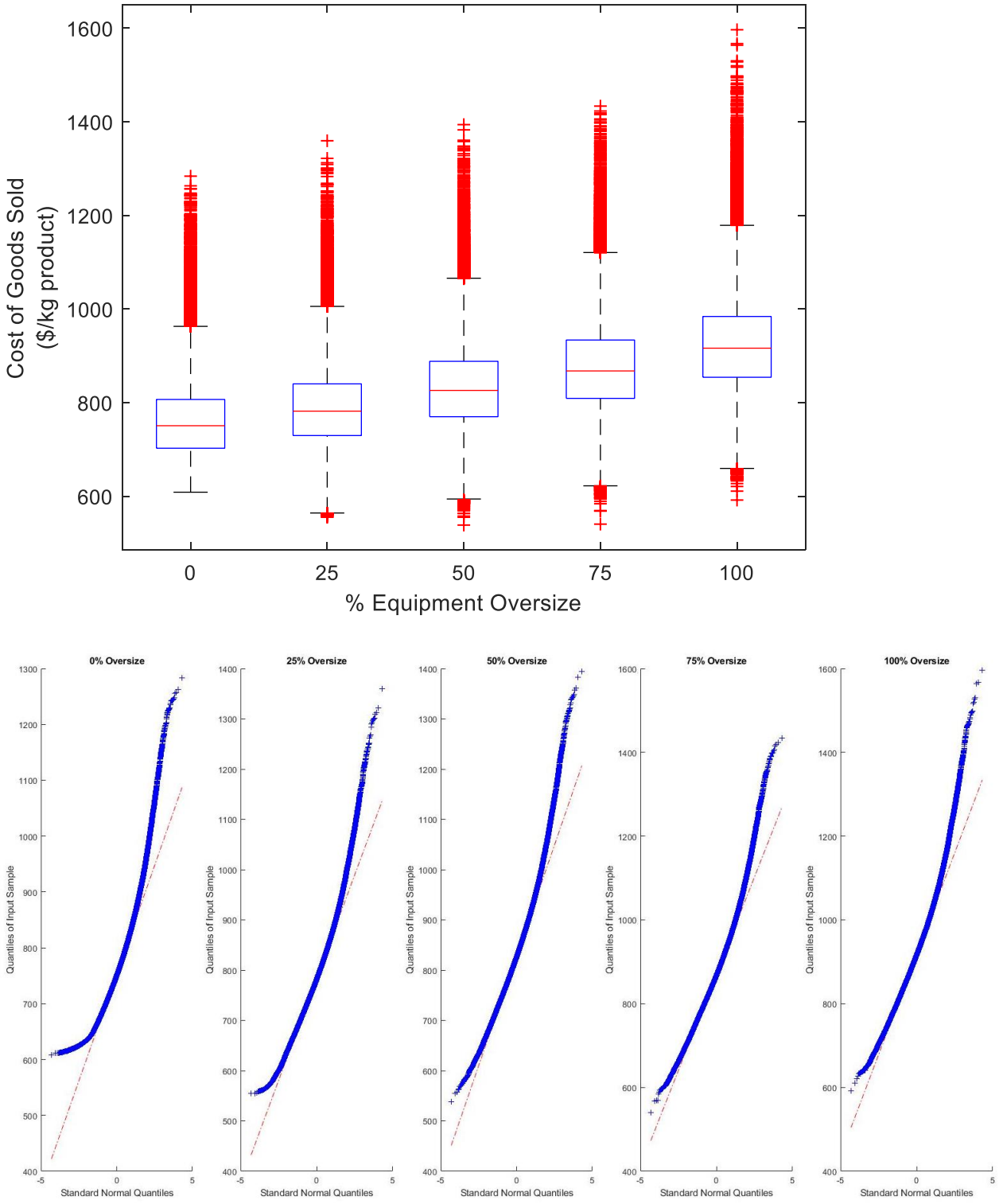

Figure S6.28. Box plots (top) and Q-Q plots (bottom) for cost of goods sold

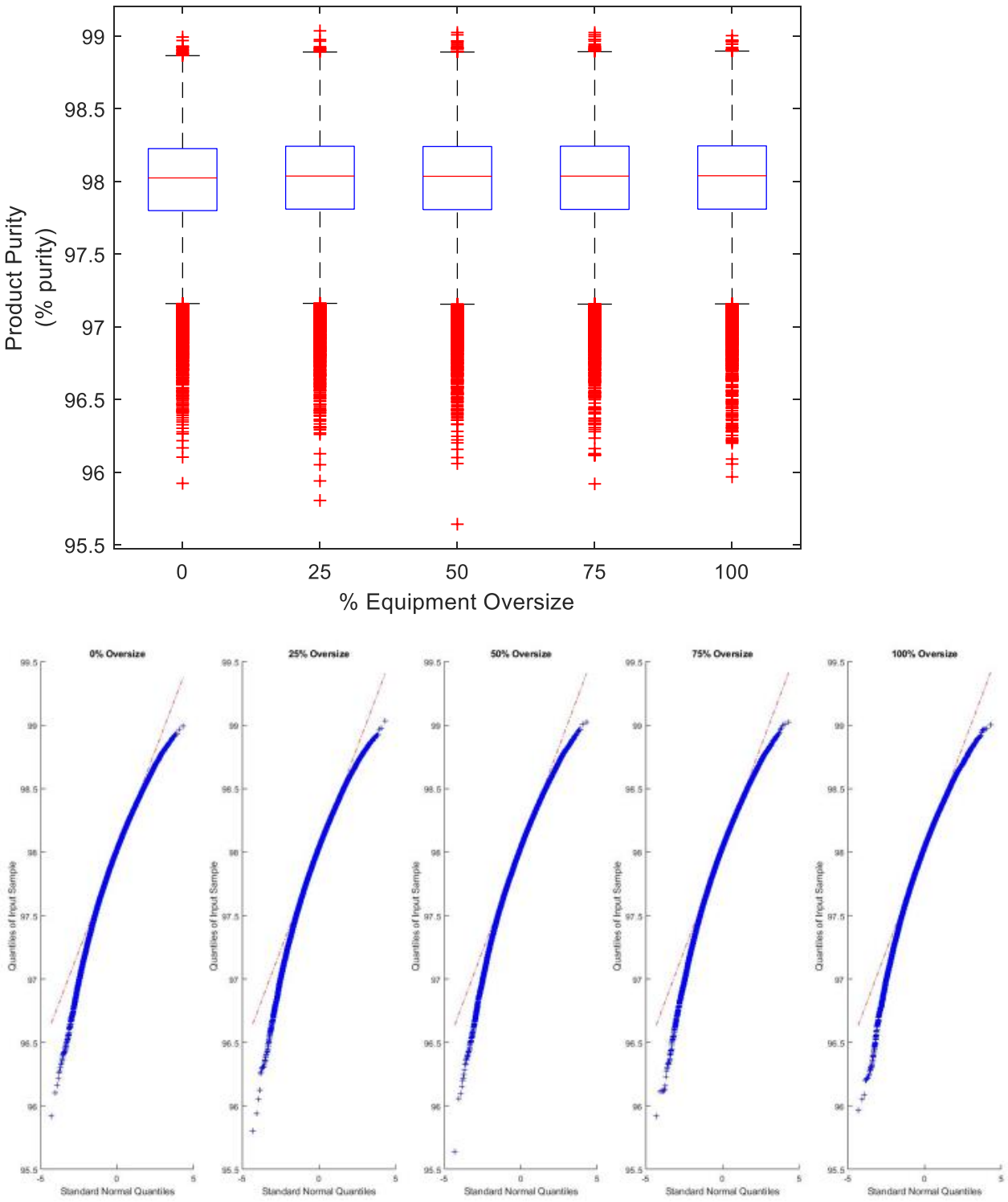

Figure S6.29. Box plots (top) and Q-Q plots (bottom) for product purity

6.5.7. Two-Sample t-Tests for Means

In the following section the test statistic and p-value results of the two-sample and two-sided t-tests assuming unequal variance ($\alpha = 0.05$) performed to evaluate equality of forecast variable and effective input parameter mean output between the equipment oversizing scenarios (0, 25, 50, 75, 100%) are tabulated for reference. P-values of an order of magnitude E-300 and smaller have been represented as "0" in the tables.

Note: results in which there is insufficient evidence to conclude a difference in means are bolded.

Table S6.7. Internal Rate of Return, $1,138/g selling price (test statistic; p-value)

	0%	25%	50%	75%	100%
0%	--				
25%	30; 2.3E-194	--			
50%	78; 0	47; 0	--		
75%	120; 0	87; 0	41; 0	--	
100%	170; 0	140; 0	89; 0	48; 0	--

Table S6.8. Internal Rate of Return, $2,275/g selling price (test statistic; p-value)

	0%	25%	50%	75%	100%
0%	--				
25%	27; 2E-159	--			
50%	75; 0	47; 0	--		
75%	110; 0	84; 0	37; 1.1E-290	--	
100%	160; 0	130; 0	83; 0	46; 0	--

Table S6.9. Internal Rate of Return, $4,225/g selling price (test statistic; p-value)

	0%	25%	50%	75%	100%
0%	--				
25%	27; 2.2E-163	--			
50%	72; 0	43; 0	--		
75%	110; 0	81; 0	38; 0	--	
100%	156; 0	130; 0	83; 0	45; 0	--

Table S6.10. Annual Throughput (test statistic; p-value)

	0%	25%	50%	75%	100%
0%	--				
25%	49; 0	--			
50%	59; 0		--		
75%	60; 0	11; 6.2E-30	**1.2; 0.23**	--	
100%	61; 0	11; 1.2E-29	**1.1; 0.27**	**0.10; 0.92**	--

Table S6.11. Cost of Goods Sold (test statistic; p-value)

	0%	25%	50%	75%	100%
0%	--				
25%	56; 0	--			
50%	140; 0	84; 0	--		
75%	210; 0	160; 0	745; 0	--	
100%	300; 0	240; 0	160; 0	82; 0	--

Table S6.12. Product Purity (test statistic; p-value)

	0%	25%	50%	75%	100%
0%	--				
25%	7.1; 1.0E-12	--			
50%	6.6; 4.7E-11	**0.55; 0.58**	--		
75%	6.1; 1.2E-09	**1.0; 0.31**	**0.46; 0.64**	--	
100%	7.3; 4.0E-13	**0.14; 0.89**	**0.69; 0.49**	**1.1; 0.25**	--

Table S6.13. Effective CEX Recovery of Product (test statistic; p-value)

	0%	25%	50%	75%	100%
0%	--				
25%	26; 1.6E-144	--			
50%	25; 1.4E-140	**0.28; 0.78**	--		
75%	26; 3.3E-148	**0.41; 0.68**	**0.69; 0.49**	--	
100%	25; 6.7E-142	**0.21; 0.83**	**0.07; 0.94**	**0.62; 0.54**	--

Table S6.14. Field Growth Yield (test statistic; p-value)

	0%	25%	50%	75%	100%
0%	--				
25%	74; 0	--			
50%	87; 0	19; 2.6E-76	--		
75%	86; 0	19; 1.3E-79	**0.64; 0.52**	--	
100%	86; 0	19; 5.0E-82	**0.97; 0.33**	**0.33; 0.75**	--

6.5.8. Kolmogorv-Smirnov Tests for Distributions

In the following section the test statistic and p-value results of the two-sample and two-sided Kolmogorv-Smirnov test performed to evaluate equality of forecast variable and effective input parameter distribution output between the equipment oversizing scenarios (0, 25, 50, 75, 100%) for which mean output is not statistically distinct (bolded in the above section) are tabulated for reference.

Note: results in which the null hypothesis (distribution 1 = distribution 2) is rejected (p-value < 0.05) are bolded.

Table S6.15. Annual Throughput (test statistic; p-value)

	50%	75%	100%
50%	--		
75%	5.7E-3; 0.28	--	
100%	5.4E-3; 0.36	6.0E-3; 0.23	--

Table S6.16. Product Purity (test statistic; p-value)

	25%	50%	75%	100%
25%	--			
50%	4.5E-3; 0.58	--		
75%	4.4E-3; 0.61	4.8E-3	--	
100%	4.1E-3; 0.69	6.3E-3	6.1E-3; 0.22	--

Table S6.17. Effective CEX Recovery of Product (test statistic; p-value)

	25%	50%	75%	100%
25%	--			
50%	4.3E-3; 0.65	--		
75%	4.9E-3; 0.48	4.5E-3; 0.59	--	
100%	3.6E-3; 0.82	2.8E-3; 0.98	3.2E-3; 0.92	--

Table S6.18. Effective Field Growth Yield (test statistic; p-value)

	50%	75%	100%
50%	--		
75%	**3.3E-2; 2.2E-16**	**--**	
100%	**3.3E-2; 2.2E-16**	3.7E-3; 0.81	--

Chapter 7. Molecular pharming to support human life on the Moon, Mars, and beyond

"Let your food be thy medicine and medicine be thy food."

-Hippocrates (400 BC);
Widely interpreted as referring to the importance of dietary nutrition and not molecular pharming… but you never know!

This chapter is based on the following publication:

McNulty, M.J., Xiong, Y. (Mary), Yates, K., Karuppanan, K., Hilzinger, J.M., Berliner, A.J., Delzio, J., Arkin, A.P., Lane, N.E., Nandi, S., and McDonald, K.A. (2021). Molecular pharming to support human life on the moon, mars, and beyond. *Crit. Rev. Biotechnol.*, 1–16. doi: 10.1080/07388551.2021.1888070.

Abstract

Space missions have always assumed that the risk of spacecraft malfunction far outweighs the risk of human system failure. This assumption breaks down for longer duration exploration missions and exposes vulnerabilities in space medical systems. Space agencies can no longer reduce the majority of the human health and performance risk through the crew member selection process and emergency re-supply or evacuation. No mature medical solutions exist to address this risk. With recent advances in biotechnology, there is promise for lessening this risk by augmenting a space pharmacy with a biologically-based space foundry for on-demand manufacturing of high-value medical products. Here we review the challenges and opportunities of molecular pharming,

the production of pharmaceuticals in plants, as the basis of a space medical foundry to close the risk gap in current space medical systems. Plants have long been considered an important life support object in space and can now also be viewed as programmable factories in space. Advances in molecular pharming-based space foundries will have widespread application in promoting simple and accessible pharmaceutical manufacturing on Earth.

7.1. Re-Thinking Human Health for Deep Space Missions

Humanity has collectively returned its gaze to the stars as space agencies and companies around the world work to develop new strategies to extend human presence farther into the universe. To get there, we need to transition from Earth-reliant to Earth-independent mission architecture. Agencies like the National Aeronautics and Space Administration (NASA) and European Space Agency (ESA) have developed exceptional life support systems for Earth-reliant human missions into space[194]. Carefully planned medicine, food, and environmental control re-supply shuttles working in concert with on-board environmental control and life support systems maintain a habitable environment for astronauts in the International Space Station (ISS)[195].

But as space missions get longer and probe deeper into the solar system – to the Moon, to Mars, and beyond – frequent re-supplies for life support systems will become increasingly burdensome. Current exploration medical capabilities are particularly vulnerable to a lower rate of resupply and longer missions. The list of necessary supplies to address persistent exposures of space travel adds up quickly: including countermeasures for increased radiation[196,197], bone loss[198,199], kidney stones[200,201], vision impairment[202], and adverse behavioral conditions[203] to name a few. The list of supplies begins to look unmanageable when you add in intermittent, or even unanticipated, exposures such as microbial infection[204–206], and spaceflight-induced genome instability and metabolic changes[207]. As mission duration increases, the risk of a low probability medical condition is amplified; when an astronaut is on Mars and the closest hospital or medical re-supply is at least 200 days of interplanetary travel away[208], it is critical that astronauts are medically self-sufficiency.

Furthermore, recent literature highlights systemic vulnerabilities in space-flown pharmaceutical life support in the biased and underreported historical data of in-flight pharmaceutical use and

efficacy, limited fidelity of current ground-analog models, and in-flight instability of drug formulations[209]. Of the small molecule solid formulations tested thus far, three-quarters will have degraded by the end of the proposed first Mars mission duration[208]. There has been no spaceflight testing of biologics, a critical category of pharmaceuticals known to be less stable than small molecule drugs[210,211]. These issues highlight the need to develop platform technologies for on-demand production of medicines.

7.2. Defining a Medical Foundry for Space Exploration

The medical systems of future space exploration will need to be reconfigured to guarantee astronaut health. The contemporary standard is the NASA-provided ISS crew health care system (CHeCS) consisting of three sub-systems: 1) the countermeasures system (CMS) composed of exercise hardware and monitoring devices, 2) the environmental health system (EHS) composed of hardware for environmental monitoring, and 3) the health maintenance system (HMS) composed of a medical kit for supporting routine minor medical needs for up to 180 days[212]. Earth-reliant medical systems like CHeCS will need to be augmented with medical foundries for self-sufficiency in Earth-independent space mission architectures. A space medical foundry will expand mission capabilities to include high-value medical product manufacturing, of which pharmaceuticals will be a critical product class. This is particularly important for extended duration exploration, and settlement, of extraterrestrial bodies such as the Moon and Mars.

A space foundry, of which a medical foundry is a subset, must be capable of utilizing a limited set of inputs (ideally *in situ* resources with minimal flown resources) to generate a wide spectrum of outputs and must be able to do so in a simple, closed loop. Recent literature have detailed a compelling narrative for the use of biotechnology to answer these challenges[208,213,214]. The Center

for Utilization of Biological Engineering in Space (https://cubes.space) is a multi-university effort to realize the inherent mass, power, and volume advantages of space biotechnology and advance the practicality of a nearly closed loop, photoautotrophic factory for production of food, pharmaceuticals, and materials on a Mars mission.

An alternative method for pharmaceutical production is chemical synthesis. In producing small molecule pharmaceuticals, chemical synthesis is often advantageous on Earth. However, as stereochemical complexity and size of the target pharmaceutical increases, chemical synthesis often becomes dramatically less feasible and attractive. For perspective, there are examples of chemical synthesis used commercially to produce pharmaceuticals as large as peptides (5-50 amino acids)[215,216], but antibodies, an example class of life-saving pharmaceuticals produced only in biological systems (termed "biologics"), are two orders of magnitude larger (~1,400 amino acids) than that. Chemical synthesis of pharmaceuticals can also be contrasted with biological production as having highly reaction-specific inputs and complex synthesis steps, often requiring use of organic solvents and generating substantial waste by-products, all of which are undesirable attributes for space applications. Chemical synthesis may be necessary for a robust medical foundry for space, indeed it will likely be required to synthesize nucleic acids to mobilize biological production in space[217], but it will not be sufficient to produce all countermeasures.

Space biotechnology has primarily focused on microbes[208,213], fungi[218], and plants[213,219]. From this perspective, we review the potential utility of plants as a molecular medical foundry for production of pharmaceuticals in deep space and contrast this with the capabilities of alternative biological organisms.

7.3. Plants in Space

Plants are an established facet of space mission architecture, with research dating back to the 1950s[220]. Most recently, a study on red romaine lettuce grown in the International Space Station (ISS) using the Vegetable Production System (Veggie) has reported that leafy vegetable crops can be grown and consumed safely in the ISS as a dietary supplement[221].

Resource flexibility is essential in the confined environments of a space mission, and researchers have shown that plants serve as versatile assets in a space mission life support system. Up to this point, studies have focused on the value of plants to harness solar energy and provide nutrients, water treatment, air treatment, and behavioral health[220–224]. Accordingly, research into advancing the capabilities of plants for space has primarily focused on those key areas. What has not been captured in published research is the potential of plants to provide astronauts with pharmaceuticals and other high value products, which is formally known as molecular pharming (Figure 7.1)[225].

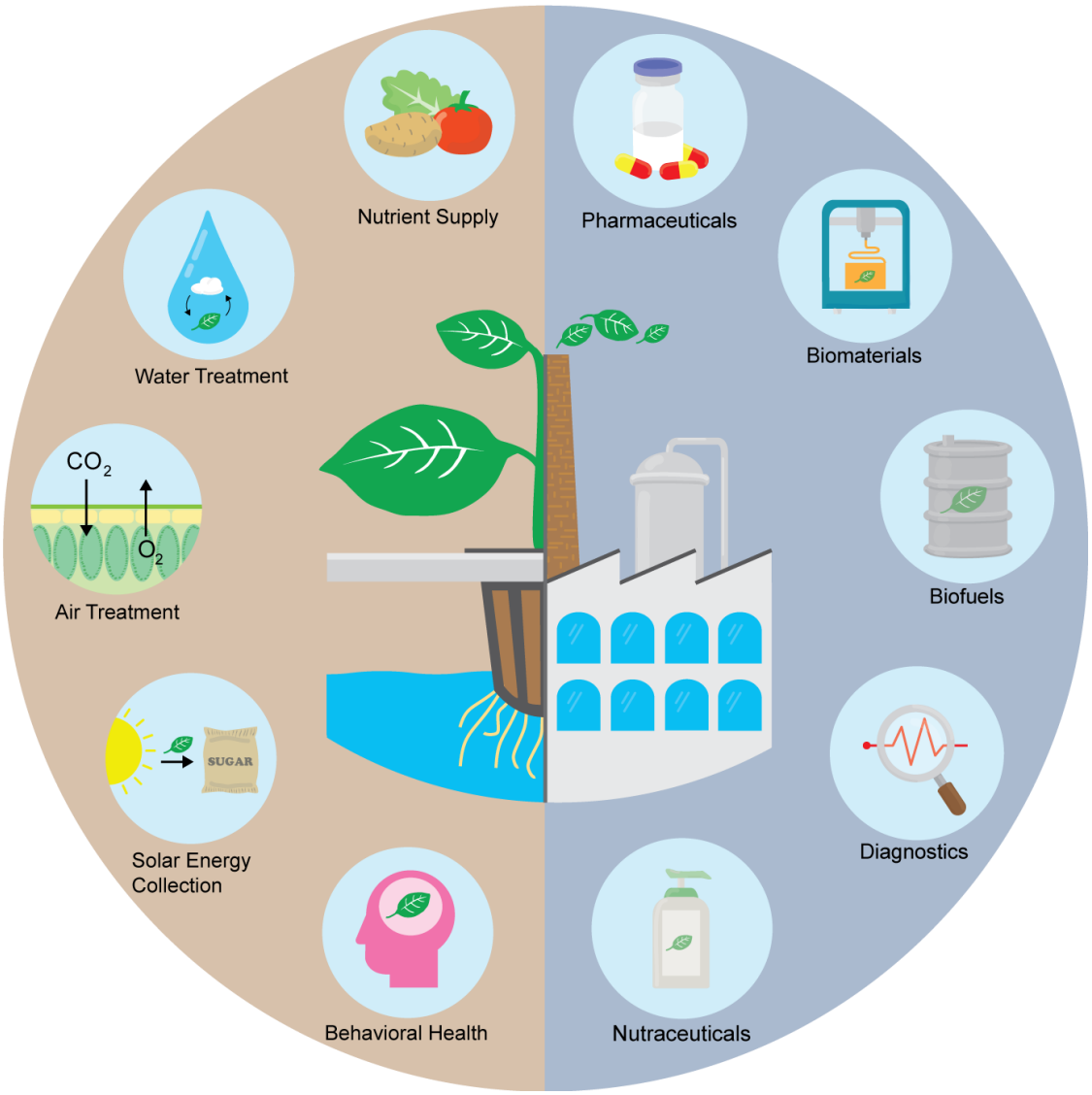

Figure 7.1. Molecular pharming embodies the perspective that plants are chemical factories. Viewing plants as factories vastly expands the bioregenerative life support capabilities of plants in space. Here we focus on molecular pharming of pharmaceuticals.

7.4. Supporting Life with Molecular Pharming

Humans have looked to plants as a source of healing for thousands of years[20]. To date, there are over 120 commercially available drugs consisting of distinct chemical substances that have been derived from plants[226]. This list includes widely used medications such as aspirin[227], the most

commonly used drug in the world, paclitaxel[228], which is used to treat various forms of cancer, and artemisinin[170], an antimalarial compound.

The breadth of therapeutically-relevant molecules that we can now produce in a plant to support human life has exploded with recombinant DNA technology. Plants have been used to produce a wide variety of complex products for supporting human life – ranging from products as diverse as diagnostic reagents and therapeutic proteins, to biomaterials and biofuels. Pioneering work in the past twenty years on plant-based production systems has positioned molecular pharming competitively for commercial applications of these diverse products on Earth[23,41,95,100,185,229]. Continuing those advances, we focus on producing pharmaceuticals as a high-priority application of molecular pharming to mitigate human health risks in extended deep space exploration.

The first commercial therapeutic protein to be produced recombinantly in plant cells (Elelyso®) was approved for enzyme replacement therapy in 2012[50,131]. While this product is produced in plant cell culture, it has established a regulatory pathway for addressing concerns with plant-based production in general. There is currently a wide range of whole plant-produced pharmaceuticals in commercial pipelines; perhaps most notably, Medicago's clinical program consists of an influenza vaccine in Phase 3 trials (ClinicalTrials.gov Identifier: NCT03739112) and several other vaccine candidates in earlier stages. Molecular pharming has also found commercial success in other application areas – for example in diagnostic reagents, with avidin produced in maize[230], veterinary medicine, with canine interferon-alpha produced in strawberry[231], nutraceuticals, with human growth factors produced in barley[232], and commodity chemicals, with cell culture media components produced in rice[233].

7.4.1. Pairing Production Strategies with Disease States

Molecular pharming with whole plants can be performed by using one of two strategies: transient production using gene delivery systems to introduce genes for the plant to temporarily transcribe and translate on-demand, or transgenic production using plants with recombinant genes inserted into the genome for stable translation (Figure 7.2). Either strategy can be executed to produce recombinant products using a simple process flow.

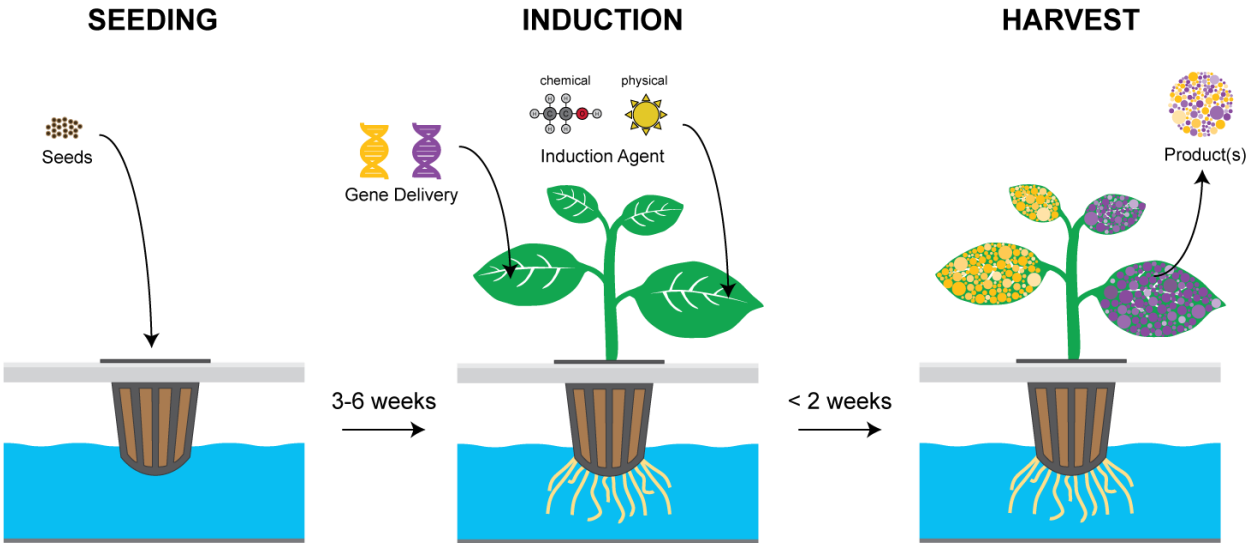

Figure 7.2. The simplicity of molecular pharming, illustrated. Producing recombinant products can be induced via gene delivery (transient production) or an induction agent (inducible transgenic production). Recombinant products accumulate in constitutive transgenic production without an induction step.

Transient production is a strategy that can provide on-demand transformation of food into a medical, or some other high-value product, resource. This enables a rapid response in which initiation of production is linked to the exceeding of some risk threshold, be it triggered by the emergence of a diagnosed disease state or an increased probability of occurrence. This allows stockpiles to be minimized for low frequency disease states, and perhaps most importantly, builds

capability to respond to unanticipated disease states. Key parameters of transient production to meet these capabilities are the production lead time (how fast can a dose of medicine be produced), the specific productivity (how much biomass is needed for a dose of medicine), and the manufacturing resources (which equipment and materials are needed for production). There are a variety of established transient production systems that employ both biotic and abiotic methods as shown in Figure 7.3. Table 7.1 summarizes key process differences in these transient production systems. Selecting the most effective transient production system depends on the disease state (e.g., a small time-to-treatment window) and the exploration mission architecture (e.g., available resources).

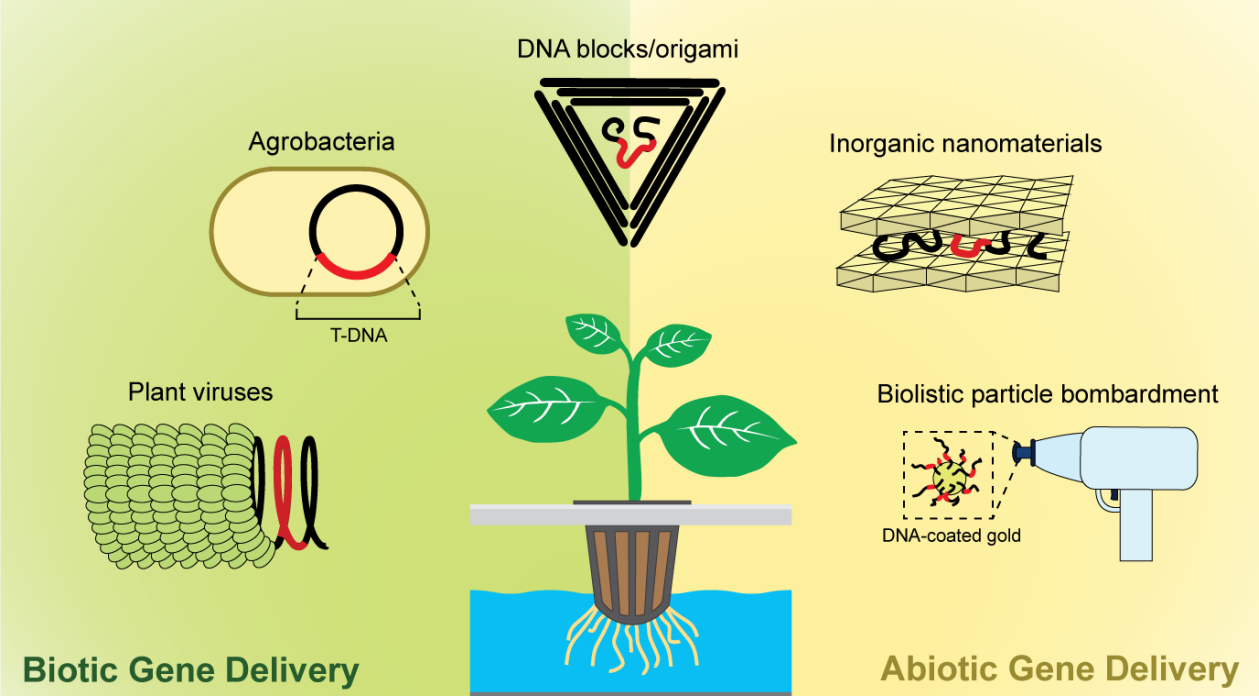

Figure 7.3. A look at previously established biotic and abiotic methods (also referred to as indirect and direct methods, respectively) for transient expression of recombinant products in plant systems.

Table 7.1. A comparison of key attributes between molecular pharming-based transient production methods. Level of expertise and equipment requirement rankings were determined using working process knowledge and the cited reference material.

	Plant viruses [234]	**Agrobacteria** [235]	**DNA blocks/origami** [236]	**Inorganic nanomaterials** [237]	**Biolistic particle bombardment** [238]
Mode of Administration	Mechanical transmission	Vacuum, syringe, spray	Vacuum, syringe	Root drenching	Gas-pressured gene gun
Vehicle Size	10 – 500 nm	1,000 – 3,000 nm	100 – 500 nm	1 – 60 nm	500 – 1,600 nm
Host Range	Virus-specific by plant family (can be more; TMV infects 11 families)	Dicot and certain monocot species	Unrestricted*	Unrestricted*	Unrestricted*
Insert Size	<10 kbp	<150 kbp	Unrestricted*	Unrestricted*	<25 kbp*
Level of Expertise	Low	Medium	Medium	Low	Low
Equipment Requirements	Low	Medium	Low	Low	Medium

*Based on limited research data available; potential limitations may be uncovered with further investigation.

Transgenic production is the simplest form of molecular pharming. Pharmaceutical production capability hardwired into the genome of the plant through either nuclear or plastid engineering[239]. No additional manufacturing resources beyond those used for plants as a traditional bioregenerative life support object are needed, except an induction agent (e.g., heat, ethanol) for inducible promoter-controlled transgenics[240]. This allows for simple and sustained production of pre-determined molecular target(s) for which a consistent demand is anticipated. Transgenic plants for medical countermeasure production will most likely be distinct resources from food crops

unless strategies such as inducible promoters or tissue-specific expression (e.g., pharmaceuticals produced only in inedible biomass) are employed.

Combined, transient and transgenic production systems have the potential to cover the breadth of pharmaceutical production needs for deep space missions. Anticipated human health-impacting exposures in deep space missions include intermittent and persistent modes, within which both acute and chronic disease states are possible.

Chronic disease states needing a constant supply of medical countermeasures are most likely best addressed by using the simpler manufacturing of transgenic production. Transient production is also a viable strategy for meeting the medical needs of chronic disease states; it often yields higher specific productivity on a product per biomass basis[241]. However, the higher resource demand of production and concerns of long-term pharmaceutical stability (if stockpiles were generated using transient production) raise potential disadvantages in transient production for chronic disease states, such as microgravity-induced osteopenia.

For acute disease states above a certain risk level, defined by both likelihood of occurrence and severity of mission impact, it may be valuable to generate transgenic plants to produce countermeasures. On the other hand, transient production may be a more cost-effective strategy for reducing mission risk associated with lower risk, and unanticipated, disease states. Here we reiterate that providing medical countermeasures for unanticipated disease states should not be underestimated.

The delineation of best use cases for transgenic and transient production system selection depends on mission architecture and the specific resource availability. The decision tree shown in Figure

7.4 provides a foundational logic framework for evaluating and selecting an appropriate molecular pharming production system on a situational basis.

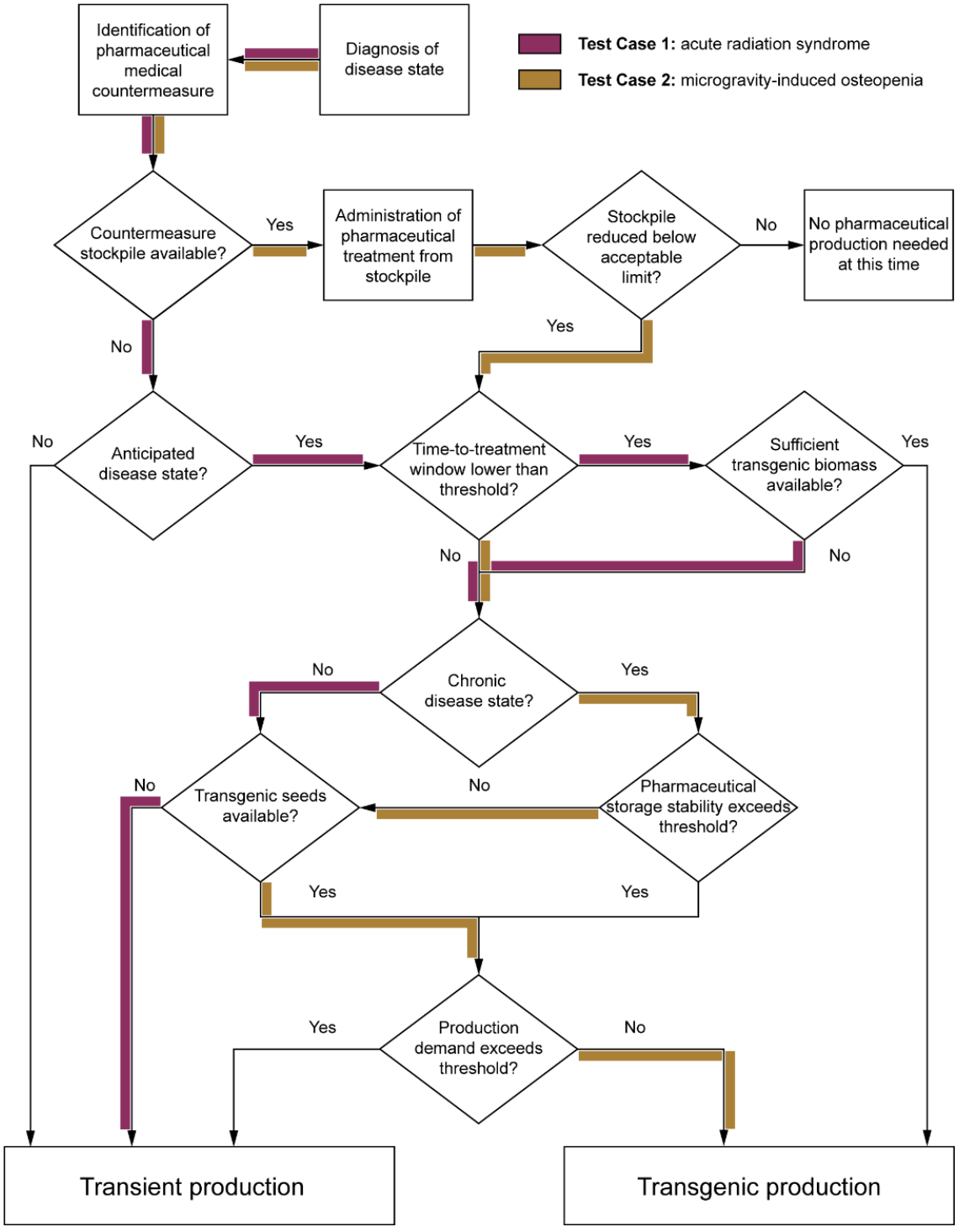

Figure 7.4. A decision tree for selecting a molecular pharming production strategy. This assumes that transient production is a more cost-efficient strategy above some threshold pharmaceutical demand, which is driven by the notion that transient production tends to yield higher product accumulation. This threshold depends on mission architecture, available resources, and the impact of the disease state to mission outcome. Two test cases of hypothetical disease state diagnoses are included; supporting information for the test cases are included in Supplementary Information.

7.4.2. A Test Case for Molecular Pharming in Space

Consider a deep space exploration mission in which plants are grown for their previously established utilities and a crew of six astronauts subsists on a diet supplemented with a single serving, 100 g fresh weight (FW), of lettuce or potato per crew member per day. The primary purpose for growing this single serving of plant-based food per day on an extended space mission is to meet the Food and Nutrition Board of the Institute of Medicine's Recommended Dietary Allowance (RDA) of nutrient. The current stated shelf life of pre-packaged space food is only 18 months[242], and degradation of key nutrients such as thiamine (vitamin B1) is well documented[243–245]. Just as when sailors suffered the effects of missing vitamin C on long sea voyages, it will be critical to avoid vitamin deficiencies as we explore deep space. Figure 7.5a and b shows the macronutrient and labile vitamin contributions of the daily single serving of lettuce or potato as a percentage of recommended dietary allowance. A supplement selected from a variety of food crops would be most effective to meet the RDA, as well as to minimize menu fatigue[246].

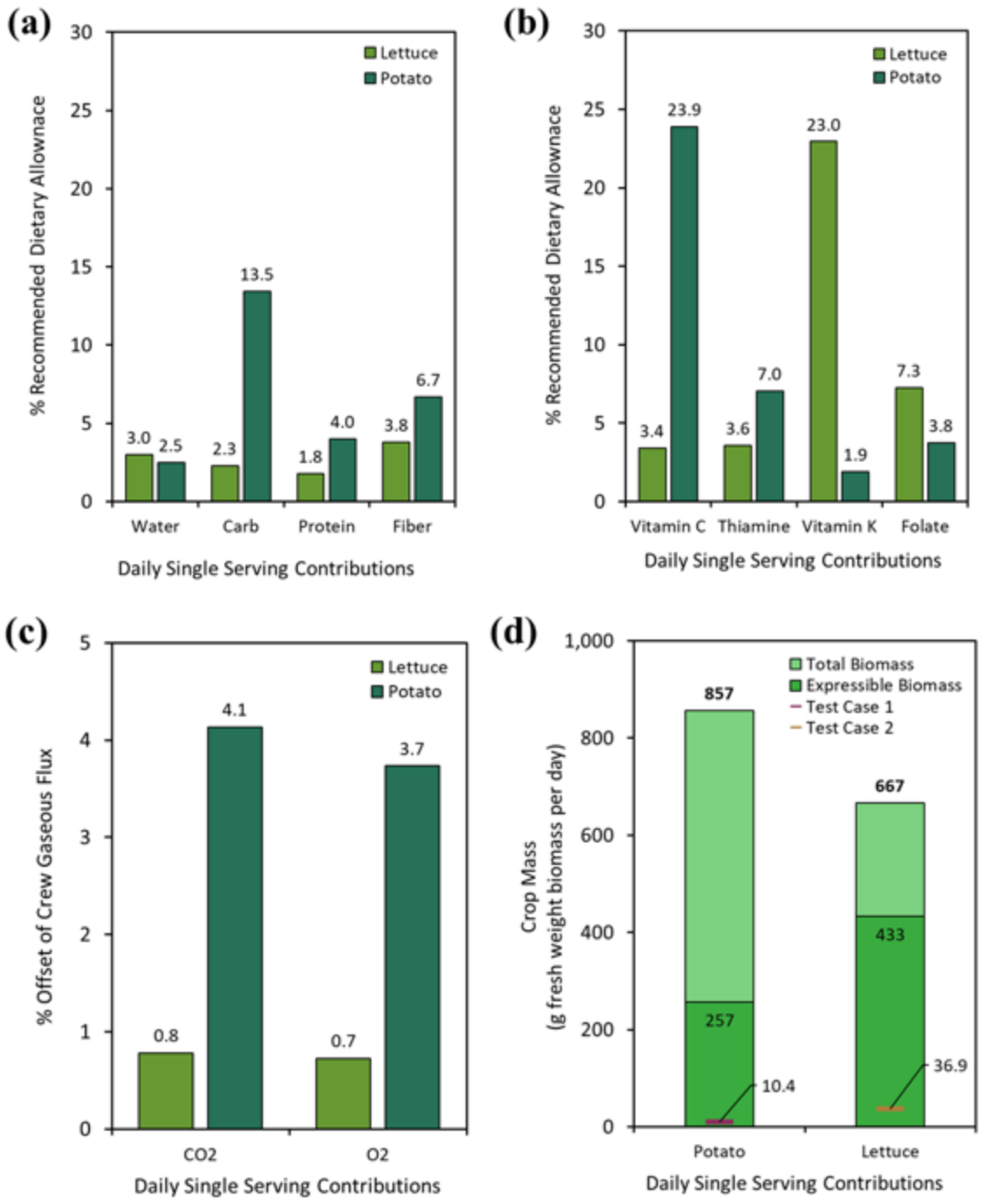

Figure 7.5. Cultivating a daily single serving (100 g fresh weight) of crop, either lettuce or potato, to supplement an astronaut's diet. Contributions of the daily single serving to Recommended Dietary Allowance are shown for select (a) macronutrients and (b) labile vitamins. (c) The biomass for a daily single serving supports air revitalization by partially offsetting human gaseous metabolic flux. (d) The biomass for a daily single serving could be more than sufficient for molecular pharming production of pharmaceutical-based medical countermeasures, as illustrated by crop mass requirements of Test Case 1 (granulocyte stimulating colony factor, 1 dose, produced in potato) and Test Case 2 (parathyroid hormone residue 1-34, 6 doses, produced in lettuce).

Growing a daily single serving supplement of plant-based food is estimated to occupy 4.6 and 5.7 m^2 of cultivation area for lettuce and potato, respectively. This considers the plant inventory needed for sustained production of a single serving per day. The actual cultivation footprint is expected to be significantly smaller than the cultivation area, as hydroponic cultivation is typically done with multi-layered growth stages. The plant cultivation calculations were performed according to values listed in NASA's Baseline Values and Assumptions Document[247]. Supporting information for the assumptions and calculations can be found in Supplementary Information (S7.2. Supplementary Tables).

In addition to supplying nutrients, this single serving will assist in other aspects of life support. Plant growth assists in air revitalization, offsetting crew carbon dioxide and oxygen flux by ~1% (lettuce) and ~4% (potato) (Figure 7.5c). It also serves to revitalize water as 9.7 (lettuce) and 22.8 (potato) liters per day of clean water are released in gaseous form via transpiration, most of which can be recycled for crop cultivation unless needed in other operations, such as for pharmaceutical formulation. These simple calculations highlight the auxiliary value of plants for bioregenerative life support.

The contributions to all aspects of life support depend highly on the crop species and cultivation environment. For example, a previous study using a closed human/plant system has shown experimentally that 11.2 m^2 of wheat grown at high light intensity (1,500 µmol m^{-2} s^{-1}) supplies sufficient oxygen for one person[248]. Wheat is one of the most productive crops for oxygen production, which is amplified by the high light intensity used and its tolerance of a 24-hour light

cycle. This crop cultivation strategy has been demonstrated to provide ~13 times more oxygen than lettuce and ~3 times more than potato. In addition to traditional life support metrics like oxygen productivity, crop selection for molecular pharming must also take into account factors such as efficiency of transformation (e.g., wheat is difficult to transform and generally yields low product accumulation[249]) and characteristics of the host cell protein compared to the product target.

Now we look at two test cases in which the biomass generated for this daily single serving can be applied to molecular pharming for manufacturing of pharmaceutical countermeasures:

> Test Case 1: Transient production of one dose of granulocyte stimulating factor (G-CSF) from 42 g FW of potato leaves per crew member (this is equivalent to leaf mass concomitant with a single serving of potato tuber) purified as an injectable countermeasure to acute radiation syndrome, representative of an acute disease state.
>
> Test Case 2: Transgenic production of a single dose per crew member (six doses total) of parathyroid hormone residue 1-34 (PTH) from 100 g FW lettuce leaves per crew member (this is equivalent to leaf mass less than a single serving of lettuce) purified as an injectable countermeasure to microgravity-induced osteopenia, representative of a chronic disease state.

Table 7.2 summarizes the key assumptions that were built into the two test cases. The logic for selection of the production method is shown in Figure 7.4 and further described in Supplementary Information (S7.1.1 Decision Tree Walkthrough).

Table 7.2. A list of assumptions used in the molecular pharming test case calculations. BLA, biologics license application. NDA, new drug application.

	Test Case 1	**Test Case 2**
Disease State	Acute radiation syndrome (acute disease)	Microgravity-induced osteopenia (chronic disease)
Countermeasure	Granulocyte stimulating factor	Parathyroid hormone residue 1-34
FDA-Approved Product	NEUPOGEN® (filgrastim) BLA: 103353	FORTEO® (teriparatide) NDA: 021318
Medication Demand	300 µg (1 doses; 300 µg/dose)	120 µg (6 doses; 20 µg/dose)
Production Method	Transient production in potato leaves	Transgenic production in lettuce leaves
Expression Level*	250 µg drug/g potato leaf fresh weight	10 µg drug/g lettuce leaf fresh weight
Expressible Biomass	23% total biomass fresh weight	65% total biomass fresh weight
Drug Delivery	Intravenous injection (50% drug loss in purification processes)	Intravenous injection (50% drug loss in purification processes)

*Conservative estimates based on molecular pharming expression levels widely reported in literature. The estimates also reflect the general trend of lower expression levels in transgenic production as compared to transient expression.

From the perspective of molecular pharming, lettuce[250,251] serves as a fast-growing crop with a small cultivation footprint in which the edible biomass is also the expressible biomass capable of producing pharmaceuticals. Potato[252,253] represents a slow-growing crop that has the advantage of distinct edible biomass (tubers) and expressible biomass (leaves); molecular pharming would not significantly impact the total available food resource. Leaves detached from the intact plant are capable of providing comparable pharmaceutical yield to those from the intact plant[251,254,255]. Production of pharmaceuticals in inedible biomass is one way to create physical separation of the food and pharmaceutical streams while maintaining resource flexibility. However, there are

situations in which it may be advantageous for merged food and pharmaceutical streams; there are reports in literature on oral delivery of pharmaceuticals in both lettuce and potato tuber[256–258]. While promising, this technology is still in early stages of development.

As shown in Figure 7.5d, only 10.4 g FW (1.2% of the total crop biomass FW, 4.0% expressible biomass FW, 1.7% food resource biomass FW) is needed for the Test Case 1 acute disease state countermeasure in potato, while 36.9 g FW (5.5% of total crop biomass FW, 8.5% expressible biomass FW, 5.8% food resource biomass FW) is needed for the Test Case 2 chronic disease state countermeasure in lettuce. While these test cases are driven by conservative assumptions of performance well-established in literature, it is important to note that biomass requirements are highly dependent on the rate of pharmaceutical accumulation (i.e., expression level), medication dose size, and drug delivery modality. Figure 7.6a illustrates how the total crop biomass demand differs between the two test cases based on the medication demand (dose size and number of doses) and over a range of conservatively estimated molecular pharming expression levels, while Figure 7.6b shows how the biomass requirements demands depend on drug delivery modality.

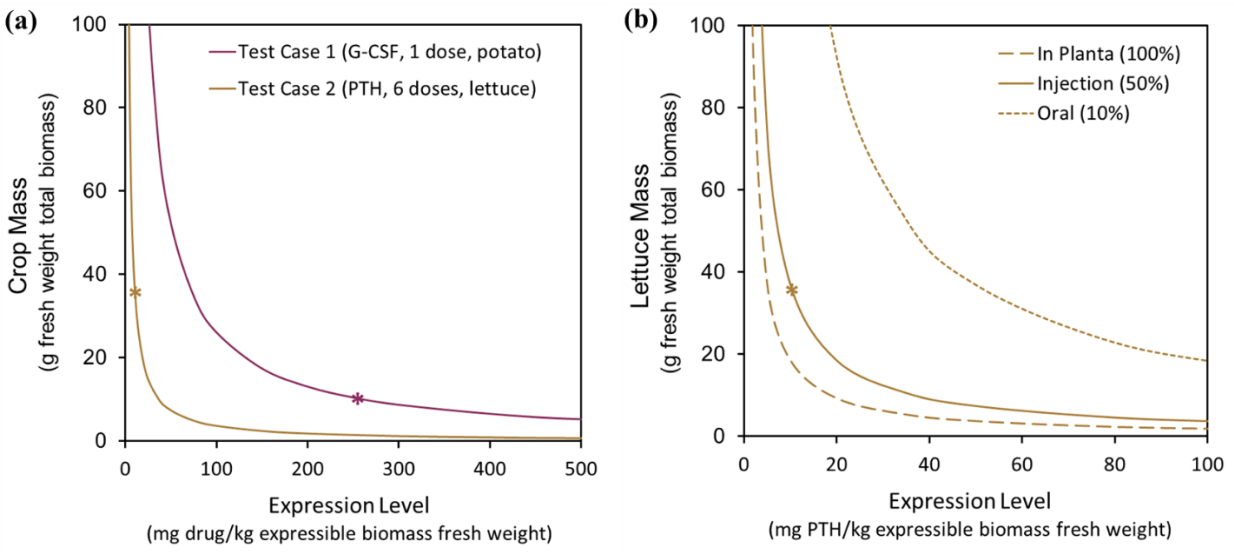

Figure 7.6. Plant cultivation requirements for molecular pharming are largely controlled by the product expression level, medication dosage, and medication delivery modality. (a) Test Case 1 and Test Case 2 sensitivity of crop mass demands to variation in pharmaceutical expression level. (b) Test Case 2 sensitivity of lettuce mass demands to selection of drug delivery modality, which we are representing as an approximated % availability of the produced drug. * signifies the expression level assumed in the test cases. G-CSF, granulocyte colony stimulating factor; PTH, parathyroid hormone residue 1-34.

7.5. Comparing Molecular Medical Foundries for Space

Since the founding of modern biotechnology with Cohen and Boyer's discovery of recombinant DNA technology in 1973[259], biological organisms have risen to prominence as the primary means for producing high-value pharmaceutical proteins and other products, most of which are too complex to be economically and sustainably produced using current chemical synthesis approaches. In the half-century since inception of recombinant DNA technology, a plethora of biological platforms have been engineered as factories of recombinant products – microbial culture, eukaryotic (mammalian, insect, yeast, plant) cell culture, live animals, cell lysates, and whole plants. Table 7.3 shows a comparison of current pharmaceutical production platforms based on attributes relevant to their deployment for human health in space. Details of the category

definition and system rankings are included in Supplementary Information (S7.1.2 Supporting Production Platform Comparisons). There are also new platforms on the horizon for production (e.g. microbiome engineering[260], gene therapy[261]) and drug delivery (e.g. microneedle-based transdermal[262]).

Table 7.3. A comparison of key characteristics for space exploration of biological platforms for pharmaceutical production.

System		In-Situ Resource Utilization	Just-In-Time Response	Operational Simplicity	Product Range	Crew & Planetary Safety
Bioreactor systems	Insect cell	★☆☆☆☆	★★☆☆☆	★★☆☆☆	★★★☆☆	★★☆☆☆
	Mammalian cell	★☆☆☆☆	★★☆☆☆	★★☆☆☆	★★★★★	★★☆☆☆
	Plant cell	★★★☆☆	★★☆☆☆	★★☆☆☆	★★★★☆	★★★★☆
	Bacteria, autotrophic	★★★★☆	★★★☆☆	★★★☆☆	★☆☆☆☆	★★★☆☆
	Bacteria, heterotrophic	★★☆☆☆	★★★☆☆	★★☆☆☆	★☆☆☆☆	★★☆☆☆
	Yeast	★☆☆☆☆	★★★☆☆	★★☆☆☆	★★★☆☆	★★★★☆
	Cell-free expression	★☆☆☆☆	★★★★☆	★★★☆☆	★★★☆☆	★★★☆☆
Non-bioreactor systems	Transgenic animals	★☆☆☆☆	★☆☆☆☆	★☆☆☆☆	★★★★★	★★★☆☆
	Transgenic plants	★★★★★	★★☆☆☆	★★★★★	★★★★☆	★★★★★
	Transient plants	★★★★☆	★★★★☆	★★★★☆	★★★★☆	★★★★☆

Commercial biopharmaceutical manufacturing on Earth is dominated by microbial fermentation and mammalian cell culture. Spread across over 1,700 production facilities globally, there is a commercial production capacity of 4.8 million liters for microbial fermentation and 15.0 million liters mammalian cell culture (online database; http://top1000bio.com/). Regulatory pathways have been well established, decades of intensive research have seen orders of magnitude increase

in productivity, and billions of dollars have been poured into developing culture-based system infrastructure.

However, this established dominance of culture-based systems does not easily translate into implementation for human health in space for several reasons. The most glaring difficulty is with cell culture behavior, both with the cell biology[263] and fluid dynamics[264], in altered gravity; operation will need to be compatible with microgravity for in-flight production and reduced gravity for a Moon or Mars mission. There is a growing body of literature on development of bioreactors with alternative containment and mixing for microgravity[265–267]. The main existing technical difficulties of culture-based systems in limited resource environments are the expensive and complex equipment requirements and the need for aseptic operation for growing the production host cells. Microbial fermenters and cell culture bioreactors are made of glass and/or a special grade (316L) stainless steel for durability and corrosion resistance[125]. Bioreactors are generally designed with a suite of capabilities, including culture agitation, aeration, sampling, in-line sensing, feedback control systems (for pH, temperature, dissolved oxygen, foaming), cleaning, and sterilization. This complex process equipment lowers general accessibility and increases workforce specialization of operators, which in turn forms another barrier to application in limited resource environments.

The equipment burden of culture-based systems is largely a result of the need to maintain a sterile cultivation environment during operation. Without adequate environmental protection, cultures are susceptible to contamination by undesired organisms. Compromised sterility of processing can lead to significant product and patient impact[268–270].

In addition to complexity, stainless steel bioreactors impose significant mass and volume penalties that might prohibit adoption in a space mission. For example, a typical glass and stainless steel

stirred tank reactor for 1L working volume (HyPerforma Glass Bioreactors, ThermoFisher Scientific) of culture weighs 3.7 kg, not including liquid culture mass and auxiliary reactor components (e.g., probes, spargers, agitator, heating jacket).

A growing trend in culture-based systems is to employ single-use technology for cost-savings in cleaning validation, capital costs, and time[271]. Single-use technology for culture-based systems typically consists of a multi-layered plastic bag used in lieu of, or with support of, a stainless steel vessel. Of specific importance to space missions, these savings could also translate into significant reductions in mass and volume requirements. However, as the name "single-use" states, these plastic bioreactor housings are only used once, introducing significant consumable and waste streams to the pharmaceutical foundry. Therefore, single-use technology may introduce reliance on a stable supply chain for consumables that could strain feasibility in a limited resource environment. The use of recyclable materials (e.g., biopolymers) for single-use technology has not been commercially implemented but would serve to alleviate these concerns. The hindrance of consumable waste is offset by reduced cleaning requirements and should be evaluated within a mission architecture. For example, if pharmaceutical production is projected to be below a threshold capacity, then the extra consumables required to be flown may be acceptable.

Exceptional to the typical culture-based system vulnerabilities, microbial, oxygenic photoautotrophic cultures (i.e., microalgae[272,273] and cyanobacteria[274,275]) represent a promising subset of culture-based systems that may be better equipped for supporting human life in space. They share many of the same benefits of molecular pharming; these organisms are able to use available *in situ* resources (i.e., light and CO_2) as feedstocks, and some have been shown to be quite tolerant to a range of water qualities (e.g., polluted water)[276]. Additionally, some of these species have unique advantageous characteristics: they can serve as a food resource, grow under

conditions that minimize probability of contamination, and even be used as biofertilizer to improve soil quality and crop productivity[277–279].

A subset of these organisms, including the microalgal species *Chlamydomonas reinhardtii* and *Chlorella vulgaris*, and the cyanobacterial species *Arthrospira platensis* (commonly sold under the name spirulina), is categorized by the U.S. Food and Drug Administration as being Generally Recognized as Safe (GRAS), whereby these organisms are considered edible and are sold commercially as food and nutritional supplements[279,280]. The edible nature of these organisms presents a potential boon to pharmaceutical foundries in space in that if the target production molecules are bioavailable through simply eating the wet or dry biomass of the production host, no downstream purification is needed.

The microbial nature of these organisms provides potential advantages to plant systems. First, microalgae (in particular *C. reinhardtii*) and cyanobacteria have genetic tools that are typically more advanced than those of plants[280–282]. Although tools for engineering *A. platensis* have been reported[283], engineering this organism has remained a challenge in the field. To this end, we have recently developed a genetic toolkit for creating stable mutants of *A. platensis* (Hilzinger, Arkin, *et al.* Unpublished) that will help unlock this organism for metabolic engineering goals. Second, these organisms have faster growth rates than plants, which enable shorter times to reach the biomass necessary for molecular harvesting. Third, the larger metabolic diversity of microalgae and cyanobacteria compared to plants could help to metabolically engineer target molecules that are difficult or impossible to produce in plants using current technologies[280].

Therefore, these organisms may be well suited for pharmaceutical production, or for enhancing nutritional load through vitamin supplementation. Thus, GRAS-status microbial oxygenic photoautotrophs are poised to become edible molecular pharming hosts for space missions. As these technologies continue to mature, a detailed techno-economic comparison between plants, microalgae, and cyanobacteria will be needed.

It may be that a robust pharmaceutical foundry for space ends up being less about selecting one system and more about selecting a network of systems. It is important that interconnectivity and synergy of different platforms be considered for biological-based production of pharmaceuticals and other high-value products to support human life (e.g., biomaterials).

A main distinguishing feature of whole plants as a pharmaceutical production platform is the freedom from complex equipment housing during operation; the supracellular structure of a plant serves as its own natural "bioreactor" for operational control (e.g., nutrient distribution) and protection against contamination. This effectively means that molecular pharming can be employed with lower complexity process control systems and equipment. Figure 7.7a and b illustrate the simplicity and linear scalability of producing pharmaceuticals in whole plants as compared to culture-based systems. However, an equivalent system mass (ESM) comparison of molecular pharming and culture-based systems for spaceflight is needed to rigorously evaluate the perceived advantage of molecular pharming simplicity.

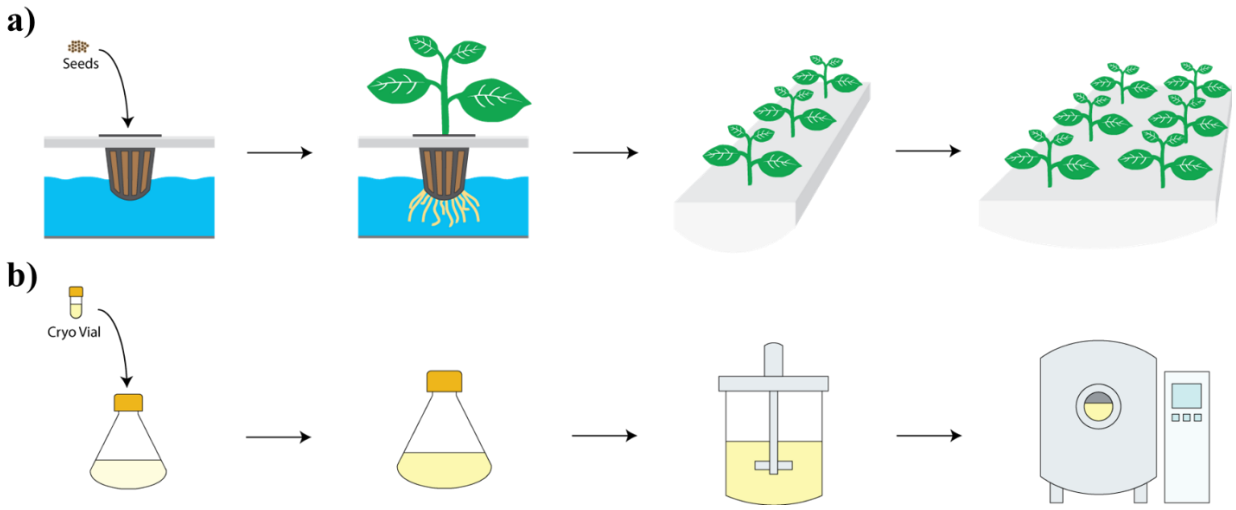

Figure 7.7. An illustration of the upstream manufacturing processes required for (a) whole plant molecular pharming, and (b) cell culture or fermentation-based biopharmaceutical production. Whole plant molecular pharming uses hydroponic or soil-based plant growth receptacles that scale linearly with demand, whereas cell culture and fermentation-based manufacturing use a series of bioreactors whose geometries are dependent on scale.

This self-regulating behavior also suggests that plants may serve as a more robust production platform with higher tolerance to input quality variation for a given output product quality. In literature, the strength of molecular pharming production tolerance as compared to culture-based systems is yet unproven, but would be a valuable avenue of research to directly investigate.

7.6. The Future of Plant-Based Foundries in Space

For decades, plants have been identified as important life support objects for human health in space. Here we have presented the need for an Earth-independent pharmaceutical life support system and identified molecular pharming as a strategy to tap into the power of plants to serve as a pharmaceutical (and other high-value product) foundry to meet that need. Molecular pharming in space has the potential to provide manufacturing capacity to respond to both acute and chronic

disease states in space with a relatively small amount of plant biomass. Selecting the set of the most appropriate molecular pharming-based production strategies should be done within a reference mission architecture, which considers key attributes that we have laid out.

There are many ways to envision pharmaceutical foundries for interplanetary use. Chemical synthesis is limited in production targets and in reagent supply but may be necessary when biology is not sufficient or capable (e.g., nucleic acid synthesis). Translating culture-based systems from Earth to space utility faces challenges of cell biology, fluid dynamics, feedstock sustainability, mass/volume penalties, and crew training. Their relatively high productivity may position them as an effective platform for settlement missions to sustain larger populations. Autotrophic cultures are exceptional solutions to several challenges of traditional culture-based systems and have more potential as a near-term platform.

More thorough investigation is needed to select an appropriate set of pharmaceutical foundries. Process mass intensity (PMI) is a metric recently adopted by the biopharmaceutical industry to measure the environmental footprint of production[63]. PMI is defined as the total mass in kg of raw material and consumable inputs to produce 1 kg of active pharmaceutical ingredient. PMI can serve as a useful reference point when performing ESM analyses of pharmaceutical foundries in space. ESM analyses are typically performed to evaluate and optimize space mission payloads to minimize launch cost (or mission objective success) as a function of mass, volume, power, cooling, and crew time needs [284]. Pharmaceutical foundry considerations will also need to include medical risk and patient outcomes. NASA's exploration medical system trade study tools, which includes a systems engineering model and a medical risk analysis model, have the potential to serve as a foundation for this analysis[285].

There are many obstacles ahead before making pharmaceutical foundries in space a reality.

What has not been thoroughly discussed in this review is the downstream processing of a molecular medical foundry, which will depend on the purity needed for the pharmaceutical formulation, delivery method, production host, etc. Downstream processing, the purification of the target molecule from the production host, is a resource-intensive aspect of biopharmaceutical production across all platforms. There is a lack of downstream processing technology that translates well from Earth-based constraints to those of space, such as a high quantity of consumables, raw materials, equipment, and cleaning costs. This bottleneck will need to be addressed for pharmaceutical foundries in space to succeed. One approach is to conduct research on novel drug delivery modalities (e.g., plant-encapsulated oral administration[286]) to reduce the need for downstream processing, and another is to diminish the resource demands of the processing itself (e.g., bioregenerative and recyclable processing reagents). A growing emphasis on distributed and just-in-time pharmaceutical production for healthcare on Earth is already driving solutions to these downstream challenges[287].

The other major hurdle is in regulatory compliance. Production and administration of pharmaceuticals in space will require extensive quality control; manufacturing a small molecule might have 50 critical tests, while manufacturing a biologic may have over 250[288]. Here, the advent of personalized medicine on Earth will illuminate a path forward. The shift from mass produced to individualized patient-specific medicine hinges on re-structuring the path to regulatory approval and quality control[289].

While there are many challenges ahead that need to be addressed to pave the way for Earth-independent life support, the rewards of this pursuit will include great insights into supporting life on Earth and beyond. Understanding this value, we aim to highlight the critical importance (and long lead time) of developing Earth-independent systems in the future of human exploration. We

illustrate that molecular pharming provides a diverse production toolset that could be used to establish a robust molecular medical foundry subsisting on a small fraction of food crop needs. In addition to advocating for molecular pharming as a synergistic asset of space life support systems, we focus on the need for multi-faceted utilization of resources in limited environments like space and extraterrestrial bodies.

7.7. Supplementary information

7.7.1. S7.1 Supplementary Text

7.7.1.1. S7.1.1 Decision Tree Walkthrough

The decision tree for selecting a molecular farming production strategy is applied to two different test cases of a diagnosed disease state where a pharmaceutical medical countermeasure has been identified as appropriate. The decision tree does not consider alternative or auxiliary non-pharmaceutical countermeasures. As this is the first decision tree to operationalize a molecular medical foundry for space, we chose to develop this first iteration in isolation from other medical systems and aspects of mission architecture. The following is a description of the assumptions and logic applied to navigate the two hypothetical test cases to an appropriate molecular pharming production strategy.

7.7.1.1.1. S7.1.1.1 Test Case 1: acute radiation syndrome

Acute radiation syndrome is selected as a test case based on NASA's evidence report for risk of acute radiation syndromes due to solar particle events[290]. Here we detail our introduction of the disease state and subsequently detail the progression of the medical response and decision making that ultimately results in transient production of filgrastim in potato leaves, as described in the main text body.

Introduction of disease state

We assume that one crew member develops acute radiation syndrome after receiving a whole body dose of 3.25 Gy ionizing radiation, as recorded by an on-person physical dosimeter, from a major solar particle event (SPE) during extravehicular activity (EVA) outside of low-Earth orbit, where

the protective magnetosphere of Earth is absent. The expected frequency of SPEs is highly dependent on the solar cycle, but individual SPEs are not able to be predicted.

Diagnosis of disease state

The illness primarily presents in the hematopoietic syndrome and is diagnosed by a combination of physical dosimeter readings (on the crew member at the time of exposure), clinical manifestations of nausea, vomiting, and fatigue, and a blood test indicating a neutrophil count decreased to less than 1.5×10^9 per liter of blood (neutropenia).

Identification of pharmaceutical medical countermeasure

The crew physician prescribes the radiation mitigator, filgrastim (NEUPOGEN®, Amgen) to increase circulating neutrophil levels to override the myelosuppressive doses of radiation.

Countermeasure stockpile available?

There is not a countermeasure stockpile of filgrastim (or an effective alternative radioprotectant/mitigator) available, which could be a result of a multitude of root causes (e.g. use-based depletion of medication, spaceflight-induced accelerated drug expiry).

Anticipated disease state?

Acute radiation syndrome is an anticipated disease state, based on the established body of literature on the matter[291].

Time-to-treatment window lower than threshold?

At a dose of 3.25 Gy, there is a 50% mortality rate within 60 days barring appropriate medical intervention[292]. Cause of death is generally due to complications arising from extensive hematopoietic damage. The time-to-treatment threshold in this decision tree is not strictly defined due to the influence of a given reference mission architecture on this value. However, the threshold will be largely based on the response time of transgenic plant production, which would likely be >3 weeks. The time-to-treatment in this test case will have a significant impact on patient outcome, and thus impact mission success through impaired crew member capability, and so is high priority is assigned here to minimize time-to-treatment.

Sufficient transgenic biomass available?

Filgrastim-producing transgenic seeds are not flown as part of the mission, and thus there is not sufficient transgenic biomass available.

Chronic disease state?

Acute radiation syndrome is an acute disease state.

Transgenic seed available?

Filgrastim-producing transgenic seeds are not flown as part of the mission.

7.7.1.1.2. S7.1.1.2 Test Case 2: microgravity-induced osteopenia

Microgravity-induced osteopenia is selected as a test case based on NASA's evidence report for risk of early onset osteoporosis due to space flight[293]. Here we detail our introduction of the disease state and subsequently detail the progression of the medical response and decision making that ultimately results in transgenic production of teriparatide in lettuce leaves, as described in the main text body.

Introduction of disease state

Microgravity-induced osteopenia is established as a chronic disease state that cannot be completely mitigated through exercise- or nutrition-based countermeasures (e.g., the Advanced Resistive Exercise Device used on the International Space Station) and affects all six crew members. Throughout spaceflight and reduced gravity conditions the crew will experience areal bone mineral density (aBMD) T-scores between -1 and -2.5 (classified as osteopenia by the World Health Organization) but may also report T-scores < -2.5 (classified as osteoporosis). These lower aBMD scores will increase fracture risk.

Diagnosis of disease state

Enabling surveillance technology for real-time tracking of space flight-induced bone loss is currently a gap. There will be technological advances that fill this gap. The disease state will be diagnosed through routine monitoring and will additionally present in fragility fractures, most likely during strenuous EVA.

Identification of pharmaceutical medical countermeasure

Reports show that spaceflight suppresses circulatory levels of parathyroid hormone (PTH), which in turn suppresses calcium absorption in the intestines and kidney[294]. The crew physician prescribes teriparatide (FORTEO®, Eli Lily and Company), which is recombinant human PTH residues 1-34, to treat severe bone loss and to facilitate fracture healing.

Countermeasure stockpile available?

There is an available stockpile of teriparatide based on the known risk of spaceflight-induced bone loss.

Stockpile reduced below acceptable limit?

The administration of teriparatide from the stockpile has reduced the available drug quantity to below the acceptable limit. As this disease state is expected to be both highly likely and highly impactful to chances of mission success, the crew will produce additional teriparatide to replenish the stockpile.

Time-to-treatment window lower than threshold?

The time-to-treatment window is not lower than the threshold. The purpose of production is to replenish the drug stockpile for future use.

Chronic disease state?

Microgravity-induced osteopenia is a chronic disease state.

Pharmaceutical storage stability exceeds threshold?

As mentioned in the main body of the manuscript, stability of biologics in spaceflight is completely untested. We do know that biologics are generally less stable than small molecule drugs, which have been shown, in limited capacity, to experience spaceflight-accelerated degradation. We assume that the stability of teriparatide does not exceed the threshold, which we anticipate would be a complex and transient value in practice.

Transgenic seeds available?

Teriparatide-producing transgenic seeds are flown as part of the mission.

Production demand exceeds threshold?

The production demand for replenishment of the teriparatide stockpile does not exceed the threshold. This is consistent with the assumption that storage stability does not exceed the

threshold; a less stable pharmaceutical will need to be produced in smaller quantities and higher frequency to serve as an effective countermeasure to a chronic disease state.

7.7.1.2. S7.1.2 Supporting Production Platform Comparisons

7.7.1.2.1. S7.1.2.1 Defining Space Exploration Characteristics

The following are definitions of the pharmaceutical production characteristics used to rank the various biological platforms for space exploration utility:

In-Situ Resource Utilization

> The capacity of the production platform to make use of resources expected to be available on a space exploration mission to an extraterrestrial planetary body. These resources include sunlight, atmospheric gases, water, and regolith.

Just-In-Time Response

> The capacity of the production platform to produce pharmaceuticals in a rapid response manner, whether it be in counteraction to an anticipated or unforeseen threat. This considers the speed of production for scenarios when the gene delivery system, or capable transgenic organism, is ready at hand and also when the gene delivery system or organism must be engineered mid-mission.

Operational Simplicity

A combination of the equipment complexity and the workforce specialization required to manufacture pharmaceuticals using the production platform. This considers control systems, robustness of operation (including multiple states of input material quality and altered gravity), ability to scale-up production as much as for early settlement missions, and specific productivity (production of a given amount of pharmaceutical per unit volume production system per unit time).

Product Range

The capacity of the production platform to generally produce a range of pharmaceutical product (from small molecule to simple peptide to secretory antibodies). The major consideration in this category is glycosylation, an essential post-translational modification where sugar moieties are attached to a therapeutic protein. Ability of the production platform to produce generally cytotoxic pharmaceutical products is also considered.

Crew & Planetary Safety

The likelihood of the production platform contamination and release and the impact on crew safety and planetary protection.

7.7.1.2.2. S7.1.2.2 Key Production Platform Resources

Here we include relevant resources which, used in conjunction with working process knowledge, were used to rank each generalized biological platform for pharmaceutical production in space exploration – insect cell[295–297], mammalian cell[298–300], plant cell[134,301,302], autotrophic bacteria[303–305], heterotrophic bacteria[306–308], yeast[309–311], cell-free expression[312–314], transgenic animal[315–317], transgenic plant[95,318,319], and transient plant[320–322].

7.7.2. S7.2. Supplementary Tables

The following tables contain the information used in the crop cultivation calculations and graphical representations for “A Test Case for Molecular Pharming in Space.”

7.7.2.1. S7.2.1 Crop Characteristics

Crop characteristics and requirements for lettuce and potato compiled from NASA's Baseline Values and Assumptions Document 2018[247]. DW, dry weight. FW, fresh weight.

Parameter		Units	Lettuce	White Potato
Harvest Index		%	90	70
Edible Biomass Productivity	Dry Basis	g DW/m^2/day	6.57	21.06
	Fresh Basis	g FW/m^2/day	131.35	105.3
	Fresh Basis Water Content	%/100	0.95	0.8
Inedible Biomass Productivity	Dry Basis	g DW/m^2/day	0.73	9.03
	Fresh Basis	g FW/m^2/day	7.3	90.25
	Fresh Basis Water Content	%	0.9	0.9
Total Biomass (Edible + Inedible), Dry Basis	Nominal	g DW/m^2/day	7.3	30.08
	High	g DW/m^2/day	7.9	50
Carbon Content		%	40	41
Metabolic Reactants & Products	O_2 Production	g/m^2/day	7.78	32.23
	CO_2 Uptake	g/m^2/day	10.7	45.23
	H_2O Uptake	kg/m^2/day	2.1	4
Support Requirements	Water Use per Dry Biomass	L/g DW	0.34	0.15
	Stock Use per Dry Biomass	L/g DW	0.034	0.022
	Acid Use per Dry Biomass	g acid/g DW	0.0618	0.0428
Light Requirements	Photosynthetic Photon Flux	mol/m^2/day	17	28
	Diurnal Photoperiod	hr/day	16	12
Growth Period		days	28	132
Nominal Planting Density		plants/m^2	19.2	6.4
Nominal Biomass per Plant at Harvest		g DW/plant	10.6	620.4

7.7.2.2. S7.2.2 Recommended Dietary Allowances

Recommended dietary allowances and adequate intakes for key macro- and micronutrients, as described by the Food and Nutrition Board of the Institute of Medicine, National Academy of Sciences[323].

Nutrient		Male (31-50 years)	Female (31-50 years)	Average
Macronutrient	Water (g)	3.7	2.7	3.2
	Carbohydrate (g)	130	130	130
	Protein (g)	56	46	51
	Fiber (g)	38	25	31.5
Micronutrient	Vitamin C (mg)	90	75	82.5
	Thiamine (mg)	1.2	1.1	1.15
	Vitamin K (µg)	120	90	105
	Folate (µg)	400	400	400

7.7.2.3. S7.2.3 Crop Nutrition

Average nutritional intake from a single serving (100 g FW) of lettuce and potato for key macro- and micronutrients, as described by the U.S. Department of Agriculture in the FoodData Central database[324].

Nutrient		Lettuce (lettuce, raw)	Potato (flesh and skin, raw)
Macronutrient	Water (g)	95.64	79.25
	Carbohydrate (g)	2.97	17.49
	Protein (g)	0.9	2.05
	Fiber (g)	1.2	2.1
Micronutrient	Vitamin C (mg)	2.8	19.7
	Thiamine (mg)	0.041	0.081
	Vitamin K (µg)	24.1	2
	Folate (µg)	29	15

Chapter 8. Evaluating the cost of pharmaceutical purification for a long-duration space exploration medical foundry

"…it will not be the engineering problems but rather the limits of the human frame that will make the final decision as to whether manned space flight will eventually become a reality."

-Wernher von Braun, 1951

This chapter is based on the following publication:

McNulty M.J., Berliner A.J., Negulescu P.G., McKee L., Hart O., Yates K., Arkin A.P., Nandi S., and McDonald K.A. (2021) Evaluating the Cost of Pharmaceutical Purification for a Long-Duration Space Exploration Medical Foundry. *Front Microbiol.* 0:3056. doi:10.3389/FMICB.2021.700863

Abstract

There are medical treatment vulnerabilities in longer-duration space missions present in the current International Space Station crew health care system with risks, arising from spaceflight-accelerated pharmaceutical degradation and resupply lag times. Bioregenerative life support systems may be a way to close this risk gap by leveraging *in situ* resource utilization (ISRU) to perform pharmaceutical synthesis and purification. Recent literature has begun to consider biological ISRU using microbes and plants as the basis for pharmaceutical life support

technologies. However, there has not yet been a rigorous analysis of the processing and quality systems required to implement biologically-produced pharmaceuticals for human medical treatment. In this work, we use the equivalent system mass (ESM) metric to evaluate pharmaceutical purification processing strategies for longer-duration space exploration missions. Monoclonal antibodies, representing a diverse therapeutic platform capable of treating multiple space-relevant disease states, were selected as the target products for this analysis. We investigate the ESM resource costs (mass, volume, power, cooling, and crew time) of an affinity-based capture step for monoclonal antibody purification as a test case within a manned Mars mission architecture. We compare six technologies (three biotic capture methods and three abiotic capture methods), optimize scheduling to minimize ESM for each technology, and perform scenario analysis to consider a range of input stream compositions and pharmaceutical demand. We also compare the base case ESM to scenarios of alternative mission configuration, equipment models, and technology reusability. Throughout the analyses, we identify key areas for development of pharmaceutical life support technology and improvement of the ESM framework for assessment of bioregenerative life support technologies.

8.1. Introduction

8.1.1. The need for a pharmaceutical foundry in space

Surveying missions to Mars, like the InSight lander[a325] launched in 2018 and Perseverance rover[b] in 2020, directly support the objectives of NASA's long-term Mars Exploration Program[c]: an effort to explore the potential for life on Mars and prepare for human exploration of Mars. The maturation of the program requires redefining the risks to human health as mission architectures transition from the current 'Earth Reliant' paradigm used on the International Space Station (ISS) to the cislunar space 'Proving Grounds' and finally to deep-space 'Earth Independent' mission architectures, as defined in NASA's report titled, "Journey to Mars: Pioneering Next Steps in Space Exploration"[d].

Human missions to Mars will be 'Earth Independent', meaning there will be very limited emergency evacuation and re-supply capabilities along with substantially delayed communications with the Earth-based mission team. The NASA Human Research Roadmap[e] currently rates most human health risks, which include 'risk of adverse health outcomes & decrements in performance due to inflight medical conditions' and 'risk of ineffective or toxic medications during long-duration exploration spaceflight', as either medium or high risk for a Mars planetary visit/habitat mission. Risk ratings are based on failure mode and effects analysis and on hazard analysis using dimensions of severity, occurrence, and detectability. A recent review highlights the current understanding of the primary hazards and health risks posed by deep space exploration as well as the six types of countermeasures: protective shielding, biological and environmental temporal

[a] https://mars.nasa.gov/insight/mission/overview/
[b] https://mars.nasa.gov/mars2020/mission/overview/
[c] https://mars.nasa.gov/
[d] http://go.nasa.gov/1VHDXxg
[e] https:// humanresearchroadmap.nasa.gov/Risks/

monitoring, specialized workout equipment, cognition and psychological evaluations, autonomous health support, and personalized medicine[326].

Of these countermeasures, it could be argued that medicine is the most crucial and least advanced towards mitigating space health hazards. There is very limited information on, and few direct studies of, pharmaceutical usage, stability, and therapeutic efficacy (i.e., pharmacokinetics, pharmacodynamics) in spaceflight or in a Mars surface environment[209]. Furthermore, flown stores of pharmaceuticals face two additional barriers: 1) radiation-accelerated degradation[327], and 2) addressing a myriad of low occurrence and high impact health hazards without the ability to fly and maintain potency of therapeutics for all of them. In these circumstances, it is often more beneficial to build robustness to these low occurrence health hazards rather than to try to predict them. It is therefore imperative that on-planet and/or in-flight pharmaceutical production be developed to bridge this risk gap. These pharmaceutical foundry technologies will supplement, not replace, the flown pharmaceutical formulary designed to treat anticipated medical threats during space missions.

Pharmaceuticals are produced either chemically or biologically. A recent review of pharmaceutical production for human life support in space compares these two methods, highlighting the need for biological production in order to address many low occurrence and high impact health hazards (e.g., sepsis, ear infection, glaucoma) and further comparing different biological production systems[328]. One major advantage of biological production is the efficiency in transporting and synthesizing genetic information as the set of instructions, or sometimes the product itself, to meet the therapeutic needs for a variety of disease states. The emerging field of Space Systems Bioengineering[329] encapsulates this need for biological production, of which pharmaceuticals is identified as an important subset.

8.1.2. The bottleneck of space foundries: purification

Biopharmaceuticals must be purified after accumulation with the biological host organism, or cell-free transcription-translation reaction, in order to meet requirements for drug delivery and therapeutic effect[127]. The majority of commercial biopharmaceutical products are administered via intravenous and subcutaneous injection[330]. Biopharmaceutical formulations for injection requires high purity (>95%) product, as impurities introduced directly into the bloodstream can trigger significant immune responses and reduce efficacy[331].

Downstream processing of biopharmaceuticals is therefore usually a resource-intensive section of overall processing, being cited as high as 80% of production costs (and contributions of input mass) for monoclonal antibody (mAb) therapeutics produced using mammalian cell cultures[63,332]. In addition to the processing burden for biopharmaceutical injectables, there are also often substantial storage costs involving complex supply chain and storage management with stability requirements for factors including temperature, time, humidity, light, and vibration[333]. There are several approaches being pursued to overcome the challenges and costs associated with downstream processing and formulation.

First are the tremendous efforts in process intensification[334]. While the highly sensitive nature of biopharmaceuticals to minor process changes has introduced barriers and complexities to innovation through process intensification that have not been realized in non-healthcare biotechnological industries, there have been significant strides made in the past decade in the areas of process integration[335], automation[336], and miniaturization[337,338].

Another route that researchers are pursuing to reduce downstream processing costs and resources is a biological solution to processing technology. In the same vein that the biopharmaceutical industry sprung out of researchers leveraging the power of biology to produce therapeutically relevant molecules that were inaccessible or excessively costly by means of chemical synthesis, researchers are now also trying to apply that same principle to purifying therapeutically relevant molecules. The simplicity of production, reagents that can be produced using self-replicating organisms, and potential recyclability of spent consumables are significant advantages of biological purification technology for space or other limited resource applications. Examples of primary biological technologies include fusion tags[339], stimuli-responsive biopolymers[340], hydrophobic nanoparticles[341], and plant virus nanoparticles[342,343].

Lastly, there are vast efforts to establish alternative drug delivery modalities[344]. Other modalities that do not require injection and which might be more compatible to administration in limited resource environments, such as oral consumption, nasal spray, inhalation, and topical application, have long presented challenges in biopharmaceutical stability (e.g., denaturation in stomach acid) and delivery to the active site (e.g., passing the gut-blood barrier) that minimize product efficacy and necessitate costly advanced formulations and chemistries[345].

A particularly promising drug delivery technique to circumvent downstream processing burdens is to sequester the active pharmaceutical ingredient in the host cells of the upstream production system as a protective encapsulation in order to facilitate bioavailability through oral delivery[346]. It represents an opportunity to greatly lower the cost of *in situ* production of human medicine for a space mission. This technique presumes that the host system is safe for human consumption, and so naturally lends itself to utility in systems such as yeast and plant production hosts. Oral delivery via host cell encapsulation has been recently established as commercial drug delivery modality

with the US Food and Drug Administration approval of Palforzia as an oral peanut-protein immunotherapy[347]. However, this solution is not necessarily amenable to the diversity of pharmaceutical countermeasures that may be required, especially for unanticipated needs in which the product may not have been evaluated for oral bioavailability.

8.1.3. Space economics

In 2011, the space shuttle program was retired due to increasing costs, demonstrating that reduction of economic cost is critical for sustaining any campaign of human exploration[348]. Although recent efforts in reducing the launch cost to low earth orbit by commercial space companies have aided in the redefinition of the space economy[349], the barrier to longer term missions, such as a journey to Mars, is still limited by the extreme financial cost in transporting resources. Additionally, it has been shown that as the mission duration and complexity increases – as expected for a human mission to Mars – the quantity of supplies required to maintain crew health also increases[247]. In the case of meeting the demand for medication, biopharmaceutical synthesis has been proposed as an alternative to packaging a growing number of different medications[208,328]. Assuming that both technologies can meet mission demand, selection of the production-based biotechnology platform will be dependent on its cost impact. It is therefore critical that the cost model of biopharmaceutical synthesis accounts for and minimizes the cost of any and all subprocesses, including those for purification.

The current terrestrial biopharmaceutical synthesis cost model does not align with the needs for space exploration environments. For example, the literature highlights the high cost of Protein A affinity chromatography resin ($8,000 – $15,000/L) and the need to reduce the price[350]. However, the purchase cost of chromatography resin is not nearly as critical in space environment

applications where the major costs are more closely tied to the physical properties of the object (mass, volume, refrigeration requirements, etc.), as a result of fuel and payload limitations and the crew time required for operation[351]. The distinct cost models of space and terrestrial biopharmaceutical production may increase the burden of identifying space-relevant processing technologies and may also limit direct transferability of terrestrial technologies without attention given to these areas.

On the other hand, changing incentives structures relating to sustainability and the advent of new platform technologies are rapidly increasing alignment and the potential for technology crossover. For example, companies like On Demand Pharmaceuticals (ondemandpharma.com), EQRx (eqrx.com), and the kenUP Foundation (kenup.eu), initiatives leading to industry adoption of environmental footprint metrics such as E-factor[352] and Process Mass Intensity (PMI)[63], and diffusion from the adjacencies of green and white biotechnology[353] all promote development of accessible and sustainable technologies. As these trends pertain to space-relevant processes, these examples can also be viewed as driving more closed loop systems composed of simpler components.

8.1.3.1. Reference mission architecture

The evaluation of biopharmaceutical system cost for space applications requires the establishment of a reference mission architecture (RMA) as a means for describing the envelope of the mission scenario and distilling initial technology specifications which relate to the proposed subsystem in question[354]. This RMA can be used to orient and define the specific mission elements that meet the mission requirements and factor into the calculations of cost for deploying biopharmaceutical technologies. Ultimately, the RMA provides the means to determine and compare cost given

specification of mission scenarios that utilize the technology in question. We envision developing and integrating biotechnological capabilities back-ended by purification and quality systems into standard methods composed of a series of unit procedures that maintain astronaut health via the Environmental Control and Life Support Systems (ECLSS)[355]. In this study, we begin to build towards this vision by proposing a high-level RMA that specifies a biopharmaceutical demand partially fulfilled through biomanufacturing over the course of a defined production window.

8.1.3.2. Equivalent system mass

In planning for future human exploration missions, technology choices and life-support systems specifications are often evaluated through the metric of the equivalent system mass (ESM)[284]. Driven by the economic factor of cost in dollars required to transport mass into orbit, the ESM framework accounts for non-mass factors such as power, volume, and crew-time by relating them to mass through predetermined equivalency factors. ESM has been used to evaluate the mass of all of the resources of a larger system including water, shielding materials, agriculture and recycle loop closure. Currently, ESM remains the standard metric for evaluating advanced life support technology platforms[356,357]. In the Space Systems Bioengineering context of realizing a biomanufactory on the surface of Mars[329], recent advances in extending this metric have been proposed in the form of extended equivalent system mass which attempts to address complexities stemming from multiple transit and operations stages, as would be required to support a crewed mission to Mars[358]. It also accounts for uncertainties inherent in mission planning such as technology failures and their downstream effects as propagated through a mission such as refrigeration failures in systems housing medicine that requires specific cooling. Such advances in the ESM framework aid in the assessment of biopharmaceutical technologies as elements in the

context of proposed ECLSS given the inherent stochastic nature of human health, especially in a space environment[359]. Here, we calculate ESM at multiple mission segments across which biopharmaceutical purification is deployed.

8.2. Materials & Methods

8.2.1. Unit procedure selection

8.2.1.1. Protein A-based affinity capture step

The medical significance of mAb therapies and the highly developed and specialized purification technology provide a fertile ground for techno-economic feasibility analysis of an ISRU-based pharmaceutical foundry for space. The first reason is that there are mAb therapies commercially approved or in development for multiple important disease states of spaceflight including osteoporosis[360], migraines/headaches[361], seizure[362], pneumonia[363], ocular herpes[364], otitis media[365], various oncological indications[366], and fungal infections[367]. A second reason is that degradation products of mAb therapies are known to result in, not just reduced efficacy, but also deleterious effects (e.g., harmful immune reactions in patients) that further compound concerns of pharmaceutical stability over a long-duration mission[368]. Thirdly is that a common manufacturing system can be used to produce treatments for a variety of indications which is highly advantageous in mass and volume savings for spaceflight. And fourthly, the economic incentive of research into mAb purification technology has resulted in a plethora of technologies, enabling this analysis to include head-to-head comparisons between multiple mAb capture steps of different origins (e.g., biotic, abiotic) and different processing mechanisms (e.g., bind-and-elute mode liquid chromatography, precipitation). It is in comparing the differences between these technologies that

we can uncover general insights into the desired components of a pharmaceutical foundry for space.

Monoclonal antibody therapy is a platform technology that supports human health across a diversity of medical indications with a generally maintained molecular structure, in large part due to the coupling of high target selectivity in the two small and highly variable complementarity-determining regions located in the antigen-binding fragments[369] and control of the biological action on that target (i.e., effector function) through the generally conserved fragment crystallizable (Fc) region[370]. This otherwise high structural fidelity conserved across mAb therapy products (which are primarily of the immunoglobulin G class) spans a wide variety of therapeutic indications and creates an opportunity for generic mAb production process flows, which include technologies devised specifically for mAb production[371]. This specialized manufacturing, which is most notable in the use of the affinity capture step targeting the Fc region of an antibody with the use of the protein-based ligands derived from the *Staphylococcus aureus* Protein A molecule, can be tuned for highly efficient purification of mAb and antibody-derived (e.g., Fc-fusion protein) class molecules[350]. Therefore, we have decided to investigate the Protein A-based affinity capture step in isolation as a starting point for understanding the costs of a potential pharmaceutical foundry in space.

It is worth noting that other similar protein ligands, such as Protein G and Protein L, are also widely used for their ability to capture different types of immunoglobulin classes and subclasses more efficiently[372].

8.2.1.2. Abiotic and biotic Protein A-based unit procedures

We chose to analyze six Protein A-based capture step procedures: three commercially available abiotic technologies (pre-packed chromatography (CHM), spin column (SPN), magnetic bead (MAG)) and three development-stage biotic technologies (plant virus-based nanoparticle (VIN), elastin-like polypeptide (ELP), and oilbody-oleosin (OLE)) (Figure 8.1). Commercial technology procedures are based on product handbooks while the procedures of developing technologies, which we would classify as Technology Readiness Level 2 per NASA's guidelines, are based on reports in literature. This set of procedures was selected to survey a wide range of operational modalities, technological chassis, and perceived advantages and disadvantages (Table 8.1).

All six of the unit procedures are operated in bind-and-elute mode, in which a clarified mAb-containing liquid stream is fed into a capture step containing Protein A-based ligand, which selectively binds the mAb and separates the mAb from the bulk feed stream. The mAb is eluted from the Protein A-based ligand and recovered using a low pH buffer to dissociate the mAb from the ligand. Finally, the low pH environment of the recovered mAb is pH neutralized for future processing or storage. The analysis does not consider differences in mAb processing upstream or downstream of the affinity capture step that may arise from differences in the unit procedure operations.

CHM is a chromatography system consisting of a liquid sample mobile phase which is pumped through a pre-packed bed of Protein A-fused resin beads housed in a column. SPN is a similar system, in which a Protein A-fused resin bead bed has been pre-packed into a plastic tube housing and the mobile phase flow is controlled via centrifugation of the plastic tube. MAG is a slurry-based magnetic separation system that uses superparamagnetic particles coated with Protein A-fused resin mixed as a slurry with the feed mAb stream for capture and elution of the mAb by

magnet. VIN is a sedimentation-based system that uses plant virion-based chassis fused with Protein A-based ligands in suspension for capture of the mAb and centrifugation, assisted by the sedimentation velocity contribution of the chassis, to isolate and elute the mAb. ELP is a precipitation-based system that uses stimuli-responsive biopolymers fused with Protein A-based ligands in suspension for capture of the mAb and external stimuli (e.g., temperature, salt) to precipitate the bound complex and elute the mAb. OLE is a liquid-liquid partitioning system that uses oil phase segregating oleosin proteins fused with Protein A-based ligands to capture mAb in the oil phase and then elute the mAb into a clean aqueous phase.

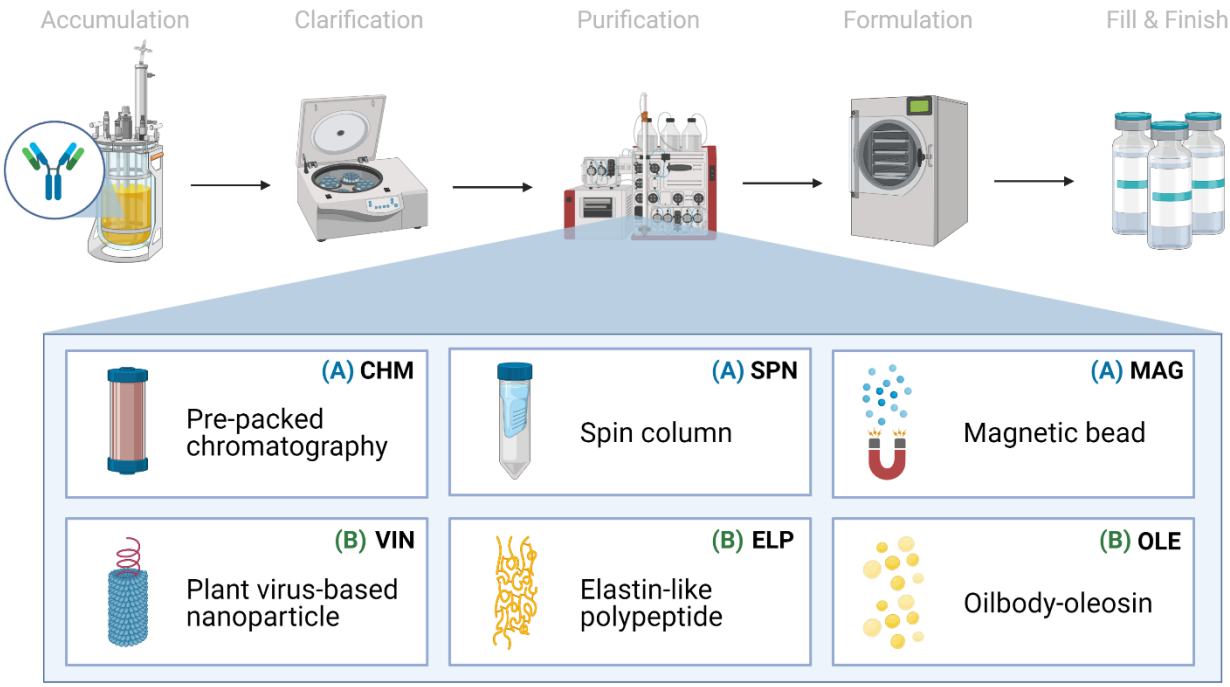

Figure 8.1. Monoclonal antibody production consists generically of product accumulation, clarification, initial purification, formulation, and fill & finish. Here we investigate six technologies for the capture step within the first purification step in a space mission context using extended equivalent system mass. The manufacturing origin of the capture reagent is denoted as either (A) abiotic or (B) biotic.

Table 8.1. List of Protein A-based monoclonal antibody capture step unit procedures included for analysis.

Unit Procedure ID	Method	Technology Used	Reference
Pre-packed chromatography[(A)]	Liquid chromatography	Pre-packed HiTrap MabSelect SuRe column of novel alkali-tolerant recombinant Protein A-based ligand coupled with an agarose matrix	Vendor handbooks[373–375]
Spin column[(A)]	Centrifuge-assisted liquid chromatography	Pre-packed Protein A HP SpinTrap spin column containing Protein A Sepharose High Performance	
Magnetic bead[(A)]	Magnetic separation	Protein A Mag Sepharose superparamagnetic beads coupled with native Protein A ligands	
Plant virus-based nanoparticle[(B)]	Sedimentation complex	Plant virion, *Turnip vein clearing virus*, presenting a C-terminal coat protein fusion display of Protein A (domains D & E)	Werner et al. 2006[342]
Elastin-like polypeptide[(B)]	Inverse transition cycle	Elastin-like polypeptides (78 pentapeptide (VPGVG) repeats) fused with Z domain, an engineered B domain of Protein A	Sheth et al. 2014[340]
Oilbody-oleosin[(B)]	Liquid-liquid partition	*Arabidopsis* oleosin fused at the N-terminal with an engineered Protein A(5)	McLean et al. 2012[376]

[A]abiotic technology; [B]biotic technology

8.2.2. Techno-economic evaluation

Techno-economic evaluations are performed using the recently proposed equations for ESM that include calculation of costs at each mission segment[358]. Equivalent system mass (ESM) for the mission ESM_0 is defined as

$$\mathrm{ESM}_0 = \sum_{k}^{\mathcal{M}} L_{eq,k} \sum_{i}^{A_k} \left[\left(M_{k_i} \cdot M_{eq,k} \right) + \left(V_{k_i} \cdot V_{eq,k} \right) + \left(P_{k_i} \cdot P_{eq,k} \right) + \left(C_{k_i} \cdot C_{eq,k} \right) + \left(T_i \cdot D_k \cdot T_{eq,k} \right) \right]$$

$$= \mathrm{ESM}_{0,pd} + \mathrm{ESM}_{0,tr1} + \mathrm{ESM}_{0,sf} + \mathrm{ESM}_{0,tr2}$$

where M_i, V_i, P_i, C_i, T_i are the initial mass [kg], volume [m^3], power requirement [kW], cooling requirement [kg/kW], and crew-time requirement [CM-h/h], M_{eq}, V_{eq}, P_{eq}, C_{eq}, T_{eq} are the equivalency factors for mass [kg/kg] (which is set to 1 in this study), volume [kg/m^3], power [kg/kW], cooling [kg/kW], and crew time [kg/CM-h], respectively, L_{eq} is the location equivalency factor [kg/kg] that accounts for costs associated with mass transport occurring at a particular mission segment (e.g., orbital maneuvers required for the return transit), and D is the duration of the mission segment [day] over a set of subsystems $i \in A$ and set of mission segments $k \in \mathcal{M}$. The mission ESM in this study is specifically defined as the sum of subtotal ESM for each mission segment within the scope of the reference mission architecture defined in this study (pre-deployment $\mathrm{ESM}_{0,pd}$, crewed transit to Mars $\mathrm{ESM}_{0,tr1}$, Mars surface operations $\mathrm{ESM}_{0,sf}$, and return crewed transit to Earth $\mathrm{ESM}_{0,tr2}$).

The mission timeline depicted in Figure 8.2 provides insight into the proposed RMA and downstream crew needs and mAb production horizon. Here we assume a total mission duration of 910 days. First, a crew of 6 will travel from Earth to low Earth orbit, then board an interplanetary craft for a 210-day journey to Martian orbit, where the crew will descend to the surface in a separate craft, allowing the large transit vehicle to remain in orbit. Once on Mars, the crew will perform surface operations for 600 days. Following surface operations, the crew will leave Mars in a fueled ascent craft, board the interplanetary vehicle, and return to Earth orbit in 200 days. The mission timeline, crew size, and ESM equivalency factors are consistent with the recent RMA presented for inclusion of biomanufacturing elements[358].

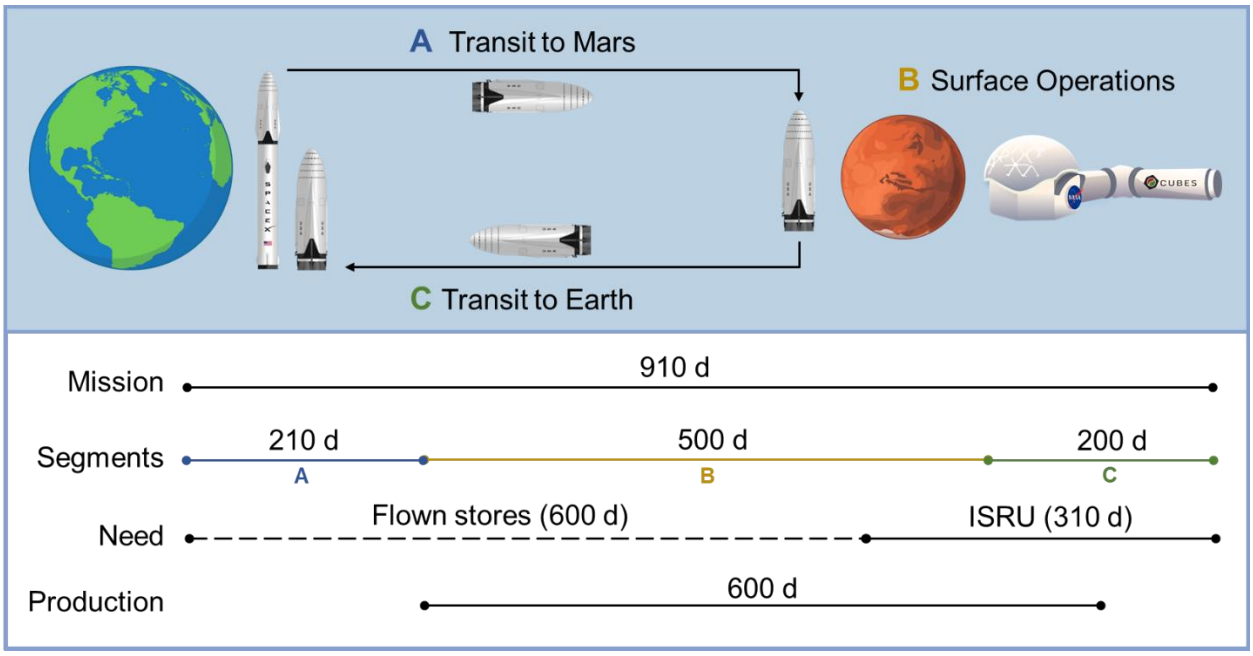

Figure 8.2. An illustration of the reference mission architecture in which (A) a crewed ship is launched from the surface of Earth and lands on Mars and (B) assembles a pre-deployed habitat on the Martian surface to perform operations before (C) a return transit to Earth on the same ship. Pharmaceutical needs are supported by flown stores until partway through surface operations, at which point needs are met by pharmaceuticals produced using *in situ* resource utilization. Production is initiated prior to the need window to ensure adequate stocks are generated by the time it is needed. Rocket artwork adapted from Musk, 2017[377]. Habitat artwork by Davian Ho.

The mission demand for mAb therapies is assumed to be 30,000 mg over the entirety of the mission (supporting logic detailed in Supplementary Information, Table S8.1). Key mission and pharmaceutical reference mission architecture details and assumptions are listed in Table 8.2. Pharmaceutical stores and production resources are assumed to be flown with the crew transit (no pre-deployment in order to maximize shelf-life). We assume that the production resources are stable throughout the mission duration. We conservatively assume (in the face of insufficient spaceflight stability data for biologics for a more refined estimate) that the first 600 days of pharmaceutical demand will be met through flown stores (20,000 mg), at which point pharmaceutical ISRU manufacturing is needed (10,000 mg) to alleviate the impact of accelerated

pharmaceutical degradation and provide supplementary medication. The pharmaceutical production window opens prior to the ISRU demand timeframe and persists through a portion of the return transit (up to mission day 810) to reflect the expected life support advantage of maintaining capabilities to counter unanticipated needs or threats. We assume that the Protein A-based unit procedures consistently yield 98% recovery of mAb from the input stream.

Table 8.2. Key mission and pharmaceutical reference mission architecture details and assumptions. mAb, monoclonal antibody.

Mission scope	
Pre-deployment	N/A
Transit to Mars	210 days
Surface operations	500 days
Return transit	200 days
Total mission duration	910 days
Crew size	6 crew members
Pharmaceutical scope	
Mission demand, mAb	30,000 mg
Biomanufacturing, mAb	10,000 mg
Capture step recovery	98%
Production window	600 days
Feed mAb concentration	1 mg/mL
Molecular weight, mAb	150 kDa

8.2.3. Unit procedure simulation

Deterministic models for each unit procedure were developed in Microsoft Excel (Supplementary Information, Spreadsheet S8.1) using reference protocols cited in Table 8.1 as a series of

executable operations, each containing a set of inputs defined by cost categories (labor, equipment, raw materials, consumables) that are correspondingly populated with characteristic ESM constituent (mass, volume, power, cooling, labor time) values (model composition illustrated in Supplementary Information, Figure S8.1). Unit procedures have been defined as the smallest single execution (i.e., unit) of the secondary purification capture step procedure according to the reference protocol. We define the unit capacity by volume according to the equipment and consumables used (e.g., 2 mL maximum working volume in a 2 mL tube) and by mAb quantity according to the binding capacity for the given method (e.g., 1 mg mAb/mL resin) (Supplementary Information, Table S8.2). Unit procedures with no explicit working volume constraints (i.e., the liquid solution volume for biotic technologies) have been defined with a maximum unit volume of 2 mL. ESM-relevant characteristics of individual inputs (e.g., equilibration buffer, 2 mL tube) are defined based on publicly available values, direct measurements taken, and assumptions (which are explicitly identified in the spreadsheet).

There are several model features that we have considered and decided not to include within the scope of analysis. Packing and containers for the inputs are not included for three reasons: 1) the contributions of the container are considered negligible as compared to the input itself (e.g., container holding 1 L buffer as compared to the 1 L of liquid buffer); 2) materials flown to space are often re-packaged with special considerations[378]; and 3) the selection of optimal container size is non-trivial and may risk obscuring more relevant ESM findings if not chosen carefully. We do not consider buffer preparation and assume the use of flown ready-to-use buffers and solutions. Furthermore, refrigeration costs of the input materials and costs that may be associated with establishing and maintaining a sterile operating environment (e.g., biosafety cabinet, 70% ethanol in spray bottles) are expected to be comparable between unit procedures and not considered.

Impacts of microgravity on unit procedure execution are not considered for the return transit production. Refrigeration costs associated with low temperature equipment operation (e.g., centrifugation at 4 °C) are included in the equipment power costs.

Inputs common across unit procedures are standardized (Supplementary Information, Table S8.3). One operational standardization is the inclusion of pH neutralization of the product stream following the low pH elution mechanism, which was explicitly stated in some procedures while not in others. Input quantities are scaled from a single unit to determine the number of units required to meet the reference mission architecture specifications. The ESM constituent inputs (mass, volume, power, cooling, labor time) are converted into equivalent mass values using RMA equivalency factors (Supplementary Information, Table S8.4).

8.3. Results & Discussion

8.3.1. Standardization of manufacturing efficiency

Given the limited granularity of the presented reference mission architecture, which was scoped as such to reflect the lack of literature presenting an overarching and validated Concept of Operations for a Transit to Mars[379], we do not define strict manufacturing scheduling criteria for pharmaceutical production. Construction of a detailed pharmaceutical production RMA is hindered by uncertainty in the number and identity of mAb therapy products that would be included within mission scope, the decay rate of mAb therapy stores in the mission environments, and a reasonable basis for building robustness to unanticipated disease states. Rather, we choose to establish an objective comparison between unit procedures by normalizing for scheduling-associated manufacturing efficiencies. We accomplish this by first identifying the number of

batches per mission (and thus batch size) needed to meet the mAb demand (base case of 10,204 mg mAb feed assuming 98% recovery) that minimizes the ESM output for a given unit procedure, and then running the simulation of pharmaceutical production at that number of mission batches, as shown in Figure 8.3a and tabulated in Supplementary Information, Table S8.5.

In Figure 8.3b – e, we visualize a deconstruction of ESM output, using the VIN unit procedure as an example, by key performance metrics that vary with a scheduling dependence in order to illustrate the significance of batch optimization in unit procedure comparison. The processing of a given batch volume and mAb quantity is allocated into a number of units, as determined by the volume and mAb quantity constraints of a given unit procedure, and a number of use cycles per batch, as determined by the capacity of the equipment specified in the given unit procedure. We show how the variation in ESM output over the number of mission batches maps to extent of unit vacancy or underutilization (Figure 8.3b), extent of operational equipment (e.g., centrifuge) vacancy or underutilization (Figure 8.3c), and number of required use cycles (Figure 8.3d). We also show an oscillatory behavior in the scheduling (i.e., total mAb purified per mission, % purified at surface operations) that quickly dampens as number of mission batches increases (Figure 8.3e). This behavior is a result of the assumption that the mAb feed stream is coming from a discrete upstream production batch (e.g., batch-mode bioreactor) that does not output partial batch quantities, as opposed to a continuous upstream production for which there are no defined batches. Accordingly, partial batch needs are met by the processing of a full batch.

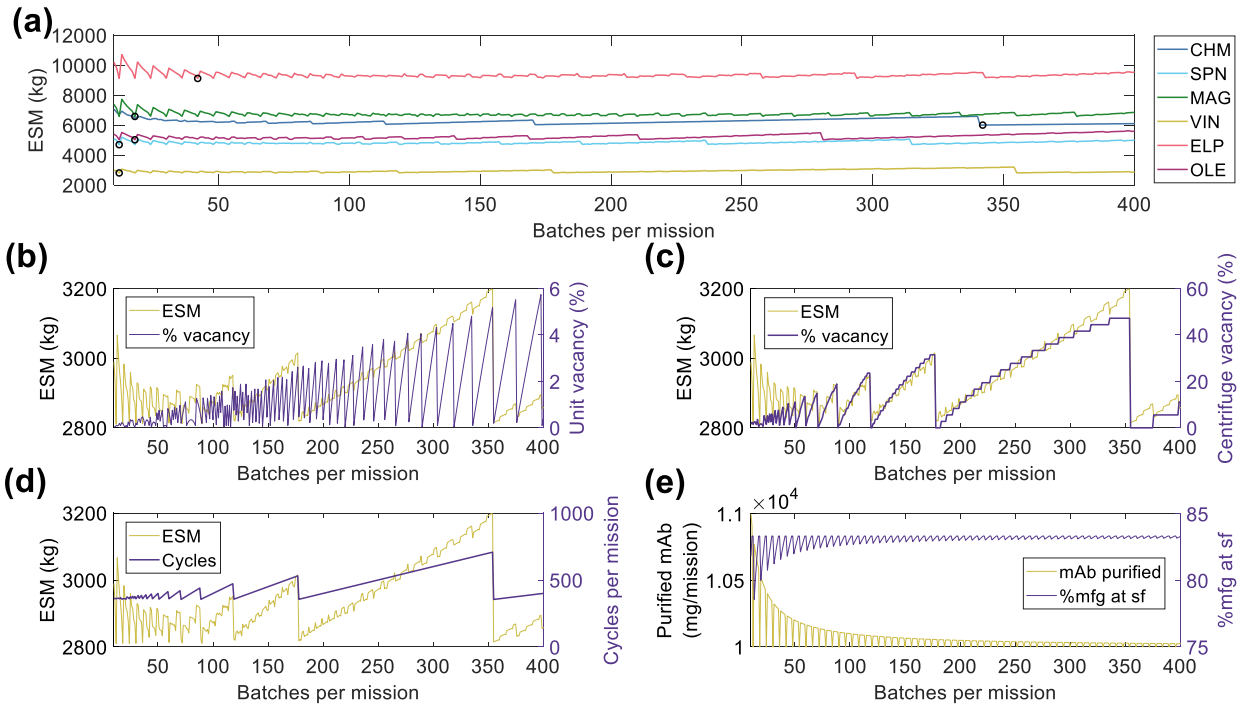

Figure 8.3. (a) Scheduling optimization for the establishment of base case scenarios for each unit procedure. The value for number of batches corresponding to the minimum equivalent system mass for each unit procedure, as indicated by black circle (○) markers. Key operational parameters impacted by mission scheduling (shown using the VIN procedure) include (b) unit underutilization or vacancy, (c) equipment underutilization or vacancy, in this case represented by the centrifuge as the bottleneck, (d) the number of use cycles, and (e) the total quantity of monoclonal antibody (mAb) per mission and per surface operation (sf). CHM, pre-packed chromatography; SPN, spin column; MAG, magnetic bead; VIN, plant virus-based nanoparticle; ELP, elastin-like polypeptide; OLE, oilbody-oleosin.

8.3.2. Base case scenario

The ESM and output metrics of the base case scenario (10,000 mg mAb demand, 1 mg mAb/mL feed concentration, 98% recovery) for each of the six unit procedures are shown in Figure 8.4a-f. From this viewpoint of an ESM output for an isolated unit procedure outside the context of a full purification scheme, the ESM ranked from lowest to highest are VIN < SPN < OLE < CHM < MAG < OLE. However, we reason that it is more important to understand the model inputs that influence the ESM output rankings than to use the rankings in this isolated subsystem analysis to

make technology selection choices, which requires the context of a full pharmaceutical foundry and of linkages to other mission elements.

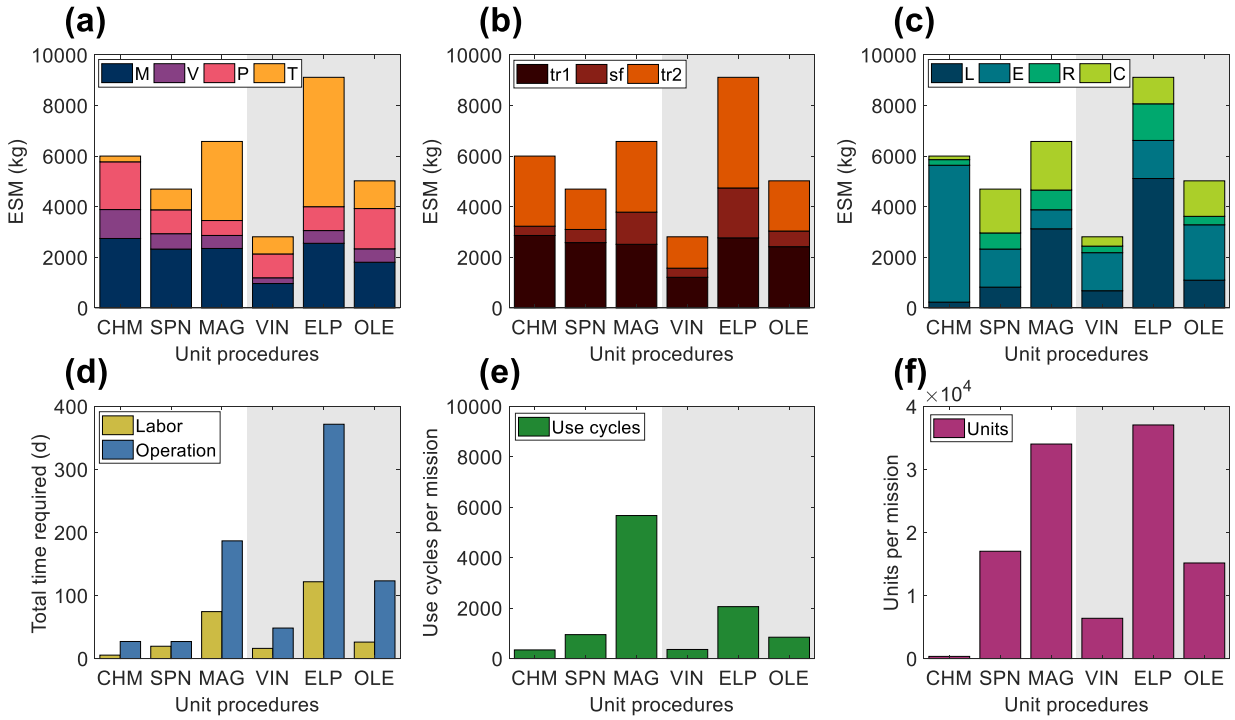

Figure 8.4. Base case equivalent system mass results broken down by (a) mass (M), volume (V), power (P), and labor time (T) constituents, (b) transit to Mars (tr_1), surface operations (sf), and return transit (tr_2) mission segments, and (c) labor (L), equipment (E), raw materials (R), and consumables (C) cost category for the six tested Protein A-based monoclonal antibody affinity capture step unit procedures segregated by abiotic (white background) and biotic (grey background) technologies. Also shown are the (d) labor and operation times, (e) number of use cycles, and (f) number of units required for each unit procedure to meet the reference mission demand. CHM, pre-packed chromatography; SPN, spin column; MAG, magnetic bead; VIN, plant virus-based nanoparticle; ELP, elastin-like polypeptide; OLE, oilbody-oleosin.

We observe that mass costs are generally the primary contributor to ESM output, except for the MAG and ELP procedures in which labor time costs are larger. The mass costs are not closely associated to any given cost category across unit procedures, but rather the breakdown of mass costs varies widely by unit procedure.

Power costs (kW) are disproportionately high given that the static nature of ESM assumes constant usage, and thus energy (kW·h) in this context (i.e., the power supply to the equipment is not turned off in this analysis). These costs represent an upper bound assuming that the power supply system capacity is sized to support a maximal power consumption in which all power-drawing elements are simultaneously in operation. Time of power usage as a fraction of duration are as follows: CHM (99%) > MAG (78%) > ELP (48%) > SPN (45%) > OLE (42%) > VIN (30%). The lower use fraction unit procedures are therefore paying a relatively higher cost per unit power demand in this current method. The electrical needs of the equipment used by the unit procedures are within NASA-proposed Mars mission RMA bounds, with energy use across all unit procedures would peak at ~1% of a proposed Mars transfer vehicle electric capacity (50 kWe) or ~5% of the habitat capacity (12 kWe) of a reference stationary surface nuclear fission power reactor[380].

The mission segment breakdown of ESM illustrates the relatively high costs of pharmaceutical manufacturing capabilities for transit, even for the transit to Mars (tr_1) in which there is no actual production taking place. There is a strong economic incentive to limit the amount of supplies flown on tr_1. Alternatives such as the pre-deployment of reagents and consumables and limiting of production to surface operations on Mars (which has lower RMA equivalency factors for mass and volume than transit operations) must be balanced against the risk to human health posed by removing pharmaceutical production capabilities from a mission segment and potentially exposing the supplies to longer storage times that could challenge shelf lives.

Labor and operation times are important parameters in the broader mission and pharmaceutical foundry context. These unit procedures represent a single step of pharmaceutical production, which if realized in a space mission context, would, in turn, need to be a small portion of a crew member's time allocation. Assuming 40-hour work weeks for crew members, the labor time spans

a range of ~1% (CHM) to ~14% (ELP) of the available crew time over the 600-day production window. It is not feasible to operationalize with such high labor and operation times at this scale of production, particularly as they stand for MAG and ELP. While strategies such as batch staggering and concurrency can be used to reduce durations, advanced automation will almost certainly need to be built into the core of a pharmaceutical foundry.

A prevailing trend throughout the unit procedures is that the number of unit executions and use cycles required by a given unit procedure are positive correlated with the ESM output value, except for the equipment cost-dominant and higher unit capacity CHM procedure. The equipment modeled in the analysis for CHM and the other unit procedures are almost certainly not space-ready and could be further designed to reduce mass and volume and increase automation to reduce crew labor time. The increased equipment costs in the CHM procedure are primarily due to automation and monitoring hardware for running liquid chromatography, which is reflected in the minimal labor costs of the CHM procedure. Miniaturization efforts, such as those focusing on microfluidic systems[381–383], are emerging as a potential path towards mitigating the high equipment costs associated with highly automated and tightly controlled manufacturing, which are crucial for freeing up valuable crew time.

The number of unit executions is determined by the binding capacity of the technology and the nominal unit size. This indicates that the unit capacity for purification is an important consideration and influential factor. Unit sizing is an important consideration that is valuable to assess more holistically within the broader pharmaceutical production and mission context.

The number of use cycles is determined by the number of unit executions required and by the maximal unit capacity of the equipment items (e.g., if you presume that an 18-slot centrifuge is the equipment bottleneck then the effective number of batches is the number of units required

divided by 18). Therefore, it can be understood that the equipment unit capacity is a critical parameter in tuning the number of use cycles and, by extension, the labor costs. For processes with lower labor costs, due to the intrinsic nature of the procedure or through automation of labor, equipment unit capacity will still influence the total duration and production throughout. The MAG and ELP procedures yield both high labor and duration times and are thus particularly sensitive to the equipment capacity.

8.3.2.1. Contextualizing ESM with supporting evaluations

Having acknowledged shortcomings of ESM as a decision-making tool for comparison of alternative approaches in isolated subsystems, we propose that supplementary evaluations can assist in contextualization. A primary gap of an isolated subsystem ESM analysis is a lack of information on the holistic usefulness or cost of a given employed resource, which could include its synergy with other mission subsystems and its extent of recyclability, or waste loop closure, within the mission context. For example, the isolated subsystem analysis does not capture information on the broad applicability that a centrifuge might have for use in other scientific endeavors, nor do the ESM outputs reflect the > 93% recyclability of water achieved by the recycler on the ISS[384] that may be generalizable to future missions.

The use of environmental footprint metrics, such as PMI, may be one valuable step towards capturing missed information on recyclability. PMI is a simple metric of material efficiency defined as the mass of raw materials and consumables required to produce 1 kg of active pharmaceutical ingredient. The study by Budzinski et al. introducing PMI for biopharmaceuticals presents data from 6 firms using small-scale (2,000 – 5,000 L reactor) and large-scale (12,000 – 20,000 L reactor) mAb manufacturing operations, finding an average 7,700 kg of input is required

to produce 1 kg of mAb[63]. Figure 8.5a presents PMI evaluation for the six capture steps included in analysis, which result in PMI outputs as low as 2,390 kg of input (CHM) and as high as 17,450 kg of input (MAG) per 1 kg of mAb. A comparison of these outputs to those of Budzinski et al. indicates that we may be observing roughly similar values after accounting for the high cost of initial purification in the study, representing ~60% of the total PMI reported, the elevated feed mAb concentration (i.e., cell culture titer) of 1 – 5.5 g mAb/L, and adjustments for economies of scale when operating at such low cycle volumes (Figure 8.5b). Consumable costs appear to be the most sensitive to scale, which represents ~1% total PMI on average in the values reported by Budzinski et al. and ranges from 35% (CHM) to 77% (OLE) here. Budzinski et al. also go one step further to distinguish water as a separate category from raw materials and report that >90% of the mass is due to water use. Here we assume pre-made buffers and do not directly add water in this study, so we refrain from a similar calculation, but it is worth noting that the extent of water use may also serve as a reasonable starting surrogate for extent of achievable recyclability in a space mission context.

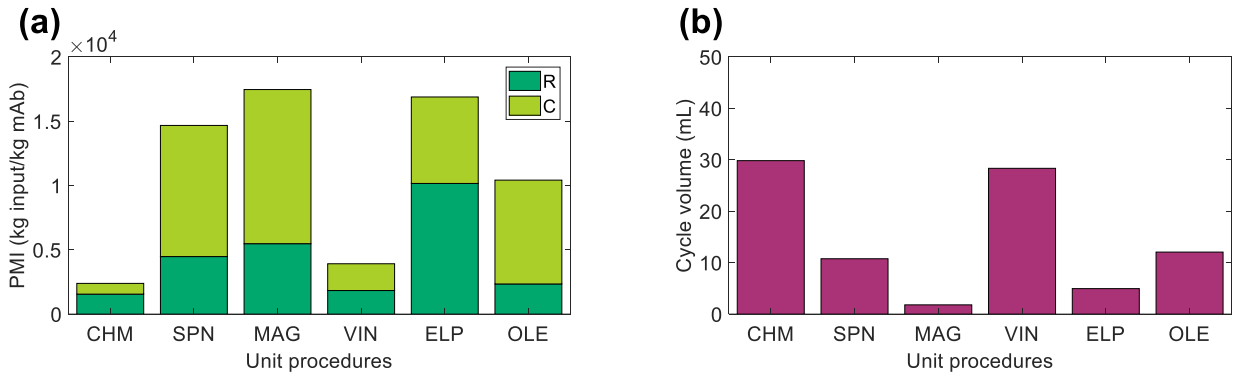

Figure 8.5. Process mass intensity (PMI) evaluation of the unit procedures broken down by raw materials (R) and consumables (C) contributions. CHM, pre-packed chromatography; SPN, spin column; MAG, magnetic bead; VIN, plant virus-based nanoparticle; ELP, elastin-like polypeptide; OLE, oilbody-oleosin.

8.3.3. Scenario analysis

We analyzed the specific ESM output broken down by cost category for the six unit procedures over a range of input stream mAb concentrations (Figure 8.6) and mission demand for mAb (Figure 8.7). Specific ESM, termed cost of goods sold in traditional manufacturing analyses, is the ESM output required to produce 1 mg mAb. This is used in the scenario analyses to normalize ESM output across variation in mission demand for mAb. The optimal number of batches per mission was found and used for each unit procedure and scenario tested (Supplementary Information, Tables S8.7 – S8.8).

We observe the general and expected trends that specific ESM decreases with an increasing feed stream mAb concentration and mission demand. The CHM procedure exhibits notably limited sensitivity to feed stream mAb concentration, which can be attributed to the equipment-dominated cost profile, fixed column size, and nature of the governing reference protocol that does not specify restrictions on sample load volume. Depending on the pre-treatment of the feed stream, it may be more reasonable to impose constraints on the sample load volume. In contrast, the specific ESM output of the CHM procedure is the most sensitive to mission mAb demand with higher demand increasingly offsetting the fixed capital costs. The CHM procedure is also the largest capacity unit modeled in the analysis (i.e., CHM capacity is 30 mg mAb/unit as compared to 2.7 mg mAb/unit for MAG, the next highest capacity unit) and is accordingly expected to scale well with demand.

The SPN, ELP, OLE procedures exhibit behaviors in which the specific ESM output abruptly plateaus with an increasing feed stream mAb concentration. This observation can be attributed to the unit procedure operating in a mAb binding capacity-limited regime (as opposed to volume-limited for more dilute feeds) which also then controls and maintains unit procedure throughput (e.g., the ELP number of units, 37,044, and use cycles per mission, 2,058, is constant at and above

0.35 mg mAb/mL input stream concentration). This can be de-bottlenecked via technology (e.g., improved chemistry of the capture step unit leading to higher binding capacity) or methodology (e.g., increased concentration of the capture step unit leading to higher binding capacity) improvements.

Low demand scenarios are particularly relevant for examination in a space health context, as small capacity redundant and emergency utility is a likely proving ground for inclusion of a space pharmaceutical foundry. At the lower boundary of the tested range (1,000 mg mAb/mission), we see the ESM outputs from lowest to highest are re-ordered as MAG < VIN < SPN < OLE < ELP < CHM. Minimization of equipment costs are particularly important in this regime, and it is observed that, indeed, the ESM output near completely aligned with the ranking of equipment cost (MAG < VIN < SPN < ELP < OLE < CHM). It is likely that other non-ESM factors such as integration with other flown elements will understandably influence the design and composition of early and low capacity flown pharmaceutical foundries.

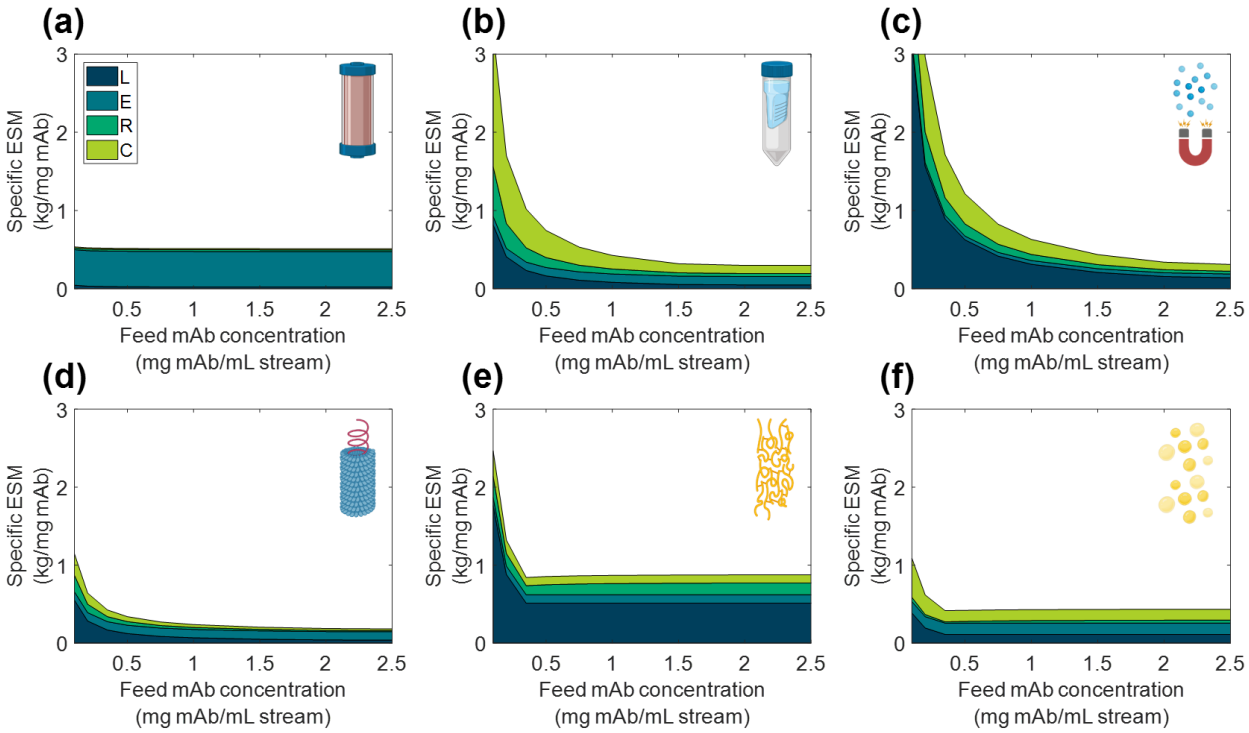

Figure 8.6. Specific equivalent system mass (per unit mass monoclonal antibody produced) broken down by labor (L), equipment (E), raw materials (R), and consumables (C) cost categories as a function of feed monoclonal antibody (mAb) concentration for (a) CHM, (b) SPN, (c) MAG, (d) VIN, (e) ELP, and (f) OLE. CHM, pre-packed chromatography; SPN, spin column; MAG, magnetic bead; VIN, plant virus-based nanoparticle; ELP, elastin-like polypeptide; OLE, oilbody-oleosin.

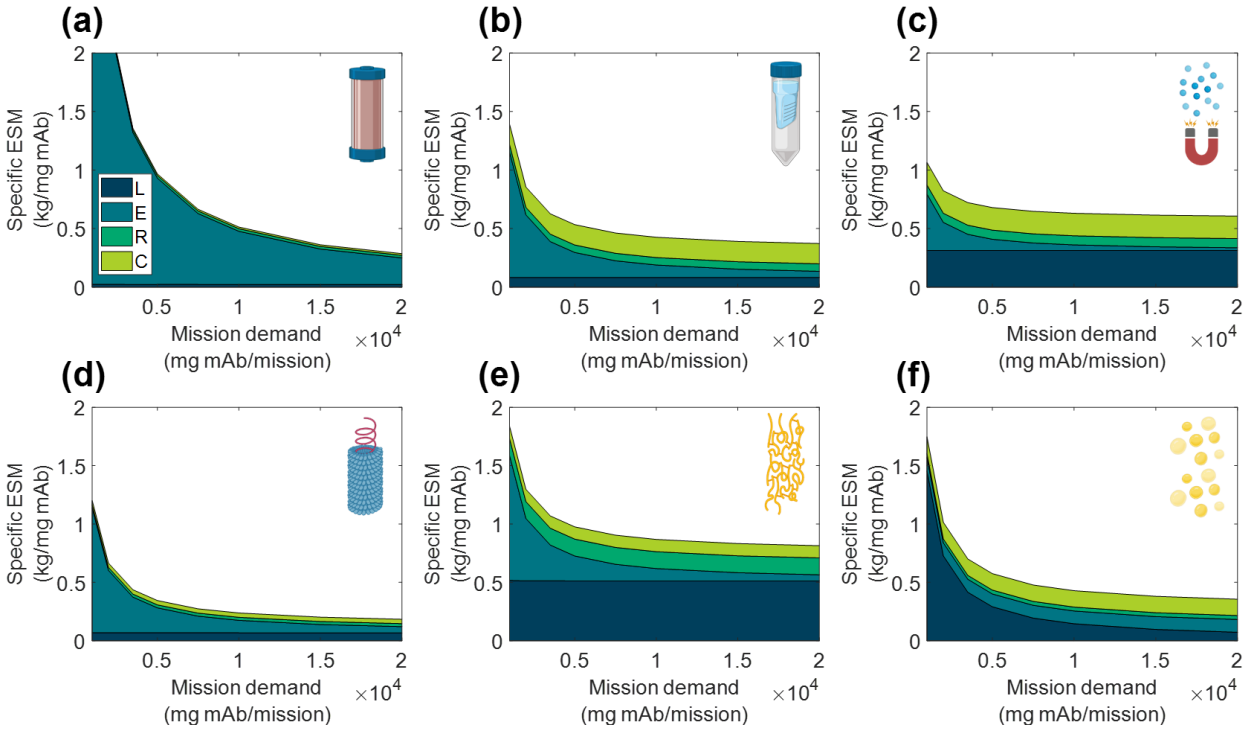

Figure 8.7. Specific equivalent system mass (per unit mass monoclonal antibody produced) broken down by labor (L), equipment (E), raw materials (R), and consumables (C) cost categories as a function of mission production demand for monoclonal antibody for (a) CHM, (b) SPN, (c) MAG, (d) VIN, (e) ELP, and (f) OLE. CHM, pre-packed chromatography; SPN, spin column; MAG, magnetic bead; VIN, plant virus-based nanoparticle; ELP, elastin-like polypeptide; OLE, oilbody-oleosin.

8.3.4. Alternate scenarios

8.3.4.1. Mission configurations

We explored variations to the base case RMA for all six unit procedures including scenarios in which the pharmaceutical manufacturing resources are shipped prior to the crew in pre-deployment, (+)pd, the production window has been truncated to close with the end of surface operations, (-)tr_2, and a combination of the two prior modifications, (+)pd (-)tr_2 (Figure 8.8). Costs of pre-deployment are included in the analyses and mission demand is kept constant regardless of the production window.

In all cases the ESM totals were reduced from the base case. Additionally, the general trend held that (-)tr_2 scenario resulted in lower ESM totals than (+)pd scenario except for SPN, in which the increased raw material and consumable costs of (-)tr_2 were sufficiently large to outweigh the reduction in equipment and labor costs of (+)pd. The combination (+)pd (-)tr_2 scenario resulted in the lowest ESM totals at a fraction of the base case (as high as 39% reduction in SPN and as low as 21% reduction in ELP).

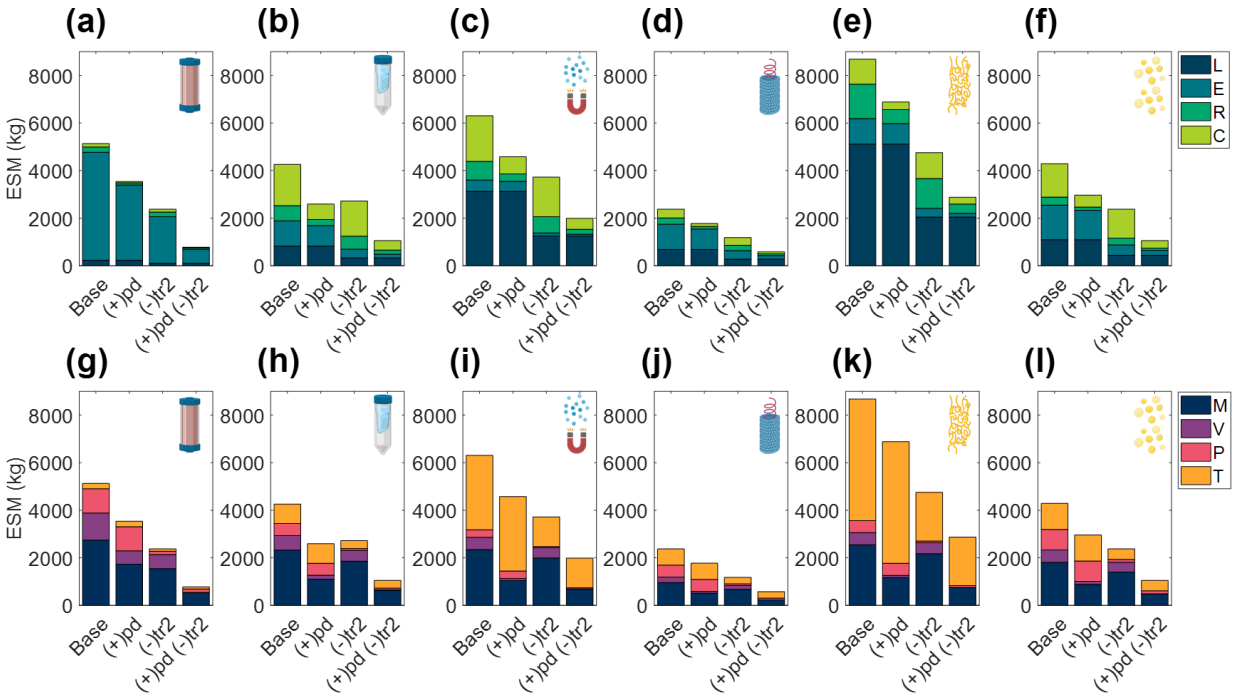

Figure 8.8. Evaluation of extended equivalent system mass values in various mission configurations broken down by labor (L), equipment (E), raw materials (R), and consumables (C) cost categories cost category and mass (M), volume (V), power (P), and labor time (T) constituents for CHM, (a, g), SPN, (b, h), MAG, (c, i), VIN, (d, j), ELP (e, k), and OLE, (f, l). Configurations include the base case scenario of manufacturing resources flown with the crew for pharmaceutical production on the surface and return transit (Base), and alternatives in which the manufacturing resources are flown prior to the crew in pre-deployment, (+)pd, the production window is limited to surface operations, (-)tr_2, and a combination of the two previously stated alternatives, (+)pd (-)tr_2. CHM, pre-packed chromatography; SPN, spin column; MAG, magnetic bead; VIN, plant virus-based nanoparticle; ELP, elastin-like polypeptide; OLE, oilbody-oleosin.

8.3.4.2. Equipment & unit throughput

Acknowledging the significance of the equipment capacity on ESM output, we further explored this contribution by comparing the base case ESM output of the centrifuge-utilizing procedures (SPN, VIN, ELP, OLE) to that resulting from the use of alternative centrifuge models (Supplementary Information, Table S8.9). This effectively results in a trade of equipment costs and batch throughput. The optimal number of batches per mission was found and used for each unit procedure and interval tested (Supplementary Information, Table S8.10).

We observe in Figure 8.9 that the ESM values increased with the size of the centrifuge model, 12-slot < 18-slot (base) < 48-slot. The labor and consumables savings of higher batch throughput were outweighed by the higher equipment costs (including higher power costs). Operation duration is an important metric relevant to a pharmaceutical foundry that is not well reflected in ESM that is also impacted by this alternative scenario. The exception to this trend is the 48-slot condition for the ELP procedure, in which a lower consumable cost related to the number of use cycles per mission (i.e., pipette tips, tubes, gloves) sufficiently lowered the total ESM below the 18-slot condition.

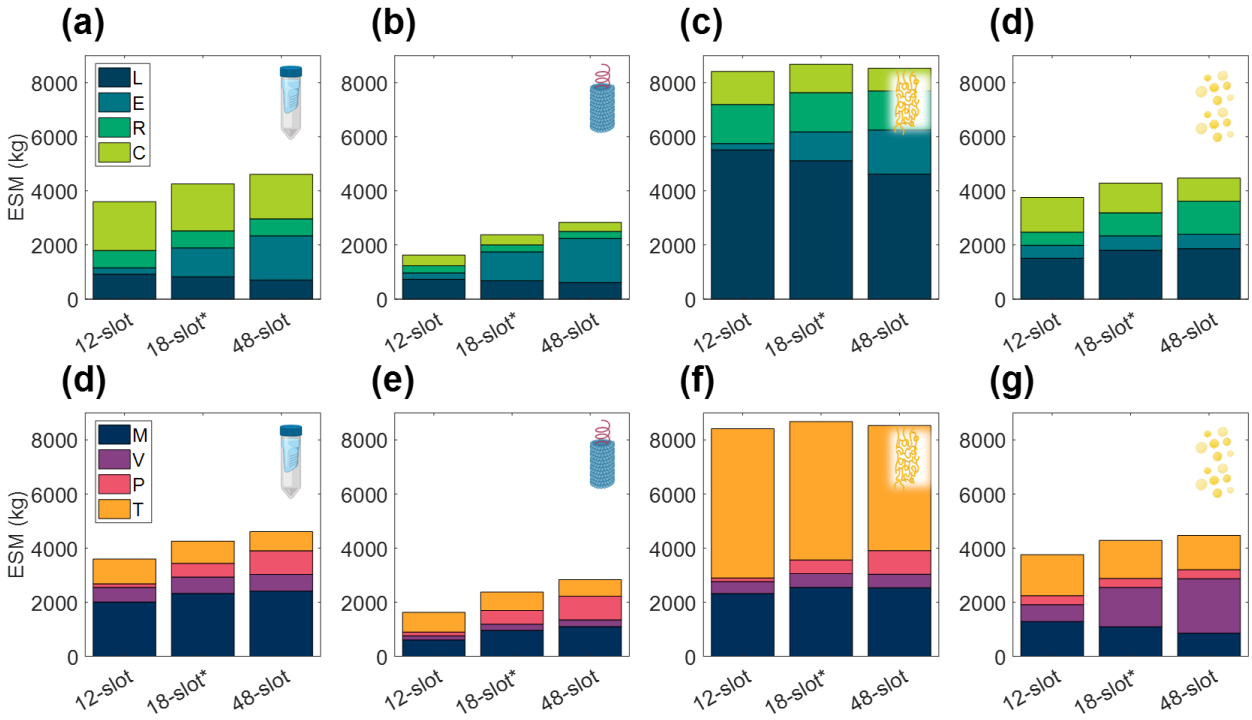

Figure 8.9. Changes in extended equivalent system mass values with different capacity centrifuge models broken down by labor (L), equipment (E), raw materials (R), and consumables (C) cost categories and mass (M), volume (V), power (P), and labor time (T) constituents for SPN (a, d), VIN (b, e), ELP (c, f), and OLE (d, g). SPN, spin column; VIN, plant virus-based nanoparticle; ELP, elastin-like polypeptide; OLE, oilbody-oleosin.

8.3.4.3. Technology reusability

The number of use cycles for liquid chromatography resins is an important economic parameter in commercial pharmaceutical manufacturing[385]. Here we explore the impact of use cycles on the CHM and ELP procedures in a space mission context, looking at no reuse nor regeneration operation of the purification technology, (-)Reuse, and at an increased number of use cycles, (+)Reuse (Figure 8.10).

We observe that the terrestrial importance of use cycles does not prevail in this isolated ESM evaluation in a space context. The high purchase costs of resin are not considered in ESM and the impact of the reuse cycles is reduced to the mass and volume savings of the pre-packed column

consumable. There is a minor decrease in ESM of the (+)Reuse over the base case scenario, but both of these result in substantially higher ESM than the (-)Reuse scenario, particularly for the ELP procedure, in which the regeneration operation has been removed in addition to the reusability of the technology.

These results echo the trend of single-use technology in commercial biotechnology in which manufacturers look to disposable plastic bioreactor and buffer bags as a means to reduce cleaning and validation costs[386]. It would be valuable to further consider the utilization of single-use technology in a space pharmaceutical foundry, and in other space systems bioengineering applications, but it is important to point out the limited scope of this ESM analysis. Here we reiterate that the single unit procedure scope establishes a modular basis for pharmaceutical foundry ESM evaluation but does not realize the true circular economy advantages of reuse, which may be considerable for the regeneration step, and of biological systems for production of the purification reagent in general.

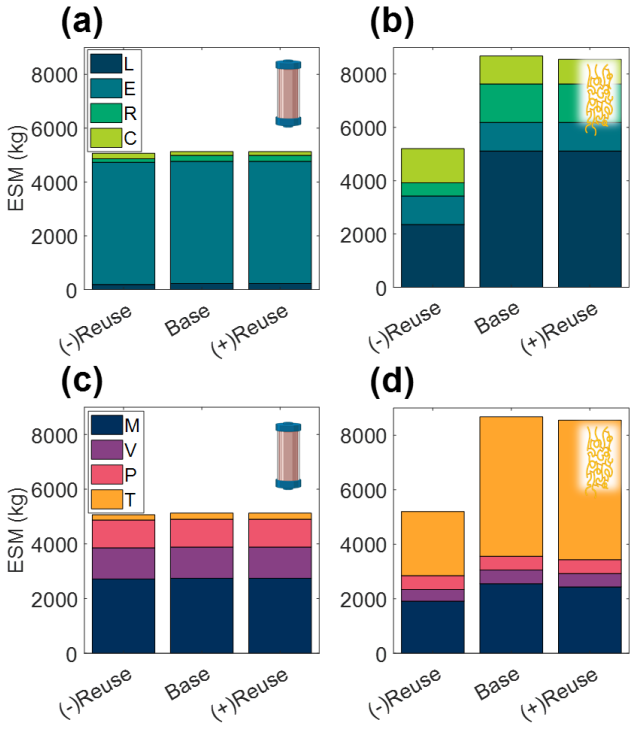

Figure 8.10. Changes in extended equivalent system mass values with reusability of purification technology broken down by labor (L), equipment (E), raw materials (R), and consumables (C) cost categories and mass (M), volume (V), power (P), and labor time (T) constituents for CHM (a, c), and ELP (b, d). (-)Reuse considers the technology as single-use and accordingly discards the unit procedure cleaning operations; (+) Reuse considers additional reuse cycles of the technology. CHM, pre-packed chromatography; ELP, elastin-like polypeptide.

8.4. Conclusion & Future Directions

In this study, we have introduced and applied the ESM framework to biopharmaceutical processing as a first step towards modeling and understanding the costs of Space Systems Bioengineering and, more specifically, of a long-duration space exploration medical foundry, which we believe may one day constitute a critical bioregenerative component of ECLSS for humans to be able to explore the surface of Mars. We have observed that the static behavior of ESM, while certainly maintaining usefulness in early-stage analyses, may stymie later-stage analyses of bioregenerative life support technologies, which tend to behavior more dynamically than traditional abiotic counterparts. In the future, higher fidelity analyses may be performed using tools such as HabNet[387], although the use of such dynamic mission design and modeling tools will require additional software engineering efforts. As it stands now, our techno-economic calculations both satisfy the three fundamental aspects for life support modeling[388] and provide helpful directions for future efforts to incorporate purification processes in space systems bioengineering.

The mAb affinity capture step represented an ideal starting point for biopharmaceutical purification cost analysis given the breadth of the mAb treatments for space-important health indications, the fact that mAb purification is considered a platform technology, and the diversity of affinity capture technologies. However, there are additional processing categories, such as size exclusion, ion exchange, and hydrophobic interaction unit procedures, which could be similarly studied in isolation for their general relevance in biopharmaceutical manufacturing. Establishing

a unit procedure knowledge base for space-relevant economics of biopharmaceutical purification would provide additional benefit to the community.

We acknowledge that the ESM analysis performed in this study utilizes current Earth-based technologies, not Mars-designed processes, and that as technologies evolve and expand the analysis will need to be updated. The need to revisit and update ESM analyses periodically as technology develops is standard practice. This is well illustrated in a recent ESM analysis of plant lighting systems that compares solar fiber optics to photovoltaic-powered light emitting diode hybrid systems[389]. The study results reversed decade-old trade study outcomes in which solar fiber optics scored more favorably, citing rapid advances in solar photovoltaics and light emitting diode technologies.

Furthermore, the analysis presented does not encapsulate potentially significant characteristics of the unit procedures at the interfaces of the upstream and downstream biomanufacturing elements. For example, at the upstream interface the biotic unit procedures (VIN, ELP, OLE) have been reported in literature to be effective capture mechanisms in "dirtier" feed solutions, perhaps absolving the need for more complex pre-capture clarification steps by virtue of process integration. At the downstream end, the eluate of the CHM unit procedure can be directly fed to the subsequent processing step, which would be particularly amenable for other column-based unit procedures, resulting in lower labor time and manufacturing duration. We also do not account for the uncertainty in performance associated with the developmental state of the technology. There have been substantially lower research and development investments in the biotic technologies than in the commercially available abiotic technologies; one may reasonably assume that there is more potential for improvements through biotic unit procedure optimization, while also considering that a larger driving force in abiotic unit procedure optimization for commercial

terrestrial operations may balance or outweigh this. Forecasting on the technology development dynamics in the context of these, and other, forces could provide significant additional insights.

Several overarching lessons on the development required for deployment of pharmaceutical purification technology to support human health in space can be gleaned from the cost breakdown of the ESM framework employed in this study. The high mass costs for the mAb capture technologies investigated suggest strong incentives to pursue efforts in miniaturization to reduce not only equipment mass, but also reagent mass, as preparation for pharmaceutical foundries in space. The high labor costs and duration of some of the technologies studied likewise suggests that automatization of biopharmaceutical purification would be impactful. Automatization could also conceivably be valuable in reducing mass costs associated with manual manipulation, such as pipette tips and gloves, and those associated with ensuring sterile operation. We also underline the importance of scheduling and equipment sizing optimization; for example, the ESM penalty for capturing the mission demand of mAb with the VIN unit procedure yielded up to 40% higher total ESM for non-optimal scheduled manufacturing batches. Given the advantage of *in situ* manufacturing to respond to uncertainty in mission medicine demand, further research to explore scheduling and equipment sizing under uncertainty would provide valuable insight.

There are a series of challenges facing pharmaceutical foundries in space beyond processing. Perhaps the most daunting of these is the incompatibility of existing pharmaceutical regulatory compliance frameworks with the design constraints of *in situ* manufacturing. There are currently dozens to hundreds of analytical tests required to confirm process and product quality prior to release of the pharmaceutical for administration to human patients[288], which translates into a highly burdensome cost for *in situ* manufacturing of pharmaceuticals in space. Fortunately, there is a strong and parallel terrestrial need to reduce the burden of regulatory compliance while

maintaining standards of quality assurance and control for personalized medicine, an individualized and patient-specific approach to medical care with widespread support. As mentioned earlier, trends of distributed and sustainable biomanufacturing on Earth provide additional support for reducing ESM-relevant costs.

The analyses presented in this study motivate future investigation into the ESM output of a complete pharmaceutical foundry for a more complete comparison to other ECLSS needs and subsequent formal evaluations of medical risk (i.e., loss of crew life, medical evacuation, crew health index, risk of radiation exposure-induced death from cancer) mitigation as a balance to the ESM costs. The Integrated Scalable Cyto-Technology system[338], reported in literature as capable of "end-to-end production of hundreds to thousands of doses of clinical-quality protein biologics in about 3 d[ays]," is an automated and multiproduct pharmaceutical manufacturing system that may serve well as a starting point for a complete pharmaceutical foundry evaluation. While downstream costs are typically a large proportion of terrestrial biopharmaceutical production costs, they may represent an even higher proportion of the overall ESM costs. ESM is more closely aligned to PMI as a metric than to cost of goods sold in dollars, suggesting that downstream contributions to ESM may similarly dominate. Budzinski and team found that downstream operations contributed 82% of the total PMI for commercial mAb production[63].

Assembly of a complete pharmaceutical foundry ESM model would also enable investigation of more nuanced RMA design considerations, such as those relating to the influence of a fixed set, or anticipated probability distribution, of pharmaceutical product diversity and batch size on optimal system composition to meet given medical risk thresholds.

As stated in the original presentation of ESM theory and application, comparison of multiple approaches for a given subsystem with ESM, such as we are studying with the capture step of a

mAb pharmaceutical foundry, should satisfy the same product quantity, product quality, reliability, and safety requirements[390]. Of these assumptions, the product quality and safety requirements prove challenging for implementation in pharmaceutical foundry comparisons. It is worth noting that reliability is not considered in the scope of this preliminary study, given the varying technology readiness levels of the unit procedures, but that it should be included in future analyses of full purification schemes. By extension, the impact of microgravity and reduced gravity on reliability and unit operation performance, while not investigated in this study, is an important and complex consideration, that requires significant research to address. Similarly, stability of the production resources over the course of a mission duration should be further considered in future works. High product sensitivity to process changes, and the large battery of testing sometimes required to observe them (the extent of which will also change with the processes employed), creates a situation where ESM comparisons of pharmaceutical foundries that serve as technology decision making tools will absolutely need to meet this requirement, albeit at a considerable cost and/or complexity of execution.

The assessment of equivalent safety requirements, to the best of the knowledge of the authors, has been approached thus far in an ad hoc and qualitative manner, relying on extensive subject manner expertise and working process knowledge. One promising route to strengthening these critically important safety assessments would be to implement a formal assessment framework based on the environmental, health, and safety (EHS) assessment proposed by Biwer and Heinzle[61], in which process inputs/outputs are ranked based on a series of hazard impact categories (e.g., acute toxicity, raw material availability, global warming potential) and impact groups (e.g., resources, organism). The key to a systematic space health-centric safety assessment like this is to establish space-relevant EHS impact categories (e.g., planetary protection, crew and ship safety). An improvement

of the EHS underpinnings has the potential to provide significant benefits to future ESM analyses in the increasingly complex mission architecture of longer-duration missions.

8.5. Supplementary Material

Supplementary Table S8.1. Example commercially approved monoclonal antibody (mAb) therapies of relevance to human health in space that have been considered in the determination of the reference mission pharmaceutical demand. Need basis is defined per the listed indication and FDA label. Demand estimates are derived by multiplying the FDA-approved need basis by the crew size and the duration of the demand. Asterisk (*) denotes an antibody drug conjugate.

mAb	Indication	Dose	Need Basis
Erenumab-aooe (FDA Label)	Migraine headache prevention	70 mg (or 140 mg)	1 dose/month
Romosozumab (FDA Label)	Bone regeneration	210 mg	1 dose/month
Gemtuzumab ozogamicin* (FDA Label)	Acute myeloid leukemia	6 mg/m^2; 3 mg/m^2; 2 mg/m^2	day 1/day 8/every 4 weeks; 1 course/year

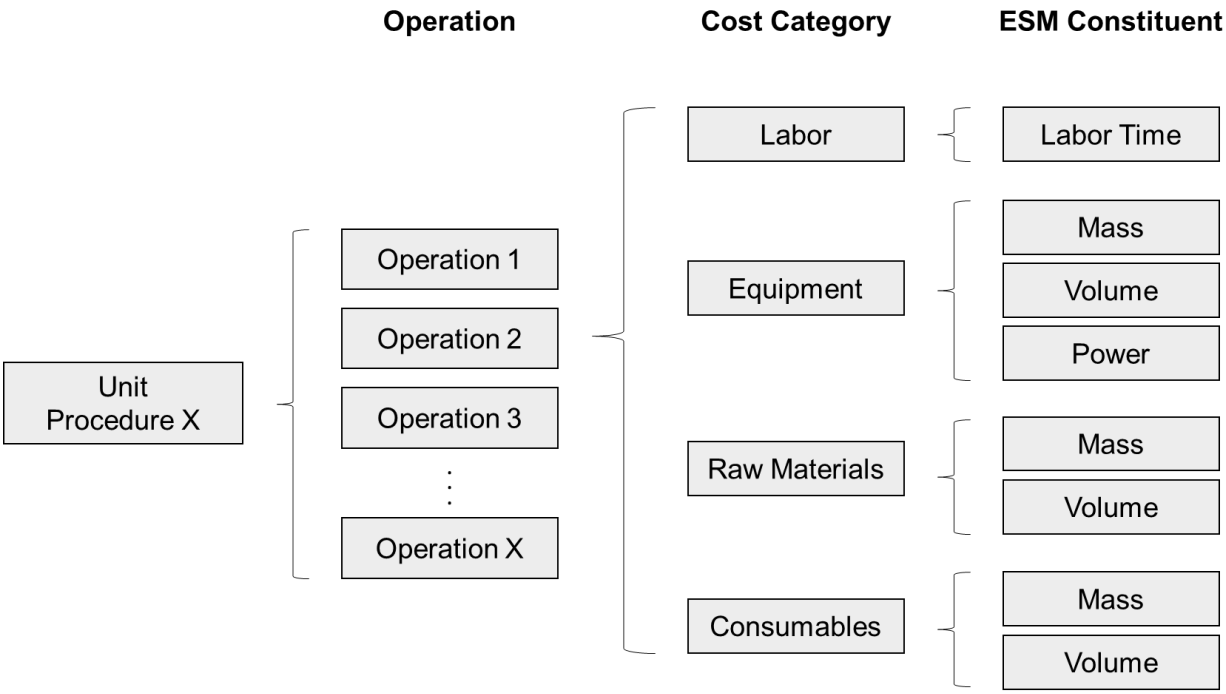

Supplementary Figure S8.1. Schematic of deterministic unit procedure model construction grouped by operation, cost category, and equivalent system mass (ESM) constituent.

Supplementary Table S8.2. Unit procedure assumptions for maximal feed stream volume and monoclonal antibody (mAb) binding capacity.

Unit Procedure	Code	mAb Binding Capacity	Maximal Feed Stream Volume
Pre-packed chromatography	CHM	30 mg/mL resin	N/A
Spin column	SPN	1 mg/column	0.6 mL
Magnetic bead	MAG	27 mg/mL bead slurry	0.3 mL
Plant virus-based nanoparticle	VIN	4 mg/mL stock solution	2 mL*
Elastin-like polypeptide	ELP	0.42 mg/mL stock solution	0.8 mL*,¥
Oilbody-oleosin	OLE	6.74 mg/mL stock solution	0.1 mL*,γ

* based on 2 mL unit volume; actual feed stream volume added is based on the amount of stock solution required and thus mAb quantity in the feed stream.
¥ reduced from 2 mL maximal to account for volume needed for salt solution addition (0.4 mL) and required 1:1 volume ratio of ELP:mAb.
γ reduced from 2 mL maximal to account for required 1:20 volume ratio of OLE:mAb.

Supplementary Table S8.3. Labor time standardizations applied to common operations across unit procedures.

Operation	Value	Unit
Monitoring	0.05	labor hour/hour
Preparation (incubation + centrifugation)	1.0	min/effective batch
Pipetting liquid	0.5	min/solution type
	0.1	min/additional unit/effective batch
Resuspending pellet	1	min/unit

Supplementary Table S8.4. Equivalency factor values used to generate equivalent system mass values from constituents of mass, volume, power, cooling, and labor.

Segment	L_{eq} (kg/kg)	M_{eq} (kg/kg)	V_{eq} (kg/m^3)	P_{eq} (kg/kW)	C_{eq} (kg/kW)	T_{eq} (kg/CM-h)
Pre-deployment (Pd)	2.77	1	9.16	237	40	0.7
Transit to Mars (Tr1)	10	1	133.8	136	50	0.7
Surface Operation (Su)	1	1	9.16	228	145	0.7
Return Transit (Tr2)	10	1	133.8	136	50	0.7

Supplementary Table S8.5. Optimal number of batches per mission in the base case scenario for each unit procedure, as determined via minimization of equivalent system mass.

Unit procedure	Optimal number of batches per mission
CHM	342
SPN	948
MAG	5670
VIN	360
ELP	2058
OLE	846

Supplementary Table S8.6. Mars surface mission equivalency factor values used by Zabel, 2020 of a space greenhouse.

Segment	M_{eq} (kg/kg)	V_{eq} (kg/m^3)	P_{eq} (kg/kW)	C_{eq} (kg/kW)	T_{eq} (kg/CM-h)
Surface Operation (Su)	1.0	215.5	87.0	146.0	0.465

Supplementary Table S8.7. Optimal number of effective batches per mission in the mAb stream composition scenario analysis conditions for each unit procedure, as determined via minimization of equivalent system mass.

mg/mL	0.10	0.20	0.35	0.50	075	1.00	1.50	2.00	5.00
CHM	342	342	342	342	342	342	342	342	342
SPN	9450	4728	2700	1896	1260	948	630	568	568
MAG	56694	28350	16200	11340	7560	5670	3780	2838	1134
VIN	2910	1494	882	639	450	360	264	216	132
ELP	7092	3546	2058	2058	2058	2058	2058	2058	2058
OLE	2988	1494	854	846	846	846	846	846	846

Supplementary Table S8.8. Optimal number of batches per mission in the mAb demand scenario analysis conditions for each unit procedure, as determined via minimization of equivalent system mass.

Demand x 10^3 (mg mAb/mission)	1.0	2.0	3.5	5.0	7.5	10.0	15.0	20.0	30.0
CHM	36	70	120	172	257	342	512	682	1022
SPN	96	192	336	474	714	948	1422	1890	2844
MAG	568	1134	1988	2838	4260	5670	8508	11340	17010
VIN	36	72	126	180	270	360	533	714	1068
ELP	210	414	726	1032	1548	2058	3090	4116	6174
OLE	86	170	300	422	632	846	1264	1692	2532

Supplementary Table S8.9. List of centrifuge models used in the alternative centrifuge scenario.

Model	Vendor	Capacity	Mass (kg)	Dimensions (cm)	Power (kW)
MiniSpin	Eppendorf	12	3.7	22.5 x 23.0 x 13.0	0.085
5418R	Eppendorf	18	22	0.0345	0.320
5427R	Eppendorf	48	30	31.9 x 54.0 x 25.4	0.550

Supplementary Table S8.10. Optimal number of effective batches per mission in the centrifuge model alternative scenario conditions for each analyzed unit procedure, as determined via minimization of equivalent system mass.

Centrifuge model	MiniSpin	5418R	5427R
SPN	1422	948	360
VIN	533	360	137
ELP	3090	2058	774
OLE	1264	846	317

Chapter 9. Affinity sedimentation and magnetic separation with plant-made immunosorbent nanoparticles for therapeutic protein purification

"Love is the only thing that can turn an enemy into a friend."

-Martin Luther King Jr.
Helping me to explain to visitors the prominently displayed golden statue of a plant virus on my office desk.

This chapter is based on the following pre-print publication:

McNulty M.J., Schwartz A., Delzio J., Karuppanan K., Jacobson A., Hart O., Dandekar A., Giritch A., Nandi S., Gleba Y., and McDonald K.A. (2021) Affinity sedimentation and magnetic separation with plant-made immunosorbent nanoparticles for therapeutic protein purification. *bioRxiv*. doi:10.1101/2021.11.05.467285

Abstract

The virus-based immunosorbent nanoparticle is a nascent technology being developed to serve as a simple and efficacious agent in biosensing and therapeutic antibody purification. There has been particular emphasis on the use of plant virions as immunosorbent nanoparticle chassis for their diverse morphologies and accessible, high yield manufacturing via crop cultivation. To date,

studies in this area have focused on proof-of-concept immunosorbent functionality in biosensing and purification contexts. Here we consolidate a previously reported pro-vector system into a single *Agrobacterium tumefaciens* vector to investigate and expand the utility of virus-based immunosorbent nanoparticle technology for therapeutic protein purification. We demonstrate the use of this technology for Fc-fusion protein purification, characterize key nanomaterial properties including binding capacity, stability, reusability, and particle integrity, and present an optimized processing scheme with reduced complexity and increased purity. Furthermore, we present a coupling of virus-based immunosorbent nanoparticles with magnetic particles as a strategy to overcome limitations of the immunosorbent nanoparticle sedimentation-based affinity capture methodology. We report magnetic separation results which exceed the binding capacity of current industry standards by an order of magnitude.

9.1. Introduction

Virus-based nanomaterials are proving to be uniquely accessible, precise, and efficacious solutions to problems in fields ranging from energy to medicine[391]. Plant viruses serve as a particularly interesting biologically-derived nanomaterial for their inherent advantages of host specificity-related human safety[392], simplicity of *in planta* cultivation[393], and wide variety of particle architectures and functionalities[394]. Plant viral nanoparticles and virus-like particles have been studied for diverse biotechnical applications including gene therapy[395,396], vaccines[397,398], medical imaging[399,400], drug delivery[401,402], and biosensors[403,404].

The concept of a plant virus-based immunosorbent nanoparticle (VIN), a plant virus or virus-like particle displaying antibody-binding proteins, has been proposed to capture antibodies for biosensing[343,405] and therapeutic antibody purification[342]. This nascent technology is one approach to address the need to reduce capital intensity for equitable and accessible antibody-related healthcare solutions, which could be harnessed to treat more prevalent diseases with availability of inexpensive and adequate production and purification capacity[184]. Purification can cost up to 80% of the total manufacturing expenses for antibody and other biopharmaceutical products[406]. The simple and bioregenerable VIN technology is also one that may transcend terrestrial needs as humankind considers extended duration space exploration and is faced with stringent life support system requirements in perhaps the most limited resource environment that humans will face[208,407]. Recent literature highlights the potential of plant-based manufacturing to close human health risk gaps for manned exploration missions[328].

Initial VIN research has primarily focused on nanomaterial design, considering three plant virion chassis (potato virus X[343], bamboo mosaic virus[405], turnip vein clearing virus (TVCV)[342]) and several ligand display strategies, including multiple fusion sites on the coat protein, linker

inclusions, modulations of ligand display density, and two different immunosorbent ligands (both based on functional fragments of *Staphylococcus aureus* Protein A). Additional research is needed to evaluate broader functionalities of VIN technology, characteristics for reliable biomanufacturing, and compatibility with advanced multi-material configurations.

There have been multiple approaches to engineering virus-based nanomaterials into multi-material configurations including layer-by-layer assembled thin biofilms[408], electrospun nanofibers[409], and bio-functionalized magnetic particles, to name a few. Within these approaches, bio-functionalized magnetic particles have been distinguished at large as an important platform within biosensing[410], and protein purification[411]. However, the virus-based nanomaterial research exploring bio-functionalized magnetic particles to date has been limited to gene therapy[412,413] and molecular imaging[414,415]. Given the demonstrated ability of virus-based nanomaterials as reagents to enhance target binding and sensitivity over traditional ligands[416–418] we perceive a general synergy and advantage in developing virus-functionalized magnetic particles for sensing and protein purification.

In this study we present a new vector for production of VINs, develop an optimized purification process for VINs that is generalizable to other plant virus-based nanomaterials, characterize key functional VIN properties, and in the process, identify potential limitations of the VIN methods used to date. In response to identification of these limitations, we present a novel VIN-magnetic particle coupled system to overcome these limitations. Preliminary results suggest enhanced immunosorbent characteristics as compared to commercial immunosorbent magnetic particle standards and also provides new perspectives for utilization of plant virus-based nanomaterials.

9.2. Results

9.2.1. Production of a plant virus-based immunosorbent nanoparticle

Intact VINs consisting of an assembled tobamovirus, TVCV, presenting a C-terminal coat protein fusion to a flexible linker domain $(GGGGS)_3$ coupled to a *S. aureus* Protein A fragment (domains D and E) were successfully produced in *Nicotiana benthamiana* plants via agroinfiltration and subsequently purified to a moderate extent (Figure 9.1a – d). An illustration of the construct schematic and results of the PCR and DNA sequence verification of the transformation are included in Supporting figures: Figure S9.1, Figure S9.2 and Supporting table: Table S9.1. The vector used here simplifies previously published *A. tumefaciens* vectors[342] by combining multiple provectors into a single vector capable of producing intact VINs.

Agroinfiltrated *N. benthamiana* plants showed signs of viral infection typical of tobamoviruses (yellowing of leaves, stunted growth; data not shown). The coat protein fusion was expressed at high levels (~ 0.3 g VIN / kg leaf fresh weight, per total soluble protein results of purified VIN) in *N. benthamiana* plants collected 6-14 days post-infiltration. Furthermore, transmission electron microscope (TEM) images show that fully assembled virion particles were formed (Figure 9.1b-c).

SDS-PAGE results confirm that there is a band at the expected size of the VIN coat protein Fc-affinity ligand fusion (CP-FcAL) (~33.5 kD) and Western blot results confirm that it is an identity match for the expected CP-FcAL (via anti-protein A antibody). We did not observe bands corresponding to unfused Fc-affinity ligand on SDS PAGE gels or in Western blots, although SDS-PAGE results do present the possibility of a minor presence of CP-FcAL degradation products. The CP-FcAL protein identity was also confirmed using mass spectrometry (Supporting figure: Figure S9.3).

In addition to agroinfiltration, we also demonstrated that mechanical transmission using the VINs generated by agroinfiltration is a viable route for production of fully assembled and functional plant virus-based immunosorbent particles. Mechanical transmission of the solution containing fully assembled VINs yielded systemic plant infection and morphological change (Figure 9.1e – g), indicating that the VINs retain systemic mobility with the immunosorbent fusion protein. Agroinfiltration-based VIN expression induced comparable *N. benthamiana* plant morphology (data not shown).

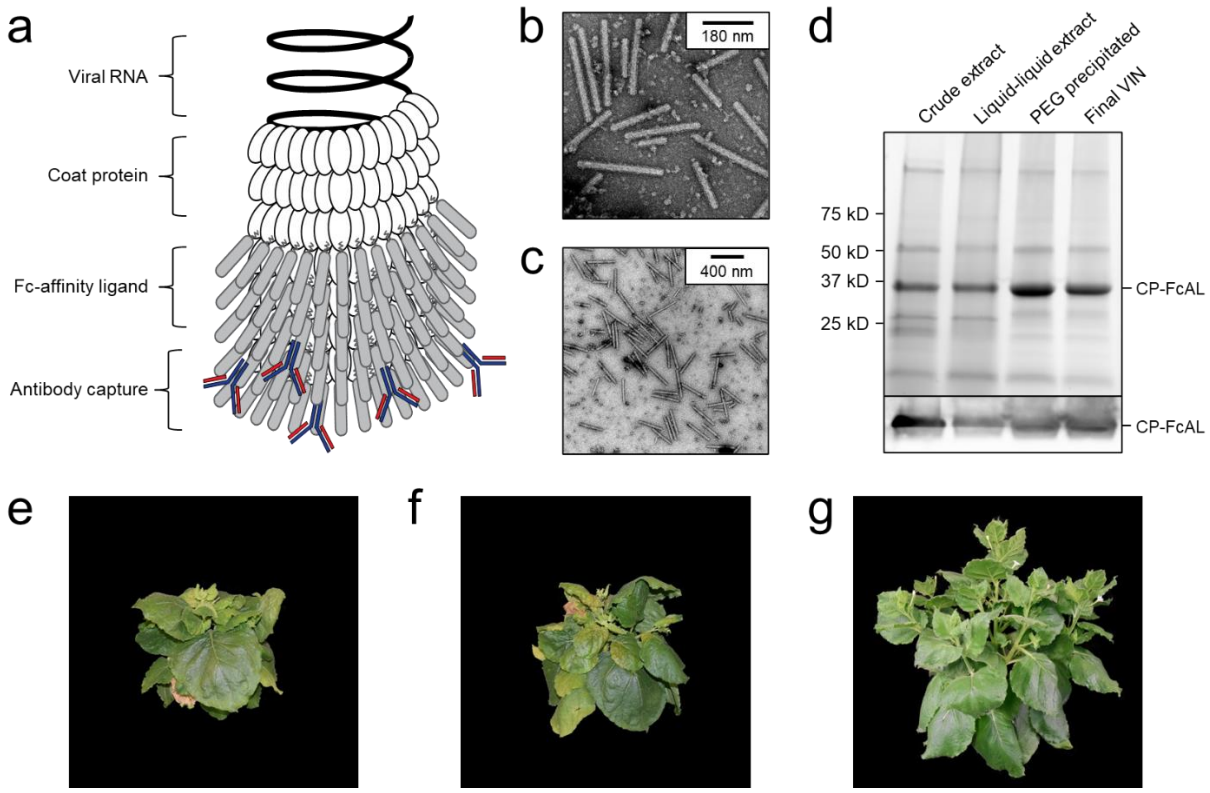

Figure 9.1. Production of a plant virus-based immunosorbent nanoparticle (VIN). (a) An illustrative depiction of a VIN. The native plant virus (viral nucleic acid encapsulated by coat protein) is fused via a peptide linker to an Fc-affinity ligand, which confers immunosorbent functionality to the plant virus. (b, c) Negative stain transmission electron microscope images of VIN in crude plant extract solution produced via agroinfiltration in *N. benthamiana* plants. (d) Reducing condition SDS-PAGE (upper) and Western blot (lower) of the VIN preparation marked at the band height corresponding to VIN coat protein Fc-affinity ligand fusion (CP-FcAL). Representative photographs of 7-week-old *N. benthamiana* plants incubated in a controlled environment facility for 14 days post-infection with mechanically transmitted (e) VIN (produced

using vector pICH25892), and (f) wild-type tobacco mosaic virus, as compared to (g) uninfected healthy plants.

9.2.2. Fc-protein capture and elution

Protein A is well known to bind strongly with the conserved fragment crystallizable (Fc) region of many species and subclass variants of IgG. We show that VINs retain general immunosorbence for several species and subclasses of IgG (Supporting figure: Figure S9.4).

Next, we demonstrate that VINs are capable of capturing and then eluting human immunoglobulin G (hIgG) using a low pH elution mechanism (Figure 9.2a – b). VINs produced using mechanical transmission were also shown to retain immunosorbent functionality (Supporting figure: Figure S9.5). Tests using bovine serum albumin (BSA) as the target capture protein confirm that sedimentation of the target protein, and largely that of the VIN, required specific binding interactions (Figure 9.2c). It was also observed that VINs would sediment in the absence of binding target proteins at centrifugation of 20,000 x g for 90 minutes (Supporting figure: Figure S9.6).

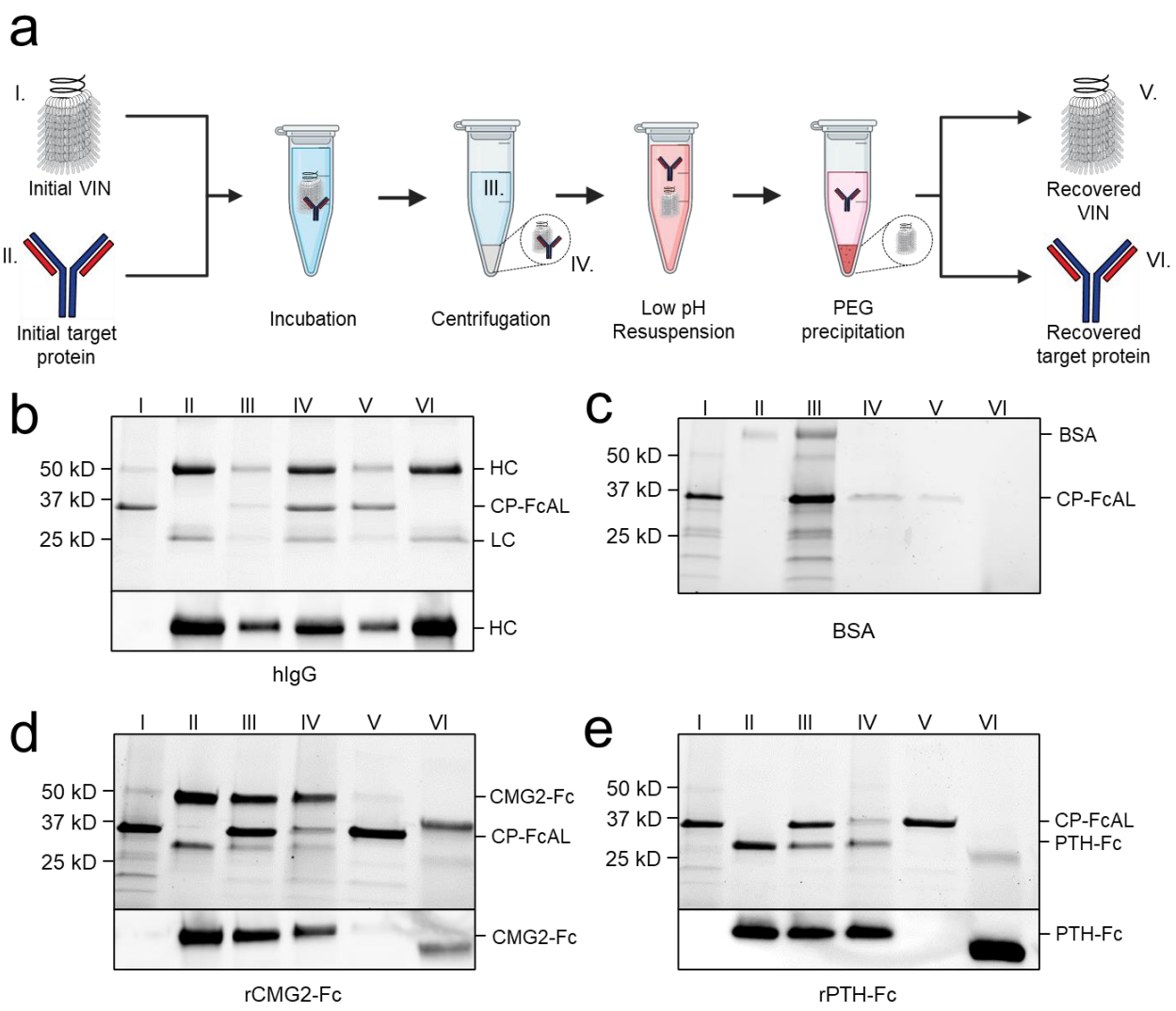

Figure 9.2. Plant virus-based immunosorbent nanoparticle (VIN)-based capture and elution of Fc-proteins from a purified solution. (a) An illustration of the VIN-based capture and elution that indicates sample points. SDS-PAGE (top) and Western blot (bottom) results of VIN-based capture and elution with pre-purified targets of (b) human immunoglobulin G (hIgG) – reduced into heavy chain (HC) and light chain (LC) constituents, (c) bovine serum albumin (BSA), (d) plant-expressed recombinant capillary morphogenesis protein Fc-fusion (rCMG2-Fc), and (e) plant-expressed recombinant parathyroid hormone Fc-fusion (rPTH-Fc). Lane definitions: I – initial VIN added; II – initial target added; III – VIN/target supernatant (loss); IV – VIN/target pellet resuspension (capture) (2x); V – recovered VIN (a,b – 2x; d,e – 4x); VI – recovered target protein (eluate) (5x).

VINs are also capable of capturing and eluting Fc-fusion proteins (Figure 9.2d – e). We successfully tested two pre-purified plant-expressed Fc-fusion proteins with VIN-based capture and elution: recombinant capillary morphogenesis protein Fc-fusion (rCMG2-Fc) and recombinant

parathyroid hormone Fc-fusion (rPTH-Fc). We observed that the biophysical characteristics (e.g., molecular mass, Svedberg coefficient) of the domain fused to the Fc region is critical to the sedimentation step (denoted III in Figure 9.2a) performance.

The hIgG sedimentation conditions (12,000 x g, 10 minutes) were not adequate for rCMG2-Fc (100 kDa) and rPTH-Fc (55 kDa). We determined that 20,000 x g for 20 minutes was adequate for sedimentation of the rPTH-Fc when bound to VINs (Supporting figure: Figure S9.7) and accordingly used this as an adequate centrifugation condition during operation with the larger rCMG2-Fc. Similarly, the smaller sizes of the Fc-fusion proteins as compared to the hIgG required a higher PEG concentration (25% w/v) for the PEG-based buffer exchange step (screening data not shown). Further optimization is required to remove residual PEG in this higher concentration method, as can be observed by the PEG interference of electrophoresis (lanes VI in Figure 9.2d – e), although it has been shown that the presence of PEG does not impede performance of subsequent downstream processing operations including ion exchange and affinity chromatography[419].

9.2.3. Process characterization

We evaluated process performance from the perspective of nanomaterial stability, capture and elution functionality, and particle integrity. VINs are stable throughout the freeze-thaw process for up to 12 cycles without noticeable degradation of CP-FcAL when stored at either -20 °C or -80 °C. Long-term stability of VINs was evaluated over a series of timepoints (2 weeks, 4 weeks, 8 weeks), temperatures (-20 °C, 4 °C, 20 °C), and protease inhibitors (none, 2 mM ethylenediaminetetraacetic acid (EDTA) and 1 mM phenylmethylsulfonyl fluoride (PMSF)) (Supporting figure: Figure S9.8). VIN CP-FcAL were intact over the duration evaluated at -20 °C

and 4 °C, while the addition of protease inhibitors was shown to prolong stability at 20 °C, with no discernable degradation observed for up to 2 weeks (Supporting figure: Figure S9.8).

Next, we demonstrated that the VIN functionality is retained when using samples of hIgG spiked into wild-type *N. benthamiana* plant extract (Figure 9.3a). Comparable performance was observed when crude *N. benthamiana* extracts of VIN were used in conjunction with antibodies spiked into crude *N. benthamiana* extracts (Supporting figure: Figure S9.9). Furthermore, we were able to demonstrate that the VINs recovered from a single capture and elution cycle can be reused for an additional cycle (Figure 9.3b). A minor fraction of hIgG was recovered with the VIN in both cycles, suggesting that hIgG recovery could be improved by optimization of the elution step (e.g., CP-FcAL binding affinity, buffer composition). The VIN recovered from the second use cycle could not be used for a third cycle with the established sedimentation conditions.

Accordingly, VIN particle integrity was investigated to probe limitations of the sedimentation method. We first compared VINs generated by two different methods of plant extraction, a blender or liquid nitrogen-assisted mortar and pestle (Figure 9.3c – d). We observed a statistically significant difference in the mean particle length between the two extraction methods ($p < 0.001$), with blender-based extraction resulting in a shorter mean VIN length (blender: $\bar{x}$ = 217 nm, σ = 84 nm, N = 428; mortar and pestle: $\bar{x}$ = 239 nm, σ = 80 nm, N = 558).

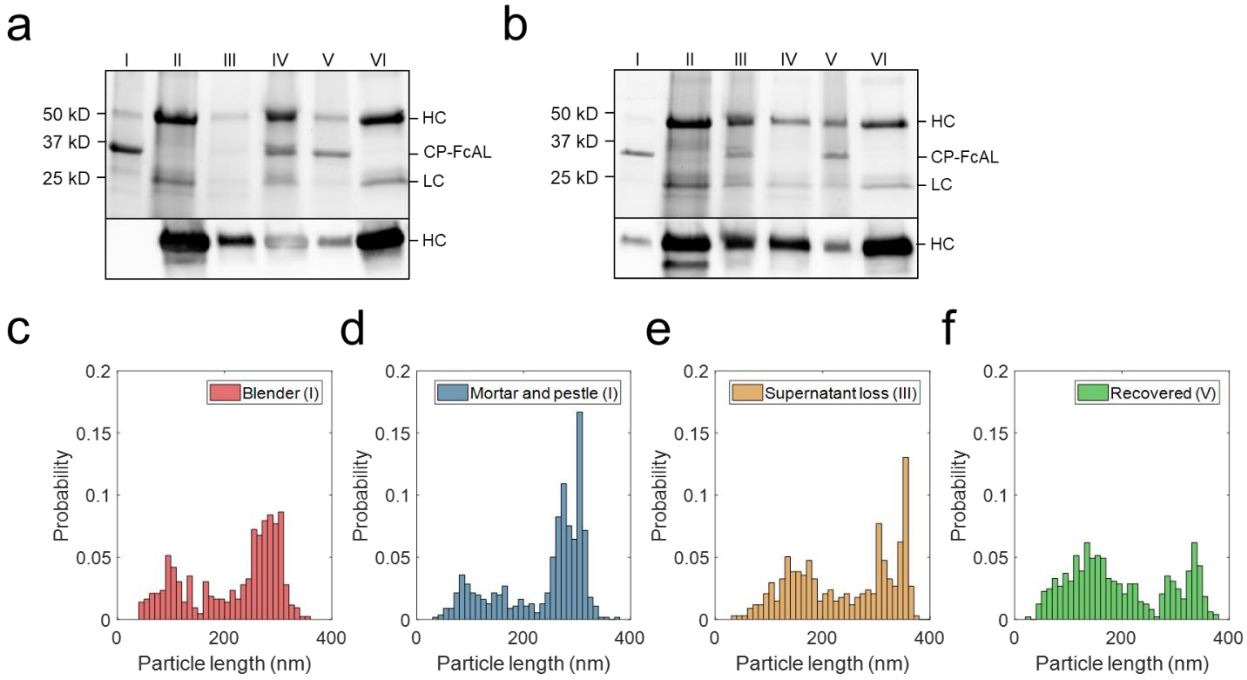

Figure 9.3. Plant virus-based immunosorbent nanoparticle (VIN)-based capture and elution of human immunoglobulin G (hIgG) from crude solution over multiple use cycles. (a) VIN-based capture and elution using a sample of hIgG in crude *N. benthamiana* plant extract, and (b) a second capture and elution cycle of the VIN recovered after the first use cycle. Lane definitions: I – initial VIN added; II – initial target added; III – VIN/target supernatant (loss); IV – VIN/target pellet resuspended (capture) (2x); V – recovered VIN (2x); VI – recovered target (eluate) (5x). Gels are marked with band heights corresponding to VIN coat protein Fc-affinity ligand fusion (CP-FcAL) and hIgG heavy chain (HC) and light chain (LC) constituents. Particle length analysis of negative stain transmission electron microscope images for (c) blender-extracted VIN, (d) liquid nitrogen-assisted mortar and pestle-extracted VIN, (e) VIN in the supernatant lost during the VIN-target complex sedimentation stage, and (f) recovered VIN post-elution. Data from parts e – f are generated using mortar and pestle extracted VIN and the naming convention I, III, and V corresponds to that established in Figure 9.2a.

We then investigated the VIN particle lengths at steps throughout the capture and elution with initial VIN generated using liquid nitrogen-assisted mortar and pestle extraction, focusing on the VINs lost in the supernatant during the VIN-hIgG complex sedimentation step (Figure 9.3e) and the final recovered VINs (Figure 9.3f), denoted III and IV in Figure 9.2a, respectively. There is an observed statistically significant difference in the mean particle length for the initial VINs, VINs

lost in the supernatant ($\bar{x}$ = 241 nm, σ = 94 nm, N = 337), and final recovered VINs ($\bar{x}$ = 196 nm, σ = 93 nm, N = 486) (I & III, $p = 0.039$; I & IV, $p < 0.001$; III & IV, $p < 0.001$) .

9.2.4. Process development

The appreciable level of impurities present in the purified VIN solutions, as well as an interest in improving scalability of the processing by removing the chloroform-based liquid-liquid extraction step, motivated an investigation into process development of the VIN purification. We performed a 2-factor 2-level process optimization of the extraction step (buffer composition – 50 mM sodium acetate 86 mM NaCl pH 5.0, 100 mM potassium phosphate pH 7.0; protease inhibitors – none, 2 mM EDTA + 1 mM PMSF) followed by an addition of a heat hold step that was investigated with a temperature screening (30 – 70 °C) after each processing operation (Figure 9.4a).

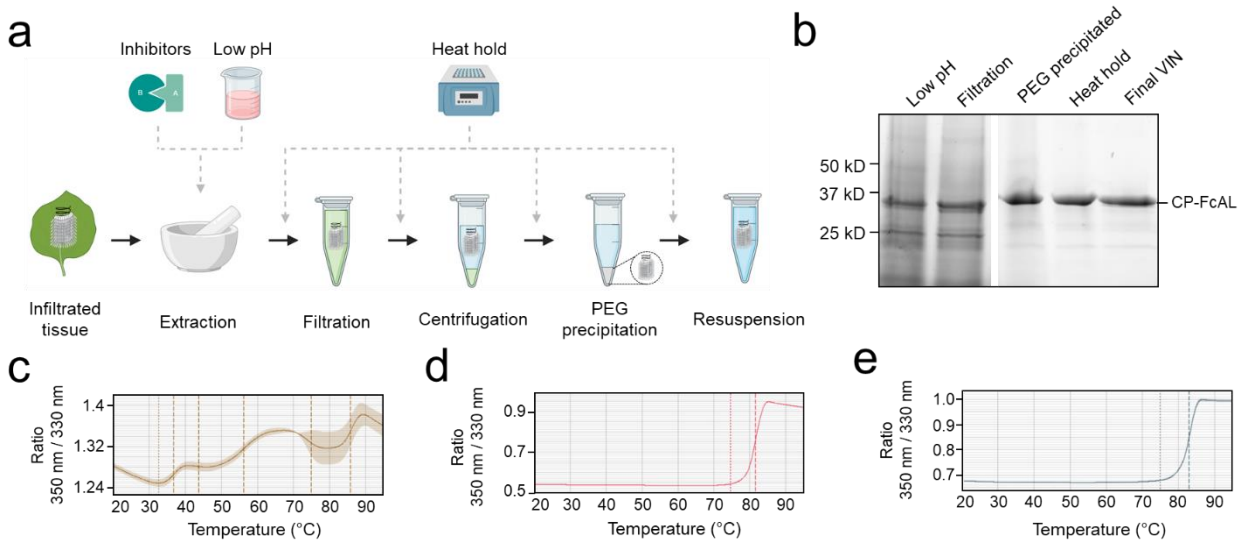

Figure 9.4. A summary of the plant virus-based immunosorbent nanoparticle (VIN) preparation process improvement conducted in this study. (a) An illustration of the VIN preparation stages and the experimental design tested, and (b) SDS-PAGE results of the optimized VIN preparation scheme shown marked at the band height corresponding to VIN coat protein Fc-affinity ligand fusion (CP-FcAL). Nano differential scanning fluorimetry assessment of protein thermostability is shown for (c) crude extract at pH 5, (d) VIN prepared according to the optimized scheme, and

(e) VIN prepared according to the baseline purification scheme, using the intrinsic tryptophan and tyrosine residue fluorescence at 350 nm and 330 nm.

Results of the process optimization conditions tested, including verification of bind-and-elute functionality of VIN produced from the different purification schemes, can be found in Supporting figures: Figure S9.10, Figure S9.11, and Figure S9.12.

The chloroform-based liquid-liquid extraction step was removed from the processing scheme with comparable or improved VIN recovery and purity upon inclusion of a low pH extraction and 60 °C heat hold post-PEG precipitation (Figure 9.4b). Interestingly, the addition of protease inhibitors to the extraction buffer reduced VIN recovery and increased the presence of what appears to be degradation products. Similarly distinct from wild-type virion processing, the heat hold resulted in significant VIN loss when introduced at processing steps prior to PEG precipitation. This behavior can be attributed to the FcAL presentation, as wild-type tobacco mosaic (wt-TMV) is routinely processed with early-stage processing heat holds[420].

Nano differential scanning fluorimetry results (Figure 9.4c – e) indicate that the VINs prepared according to either protocol detailed in this study exhibit a melting temperature of ~82 °C, supporting that the improved protocol does not introduce discernible differences in VIN CP-FcAL stability. There are multiple distinct conformational shifts within the crude solution consistent with the heterogeneity of solution.

9.2.5. Magnetic separation with VIN

Figure 9.5a illustrates the basic concept and utility of the VIN-coupled magnetic particles (VIN-MPs) generated in this study and Figure 9.5b – c displays TEM images of the intact VIN-MPs

complex. A magnetic separation-based capture and elution method was developed with hIgG spiked into phosphate buffered saline (PBS) (not shown) and crude *N. benthamiana* plant extract that confirms the VIN immunosorbent functionality in this novel configuration (Figure 9.5d). A faint presence in the elution that may indicate that some minor amount of VIN is recovered in addition to the target hIgG.

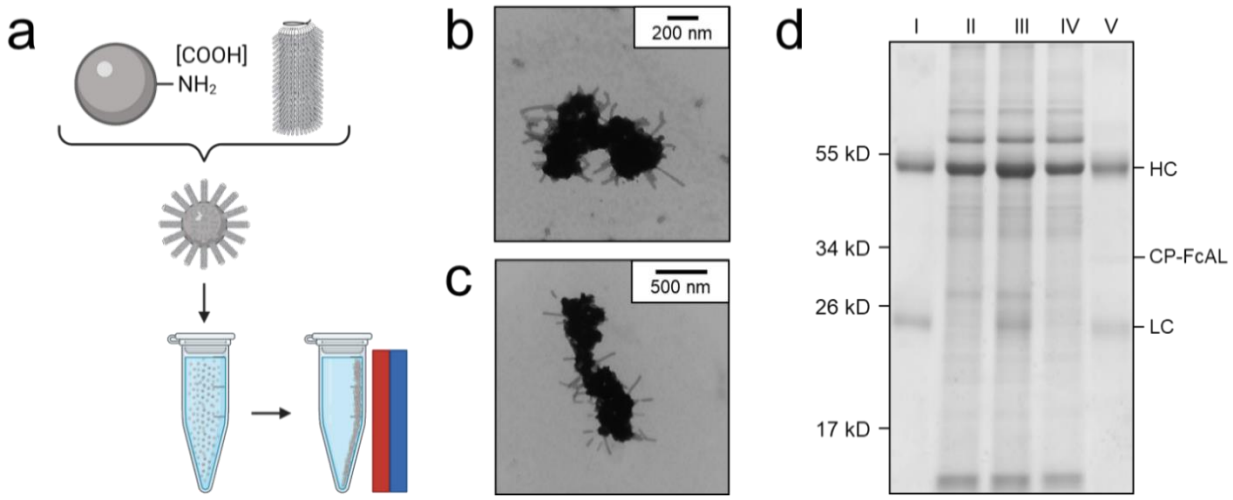

Figure 9.5. Production of plant virus-based immunosorbent nanoparticles coupled with magnetic particles (VIN-MPs). (a) An illustrative depiction of VIN-MPs. (b, c) Negative stain transmission electron microscope images of VIN-MPs generated using amine-terminated magnetic particles and 5% glutaraldehyde (VIN-MP-NGs). (d) Reducing condition SDS-PAGE of human immunoglobulin G (hIgG) bind-and-elute using VIN-MP-NGs and magnetic separation. Gels are marked with band heights corresponding to VIN coat protein Fc-affinity ligand fusion (CP-FcAL) and hIgG heavy chain (HC) and light chain (LC) constituents. Lane definitions: I – initial hIgG added; II – *N. benthamiana* plant extract; III – hIgG spiked into *N. benthamiana plant* extract; IV – non-bound supernatant after magnetic separation with VIN-MPs; V – hIgG elution from VIN-MPs.

The VIN-MP were either coupled with amine-terminated (VIN-MP-N) or carboxyl-terminated (VIN-MP-C) superparamagnetic particles. The VIN-MP-N coupled at significantly higher densities (> 0.2 mg VIN/mg MP) than the VIN-MP-C (≤ 0.1 mg VIN/mg MP) and resulted in higher hIgG capture. Therefore, VIN-MP-N were selected as the basis for additional study.

Two different coupling agents were tested: glutaraldehyde (VIN-MP-NG) and 1-Ethyl-3-(3-dimethylaminopropyl)carbodiimide (EDC) (VIN-MP-NE). Furthermore, we screened a range of EDC concentrations for use in the VIN-MP-NE synthesis reaction. We observed that the coupling density of VINs to MPs could be tuned with the concentration of EDC used in the covalent coupling reaction (Figure 9.6a). We also observed that the VIN concentration in the reaction medium could be used to tune coupling density (data not shown).

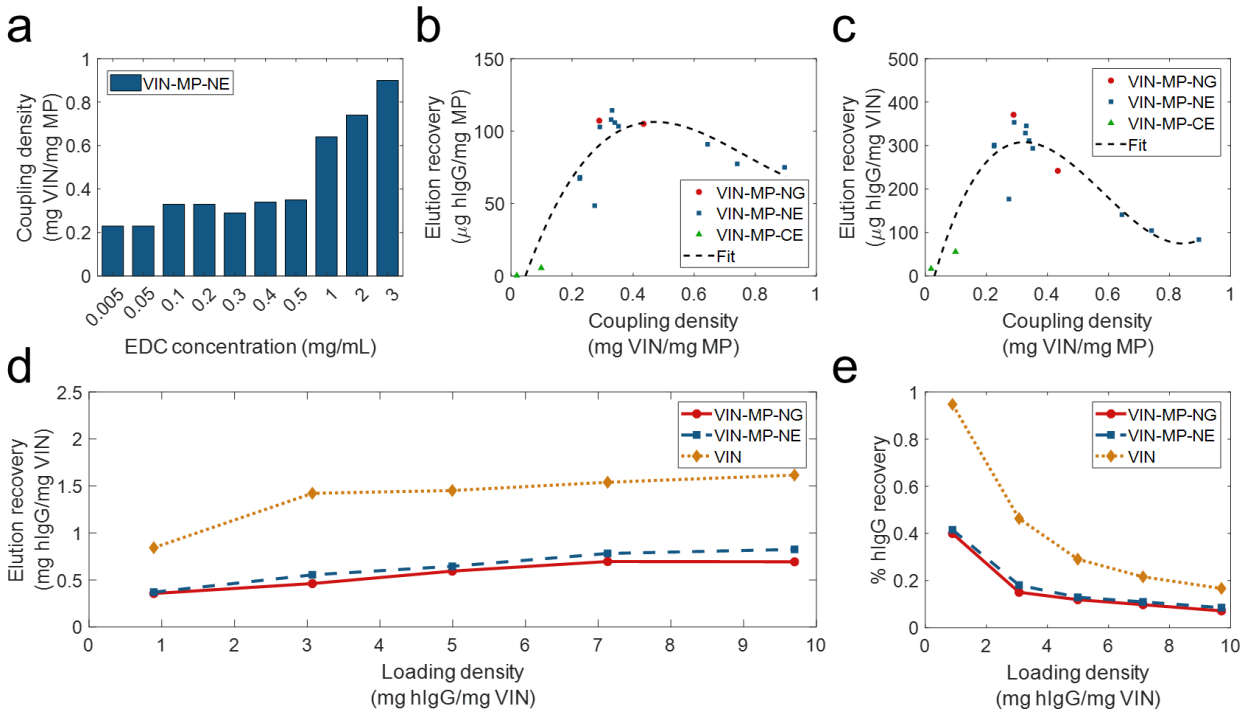

Figure 9.6. Screening and evaluation of plant virus-based immunosorbent nanoparticle-coupled magnetic particle (VIN-MP) coupling density and human immunoglobulin G (hIgG) elution. (a) 1-Ethyl-3-(3-dimethylaminopropyl)carbodiimide (EDC) concentration used during coupling and resultant coupling density for amine-terminated magnetic particles. VIN-MP coupling density and hIgG elution recovery for both amine- and carboxyl-terminated magnetic particles (b) per MP mass basis, and (c) per VIN mass basis. Fits are generated as 3rd order polynomials. Elution recoveries of hIgG from PBS are shown over a range of hIgG loading densities for amine-terminated MP (VIN-MP-N) with 5% glutaraldehyde coupling (VIN-MP-NG), 0.5 mg/mL EDC coupling (VIN-MP-NE), and uncoupled VIN in free suspension (d) per VIN mass basis, and (e) as an extent of the loading density and of hIgG from PBS.

We observed a non-monotonic relationship between coupling density and hIgG binding/elution load per mass of MP (Figure 9.6b). An optimal coupling density of 0.3 – 0.4 mg VIN/mg MP was identified. The hIgG binding/elution load per mass of VIN was consistent at approximately 0.3 mg hIgG/mg VIN below a coupling density of 0.4 mg VIN/mg MP, above which a negative correlation between coupling density and hIgG binding/elution load per mass of VIN is observed (Figure 9.6c). This suggests that higher coupling densities may provide less available hIgG binding sites due to steric hinderances or electrostatic interactions.

A comparison of VIN capture and elution performance with hIgG in PBS is shown in Figure 9.6d-e for magnetic separation using VIN-MP and sedimentation separation using uncoupled VIN over a range of hIgG loading densities. The VIN-MP hIgG elution recovery normalized by mass of VIN is approximately 35-55% of that of the uncoupled VIN.

Sedimentation and magnetic separation-based operations were further compared in purification of plant-expressed monoclonal antibody (mAb) A20 from crude *N. benthamiana* plant extract (Figure 9.7). Non-reducing condition SDS-PAGE results indicate that fully assembled mAb A20 is produced and recovered by VIN in elution. The relative extents of mAb A20 elution recovery for uncoupled VIN and VIN-MP are consistent with the hIgG in PBS results.

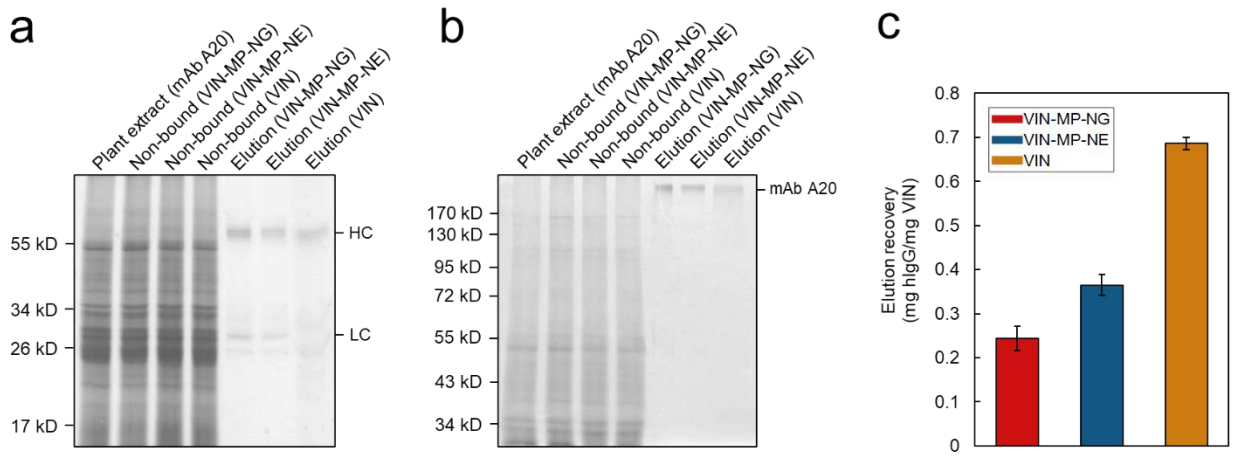

Figure 9.7. Capture and elution of plant-expressed monoclonal antibody (mAb) A20 by sedimentation with uncoupled plant virus-based immunosorbent nanoparticle (VIN) and magnetic separation with VIN-coupled magnetic particle (VIN-MP). (a) Reducing and, (b) non-reducing SDS-PAGE results of the non-bound supernatant and elution recovery of plant-expressed mAb A20 for VIN-MP with 5% glutaraldehyde coupling (VIN-MP-NG), 0.5 mg/mL 1-Ethyl-3-(3-dimethylaminopropyl)carbodiimide coupling (VIN-MP-NE), and uncoupled VIN in free suspension. Gels are marked with band heights corresponding to mAb A20 heavy chain (HC) and light chain (LC) constituents (reduced) or to dimerized mAb A20 (non-reduced). (c) Elution recovery of plant-expressed mAb A20 for VIN-MP-NG, VIN-MP-NE, and uncoupled VIN in free suspension. Error bars represent a single standard deviation of technical triplicate measurements.

9.3. Discussion

9.3.1. Biotic purification technologies

Virus-based nanomaterials present promising characteristics as an alternative technological platform to traditional chemical methods of biopharmaceutical purification in their inexpensive and scalable production coupled with their high replication fidelity, biophysical properties, stability, and accessible modifications leading to wide-ranging functionality. There are safety and regulations concerns of commercializing self-replicating technology, but this barrier has been addressed by researchers by removing the requisite replication machinery, as is done to generate virus-like particle technology[421,422], using a plant virus to avoid human infection[398], designing the virus-based nanomaterial to rapidly shed the transgenic gene inserts[34], and/or inactivating the virus[423]. As these methodologies are well established, we do not address virus nanoparticle containment strategies within the scope of VIN process development.

A range of biotic technologies beyond virus-based nanomaterials have been developed and studied for biopharmaceutical purification[424,425]. These can be classified by utility as fusion tags (e.g., inteins[426], carbohydrate binding modules[427]), thermo-responsive biopolymers (e.g., elastin-like polypeptides[428]), and hydrophobic nanoparticles (e.g., polyhydroxyalkanoates[429], oleosins[430],

hydrophobins[341]). Fusion tags have by and large been the most widely adopted biotic purification technology for the accessibility they present to early-stage research labs. However, they are limited as a platform technology by the influence of product-specific characteristics, complications of tag cleavage, and generally unfavorable commercial-scale economics (Fc-fusion tags being a notable exception to most of these limitations)[339]. There has been some adoption and maturation of the other biotic technologies that overcome these limitations, with an observed emphasis on elastin-like polypeptides (ELPs)[340,428] and oleosins[376]. VINs represent another contender within this group of technology, albeit at a more nascent stage of development. Advantages of VIN technology include the simplicity of production (ELP: culture-based system; VIN: plant-based system) and within that the projected high yield per hectare (oleosin: < 1 kg/hectare; VIN: 200+ kg per hectare)[342] that position VINs as inexpensive purification reagents.

Mechanical transmission-based production of VINs, as we have demonstrated, could be considered for economical manufacturing for its enhanced simplicity over agrobacterium-based methods and its reliability and stability over transcript-based methods. A main barrier to this strategy is the variability and escape of the VIN functionality over the course of multiple virion replication and plant passage cycles. One strategy to alleviate these concerns would be to embed selective pressures into the processing procedure, although this would introduce yet unsolved barriers within quality assurance and quality control that would hinder commercialization. Studies have shown the use of selective pressures during production can cause viruses to sacrifice reproductive fitness for selected characteristics (e.g., thermal and structural stability)[431] and that genetic stability of virus-based nanomaterials can be achieved[432].

9.3.2. Affinity sedimentation processing

Affinity sedimentation shares several characteristics with affinity precipitation, which provides potential benefits of low cost and buffer usage[433], ability to achieve high concentration factors[434], high throughput[435], and minimal concerns of fouling at the expense of higher recovery and selectivity generally achieved by a chromatographic counterpart[436], which can consist of as much as 50% of the total pharmaceutical manufacturing costs[128]. Affinity sedimentation and precipitation methods also exhibit generally higher tolerance to variation in feed streams, as we have shown with VINs through processing of crude plant extract, making them well-suited to early-stage downstream processing.

Biotic purification technologies have been applied in a diverse range of processing strategies including liquid chromatography, inverse transition cycling, aqueous two-phase partitioning, and affinity precipitation. The uncoupled VIN application methodology presented here is based on what we are terming as pseudo-secondary effect affinity sedimentation, in which the affinity interaction and sedimentation mechanisms are partially coupled with a dependence of the sedimentation on affinity interaction (i.e., VIN-target protein complex characteristics influence sedimentation velocity). We derive this terminology from affinity precipitation processing which has distinguished methodologies as either primary effect (coupled affinity/precipitation) or secondary effect (independent affinity/precipitation)[433].

We performed initial work to identify centrifugation conditions as a function of target protein characteristics and loading (e.g., antibody versus Fc-fusion protein), but it may be valuable in future works to develop a model to understand this relationship more deeply between the VIN-target protein complex morphology and sedimentation velocity. It was qualitatively observed that Fc-fusion protein recovery was lower than that of hIgG regardless of centrifugation conditions.

We hypothesize that lower binding affinities and differing biophysical characteristics of the VIN-Fc-fusion protein complex are contributing to these observed differences. However, future work is required to elucidate these underlying mechanisms.

A semi-quantitative comparison of hIgG binding capacity between the VINs prepared at two levels of purity (data not shown) indicates that there may be a minor reduction in binding capacity between these conditions, likely associated with non-specific blocking by various expected plant host impurities including proteins, salts, polysaccharides, and phenolics[437]. However, there was no discernable impact of the solution type (crude extract or purified solution) on reusability of the VINs for an additional cycle of capture and elution.

While protein solids, such as those formed in precipitation and sedimentation, have been shown to be stable in long term storage[127], here we show that sedimentation impacts VIN structural integrity and presumably contributes to the unstable performance over multiple reuse cycles. From these results, one may infer the importance of fully intact VIN on sedimentation characteristics and thus centrifugal recovery. The mechanism of particle breakage is suspected to be mechanically induced during pellet resuspension and not a direct result of the protein pellet formation from sedimentation. The mechanical properties of viruses have been studied extensively using computational and physical methods[438,439]. TMV, another stiff rod-like virus in the same genus as the TVCV used for the VIN in this study, has been attributed a Young's modulus of 6 ± 3 GPa[440], although mixed reports suggest the value could be lower[441]. Furthermore, there are reports on icosahedral virions that demonstrate minor changes in coat protein composition resulting in significant modulation of mechanical properties[442].

Thus, we hypothesize that the presumably stiff TVCV rod-like particle basis combined with increased drag by the loose affinity ligand display sheath (using the largest genetically inserted

virion coat protein presentation to date) surrounding the VIN enhances its vulnerability to applied shear stress during pellet resuspension via repeated pipette tip aspiration. It may be that a smaller affinity ligand presentation, such as an affibody[443] or synthetic peptide[444], would decrease particle breakage (but also necessitate more aggressive centrifugation conditions with the smaller virion size). Gentler resuspension methods with lower shear would also be worth investigating to decrease breakage. Similar shear sensitivity in pipette-based resuspension has been shown for larger biomolecule systems such as with cell-based pelleting, wherein higher pellet compaction and tip velocities were shown to result in cell losses[445]. Pellets formed during VIN processing and use were highly compacted and required considerable pipetting for complete resuspension, suggesting that pipette-based resuspension could have also played a role of particle degradation in this system. Gentler resuspension techniques should be explored in the future to improve particle integrity during operation.

In this study, we investigated stability of the VINs over long term storage, multiple freeze-thaw cycles, and at elevated temperatures, primarily focusing on coat protein fusion primary structure. Additional stability concerns include impact to protein secondary structure, virion particle structure, and nucleic acid integrity. Exposure to multiple freeze-thaw cycles has been shown to degrade virion nucleic acid and infectivity[446]. Thermostability was confirmed at the level of secondary protein structure via performance check of bind-and-elute functionality, which led to the integration of a high heat hold into the VIN purification scheme.

9.3.3. VIN process development

The process development investigation presented here provides insights on the differences between wild-type plant virions and protein display plant virions, which is relevant technology for

a host of biomedical applications. The improved process can serve as a roadmap for future virus-based nanomaterial purification. We observed that the protein presentation confers additional processing sensitivities to the virion (which is otherwise described as a glassy surface), likely due to the interactions between the presented ligand and *N. benthamiana* plant host cell impurities, noticeable in the heat hold of crude solution and the inclusion of protease inhibitors to extraction.

We observed that the two effective unit procedure modifications, low pH extraction and heat hold post-PEG precipitation, possess low orthogonality in impurity clearance mechanisms for the starting stream used although there is still discernable benefit in combining the methods as observed by the improvement in SDS-PAGE band purity.

The process development in this work focused on addition and removal of unit procedures at a high-level to inform process design. There is value in future research performing parameter optimization with an emphasis on maximizing recovery and purity with a fixed purification scheme.

9.3.4. Magnetic separation

The VIN-MP results presented in this study, representing the first virus-based nanomaterial system coupled with MPs for protein purification, reflect a greater than 25x increase in binding capacity compared to current industry standards for affinity protein capture with magnetic particles – Pierce™ Protein A Magnetic Beads (≥ 40 µg rabbit IgG/mg MP) (ThermoFisher Scientific), SureBeads™ Protein A Magnetic Beads (≥ 6 µg IgG/mg MP) (Bio-Rad Laboratories), VIN-MP (> 1,000 µg hIgG/mg MP).

These exciting results provide strong evidence for the sensitivity-enhancing properties of virus-based nanomaterials and their usefulness as ligand scaffolding in biotechnological applications.

Furthermore, the VIN-MP system served to decouple the affinity and separation mechanisms of processing, as compared to the partially coupled behavior in VIN sedimentation operation, thereby increasing the process robustness to changes in the sample solution, including the diversity and concentration of the target protein. Additional investigation is required to experimentally assess this capability in a larger set of processing conditions. Investigation of the reusability of VIN-MP and for magnetic separation and particle integrity over operation is also of importance for future testing. Preliminary results suggest there may be a minor presence of VIN in the eluate. Two possible means of explaining this observation are proteolytic cleavage along a covalently bonded FcAL resulting in detachment of the VIN from MP or minor particle breakage from resuspension of the VIN-MP after magnetic separation resulting in the presence of VIN fragments.

The uncoupled VIN sedimentation operation demonstrated 2-3 times higher capture capacity per VIN mass than the VIN-MP system. The uncoupled VIN operation also resulted in hIgG recoveries as high as 95% of the feed, whereas VIN-MP operation was maximal at 42% recovery of the feed hIgG (Figure 9.6). It will be important to identify the cause for the lower recovery in future development by additional screening of lower hIgG concentrations and optimization of the capture and elution methodology.

Higher capture capacity may be particularly advantageous for large-scale protein purification – an area for which affinity precipitation[447] and magnetic separation[411] are receiving growing interest. However, given the nature of VINs as inexpensive and simply produced reagents, the value of maximizing Fc-protein binding per VIN in a small-scale commercial application (as is the current

niche of magnetic particle purification) is most likely weighted less than factors such as Fc-protein recovery, process duration, labor time, amenability to automation, and equipment costs.

For perspective on these other factors, consider that our recently published study on evaluating the costs of the affinity capture step of mAb purification[448] yielded results that the unit costs of magnetic separation (modeled using an industry standard technology with a comparable capture and elution protocol) were lower than uncoupled VIN sedimentation in process duration (73% reduction), labor time (30% reduction), and equipment mass (71% reduction) when processing a single lab-scale sample (2 mL volume tube). These results support the favorable position of VIN-MP in comparison to uncoupled VIN sedimentation for lab-scale applications.

9.4. Summary and future directions

Virus-based nanomaterials provide a highly diverse and tunable technology that can be adapted to overcome the limitations of the application methodology. For example, the length of a rod-like plant virus such as the one used in this study, TVCV, is proportional to the length of the viral genomic information and, as such, the length can be modulated through the addition or subtraction of genomic information (e.g., addition of non-functional genomic information can be used to increase virion particle length)[449]. Increasing VIN length in this manner is one approach to investigate for increasing the binding site occupation in the VIN-MP system. Other techniques useful for VIN performance optimization include density modulation of the protein display[450] and a multi-ligand protein display[342]. Last not least, use of affinity ligands other than Protein A domains, in particular, affibodies evolved from Protein A/Z domains[451], should expand the usability of the technology beyond monoclonal antibody binding/capture[452].

In this study, we have presented the development of a virus-based nanomaterial to serve as a protein purification reagent, characterized performance using a pseudo-secondary effect affinity sedimentation bind-and-elute protocol, expanded functionality to Fc-fusion proteins, identified limitations of the technology operated in that procedure, and developed a magnetic particle coupled system for magnetic separation to improve processing. This provides further evidence supporting virus-based nanomaterials as simple and inexpensive reagents for protein purification and suggests a path forward for technological development.

9.5. Experimental procedures

9.5.1. Gene constructs

The viral expression vector used in this study is based on previously reported TVCV-based vectors[342]. The viral expression vector used here (pICH25892; plasmid kindly provided by Nomad Biosciences GmbH) is an assembly of the previously reported 5' provector containing the TVCV coat protein (minus the stop codon) fused to a C-terminal glycine-rich flexible linker (pICH20701) and the 3' provector containing the D and E antibody-binding domains from *S. aureus* protein A with short flanking sequences (amino acids 29 – 161; GenBank accession no. J01786) (pICH21767).

9.5.2. Production of VIN

VINs were primarily produced via whole plant agroinfiltration using *A. tumefaciens* containing viral expression vector pICH25892 according to a previously reported method with minor modifications[453]. A final cell density of OD_{600} = 0.2 was used for agroinfiltration. Post-infiltration

plants were cultivated at 60% relative humidity with a 16-hour photoperiod, 23 °C/20 °C temperature regime, and a photosynthetic photon flux density of 425 µmol/(m^2·s) derived from a combination of high-pressure sodium, high-pressure metal halide, and incandescent lights for a duration of 6-12 days post-inoculation.

VINs were also produced via direct mechanical transmission of intact VINs. A total volume of 300 µL of purified VIN solution (~0.1 mg/mL) was applied per plant in aliquots of 100 µL for each of three middling leaves. An abrasive powder (Celite) was lightly sprinkled on each leaf and each leaf was gently rubbed by hand. The surfaces of the leaves were rinsed with water at 20 minutes post-inoculation to remove excess inoculation reagents.

9.5.3. Purification of VIN

VIN-expressing *N. benthamiana* leaf tissue was stored at -80 °C after harvest and processed with minor modifications to a previously reported protocol[342]. A single round of PEG-assisted precipitation step was performed rather than two. Extraction was performed using either a blender (NutriBullet; NutriBullet, LLC, Pacoima, CA) or liquid nitrogen-assisted mortar and pestle with 0.1 M potassium phosphate pH 7.0 extraction buffer at a 3:1 buffer volume to biomass weight extraction ratio. In the case of the mortar and pestle method, the homogenized leaf powder was mixed with the buffer and nutated for 30 minutes at 4 °C for extraction.

9.5.4. Binding and elution of Fc-proteins

Binding and elution of Fc-proteins was performed according to a previously reported protocol[342]. Four different target Fc-proteins were used in this study: hIgG (Sigma-Aldrich, St. Louis, MO),

plant-expressed rCMG2-Fc)[454], plant-expressed rPTH-Fc (unpublished data), and using the magnICON® system[455], plant-expressed mAb A20 (subclass: IgG2a/kappa, species: mouse)[456,457]. Development of target protein-specific modifications to the method are detailed in results.

9.5.5. Coupling VIN with magnetic particles

VIN-MP were generated by covalent attachment of VIN to primary amine-terminated superparamagnetic iron oxide particles (Product No. I7643, Sigma-Aldrich, St. Louis, MO, USA), VIN-MP-N, or carboxyl-terminated superparamagnetic iron oxide particles (Product No. I7518, Sigma-Aldrich, St. Louis, MO, USA), VIN-MP-C, both of approximately 1 µm size, was performed according to the methods detailed in the product data sheets using ~2 mL total reaction volumes. VIN stock solutions at ~3-6 mg/mL concentration in 10 mM potassium phosphate buffer pH 7.0 were used in coupling. Coupling efficiency was measured using A280 values for amine-terminated particles and Bradford assay soluble protein values for carboxyl-terminated particles.

9.5.6. Binding and elution of Fc-proteins with VIN-magnetic particles

A VIN-MP solution was prepared by resuspending 2.5 mg of VIN-MP in 0.5 ml of 0.1 M sodium phosphate buffer pH 8.0 binding buffer. Further, the particles were magnetically separated; the supernatant was aspirated and discarded (repeated three times).

Crude protein extracts from *N. benthamiana* leaves (leaf juice press extraction followed by microfiltration with filter paper) in binding buffer were spiked with various amounts of hIgG. A volume of 100 µL hIgG-containing crude extract was added to the VIN-MP solution. The mixture was briefly vortexed and then incubated nutating at 4 °C for 30 minutes. The incubated solution

was then magnetically separated and washed three times with binding buffer. The binding buffer was removed after wash and 50 µl of 0.2 M glycine buffer pH 2.5 elution buffer was added. The solution was briefly vortexed to resuspend magnetic particles and further incubated nutating at 4 °C for 5 min. Particles were again magnetically separated and the supernatant was collected as the eluate. The eluate was then pH neutralized with 13 µl of 1.5 M Tris-HCl buffer pH 8.8. The elution and neutralization steps were repeated three times and pooled together.

9.5.7. Protein analysis

Protein concentration was measured using Bradford and Pierce Modified Lowry assays.

Sample protein compositions were analyzed by SDS-PAGE and Western blot. SDS-PAGE samples were loaded using constant volume (30 µL). Western blot analysis was performed using a primary antibody of rabbit anti-protein A (1:25,000 dilution) (Sigma-Aldrich, St. Louis, MO) and a secondary antibody of goat anti-rabbit IgG-HRP (1:3,000 dilution) (Southern Biotech, Birmingham, AL) for detection of VIN CP-FcAL. A secondary antibody of goat anti-human IgG-HRP (1:2,500 dilution) was used to detect human IgG, rCMG2-Fc, and rPTH-Fc.

Dot blots were performed using 5 µL liquid samples and 0.45 µm nitrocellulose membrane. The positive control consisted of 100 – 500 ng recombinant Protein A (ThermoFisher Scientific, Santa Clara, CA). The negative control consisted of ~2 µg wt-TMV from purified *N. benthamiana* solution. VIN samples consisted of ~100 µg of VIN from purified *N. benthamiana* solution based on total soluble protein assay results. Several secondary antibody conditions were used: rat anti-mouse IgG-HRP (1:1,000 dilution) (ThermoFisher Scientific), rabbit anti-goat IgG-HRP (1:3,000 dilution) (Invitrogen, Carlsbad, CA), and goat anti-human IgG-HRP (1:3,000 dilution).

9.5.8. Electron microscopy

Carbon film on 300 mesh copper discs (Ted Pella, Redding, CA, USA) were prepared for increased hydrophilicity by glow discharge at 30 mA for 30 seconds on a glass slide. 5 µL liquid VIN solution samples were loaded onto the prepared disc, incubated 30 seconds, and then blotted with filter paper. Negative stain was applied in five sequential rounds of 5 µL uranyl sulfate loading, 30 second incubation, and filter paper blotting. TEM was performed using a JEM-1230 transmission electron microscope (JEOL, Peabody, MA, USA).

The lengths of VIN particles imaged by TEM were manually measured using straight line analysis with ImageJ (National Institutes of Health, Bethesda, MD, USA). Statistically significant differences in mean particle lengths of different VIN solutions were determined by equal variance two sample t-test ($\alpha = 0.05$). The equal variance assumption was evaluated by two sample F-test ($\alpha = 0.05$).

9.6. Supporting information

9.6.1. Construct schematic and sequence verification

The following is additional detail of the construct schematic and sequence verification performed. Figure S9.1 displays an illustration of the recombinant *Turnip vein clearing virus* genome prepared as a T-DNA insertion for transformation into *Agrobacterium tumefaciens*. Table S9.1 displays the primer set used and Figure S9.2 displays the PCR-based DNA sequence confirmation first in *Escherichia coli* and subsequently in *A. tumefaciens*.

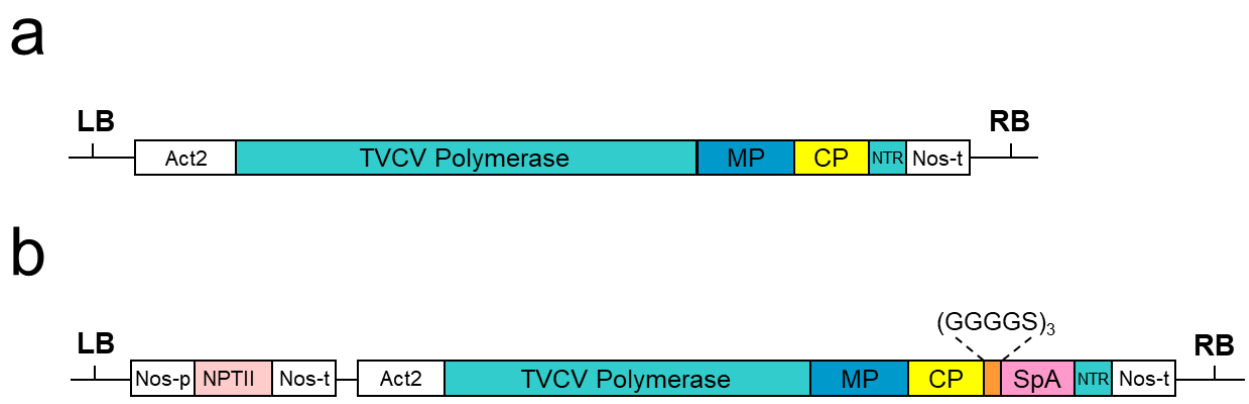

Figure S9.1. *Agrobacterium tumefaciens* T-DNA vector constructs for (a) wild-type TVCV (not used; shown for reference), and (b) TVCV-based immunosorbent nanoparticle. Act2, actin promoter; MP, movement protein; CP, coat protein; NTR, 3' non-translatable region; Nos-p (-t), nopaline synthase gene promoter (terminator); NPTII, kanamycin resistance gene; SpA, Staphylococcal protein A-based Fc-affinity ligand; LB, left border of T-DNA; RB, right border of T-DNA.

Table S9.1. Forward and reverse primers used to verify the vector construct DNA sequence after the bacterial transformation events. The set of primers was designed to generate an amplicon (922 nt) that spans from the start of the coat protein to the end of the Fc affinity ligand.

Primer	Length (bp)	Sequence
Forward	30	ATGTCTTACAACATTACAAACCCGAATCAG
Reverse	30	TTCACTCCTTGTTAAAGTTGTTATCTGCCT

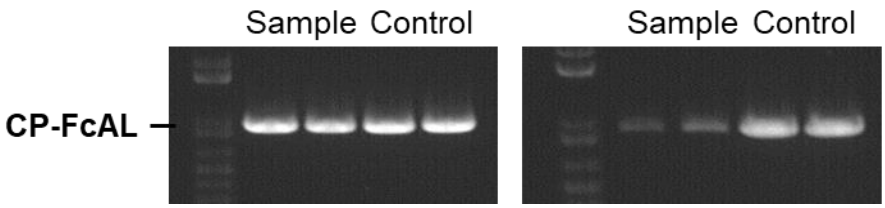

Figure S9.2. DNA gel electrophoresis image of PCR results verify presence of the coat protein Fc-affinity ligand nucleic acids in the transformation of *E. coli* (left) and *A. tumefaciens* (right). The synthesized template DNA is used as control.

9.6.2. Mass spectroscopy of coat protein fusion

The following is information on the protein sequence verification performed. Figure S9.3 shows comparison of the amino acid sequence predicted from the plasmid map (termed control) aligned with the submitted gel electrophoresis band cut VIN sample (termed sample). The sample data was generated by mass spectrometry analysis performed by the UC Davis Proteomics Core (https://proteomics.ucdavis.edu/). Mass spectroscopy data was analyzed using the software Scaffold 4.0 (Proteome Software, Inc., Portland, Oregon).

The mass spectrometry results yielded 78% amino acid coverage (238/306) and 2,203 total spectra at 99.0% minimum with a protein threshold of 5.0% false discovery rate (FDR) and protein decoy FDR of 0.6%, and a peptide threshold of 1.0% FDR and peptide decoy FDR of 0.06%. Results include full coverage of both the N- and C-terminus sequence of the fusion protein (CP + Protein A).

CP (N-terminal) **Surface-exposed loop**

Control: MSYNITNPNQYQYFAAVWAEPIPMLNQCMSALSQSYQTQAARDTVRQQFSNLLSAVVTPSQRFPDTGS
Sample: MSYNITNPNQYQYFAAVWAEPIPMLNQCMSALSQSYQTQAAR - - - - QQFSNLLSAVVTPSQRFPDTGS

TVCV Coat Protein

Control: RVYVNSAVIKPLYEALMKSFDTRNRIIETEEESRPSASEVANATQRVDDATVAIRSQIQLLLSELSNGHGYMN
Sample: RVYVNSAVIKPLYEALMKSFDTRNRIIETEEESRPSASEVANATQRVDDATVAIRSQIQLLLSELSNGHGYMN

CP (C-terminal) **Flexible Linker**

Control: RAEFEALLPWTTAPATGGGGSGGGGSGGGGSGGVTPAANAAQHDEAQQNAFYQVLNMPNLNADQRN
Sample: R - N

Protein A, Domain D + E

Control: GFIQSLKDDPSQSANVLGEAQKLNDSQAPKADAQQNNFNKDQQSAFYEILNMPNLNEAQRNGFIQSLKD
Sample: GFIQSLKDDPSQSANVLGEAQKLNDSQAPKADAQQNNFNKDQQSAFYEILNMPNLNEAQRNGFIQSLKD

Control: DPSQSTNVLGEAKKLNESQAPKADNNFNKE
Sample: DPSQSTNVLGEAKKLNESQAPKADNNFNKE

Figure S9.3. Mass spectroscopy amino acid analysis coverage of a gel cut VIN sample compared to the plasmid map sequence. CP, coat protein; TVCV, turnip vein clearing virus.

9.6.3. Supporting immunosorbence characterization

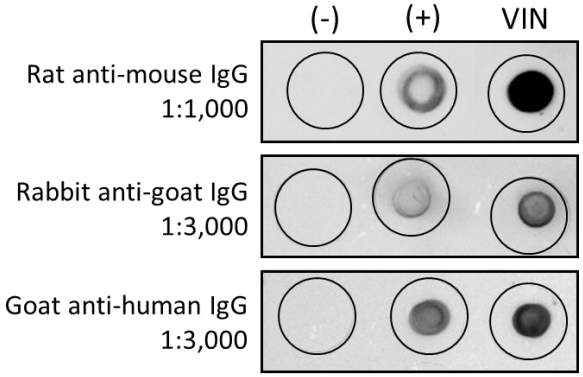

Figure S9.4. Dot blot assay portrays the negative control (-), wild-type TMV, positive control (+), recombinant Protein A, and VIN binding to Immunoglobulin G from rat, rabbit, and goat. The assay only used secondary antibodies, given the nature of the immunosorbent probe.

The following is functionality verification of VINs produced via mechanical transmission. Figure S9.5 depicts the bind-and-elute operation performed with VIN produced via mechanical inoculation of *Nicotiana benthamiana* plants. There is a visible difference in the purified VIN solution produced via mechanical transmission, in what we suspect is a discernable increase in coat protein degradation products given by the band at ~25 kD.

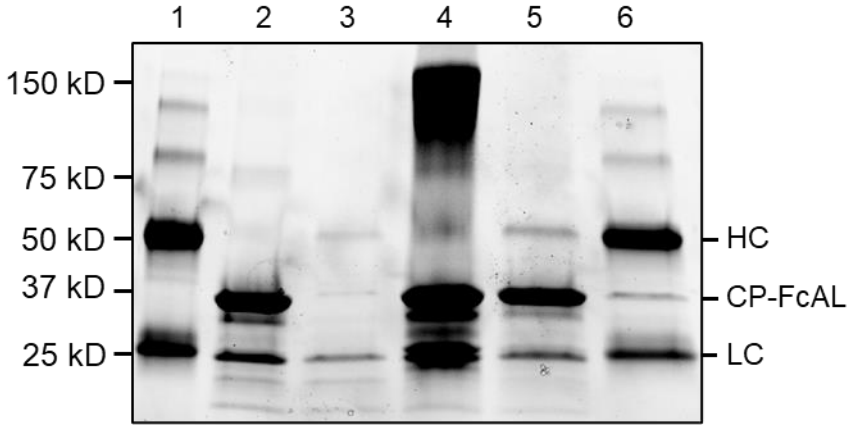

Figure S9.5. SDS-PAGE of mechanical transmission-generated VIN bind-and-elute with human antibody. Description of lanes are 1 – initial human antibody, 2 – initial VIN, 3 – centrifuge supernatant (waste stream), 4 – resuspended pellet, 5 – recovered VIN, 6 – recovered human antibody. CP, virus coat protein; FcAL, Fc-affinity ligand; HC, antibody heavy chain; LC, antibody light chain.

We observed that centrifugations of 20,000 x g for 90 minutes at 4 °C were sufficient to pellet the VINs in the absence of a suitable population of target protein to bind with, as demonstrated in Figure S9.6 by the use of bovine serum albumin (BSA) as a negative control target protein substitution and the complete diversion of BSA to the supernatant loss lane.

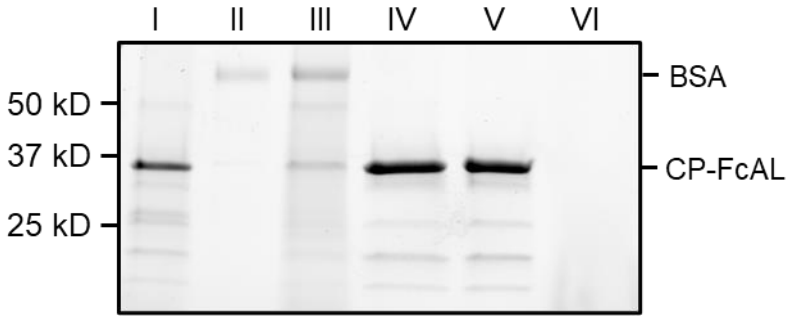

Figure S9.6. SDS-PAGE results of the VIN-based bind-and-elute procedure with a target of bovine serum albumin (BSA) using a centrifugation condition of 20,000 x g for 90 minutes at 4 °C. Lane definitions: I – initial VIN added; II – initial BSA added; III – VIN/BSA supernatant (loss); IV – VIN/BSA pellet resuspended; V – recovered VIN; VI – recovered BSA from resuspended pellet.

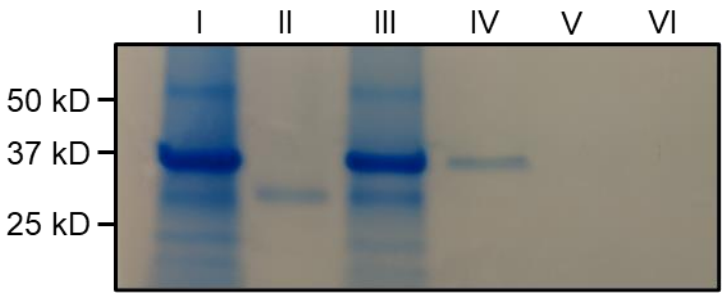

Figure S9.7. SDS-PAGE results of VIN-based capture and elution of the pre-purified plant-expressed recombinant parathyroid hormone Fc-fusion (rPTH-Fc) using centrifugation conditions of 10,000 x g, 10 minutes, 4 °C. Lane definitions: I – initial VIN added; II – initial rPTH-Fc added; III – VIN/PTH-Fc supernatant (loss); IV – VIN/rPTH-Fc pellet resuspension (capture); V – recovered VIN; VI – recovered rPTH-Fc(eluate).

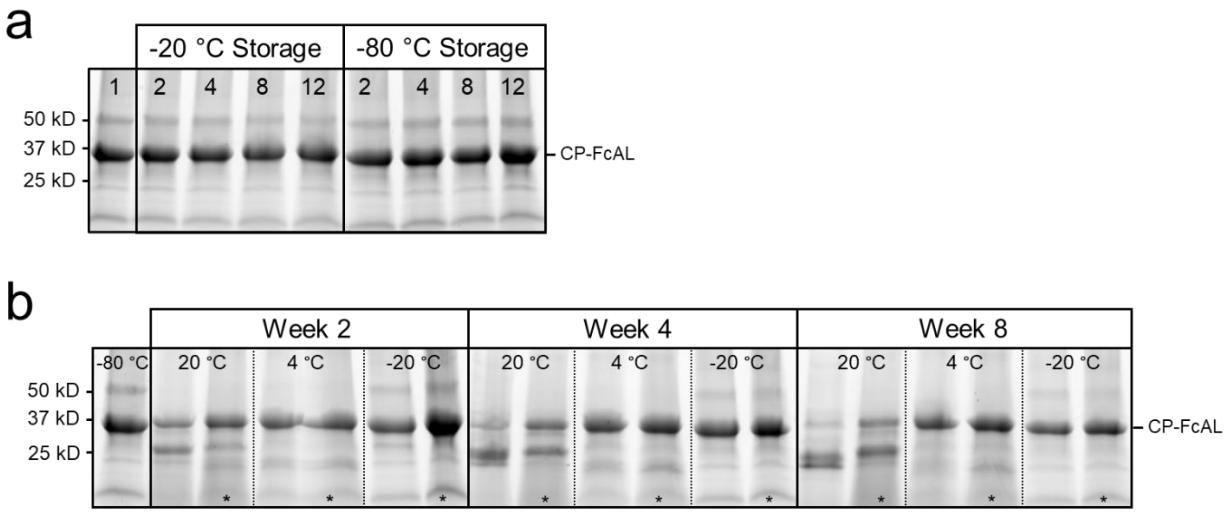

Figure S9.8. (A) The effect of freeze-thaw (FT) cycles (2, 4, 8, 12) on the stability of the VIN coat protein Fc-affinity ligand fusion using both -20 °C and -80 °C storage conditions shown by SDS-PAGE. The initial stock (FT cycle 1) is preserved in -80 °C storage. (B) Long-term storage stability of the VIN coat protein Fc-affinity ligand fusion at 20 °C, 4 °C, and -20 °C temperature conditions with and without protease inhibitor additives. Lanes with an asterisk (*) have 2 mM EDTA and 1 mM PMSF protease inhibitors added to the storage solution.

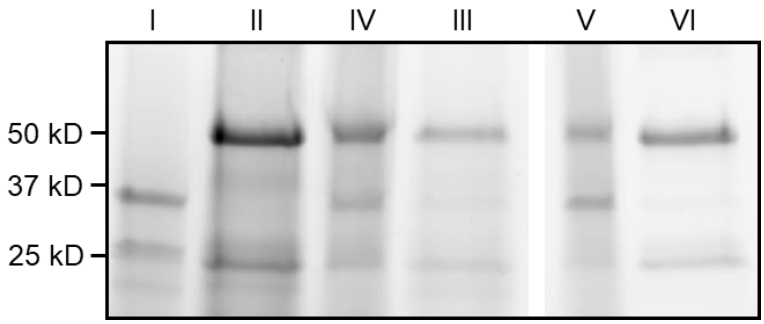

Figure S9.9. SDS-PAGE results of VIN-based capture and elution of using crude *N. benthamiana* plant extract containing VIN and a sample of hIgG spiked into crude *N. benthamiana* plant extract. Lane definitions: I – initial VIN added; II – initial target added; III – VIN/target supernatant (loss); IV – VIN/target pellet resuspended (capture) (2x); V – recovered VIN (2x); VI – recovered target (eluate) (5x).

9.6.4. Process development study results

The following is additional detail that highlights some of the key experiments performed as part of the VIN purification and use process development. Figure S9.7 shows the results the of 2-factor 2-level study design for extraction optimization of the VIN purification. Figure S9.8 displays the results of a temperature screen performed for various VIN and wild-type *Tobacco mosaic virus* (wt-TMV) solutions as part of a thermostability assessment. Figure 9.9 displays the bind-and-elute assessment which was used to confirm retention of functionality for the different VIN preparations.

Interestingly, the addition of protease inhibitors to the extraction buffer resulted in increased losses to VIN recovery. Corresponding with other published studies, the use of a low pH extraction buffer improved impurity clearance and thus VIN purity. The temperature screen shows the difference in apparent stability and/or presence of VIN in solution compared between the final VIN solution and the crude post-extraction solution, illuminating an unexpected instability of the VIN in crude solution. This difference in temperature screen results between the crude and purified solution was not observed for wt-TMV. The authors did not extend this study further to assess whether this can be attributed to impurity-enhanced degradation or sedimentation of the VIN.

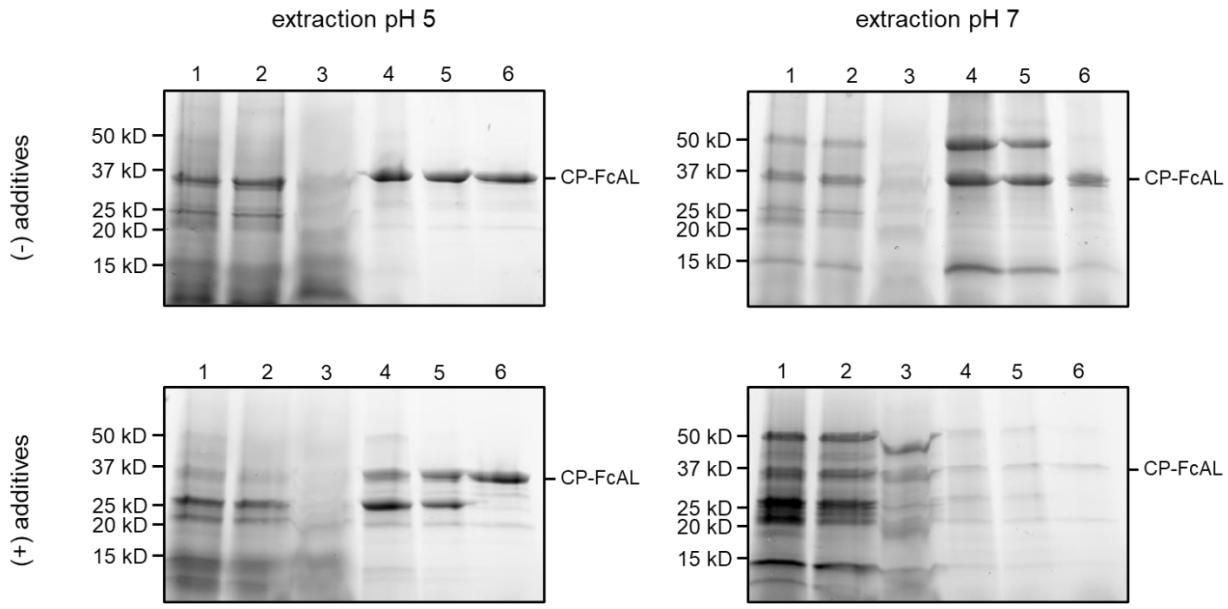

Figure S9.10. Process development observations via SDS-PAGE for a 2-factor 2-level study design to test extraction conditions (buffer pH and buffer additives). Buffer additives are 2 mM EDTA and 1 mM PMSF. Lane definitions: 1 – crude extraction; 2 – clarification; 3 – PEG precipitation (supernatant); 4 – PEG precipitation (pellet); 5 – post-PEG centrifugation (supernatant); 6 – final VIN solution.

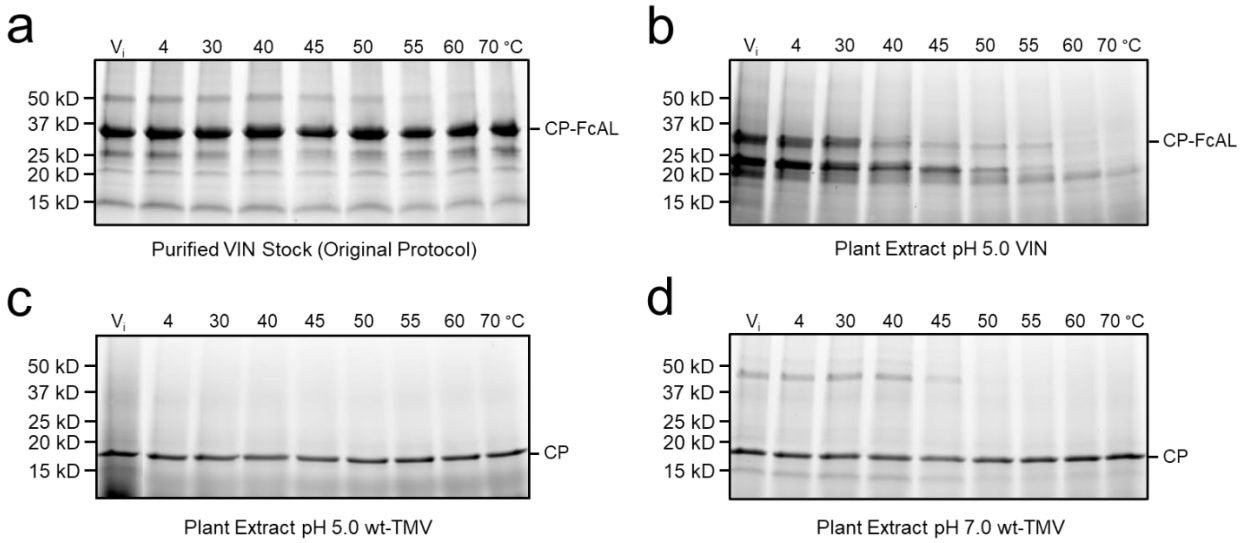

Figure S9.11. Key thermostability assessment results visualized with SDS-PAGE after five minute temperature holds ranging from 4 °C to 70 °C of (A) VIN purified using the original protocol, (B) VIN in crude plant extract at pH 5.0 with additives, (C) wt-TMV in crude plant extract at pH 5.0 with additives, and (D) wt-TMV in crude plant extract at pH 7.0 with additives. Samples are lightly centrifuged (5,000 x g for 5 minutes at 4 °C) after heat hold to clear aggregates from suspension. V_i, initial virus solution.

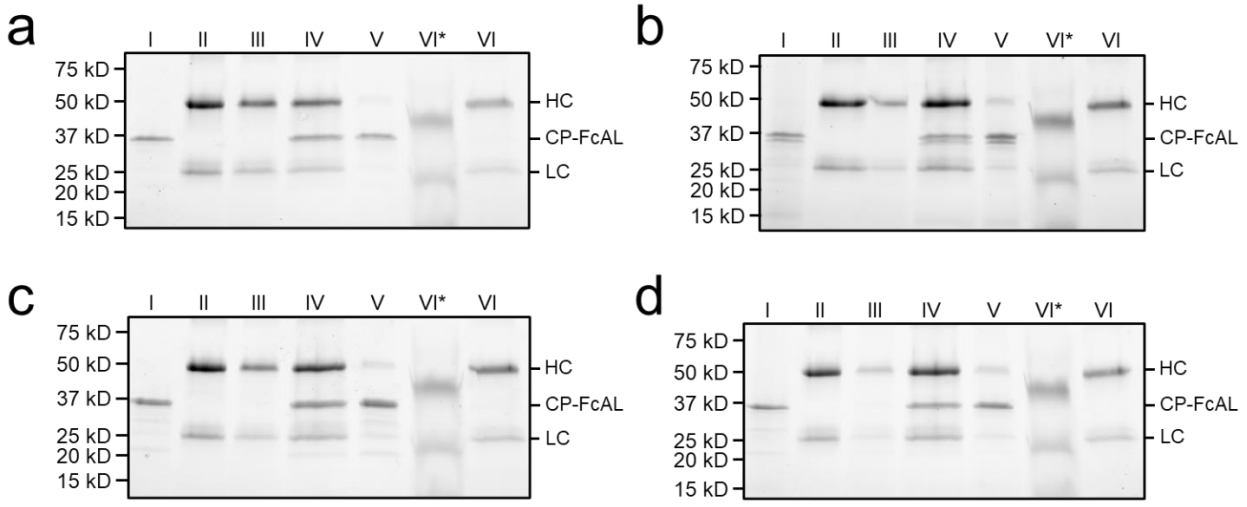

Figure S9.12. Performance verification of VIN bind-and-elute functionality for those generated through the three most promising process improvement workflows of (a) low pH extract with a heat hold, (b) neutral pH extraction with a heat hold, (c) low pH extract plus buffer additives with heat hold, and (d) the original protocol methodology. Lanes are labeled according to the naming convention outlined in Figure 4a with the addition of VI*, which is the intermediary step containing PEG 6,000 prior to target protein buffer exchange.

Chapter 10. Functionalizing silica sol-gel with entrapped plant virus-based immunosorbent nanoparticles

"Spiders' webs only have to be large enough to catch flies."

-Neil Gaiman

This chapter is based on the following pre-print publication:

McNulty M.J., Hamada N., Delzio J., McKee L., Nandi S., Longo M.L., and McDonald K.A. (2021) Functionalizing silica sol-gel with entrapped plant virus-based immunosorbent nanoparticles. *bioRxiv*. doi:10.1101/2021.11.12.468100

Abstract

Advancements in understanding and engineering of virus-based nanomaterials (VBNs) for biomedical applications motivate a need to explore the interfaces between VBNs and other biomedically-relevant chemistries and materials. While several strategies have been used to investigate some of these interfaces with promising initial results, including VBN-containing slow-release implants and VBN-activated bioceramic bone scaffolds, there remains a need to establish VBN-immobilized three dimensional materials that exhibit improved stability and diffusion characteristics for biosensing and other analyte-capture applications. Silica sol-gel chemistries have been researched for biomedical applications over several decades and are well understood; various cellular organisms and biomolecules (e.g., bacteria, algae, enzymes) have been

immobilized in silica sol-gels to improve viability, activity, and form factor (i.e., ease of use). Here we present the immobilization of an antibody-binding VBN in silica sol-gel by pore confinement. We have shown that the resulting system is sufficiently diffuse to allow antibodies to migrate in and out of the matrix. We also show that the immobilized VBN is capable of antibody binding and elution functionality under different buffer conditions for multiple use cycles. The promising results of the VBN and silica sol-gel interface indicate a general applicability for VBN-based bioseparations and biosensing applications.

10.1. Introduction

Virus-based nanomaterials (VBNs) are being studied for various medical applications as versatile nanomachines that can be manufactured at an industrial scale with high fidelity and low costs[391,423]. Reports in literature have primarily focused on the design of novel VBNs. With sufficient novelty and value of VBNs having been demonstrated in several application areas, there is a need to consider more advanced VBN-based systems to leverage the potential of existing VBNs and move this technological platform towards the clinic and market.

To date, several studies have explored VBNs as structural and/or functional elements within larger system arrangements. Recent examples include: hot-melt extrusion of trivalent vaccine candidates mixed into slow-release PLGA implants[458]; surface conjugation of osteogenic VBN nanofibers to the surface of 3D-printed bioceramic bone scaffolding[459]; electrostatic layer-by-layer assembly of free-standing VBN biofilms[408]; surface adsorption of immunosorbent VBNs onto gold sensor chips[343]; magnetic particle conjugation to immunosorbent VBNs for protein purification[40].

Silica sol-gel chemistries represent an alluring set of matrices for bioencapsulation and more advanced VBN-based systems. Extensive literature supports favorable silica sol-gel chemistry characteristics of high structural uniformity, stability, pore size tunability, optical properties, and biodegradability for various biomedical applications[460,461]. A range of live cells[462–464] and enzymes[465–467] have been studied for bioencapsulation in silica sol-gel matrices to stabilize viability and activity as well as to improve ease of use for the intended application. There have not yet been any such studies using VBNs, with the exception of a study of viral encapsulation focused on extended release of viral vectors for gene therapy[468].

In this study we present entrapment and utility of plant virus-based immunosorbent nanoparticles (VINs) in silica sol-gel matrices by pore confinement, representing a novel system configuration

for VBNs in general. VINs display antibody-binding proteins on their external coat protein surface, and they have been used as simple and bioregenerable reagents for biosensing and therapeutic antibody purification[342,343,405]. This entrapment of VINs represents the first use of plant virus-based VBNs in a silica sol-gel matrix and the first application of VBN technology for utility in an intact silica sol-gel matrix. We demonstrate that the silica sol-gel matrix can immobilize these large biomolecules over a long-duration (~30 days) in an environment that preserves their immunosorbent capture and elution functionalities and is sufficiently diffusive for antibodies to freely enter and leave the matrix. We also show that the silica sol-gel encapsulated VINs can be used to purify antibodies from a complex mixture, in this case, crude *Nicotiana benthamiana* plant extract (representing the production of therapeutic antibodies in plants, formerly known as molecular pharming[455]), to overcome reusability and bioprocessing challenges encountered when using VINs in solution to purify antibodies.

10.2. Materials & Methods

10.2.1. Virion production

Turnip vein clearing virus (TVCV) presenting a coat protein display of the D and E domains of *Staphylococcus aureus* Protein A was used as the plant virus-based immunosorbent nanoparticles. The VINs were produced according to a previously reported study by agroinfiltration of *N. benthamiana* plants using expression vector pICH25892 and processed with a polyethylene glycol (PEG)-based purification scheme[40]. Final yield was approximately 300 mg VIN per kg *N. benthamiana* leaf tissue, as determined by Bradford total soluble protein assay.

Wild-type tobacco mosaic virus (wt-TMV) was produced via mechanical inoculation of ~5-week old *N. benthamiana* plants by lightly sprinkling three leaves per plant with Celite® 545 (Millipore Sigma, Burlington, MA, USA) as an abrasive aid and gently rubbing 100 µL of 0.01 mg/mL wt-TMV in 0.01 M potassium phosphate buffer pH 7.0 per each of the three leaves. The plant leaves were washed with water 20 minutes after inoculation. Leaf tissue was collected after infection symptoms presented ~1 week post-inoculation and frozen at -80 °C for storage.

Extraction of wt-TMV from frozen *N. bethamiana* leaf tissue was performed with a 5:1 (w/v) extraction ratio with 0.1 M potassium phosphate pH 7.0 with 0.1% (v/v) beta-mercaptoethanol using a chilled mortar and pestle. The plant extract was filtered through three-layered cheese cloth, mixed with equal parts chloroform and n-butanol up to 1:1 (v/v) ratio, centrifuged at 8,000 x g and 4 °C for 10 minutes, and the upper aqueous phase layer was collected. PEG-based precipitation was performed by addition of 4% (w/v) PEG 8,000 and 1% (w/v) NaCl, incubation of the mixture for 30-60 minutes at 4 °C, and centrifugation at 8,000 x g and 4 °C for 15 minutes. The pellet was resuspended in 50 mM Tris-HCl pH 7.0 with a glass rod and let to sit at 4 °C for 30-60 minutes. The resuspended solution was centrifuged again at 8,000 x g and 4 °C for 10 minutes. The resulting supernatant was then ultracentrifuged at 50,000 RPM and 4 °C for 90 minutes using a 70.1 Ti rotor (Beckman Coulter, Brea, CA, USA) with 1 mL 15% sucrose cushion per tube. The pellet was resuspended again in 50 mM Tris-HCl pH 7.0 with a glass rod and let to sit at 4 °C overnight. The resuspended solution was added on top of a 10 – 40% (w/v) sucrose gradient and ultracentrifuged at 30,000 RPM and 4 °C for 90 minutes using a SW40 swinging bucket rotor. A 50% sucrose solution was used as a plug to fractionate and collect the wt-TMV containing solution.

Purification of wt-TMV was also performed according to the VIN purification protocol. Final yield was ~ 800 mg wt-TMV per kg *N. benthamiana* leaf tissue, as determined by UV absorbance A_{260nm} spectroscopy measurements.

The fluorescent reporter particle used in this study, a chemical conjugation of the Cyanine 5 fluorophore to the exterior of the wt-TMV coat protein (Cy5-TMV), was generated using purified wt-TMV and a two-step reaction composed of a diazonium coupling and click reaction step according to a method presented by Bruckman and Steinmetz[42]. Spin filters were used to separate the Cy5-TMV from leftover reaction reagents. Fluorophore dye loading is calculated using extinction coefficients at 260 nm of ε_{Cy5} = 250,000 mL/cm/mg [42] and ε_{TMV} = 3 mL/cm/mg [469].

10.2.2. Silica sol-gel synthesis

The silica sol-gel synthesis was performed according to the method for entrapment of liposomes in silica gel detailed by Zeno and team[470]. In brief, 3.8 mL of tetramethyl orthosilicate (TMOS) was added dropwise to 2.75 mL of 0.002 M HCl in a beaker chilled by an ice bath. This mixture was tip sonicated for 15 minutes, added to a round-bottom flask, and rotary evaporated at 340 mbar reduced pressure and 50 °C for 2-3 minutes before being passed through a 0.22 µm filter to yield the final silica sol. The sol was combined with 3 parts PBS by volume and 1 part of a PBS solution containing either VIN, wt-TMV, or Cy5-TMV at ~0.300 mg/mL concentration (according to total soluble protein measurement for VIN or UV-vis measurement for TMV).

The prepared solution was aliquoted as 40 µL droplets (or 2 µL droplets for the fluorescent microscope imaging) onto parafilm at room temperature for gel bead formation. Post-gelation (~1 hr) beads were submerged in equilibration buffer (PBS pH 7.0) at 4 °C prior to use.

10.2.3. Binding and elution of human immunoglobulin G

The binding and elution of human immunoglobulin G (hIgG) with gel beads was performed following a series of processing steps for batch operation: equilibration, sample loading, impurity wash, and elution. Equilibration consists of a 150 µL PBS buffer bath to submerge each 40 µL gel bead, which was individually contained in a 2 mL tube, that was nutated at 4 °C for a minimum duration of 24 hours and exchanged with fresh PBS buffer a minimum of four times throughout the duration. Previous reports in literature have provided 24 hours of equilibration prior to silica sol-gel use[471], presumably to ensure stabilization of internal pore charges.

The hIgG samples were prepared as 80 µL of 0.25 mg/mL hIgG in either PBS or 0.22 µm filtered *N. benthamiana* extract. The clarified *N. benthamiana* extract was prepared by 3:1 (v/w) chilled mortar and pestle extraction of 6-week-old *N. benthamiana* leaf tissue frozen at -80 °C, filtration through 4-layered cheesecloth, centrifugation at 8,000 x g and 4 °C for 15 minutes, and an additional filtration through a dead-end 0.22 µm syringe filter. For sample loading, all equilibration buffer was removed and the 80 µL of sample was added to submerge the silica sol-gel bead, which was kept at 4 °C nutating for 24 hours.

Impurity wash consisted of a minimum of four buffer exchanges into fresh PBS buffer over a period of no less than 24 hours at 4 °C while nutating.

Elution consisted of PBS buffer removal, addition of 80 µL 0.1 M glycine buffer pH 2.5, incubation for 4 hours at 4 °C while nutating, recovery of the elution solution, and pH neutralization with 0.1 volumes of 0.1 M Tris-HCl pH 9.0.

10.2.4. Protein analysis

Protein analyses using methods of the Bradford assay, SDS-PAGE, western blot, and transmission electron microscopy (TEM) were performed according to previously reported methods[40]. UV-vis measurements were made using a Quartz SUPRASIL® quartz cuvette (Hellma Analytics, Plainview, NY, USA) and a SpectraMax® M4 spectrophotometer (Molecular Devices, San Jose, CA, USA). Fluorescence microscopy was performed with an Eclipse 80i microscope (Nikon, Tokyo, Japan) equipped with a 4x objective. Immediately before imaging, Cy5-TMV loaded beads were transferred from a PBS bath to a slide and excess PBS was removed with a pipette. All images were collected using the same exposure time.

10.3. Results

An illustration of the silica sol-gel functionalization with entrapped plant virus-based immunosorbent nanoparticles and the example use case presented in this study is depicted in Figure 10.1.

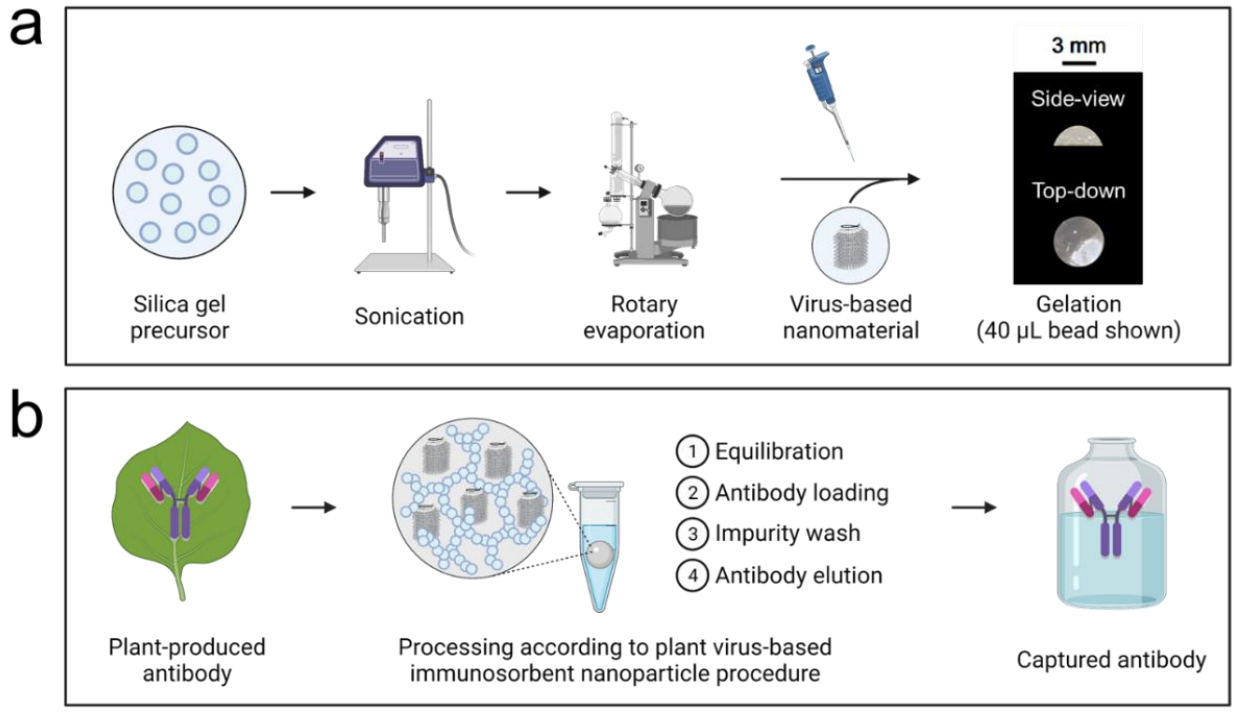

Figure 10.1. Illustrated schematics of (a) synthesis of sol-gel functionalized with entrapped virus-based nanomaterials (including example photographs of gels synthesized in this study), and (b) the example use case presented in this work of gel-entrapped plant virus-based immunosorbent nanoparticles for affinity purification of plant-made antibodies.

Firstly, a fluorescent reporter VBN was developed to investigate silica sol gel entrapment. As shown in Figure 10.2a, we produced wt-TMV *in planta* and purified the wt-TMV to ultra-high levels of purity. We then generated Cy5-TMV as a reporter system using previously developed methods to conjugate Cyanine 5 fluorophore to the exterior surface of wt-TMV coat[42]. UV-Vis absorbance spectroscopy 200 – 700 nm spectrums of wt-TMV and Cy5-TMV are comparable to the spectrum results of the previously reported study (Figure 10.2b). Notably differences of the Cy5-TMV from the wt-TMV include the introduction of an absorbance peak at around 324 nm, which is consistent with the introduction of a diazonium bond (needed for the alkyne addition reaction), and another peak at around 646 nm, which is consistent with the sulfo-Cy5 azide

absorbance. We estimate a dye loading of ~32%, which is to say that on average ~680 of an estimated 2,130 coat proteins per assembled virion were conjugated with a Cy5 fluorophore on the exterior surface. Negative stain TEM images were used to confirm structural integrity of the Cy5-TMV (Figure 10.2c).

Plant virion entrapment due to crosslinking physical immobilization during silica sol-gel bead synthesis was then assessed using the Cy5-TMV reporter system. Normalized areal fluorescence measurements are shown over the course of a 48-hour study in Figure 10.2d. Representative fluorescence microscopy images used in the quantitative measurements are shown in Figure 10.2e. Fluorescence results indicate that the initial Cy5-TMV concentration in the silica sol-gel matrix was maintained throughout the period of examination. There were appreciable decreases in gel bead volume due to minor breakages and shrinkage over the course of multiple microscope images (Supplementary Information, Figure S10.1). We attribute this observed behavior to the small bead size (2 µL), forceps manipulation, and multiple exposures to a dry environment used for fluorescent microscope imaging. This observation of areal shrinkage was not noted in the beads used for functional testing (40 µL).

There was no evidence of VIN or wt-TMV lost in the PBS wash buffer during standard equilibration to suggest incomplete entrapment. However, we performed an experiment using lower wash buffer volumes (1 vol buffer: 1 vol gel) to improve the limit of detection and found that < 10% of the initial VIN or wt-TMV mass added to the gel was recovered in the wash buffer during equilibration, peaking at an initial brief wash timepoint and decaying rapidly from there (Supplementary Information, Figure S10.2). This suggests that a small amount of the VIN or wt-TMV was not adequately entrapped during sol-gel synthesis and that it can be readily cleared from solution.

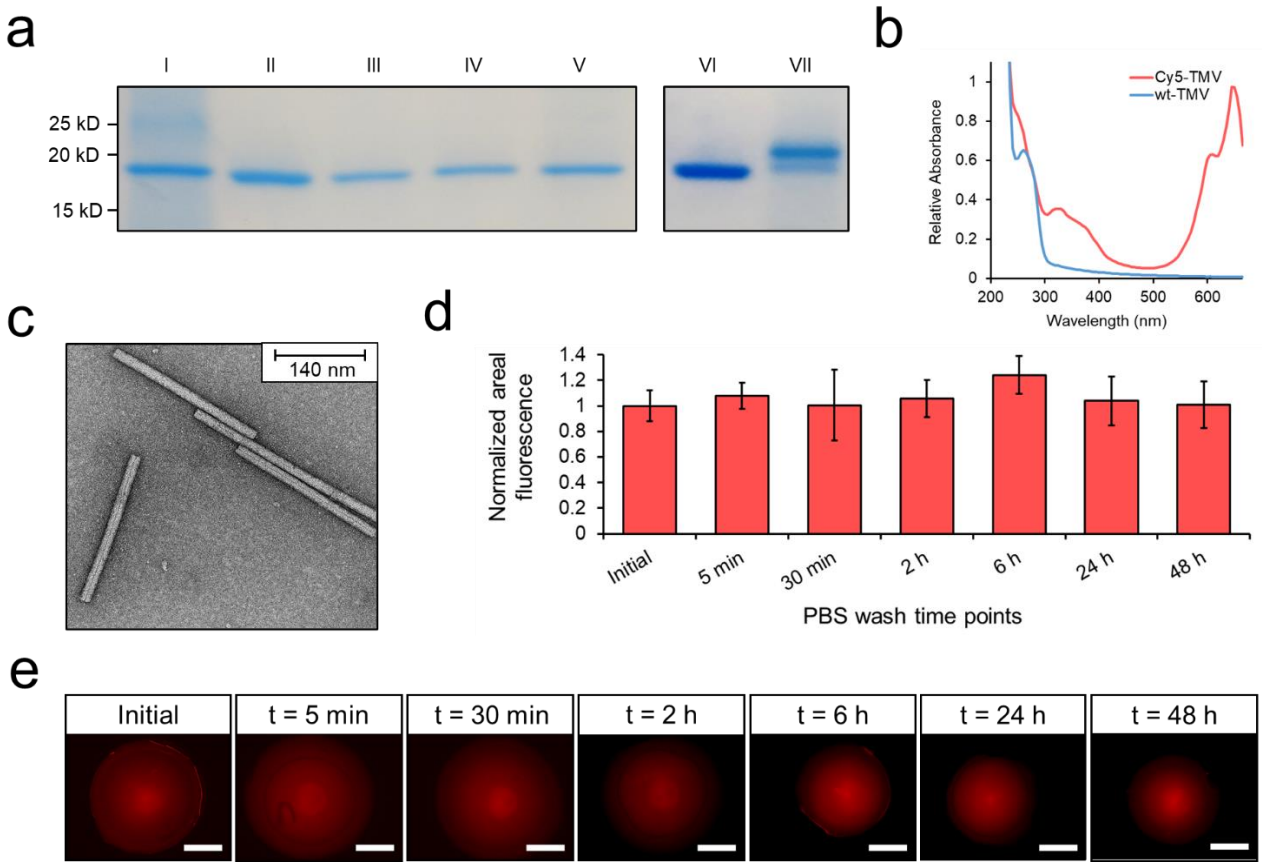

Figure 10.2. Purification and immobilization of fluorescently labelled plant virions (a) SDS-PAGE results of an ultracentrifuge-based purification of wt-TMV from *Nicotiana benthamiana* leaf tissue, which is then chemically conjugated with Cy5 dye in a two-step reaction to generate Cy5-TMV. Lane definitions: I – filtered plant extract, II – PEG-precipitated pellet resuspension, III – microfuge pellet, IV – ultracentrifuge pellet resuspension, V – ultracentrifuge wash, VI – initial wt-TMV pre-conjugation, VII – Cy5-TMV post-conjugation. (b) UV-Vis absorbance spectra of wt-TMV and Cy5-TMV. (c) Negative stain transmission electron microscope image of the Cy5-TMV. (d) Normalized areal fluorescence per 2 µL volume silica bead containing Cy5-TMV over 48 hours. Beads were exchanged into fresh PBS buffer after each measurement. Error bars represent one standard deviation with biological triplicate. (e) Fluorescent microscope images of the silica sol-gel beads containing Cy5-TMV over 48 hours of submerged gel wash. Scale bars represent 500 µm.

The bind-and-elute immunosorbent functionality of the VIN-entrapped silica sol-gel beads was then examined in this study. Assessment of this functionality using samples of hIgG in PBS and hIgG in clarified *N. benthamiana* plant extract is shown in each condition for two consecutive cycles of bind-and-elute in Figure 10.3. The results show that the VIN-entrapped beads yielded a

high recovery of hIgG in the elution step for both the PBS and plant extract conditions, whereas the TMV-entrapped beads did not.

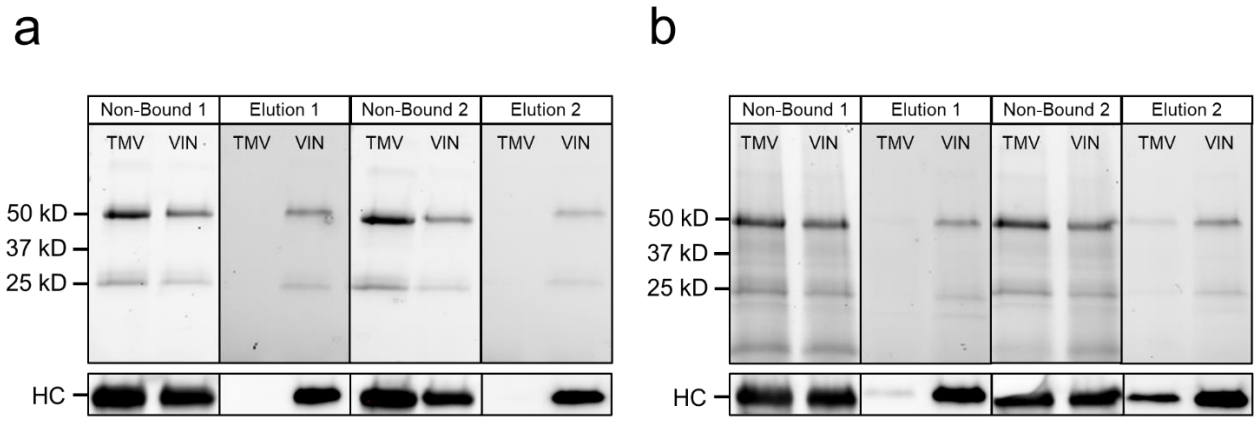

Figure 10.3. Use of silica sol-gel functionalized with entrapped plant virus-based immunosorbent nanoparticles (VIN) to purify monoclonal antibodies. Reducing condition SDS-PAGE (upper) and western blot (lower) results of the non-bound liquid sample after loading and low pH elution of human immunoglobulin G for a first and second use cycle shown for a sample loading consisting of human immunoglobulin G spiked into a solution of (a) clean PBS and (b) sterile-filtered *Nicotiana benthamiana* extract. Lanes are loaded with fixed volume. HC, heavy chain of the human immunoglobulin G.

The small amount of hIgG in the elution for the wt-TMV negative control using *N. benthamiana* extract (Figure 10.3b) indicates that the bind-and-elute functionality cannot be solely ascribed to specific Protein A-Fc interactions. Additional negative controls of silica sol-gel synthesized with bovine serum albumin and with no proteinaceous solution also corroborate these results (data not shown). The hIgG recovered in the elution for the plant extract-containing sample condition indicates some degree of non-specific binding interactions which may be present. Minor yellowish coloration of the gel bead, which closely resembled the color of the loaded sample, after impurity washing provides visual support for this observation (data not shown).

The second use cycle of hIgG recovery in elution indicates that the VIN functionality is preserved over multiple uses. A three-week lag period between the gel synthesis and completion of the

second use cycle also provides additional support for the entrapment and stability of VIN in the silica sol-gel environment. An increase in hIgG recovery for the second use cycle elution of the wt-TMV bead and plant extract-containing sample condition is observed, which may indicate an undesired behavior for performance such as incomplete hIgG elution from the first use cycle or an additive effect of the non-specific binding mechanism between the first and second use cycle such as what may be observed should a subset of the plant extract constituents accumulatively bind to the silica sol-gel matrices.

The hIgG captured from the plant extract sample was recovered at ~60% purity in both use cycles, based on gel densitometry measurement. The SDS-PAGE results qualitatively support that the hIgG purity was significantly increased from the capture and elution procedure. A reduction in recovery for the second use cycle was observed for hIgG in PBS (~50% first elution) and in plant extract (~80% first elution).

A substantial fraction of the hIgG sample loaded was not bound in either the VIN or wt-TMV conditions. We attribute this to the excess loading concentration, which was used in this proof-of-concept study to determine maximal elution given the employed gel synthesis and operational configuration. Each gel bead was synthesized containing a total of ~3 μg VIN, which, based our previous study of VIN in free solution recovering ~1.5 mg hIgG/mg VIN in excess hIgG conditions, can be estimated to correspond to a binding capacity of ~4.5 μg hIgG. Each gel was incubated in a liquid bath containing ~20 μg hIgG. Based on Bradford total soluble protein assay results, we recovered ~1.9 μg hIgG from PBS for the first cycle elution from the immobilized VIN sol-gel bead, corresponding to ~10% hIgG recovery of the initial sample load. This binding capability represents ~42% of that of VIN in free solution.

10.4. Discussion

In this study, we report encouraging proof-of-concept results for novel VBN entrapment and functionality within the pores of silica sol-gel matrices with broad applicability in protein purification and biosensing. VIN-containing silica sol-gel beads were used to capture hIgG from PBS or plant extract and elute the hIgG in a low pH environment for two consecutive use cycles spanning approximately 30 days post-synthesis. The high surface area to volume ratio of the rod-like VBNs used in this study proved to be an amenable geometry for pore entrapment with considerable active binding site availability without the need for significant optimization.

Future work to investigate the significance of VBN morphology on performance would be valuable for understanding the possible VBN silica gol-gel design space. Relevant characteristics for investigation include the geometry of the virion, either rod-like or icosahedral, the rigidity of the geometry, given that rod-like virions can be classified as stiff (e.g., tobacco mosaic virus) or flexible (e.g., potato virus X), and the size of the virion, which can be readily extended in rod-like virions through genome augmentation.

Non-specific binding interactions of the hIgG to the silica sol-gel were observed in this study, as observed for the wt-TMV and plant extract sample condition. We hypothesize that constituents of the plant extract bind to the silica sol-gel and in turn the extract-gel complex increases the non-specific binding interactions with hIgG. Additionally, we hypothesize that the low pH elution conditions (pH 2.5) and the isoelectric points of the silica sol-gel matrix (pH 2.0 for silica) and hIgG (> pH 6.0) may generate a non-specific binding environment that could result in incomplete hIgG elution into the bulk liquid. This behavior was not observed in the experimental execution of this study but should be considered in the future. The isoelectric points of wt-TMV coat protein, pH ~4[472], and VIN coat protein fusion, pH ~3.7 as estimated using Expasy

(web.expasy.org/compute_pi/), are both net negatively charged at the neutral gelation condition and not expected to non-specifically bind with the silica sol-gel matrix. We do suggest that future works more rigorously resolve concerns of non-specific binding interactions through optimization of silica sol-gel composition, perhaps considering doping (3-aminopropyl) triethoxysilane into the formulation, as has been successfully employed in previous studies[473].

The reduction of effective binding capacity for silica sol-gel entrapped VIN was within the range of previously reported reductions in enzyme activity; silica sol-gel entrapped horseradish peroxidase and glucose-6-phosphate dehydrogenase enzymes were reported to exhibit specific activity of 73% and 36% of the specific activities of the free enzymes, respectively[471]. Further investigation is required to understand the relative contributions of protein activity modulation, such as from VIN exposure to gelation conditions or the internal pore environment pH, and loss of accessibility of the active site, such as from diffusional limitations in the sol-gel matrix or partitioning of VIN into hIgG-inaccessible silica sol-gel matrix pores.

The findings of this study were consistent with the results of Kangasniemi and team for extended release of adenovirus from silica sol-gel in finding that the VBNs in silica sol-gel were stable for extended durations (weeks to months) and could be evenly distributed in the sol-gel post-entrapment, as noted by the nearly linear VBN release profile during *in vitro* silica dissolution in their study[468]. The fundamental difference in observations was that Kangasniemi and team showed VBN activity to be retained for VBN that were released into free solution via silica dissolution, whereas this study reports VBN activity while entrapped within the silica sol-gel matrices. Our work also presents the first entrapment of plant virus-based VBN in silica sol-gel, which can be used in a wide variety of applications not amenable to mammalian virus-based VBN due to

inherent advantages of safety (e.g., non-infectious to humans) and inexpensive and simple production.

The VIN silica sol-gel system presented in this study could serve as the foundation for a robust and reusable platform for biosensing. For example, the VIN system could be readily configured for immunosensing, in which the desired detection antibody would be first introduced to and fixed (via non-covalent bonding) in the VIN-entrapped gel matrix, allowing the subsequent addition of the desired analyte solution for sensing. The detection antibody could be removed via low pH elution and the same VIN-entrapped gel could be reused with a different detection antibody, as desired. This hypothesized example system may provide means for easy reuse and flexibility of sensing targets as well as an enhanced sensitivity over antibody-only systems due to the increased sensing surface area of the structural scaffolding of the VIN. This hypothesis of the potential for increased sensitivity is strongly supported by our recently reported results that VIN coupled to magnetic particles could achieve ~25x higher binding capacity of antibodies as compared to current industry standards for affinity protein capture with magnetic particles on a per unit mass basis[40].

Future works to further exploit the advantages of the highly tractable silica sol-gel chemistries for more sophisticated geometries and fine-tuned pore architecture would be valuable. For example, a previous study showed synthesis of bimodal pore distribution silica sol-gel in monolithic nanoflow columns in which the smaller pores are used to entrap the ligand to functionalize the column and the larger pores promote bulk flow and diffusion of the target molecule to the ligand active site[474]. This system architecture could be valuable for developing scale-down VBN-based bioseparation or biosensing technologies.

10.5. Supplementary information

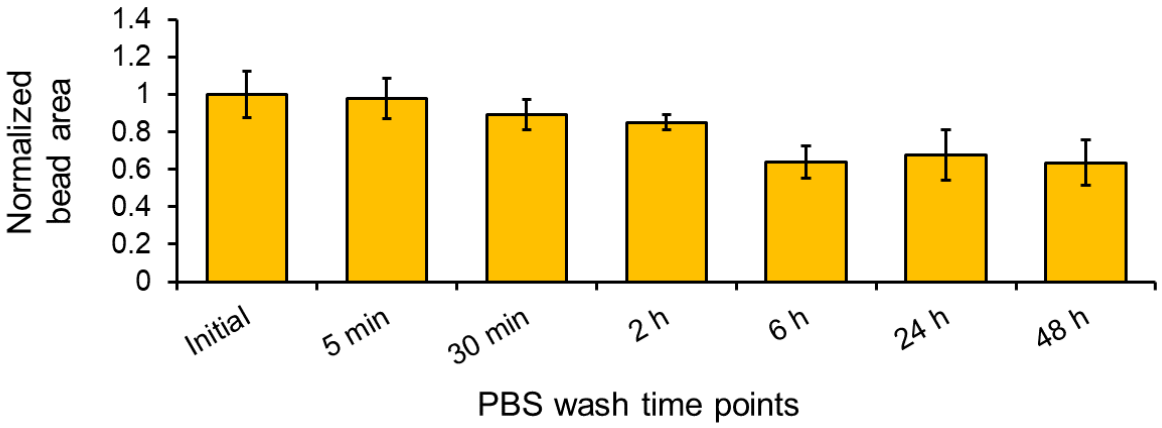

Figure S10.1. Normalized bead area over time for 2 µL volume silica bead containing Cy5-TMV over 48 hours. Beads were exchanged into fresh PBS buffer after each measurement. Error bars represent one standard deviation with biological triplicate.

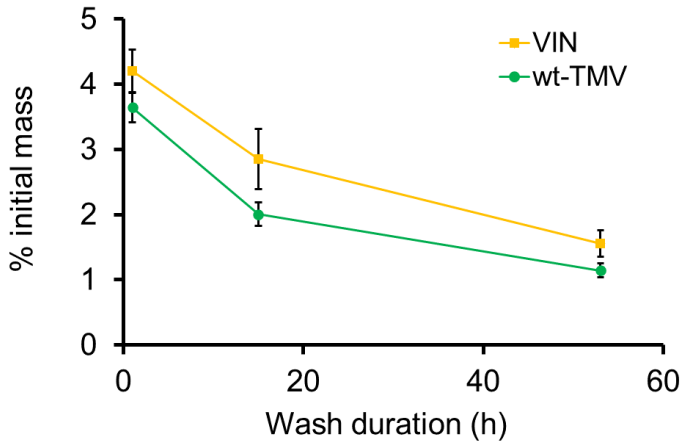

Figure S10.2. UV-vis A_{280} measurements of the PBS wash solution over ~2 days of equilibration reported as a fraction of the initial A_{280} measurement for the VIN or wt-TMV added into the silica sol-gel synthesis. The PBS wash solution was collected at each sample timepoint and exchanged with fresh buffer. This experiment was conducted using 1 volume PBS wash solution per volume silica sol-gel to improve limit of detection. The retention of the PBS wash solution in the buffer exchange (~50% total wash solution) dictates that these results represent an upper bound of the initial mass lost during washing. Error bars represent 1 S.D. using biological triplicate.

Chapter 11. Development of a recirculating system with virus-based nanomaterials as a process integration strategy

"I regarded home as a place I left behind in order to come back to it afterward."

-Ernest Hemingway;
Since the discovery of viruses via Chamberland filter-candle, we continue to return to filtration to innovate in virology and its applications.

This chapter is not based on a previously published article. The works presented in this chapter serve as foundational for a future peer-reviewed journal publication when augmented with additional experimental characterization investigations and analysis. The author list for the works presented in this chapter is as follows:

Matthew J. McNulty[1], Justin Wong[1], Liber McKee[1], Kevin Yates[1], Patrick G. Negulescu[1], Katherine Haddad[1], Somen Nandi[1,2], and Karen A. McDonald[1,2]

[1]Department of Chemical Engineering, University of California, Davis, CA, USA

[2]Global HealthShare® Initiative, University of California, Davis, CA, USA

Abstract

Chromatographic separations are ubiquitously employed in industrial protein purification applications. However, concerns of cost and bottlenecking process throughput motivate development of alternative technologies for commercial large-scale protein purification. With the

looming rise of personalized medicine and point-of-care technologies, there is a growing interest in technologies capable of scale-out, increasing production scale through the number of units rather than the size of the unit, as is traditionally considered in scale-up. Virus-based nanomaterials is an emerging technology platform that has potential in both scale-up and scale-out with the generally high stability and inexpensive production of the technology.

In this study we present a proof-of-concept process for a novel process integration strategy that combines mAb capture, concentration, and purification using plant virus-based immunosorbent nanoparticles (VINs) circulating in a tangential flow filtration retentate loop. We have reported on the high-fidelity production of VINs as inexpensive and high capacity bioregenerable affinity reagents. The VINs used in this study are significantly larger biomolecules (~300 nm x 30 nm) than the mAb target, enabling large pore size filters (>1,000 kD) and high flow rates that would not be possible with the smaller pore sizes required for existing methods. The unique biophysical nature of the VINs as a capture agent may also be useful in microfluidic scale-down approaches.

11.1. Introduction

Packed-bed liquid chromatography unit procedures are dominant purification technologies in biopharmaceutical industry[475]. And none is perhaps as well established as Protein A affinity chromatography for monoclonal antibody (mAb) capture[476]. However, relatively high resin costs (Protein A affinity resin: $8,000 - $15,000 per liter[350]), low throughput, and complex scalability motivate the research and development of novel purification unit procedures[477]. Some of these technologies have maintained a similar form factor (i.e., a liquid mobile phase passing through a column of stationary solid phase) throughout innovation, such as with membrane chromatography[478] and monolithic chromatography[479]. While encouraging developments suggest that improvements to the stationary phase material characteristics may improve throughput, it generally remains an issue that bottlenecks the biomanufacturing[435]. Other development efforts seek to establish different system configurations that may not consist of a mobile liquid phase passed by a stationary solid phase to improve throughput, such as with what has been done with magnetic separation[411] and precipitation[433].

Continuous countercurrent tangential chromatography (CCTC), in which a resin slurry is flowed through a series of static mixers and hollow fiber membrane modules countercurrent to the direction of buffer flow (permeate), has emerged as a promising alternative to batch column chromatography operation[480–482] with reports in literature of five-to-tenfold increases in productivity[483,484].

Continuous precipitation, in which the active pharmaceutical ingredient (API) is precipitated and then washed using tangential flow filtration, is an analogous method to CCTC for precipitation-based API capture that has also received attention in recent literature[485,486]. No direct performance

comparisons of this method to conventional batch column chromatography operation, nor to CCTC, have been reported, to the best of our knowledge.

Interestingly, the biologically-derived elastin-like polypeptide-Z domain fusion (ELP-Z) was investigated as a technological basis for continuous precipitation[428]. Unfortunately, the precipitate and TFF system characteristics were not compatible, leading to fouling problems, and as a result the study primarily focused on proof-of-concept work using dead-end flow filtration.

In this study we present a method for recirculating plant virus-based immunosorbent nanoparticles (VINs) within a tangential flow filtration retentate loop that functions as a process integration of mAb capture, concentration, and purification. This work leverages the results of earlier studies to design a system that takes advantage of the unique characteristics of VIN as an inexpensive and high capacity bioregenerable affinity reagent. We demonstrate that the large size of the VIN (~300 nm x 30 nm) enables large pore size filters (>1,000 kD) and high flow rates for a unique all-in-one approach to mAb capture, concentration, and purification.

11.2. Materials and Methods

11.2.1. Production and purification of plant virus-based immunosorbent nanoparticles

The VIN production and purification methods used in this study were based on previously reported methods[40]. In brief, VINs were produced by agroinfiltration of 5 – 6-week-old greenhouse-grown *Nicotiana benthamiana* plants with expression vector pICH25892 at OD_{600} = 0.2, incubation for 7 – 9 days post-induction, and post-harvest leaf tissue storage at -80 °C. Extraction from frozen leaf tissue was performed using a chilled mortar and pestle with 3 parts 0.1 M sodium acetate 0.86 M NaCl pH 5.0 buffer:1 part leaf tissue (volume/fresh weight mass). The crude extract solution was

clarified through 4-layered cheesecloth and then centrifuged at 10,000 x g for 10 minutes at 4 °C. The pellet was discarded and the clarified supernatant solution was mixed with 4% mass polyethylene glycol 6,000, nutated for 30 – 60 minutes at 4 °C, and then centrifuged at 12,000 x g for 10 minutes at 4 °C. The supernatant was discarded and the pellet was resuspended in 1/5 volume phosphate buffered saline (PBS) buffer by gentle glass rod abrasion followed by >60 minutes rest at 4 °C. A final centrifuge step at 10,000 x g for 20 minutes at 4 °C was used to clear any non-solubilized solids. VIN concentration (per total soluble protein content assay) in the final solution corresponded to an expression level of ~0.3 mg/kg leaf fresh weight[40].

11.2.2. Tangential flow filtration operation

This study used an ÄKTA flux tangential flow filtration system (Cytiva, Marlborough, MA, USA) and a Pelicon® XL 1,000 kD and 50 cm^2 filtration area cassette with Ultracel® membrane (MilliporeSigma, Burlington, MA, USA) was used for all tangential flow filtration (TFF) operations. The TFF system was assembled and calibrated per vendor instructions prior to operation. Double-distilled water was pumped through membrane module for initial normalized water permeability testing and subsequently tested again after each cleaning cycle to ensure adequate recovery and cleanliness prior to reuse. All buffers were 0.22 µm filtered prior to being introduced to the TFF system. The feed flow rate was set to 30-50 mL/min for all steps of TFF operation.

A sample of ~14 mL purified VIN solution (~4.2 mg VIN) pre-mixed for 30 – 60 minutes at 4 °C with a solution containing 4.2 mg of human immunoglobulin G (hIgG) from human serum (Sigma-Aldrich, St. Louis, MO, USA) was loaded into the TFF feed tank for each run. In first set of TFF runs, the hIgG solution simply consisted of a 5 mg hIgG/mL phosphate buffered saline (PBS)

solution. In the second set of runs, the hIgG solution consisted of hIgG spiked into 6 mL of clarified *Nicotiana benthamiana* plant extract, simulating a feedstock based on plant-based antibody manufacturing with an extraction ratio of 3 volumes buffer to 1 mass unit of leaf fresh weight and expression level of ~2 g/kg leaf tissue fresh weight. In brief, this clarified plant extract was prepared from six-week-old wild-type greenhouse-grown plant leaves extracted in 3 parts PBS buffer:1 part leaf tissue (v/w) using a chilled mortar and pestle, passed through four-layered cheesecloth, centrifuged at 10,000 x g for 15 minutes at 4 °C, and 0.22 µm filtered.

After the VIN and hIgG sample was loaded into the TFF feed tank, bringing the working volume up to 20 or 26 mL, the liquid in the system was then recirculated with the permeate line closed for five (5) volumes.

An initial concentration step was performed for the second set of runs using a simulated plant-based antibody manufacturing feedstock to reduce the working retentate volume down to 20 mL (concentration factor of 1.3).

The impurity removal stage was performed as five (5) batch diavolumes of PBS pH 7.0 buffer. The pH adjustment stage was performed as a bulk addition of all five (5) diavolumes of 0.1 M glycine buffer pH 2.45 recirculated with the permeate line close for five (5) volumes. The permeate line was opened for the product recovery step and the permeate was collected in 5 mL fractions.

The cleaning began with a draining of the remaining retentate volume. PBS buffer was added, recirculated, and drained. A caustic cycle followed with 0.1 M NaOH circulated for 20 minutes with the permeate line open, an additional 30 minutes of circulation with the permeate line closed, and then a final 20 minutes of circulation with the permeate line open. The TFF cassette was stored primed with NaOH in a sealed container in 4 °C.

11.2.3. Protein analysis

Protein analysis was performed using the Bradford total soluble protein assay, sodium dodecyl sulphate-polyacrylamide gel electrophoresis (SDS-PAGE), western blot, and UV-vis absorbance according to previously reported methods[40,43].

11.3. Results

An illustration and system schematic of the virus combined VIN TFF circulatory system presented in this study is depicted in Figure 11.1. The VIN TFF mAb affinity filtration and capture process was carried out using in the following steps in sequence: (1) an incubation at neutral pH for binding of the VIN and mAb in solution, (2) concentration of the neutral pH solution containing VIN-mAb complexes, (3) diafiltration into clean neutral pH buffer to remove impurities from solution, (4) addition of low pH solution and recirculation with a closed permeate line, (5) concentration of the low pH solution containing unbound VIN and mAb to recover the mAb product in the permeate.

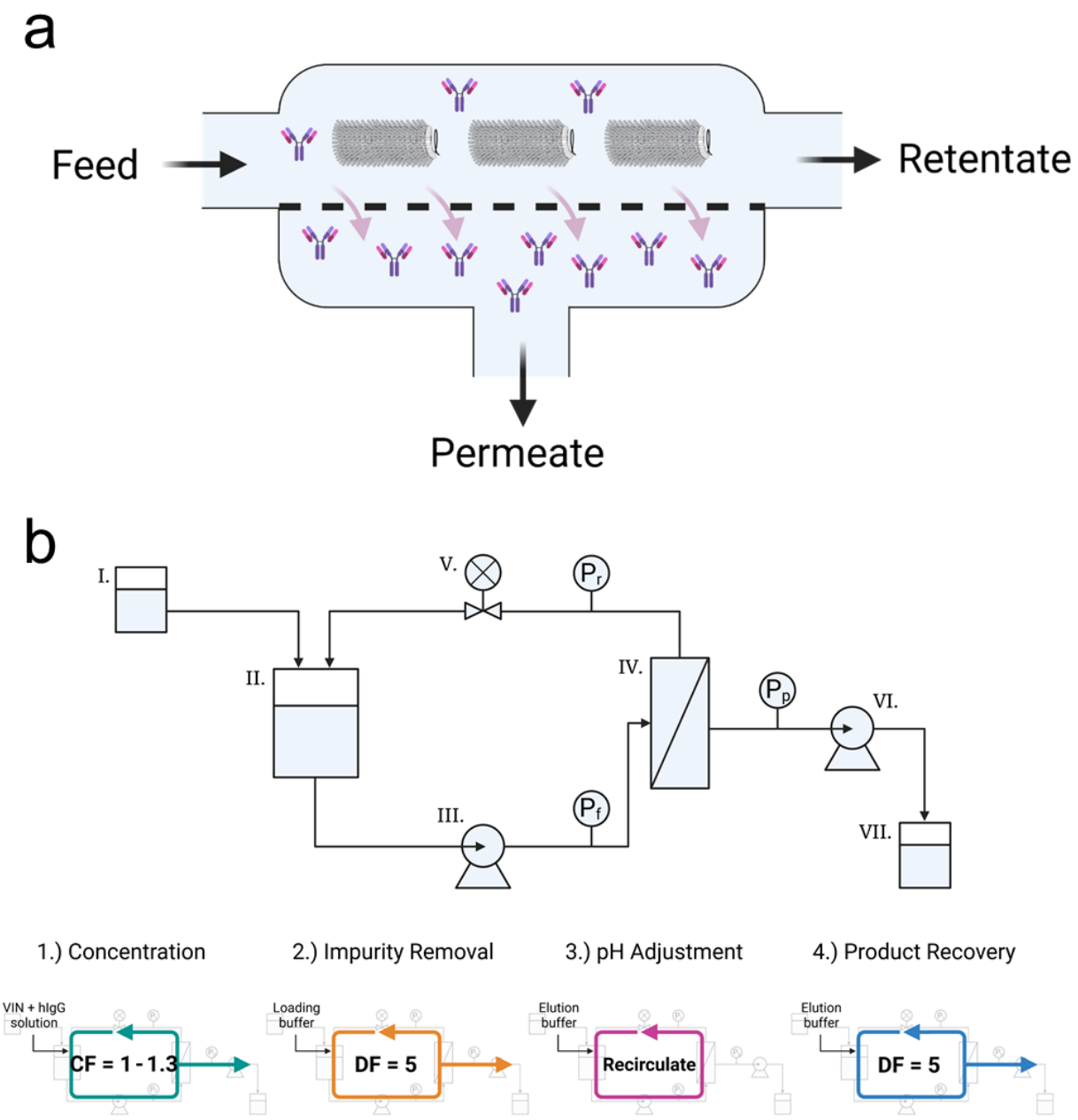

Figure 11.1. (a) An illustration of the plant virus-based immunosorbent nanoparticle (VIN)-circulating tangential flow filtration system in which the VIN are maintained in the retentate loop by size exclusion and the product is able to freely diffuse to the permeate when unbound from the VIN. (b) A schematic overview of the experimental equipment set-up and operations. I – buffer feed tank, II – storage tank, III – feed pump, IV – membrane module, V – retentate pressure valve, VI – permeate pump, VII – permeate collection vessel. CF, concentration factor; DF, diafiltration factor.

Figure 11.2 shows SDS-PAGE and western blot which indicate successful proof-of-concept for the outlined novel method of VIN TFF mAb affinity filtration and capture. VIN were successfully purified using simple processing methods. The presence of VIN coat protein Fc-affinity ligand (CP-FcAL) fusion proteins in TFF retentate samples, and the lack of VIN in the permeate line fractions collected in the impurity removal and product recovery stage, indicate that the VIN were successfully retained within the retentate circulatory loop.

Most of the hIgG remained within the retentate loop throughout the impurity removal stage, as would be expected for hIgG bound with VIN CP-FcAL, and was recovered in the permeate during product recovery, in which the low pH conditions has been shown to promote hIgG and VIN dissociation.

A minority of the hIgG, as detected in the western blot, and potentially a minority of the VIN, as could be detected in the SDS-PAGE result, were observed in permeate during the impurity removal stage (Figure 11.2b, fractions F1 – F10). Additional work is required to determine if the VIN is present in the permeate, but if so, this could suggest that a small fraction of the VIN, perhaps smaller particle fragments (a previous study found a particle length distribution of $\bar{x}$ = 239 nm, σ = 80 nm[40]), was capable of passing through the membrane at the 1,000 kD molecular weight cut off (MWCO).

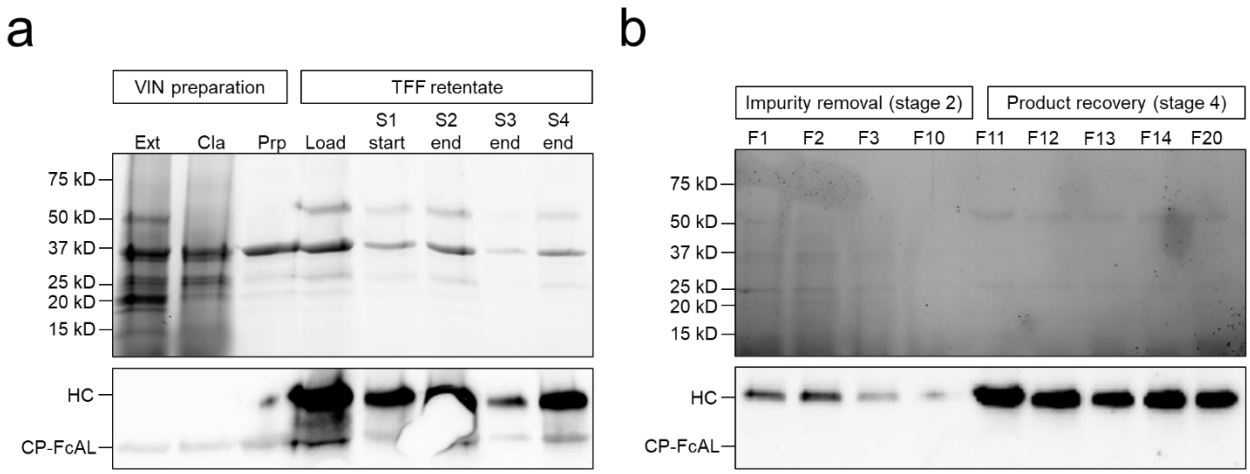

Figure 11.2. SDS-PAGE and western blot results of the combined plant virus-based immunosorbent nanoparticle (VIN) tangential flow filtration (TFF) circulatory system, shown for a proof-of-concept sample load of purified human immunoglobulin G. (a) VIN preparation and TFF retentate samples. (b) TFF permeate samples for the impurity removal and product recovery stages. Ext – extraction step; Cla – clarification step; Prp – final prepared stock solution; S – stage of operation (per Figure 1); F – permeate fraction (5 mL each); HC, IgG heavy chain; CP-FcAL, VIN coat protein Fc-affinity ligand.

As shown in Figure 11.3, the permeate flux was maintained between ~75 – 120 LMH throughout operation. In between the impurity removal and product recovery stages, the addition and recirculation of a single bolus consisting of five (5) diavolumes of low pH elution buffer with a closed permeate line likely contributed to the increased flux observed at the start of product recovery. The additional volume, removal of a transmembrane pressure (TMP) driving force, and a change in the pH of the liquid environment all likely contributed to perturbation and clearance of the protein aggregate on the membrane[487].

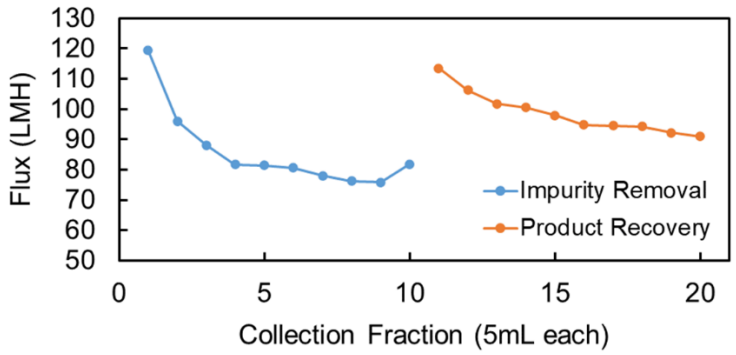

Figure 11.3. Permeate flux data for the combined plant virus-based immunosorbent nanoparticle tangential flow filtration system over impurity removal and product recovery stages.

Figure 11.4 displays permeate measurements of UV absorbance for each fraction collected during the impurity removal stage. We observed a 96% reduction in absorbance measurement by the end of the impurity removal stage, indicating that the majority of the impurities present in the prepared VIN solution had been cleared. This reduction is consistent with general performance expectations of TFF batch diafiltration. The liquid hold-up volume in the permeate line was collected as part of the first fraction, contributing to a lower absorbance measurement and conservative estimate of impurity clearance.

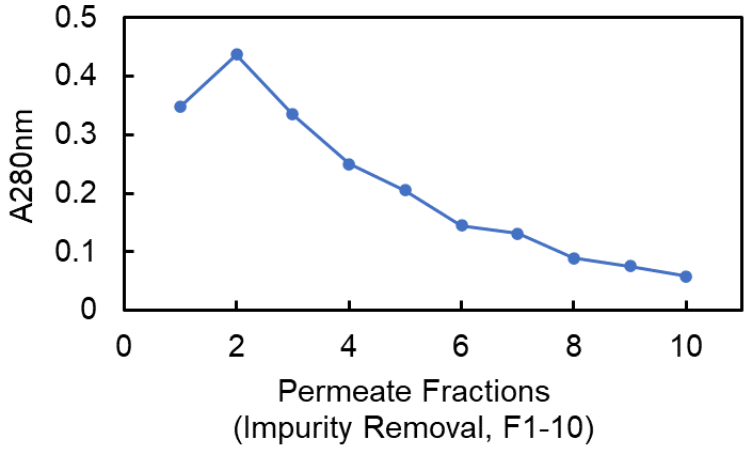

Figure 11.4. UV-vis A280 absorbance measurements for the tangential flow filtration permeate fractions for the impurity removal stage. Fractions are collected in increments of 0.5 diavolumes.

The VIN TFF method presented in this study was also efficacious for VIN-based capture and elution of hIgG from clarified *N. benthamiana* plant extract solution. Figure 11.5 shows the SDS-PAGE and western blot results from the VIN TFF method executed in this more process-relevant set of conditions. As with the purified hIgG binding and recovery, we observe the presence of VIN CP-FcAL in the TFF retentate samples, and the lack of VIN in the permeate line fractions collected during operation, indicating the VIN were again successfully retained in the retentate circulatory loop. The hIgG was largely retained during the impurity removal stage and eluted into the permeate during the product recovery stage. Interestingly, the pattern of bulk hIgG clearance in early volumes of the collected permeate fractions was more representative of the expected clearance during TFF diafiltration than was observed for the earlier study using purified hIgG.

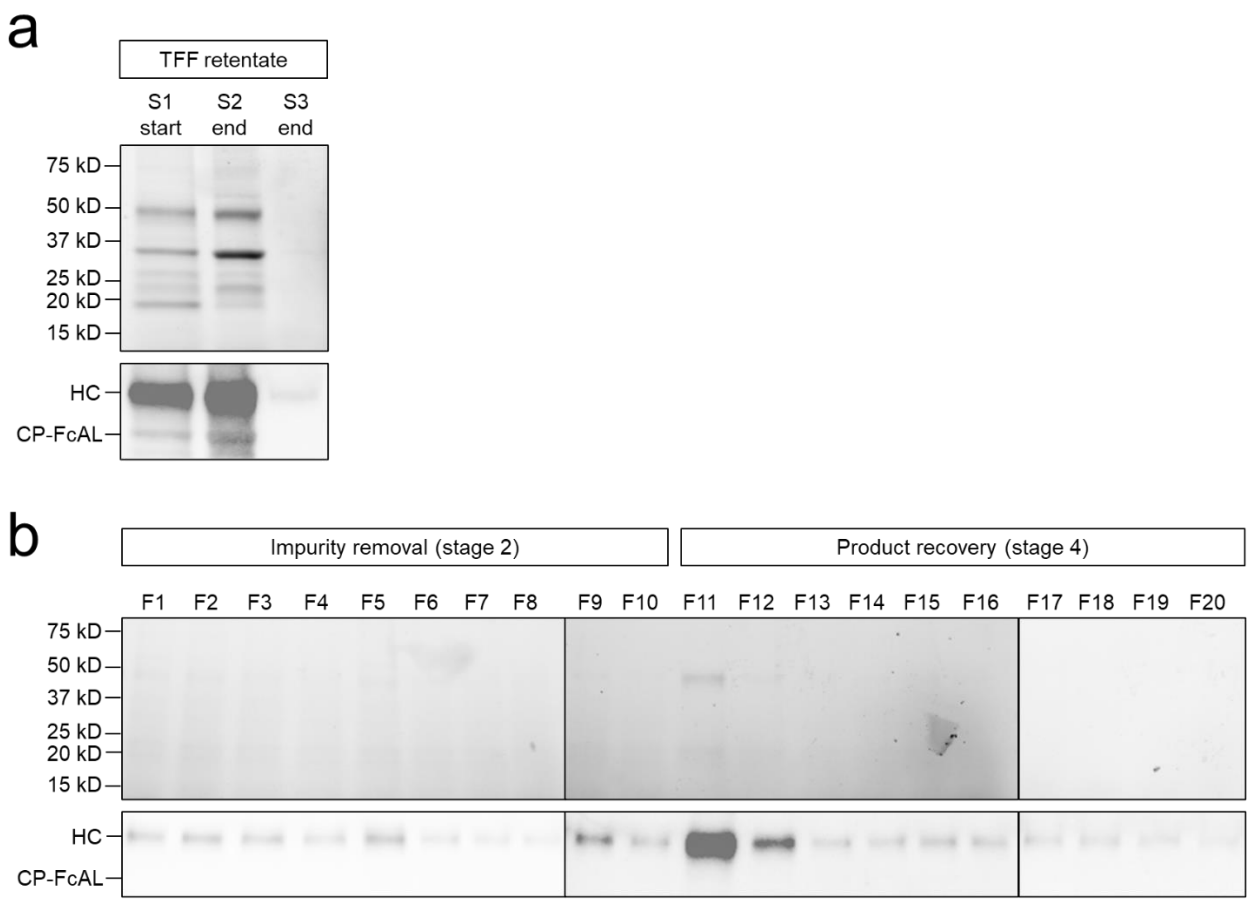

Figure 11.5. SDS-PAGE and western blot results of the combined plant virus-based immunosorbent nanoparticle (VIN) tangential flow filtration (TFF) circulatory system, shown for a sample load of human immunoglobulin G in clarified *N. benthamiana* plant extract. (a) TFF retentate samples. (b) TFF permeate samples for the impurity removal and product recovery stages. S – stage of operation (per Figure 1); F – permeate fraction (5 mL each).

11.4. Discussion

VIN technology is emerging as a model class of virus-based nanomaterial for which a range of novel and advanced system configurations have been reported. Two first-in-class advanced system configurations for plant virus-based nanomaterials, namely magnetic particle conjugation[40] and silica sol-gel entrapment[43], have been in reported in the past year (in addition to the novel affinity sedimentation method first reported in 2006[342]) with promising results (e.g., a reported 25x increase in binding capacity for VIN-coupled magnetic particles compared to commercial

standards for antibody-binding magnetic particle) reflecting the advantages of integrating virus-based nanomaterial into existing pharmaceutical purification and biosensing systems.

In this study, we report promising proof-of-concept results for a new advanced system configuration – VIN-circulating TFF-based mAb affinity capture and recovery. The VIN were circulated in the TFF retentate at neutral and low pH buffer without fouling the cassette membrane. VIN-hIgG binding and complex formation was demonstrated in PBS or clarified plant extract as a mechanism to retain hIgG in the retentate loop when using a 1,000 kD MWCO membrane that would have otherwise rapidly cleared hIgG into the permeate. Diafiltration with low pH buffer was shown as a mechanism to adequately promote VIN-hIgG dissociation and subsequent recovery of hIgG in the permeate.

Works to complete this proof-of-concept study would include collection of additional characterization data to strengthen existing results. Valuable additional data to collect for completing this study would include TMP measurements, total soluble protein content measurements of the retentate and permeate collection fractions, dynamic light scattering measurement of the average particle hydrodynamic radius in the retentate throughout operation to investigate the potential for VIN particle rupture and VIN fragment clearance into the permeate. Accordingly, this characterization could serve as a foundation for future studies on reusability of the VIN for additional rounds of hIgG capture and purification.

There are several directions that could be taken to further develop the VIN-TFF method. There are several components of the system operation that could be clearly improved on. A smaller MWCO cassette membrane, such as 300 kD, could be used to investigate and/or minimize chances of VIN, and hIgG, escape into the permeate. Rather than batch diafiltration, the VIN-TFF operations could be carried out using constant volume diafiltration to improve the rate of impurity and product

clearance[488]. Buffer compositions could be optimized through addition of detergents or salts (e.g., guanidine HCl[489]) to minimize attractive electrostatic interactions leading to high viscosity and protein aggregation[490]. A study of the flux-TMP profile could be carried out to identify the optimal fixed TMP for operation, which is generally at the transition point between pressure-dependent and -independent regions of the profile to maximize flux (to reduce process time) while minimizing antibody aggregation[491]. An improved understanding of the operating range of the permeate flux, a key factor considered in equipment sizing and large-scale economic potential[492], would aid in defining future directions from there. It could also be important to investigate VIN-TFF performance when VIN has been pre-loaded into the TFF followed by the desired mAb solution afterwards, which is one route for removing the mixing and incubation step present in the current methodology to improve speed of operation. It is also worth considering the extent of VIN purification required prior to loading of the VIN into the TFF to similarly reduce overall processing requirements.

Another promising route for development of the VIN-TFF is scale-down. Initial studies of VIN stability over a duration of eight (8) weeks found no discernable differences in the VIN CP-FcAL at 4 °C, suggesting that VIN would be amenable for more distributed use cases[40]. In recent years, there have been reports of microfluidic devices integrated with TFF elements for biological separation and diagnostic applications[493–495]. If proven successful, a VIN-TFF microfluidic concept would serve as one unit operation module that could be integrated into the new and upcoming concept of "therapeutics-on-a-chip" device for point-of-care protein production[496,497].

The VIN-TFF system reported in this study has unique advantages over the previously reported VIN system configurations. It improves upon the original VIN processing methodology of centrifugation-assisted sedimentation requirements for significant labor and may be a strategy to

overcome the VIN particle breakage of the sedimentation method that limits reusability and material uniformity. The VIN-conjugated magnetic particle and VIN-functionalized silica sol-gel systems both provide simple strategies for isolating the VIN from bulk solution at the cost of a reduction in VIN active site availability for binding, whereas the VIN-TFF system theoretically maintains the VIN in solution with full active site availability and binding capacity. The other VIN system configurations are not without their own particular merits, as have been outlined in their respective works, but this is to say that the proof-of-concept VIN-TFF system developed in this study lays the foundation for development of a system that maximizes the VIN binding capacity and provides opportunity in both scale-up and scale-down.

The advantages of this novel VIN-TFF system configuration are not constrained to VINs specifically but are also expected to be broadly applicable to other virus-based nanomaterials.

Chapter 12. From farmers to astronauts: Engineering a hand-powered centrifuge for limited resource environments

"Yes, of course duct tape works in a near-vacuum. Duct tape works anywhere. Duct tape is magic and should be worshiped."

-Andy Weir

This chapter is not based on a previously published article. The works presented in this chapter serve as foundational for a future peer-reviewed journal publication when augmented with additional experimental investigation and analysis. The author list for the works presented in this chapter is as follows:

Matthew J. McNulty[1], Kevin Yates[1], Dylan Estrada[1], Amar Zagdragchaa[2], Justin Mahley[2], Kha Ton[1], Somen Nandi[1,3], William Miller[2], Devoun Stewart[2], and Karen A. McDonald[1,3]

[1]Department of Chemical Engineering, University of California, Davis, CA, USA

[2]Department of Chemistry, Sacramento City College, Sacramento, CA, USA

[3]Global HealthShare® Initiative, University of California, Davis, CA, USA

Abstract

Many research, diagnostic, and manufacturing workflows rely on a centrifuge for separations. New frontiers in limited resource environments like pathogen biosensing in agriculture and increased human presence in outer space strain the feasibility of the current workflow paradigm and motivate

new adaptations and accommodations. A range of novel centrifuge designs have been proposed over the years to accommodate different resource limited environments. One breakthrough design several years ago was the nonlinear oscillatory paperfuge, which brought an ultralow cost solution to blood plasma fractionation and malaria diagnostics. In this study, we expand upon the concept of nonlinear oscillatory centrifugation using 3D-printed parts and a system with a volumetric capacity of up to six 2 mL tubes. We characterize the general centrifuge performance, apply it for two test cases of liquid-solid separation and filter extraction, screen the impact of critical design parameters, and perform multivariate optimization of the design.

12.1. Introduction

Centrifugation is a critical operation in many biotechnical workflows, ranging from medical diagnostics to scientific discovery to manufacturing. The new frontiers of biotechnology are expanding to increase accessibility to limited resource environments and venture into unexplored territories. These limited resource frontiers include remote field sites, communities recovering from natural calamity, wartime battlefields, and deep space. There is a parallel need for the biotechnical workflows to adapt to the new constraints of these environments. Traditional commercial centrifuges are not well-suited to these constraints or environments because of a high cost, large size, and reliance on steady electricity. In recent years, researchers have begun working to meet this need and a series of limited resource centrifuge designs have been reported (Table 12.1). These centrifuge designs are as varied in their use cases, from blood fractionation to virus detection assay, as they are in their design inspiration, from salad spinners to bike wheels to fidget spinners.

Table 12.1. A list of centrifuges designed for limited resource environment applications. RCF, relative centrifugal force.

ID	Volumetric Capacity	Material/Construction Complexity/Cost	Cost [mass (g), currency ($)]	Average RCF Output
Paperfuge[498]	< 80 µL	Paper, string, and plastic	~2 g $0.20	< 30,000 x g
3Dfuge[499]	< 8 mL	3D printed parts, string	~20 g $1.00	Unknown (2,100 x g max, oscillating)
Traditional Gear[500]	< 9 mL	3D printed parts	~550 g $25	< 550 x g
Salad Spinner[501]	< 420 µL	Pre-assembled salad spinner; plastic parts	~1,200 g $35	< 31 x g
Egg Beater[502]	< 2 mL	Egg beater, tubing, paper	~91 g $8-20	< 150 x g

OPN Minifuge*,[503]	< 3 mL	Hardware store goods, electrical circuitry	unknown g $15-45	129 x g
Dremelfuge*,#	< 9 mL	Dremel-300, 3D printed parts	> 550 g > $300	51,520 x g
Bearing-Based Hand Spinner[504]	< 80 µL	3D printed parts, ball bearings	~36 g $0.04-10	< 273 x g
Fidget-Spinner[505]	< 80 µL	Fidget spinner, tape, tubing	~ 68 g ~ $10	~ 60 x g
Spokefuge$^{\gamma}$	< 2 mL	Bicycle, 3D printed parts	~11,000 g ~$100	~ 6 x g**
Handyfuge[506]	< 3 mL	Hand-crank flashlight, tube holder	~85 g $5	500 x g

*****Requires electrical power input
source: https://www.thingiverse.com/thing:1483
γ source: https://www.wired.com/2014/12/clever-bike-powered-centrifuge-developing-countries/
**Not available. Estimated based on average bike tire size (26") and bike speed (10 MPH)

Perhaps most notable in its ulta-low cost ($0.20) and ultra-high speeds (<125,000 RPM; 30,000 RCF), the "paperfuge" developed by Bhamla and team is a paper-based and hand-powered centrifuge that exploits the mechanics of a simple buzzer toy[498]. They demonstrated that the paperfuge device can be used to fractionate a blood sample in as little as 1.5 minutes. The paperfuge marked a defining moment in medical diagnostic accessibility. However, the volume constraints of the capillary tubes limited the application areas primarily to low volume blood-based samples.

Earlier last year, Bhamla extended this work with the "3D-fuge," a 3D-printed centrifuge disk also based on the buzzer toy mechanics[499]. The 3D-fuge has been adapted to accommodate larger liquid volumes (up to 2 mL per sample; 8 mL per centrifuge). With this expanded capacity, they demonstrated proof-of-concept nucleotide extraction and bacterial pelleting feasibility.

In this work, we further expand upon the concept of a 3D-printed centrifuge based on the buzzer toy with more in-depth characterization, centrifuge design optimization, and two use cases. We further investigate the relationship between the applied human input force and the angular velocity profile, screen the influence of critical design parameters, perform multivariate optimization of the design, and benchmark performance against a traditional benchtop centrifuge. We demonstrate that this 3D-printed centrifuge design holds promise for advancing limited resource environment centrifugation capabilities in liquid-solid separation and filter extraction.

12.2. Materials & Methods

12.2.1. Hand-powered centrifuge

The hand-powered centrifuge consists of a 3D-printed plastic disc and two handles, along with a length of string threaded through the disc and handles. The centrifuge design is based on the design popularized by Bhamla in 2017 with the paperfuge[1], which was further expanded upon with the 3D-fuge in 2019[499]. The parts were printed using 2.85 mm polylactic acid (PLA) filament with an Ultimaker 2+ 3D printer equipped with a 0.4 mm nozzle with a layer height of 0.15 mm. Braided nylon mason line #1 (T.W. Evans Cordage Co., Inc., Cranston, RI) was used as the string.

12.2.2. Testing platform

A testing platform was constructed to characterize and optimize the performance of the hand-powered centrifuge. The testing platform is a guided rail system designed to measure applied human input force using a force transducer (S-type load cell 0-100kg; Phidgets, catalog ID: CZL301C) and angular velocity using a laser tachometer. Additional details of the force transducer

and laser tachometer configurations are included in Supplementary Information (Text S12.1 – S12.2). Calibrations of the testing platform measurements were tested using spring gauges (force measurement) and a cell-phone camera at 240 frames-per-second (angular velocity measurement) (Supplementary Information, Figure S12.1).

The two handles of the HPC are affixed to the guided rail system. One handle is attached to a sliding track that can move freely in a single axis. The other handle is attached to a stationary force transducer configuration at one end of the rail. Adjacent to the stationary force transducer is the laser tachometer system.

12.2.3. Centrifuge performance

Centrifuge performance was benchmarked using an effective relative centrifugal force (RCF) obtained over a minimum of three (3) sets of five (5) consecutive oscillatory periods (each including a single cycle of both positive and negative direction disc spinning) in which the corresponding human-applied normal force reaches a maximum of 60 N +/- 10% (54 – 66 N) per human-driven pull. Two human-driven pulls are required for one complete oscillatory period. A measure of effective RCF was previously established and shown for the paperfuge design to closely approximate the bioseparation capability of a benchtop centrifuge at that RCF[498]. Effective RCF is defined as,

$$effective\ RCF = \frac{R_d \langle \omega^2(t) \rangle}{g}$$

where R_d is disc radius (in m), ω is angular velocity (in rad/s), and g is acceleration due to gravity (in m/s^2).

Data for the benchtop centrifuge standard curves were collected using biological triplicate at RCF values of 50 x g, 100 x g, 200 x g, 300 x g, 500 x g, and 750 x g. A power regression was used to generate the standard curve for mapping HPC performance to benchtop centrifuge performance.

HPC operation studied for univariate analysis and multivariate optimization was executed using six 1.5 mL tubes slotted in the disc each containing 1.2 mL of water.

12.3. Results & Discussion

12.3.1. Hand-powered centrifuge

A hand-powered centrifuge (HPC) based on the previously reported paperfuge concept was designed and 3D-printed for bioseparations of liquid samples up to 2 mL in volume, as shown in Figure 12.1. The HPC device is composed of a central disc (that can be slotted with sample tubes) connected to two sets of handles via a singular loop of thread inserted through the central disc and handle holes. This design generates a spinning of the centrifuge disc, and thus the relative centrifugal force driving the bioseparations, through a normal applied force by the human operator on both hands to establish a pattern of non-linear oscillation consisting of successive string winding and unwinding, alternating between the positive and negative rotational direction with each winding-unwinding cycle. The human operation of the HPC is simple and teachable, yet in our experience we found that human operators required a minor initial training to understand proper technique.

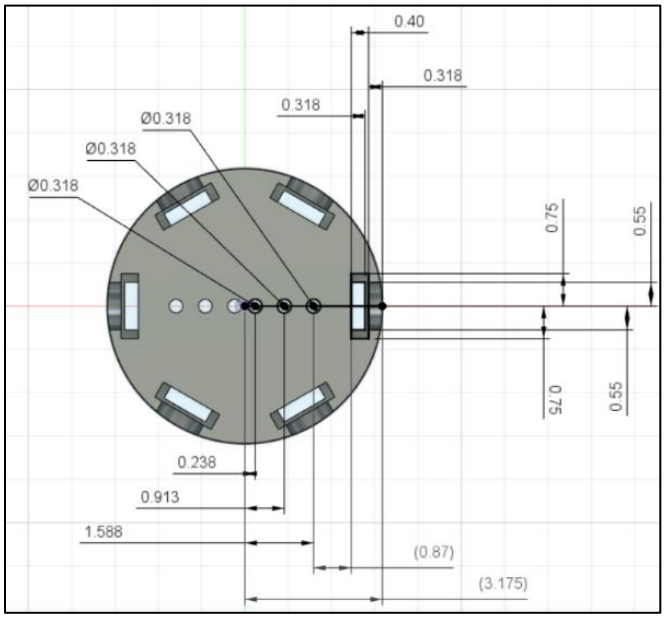

Figure 12.1. An engineering design diagram of the base case hand-powered centrifuge disc. Measurement are shown in centimeters.

Given the inherent variation in the human operation of the HPC, a testing platform was designed and constructed for the standardization of the HPC operation and measurement of key performance data (normal applied force, angular velocity), as shown in Figure 12.2. The normal applied human force on the handle of the mobile platform slotted in the guiderail system, as measured by the S-type load cell, was sampled every 20 milliseconds and displayed graphically on a nearby computer monitor in real time to inform pulling force corrections for the operator. Angular velocity, as measured by the laser tachometer and stored with the data logger, was sampled every 20 milliseconds. With this sampling frequency, the bottleneck on angular velocity resolution became effectively bounded by the dynamic combination of the reflective tape spacing and the angular velocity of the disc.

One variable that we did not control for with the testing platform was the relaxation distance allotted per pull cycle, which is to say that we did not impose a strict measure of distance along the guided rail system that the mobile platform would be moved closer to the load cell to allow string winding after completion of the pull. Future works may consider means for establishing control of this variable, which in turn influences extent of string winding and ultimately angular velocity.

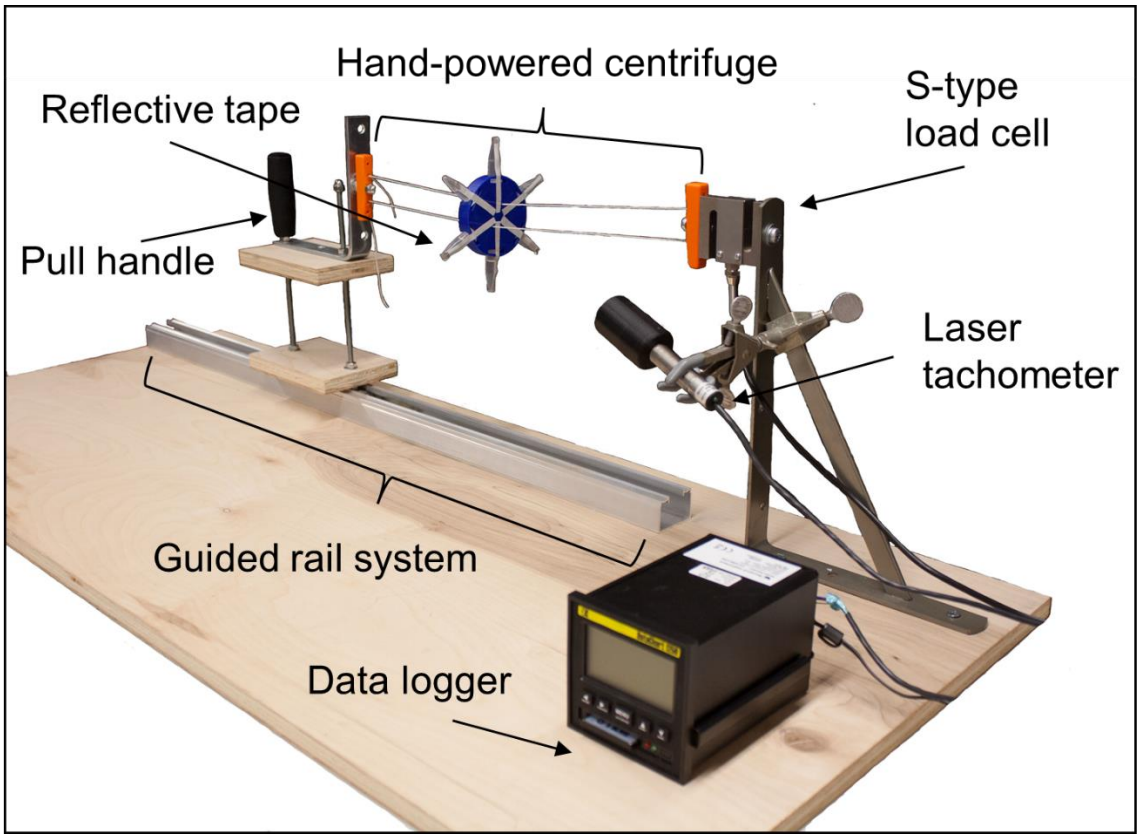

Figure 12.2. An annotated photograph of the physically constructed testing platform configuration used to maintain regular centrifuge operation and measure applied force and centrifuge angular velocity.

Sample output data from HPC operation with the testing platform is shown in Figure 12.3. The HPC was found to be capable of achieving an effective RCF upwards of 100 x g with a reasonably mild human input characterized by a peak pull force of 60 N.

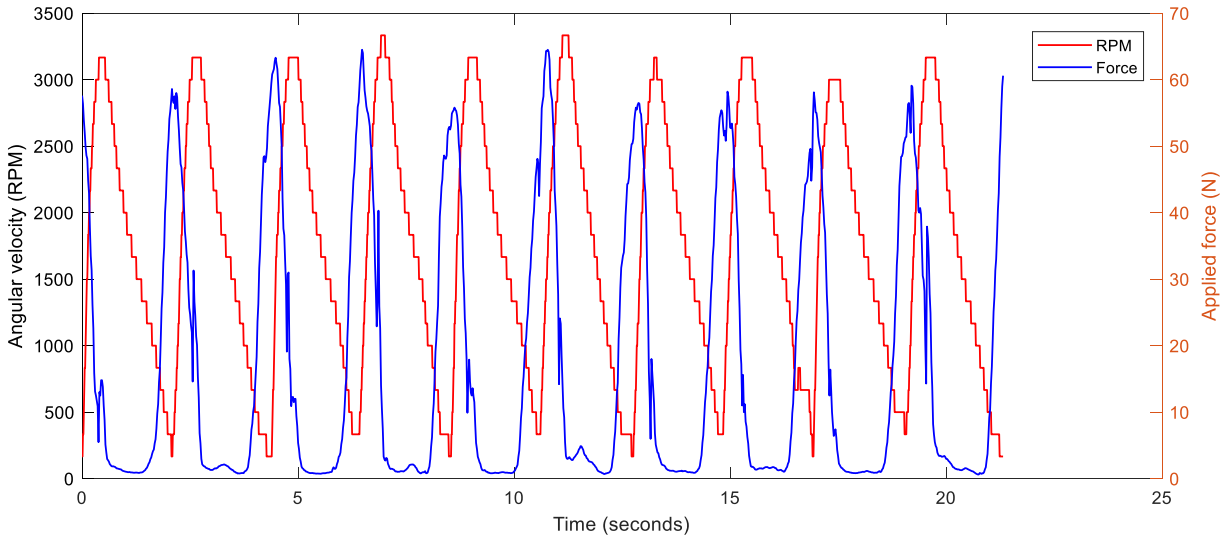

Figure 12.3. An example set of data collected during hand-powered centrifuge operation for applied force and the absolute value of angular velocity.

12.3.2. Bioseparation test cases: liquid-solid & filter extraction

We tested the performance of the base case HPC design in two major classes of bioseparations, liquid-solid separation and filter extraction, relevant to the volume scale of the HPC and we benchmarked this against the performance of a traditional benchtop centrifuge. This allowed us to compare the efficiency of bioseparation for a given effective RCF of the HPC operation to the efficiency of bioseparation for an equivalent RCF generated by benchtop centrifugation.

The results of the liquid-solids separations capability of the HPC, as tested using a system of 1.2 mL of lettuce leaf extract in phosphate buffered saline (PBS) pH 7.0 per 1.5 mL tube, are shown in Figure 12.4. The lettuce leaf extract was prepared by thorough pestle pulverization of the leaf

tissue in the tube. The reduction in optical density (OD) corresponds to the extent of sample sedimentation, so a lower OD represents a greater extent of sedimentation. We show that the HPC can reasonably reduce sample OD by approximately 40 – 60% over the course of five (5) minutes of operation. However, the HPC significantly underperformed in comparison to the sedimentation obtained for an equivalent RCF with a traditional benchtop centrifuge. This extent of underperformance increased with the effective RCF and peak applied force used in HPC operation.

We observed that the complex mixture of lettuce extract had several different sedimentation layers (data not shown). The bottom-most layer of sediment, of a whiteish hue, formed a compact and solid pellet, while other of the greener colored sediments were observably less dense and less solid. In this context, we hypothesize that the pellet perturbations experienced in the directional oscillations of normal HPC operation were sufficient to largely disrupt sedimentation of some of the green sediment species but did not interfere with sedimentation of other species. From this, we gather that the efficiency in use of HPC for liquid-solid separations is largely dependent on the characteristics of the sediment formed during operation.

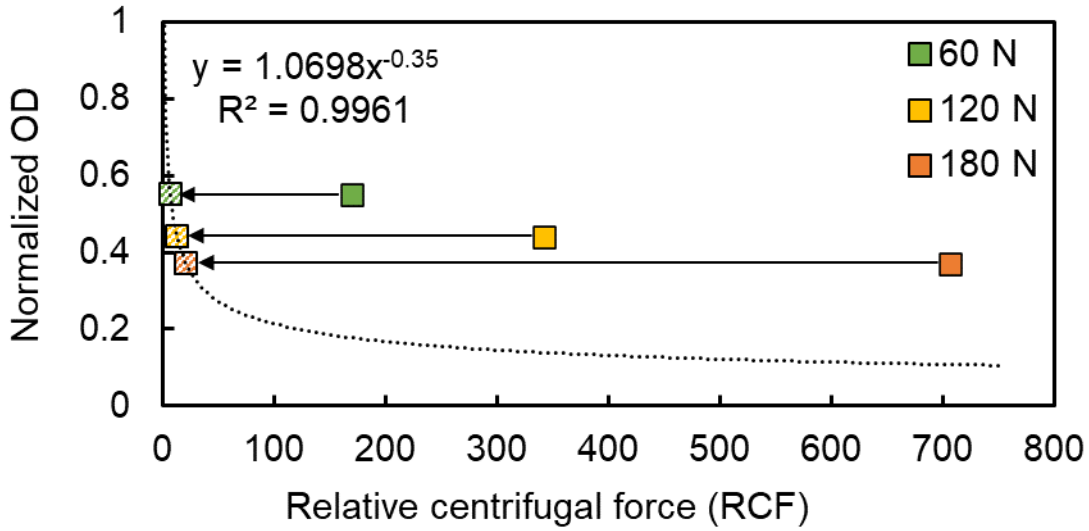

Figure 12.4. An evaluation of the liquid-solids separations capability of the hand-powered centrifuge operated at a given average relative centrifugal force (RCF) (solid box) as compared to standard curve generated with benchtop centrifuge performance (dotted line) using a model system of *Lactuca sativa* cv. Crisphead plant extract in phosphate buffered saline pH 7.0 solution. Three hand-powered centrifuge conditions for peak applied force were tested (60 N, 120 N, 180 N). All samples were centrifuged for 5-minute durations. The hashed boxes represent the equivalent benchtop centrifuge RCF that would be required to achieve equivalent separations as to the hand-powered centrifuge based on interpolation of the benchtop standard curve results. Effective RCF values for the hand-powered centrifuge performance are based on angular velocity data for the full 5-minute span. Optical density (OD) results are normalized to the OD of the initial plant extract solution.

The results of the filter extraction capability of the HPC, as tested using a system of water and 100 kD membrane spin filters set in 2 mL tubes, are shown in Figure 12.5. The tube slots of the HPC disc were re-designed to fit the shape of the spin filter. A total of 500 µL water was added per spin filter and the permeate volume represents the extent of water that had been extracted through the filter. We show that the HPC can extract 30 – 180 µL water through the filter over the course of five (5) minutes of operation. In contrast with the results of liquid-solids bioseparations, the HPC overperformed in comparison to the filter extraction obtained for an equivalent RCF with a traditional benchtop centrifuge. This overperformance was observed for all three of the peak applied force conditions tested for HPC operation.

The high performance of the HPC in this test case suggests that the HPC may be particularly amenable technology for limited resource environment filter extractions, which would include nucleic acid purification, water and soil samples, and more. These results may suggest that the peak RCF (529 x g for the 60 N run, 911 x g for the 120 N run, 1,397 x g for the 180 N run) has a disproportionate effect on the rate of water clearance through the spin filter.

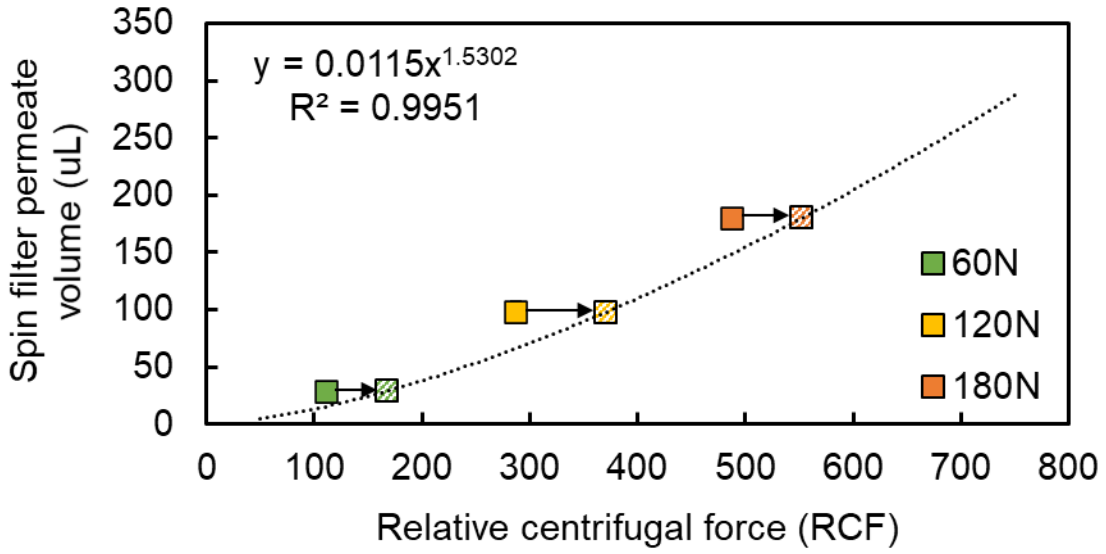

Figure 12.5. An evaluation of spin filter extraction capability of the hand-powered centrifuge at a given average relative centrifugal force (RCF) (solid box) as compared to standard curve generated with benchtop centrifuge performance (dotted line) using a model system of water filtration. Three hand-powered centrifuge conditions for peak applied force were tested (60 N, 120 N, 180 N). All samples were centrifuged for 5-minute durations. The hashed boxes represent the equivalent benchtop centrifuge RCF that would be required to achieve equivalent separations as to the hand-powered centrifuge based on interpolation of the benchtop standard curve results. Effective RCF values for the hand-powered centrifuge performance are based on angular velocity data for the full 5-minute span.

The results of the two test cases together strongly suggest that the previously defined equation of effective RCF does not consistently capture HPC bioseparations capability in terms of traditional benchtop centrifuge. Due to the unique mechanism of rotation and separation, the performance should be closely evaluated for a new application.

12.3.3. Univariate sensitivity analysis of HPC design

We performed univariate sensitivity analysis to investigate the impact of a set of six (6) independent variables of the HPC design on two key dependent variables of HPC performance –

effective RCF and frequency of oscillation. The low, base, and high values selected for each of the independent variables of HPC design are shown in Table 12.2. The low and high values were determined based on working process knowledge and inherent design constraints (e.g., the low value for disc radius was determined as the minimum radius required for maintaining six (6) tube slots in the disc).

Table 12.2. Independent variable ranges evaluated in single-factor experiments for hand-powered centrifuge design.

Parameter	Lo	Base	Hi
Disc radius, DR (cm)	28	32	45
Disc hole distance from the origin, DH (cm)	2.25	15	22
Handle hole distance from the origin, HH (cm)	2.25	15	25
Disc mass, DM (% PLA inlay)	5	20	80
String length disc to handle, SL (cm)	16.5	20.6	24.8
Peak applied force, FP (N)	40 +/- 10%	60 +/- 10%	80 +/- 10%

The results of the univariate analysis are shown in Figure 12.6. A statistically significant difference in effective RCF was observed across most of the independent variables tested. The run-to-run variation in effective RCF during HPC operation is considerable, as expected.

We observed that a smaller disc radius resulted in higher effective RCF and higher frequency. A smaller disc hole distance from the origin yielded lower effective RCF and lower frequency. The handle hole distance from the origin did not yield significantly different effective RCF values, but a smaller distance was associated with a lower frequency. Higher disc mass resulted in higher

effective RCF, and both the low and high values were associated with a lower frequency than the base. A shorter string length yielded higher effective RCF and higher frequency. And lastly, a larger pull force resulted in higher effective RCF and higher frequency.

String type is an independent variable that was not tested but should be considered in future investigations. We suspect that the properties of the string (e.g., compressibility, thickness) may significantly impact the HPC operation, particularly in regard to the extent of formation of super-coiled structures during winding.

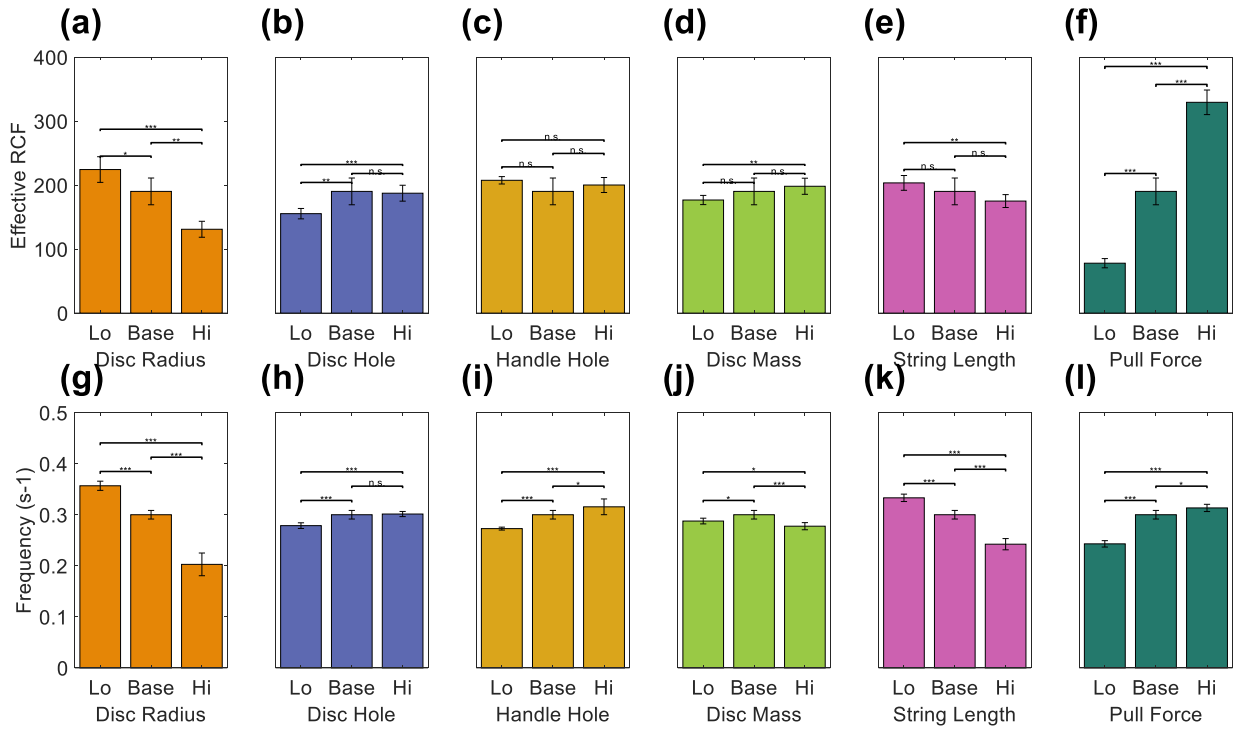

Figure 12.6. Univariate analysis results display differences in effective relative centrifugal force (RCF) and frequency over variations in disc radius (a, g), disc hole distance from the origin (b, h), handle hole distance from the origin (c, i), disc mass (d, j), string length (e, k), and average normal pull force (f, l). Error bars represent a minimum of triplicate measurements. Statistical significance was evaluated by two-sample two-tailed t-test at $p \leq 0.05$ (*), $p \leq 0.01$ (**), $p \leq 0.001$ (***). n.s., insufficient evidence to conclude statistically significant difference (i.e., $p > 0.05$).

12.3.4. Multivariate optimization of HPC design

We performed a three-factor optimization of the HPC performance, defined as the response of effective RCF in this analysis, considering the following independent variables: disc radius, disc hole distance from the origin, and handle hole distance from the origin. These three variables were selected by inspection results from the univariate analysis and an interest in investigating the interaction between Disc hole distance from the origin (DH) and Handle hole distance from the origin (HH), which we suspected contributed to the effective RCF in large part due to the terminal twisting angle of the disc. A Box-Behnken design was employed for the design of experiments for the experimental efficiency and response surface methodology was used for optimization. Independent variable values used in this study are listed in Table 12.3. The Box-Behnken experimental design and response values for effective RCF are listed in Supplementary Information, Table S12.2.

Table 12.3. Independent variable values assigned for the three-level multivariate analysis.

Parameter	-1 (cm)	0 (cm)	1 (cm)
Disc radius, DR	30	37.5	45
Disc hole distance from the origin, DH	2.25	12.125	22
Handle hole distance from the origin, HH	2.25	13.625	25

We predicted response of the effective RCF by multiple regression analysis on the experimental data using the following second-order polynomial equation containing regression coefficients for intercept, linear, quadratic, and interaction terms:

$$effective\ RCF = 156.08 - 17.036X_1 + 10.72X_2 + 20.926X_3 - 2.4563X_1X_2 + 1.2863X_1X_3 - 6.968X_2X_3 - 5.742X_1^2 + 22.348X_2^2 - 24.457X_3^2$$

where X_1, X_2, and X_3 were the normalized [-1, +1] coded values of the three independent variables DR, DH, and HH, respectively. The regression was graphically represented by response surface and contour plots in Figure 12.7. The plots were generated by fixing one of the independent variables at its zero (0) level, representing the center value of its testing range.

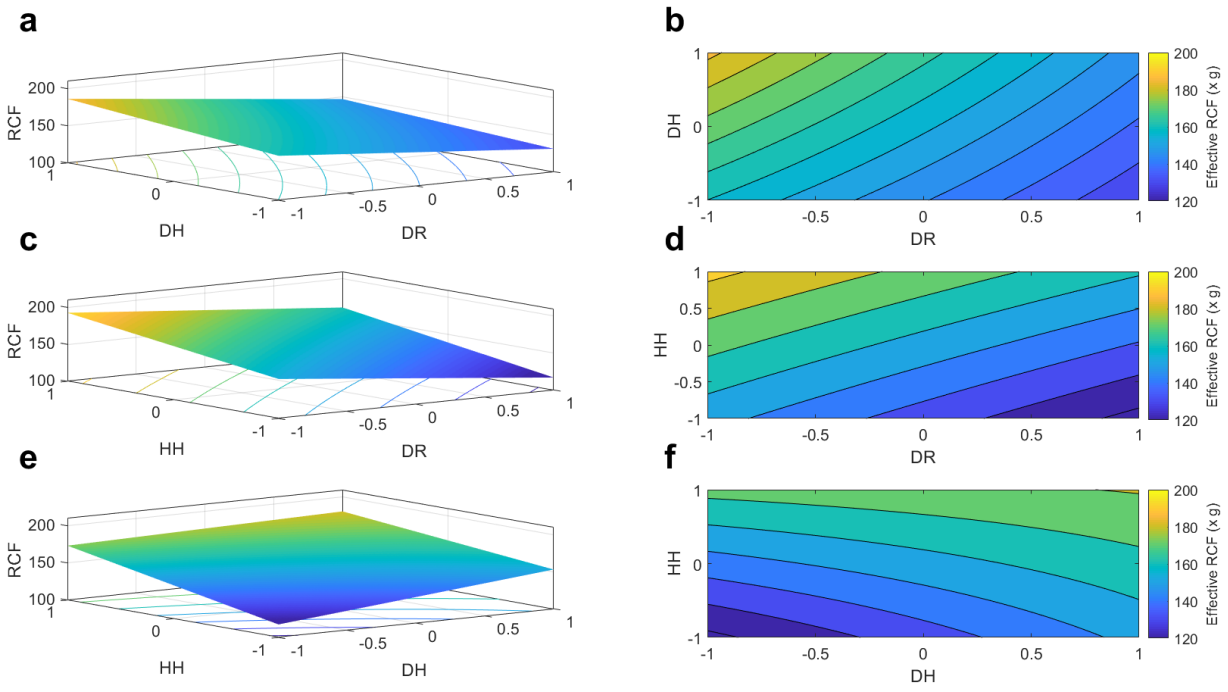

Figure 12.7. Response surface and contour plots to visualize the regression model. Response surface and contour plots of effective relative centrifugal force (RCF) as a function of (a, b) disc radius (DR) and disc hole distance from the origin (DH), (c, d) DR and handle hole distance from the origin (HH), and (e, f) DH and HH.

The R^2 value (0.867) and adjusted-R^2 value (0.629) of the model suggest a reasonable fit with the experimental data, however the significance of the model was tested and shown to be lacking by analysis of variances (ANOVA), as shown in Supplementary Information, Table S12.3. The F-value of the overall significance (3.63) and associated p-value (0.085) indicated that the regression model was not a better fit than the intercept-only model. Additionally, the F-value for the lack of fit and associated p-value also indicate invalidity of the model. The majority of the individual coefficients were not shown to be significant ($p \leq 0.05$), however the two linear terms X_1 (0.050) and X_3 (0.025) were shown to be significant. It may be that the inherent variation in HPC human operation was sufficiently noisy, and the controls we implemented via the testing platform and criterion were insufficiently robust, as to obscure the signal of the data. This provides motivation for future study of inter- and intra-operator variation. Future works to improve the significance of the model would include data transformation, additional data coverage and/or replication, and investigating different independent variables.

In contrast to these findings, it is worth noting that an added variable plot for the whole model (which excludes the intercept term), as shown in Supplementary Information, Figure S12.2, illustrated that the model was significant (as evaluated because a horizontal line cannot be fit between the confidence bounds).

The optimal values of the three independent variables were found to be DR = 30 cm, DH = 22 cm, HH = 16.6 cm by solving for the maximum effective RCF using the regression equation. The optimum set of values is plotted within the context of the Box-Behnken design, as shown in Supplementary Information, Figure S12.3. The optimal was identified in a region of low data coverage for the design, representing an area of greater uncertainty in the model. The performance of an HPC with the optimal set of values has not yet been printed and evaluated. Future works that

consider this multivariate analysis will need to perform this verification assessment. Additionally, if this value is found to optimal, it may be advantageous to feed the model with additional data in that region of the design space to ensure the optimal is correctly identified.

12.4. Supplementary information

12.4.1. Supplementary tables

Table S12.1. A summary of the printing parameters used with the Ultimaker 2+ 3D printer equipped with a 0.4 mm nozzle for printing of the hand-powered centrifuge (HPC) disc, handles, and testing platform components.

Item	Printing Parameters					
	Material	Extruder Temperature (℃)	Bed Temperature (℃)	Layer Height (mm)	Infill Density (%)	Raft
HPC handle	PLA	210	N/A	0.15	Variable	yes
HPC disk	PLA	210	N/A	0.15	Variable	yes
Tachometer bracket	Nylon	250	75	0.2	15	yes
Tachometer sensing tip shield	Nylon	250	75	0.2	20	no

Table S12.2. Box-Behnken experimental design and response values for effective relative centrifugal force (RCF). DR, disc radius; DH, disc hole distance from the origin; HH, handle hole distance from the origin.

Run #	DR	DH	HH	Effective RCF (x g)	
				Mean	S.D.
1	-1	-1	0	195.42	10.48
2	-1	1	0	210.59	11.88
3	1	-1	0	139.70	3.48
4	1	1	0	145.05	10.23
5	-1	0	-1	113.43	3.31
6	-1	0	1	145.85	5.00
7	1	0	-1	103.34	10.28
8	1	0	1	140.91	13.31
9	0	-1	-1	106.34	7.79
10	0	-1	1	168.99	10.47
11	0	1	-1	152.89	5.63
12	0	1	1	187.67	7.77
13	0	0	0	156.08	13.76

Table S12.3. Results of analysis of variances (ANOVA) for effective relative centrifugal force.

Source		Sum of squares	DF	Mean square	F-value	p-value
Total		13230	14	944.98		
Model		11475	9	1275	3.6333	0.084581
	Linear	6744.4	3	2248.1	6.4064	0.036415
	Nonlinear	4730.7	6	788.45	2.2468	0.19614
Residual		1754.6	5	350.92		
	Lack of fit	1754.6	3	584.87	Inf	0
	Pure error	0	2	0		
X_1		2321.8	1	2321.8	6.6162	0.049902
X_2		919.3	1	919.3	2.6196	0.16647
X_3		3503.3	1	3503.3	9.9832	0.025106
X_1X_2		24.133	1	24.133	0.068771	0.8036
X_1X_3		6.6186	1	6.6186	0.018861	0.89613
X_2X_3		194.21	1	194.21	0.55343	0.49038
X_1^2		121.74	1	121.74	0.3469	0.58147
X_2^2		1844	1	1844	5.2548	0.070443
X_3^2		2208.5	1	2208.5	6.2935	0.053915

12.4.2. Supplementary text

Text S12.1. An overview of the force transducer configuration within the testing platform.

We used a force transducer configuration for measurement of applied normal force during HPC performance characterization. An S-type load cell (rated 0-100kg; Phidgets, catalog ID: CZL301C) is affixed to the testing platform with a mounting bracket. The load cell is connected to a Wheatsone Bridge (Phidgets, catalog ID: DAQ1500_0) for signal amplification and translation. This is connected to a desktop computer using a USB-powered VINT Hub (Phidgets, catalog ID: HUB0000_0).

The load cell data are converted from resistivity measurements into force measurements using a standard curve, which we generated using a set of scale calibration weights (0.1 – 10 kg). Spring gauges (1 – 50 N) were used for measurement validation.

We used a custom Python script to set the parameters of the test (total duration of the test, sampling time interval, target pull force), initialize data collection, view real-time pull force measurements on a graphical interface that illustrates the +/- 10% bounds of the target pull force that we had set as operational restraints, and saves the test run measurements to a data file for future analysis.

Text S12.2. An overview of the laser tachometer configuration within the testing platform.

We used a laser tachometer configuration for measurement of angular velocity during HPC performance characterization. A remote optical LED sensor (catalog ID: 6180-057, Monarch Instruments) is affixed to the testing platform with a burette clamp. A custom 3D-printed protective light shield is screwed onto the sensing tip to protect the sensing mechanic from indoor fluorescent light signal interference. Strips of reflective tape (catalog ID: 6180-070, Monarch Instruments) are applied onto the hand-powered centrifuge disk along the length of each of the six tubes and tube slots. The sensor tip is aimed at the hand-powered centrifuge disk at an angle of 15-30° from perpendicular to avoid light reflection not associated with the reflective tape signal.

The sensor was connected to a DataChart DC1250 (catalog ID: DC1250, Monarch Instruments) for data collection and storage on an external removable card. The Navigator software (catalog ID: 5380-260, Monarch Instruments) is used to export the raw data into a readable form for future analysis.

12.4.3. Supplementary figures

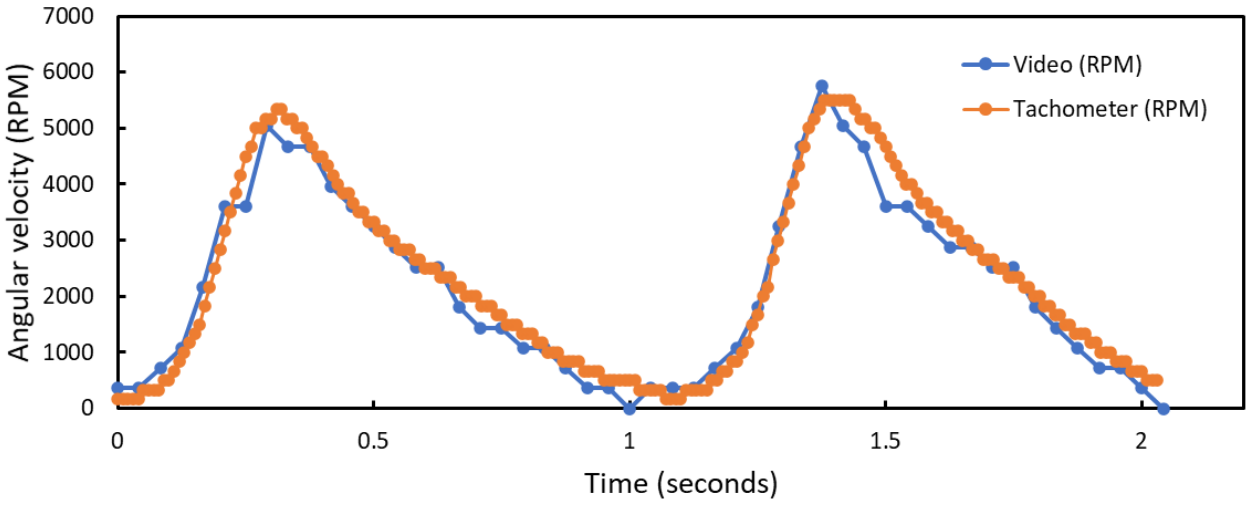

Figure S12.1. An overlay of laser tachometer and 240 frames-per-second cell-phone camera measurements of hand-powered centrifuge angular velocity.

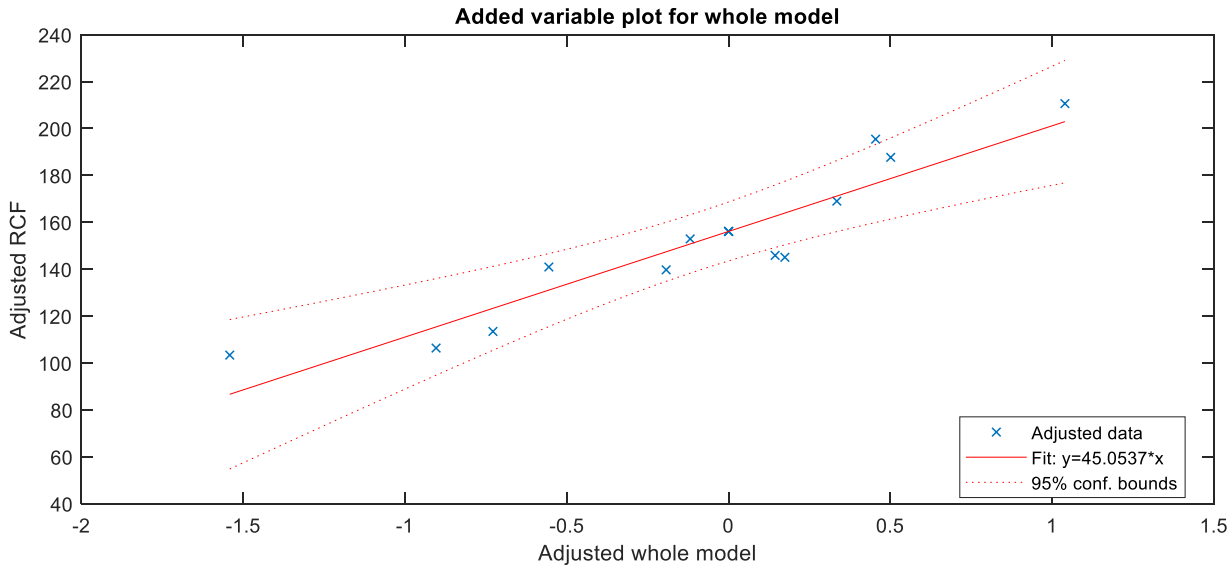

Figure S12.2. An added variable plot for the whole model for response of effective relative centrifugal force (RCF).

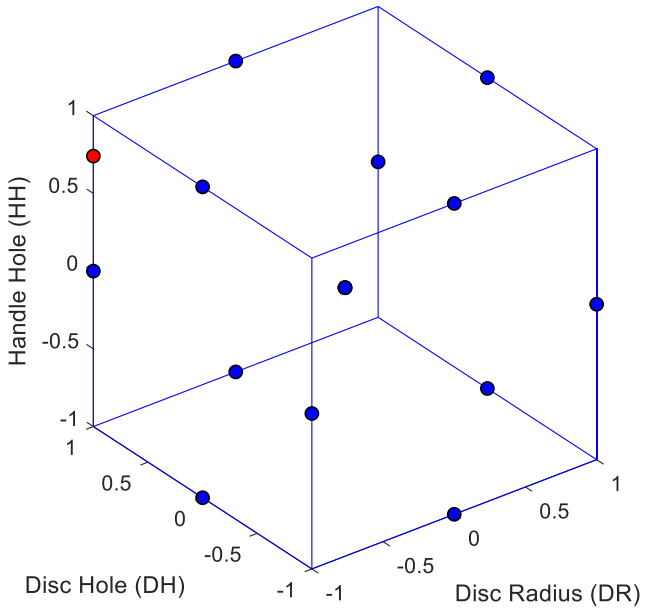

Figure S12.3. An illustration of the three-factor Box-Behnken design with experimental runs represented by blue dots. The red dot represents the predicted optimal conditions for maximizing effective relative centrifugal force.

Chapter 13. Future Works

"Hold fast to dreams
For if dreams die
Life is a broken-winged bird
That cannot fly.
Hold fast to dreams
For when dreams go
Life is a barren field
Frozen with snow."

-Langston Hughes;
Also, what I try to remind myself of when I think about the chances of these future works being completed or otherwise useful to the world.

This concluding chapter is structured as a series of subsections each detailing a research investigation and/or concept that has been explored in considerable depth, worthy of inclusion for the reader, but which has not been completed within the scope of the body of work of this dissertation.

13.1. Monolith purification of virus-based nanomaterials

Summary statement: Monolithic chromatography is an emerging purification technology with advantageous characteristics for purifying larger biomolecules. There is a high value to be had in developing monolithic chromatographic purification methods for plant virus-based immunosorbent nanoparticles (VINs), as an exemplar for plant virus-based nanomaterials, using this technology. Existing purification methodologies face issues of

throughput, low final purity, expensive equipment, and long durations. Rational engineering design approaches can be used to streamline the process development.

Commercial biomanufacturing is being challenged by the emergence of larger biomolecule products. Biomedicals sectors such as gene therapy, vaccine development, and medical imaging have research pipelines rich with biological product platforms based on viral nanoparticles (VNPs) and other larger biomolecules. Traditional downstream unit operations, such as resin-based liquid chromatography columns, are often still used for purification of these large biomolecules. In these situations, process performance is significantly impaired when compared to the intended use case of protein separation. The low diffusivity of larger biomolecules within the resin results in slow chromatographic binding and elution kinetics, which in turn results in reduced binding capacity, resolution of separation, and process throughput.

Monolithic chromatography represents an alternative solution to larger biomolecule purification[507]. Mass transport is dictated by convective flow in monolithic chromatography, whereas transport in resin-based chromatography is largely controlled by diffusion in the resin bead pores where the functional ligands reside. Monolithic chromatography has been successfully employed for purification of larger biomolecules including VNPs based on adeno-associated viruses, influenza viruses, lentiviruses, and bacteriophages[508–512]. However, while there is literature reporting purification of wild-type plant virions using monolithic chromatography[513–515], purification of plant VNPs has not been previously established in literature. Plant VNPs are currently being explored for utility in vaccines, medical imaging contrast agents, drug delivery vehicles, biosensors, and pharmaceutical purification. They continue to play a key role in the

advent of larger biomolecule products – upstream production is simple, inexpensive, and scalable using plant-based cultivation and they are non-pathogenic in humans, an important safety consideration in commercialization. As of now, purification of plant VNPs is primarily reported using resin-based chromatography or molecular biology-based unit operations including sucrose gradient-based ultracentrifugation.

We are proposing an investigation into the use of monolithic chromatography in the purification scheme of tobamovirus-based plant VNPs to improve and de-bottleneck current manufacturing strategies, which are limited in throughput by low flowrates and recovery of resin-based chromatography or the low capacity and long operational time of ultracentrifugation. Figure 13.1.1 illustrates the difference in prospective workflows for purification of plant VNPs via "classic" ultracentrifugation-based and novel monolithic chromatographic-based methodologies. Figure 13.1.2 displays the differences in isoelectric point and molecular weight between the VIN and soluble *Nicotiana tabacum* host cell proteins, representing impurities. These differences should be exploited in the process development of a purification scheme. Furthermore, Figure 13.1.3 shows a generic decision tree for process development of the pre-monolithic chromatography purification steps that guides development based on molecule properties. In combination, a proper pre-treatment and set of monolithic chromatographic steps could be assembled for efficient VIN purification.

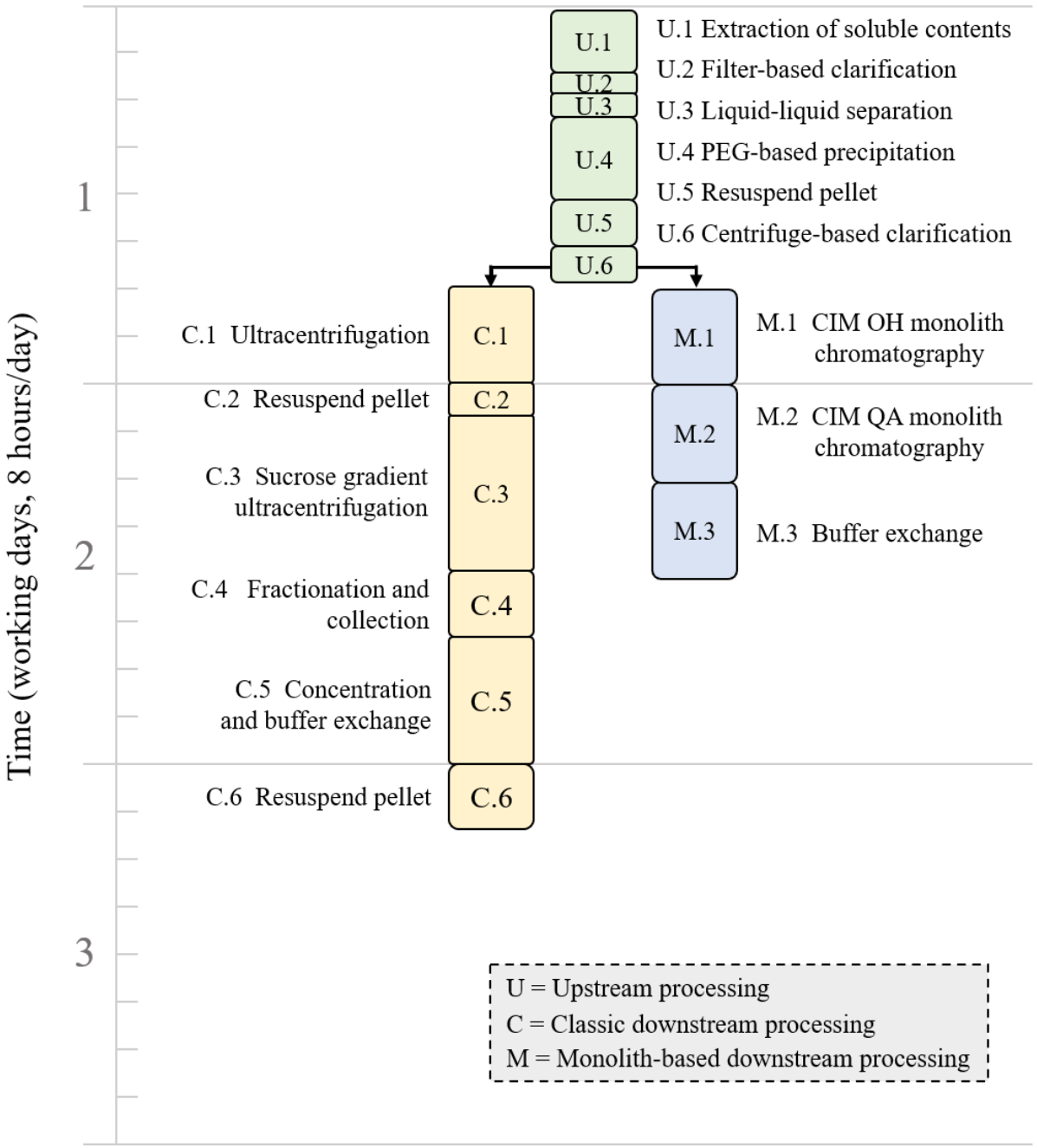

Figure 13.1.1. A comparison of a "classic" molecular biologist approach to purification of plant virus-based nanomaterials to an engineering monolithic chromatography-based purification. The "classic" approach and timeline is based on unpublished data; the monolith approach and timeline are estimated using working process knowledge and prediction of an optimal purification scheme. CIM, convective interaction media; PEG, polyethylene glycol; OH, hydroxy (hydrophobic interaction ligand); QA, quarternary amine (strong anion exchange ligand).

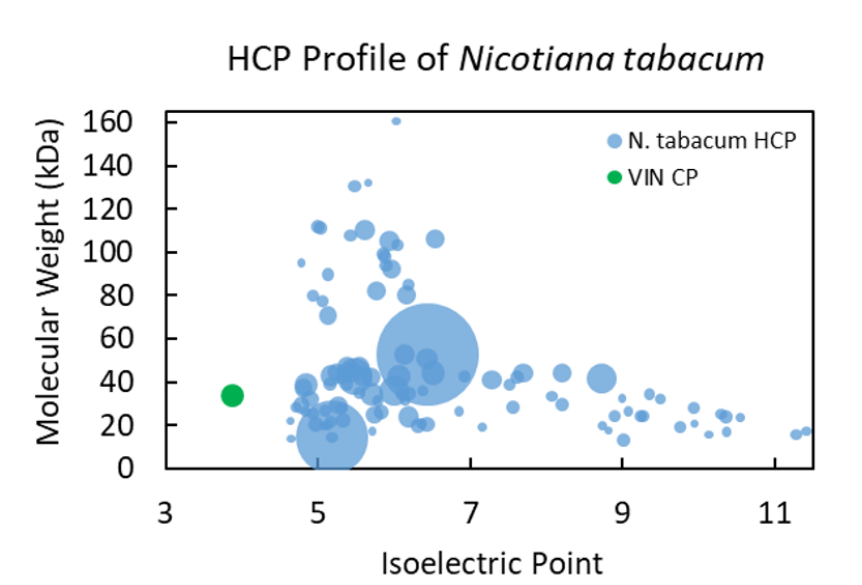

Figure 13.1.2. Biophysical properties (molecular weight, isoelectric point) and relative abundance by bubble size of the host cell protein (HCP) profile of 47-day-old *Nicotiana tabacum* leaf tissue extracted in neutral pH buffer. Data obtained from existing literature[516]. The target molecule, the plant virus-based immunosorbent nanoparticle (VIN) studied in this dissertation, assembled as a fully-formed polymer unit is significantly larger than the host cell impurities. The VIN coat protein (CP), the monomer unit, is shown for purposes of scale.

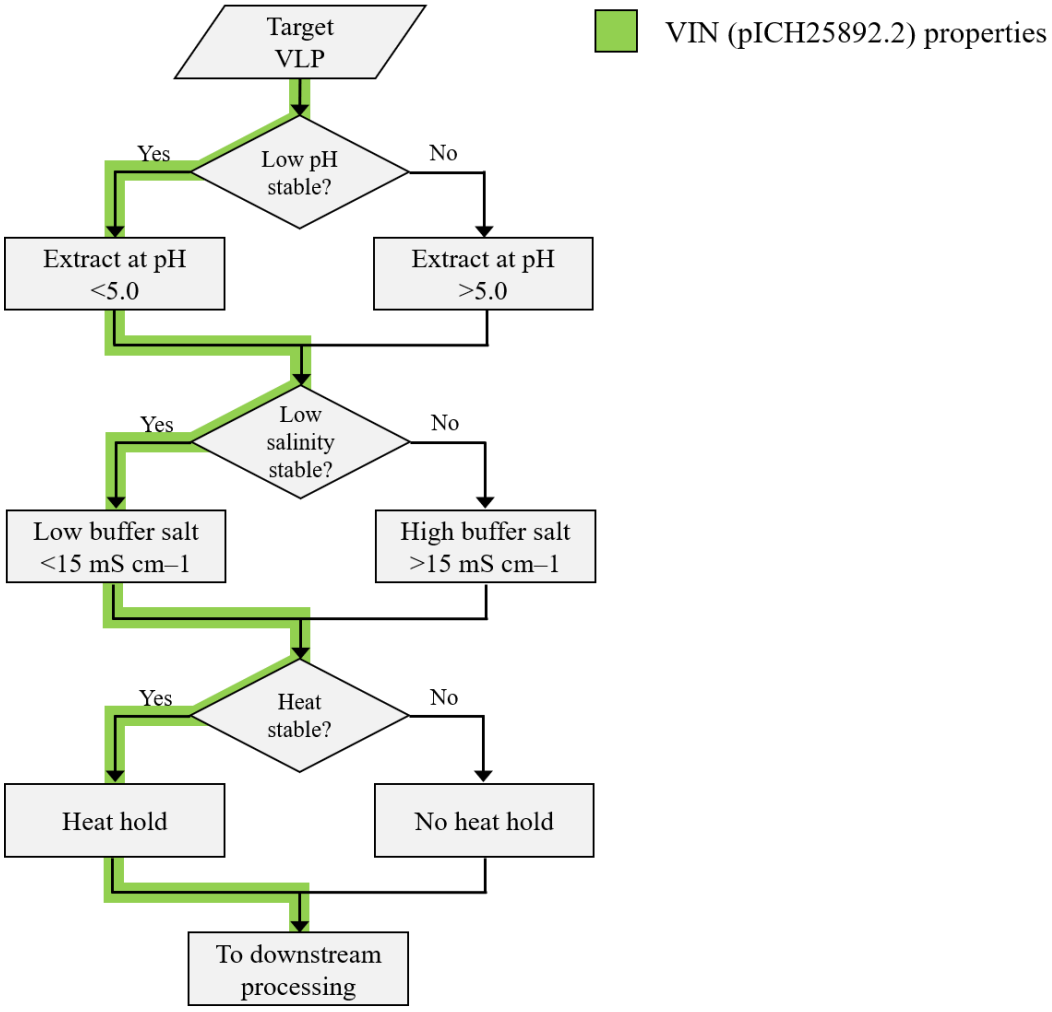

Figure 13.1.3. A proposed decision tree for designing the downstream processing composition for a given plant-made virus-like particle (VLP). Adapted from an existing report in literature[517]. An example walkthrough of the decision tree is highlighted in green using the properties of the plant virus-based immunosorbent nanoparticle (VIN) studied in this dissertation.

13.2. Stability of plant virus-based immunosorbent nanoparticles under selective pressure

Summary statement: Production of the plant virus-based immunosorbent nanoparticle studied in this dissertation, and plant virus-based nanomaterials in general, are produced using agroinfiltration or plasmid infection methods. While these methods result in generally uniform and high accumulation level production, virion infection represents a less resource intensive method of production that is generally not considered because of concerns of inconsistency and genetic instability. We consider the possibility that selective pressures can be built into the plant virus-based nanomaterial processing methodology that could mitigate the traditional concerns of virion infection-based production. Results are detailed for the method development for RNA-sequencing that may be used in the proposed investigation.

13.2.1. Introduction

Plant virus-based immunosorbent nanoparticles (VINs) are a promising platform technology for pharmaceutical purification in limited resource environments such as deep space exploration or rural Earth. Current VIN production is accomplished via *Agrobacterium tumefaciens*-based delivery. This methodology is preferred for laboratory experimentation, as the sequence is highly conserved for repeated production of the same target VIN. However, in practical application this requires -80C freezer stocks of bacteria, bacterial culture (growth media, sterile environment, shakers/fermenters, incubation chamber), and a vacuum chamber.

In review of agrobacterium-based delivery, a DNA sequence encoding the VIN is loaded into the T-DNA region of the agrobacterium's disarmed tumor-inducing plasmid. The agrobacterium is grown to inoculation density in a fermentation culture, spun down, and resuspended in infiltration buffer. Mature plants are submerged in the infiltration solution and a vacuum is pulled. Upon vacuum release, the infiltration solution rushes into the interstitial space of the leaf tissue. Within this space the agrobacterium transfers the T-DNA region into the plant cells where the DNA is used to produce VIN.

An alternative production strategy more conducive to limited resource environments, with less complex material and environment requirements, would be highly beneficial to advancing the technology readiness level (TRL) of VIN technology. Relevant production options are reviewed in Figure 13.2.1.

1.) Agroinfiltration

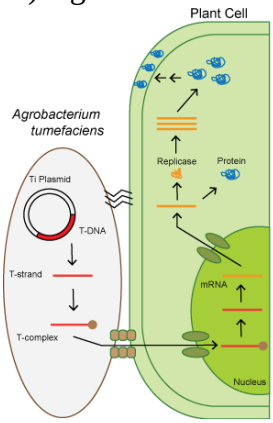

(+) Leaf-to-leaf homogeneity
(+) Short incubation
(–) Bacterial culture
(–) High process complexity

2.) Plasmid Infection

(+) Medium process complexity
(+) Inter-passage genetic stability
(–) Transcript generation
(–) Vital starting stock

3.) Virion Infection

(+) Low process complexity
(+) High throughput
(–) Genetic instability
(–) Leaf-to-leaf variation

Figure 13.2.1. A review of plant virus production strategies relevant to VIN technology.

In nature, *Turnip vein clearing virus* is not compatible with insect vector transmission, as many other plant viruses are. Instead, it is transmitted from plant to plant via mechanical wounding. This mechanical transmission is a very simple method of virus production – there are no complex materials, equipment, or operations required. The current VIN within project scope is genetically modified turnip vein clearing virus (TVCV). It stands to reason that mechanical transmission could be a highly resource-effective method of VIN production. Preliminary results suggest that the TVCV-based VINs do indeed retain capability to systematically infect plant tissue (see dissertation Chapter 9 results).

Additionally, preliminary results also suggest VINs accumulated in systemically infected leaf tissue retain significant functionality (see dissertation Chapter 9 results). Despite these results, there is insufficient evidence to suggest that mechanical transmission is a viable means of consistent VIN production. Investigations and reporting thus far have been very limited in scope. The experiments have confirmed functionality but have not quantitatively measured functionality nor genetic fidelity of the VIN. There have not been longitudinal studies of these VIN characteristics over multiple consecutive passages of mechanical transmission.

It is expected that the VINs will mutate over multiple passages of mechanical transmission; plant viruses will naturally shed excess genetic bulk that reduces fitness over time. Measurements of mutation rate estimate 2.4×10^{-5} mutations/nucleotide/replication for *Tobacco mosaic virus*, a close relative of *Turnip vein clearing virus*[518]. For a given *Nicotiana benthamiana* plant at maturity for infection (up to ~15 g), we can therefore roughly estimate that the virion population will experience 8.3×10^{12} mutations per plant infection cycle. These mutations are not necessarily compounding; ~70% of mutations are deleterious and may result in lower replication fitness for that progeny virion, potentially removing the possibility of future replication. And it is critical to

note that mutation rate is not an invariable property of a virus, but rather it fluctuates with the cellular and environmental conditions. Nonetheless, natural *in planta* function dictates that the immunosorbent Fc-affinity ligand of the VIN can be viewed as a detriment to reproductive fitness as a transcriptional, translational, and steric burden. This suggests that there is a very high chance that the final VIN population of an infected plant will not be representative of, nor closely resemble, the starting inoculation population, and that this final population will likely have lower antibody binding and elution performance. It is important to note that the Fc-affinity ligand of the VIN may be well composed for stability, based on relationships established in patent literature for potato virus X (PVX)-based particles, the GC content, and insertion length (Figure 13.2.2).

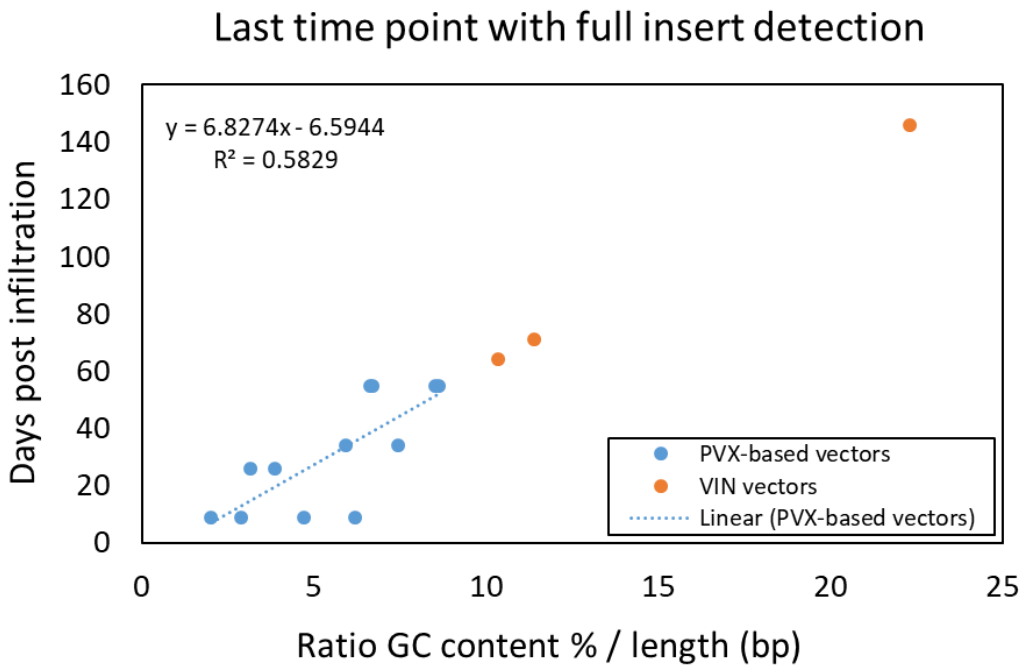

Figure 13.2.2. Recent insights on genomic stability based on patent WO 2019/053262 A1 that has been extrapolated to consider genomic stability of the plant virus-based immunosorbent nanoparticle (VIN) vector investigated in this dissertation. PVX, potato virus X.

However, what if we can align virion fitness and immunosorbent functionality? By imposing non-natural selective pressure, we can re-define which qualities of the virion contribute to fitness. Ideally, a selective pressure to control production of bioprocessing reagents in a limited resource environment would not introduce any additional resource requirements. One method to introduce a selective pressure with no resource penalty is by considering the end utility of the VIN as a bioprocessing reagent itself as a selective pressure. In the originally established VIN bioprocessing scheme, centrifugation is used to precipitate VIN-immunoglobulin G (IgG) complexes based on the high sedimentation velocity of the complex. Previous results have shown that neither the VIN nor IgG will precipitate in free unbound form (see dissertation Chapter 9 results). They also indicate that IgG will not complex to significant degree with VIN, or similar virus-based particles, non-specifically. This VIN-IgG complex-dependence provides a simple manner to isolate functional VIN from non-functional.

There is an existing body of literature to suggest that viruses and virus-based nanomaterials are capable of trading reproductive fitness for other characteristics under selective pressure[432,519]. For example, a study demonstrated trade of reproductive fitness of a RNA virus (bacteriophage) for increased viral enzyme stability in a novel temperature environment that imposed detrimental outcomes on native virion populations[431]. Another study found that insertions for antigen presentation in live viral vaccine candidates were genetically stable over 11 generations of *in vitro* passaging[520].

Natural *in planta* fitness and VIN antibody-binding functionality are in opposition. The purpose of the selective pressures is to re-define fitness as in alignment with antibody-binding functionality, rather than with reproductive capability.

13.2.2. Methodology development

Here we propose a study design to assess mechanical transmission as a VIN production methodology and then detail the progress made in development of the necessary methodologies required for execution of the study. The high-level study objective can be decomposed into three investigations: a) single plant passage VIN characteristics, b) changes in VIN biophysical and genetic characteristics over multiple plant passages, and c) the use of selective pressures to maintain and/or improve antibody-binding functionality across multiple plant passages. Figure 13.2.3 summarizes the experimental design in a visual representation. A comparison of two conditions for virion preparation, with distinct selective pressures, in each of these investigations could allow for parsing of the impact of the selective pressure characteristics. The first condition is to passage crude plant sap from the upper plant leaves collected post-infection; this condition selects for VIN capable of system mobility (assuming that the lower plant leaves are the target of mechanical transmission). System mobility would likely also ensure characteristics such as full virion assembly and low propensity for aggregation. The second condition, building upon the first condition, would then be to passage VIN that had been purified from the crude plant sap from the upper plant leaves and also then collected from the pellet of a centrifugation in a sample containing IgG. The presence of the VIN in the pellet would suggest that the VINs in that population are capable of binding to the IgG. This additionally selects for VIN functionality and could be extended to the analysis of VIN quantity in the pellet to track more fine-tuned changes in functionality. If significant changes in functionality are observed, then more stringent centrifugation conditions (i.e., shorter duration or lower relative centrifugal force centrifugation) could be applied to select for improved functionality.

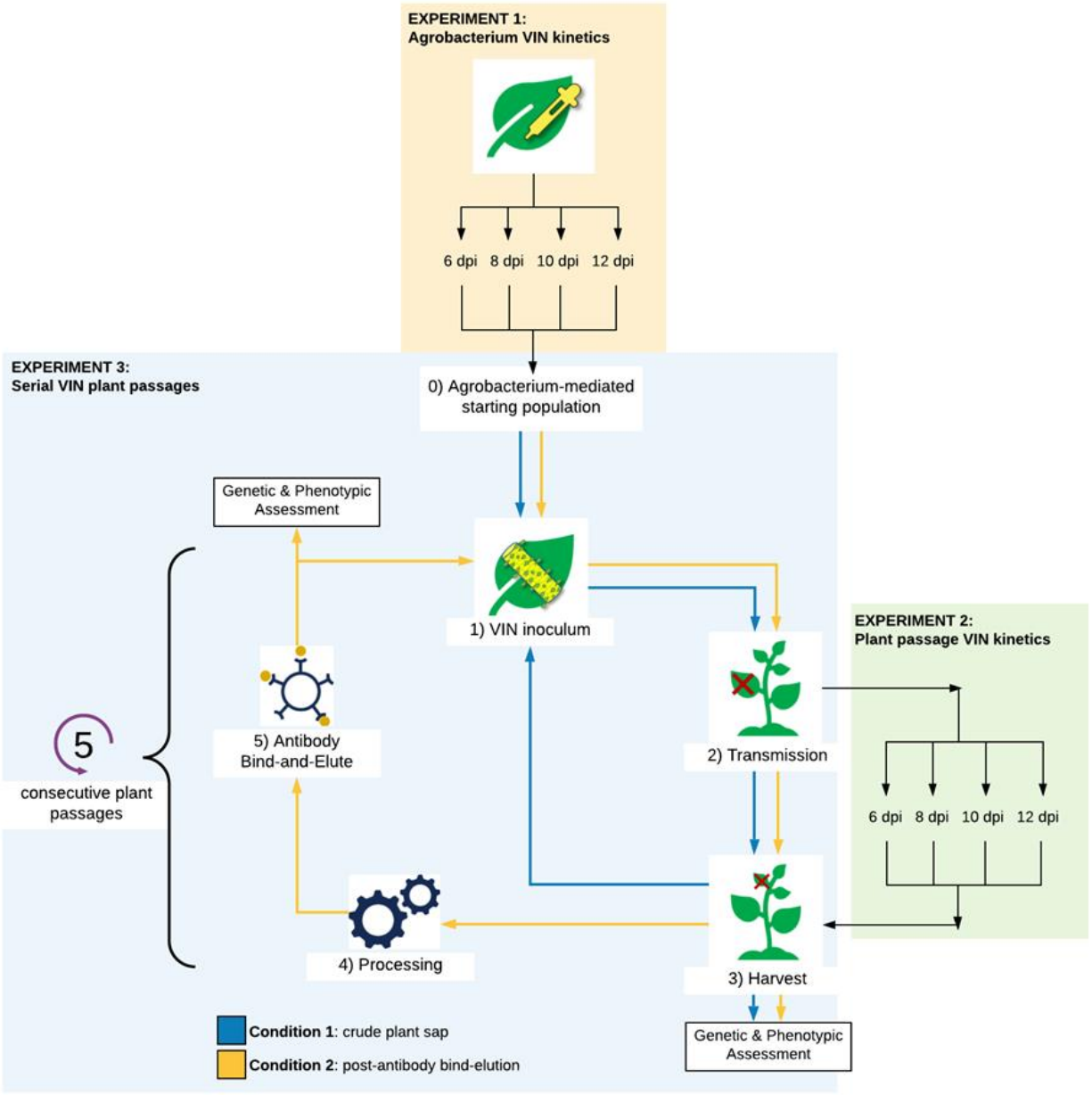

Figure 13.2.3. A visual representation of the proposed experimental design

The methodologies necessary to generate the VIN samples (of infected plant tissue and purified aqueous solution) over five (5) consecutive plant passages have already been detailed earlier in this dissertation. The focus of the preliminary methodology development is on the preparation for RNA-sequencing, which could be used to assess the mutational landscape outcomes of the two

different selective pressures employed through plant passaging. Additionally, reverse transcription quantitative PCR (RT-qPCR) would also be needed for the kinetic studies but was not included in the scope of the preliminary method development.

The preparation for RNA-seq can be broken down as 1) RNA purification, 2) RNA-seq library prep, and 3) RT-qPCR.

RNA purification consists of extraction and characterization. Extraction was performed either with the RNeasy Mini kit (for purified aqueous solution samples) or the RNeasy Plant Mini kit (for infected plant tissue samples). Infected tissue samples were first disrupted by liquid nitrogen-assisted mortar and pestle grinding. RNA characterization consisted of UV-vis measurements of purity (A_{260}/A_{230} of ~2.0 – 2.2; A_{260}/A_{280} of ~2.0; spectra peak should be at 260 nm), Qubit RNA measurement of quantity (with the Qubit High Sensitivity RNA Assay kit), and Agilent 2100 Bioanalyzer measurement of quality (with the RNA Pico 6000 kit). It is important to note that the output of the Agilent 2100 Bioanalyzer measurement of quality (see example output in Figure 13.2.4), the RNA Integrity Number (RIN), is based on the relative abundance of multiple host organism ribosomal RNAs and thus not appropriate for measurement of RNA extracted from the purified aqueous solution condition. Preliminary RNA characterization results generated during method development are summarized in Table 13.2.1. The low A260/A230 ratio observed for sample 2B is suspected to be due to residual guanidine thiocyanate from the RNA lysis buffer, which has been shown by Qiagen not to compromise reliability of downstream applications.

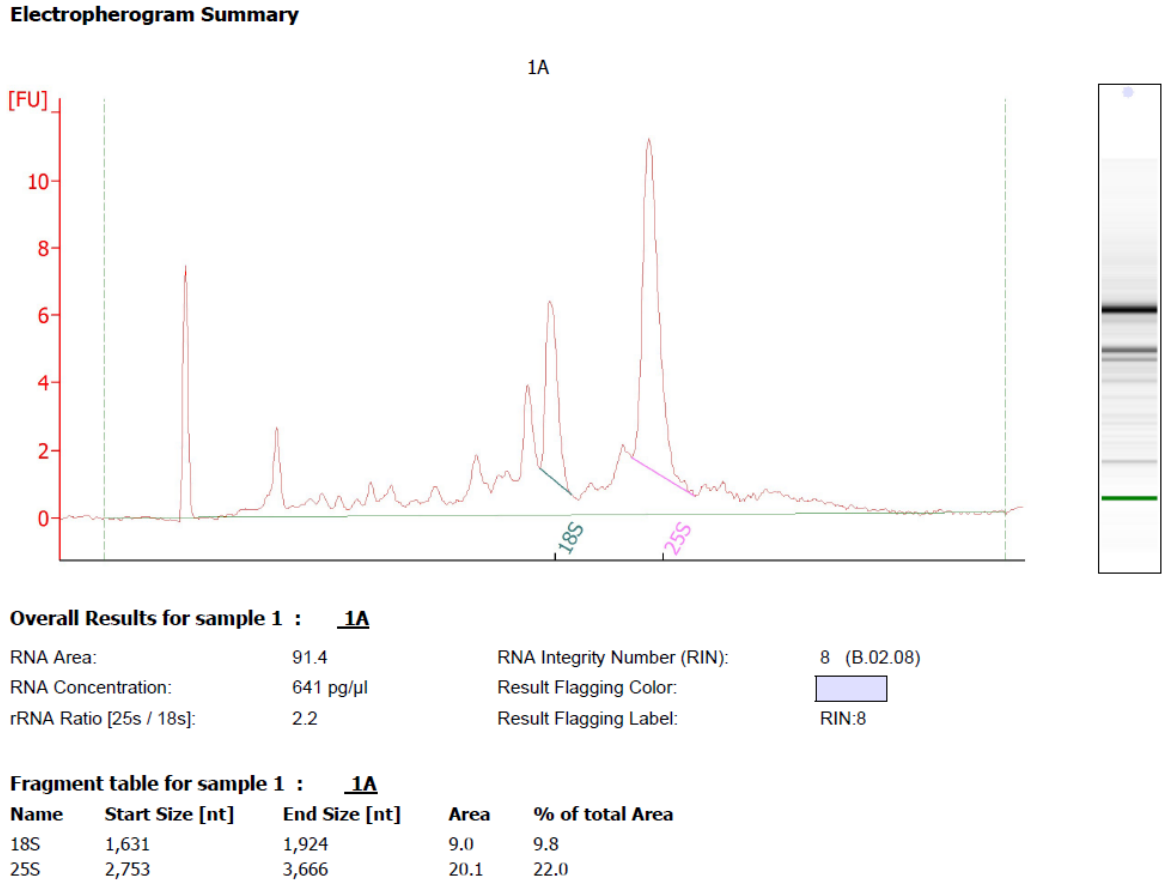

Figure 13.2.4. Sample electropherogram summary generated using the Agilent 2100 Bioanalyzer with the RNA 6000 Pico kit for the measurement of extracted VIN RNA quality.

Table 13.2.1. Tabular summary of the RNA extraction results obtained for method development purposes. The A/B denotion of the sample ID refers to the extraction buffer composition; A refers to the standard kit buffer, while B refers to the standard kit buffer with an addition of 2.5% polyvinylpyrrolidone of molecular weight 40 kD to assist in phenolics removal. Asterisk (*) indicates samples for which the RIN is not a relevant measure of quality. HS, high sensitivity; RIN, RNA integrity number.

Sample ID	Sample Source	Elution Volume		Nanodrop				Qubit HS RNA		Bioanalyzer
		NFW		RNA Conc.		260/280	260/230	RNA Conc.		RIN
1A	~100 µg tissue	60	µL	156.3	ng/µL	2.12	1.84	148.00	ng/µL	8

1B	~100 µg tissue	60	µL	51.9	ng/µL	2.05	0.25	48.60	ng/µL	6.6
2A	100 µL purified VIN	60	µL	23.1	ng/µL	2.01	0.16	18.40	ng/µL	2.6*
2B	100 µL purified VIN	60	µL	8	ng/µL	1.76	0.09	5.32	ng/µL	2.2*

The RNA-sequencing library preparation method developed in this study is an amplicon-based approach, as summarized in Figure 13.2.5. The full VIN genome is 7,308 bp in length, but we assessed in this method that assessment of the flexible linker and Fc-affinity ligand transgene insertion (447 bp length) is sufficient. This method was developed for RNA-sequencing with the iSeq100, which imposes limitations of 2 x 150 bp paired end read length. Thus, two sets of amplicons have been generated in this methodology development to span the total transgene insertion length. Unique molecular identifiers (UMIs) (8-mer length) were incorporated into the amplicon to be able to account for the amplification biases introduced by PCR in post-processing analysis, following precedent of previously reported methodologies[521–523]. Table 13.2.2 provides the primer sequences used in the library preparation. Reverse transcription primers were verified for low binding to sequences within *Nicotiana benthamiana*, *Turnip vein clearing virus*, and all other organism databases to ensure minimal non-specific amplification. The primers were designed for optimal melting temperatures, respective to the reaction enzyme and the other primers in the reaction, as well as for low homodimer, heterodimer, and hairpin energetics (> -9 kcal/mole). Reaction conditions used are based on enzyme vendor instructions and primer melting temperatures. It is important to note that PCR cycles were kept under 30 to avoid significant rate of mutations in the unique molecular identifiers. AMPure XP bead cleanup steps were added after each reaction to remove excess primers and reaction reagents. The reaction performance was

measured after each step using the 4200 TapeStation System with the D1000 ScreenTape assay to verify the nucleic acid length and quantity.

Reverse transcription reactions used a fixed 2 µL volume of template RNA (10 – 300 µg total RNA) and an incubation temperature of 53 °C. The amplification PCR reactions used a fixed 10% volume of template DNA, an annealing temperature of 69.2 °C/68.5 °C for amplicon 1/amplicon 2, an extension time of 30 seconds, and 20 PCR cycles. The index PCR reactions used 1-5 µL template DNA (10-24 ng DNA) for a 50 µL reaction, an annealing temperature of 55 °C, an extension time of 30 seconds, and 8 PCR cycles. The post-index PCR reaction bead clean ups were double-sided to remove larger and smaller products.

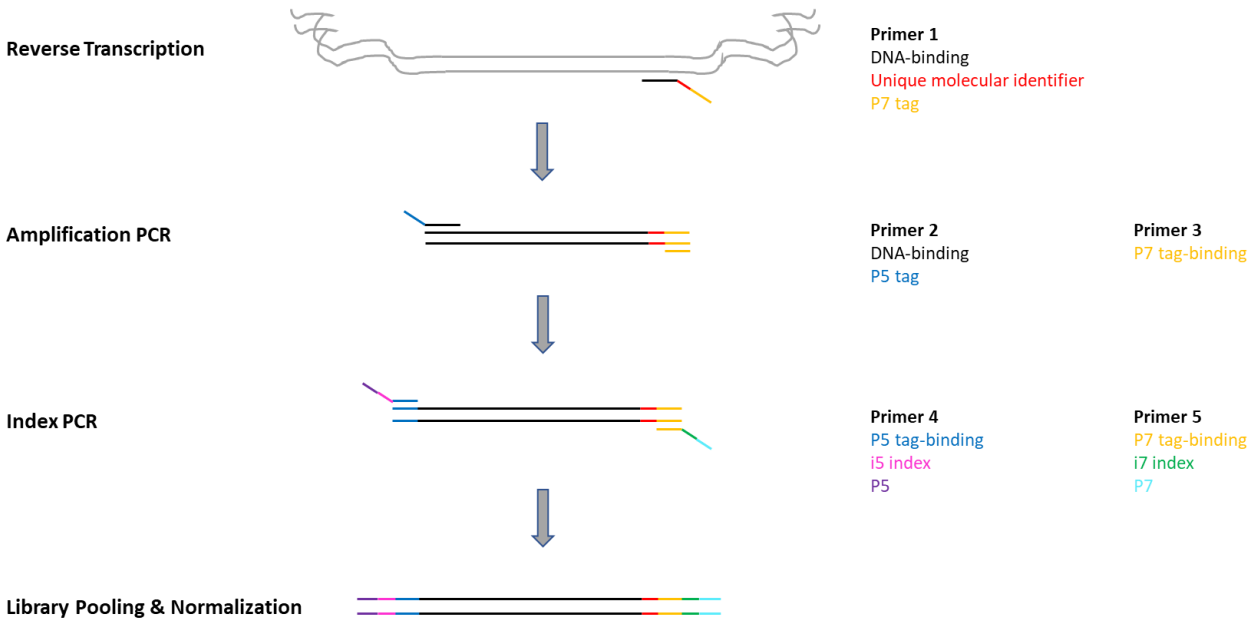

Figure 13.2.5. Visual schematic of the amplicon-based library preparation protocol used in this method development study.

Table 13.2.2. Reaction enzymes and primer sequences used in method developed for amplicon-based library preparation.

Reaction	Enzyme	Primer ID	Description	Sequence (5' -> 3')
Reverse transcription	SuperScript IV RT	Primer 1 (Amplicon 1)	DNA binding + UMI + P7 tag (reverse adapter)	GTCTCGTGGGCTCGG AGATGTGTATAAGA GACAGNNNNNNNG CACCACGCTCTAGTA AGCTTTCA
		Primer 1 (Amplicon 1)	DNA binding + UMI + P7 tag (reverse adapter)	GTCTCGTGGGCTCGG AGATGTGTATAAGA GACAGNNNNNNNT GAAGTTATTCTGCTG TGCATCAGC
Amplification PCR	Platinum SuperFi PCR DNA Polymerase	Primer 2 (Amplicon 1)	DNA binding + P5 tag (forward adapter)	TCGTCGGCAGCGTCA GATGTGTATAAGAG ACAGGAAGCTCAGA AGTTGAATGATAGTC AGGCA
		Primer 2 (Amplicon 2)	DNA binding + P5 tag (forward adapter)	TCGTCGGCAGCGTCA GATGTGTATAAGAG ACAGTGGACTACTGC GCCTGCTACA
		Primer 3 (Amplicon 1 + 2)	Partial P7 tag (3' trim; reverse adapter)	GTCTCGTGGGCTCGG AGATGTGTATA
Index PCR	Platinum SuperFi PCR DNA Polymerase	Primer 4 (Amplicon 1 + 2)	P5 + i5 index + P5 tag-binding	AATGATACGGCGAC CACCGAGATCTACAC [i5*] TCGTCGGCAGCGTC
		Primer 5 (Amplicon 1 + 2)	P7 + i7 index + P7 tag-binding	CAAGCAGAAGACGG CATACGAGAT [i7**] GTCTCGTGGGCTCGG

*i5 indices used: S501, S502, S503, S504
**i7 indices used: N701, N702, N703

The electrophoresis assay results confirmed that the generated amplicons were approximately the expected sizes (data not shown). Amplicon DNA was amplified using CLoneJET PCR cloning kit, extracted using the QIAGEN Miniprep kit, and sent out for Sanger sequencing, which confirmed that we generated the desired amplicon sequences. Given this positive confirmation, the

methodology for library preparation detailed here does appear to be adequate for the desired RNA-sequencing workflow. Future works could apply this library preparation method to VIN-containing samples to investigate questions regarding population-level genetics via RNA-sequencing.

13.3. Arbitrary protein capture using plant virus-based immunosorbent nanoparticles

Summary statement: The immunosorbent functionality of plant virus-based immunosorbent nanoparticles can be applied beyond antibody capture. For example, the plant virus-based chassis, with its large size, high aspect ratio, and high ligand density, has potential to improve existing antibody-related applications such as the widely used enzyme-linked immunosorbent assay. To this end, we have introduced the concept of arbitrary protein capture with plant virus-based immunosorbent nanoparticles through the use of antibody intermediaries. We present the successes and remaining challenges identified during a preliminary methodology development.

13.3.1. Introduction

The functionality of plant virus-based immunosorbent nanoparticles (VINs) have already been employed for antibody-related purification and diagnostics in reports from literature. The unique properties of this virus-based chassis may also serve as beneficial for developing adjacent need cases, such as for improving sensitivity of immunosorbent assays (e.g., the commonly used enzyme-linked immunosorbent assay) or for purifying an antigen, by exploiting the capability of antibody generation to target a vast array of protein epitopes, which we liberally describe as encompassing any arbitrary protein. An illustration of the general concept of VIN-based arbitrary protein capture is displayed in Figure 13.3.1.

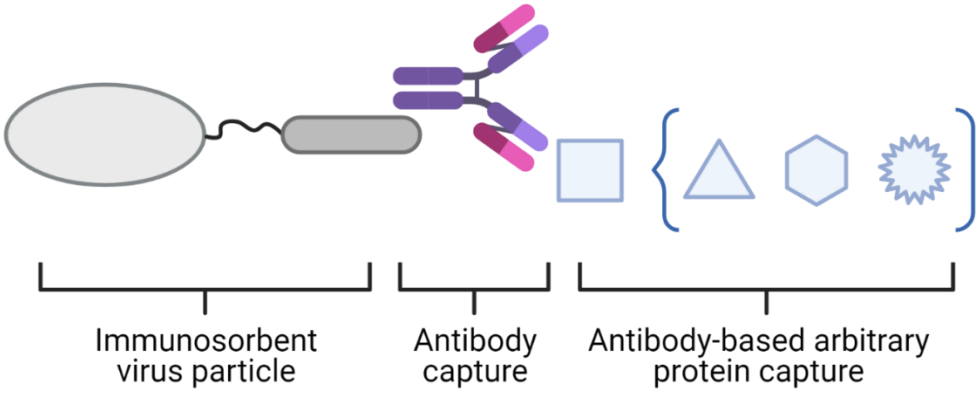

Figure 13.3.1. A conceptual illustration of a method to extend general immunosorbence for the capture of arbitrary proteins.

The method for arbitrary protein capture preliminarily presented here can be deconstructed into a series of mechanistic steps: 1) VIN-antibody-antigen complex formation, 2) isolation of the bound complex from the bulk liquid stream, 3) dissociation of the antigen from the bound complex, and 4) separation and recovery of the dissociated antigen.

13.3.2. Methodology development

Preliminary methods were developed and experimentation was performed for each of the four mechanistic steps of arbitrary protein capture and elution. We tested with two different "arbitrary proteins" – granulocyte colony stimulating factor (G-CSF) and bovine serum albumen (BSA) – and with several different antibodies, as detailed later in the method.

13.3.2.1. Mechanisms 1 & 2: VIN-antibody-antigen complex formation & isolation of the bound complex from the bulk liquid stream

We opted to jointly test the VIN-antibody-antigen complex formation mechanism and isolation of the bound complex form the bulk liquid mechanism using a sedimentation-based method derived from previously established protocols for VIN capture and elution of antibodies. Using a 1 mL working volume, we mixed a solution of 100 µL VIN (~0.3 mg/mL), 8 – 70 µL antibody (2 mg/mL), 5 – 10 µL antigen (2 mg/mL), and 830 – 892 µL with phosphate buffered saline buffer (PBS) at pH 7.0 at 4 °C for 60 minutes nutating. To evaluate potential impact of order-of-addition on complex formation, we established conditions in which one of the complex components was added after the first two components at the halfway point through the incubation period. The incubated solution was then centrifuged at 20,000 x g and 4 °C for 10 minutes. The resultant supernatant is transferred to a new tube and the pellet is resuspended in 1 mL PBS pH 7.0.

Results of the screening for impact of order-of-addition on complex formation and sedimentation with rabbit anti-BSA IgG and BSA are shown in Figure 13.3.2. The qualitative SDS-PAGE results suggest a minor reduction in complex formation and isolation when the VIN is added last at the halfway point of incubation (also supported by additional data not shown). Additional experiments should be run to assess whether this can be attributed to VIN-IgG binding inhibition in the IgG-antigen complex formation, lower incubation time for the VIN-IgG binding to occur, or to a difference in complex sedimentation characteristics.

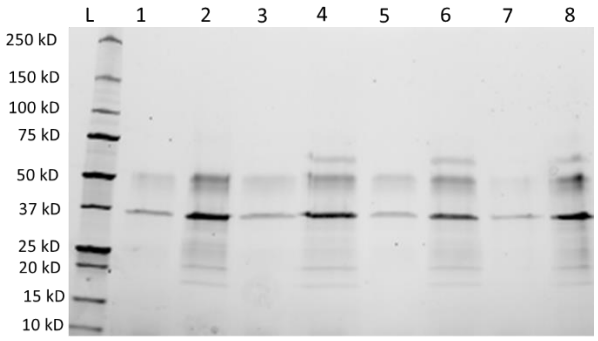

Figure 13.3.2. SDS-PAGE results of preliminary complex formation and isolation experiments using VIN (~33.5 kD in reducing conditions), rabbit anti-BSA IgG (~150 kD; 50 kD and 25 kD in reducing conditions), and BSA (~66 kD) over a range of rabbit anti-BSA IgG concentrations. Lane definitions: L – protein ladder; 1 – VIN + antibody, no antigen (pellet); 2 – VIN + antibody, no antigen (supernatant); 3 – VIN + antibody + antigen (pellet); 4 – VIN + antibody + antigen (supernatant); 5 – VIN + antibody, antigen added at midpoint (pellet); 6 – VIN + antibody, antigen added at midpoint (supernatant); 7 – antibody + antigen, VIN added at midpoint (pellet); 8 – 4x antibody + antigen, VIN added at midpoint (supernatant).

The extent of sedimentation observed in Figure 13.3.2 is significantly lower than that reported for VIN-hIgG experimentation. We hypothesize that the VIN-IgG binding affinity varies with the IgG species and subtype, as is standardly recognized for the Protein A affinity mechanism. Results of screening VIN-IgG sedimentation with varying concentrations of rabbit anti-BSA are shown in Figure 13.3.3. As expected, an increase in relative abundance of IgG to VIN increases the extent of VIN-IgG sedimentation. However, in all conditions tested the extent of IgG recovery remained below 50%.

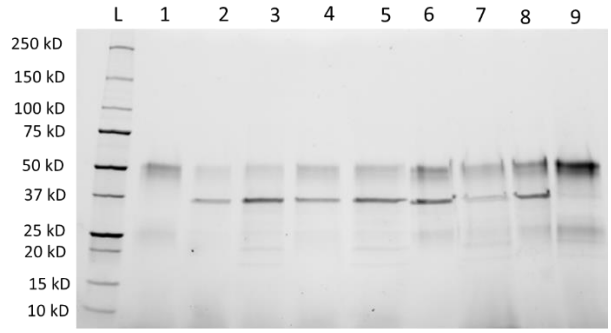

Figure 13.3.3. SDS-PAGE results of preliminary complex formation and isolation experiments using VIN (~33.5 kD in reducing conditions) and rabbit anti-BSA IgG (~150 kD; 50 kD and 25 kD in reducing conditions) over a range of rabbit anti-BSA IgG concentrations. Lane definitions: L – protein ladder; 1 – 1x antibody concentration without VIN (control); 2 – 0.5x antibody concentration (pellet); 3 – 0.5x antibody concentration (supernatant); 4 – 1x antibody concentration (pellet); 5 – 1x antibody concentration (supernatant); 6 – 2x antibody concentration (pellet); 7 – 2x antibody concentration (supernatant); 8 – 4x antibody concentration (pellet); 9 – 4x antibody concentration (supernatant).

In Figure 13.3.4, we show that VIN-IgG-G-CSF complex formation is also observed. Again, the antibody used (rat anti-G-CSF IgG2) appeared to have characteristically poor binding affinity with VIN (~33.5 kD in reducing conditions), as noted by the low extent of IgG sedimentation and recovery. In Figure 13.3.5, we show that we can use sheep anti-G-CSF IgG to achieve significantly higher rates of IgG sedimentation, and thus lower IgG loss. It is worth noting that the results in Figure 13.3.5 include preliminary proof-of-concept results for all four mechanisms.

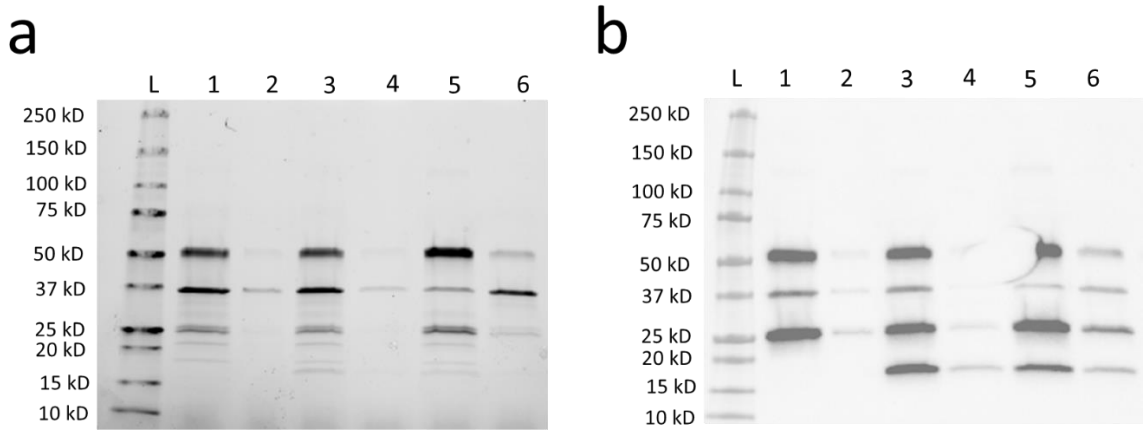

Figure 13.3.4. (a) SDS-PAGE and (b) western blot results of preliminary complex formation and isolation experiments using VIN (~33.5 kD in reducing conditions), rat anti-G-CSF IgG2 (~150 kD; 50 kD and 25 kD in reducing conditions), and G-CSF (~18.8 kD). Goat anti-rabbit IgG HRP is used for the western blot. Lane definitions: L – protein ladder; 1 – VIN + antibody, no antigen (supernatant); 2 – VIN + antibody, no antigen (pellet); 3 – VIN + antibody + antigen (supernatant); 4 – VIN + antibody + antigen (pellet) ; 5 – VIN + 2x antibody + antigen (supernatant); 6 – VIN + 2x antibody + antigen (pellet).

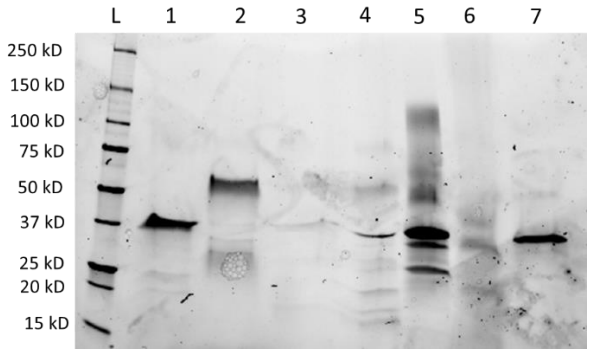

Figure 13.3.5. SDS-PAGE results of preliminary complex formation and isolation experiments using VIN (~33.5 kD in reducing conditions), sheep anti-G-CSF IgG (~150 kD; 50 kD and 25 kD in reducing conditions), and G-CSF (~18.8 kD). Here we used the capture and elution protocol for VIN sedimentation processing, in which the pelleted complex is resuspended in low pH and the VIN is then isolated using PEG precipitation. Lane definitions: L – protein ladder; 1 – initial VIN; 2 – initial IgG; 3 – initial G-CSF; 4 – supernatant loss; 5 – resuspended pellet; 6 – recovered antibody and antigen; 7 – recovered VIN.

Together, these results indicate that VIN-antibody-antigen complexes can indeed be formed and readily sedimented for two separate arbitrary proteins (BSA, G-CSF) and using three different antibody species (with varying degrees of success). Maturation of the arbitrary protein capture methodology will benefit from a more robust understanding of broad VIN-IgG interactions across different IgG variants. It may also be prudent to select a different isolation mechanism (such as the magnetic separations, silica sol-gel, and tangential flow filtration methods discussed in earlier chapters), depending on the end application of the method.

13.3.2.2. Mechanism 3: Dissociation of the antigen from the bound complex

To test mechanism 3, dissociation of the antigen from the bound complex, we designed a set of experiments using spin filters in which the selected filter pore size (300 kD) would permit unbound antibody and antigen components through the filter and into the flowthrough sample. We tested conditions of low pH, high salt, and low pH with high salt for dissociation, using pH 7 low salt as

a control condition. We selected these dissociation conditions based on a previous report of antibody-antigen dissociation in literature for Alzheimer disease diagnosis[524].

Results of the dissociation experiment are shown in Figure 13.3.6. The neutral pH condition provides additional confirmation that we are indeed observing VIN-antibody-antigen complex formation. However, the conditions intended to test dissociation mechanisms were generally inconclusive, as best represented in Figure 13.3.6. Use of higher salt concentrations (0.5 – 1 M) resulted in significant aggregation that blocked filter pores and retained the majority of protein in the retentate (data not shown). Simple considerations of mass balance highlight significant issues that were observed in recovering G-CSF from the spin filter, in either the retentate or flow through. We tested two different filter membranes (PES, regenerated cellulose) and observed similar issues in both of these systems. We have not identified the source of the G-CSF loss, although we hypothesize this to be due to non-specific filter or tube interactions.

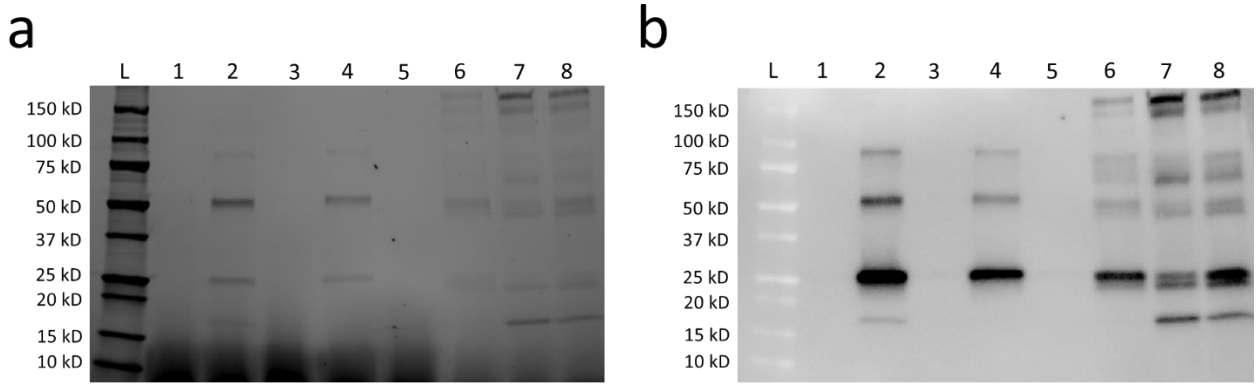

Figure 13.3.6. (a) SDS-PAGE and (b) western blot results of preliminary dissociation experiments using rat anti-G-CSF IgG2 (~150 kD; 50 kD and 25 kD in reducing conditions) and G-CSF (~18.8 kD) centrifuged in a 300 kD spin filter. Goat anti-rabbit IgG HRP is used for the western blot. Lane definitions: L – protein ladder, 1 – pH 7.0, 0.2 M salt (flow through), 2 – pH 7.0, 0.2 M salt (retentate), 3 – pH 2.5, 0.2 M salt (flow through), 4 – pH 2.5, 0.2 M salt (retentate), 5 – pH 2.5, 0.1 M salt (flow through), 6 – pH 2.5, 0.1 M salt (retentate), 7 – pH 7.0 control (not centrifuged), 8 – pH 2.5 control (not centrifuged).

The experimental results of Figure 13.3.5, while not an isolated test of the dissociation mechanism, do indicate that low pH is an adequate mechanism for dissociating at minimum the VIN from the IgG and G-CSF. Future work needs to be performed to confirm if this also adequately dissociates the IgG from the G-CSF. Additionally, it may be worthwhile to explore dissociation mechanisms that maintain the VIN-IgG binding while dissociating the antigen from the antibody. This may result in a simpler and more favorable operation for when the objective is high extent of recovery of the antigen/arbitrary protein for a downstream application.

13.3.2.3. Mechanism 4: Separation and recovery of the dissociated antigen

We employed a polyethylene glycol (PEG) precipitation methodology for separation and recovery of the dissociated antigen. PEG precipitation is a widely established methodology for separating biomolecules largely based on molecular weight. Here we have preliminarily screened a range of PEG concentrations to identify conditions that would precipitate the antibody but not the antigen. Here we use human IgG (hIgG) and BSA as a mock dissociated antibody-antigen system, given the low binding affinity between hIgG and BSA. Additionally, we selected BSA as the mock antigen for this experimentation on the rationale that BSA (66 kD) represents a soft upper bound of the antigen size below which we expect the majority of antigen sizes to lay.

We first generate an initial 1 mL working volume containing 17 µL hIgG (2 mg/mL) and 10 µL BSA (2 mg/mL) in PBS buffer pH 7.0. We use stocks of 50% PEG 6,000 and 25% NaCl to bring the solution to varying final concentrations of PEG (10 – 30%) and 1% NaCl. The PEG-containing solution is then nutated at 4 °C for 30 – 60 minutes. The rested solution is then centrifuged at 16,000 x g and 4 °C for 15 minutes after which the supernatant is removed and the pellet is resuspended in 1 mL of PBS buffer pH 7.0.

Results for the final PEG screen experiment (11 – 16%) are shown in Figure 13.3.7. We identified that 14% PEG is the optimal concentration to precipitate hIgG but not BSA. Given that the VIN precipitates at as low as 4% PEG concentration, this condition can be used to separate VIN and antibody into the same stream. Alternatively, a primary 4% PEG precipitation step could be used to first isolate the VIN and a subsequent 14% PEG precipitation step could be used to isolate the antibody and antigen, if one is interested in isolating all three complex constituents from each other.

The results we obtained suggest that we could also use lower concentrations of PEG, such as 11% PEG, to selectively precipitate the antibody. However, we qualitatively observe that the lower PEG concentrations result in lower IgG recoveries. Consequently, this would also result in an incomplete separation of antibody and antigen. Future work should be performed to exchange the isolated antigen into a PEG-free solution and to evaluate for residual antibody.

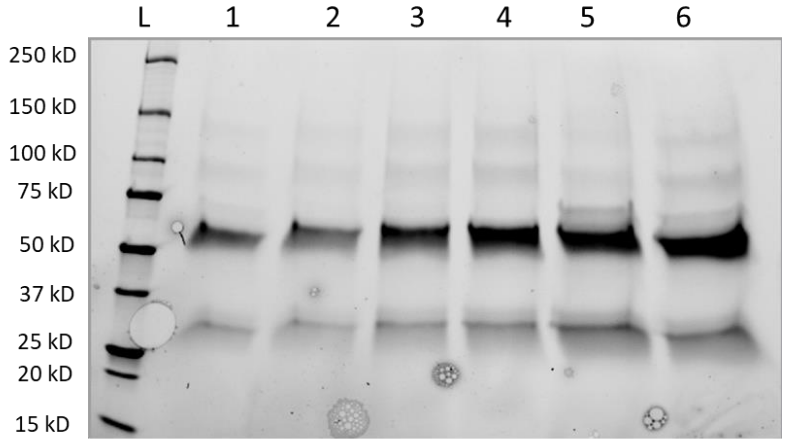

Figure 13.3.7. SDS-PAGE results of preliminary antigen separation and recovery experiments. A mock dissociated antibody (hIgG) (~150 kD; 50 kD and 25 kD in reducing conditions) and antigen (BSA) (~66 kD) system is used to screen PEG concentrations that can be used to selectively precipitate the antibody. Each lane represents the resuspended pellet post-PEG precipitation. Lane definitions: L – protein ladder; 1 – 11% PEG; 2 – 12% PEG; 3 – 13% PEG; 4 – 14% PEG; 5 – 15% PEG; 6 – 16% PEG.

13.4. Deconstructing plant virus-based immunosorbent nanoparticles into major structural components

Summary statement: The primary research focus of plant virus-based immunosorbent nanomaterials presented in this dissertation has been on bioprocessing. Here we discuss the three major structural components of the VIN and detail considerations for each of these three components that may inform future VIN construct design.

The majority of the plant virus-based immuosorbent nanoparticle (VIN) investigations in this dissertation has focused on development of novel and improved bioprocessing with VINs. A single VIN design was selected/constructed based on a previous literature reporting highly promising characteristics. This focus was intentionally defined in interest of performing research to help drive technological maturation for VINs and virus-based nanomaterials, in general.

In selection/construction of this single VIN design, significant efforts were applied in understanding the major structural components of VINs (and ligand display technology in general), how the characteristics of these components influence the resultant VIN, and in turn how this influences the bioprocessing parameters. We identified and evaluated three major structural components of VINs (as illustrated in Figure 13.4.1): 1) the viral chassis consisting of a coat protein monomer(s) that self-assembles into the full virion particle, 2) the linker domain connecting the virion particle coat protein to the functional protein display, and 3) the immunosorbent Fc-affinity ligand that directly binds with Fc-protein targets including antibodies and Fc-fusion proteins.

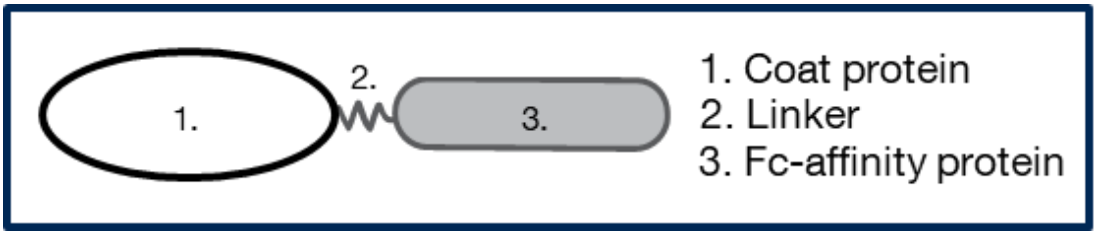

Figure 13.4.1. An illustration of the three major structural constituents of a plant virus-based immunosorbent nanoparticle.

13.4.1. Component 1: Viral chassis

Virus-based nanomaterials use viral chassis for a variety of purposes including mineralization, cargo delivery, and ligand display. Accordingly, a variety of viruses serve as ideal chassis. Examining plant viruses specifically, for inherent advantages of safety and production mentioned earlier, there are three primary archetypes of virion morphology: icosahedral, rigid helical, and flexuous helical morphologies. Beyond general morphology, there are multiple key features that should be considered, as we have highlighted in Table 13.4.1.

Starting from natural plant virions, these key features are often entangled. For example, icosahedral virions tend to be significantly smaller (e.g., cowpeas mosaic virus, ~30 nm diameter) than flexuous or rigid helical viruses (e.g., potato virus X, ~515 x 13 nm). Both tobamoviruses, such as tobacco mosaic virus and turnip vein clearing virus, and potexviruses, such as potato virus X, have been shown to be effective chassis for virus-based nanomaterials.

Table 13.4.1. A summary of select key virion chassis features for consideration in development of ligand display virus-based nanomaterials.

Viral chassis feature	Comments regarding ligand display technology
Virion morphology/shape	Higher aspect ratios will yield higher surface area to volume ratio, which can be beneficial for specific binding capacities of ligand display applications.
Virion size	Critical determinant of sedimentation velocity, conditions required for entrapment, and extent of solvent exposure on immobilized surfaces/matrices.
Number of coat proteins per virion	Defines the maximal number of ligand display sites per virus-based nanomaterial.
Number of coat protein subunits	An important consideration for ligand display spacing and multi-ligand presentation approaches.
Coat protein size/shape	Impacts ligand display spacing, sites on the coat protein for ligand fusion/conjugation, and propensity for domain-domain interactions.

13.4.2. Component 2: Linker domain

The linker domain is a critical structural component that, when discovered, drastically increased the possibilities for genetically fused ligand display technologies. Linkers can be used to improve protein folding, stability, biological activity, and accumulation levels. Prior to linker utilization, coat protein fusions for ligand display were restricted to 20 amino acids in length or less for tomaboviruses without interfering with full virion assembly[525]. Consequently, the largest coat protein fusion reported for tobamovirus ligand display, which happens to be the rod-like plant virus-based nanomaterial used in the studies reported earlier in this dissertation, has been increased to 133 amino acids in length – an astonishing > 6x increase in length compared to the no-linker approach.

Table 13.4.2 provides a summary of linker types and general associated characteristics.

Table 13.4.2. A summary of various linker types and associated general characteristics, as briefly summarized from several in-depth studies and reviews on the topic[526–528].

Linker type	Characteristics	Example (Amino Acid Sequence)
No linker	Restricted fusion size for ligand display Poor assembly	N/A
Helical	Minimal domain-domain interactions Increased thermal stability	$(EAAAK)_n$, n = 1 – 3
Flexible	Possible domain-domain interactions Dynamic binding sterics	$(GGGGS)_n$, n = 1 – 3
Long	Increased solvent exposure	$A(EAAAK)_4ALEA(EAAAK)_4A$

13.4.3. Component 3: Fc-affinity ligand

The Fc-affinity ligand is the primary determinant of the immunosorbent capability of the VIN. The high commercial value of Protein A-based affinity capture of antibodies and Fc-fusion proteins affords the design luxury of many publicly available variants and alternatives. Table 13.4.3 provides a list of critical parameters to consider throughout the selection of future Fc-affinity ligands for novel VIN constructs. Table 13.4.4 includes a list of Fc-affinity peptides/proteins that have been viewed as high potential in future Fc-affinity ligand selection.

Table 13.4.3. A list of critical Fc-affinity protein parameters highlighting associated process parameters, current output (based on construct design, pICH25892), desired output, and priority rankings.

Priority	VIN Parameter	Process Parameter	Current Output	Desired Output
High	Selectivity	Purity	≥ 90%	≥ 90%
High	Elution conditions	Raw materials	pH 2.5	Mildly acidic pH
Medium	Binding constant	Recovery	Undefined	1 μM < K_d < 1 nM

Medium	Charge density	Expression	pI 3.68	Undefined
Low	Cycle stability	Consumables	≥ 1 Cycle	> 1 Cycle
Low	Size	Expression	133-aa; 14.5kD	Small
Low	Storage stability	Shelf life	2 weeks at 4 °C (>8 weeks with protease inhibitors)	Long duration

Table 13.4.4. A list of published Fc-affinity ligands that were selected based on initial promise as candidates for future design of plant virus-based immunosorbent nanoparticles. DBC, dynamic binding capacity. PA, Protein A.

Ligand	Size	Binding, K_a	Elution pH	Comments
Protein A (PA)[529]	42 kDa	1.4×10^8 M^{-1}	3.5	Includes all five domains of Protein A
PA, Z domain[530]	6.7 kDa	5.0×10^8 M^{-1}	3.6	Synthetic derived from domain B
PA, B domain[531]	7.1 kDa	2.5×10^7 M^{-1}	3.5	Modified domain B
NKFRGKYK[532]	0.9 kDa	8.9×10^6 M^{-1}	4.0	83% purity from cell medium; DBC 5 mg/ml
Fc-III-4C[533]	1.7 kDa	4.0×10^7 M^{-1}	3.5	Multiple tryptophan; Double cyclic structure
FYWHCLDE[534]	0.9 kDa	6.7×10^5 M^{-1}	6.0	DBC 104 mg/mL; Uncertain selectivity
PA, affibody[535]	6.3 kDa	$2 – 6 \times 10^6$ M^{-1}	Not available	*In vitro* evolved anti-Protein Z affibody

13.5. A strategy for the early evolution of plant cultivation on Mars

Summary statement: Steady state approximations of plant cultivation for long-duration space missions, including Mars settlements, have been reported and refined for several decades to fit within the static mission economic metrics employed for mission architecture optimization, such as equivalent system mass. To date, there are no detailed reports available for evaluation of non-steady state dynamics of plant cultivation. Here we preliminarily propose a novel route of progression for plant cultivation as a thought experiment to begin to parse out interesting questions needed to evaluate the plant cultivation, and mission, non-steady state dynamics.

Current NASA models such as the Advanced Life Support Sizing Analysis Tool (ALSSAT) provide significant insights into optimization of mission architecture. These models provide invaluable steady state approximations for mission demands. However, the non-steady state dynamics for an *in situ* resource utilization (ISRU)-based Mars settlement mission architecture are non-negligible with potential cascading mission ramifications.

For this reason, we propose to consider an approach to non-steady state plant cultivation that accounts for settlement development dynamics and utilizes the strengths of hydroponic and regolith-derived cultivation. The typical convention has been to consider hydroponic cultivation in early plant production stages with an eventual transition to regolith-derived cultivation as the mission scales and maturates. While we acknowledge that this conventional wisdom may result in optimal economics, we also understand that there are complex system considerations involving all aspects of the reference mission architecture for selection of an ideal plant cultivation strategy and progression. Given the uncertainty in future Mars mission reference mission architectures, here we propose a novel progression of plant cultivation for a Mars settlement progression as a thought experiment to consider the value of early-stage regolith-derived cultivation, particularly in the context of a mission in which resources are generated *in situ* using biological engineering. Future works would be required to further develop the proposed strategy, evaluate the merits more technically, and identify potential high-value research and development that may be pursued.

Figure 13.5.1 provides an overview diagram of the novel plant cultivation progression proposed here.

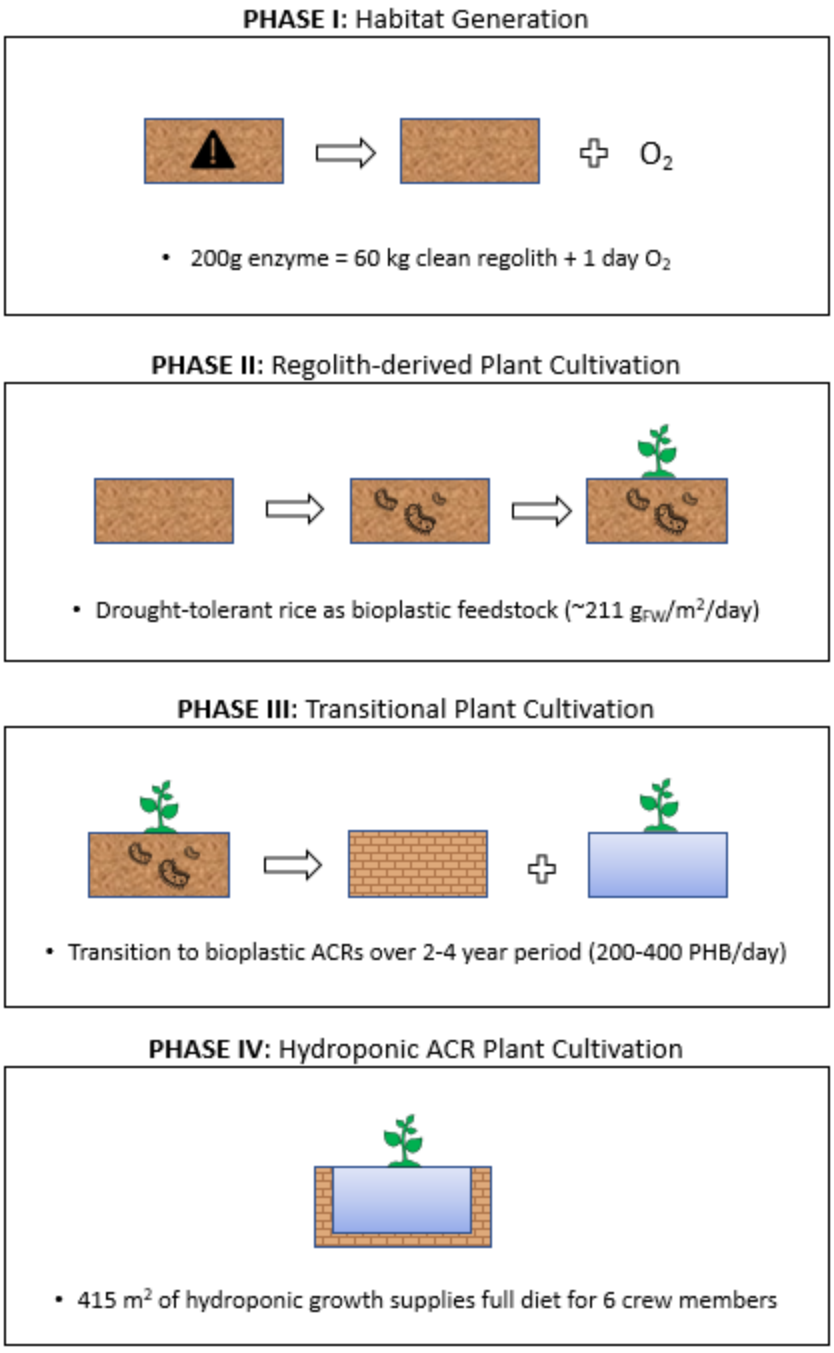

Figure 13.5.1. A diagram of a novel Mars mission plant cultivation progression.

13.5.1. PHASE I: Habitat Generation

Conditions: To begin with, the crew members will need generate a hospitable main base of operations. Key attributes the habitat must possess include 1) habitable oxygen level, 2) low

perchlorate exposure from regolith and dust, and 3) potable water source. The scenario neglects #3, as this source could take many different forms depending on landing site. For undertaking habitat construction, the crew members will have a limited supply of bioplastics. To generate additional bioplastics at a reasonable rate (assumed to be 200 – 400 g bioplastic/day), the crew members will need to heavily rely on anaerobic digestion of inedible plant tissue as feedstock (4,600 – 9,200 g biomass fresh weight; Calculation using NASA's Baseline Values and Assumptions Document (BVAD) 2018[247]). The inedible plant tissue requirements can be met with crop capacity of 12-24% full diet for six crew members (CM) on a food mass basis (equal dry weight lettuce, rice, potato; Calculation using NASA's BVAD 2018[247]).

Proposal: Initial regolith detoxification will be performed cell-free with a stock of perchlorate-reducing bacterial enzymes (perchlorate reductase & chlorite dismutase) at a rate of 1,928 μmol chlorite/mg chlorite dismutase/minute[536]. Based on perchlorate content in regolith, daily supply of oxygen per crew member can be obtained by complete reduction of perchlorate in 60 kg regolith with 100 g of each enzyme in approximately an 1 hour[537]. Information on the reusability of the enzymes is not publicly available. While it is expected to have redundant initial oxygen stores, this will stretch oxygen supplies.

13.5.2. PHASE II: Regolith-Derived Plant Cultivation

Conditions: Perchlorate readily accumulates in edible plant tissue, and thus clean regolith is required to minimize perchlorate intake[538]. Crew members will have access to 60 kg clean regolith/day/crew member for as long as enzymatic perchlorate reduction is used for full oxygen supply. Perchlorate-reducing bacterial cultures can be expected to yield 0.2 – 2.5 g perchlorate reduction/m^3/hour (based on working process knowledge).

Proposal: The clean regolith will be used as a substrate to grow crops in raised beds floored with thin water-impermeable plastic. Crop distribution will begin heavily weighted with rice, which yields the highest bioplastic feedstock productivity. Regolith-derived crop production will increase at a rate constrained by acquisition of clean regolith, water, and nutrients. Crop distribution will shift towards favoring desired food production as rising capacity lowers the difficulty of meeting bioplastic demands.

The bioplastics will be used to form crucial equipment and tools, including a vessel for growth of perchlorate-reducing bacteria as to transition from the reliance on stock enzyme solutions. These bacteria will naturally produce water and carbon dioxide as bioproducts, rather than oxygen. Plant cultivation will offset the decrease in oxygen generation. Plant-based alternatives, such as transgenic plant (e.g., switchgrass) production of bioplastic[539] to microbial production of bioplastics could provide a way to cut back on bioreactor printing requirements and supplement oxygen production.

Raised bed regolith will be seeded with starter cultures of bacteria to form a microbiome favorable for drought tolerance, thus bolstering productivity in this start-up period while water is still being acquired to hit target supply levels.

13.5.3. PHASE III: Transitional Plant Cultivation

Conditions: The crew members will have access to the tools to directly compress detoxified Martian regolith into structural building components at ambient conditions[540]. Prior phases will have generated sufficient clean regolith and plant biomass to provide a substantial crop and bioplastics capacity.

Proposal: As raised bed crop areas accumulate to near the total footprint for hydroponic vertical farming (full diet for 6 CM requires 415m^2 distributed across several vertically-stacked layers; Calculation using NASA's BVAD 2018[247]), the clean regolith processing facility will transition to the formation of structural building components in addition to use as the plant growth substrate. These structural building components will be used to create the multi-layer framework for hydroponic growth.

At full bioplastic generation (200 – 400 g/day), approximately half will be used for construction of agricultural cultivation receptacles (ACRs) for hydroponic growth. As individual ACRs are completed for hydroponic growth, regolith-based raised beds providing plant growth beyond desired capacity are decommissioned. Obsoleted regolith raised beds are repurposed as structural building components. Bioplastic generation can be increased to utilize the additional inedible plant biomass from the additional 76 – 88% biomass required for crop production to meet full diet requirements.

13.5.4. PHASE IV: Hydroponic ACR Plant Cultivation

Conditions: Sufficient ACRs have been constructed to contain 415 m^2 of plants for full diet supply. ACR designs are not finalized. To estimate bioplastic needs, we assume closed rectangular box with 3 m length x 1 m width x 0.1 m height, with 1mm wall thickness and 50% top face coverage. We will need 138 ACRs with these dimensions, which equates to a demand of 914 kg bioplastic. Based on current bioplastic projections, this would take between 6 to 12 years from the start of full bioplastic production capacity. Based on an "open bucket" ACR design based on similar cultivation area to the Breadboard project Biomass Production Chamber[541] and that 50% of the

ACRs need to be printed, the production time is 2 to 4 years. Full hydroponic implementation is not established until the end of this production time.

Proposal: As raised beds are decommissioned for replacement with hydroponic growth, the obsoleted clean regolith will be repurposed as structural building components. The regolith-derived structure bears much of the plant and water load to enable thin, and thus low bioplastic demand, ACRs (1 mm thickness). Full hydroponic growth maximizes biomass productivity and resource utilization (particularly water and plant nutrients) for optimum food, pharmaceutical, and microbial feedstock production.

References

"Ideas are like rabbits. You get a couple and learn how to handle them, and pretty soon you have a dozen."

-John Steinbeck
Who may as well have said this about references.

1. Pande V, Pandey SC, Sati D, Pande V, Samant M. Bioremediation: an emerging effective approach towards environment restoration. *Environ Sustain 2020 31*. 2020;3(1):91-103. doi:10.1007/S42398-020-00099-W

2. Callegari A, Bolognesi S, Cecconet D, Capodaglio AG. Production technologies, current role, and future prospects of biofuels feedstocks: A state-of-the-art review. *https://doi.org/101080/1064338920191629801*. 2019;50(4):384-436. doi:10.1080/10643389.2019.1629801

3. Herdt RW. Biotechnology in Agriculture. *http://dx.doi.org/101146/annurev.energy31031405091314*. 2006;31:265-295. doi:10.1146/ANNUREV.ENERGY.31.031405.091314

4. Evens R, Kaitin K. The Evolution Of Biotechnology And Its Impact On Health Care. *https://doi.org/101377/hlthaff20141023*. 2017;34(2):210-219. doi:10.1377/HLTHAFF.2014.1023

5. Wouters OJ, McKee M, Luyten J. Estimated Research and Development Investment Needed to Bring a New Medicine to Market, 2009-2018. *JAMA*. 2020;323(9):844-853. doi:10.1001/JAMA.2020.1166

6. Green GM, Read RH, Lee S, Tubon T, Hunsberger JG, Atala A. Recommendations for workforce development in regenerative medicine biomanufacturing. *Stem Cells Transl Med*. 2021;10(10):1365. doi:10.1002/SCTM.21-0037

7. Otto RD, Santagostino A, Schrader U, et al. *From Science to Operations: Questions, Choices and Strategies for Success in Biopharma*. (Otto RD, Santagostino A, Schrader U, eds.). McKinsey & Company; 2014. https://www.mckinsey.com/industries/life-sciences/our-insights/rapid-growth-in-biopharma. Accessed November 7, 2021.

8. Moosivand A, Ghatari AR, Rasekh HR. Supply Chain Challenges in Pharmaceutical Manufacturing Companies: Using Qualitative System Dynamics Methodology. *Iran J Pharm Res IJPR*. 2019;18(2):1103. doi:10.22037/IJPR.2019.2389

9. Iyengar S, Tay-Teo K, Vogler S, et al. Prices, Costs, and Affordability of New Medicines for Hepatitis C in 30 Countries: An Economic Analysis. *PLOS Med*. 2016;13(5):e1002032. doi:10.1371/JOURNAL.PMED.1002032

10. He S, Krainer KMC. The Inequity of Biotechnological Impact. *Mol Plant*. 2021;14(1):1-2. doi:10.1016/J.MOLP.2020.12.011

11. Björk B-C, Solomon D. Open access versus subscription journals: a comparison of scientific impact. *BMC Med 2012 101*. 2012;10(1):1-10. doi:10.1186/1741-7015-10-73

12. Çakmaklı C, Demiralp S, Kalemli-Özcan Şebnem, Yeşiltaş S, Yıldırım MA. The Economic Case for Global Vaccinations: An Epidemiological Model with International Production Networks. *SSRN*. January 2021. doi:10.3386/W28395

13. Figueroa JP, Hotez PJ, Batista C, et al. Achieving global equity for COVID-19 vaccines: Stronger international partnerships and greater advocacy and solidarity are needed. *PLOS Med*. 2021;18(9):e1003772. doi:10.1371/JOURNAL.PMED.1003772

14. Huggett B. Biotech's pale shadow. *Nat Biotechnol 2017 361*. 2017;36(1):20-30. doi:10.1038/nbt.4046

15. Menon BRK. The missing colours of chemistry. *Nat Chem 2021 132*. 2021;13(2):101-106. doi:10.1038/s41557-020-00632-8

16. Wingfield AH. Systemic racism persists in the sciences. *Science (80-)*. 2020;369(6502):351. doi:10.1126/SCIENCE.ABD8825

17. Socio-economic inequality in science is on the rise. *Nat 2016 5377621*. 2016;537(7621):450-450. doi:10.1038/537450a

18. Is science only for the rich? *Nature*. 2016;537(7621):466-470. doi:10.1038/537466A

19. Xie Y. "Undemocracy": inequalities in science. *Science (80-)*. 2014;344(6186):809-810. doi:10.1126/SCIENCE.1252743

20. Veeresham C. Natural products derived from plants as a source of drugs. *J Adv Pharm Technol Res*. 2012;3(4):200-201. doi:10.4103/2231-4040.104709

21. Fraley RT, Rogers SG, Horsch RB, et al. Expression of bacterial genes in plant cells. *Proc Natl Acad Sci*. 1983;80(15):4803-4807. doi:10.1073/PNAS.80.15.4803

22. Horsch RB, Fraley RT, Rogers SG, Sanders PR, Lloyd A, Hoffmann N. Inheritance of Functional Foreign Genes in Plants. *Science (80-)*. 1984;223(4635):496-498. doi:10.1126/SCIENCE.223.4635.496

23. Hiatt A, Caffferkey R, Bowdish K. Production of antibodies in transgenic plants. *Nature*. 1989;342:76-78. doi:https://doi.org/10.1038/342076a0

24. Tschofen M, Knopp D, Hood E, Stöger E. Plant Molecular Farming: Much More than Medicines. *Annu Rev Anal Chem*. 2016. doi:10.1146/annurev-anchem-071015-041706

25. Shanmugaraj B, Bulaon CJI, Phoolcharoen W. Plant Molecular Farming: A Viable Platform for Recombinant Biopharmaceutical Production. *Plants 2020, Vol 9, Page 842*. 2020;9(7):842. doi:10.3390/PLANTS9070842

26. Itakura K, Hirose T, Crea R, et al. Expression in Escherichia coli of a Chemically Synthesized Gene for the Hormone Somatostatin. *Science (80-)*. 1977;198(4321):1056-

1063. doi:10.1126/SCIENCE.412251

27. Nallet S, Wurm F, Hacker D. Recombinant Protein Production Yields from Mammalian Cells: Past, Present, and Future. *BioPharm Int*. 2008;2008(5). https://www.biopharminternational.com/view/recombinant-protein-production-yields-mammalian-cells-past-present-and-future. Accessed January 6, 2022.

28. Andersen DC, Krummen L. Recombinant protein expression for therapeutic applications. *Curr Opin Biotechnol*. 2002;13(2):117-123. doi:10.1016/S0958-1669(02)00300-2

29. De Martinis D, Rybicki EP, Fujiyama K, Franconi R, Benvenuto E. Editorial: Plant Molecular Farming: Fast, Scalable, Cheap, Sustainable. *Front Plant Sci*. 2016;7:1148. doi:10.3389/fpls.2016.01148

30. Schillberg S, Raven N, Spiegel H, Rasche S, Buntru M. Critical Analysis of the Commercial Potential of Plants for the Production of Recombinant Proteins. *Front Plant Sci*. 2019;10:720. doi:10.3389/fpls.2019.00720

31. Twyman RM, Stoger E, Schillberg S, Christou P, Fischer R. Molecular farming in plants: host systems and expression technology. *Trends Biotechnol*. 2003;21(12):570-578. doi:10.1016/J.TIBTECH.2003.10.002

32. Ma JK-C, Christou P, Chikwamba R, et al. Realising the value of plant molecular pharming to benefit the poor in developing countries and emerging economies. *Plant Biotechnol J*. 2013;11(9):1029-1033. doi:10.1111/pbi.12127

33. Ortega-Rivera OA, Shin MD, Chen A, et al. Trivalent Subunit Vaccine Candidates for COVID-19 and Their Delivery Devices. *J Am Chem Soc*. 2021;143(36):14748-14765. doi:10.1021/JACS.1C06600/SUPPL_FILE/JA1C06600_SI_001.PDF

34. Torti S, Schlesier R, Thümmler A, et al. Transient reprogramming of crop plants for agronomic performance. *Nat Plants*. 2021;7(2):159-171. doi:10.1038/s41477-021-00851-y

35. Marillonnet S, Giritch A, Gils M, Kandzia R, Klimyuk V, Gleba Y. In planta engineering of viral RNA replicons: efficient assembly by recombination of DNA modules delivered by Agrobacterium. *Proc Natl Acad Sci U S A*. 2004;101(18):6852-6857. doi:10.1073/pnas.0400149101

36. Arntzen C. Plant-made pharmaceuticals: From “Edible Vaccines” to Ebola therapeutics. *Plant Biotechnol J*. 2015;13(8):1013-1016. doi:10.1111/pbi.12460

37. Largent EA. EBOLA and FDA: reviewing the response to the 2014 outbreak, to find lessons for the future. *J Law Biosci*. 2016;3(3):489. doi:10.1093/JLB/LSW046

38. Team TPIWG for the M-NPIS. A Randomized, Controlled Trial of ZMapp for Ebola Virus Infection. *N Engl J Med*. 2016;375(15):1448. doi:10.1056/NEJMOA1604330

39. Murad S, Fuller S, Menary J, et al. Molecular Pharming for low and middle income countries. *Curr Opin Biotechnol*. 2020;61:53-59. doi:10.1016/j.copbio.2019.10.005

40. McNulty MJ, Schwartz A, Delzio J, et al. Affinity sedimentation and magnetic separation

with plant-made immunosorbent nanoparticles for therapeutic protein purification. *bioRxiv*. November 2021:2021.11.05.467285. doi:10.1101/2021.11.05.467285

41. Marillonnet S, Thoeringer C, Kandzia R, Klimyuk V, Gleba Y. Systemic Agrobacterium tumefaciens-mediated transfection of viral replicons for efficient transient expression in plants. *Nat Biotechnol*. 2005;23(6):718-723. doi:10.1038/nbt1094

42. Bruckman MA, Steinmetz NF. Chemical modification of the inner and outer surfaces of Tobacco Mosaic Virus (TMV). *Methods Mol Biol*. 2014;1108:173-185. doi:10.1007/978-1-62703-751-8_13

43. McNulty MJ, Hamada N, Delzio J, et al. Functionalizing silica sol-gel with entrapped plant virus-based immunosorbent nanoparticles. *bioRxiv*. November 2021:2021.11.12.468100. doi:10.1101/2021.11.12.468100

44. Einarson MB, Pugacheva EN, Orlinick JR. Far Western: probing membranes. *CSH Protoc*. 2007;2007(8):pdb.prot4759. doi:10.1101/pdb.prot4759

45. Ernst O, Zor T. Linearization of the Bradford Protein Assay. *J Vis Exp*. 2010;(38). doi:10.3791/1918

46. Peters MS, Timmerhaus KD, West RE. *Plant Design and Economics for Chemical Engineers*. 5th ed. McGraw-Hill Publishing Company; 2003.

47. Petrides D, Carmichael D, Siletti C, Koulouris A. Bioprocess Simulation and Economics. In: *Essentials in Fermentation Technology*. Springer, Cham; 2019:273-305. doi:10.1007/978-3-030-16230-6_9

48. Fischer R, Buyel JF. Molecular farming – The slope of enlightenment. *Biotechnol Adv*. 2020;40:107519. doi:10.1016/j.biotechadv.2020.107519

49. Holtz BR, Berquist BR, Bennett LD, et al. Commercial-scale biotherapeutics manufacturing facility for plant-made pharmaceuticals. *Plant Biotechnol J*. 2015;13(8):1180-1190. doi:10.1111/pbi.12469

50. Tekoah Y, Shulman A, Kizhner T, et al. Large-scale production of pharmaceutical proteins in plant cell culture-the protalix experience. *Plant Biotechnol J*. 2015;13(8):1199-1208. doi:10.1111/pbi.12428

51. D'Aoust M-A, Couture MM-J, Charland N, et al. The production of hemagglutinin-based virus-like particles in plants: a rapid, efficient and safe response to pandemic influenza. *Plant Biotechnol J*. 2010;8(5):607-619. doi:10.1111/j.1467-7652.2009.00496.x

52. Nandi S, Yalda D, Lu S, et al. Process development and economic evaluation of recombinant human lactoferrin expressed in rice grain. *Transgenic Res*. 2005;14(3):237-249. doi:10.1007/s11248-004-8120-6

53. Corbin JM, McNulty MJ, Macharoen K, McDonald KA, Nandi S. Technoeconomic analysis of semicontinuous bioreactor production of biopharmaceuticals in transgenic rice cell suspension cultures. *Biotechnol Bioeng*. 2020;117(10):3053–3065. doi:10.1002/bit.27475

54. McNulty MJ, Gleba Y, Tusé D, et al. Techno-economic analysis of a plant-based platform for manufacturing antimicrobial proteins for food safety. *Biotechnol Prog*. 2020;36(1). doi:10.1002/btpr.2896

55. Alam A, Jiang L, Kittleson GA, et al. Technoeconomic Modeling of Plant-Based Griffithsin Manufacturing. *Front Bioeng Biotechnol*. 2018;6:102. doi:10.3389/fbioe.2018.00102

56. Nandi S, Kwong AT, Holtz BR, Erwin RL, Marcel S, McDonald KA. Techno-economic analysis of a transient plant-based platform for monoclonal antibody production. *MAbs*. 2016;8(8):1456-1466. doi:10.1080/19420862.2016.1227901

57. Walwyn DR, Huddy SM, Rybicki EP. Techno-Economic Analysis of Horseradish Peroxidase Production Using a Transient Expression System in Nicotiana benthamiana. *Appl Biochem Biotechnol*. 2015;175(2):841-854. doi:10.1007/s12010-014-1320-5

58. Tusé D, Tu T, McDonald KA. Manufacturing economics of plant-made biologics: Case studies in therapeutic and industrial enzymes. *Biomed Res Int*. 2014;2014. doi:10.1155/2014/256135

59. Pleitt K, Somasundaram B, Johnson B, Shave E, Lua LHL. Evaluation of process simulation as a decisional tool for biopharmaceutical contract development and manufacturing organizations. *Biochem Eng J*. 2019;150:107252. doi:10.1016/j.bej.2019.107252

60. Turton R, Shaeiwitz JA, Bhattacharyya D, Whiting WB. *Analysis, Synthesis, and Design of Chemical Processes*. 5th ed. Pearson; 2018.

61. Biwer A, Heinzle E. Environmental assessment in early process development. *J Chem Technol Biotechnol*. 2004;79(6):597-609. doi:10.1002/jctb.1027

62. Heinzle E, Biwer AP, Cooney CL. *Development of Sustainable Bioprocesses: Modeling and Assessment*. Hoboken, NJ, USA: John Wiley & Sons, Ltd; 2007.

63. Budzinski K, Blewis M, Dahlin P, et al. Introduction of a process mass intensity metric for biologics. *N Biotechnol*. 2019;49:37-42. doi:10.1016/j.nbt.2018.07.005

64. Chisti Y. Modern systems of plant cleaning. *Encycl Food Microbiol*. 1999:1806-1815.

65. Bremer PJ, Seale RB. Clean-in-Place (CIP). In: *Encyclopedia of Industrial Biotechnology*. Hoboken, NJ, USA: John Wiley & Sons, Inc.; 2010. doi:10.1002/9780470054581.eib231

66. Davies S, Sykes T, Philips M, Hancock J. Hygienic design and Cleaning-In-Place (CIP) systems in breweries. In: *Brewing Microbiology: Managing Microbes, Ensuring Quality and Valorising Waste*. Elsevier; 2015:221-239. doi:10.1016/B978-1-78242-331-7.00010-1

67. World Health Organization. Foodborne Disease Burden Epidemiology Reference Group. *WHO Estimates of the Global Burden of Foodborne Diseases*.; 2015.

68. Uyttendaele M, Franz E, Schlüter O. Food Safety, a Global Challenge. *Int J Environ Res Public Health*. 2015;13(1):67. doi:10.3390/ijerph13010067

69. Scallan E, Hoekstra RM, Angulo FJ, et al. Foodborne illness acquired in the United

States--major pathogens. *Emerg Infect Dis*. 2011;17(1):7-15. doi:10.3201/eid1701.p11101

70. Bartsch SM, Asti L, Nyathi S, Spiker ML, Lee BY. Estimated Cost to a Restaurant of a Foodborne Illness Outbreak. *Public Health Rep*. 2018;133(3):274-286. doi:10.1177/0033354917751129

71. Hoffmann S, Batz MB, Morris, J. Glenn J. Annual Cost of Illness and Quality-Adjusted Life Year Losses in the United States Due to 14 Foodborne Pathogens. *J Food Prot*. 2012;75(7):1292-1302. doi:10.4315/0362-028X.JFP-11-417

72. Ferro S, Amorico T, Deo P. Role of food sanitising treatments in inducing the 'viable but nonculturable' state of microorganisms. *Food Control*. 2018;91:321-329. doi:10.1016/J.FOODCONT.2018.04.016

73. Asakura H, Igimi S, Kawamoto K, Yamamoto S, Makino S. Role of in vivo passage on the environmental adaptation of enterohemorrhagic Escherichia coli O157:H7: Cross-induction of the viable but nonculturable state by osmotic and oxidative stresses. *FEMS Microbiol Lett*. 2005;253(2):243-249. doi:10.1016/J.FEMSLE.2005.09.039

74. Gage L. Impact of Food Disinfectants on Formation of VBNC Cells in Salmonella. In: *Annual Meeting of the International Association for Food Protection*. St. Louis, Missouri: Iafp; 2016:P3-158. https://iafp.confex.com/iafp/2016/webprogram/Paper12399.html. Accessed August 9, 2018.

75. Van Houteghem N, Devlieghere F, Rajkovic A, Gómez SMO, Uyttendaele M, Debevere J. Effects of CO2 on the resuscitation of Listeria monocytogenes injured by various bactericidal treatments. *Int J Food Microbiol*. 2008;123(1-2):67-73. doi:10.1016/J.IJFOODMICRO.2007.12.002

76. Nicolò MS, Gioffrè A, Carnazza S, Platania G, Silvestro I Di, Guglielmino SPP. Viable But Nonculturable State of Foodborne Pathogens in Grapefruit Juice: A Study of Laboratory. *Foodborne Pathog Dis*. 2011;8(1):11-17. doi:10.1089/fpd.2009.0491

77. Schulz S, Stephan A, Hahn S, et al. Broad and efficient control of major foodborne pathogenic strains of Escherichia coli by mixtures of plant-produced colicins. *Proc Natl Acad Sci U S A*. 2015;112(40):E5454-60. doi:10.1073/pnas.1513311112

78. Sharma M. Lytic bacteriophages: Potential interventions against enteric bacterial pathogens on produce. *Bacteriophage*. 2013;3(2):e25518. doi:10.4161/bact.25518

79. U.S. Food & Drug Administration. GRN No. 802. https://www.accessdata.fda.gov/scripts/fdcc/?set=GRASNotices&id=802. Accessed June 3, 2019.

80. Kazanavičiūtė V, Misiūnas A, Gleba Y, Giritch A, Ražanskienė A. Plant-expressed bacteriophage lysins control pathogenic strains of Clostridium perfringens. *Sci Rep*. 2018;8(1):10589. doi:10.1038/s41598-018-28838-4

81. Stephan A, Hahn-Löbmann S, Rosche F, Buchholz M, Giritch A, Gleba Y. Simple Purification of Nicotiana benthamiana-Produced Recombinant Colicins: High-Yield Recovery of Purified Proteins with Minimum Alkaloid Content Supports the Suitability of the Host for Manufacturing Food Additives. *Int J Mol Sci*. 2017;19(1):95.

doi:10.3390/ijms19010095

82. U.S. Food & Drug Administration. GRN No. 775. https://www.accessdata.fda.gov/scripts/fdcc/?set=GRASNotices&id=775&sort=GRN_No&order=DESC&startrow=1&type=basic&search=775. Published 2018.

83. Shin JM, Gwak JW, Kamarajan P, Fenno JC, Rickard AH, Kapila YL. Biomedical applications of nisin. *J Appl Microbiol*. 2016;120(6):1449-1465. doi:10.1111/jam.13033

84. Noyes G, Viator CL, Muth MK, Brophy JE. *Costs of Food Safety Investments Prepared for Costs of Food Safety Investments Revised Final Report*.; 2015. https://www.fsis.usda.gov/wps/wcm/connect/0cdc568e-f6b1-45dc-88f1-45f343ed0bcd/Food-Safety-Costs.pdf?MOD=AJPERES. Accessed September 16, 2018.

85. Oliveira H, Azeredo J, Lavigne R, Kluskens LD. Bacteriophage endolysins as a response to emerging foodborne pathogens. *Trends Food Sci Technol*. 2012;28(2):103-115. doi:10.1016/j.tifs.2012.06.016

86. Gillor O, Nigro L, Riley M. Genetically Engineered Bacteriocins and their Potential as the Next Generation of Antimicrobials. *Curr Pharm Des*. 2005;11(8):1067-1075. doi:10.2174/1381612053381666

87. Schmelcher M, Donovan DM, Loessner MJ. Bacteriophage endolysins as novel antimicrobials. *Future Microbiol*. 2012;7(10):1147-1171. doi:10.2217/fmb.12.97

88. Schneider T, Hahn-Löbmann S, Stephan A, et al. Plant-made Salmonella bacteriocins salmocins for control of Salmonella pathovars. *Sci Rep*. 2018;8(1):4078. doi:10.1038/s41598-018-22465-9

89. Paškevičius Š, Starkevič U, Misiūnas A, Vitkauskienė A, Gleba Y, Ražanskienė A. Plant-expressed pyocins for control of Pseudomonas aeruginosa. Davis KR, ed. *PLoS One*. 2017;12(10):e0185782. doi:10.1371/journal.pone.0185782

90. Kovalskaya N, Foster-Frey J, Donovan DM, Bauchan G, Hammond RW. Antimicrobial activity of bacteriophage endolysin produced in nicotiana benthamiana plants. *J Microbiol Biotechnol*. 2015;26(1):160-170. doi:10.4014/jmb.1505.05060

91. Goodin MM, Zaitlin D, Naidu RA, Lommel SA. Nicotiana benthamiana : Its History and Future as a Model for Plant–Pathogen Interactions. *Mol Plant-Microbe Interact*. 2008;21(8):1015-1026. doi:10.1094/MPMI-21-8-1015

92. Alkanaimsh S, Karuppanan K, Guerrero A, et al. Transient Expression of Tetrameric Recombinant Human Butyrylcholinesterase in Nicotiana benthamiana. *Front Plant Sci*. 2016;7:743. doi:10.3389/fpls.2016.00743

93. Karuppanan K, Duhra-Gill S, Kailemia M, et al. Expression, Purification, and Biophysical Characterization of a Secreted Anthrax Decoy Fusion Protein in Nicotiana benthamiana. *Int J Mol Sci*. 2017;18(1):89. doi:10.3390/ijms18010089

94. Pogue GP, Vojdani F, Palmer KE, et al. Production of pharmaceutical-grade recombinant aprotinin and a monoclonal antibody product using plant-based transient expression systems. *Plant Biotechnol J*. 2010;8(5):638-654. doi:10.1111/j.1467-7652.2009.00495.x

95. Werner S, Breus O, Symonenko Y, Marillonnet S, Gleba Y. High-level recombinant protein expression in transgenic plants by using a double-inducible viral vector. *Proc Natl Acad Sci U S A*. 2011;108(34):14061-14066. doi:10.1073/pnas.1102928108

96. D'Aoust M-A, Lavoie P-O, Couture MM-J, et al. Influenza virus-like particles produced by transient expression in *Nicotiana benthamiana* induce a protective immune response against a lethal viral challenge in mice. *Plant Biotechnol J*. 2008;6(9):930-940. doi:10.1111/j.1467-7652.2008.00384.x

97. Chen Q, Lai H, Hurtado J, Stahnke J, Leuzinger K, Dent M. Agroinfiltration as an Effective and Scalable Strategy of Gene Delivery for Production of Pharmaceutical Proteins. *Adv Tech Biol Med*. 2013;1(1). doi:10.4172/atbm.1000103

98. U.S. Food & Drug Administration. *CFR - Code of Federal Regulations Title 21 Part 110*. https://www.accessdata.fda.gov/scripts/cdrh/cfdocs/cfcfr/CFRSearch.cfm?CFRPart=110.

99. Azzoni AR, Kusnadi AR, Miranda EA, Nikolov ZL. Recombinant aprotinin produced in transgenic corn seed: Extraction and purification studies. *Biotechnol Bioeng*. 2002;80(3):268-276. doi:10.1002/bit.10408

100. Pogue GP, Lindbo JA, Garger SJ, Fitzmaurice WP. Making an Ally from an Enemy: Plant Virology and the New Agriculture. *Annu Rev Phytopathol*. 2002;40(1):45-74. doi:10.1146/annurev.phyto.40.021102.150133

101. Jutras P V, Marusic C, Lonoce C, et al. An Accessory Protease Inhibitor to Increase the Yield and Quality of a Tumour-Targeting mAb in Nicotiana benthamiana Leaves. *PLoS One*. 2016;11(11):e0167086. doi:10.1371/journal.pone.0167086

102. Schuhmacher A, Gassmann O, Hinder M. Changing R&D models in research-based pharmaceutical companies. *J Transl Med*. 2016;14(1):105. doi:10.1186/s12967-016-0838-4

103. Hahn-Löbmann S, Stephan A, Schulz S, et al. Colicins and Salmocins – New Classes of Plant-Made Non-antibiotic Food Antibacterials. *Front Plant Sci*. 2019;10:437. doi:10.3389/fpls.2019.00437

104. Jensen HH, Unnevehr LJ, Gomez MI, Jensen HH;, Unnevehr LJ; *The Costs of Improving Food Safety in the Meat Sector*. Vol 225.; 1998. http://lib.dr.iastate.edu/card_workingpapers/225. Accessed September 30, 2018.

105. Ripoll G, Albertí P, Alvarez-Rodríguez J, Blasco I, Sanz A. Body size, carcass and meat quality of three commercial beef categories of 'Serrana de Teruel' breed. *Spanish J Agric Res*. 2016;14(3):e0604. doi:10.5424/sjar/2016143-9122

106. A. Estes Reynolds J. Utilization of spray wash with organic acids (peroxyacetic acid and lactic acid) and chlorinated wash in combination, utilizing direct application methods, for pathogen reduction on pork and beef carcasses in small and very small meat processing plants (r. 2005.

107. Aranha H. Virus Safety Of Biopharmaceuticals. Contract Pharma. https://www.contractpharma.com/issues/2011-11/view_features/virus-safety-of-biopharmaceuticals. Published 2011.

108. Nandi S, McDonald K. Expression of Recombinant Proteins in Plant Cell Culture. In: Hefferon K, ed. *Plant-Derived Pharmaceuticals: Principles and Applications for Developing Countries*. CAB International; 2014. https://www.cabi.org/bookshop/book/9781780643434.

109. Huang TK, McDonald KA. Bioreactor systems for in vitro production of foreign proteins using plant cell cultures. *Biotechnol Adv*. 2012;30(2):398-409. doi:10.1016/j.biotechadv.2011.07.016

110. Häkkinen ST, Reuter L, Nuorti N, Joensuu JJ, Rischer H, Ritala A. Tobacco BY-2 Media Component Optimization for a Cost-Efficient Recombinant Protein Production. *Front Plant Sci*. 2018;9:45. doi:10.3389/fpls.2018.00045

111. Tabata H. Production of Paclitaxel and the Related Taxanes by Cell Suspension Cultures of Taxus Species. *Curr Drug Targets*. 2006;7(4):453-461. doi:http://dx.doi.org/10.2174/138945006776359368

112. Ratner M. Pfizer stakes a claim in plant cell-made biopharmaceuticals. *Nat Biotechnol*. 2010;28(2):107-108. doi:10.1038/nbt0210-107

113. Almon E, Khoury T, Drori A, et al. An oral administration of a recombinant anti-TNF fusion protein is biologically active in the gut promoting regulatory T cells: Results of a phase I clinical trial using a novel oral anti-TNF alpha-based therapy. *J Immunol Methods*. 2017;446:21-29. doi:10.1016/J.JIM.2017.03.023

114. Schiffmann R, Goker-Alpan O, Holida M, et al. Pegunigalsidase alfa, a novel PEGylated enzyme replacement therapy for Fabry disease, provides sustained plasma concentrations and favorable pharmacodynamics: A 1-year Phase 1/2 clinical trial. *J Inherit Metab Dis*. 2019;42(3):jimd.12080. doi:10.1002/jimd.12080

115. Corbin JM, Hashimoto BI, Karuppanan K, et al. Semicontinuous Bioreactor Production of Recombinant Butyrylcholinesterase in Transgenic Rice Cell Suspension Cultures. *Front Plant Sci*. 2016;7(March):1-9. doi:10.3389/fpls.2016.00412

116. Corbin JM, Kailemia MJ, Cadieux CL, et al. Purification, characterization, and N-glycosylation of recombinant butyrylcholinesterase from transgenic rice cell suspension cultures. *Biotechnol Bioeng*. 2018;115(5):1301-1310. doi:10.1002/bit.26557

117. Petrides D, Carmichael D, Siletti C, Koulouris A. Biopharmaceutical Process Optimization with Simulation and Scheduling Tools. *Bioengineering*. 2014;1:154-187. doi:10.3390/bioengineering1040154

118. Rouf S., Moo-Young M, Scharer J., Douglas P. Single versus multiple bioreactor scale-up: economy for high-value products. *Biochem Eng J*. 2000;6(1):25-31. doi:10.1016/S1369-703X(00)00066-8

119. Rouf S., Douglas P., Moo-Young M, Scharer J. Computer simulation for large scale bioprocess design. *Biochem Eng J*. 2001;8(3):229-234. doi:10.1016/S1369-703X(01)00112-7

120. Xenopoulos A. A new, integrated, continuous purification process template for monoclonal antibodies: Process modeling and cost of goods studies. *J Biotechnol*.

2015;213:42-53. doi:10.1016/J.JBIOTEC.2015.04.020

121. Wilken LR, Nikolov ZL. Recovery and purification of plant-made recombinant proteins. *Biotechnol Adv*. 2012;30(2):419-433. doi:10.1016/j.biotechadv.2011.07.020

122. Mir-Artigues P, Twyman RM, Alvarez D, et al. A simplified techno-economic model for the molecular pharming of antibodies. *Biotechnol Bioeng*. 2019;116(10):2526-2539. doi:10.1002/bit.27093

123. Stoller JK, Aboussouan LS. Myths and misconceptions about α1-antitrypsin deficiency. *Arch Intern Med*. 2009;169(6):546-550.

124. Miller RG, Appel SH. Introduction to supplement: the current status of treatment for ALS. *Amyotroph Lateral Scler Front Degener*. 2017;18(sup1):1-4. doi:10.1080/21678421.2017.1361447

125. Lydersen BK, D'Elia N, Nelson KL. *Bioprocess Engineering : Systems, Equipment and Facilities*. New York, USA: Wiley; 1994.

126. Chisti Y, Moo-Young M. *Clean-in-Place Systems for Industrial Bioreactors: Design, Validation and Operation*. Vol 3.; 1994.

127. Harrison RG, Todd PW, Rudge SR, Petrides DP. *Bioseparations Science and Engineering*. 2nd ed. (Gubbins KE, Barteau MA, Lauffenburger DA, Morari M, Ray WH, Russel WB, eds.). Oxford University Press; 2015.

128. Kelley B. Industrialization of mAb production technology: the bioprocessing industry at a crossroads. *MAbs*. 2009;1(5):443-452. http://www.ncbi.nlm.nih.gov/pubmed/20065641. Accessed March 29, 2017.

129. Xu S, Gavin J, Jiang R, Chen H. Bioreactor productivity and media cost comparison for different intensified cell culture processes. *Biotechnol Prog*. 2017;33(4):867-878. doi:10.1002/btpr.2415

130. Grabowski GA, Golembo M, Shaaltiel Y. Taliglucerase alfa: An enzyme replacement therapy using plant cell expression technology. *Mol Genet Metab*. 2014;112(1):1-8. doi:10.1016/j.ymgme.2014.02.011

131. Mor TS. Molecular pharming's foot in the FDA's door: Protalix's trailblazing story. *Biotechnol Lett*. 2015;37(11):2147-2150. doi:10.1007/s10529-015-1908-z

132. Mustafa NR, de Winter W, van Iren F, Verpoorte R. Initiation, growth and cryopreservation of plant cell suspension cultures. *Nat Protoc*. 2011;6(6):715-742. doi:10.1038/nprot.2010.144

133. Kwon JY, Jeong SH, Choi JW, Pak YY, Kim D Il. Assessment of long-term cryopreservation for production of hCTLA4Ig in transgenic rice cell suspension cultures. *Enzyme Microb Technol*. 2013;53(3):216-222. doi:10.1016/j.enzmictec.2013.05.008

134. Santos RB, Abranches R, Fischer R, Sack M, Holland T. Putting the Spotlight Back on Plant Suspension Cultures. *Front Plant Sci*. 2016;7(March):1-12. doi:10.3389/fpls.2016.00297

135. Chung CH, Mirakhur B, Chan E, et al. Cetuximab-Induced Anaphylaxis and IgE Specific for Galactose- α-1,3-Galactose. 2008;11(358):1109-1117. doi:10.1126/scisignal.2001449.Engineering

136. Shaaltiel Y, Tekoah Y. Plant specific N-glycans do not have proven adverse effects in humans. *Nat Biotechnol*. 2016;34(7):706-708. doi:10.1038/nbt.3556

137. Rup B, Alon S, Amit-Cohen B-C, et al. Immunogenicity of glycans on biotherapeutic drugs produced in plant expression systems —The taliglucerase alfa story. *PLoS One*. 2017;12(10). doi:10.1371/journal.pone.0186211

138. Jurchison S. PharmAthene, Inc. Presents Phase I Clinical Trial Results and New Therapeutic Animal Model Data for Protexia(R) | BioSpace. BioSpace. https://www.biospace.com/article/releases/pharmathene-inc-presents-phase-i-clinical-trial-results-and-new-therapeutic-animal-model-data-for-protexia-r-/. Published 2009. Accessed December 9, 2019.

139. PharmAthene. United States Security and Exchange Commissions Form 10-K for the fiscal year ended December 31, 2014. 2015.

140. Saxena A, Tipparaju P, Luo C, Doctor BP. Pilot-scale production of human serum butyrylcholinesterase suitable for use as a bioscavenger against nerve agent toxicity. *Process Biochem*. 2010;45(8):1313-1318. doi:10.1016/j.procbio.2010.04.021

141. DARPA. Broad Agency Announcement Butyrylcholinesterase Expression in Plants DSO DARPA-BAA-12-31. 2012.

142. Ashani Y. Prospective of human butyrylcholinesterase as a detoxifying antidote and potential regulator of controlled-release drugs. *Drug Dev Res*. 2000;308:2000. doi:10.1002/1098-2299(200007/08)50:3/4<298::AID-DDR13>3.0.CO;2-X

143. Alkanaimsh S, Karuppanan K, Guerrero A, et al. Transient expression of tetrameric recombinant human butyrylcholinesterase in *Nicotiana benthamiana*. *Front Plant Sci*. 2016;7(June):743. doi:10.3389/fpls.2016.00743

144. Geyer BC, Kannan L, Cherni I, Woods RR, Soreq H, Mor TS. Transgenic plants as a source for the bioscavenging enzyme, human butyrylcholinesterase. *Plant Biotechnol J*. 2010;8(8):873-886. doi:10.1111/j.1467-7652.2010.00515.x

145. Kim NS, Jang SH, Yu HY, et al. Amylase and cysteine proteinase gene knockdown in rice cells using RNA interference for enhancing production of recombinant proteins. *Plant Cell Tissue Organ Cult*. 2013;114(1):97-107. doi:10.1007/s11240-013-0309-z

146. Yu D, Song M-N, Lim J-A, Kim D-I. Effects of culture media on hCTLA4Ig production and protein expression patterns in transgenic rice cell suspension cultures. *Biotechnol Bioprocess Eng*. 2008;13(4):424-430. doi:10.1007/s12257-008-0140-2

147. Park CI, Lee SJ, Kang SH, Jung HS, Kim D Il, Lim SM. Fed-batch cultivation of transgenic rice cells for the production of hCTLA4Ig using concentrated amino acids. *Process Biochem*. 2010;45(1):67-74. doi:10.1016/j.procbio.2009.08.004

148. Van Beilen JB, Poirier Y. Production of renewable polymers from crop plants. *Plant J*.

2008;54(4):684-701. doi:10.1111/j.1365-313X.2008.03431.x

149. Ismail BP, Senaratne-Lenagala L, Stube A, Brackenridge A. Protein demand: review of plant and animal proteins used in alternative protein product development and production. *Anim Front*. 2020;10(4):53-63. doi:10.1093/af/vfaa040

150. Kojima Y, Parcell J, Cain J. A Global Demand Analysis of Vegetable Oils for Food and Industrial Use: A Cross-Country Panel Data Analysis with Spatial Econometrics. In: *Agricultural & Applied Economics Association Annual Meeting*. Boston; 2016.

151. Sylvetsky AC, Rother KI. Trends in the consumption of low-calorie sweeteners. *Physiol Behav*. 2016;164(Pt B):446-450. doi:10.1016/j.physbeh.2016.03.030

152. Kesik-Brodacka M. Progress in biopharmaceutical development. *Biotechnol Appl Biochem*. 2018;65(3):306-322. doi:10.1002/bab.1617

153. McDonald KA, Holtz RB. From Farm to Finger Prick—A Perspective on How Plants Can Help in the Fight Against COVID-19. *Front Bioeng Biotechnol*. 2020;8:782. doi:10.3389/fbioe.2020.00782

154. Ma JKC, Drake PMW, Christou P. The production of recombinant pharmaceutical proteins in plants. *Nat Rev Genet*. 2003;4(10):794-805. doi:10.1038/nrg1177

155. Chen Y-S, Zaro J, Zhang D, Huang N, Simon A, Shen W-C. Characterization and Oral Delivery of Proinsulin-Transferrin Fusion Protein Expressed Using ExpressTec. *Int J Mol Sci*. 2018;19(2):378. doi:10.3390/ijms19020378

156. Laffan AM, McKenzie R, Forti J, et al. Lactoferrin for the prevention of post-antibiotic diarrhoea. *J Heal Popul Nutr*. 2011;29(6):547-551. doi:10.3329/jhpn.v29i6.9889

157. Kermode AR, Jiang L. *Molecular Pharming: Applications, Challenges and Emerging Areas*. Wiley Blackwell; 2018. doi:10.1002/9781118801512

158. Ma JK-C, Barros E, Bock R, et al. Molecular farming for new drugs and vaccines. Current perspectives on the production of pharmaceuticals in transgenic plants. *EMBO Rep*. 2005;6(7):593-599. doi:10.1038/sj.embor.7400470

159. McNulty MJ, Gleba Y, Tusé D, et al. Techno-economic analysis of a plant-based platform for manufacturing antimicrobial proteins for food safety. *Biotechnol Prog*. 2020;36(1). doi:10.1002/btpr.2896

160. Moustafa K, Makhzoum A, Trémouillaux-Guiller J. Molecular farming on rescue of pharma industry for next generations. *Crit Rev Biotechnol*. 2016;36(5):840-850. doi:10.3109/07388551.2015.1049934

161. Iizumi T, Ramankutty N. Changes in yield variability of major crops for 1981-2010 explained by climate change. *Environ Res Lett*. 2016;11(3):034003. doi:10.1088/1748-9326/11/3/034003

162. Batan LY, Graff GD, Bradley TH. Techno-economic and Monte Carlo probabilistic analysis of microalgae biofuel production system. *Bioresour Technol*. 2016;219:45-52. doi:10.1016/j.biortech.2016.07.085

163. J. Zhuang, M. A. Marchant, S. E. Nokes, H. J. Strobel. Economic Analysis of Cellulase Production Methods for Bio-Ethanol. *Appl Eng Agric*. 2007;23(5):679-687. doi:10.13031/2013.23659

164. Papavasileiou V, Koulouris A, Siletti C, Petrides D. Optimize manufacturing of pharmaceutical products with process simulation and production scheduling tools. *Chem Eng Res Des*. 2007;85(7 A):1086-1097. doi:10.1205/cherd06240

165. Martagan T, Krishnamurthy A, Leland PA, Maravelias CT. Performance guarantees and optimal purification decisions for engineered proteins. *Oper Res*. 2018;66(1):18-41. doi:10.1287/opre.2017.1661

166. Biwer A, Griffith S, Cooney C. Uncertainty analysis of penicillin V production using Monte Carlo simulation. *Biotechnol Bioeng*. 2005;90(2):167-179. doi:10.1002/bit.20359

167. Kelada KD, Tusé D, Gleba Y, McDonald KA, Nandi S. Process Simulation and Techno-Economic Analysis of Large-Scale Bioproduction of Sweet Protein Thaumatin II. *Foods*. 2021;10(4):838. doi:10.3390/foods10040838

168. Basu P, Joglekar G, Rai S, Suresh P, Vernon J. Analysis of Manufacturing Costs in Pharmaceutical Companies. *J Pharm Innov*. 2008;3:30-40. doi:10.1007/s12247-008-9024-4

169. Knödler M, Rühl C, Emonts J, Buyel JF. Seasonal Weather Changes Affect the Yield and Quality of Recombinant Proteins Produced in Transgenic Tobacco Plants in a Greenhouse Setting. *Front Plant Sci*. 2019;10:1245. doi:10.3389/fpls.2019.01245

170. Su XZ, Miller LH. The discovery of artemisinin and the Nobel Prize in Physiology or Medicine. *Sci China Life Sci*. 2015;58(11):1175-1179. doi:10.1007/s11427-015-4948-7

171. Moudi M, Go R, Yien CYS, Nazre M. Vinca alkaloids. *Int J Prev Med*. 2013;4(11):1131-1135. doi:10.2165/00128415-200711380-00080

172. Singh DP, Kumari M, Prakash HG, Rao GP, Solomon S. Phytochemical and Pharmacological Importance of Stevia: A Calorie-Free Natural Sweetener. *Sugar Tech*. 2019;21(2):227-234. doi:10.1007/s12355-019-00704-1

173. Menary J, Hobbs M, Mesquita de Albuquerque S, et al. Shotguns vs Lasers: Identifying barriers and facilitators to scaling-up plant molecular farming for high-value health products. Mor TS, ed. *PLoS One*. 2020;15(3):e0229952. doi:10.1371/journal.pone.0229952

174. Sparrow PAC, Irwin JA, Dale PJ, Twyman RM, Ma JKC. Pharma-Planta: Road testing the developing regulatory guidelines for plant-made pharmaceuticals. *Transgenic Res*. 2007;16(2):147-161. doi:10.1007/s11248-007-9074-2

175. Sparrow P, Broer I, Hood E, Eversole K, Hartung F, Schiemann J. Risk Assessment and Regulation of Molecular Farming - A Comparison between Europe and US. *Curr Pharm Des*. 2013;19(31):5513-5530. doi:10.2174/1381612811319310007

176. Faye L, Gomord V. Success stories in molecular farming-a brief overview. *Plant Biotechnol J*. 2010;8(5):525-528. doi:10.1111/j.1467-7652.2010.00521.x

177. Pei L, Schmidt M. Novel biotechnological approaches to produce biological compounds: challenges and opportunities for science communication. *Curr Opin Biotechnol*. 2019;56:43-47. doi:10.1016/j.copbio.2018.08.012

178. Tremblay R, Wang D, Jevnikar AM, Ma S. Tobacco, a highly efficient green bioreactor for production of therapeutic proteins. *Biotechnol Adv*. 2010;28(2):214-221. doi:10.1016/j.biotechadv.2009.11.008

179. Bally J, Jung H, Mortimer C, et al. The Rise and Rise of Nicotiana benthamiana : A Plant for All Reasons. *Annu Rev Phytopathol*. 2018;56(1):405-426. doi:10.1146/annurev-phyto-080417-050141

180. Spiegel H, Stöger E, Twyman RM, Buyel JF. Current Status and Perspectives of the Molecular Farming Landscape. In: *Molecular Pharming*. Hoboken, NJ, USA: John Wiley & Sons, Inc.; 2018:1-23. doi:10.1002/9781118801512.ch1

181. Yao J, Weng Y, Dickey A, Wang KY. Plants as factories for human pharmaceuticals: Applications and challenges. *Int J Mol Sci*. 2015;16(12):28549-28565. doi:10.3390/ijms161226122

182. Buyel JF. Plant Molecular Farming - Integration and Exploitation of Side Streams to Achieve Sustainable Biomanufacturing. *Front Plant Sci*. 2018;9:1893. doi:10.3389/fpls.2018.01893

183. Tsekoa TL, Singh AA, Buthelezi SG. Molecular farming for therapies and vaccines in Africa. *Curr Opin Biotechnol*. 2020;61:89-95. doi:10.1016/j.copbio.2019.11.005

184. Buyel JF, Twyman RM, Fischer R. Very-large-scale production of antibodies in plants: The biologization of manufacturing. *Biotechnol Adv*. 2017;35(4):458-465. doi:10.1016/j.biotechadv.2017.03.011

185. Ma JKC, Drossard J, Lewis D, et al. Regulatory approval and a first-in-human phase I clinical trial of a monoclonal antibody produced in transgenic tobacco plants. *Plant Biotechnol J*. 2015;13(8):1106-1120. doi:10.1111/pbi.12416

186. Hamada A, Yamaguchi KI, Harada M, Horiguchi KI, Takahashi T, Honda H. Recombinant, rice-produced yeast phytase shows the ability to hydrolyze phytate derived from seed-based feed, and extreme stability during ensilage treatment. *Biosci Biotechnol Biochem*. 2006;70(6):1524-1527. doi:10.1271/bbb.60039

187. Rocha I, Ma Y, Souza-Alonso P, Vosátka M, Freitas H, Oliveira RS. Seed Coating: A Tool for Delivering Beneficial Microbes to Agricultural Crops. *Front Plant Sci*. 2019;10:1357. doi:10.3389/fpls.2019.01357

188. Finger R, Swinton SM, El Benni N, Walter A. Precision Farming at the Nexus of Agricultural Production and the Environment. *Annu Rev Resour Econ*. 2019;11(1):313-335. doi:10.1146/annurev-resource-100518-093929

189. King A. Technology: The future of agriculture. *Nature*. 2017;544:S21-S23.

190. Avis KE, Wu VL, eds. *Biotechnology and Biopharmaceutical Manufacturing, Processing, and Preservation*. CRC Press; 1996.

191. Achilleos EC, Calandranis JC, Petrides DP. Quantifying the impact of uncertain parameters in the batch manufacturing of active pharmaceutical ingredients. *Pharm Eng*. 2006;26(34).

192. Wann M, Raper CD. A Dynamic Model for Plant Growth: Validation Study Under Changing Temperatures. *Ann Bot*. 1984;53(1):45-52.

193. Wann M, Rapper CD, Lucas HL. A dynamic model for plant growth: A simulation of dry matter accumulation for tobacco. *Photosynthetica*. 1978;12:121-136.

194. Meyer CE, Schneider WF. *NASA Advanced Exploration Systems: 2018 Advancements in Life Support Systems*.; 2018. https://ntrs.nasa.gov/search.jsp?R=20180006596.

195. Jackson S. Life Support Systems. 2016. https://www.nasa.gov/content/life-support-systems. Accessed October 30, 2017.

196. Hu S, Barzilla JE, Semones E. Acute radiation risk assessment and mitigation strategies in near future exploration spaceflights. *Life Sci Sp Res*. 2020;24:25-33. doi:10.1016/j.lssr.2019.10.006

197. Chancellor JC, Blue RS, Cengel KA, et al. Limitations in predicting the space radiation health risk for exploration astronauts. *npj Microgravity*. 2018;4(1):1-11. doi:10.1038/s41526-018-0043-2

198. Gambacurta A, Merlini G, Ruggiero C, et al. Human osteogenic differentiation in Space: Proteomic and epigenetic clues to better understand osteoporosis. *Sci Rep*. 2019;9(1):1-10. doi:10.1038/s41598-019-44593-6

199. Sibonga JD. Spaceflight-induced bone loss: Is there an Osteoporosis Risk? *Curr Osteoporos Rep*. 2013;11(2):92-98. doi:10.1007/s11914-013-0136-5

200. Kassemi M, Thompson D. Prediction of renal crystalline size distributions in space using a PBE analytic model. 1. Effect of microgravity-induced biochemical alterations. *Am J Physiol Ren Physiol*. 2016;311:520-530. doi:10.1152/ajprenal.00401.2015.-An

201. Çiftçioğlu N, Haddad RS, Golden DC, Morrison DR, McKay DS. A potential cause for kidney stone formation during space flights: Enhanced growth of nanobacteria in microgravity. *Kidney Int*. 2005;67(2):483-491. doi:10.1111/j.1523-1755.2005.67105.x

202. Zhang LF, Hargens AR. Spaceflight-induced intracranial hypertension and visual impairment: Pathophysiology and countermeasures. *Physiol Rev*. 2018;98(1):59-87. doi:10.1152/physrev.00017.2016

203. Jandial R, Hoshide R, Waters JD, Limoli CL. Space-brain: The negative effects of space exposure on the central nervous system. *Surg Neurol Int*. 2018;9(1). doi:10.4103/sni.sni_250_17

204. Taylor PW. Impact of space flight on bacterial virulence and antibiotic susceptibility. *Infect Drug Resist*. 2015;8:249-262. doi:10.2147/IDR.S67275

205. Trudel G, Shafer J, Laneuville O, Ramsay T. Characterizing the effect of exposure to microgravity on anemia: more space is worse. *Am J Hematol*. 2020;95(3):267-273.

doi:10.1002/ajh.25699

206. Sobisch LY, Rogowski KM, Fuchs J, et al. Biofilm forming antibiotic resistant gram-positive pathogens isolated from surfaces on the international space station. *Front Microbiol*. 2019;10(MAR):543. doi:10.3389/fmicb.2019.00543

207. Garrett-Bakelman FE, Darshi M, Green SJ, et al. The NASA twins study: A multidimensional analysis of a year-long human spaceflight. *Science (80-).* 2019;364(6436). doi:10.1126/science.aau8650

208. Menezes AA, Cumbers J, Hogan JA, Arkin AP. Towards synthetic biological approaches to resource utilization on space missions. *J R Soc Interface*. 2015;12(102):20140715. doi:10.1098/rsif.2014.0715

209. Blue RS, Bayuse TM, Daniels VR, et al. Supplying a pharmacy for NASA exploration spaceflight: challenges and current understanding. *npj Microgravity*. 2019;5(1):14. doi:10.1038/s41526-019-0075-2

210. Mazzeo A, Carpenter P. Stability Studies for Biologics. In: *Handbook of Stability Testing in Pharmaceutical Development*. Springer New York; 2009:353-369. doi:10.1007/978-0-387-85627-8_17

211. Reynolds T, de Zafra C, Kim A, Gelzleichter TR. Overview of Biopharmaceuticals and Comparison with Small-molecule Drug Development. In: *Nonclinical Development of Novel Biologics, Biosimilars, Vaccines and Specialty Biologics*. Elsevier Inc.; 2013:3-33. doi:10.1016/B978-0-12-394810-6.00001-0

212. Barratt MR, Pool SL. *Principles of Clinical Medicine for Space Flight*. Springer New York; 2008. doi:10.1007/978-0-387-68164-1

213. Menezes AA, Montague MG, Cumbers J, Hogan JA, Arkin AP. Grand challenges in space synthetic biology. *J R Soc Interface*. 2015;12(113):20150803. doi:10.1098/rsif.2015.0803

214. Nangle SN, Wolfson MY, Hartsough L, et al. The case for biotech on Mars. *Nat Biotechnol*. 2020;38(4):401-407. doi:10.1038/s41587-020-0485-4

215. Vlieghe P, Lisowski V, Martinez J, Khrestchatisky M. Synthetic therapeutic peptides: science and market. *Drug Discov Today*. 2010;15(1-2):40-56. doi:10.1016/j.drudis.2009.10.009

216. Uhlig T, Kyprianou T, Martinelli FG, et al. The emergence of peptides in the pharmaceutical business: From exploration to exploitation. *EuPA Open Proteomics*. 2014;4:58-69. doi:10.1016/j.euprot.2014.05.003

217. Hao M, Qiao J, Qi H. Current and emerging methods for the synthesis of single-stranded DNA. *Genes (Basel)*. 2020;11(2):116. doi:10.3390/genes11020116

218. Cortesão M, Schütze T, Marx R, Moeller R, Meyer V. Fungal Biotechnology in Space: Why and How? In: ; 2020:501-535. doi:10.1007/978-3-030-29541-7_18

219. Llorente B, Williams TC, Goold HD. The Multiplanetary Future of Plant Synthetic Biology. *Genes (Basel)*. 2018;9(7). doi:10.3390/genes9070348

220. Wheeler RM. Agriculture for Space: People and Places Paving the Way. *Open Agric*. 2017;2(1):14-32.

221. Khodadad CLM, Hummerick ME, Spencer LE, et al. Microbiological and Nutritional Analysis of Lettuce Crops Grown on the International Space Station. *Front Plant Sci*. 2020;11:199. doi:10.3389/fpls.2020.00199

222. Wolff S, Coelho L, Karoliussen I, Jost A-I. Effects of the Extraterrestrial Environment on Plants: Recommendations for Future Space Experiments for the MELiSSA Higher Plant Compartment. *Life*. 2014;4(2):189-204. doi:10.3390/life4020189

223. Nelson M, Pechurkin NS, Allen JP, Somova LA, Gitelson JI. Closed Ecological Systems, Space Life Support and Biospherics. In: *Environmental Biotechnology*. Humana Press; 2010:517-565. doi:10.1007/978-1-60327-140-0_11

224. Odeh R, Guy CL. Gardening for Therapeutic People-Plant Interactions during Long-Duration Space Missions. *Open Agric*. 2017;2(1):1-13.

225. Lomonossoff GP, D'Aoust MA. Plant-produced biopharmaceuticals: A case of technical developments driving clinical deployment. *Science (80-)*. 2016;353(6305):1237-1240. doi:10.1126/science.aaf6638

226. Fabricant DS, Farnsworth NR. The value of plants used in traditional medicine for drug discovery. *Environ Health Perspect*. 2001;109(suppl 1):69-75. doi:10.1289/ehp.01109s169

227. Desborough MJR, Keeling DM. The aspirin story - from willow to wonder drug. *Br J Haematol*. 2017;177(5):674-683. doi:10.1111/bjh.14520

228. Zhu L, Chen L. Progress in research on paclitaxel and tumor immunotherapy. *Cell Mol Biol Lett*. 2019;24(1). doi:10.1186/s11658-019-0164-y

229. Haq TA, Mason HS, Clements JD, Arntzen CJ. Oral immunization with a recombinant bacterial antigen produced in transgenic plants. *Science (80-)*. 1995;268(5211):714-716. doi:10.1126/science.7732379

230. Hood EE, Witcher DR, Maddock S, et al. Commercial production of avidin from transgenic maizecharacterization of transformant, production, processing, extraction and purification. *Mol Breed*. 1997;3(4):291-306. doi:10.1023/A:1009676322162

231. Sack M, Hofbauer A, Fischer R, Stoger E. The increasing value of plant-made proteins. *Curr Opin Biotechnol*. 2015;32:163-170. doi:10.1016/j.copbio.2014.12.008

232. Aldag C, Teixeira DN, Leventhal PS. Skin rejuvenation using cosmetic products containing growth factors, cytokines, and matrikines: A review of the literature. *Clin Cosmet Investig Dermatol*. 2016;9:411-419. doi:10.2147/CCID.S116158

233. Zhang D, Nandi S, Bryan P, et al. Expression, purification, and characterization of recombinant human transferrin from rice (Oryza sativa L.). *Protein Expr Purif*. 2010;74(1):69-79. doi:10.1016/j.pep.2010.04.019

234. Gergerich RC, Dolja V V. Introduction to Plant Viruses, the Invisible Foe. *Plant Heal*

Instr. 2006. doi:10.1094/phi-i-2006-0414-01

235. Gelvin SB. Agrobacterium-mediated plant transformation: the biology behind the "gene-jockeying" tool. *Microbiol Mol Biol Rev*. 2003;67(1):16-37, table of contents. doi:10.1128/MMBR.67.1.16-37.2003

236. Lakshmanan M, Kodama Y, Yoshizumi T, Sudesh K, Numata K. Rapid and efficient gene delivery into plant cells using designed peptide carriers. *Biomacromolecules*. 2013;14(1):10-16. doi:10.1021/bm301275g

237. Bao W, Wang J, Wang Q, O'Hare D, Wan Y. Layered double hydroxide nanotransporter for molecule delivery to intact plant cells. *Sci Rep*. 2016;6. doi:10.1038/srep26738

238. Gunadi A, Dean EA, Finer JJ. Transient transformation using particle bombardment for gene expression analysis. In: *Methods in Molecular Biology*. Vol 1864. Humana Press Inc.; 2019:67-79. doi:10.1007/978-1-4939-8778-8_5

239. Meyers B, Zaltsman A, Lacroix B, Kozlovsky S V., Krichevsky A. Nuclear and plastid genetic engineering of plants: Comparison of opportunities and challenges. *Biotechnol Adv*. 2010;28(6):747-756. doi:10.1016/j.biotechadv.2010.05.022

240. Borghi L. Inducible gene expression systems for plants. *Methods Mol Biol*. 2010;655:65-75. doi:10.1007/978-1-60761-765-5_5

241. Thomas DR, Penney CA, Majumder A, Walmsley AM. Evolution of plant-made pharmaceuticals. *Int J Mol Sci*. 2011;12(5):3220-3236. doi:10.3390/ijms12053220

242. Cooper M, Douglas G, Perchonok M. Developing the NASA Food System for Long-Duration Missions. *J Food Sci*. 2011;76(2):R40-R48. doi:10.1111/j.1750-3841.2010.01982.x

243. Zwart SR, Kloeris VL, Perchonok MH, Braby L, Smith SM. Assessment of Nutrient Stability in Foods from the Space Food System After Long-Duration Spaceflight on the ISS. *J Food Sci*. 2009;74(7):H209-H217. doi:10.1111/j.1750-3841.2009.01265.x

244. Goulette TR, Zhou J, Dixon WR, et al. Kinetic parameters of thiamine degradation in NASA spaceflight foods determined by the endpoints method for long-term storage. *Food Chem*. 2020;302:125365. doi:10.1016/j.foodchem.2019.125365

245. Cooper M, Perchonok M, Douglas GL. Initial assessment of the nutritional quality of the space food system over three years of ambient storage. *npj Microgravity*. 2017;3(1). doi:10.1038/s41526-017-0022-z

246. Smith SM, Rice BL, Dlouhy H, Zwart SR. Assessment of Nutritional Intake During Space Flight and Space Flight Analogs. *Procedia Food Sci*. 2013;2:27-34. doi:10.1016/j.profoo.2013.04.006

247. Anderson MS, Ewert MK, Keener JF. *Life Support Baseline Values and Assumptions Document*.; 2018. doi:NASA/TP-2015–218570/REV1

248. Edeen MA, Dominick JS, Barta DJ, Packham NJC. Control of air revitalization using plants: Results of the early human testing initiative phase i test. In: *SAE Technical Papers*.

SAE International; 1996. doi:10.4271/961522

249. Ramessar K, Capell T, Christou P. Molecular pharming in cereal crops. In: *Phytochemistry Reviews*. Vol 7. Springer; 2008:579-592. doi:10.1007/s11101-008-9087-3

250. Chen Q, Dent M, Hurtado J, et al. Transient protein expression by agroinfiltration in lettuce. In: *Methods in Molecular Biology*. Vol 1385. ; 2016:55-67. doi:10.1007/978-1-4939-3289-4_4

251. Joh LD, Wroblewski T, Ewing NN, VanderGheynst JS. High-level transient expression of recombinant protein in lettuce. *Biotechnol Bioeng*. 2005;91(7):861-871. doi:10.1002/bit.20557

252. Castañón S, Marín MS, Martín-Alonso JM, et al. Immunization with potato plants expressing VP60 protein protects against rabbit hemorrhagic disease virus. *J Virol*. 1999;73(5):4452-4455.

253. Zhang Y, Chen M, Siemiatkowska B, et al. A Highly Efficient Agrobacterium-Mediated Method for Transient Gene Expression and Functional Studies in Multipe Plant Species. *Plant Commun*. February 2020:100028. doi:10.1016/j.xplc.2020.100028

254. Fujiuchi N, Matsuda R, Matoba N, Fujiwara K. Removal of bacterial suspension water occupying the intercellular space of detached leaves after agroinfiltration improves the yield of recombinant hemagglutinin in a Nicotiana benthamiana transient gene expression system. *Biotechnol Bioeng*. 2016;113(4):901-906. doi:10.1002/bit.25854

255. Plesha MA, Huang T-K, Dandekar AM, Falk BW, McDonald KA. High-Level Transient Production of a Heterologous Protein in Plants by Optimizing Induction of a Chemically Inducible Viral Amplicon Expression System. *Biotechnol Prog*. 2007;23(6):1277-1285. doi:10.1021/bp070238s

256. Lamson NG, Fein KC, Gleeson JP, et al. From Farm to Pharmacy: Strawberry-Enabled Oral Delivery of Protein Drugs. *bioRxiv*. March 2020:2020.03.11.987461. doi:10.1101/2020.03.11.987461

257. Kapusta J, Modelska A, Figlerowicz M, et al. A plant-derived edible vaccine against hepatitis B virus. *FASEB J*. 1999;13(13):1796-1799.

258. Thanavala Y, Mahoney M, Pal S, et al. Immunogenicity in humans of an edible vaccine for hepatitis B. *Proc Natl Acad Sci U S A*. 2005;102(9):3378-3382. doi:10.1073/pnas.0409899102

259. Cohen SN, Chang ACY, Boyer HW, Helling RB. Construction of biologically functional bacterial plasmids in vitro. *Proc Natl Acad Sci U S A*. 1973;70(11):3240-3244. doi:10.1073/pnas.70.11.3240

260. Isabella VM, Ha BN, Castillo MJ, et al. Development of a synthetic live bacterial therapeutic for the human metabolic disease phenylketonuria. *Nat Biotechnol*. 2018;36(9):857-867. doi:10.1038/nbt.4222

261. Anguela XM, High KA. Entering the Modern Era of Gene Therapy. *Annu Rev Med*. 2019;70(1):273-288. doi:10.1146/annurev-med-012017-043332

262. Li C, Wang J, Wang Y, et al. Recent progress in drug delivery. *Acta Pharm Sin B*. 2019;9(6):1145-1162. doi:10.1016/j.apsb.2019.08.003

263. Feng M, Peng J, Song C, Wang Y. Mammalian cell cultivation in space. *Microgravity Sci Technol*. 1994;7(2):207-210.

264. Sani RL, Koster JN, eds. *Low-Gravity Fluid Dynamics and Transport Phenomena*. Washington DC: American Institute of Aeronautics and Astronautics; 1990. doi:10.2514/4.866036

265. Adam JA, Gulati S, Hirsa AH, Bonocora RP. Growth of microorganisms in an interfacially driven space bioreactor analog. *npj Microgravity*. 2020;6(1):1-7. doi:10.1038/s41526-020-0101-4

266. Walther I. Space bioreactors and their applications. *Adv Space Biol Med*. 2002;8:197-213. doi:10.1016/s1569-2574(02)08020-6

267. Gòdia F, Albiol J, Montesinos JL, et al. MELISSA: A loop of interconnected bioreactors to develop life support in Space. *J Biotechnol*. 2002;99(3):319-330. doi:10.1016/S0168-1656(02)00222-5

268. Lotfipour F, Hallaj-Nezhadi S. Microbial Quality Concerns for Biopharmaceuticals. In: *Latest Research into Quality Control*. InTech; 2012. doi:10.5772/52114

269. Merten OW. Virus contaminations of cell cultures - A biotechnological view. In: *Cytotechnology*. Vol 39. Nature Publishing Group; 2002:91-116. doi:10.1023/A:1022969101804

270. Aggarwal S. What's fueling the biotech engine - 2008. *Nat Biotechnol*. 2009;27(11):987-993. doi:10.1038/nbt1109-987

271. Jacquemart R, Vandersluis M, Zhao M, Sukhija K, Sidhu N, Stout J. A Single-use Strategy to Enable Manufacturing of Affordable Biologics. *Comput Struct Biotechnol J*. 2016;14:309-318. doi:10.1016/j.csbj.2016.06.007

272. Zhang J, Müller BSF, Tyre KN, et al. Competitive Growth Assay of Mutagenized Chlamydomonas reinhardtii Compatible With the International Space Station Veggie Plant Growth Chamber. *Front Plant Sci*. 2020;11:631. doi:10.3389/fpls.2020.00631

273. Matula EE, Nabity JA. Failure modes, causes, and effects of algal photobioreactors used to control a spacecraft environment. *Life Sci Sp Res*. 2019;20:35-52. doi:10.1016/j.lssr.2018.12.001

274. Olsson-Francis K, Cockell CS. Use of cyanobacteria for in-situ resource use in space applications. *Planet Space Sci*. 2010;58(10):1279-1285. doi:10.1016/j.pss.2010.05.005

275. Billi D, Baqué M, Verseux C, Rothschild L, de Vera JP. Desert cyanobacteria: Potential for space and earth applications. In: *Adaption of Microbial Life to Environmental Extremes: Novel Research Results and Application, Second Edition*. Springer International Publishing; 2017:133-146. doi:10.1007/978-3-319-48327-6_6

276. Sorkhoh N, Al-Hasan R, Radwan S, Höpner T. Self-cleaning of the Gulf . *Nature*.

1992;359(6391):109. doi:10.1038/359109a0

277. Singh JS, Kumar A, Rai AN, Singh DP. Cyanobacteria: A precious bio-resource in agriculture, ecosystem, and environmental sustainability. *Front Microbiol*. 2016;7(APR). doi:10.3389/fmicb.2016.00529

278. Stewart JJ, Adams WW, Escobar CM, López-Pozo M, Demmig-Adams B. Growth and Essential Carotenoid Micronutrients in Lemna gibba as a Function of Growth Light Intensity. *Front Plant Sci*. 2020;11:480. doi:10.3389/fpls.2020.00480

279. Furmaniak MA, Misztak AE, Franczuk MD, Wilmotte A, Waleron M, Waleron KF. Edible cyanobacterial genus Arthrospira: Actual state of the art in cultivation methods, genetics, and application in medicine. *Front Microbiol*. 2017;8(DEC):2541. doi:10.3389/fmicb.2017.02541

280. Torres-Tiji Y, Fields FJ, Mayfield SP. Microalgae as a future food source. *Biotechnol Adv*. March 2020:107536. doi:10.1016/j.biotechadv.2020.107536

281. Carroll AL, Case AE, Zhang A, Atsumi S. Metabolic engineering tools in model cyanobacteria. *Metab Eng*. 2018;50:47-56. doi:10.1016/j.ymben.2018.03.014

282. Gordon GC, Pfleger BF. Regulatory tools for controlling gene expression in cyanobacteria. In: *Advances in Experimental Medicine and Biology*. Vol 1080. Springer New York LLC; 2018:281-315. doi:10.1007/978-981-13-0854-3_12

283. Takeuchi R, Roberts J. Targeted Mutagenesis in Spirulina. 2017.

284. Levri JA, Fisher JW, Jones HW, et al. *Advanced Life Support Equivalent System Mass Guidelines Document ALS Equivalent System Mass Guidelines Document*. Moffett Field, CA; 2003.

285. Mindock J, Myers J, Latorella K, et al. *Exploration Medical System Trade Study Tools Overview*.; 2018.

286. Kwon K-C, Daniell H. Oral Delivery of Protein Drugs Bioencapsulated in Plant Cells. *Mol Ther*. 2016;24(8):1342-1350. doi:10.1038/mt.2016.115

287. Gomez-Marquez J, Hamad-Schifferli K. Distributed Biological Foundries for Global Health. *Adv Healthc Mater*. 2019;8(18):1900184. doi:10.1002/adhm.201900184

288. Morrow T, Felcone LH. Defining the difference: What Makes Biologics Unique. *Biotechnol Healthc*. 2004;1(4):24-29.

289. Knowles L, Luth W, Bubela T. Paving the road to personalized medicine: recommendations on regulatory, intellectual property and reimbursement challenges. *J Law Biosci*. 2017;4(3):453. doi:10.1093/JLB/LSX030

290. Carnell L, Blattnig S, Hu S, et al. *Human Health and Performance Risks of Space Exploration Missions*.; 2009.

291. Chancellor JC, Scott GBI, Sutton JP. Space radiation: The number one risk to astronaut health beyond low earth orbit. *Life*. 2014;4(3):491-510. doi:10.3390/life4030491

292. Lushbaugh CC. Reflections on Some Recent Progress in Human Radiobiology. In: Vol 3. Elsevier; 1969:277-314. doi:10.1016/b978-1-4832-3122-8.50012-3

293. Sibonga JD, Evans HJ, Smith SA, Spector E, Yardley G, Alwood J. *Risk of Early Onset Osteoporosis Due to Space Flight*.; 2017.

294. Smith SM, Heer M, Shackelford LC, et al. Bone metabolism and renal stone risk during International Space Station missions. *Bone*. 2015;81:712-720. doi:10.1016/j.bone.2015.10.002

295. Yee CM, Zak AJ, Hill BD, Wen F. The Coming Age of Insect Cells for Manufacturing and Development of Protein Therapeutics. *Ind Eng Chem Res*. 2018;57(31):10061-10070. doi:10.1021/acs.iecr.8b00985

296. Arunkarthick S, Asokan R, Aravintharaj R, Niveditha M, Kumar NKK. A Review of Insect Cell Culture: Establishment, Maintenance and Applications in Entomological Research. *J Entomol Sci*. 2017;52(3):261-273. doi:10.18474/jes17-02pt.1

297. Schneider Y-J, Agathos SN, Ikonomou L, Schneider Y-J, Agathos · S N. Insect cell culture for industrial production of recombinant proteins. *Artic Appl Microbiol Biotechnol*. 2003;62:1-20. doi:10.1007/s00253-003-1223-9

298. Fischer S, Otte K. CHO Cell Engineering for Improved Process Performance and Product Quality . In: *Cell Culture Engineering*. Wiley; 2019:207-250. doi:10.1002/9783527811410.ch9

299. Dumont J, Euwart D, Mei B, Estes S, Kshirsagar R. Human cell lines for biopharmaceutical manufacturing: history, status, and future perspectives. *Crit Rev Biotechnol*. 2016;36(6):1110-1122. doi:10.3109/07388551.2015.1084266

300. Bandaranayake AD, Almo SC. Recent advances in mammalian protein production. *FEBS Lett*. 2014;588(2):253-260. doi:10.1016/j.febslet.2013.11.035

301. Xu J, Zhang N. On the way to commercializing plant cell culture platform for biopharmaceuticals: present status and prospect. *Pharm Bioprocess*. 2014;2(6):499-518. doi:10.4155/pbp.14.32

302. Gerasimova S V., Smirnova OG, Kochetov A V., Shumnyi VK. Production of recombinant proteins in plant cells. *Russ J Plant Physiol*. 2016;63(1):26-37. doi:10.1134/S1021443716010076

303. Claassens NJ, Sousa DZ, Dos Santos VAPM, De Vos WM, Van Der Oost J. Harnessing the power of microbial autotrophy. *Nat Rev Microbiol*. 2016;14(11):692-706. doi:10.1038/nrmicro.2016.130

304. Vijayakumar S, Menakha M. Pharmaceutical applications of cyanobacteria-A review. *J Acute Med*. 2015;5(1):15-23. doi:10.1016/j.jacme.2015.02.004

305. Lau N-S, Matsui M, Abdullah AA-A. Cyanobacteria: Photoautotrophic Microbial Factories for the Sustainable Synthesis of Industrial Products. *Biomed Res Int*. 2015;2015. doi:10.1155/2015

306. Jozala AF, Geraldes DC, Tundisi LL, et al. Biopharmaceuticals from microorganisms: from production to purification. *Brazilian J Microbiol*. 2016;47:51-63. doi:10.1016/j.bjm.2016.10.007

307. Pham J V., Yilma MA, Feliz A, et al. A review of the microbial production of bioactive natural products and biologics. *Front Microbiol*. 2019;10(JUN):1404. doi:10.3389/fmicb.2019.01404

308. Baeshen MN, Al-Hejin AM, Bora RS, et al. Production of biopharmaceuticals in E. Coli: Current scenario and future perspectives. *J Microbiol Biotechnol*. 2015;25(7):953-962. doi:10.4014/jmb.1412.12079

309. Nielsen J. Production of biopharmaceutical proteins by yeast. *Bioengineered*. 2013;4(4):207-211. doi:10.4161/bioe.22856

310. Fidan O, Zhan J. Recent advances in engineering yeast for pharmaceutical protein production. *RSC Adv*. 2015;5(105):86665-86674. doi:10.1039/c5ra13003d

311. Walker RSK, Pretorius IS. Applications of yeast synthetic biology geared towards the production of biopharmaceuticals. *Genes (Basel)*. 2018;9(7). doi:10.3390/genes9070340

312. Silverman AD, Karim AS, Jewett MC. Cell-free gene expression: an expanded repertoire of applications. *Nat Rev Genet*. 2020;21(3):151-170. doi:10.1038/s41576-019-0186-3

313. Khambhati K, Bhattacharjee G, Gohil N, Braddick D, Kulkarni V, Singh V. Exploring the Potential of Cell-Free Protein Synthesis for Extending the Abilities of Biological Systems. *Front Bioeng Biotechnol*. 2019;7:248. doi:10.3389/fbioe.2019.00248

314. Tinafar A, Jaenes K, Pardee K. Synthetic Biology Goes Cell-Free. *BMC Biol*. 2019;17(1):1-14. doi:10.1186/s12915-019-0685-x

315. Bertolini LR, Meade H, Lazzarotto CR, et al. The transgenic animal platform for biopharmaceutical production. *Transgenic Res*. 2016;25(3):329-343. doi:10.1007/s11248-016-9933-9

316. Houdebine LM. Production of pharmaceutical proteins by transgenic animals. *Comp Immunol Microbiol Infect Dis*. 2009;32(2):107-121. doi:10.1016/j.cimid.2007.11.005

317. Niemann H, Kind A, Schnieke A. Production of Biopharmaceuticals in Transgenic Animals. In: *Pharmaceutical Biotechnology*. Weinheim, Germany: Wiley-VCH Verlag GmbH & Co. KGaA; 2012:71-111. doi:10.1002/9783527632909.ch5

318. Giddings G, Allison G, Brooks D, Carter A. Transgenic plants as factories for biopharmaceuticals. *Nat Biotechnol*. 2000;18(11):1151-1155. doi:10.1038/81132

319. Sack M, Rademacher T, Spiegel H, et al. From gene to harvest: Insights into upstream process development for the GMP production of a monoclonal antibody in transgenic tobacco plants. *Plant Biotechnol J*. 2015;13(8):1094-1105. doi:10.1111/pbi.12438

320. Kopertekh L, Schiemann J. Transient Production of Recombinant Pharmaceutical Proteins in Plants: Evolution and Perspectives. *Curr Med Chem*. 2017;26(3):365-380. doi:10.2174/0929867324666170718114724

321. Burnett MJB, Burnett AC. Therapeutic recombinant protein production in plants: Challenges and opportunities. *PLANTS, PEOPLE, PLANET*. 2019;2(2):121-132. doi:10.1002/ppp3.10073

322. Bamogo PKA, Brugidou C, Sérémé D, et al. Virus-based pharmaceutical production in plants: An opportunity to reduce health problems in Africa. *Virol J*. 2019;16(1):1-16. doi:10.1186/s12985-019-1263-0

323. National Institues of Health Office of Dietary Supplements. Nutrient Recommendations : Dietary Reference Intakes (DRI). https://ods.od.nih.gov/Health_Information/Dietary_Reference_Intakes.aspx. Accessed May 25, 2020.

324. U.S. Department of Agriculture Agricultural Research Service. FoodData Central. https://fdc.nal.usda.gov/index.html. Accessed May 25, 2020.

325. Overview | Mission – NASA's InSight Mars Lander. https://mars.nasa.gov/insight/mission/overview/.

326. Afshinnekoo E, Scott RT, MacKay MJ, et al. Fundamental Biological Features of Spaceflight: Advancing the Field to Enable Deep-Space Exploration. *Cell*. 2020;183(5):1162-1184. doi:10.1016/j.cell.2020.10.050

327. Du B, Daniels VR, Vaksman Z, Boyd JL, Crady C, Putcha L. Evaluation of physical and chemical changes in pharmaceuticals flown on space missions. *AAPS J*. 2011;13(2):299-308. doi:10.1208/s12248-011-9270-0

328. McNulty MJ, Xiong Y (Mary), Yates K, et al. Molecular pharming to support human life on the moon, mars, and beyond. *Crit Rev Biotechnol*. March 2021:1-16. doi:10.1080/07388551.2021.1888070

329. Berliner AJ, Hilzinger JM, Abel AJ, et al. Towards a Biomanufactory on Mars. December 2020. doi:10.20944/preprints202012.0714.v1

330. Škalko-Basnet N. Biologics: The role of delivery systems in improved therapy. *Biol Targets Ther*. 2014;8:107-114. doi:10.2147/BTT.S38387

331. Haile LA, Puig M, Kelley-Baker L, Verthelyi D. Detection of Innate Immune Response Modulating Impurities in Therapeutic Proteins. Allen IC, ed. *PLoS One*. 2015;10(4):e0125078. doi:10.1371/journal.pone.0125078

332. Rathore AS, Pathak M, Ma G, Bracewell DG. Re-use of Protein A Resin: Fouling and Economics. *BioPharm Int*. 2015;3(28). http://www.processdevelopmentforum.com/articles/re-use-of-protein-a-resin-fouling-and-economics/. Accessed March 31, 2021.

333. Sykes C. Time- and temperature-controlled transport: Supply chain challenges and solutions. *P T*. 2018;43(3):154. /pmc/articles/PMC5821242/. Accessed April 20, 2021.

334. Strube J, Ditz R, Kornecki M, et al. Process intensification in biologics manufacturing. *Chem Eng Process - Process Intensif*. 2018;133:278-293. doi:10.1016/J.CEP.2018.09.022

335. Steinebach F, Karst D, Morbidelli M. Design of Integrated Continuous Processes for High-Quality Biotherapeutics. In: *Continuous Biomanufacturing - Innovative Technologies and Methods*. Weinheim, Germany: Wiley-VCH Verlag GmbH & Co. KGaA; 2017:457-480. doi:10.1002/9783527699902.ch16

336. Pollard D, Brower M, Richardson D. Progress Toward Automated Single-Use Continuous Monoclonal Antibody Manufacturing via the Protein Refinery Operations Lab. In: *Continuous Biomanufacturing - Innovative Technologies and Methods*. Weinheim, Germany: Wiley-VCH Verlag GmbH & Co. KGaA; 2017:107-130. doi:10.1002/9783527699902.ch4

337. Adiga R, Al-adhami M, Andar A, et al. Point-of-care production of therapeutic proteins of good-manufacturing-practice quality. *Nat Biomed Eng*. 2018;2(9):675-686. doi:10.1038/s41551-018-0259-1

338. Crowell LE, Lu AE, Love KR, et al. On-demand manufacturing of clinical-quality biopharmaceuticals. *Nat Biotechnol*. 2018;36(10):988. doi:10.1038/nbt.4262

339. Bell MR, Engleka MJ, Malik A, Strickler JE. To fuse or not to fuse: What is your purpose? *Protein Sci*. 2013;22(11):1466-1477. doi:10.1002/pro.2356

340. Sheth RD, Jin M, Bhut B V., Li Z, Chen W, Cramer SM. Affinity precipitation of a monoclonal antibody from an industrial harvest feedstock using an ELP-Z stimuli responsive biopolymer. *Biotechnol Bioeng*. 2014;111(8):1595-1603. doi:10.1002/bit.25230

341. Jugler C, Joensuu J, Chen Q. Hydrophobin-protein a fusion protein produced in plants efficiently purified an anti-west nile virus monoclonal antibody from plant extracts via aqueous two-phase separation. *Int J Mol Sci*. 2020;21(6). doi:10.3390/ijms21062140

342. Werner S, Marillonnet S, Hause G, Klimyuk V, Gleba Y. Immunoabsorbent nanoparticles based on a tobamovirus displaying protein A. *Proc Natl Acad Sci U S A*. 2006;103(47):17678-17683. doi:10.1073/pnas.0608869103

343. Uhde-Holzem K, McBurney M, Tiu BDB, et al. Production of Immunoabsorbent Nanoparticles by Displaying Single-Domain Protein A on Potato Virus X. *Macromol Biosci*. 2016;16(2):231-241. doi:10.1002/mabi.201500280

344. Anselmo AC, Gokarn Y, Mitragotri S. Non-invasive delivery strategies for biologics. *Nat Rev Drug Discov*. 2018;18(1):19-40. doi:10.1038/nrd.2018.183

345. Mitragotri S, Burke PA, Langer R. Overcoming the challenges in administering biopharmaceuticals: Formulation and delivery strategies. *Nat Rev Drug Discov*. 2014;13(9):655-672. doi:10.1038/nrd4363

346. Kwon K-C, Daniell H. Low-cost oral delivery of protein drugs bioencapsulated in plant cells. *Plant Biotechnol J*. 2015;13(8):1017-1022. doi:10.1111/pbi.12462

347. Vickery BP, Vereda A, Casale TB, et al. AR101 Oral Immunotherapy for Peanut Allergy. *N Engl J Med*. 2018;379(21):1991-2001. doi:10.1056/NEJMoa1812856

348. Wall M. NASA's Shuttle Program Cost $209 Billion - Was it Worth It? | Space.

Space.com. https://www.space.com/12166-space-shuttle-program-cost-promises-209-billion.html. Published 2011.

349. Whealan George K. The Economic Impacts of the Commercial Space Industry. *Space Policy*. 2019;47:181-186. doi:10.1016/j.spacepol.2018.12.003

350. Ramos-de-la-Peña AM, González-Valdez J, Aguilar O. Protein A chromatography: Challenges and progress in the purification of monoclonal antibodies. *J Sep Sci*. 2019;42(9):1816-1827. doi:10.1002/jssc.201800963

351. Jones HW. The cost and Equivalent System Mass of space crew time. In: *SAE Technical Papers*. SAE International; 2001. doi:10.4271/2001-01-2359

352. Sheldon RA. The E Factor: Fifteen years on. *Green Chem*. 2007;9(12):1273-1283. doi:10.1039/b713736m

353. Tylecote A. Biotechnology as a new techno-economic paradigm that will help drive the world economy and mitigate climate change. *Res Policy*. 2019;48(4):858-868. doi:10.1016/j.respol.2018.10.001

354. Drake BG, Watts KD. *Human Exploration of Mars Design Reference Architecture 5.0 Addendum #2*.; 2014. http://www.sti.nasa.gov. Accessed March 7, 2021.

355. Hendrickx L, De Wever H, Hermans V, et al. Microbial ecology of the closed artificial ecosystem MELiSSA (Micro-Ecological Life Support System Alternative): Reinventing and compartmentalizing the Earth's food and oxygen regeneration system for long-haul space exploration missions. In: *Research in Microbiology*. Vol 157. Elsevier Masson; 2006:77-86. doi:10.1016/j.resmic.2005.06.014

356. Hogan JA, Kang S, Cavazzoni J, Levri JA, Finn C, Luna B. *A Simulation Study Comparing Incineration and Composting in a Mars-Based Advanced Life Support System*. Moffett Field, CA; 2000. doi:NASA Document ID 20000121172

357. Zabel P. Influence of crop cultivation conditions on space greenhouse equivalent system mass. *CEAS Sp J*. 2020;13(1):3-15. doi:10.1007/s12567-020-00317-5

358. Berliner AJ, Makrygiorgos G, Hill A. Extension of Equivalent System Mass for Human Exploration Missions on Mars. January 2021. doi:10.20944/preprints202101.0363.v1

359. Bizzarri M, Masiello MG, Cucina A, Guzzi R. Journey to Mars: A Biomedical Challenge. Perspective on future human space flight. *J Biol Sci hypotheses Opin*. 2017;1(2):15-26. doi:10.13133/2532-5876_2.6

360. Faienza MF, Chiarito M, D'amato G, et al. Monoclonal antibodies for treating osteoporosis. *Expert Opin Biol Ther*. 2018;18(2):149-157. doi:10.1080/14712598.2018.1401607

361. Schuster NM, Rapoport AM. New strategies for the treatment and prevention of primary headache disorders. *Nat Rev Neurol*. 2016;12(11):635-650. doi:10.1038/nrneurol.2016.143

362. Zhao J, Wang Y, Xu C, et al. Therapeutic potential of an anti-high mobility group box-1

monoclonal antibody in epilepsy. *Brain Behav Immun*. 2017;64:308-319. doi:10.1016/j.bbi.2017.02.002

363. Hua L, Hilliard JJ, Shi Y, et al. Assessment of an anti-alpha-toxin monoclonal antibody for prevention and treatment of Staphylococcus aureus-induced pneumonia. *Antimicrob Agents Chemother*. 2014;58(2):1108-1117. doi:10.1128/AAC.02190-13

364. Krawczyk A, Dirks M, Kasper M, et al. Prevention of Herpes Simplex Virus Induced Stromal Keratitis by a Glycoprotein B-Specific Monoclonal Antibody. BenMohamed L, ed. *PLoS One*. 2015;10(1):e0116800. doi:10.1371/journal.pone.0116800

365. Iino Y, Takahashi E, Ida S, Kikuchi S. Clinical efficacy of anti-IL-5 monoclonal antibody mepolizumab in the treatment of eosinophilic otitis media. *Auris Nasus Larynx*. 2019;46(2):196-203. doi:10.1016/j.anl.2018.07.011

366. Zahavi D, Weiner L. Monoclonal Antibodies in Cancer Therapy. *Antibodies*. 2020;9(3):34. doi:10.3390/antib9030034

367. Ulrich S, Ebel F. Monoclonal Antibodies as Tools to Combat Fungal Infections. *J Fungi*. 2020;6(1):22. doi:10.3390/jof6010022

368. Laptoš T, Omersel J. The importance of handling high-value biologicals: Physico-chemical instability and immunogenicity of monoclonal antibodies. *Exp Ther Med*. 2018;15(4):3161. doi:10.3892/ETM.2018.5821

369. Goding JW. *Monoclonal Antibodies*. 3rd ed. Academic Press; 1996. https://www.elsevier.com/books/monoclonal-antibodies/goding/978-0-12-287023-1. Accessed March 31, 2021.

370. Kang TH, Jung ST. Boosting therapeutic potency of antibodies by taming Fc domain functions. *Exp Mol Med*. 2019;51(11):138. doi:10.1038/s12276-019-0345-9

371. Sommerfeld S, Strube J. Challenges in biotechnology production - Generic processes and process optimization for monoclonal antibodies. *Chem Eng Process Process Intensif*. 2005;44(10):1123-1137. doi:10.1016/j.cep.2005.03.006

372. Choe W, Durgannavar T, Chung S. Fc-Binding Ligands of Immunoglobulin G: An Overview of High Affinity Proteins and Peptides. *Materials (Basel)*. 2016;9(12):994. doi:10.3390/ma9120994

373. *Affinity Chromatography Handbook, Vol. 1: Antibodies*.; 2021. https://cdn.cytivalifesciences.com/dmm3bwsv3/AssetStream.aspx?mediaformatid=10061&destinationid=10016&assetid=11660. Accessed March 28, 2021.

374. *Protein A HP SpinTrap Product Booklet*.; 2006. https://www.cytivalifesciences.co.jp/tech_support/manual/pdf/28906770.pdf. Accessed March 28, 2021.

375. *Protein A Mag Sepharose Xtra Protein G Mag Sepharose Xtra Affinity Chromatography Instructions for Use*.; 2020. https://cdn.cytivalifesciences.com/dmm3bwsv3/AssetStream.aspx?mediaformatid=10061&destinationid=10016&assetid=15782. Accessed March 28, 2021.

376. McLean MD, Chen R, Yu D, et al. Purification of the therapeutic antibody trastuzumab from genetically modified plants using safflower Protein A-oleosin oilbody technology. *Transgenic Res*. 2012;21(6):1291-1301. doi:10.1007/s11248-012-9603-5

377. Musk E. Making Humans a Multi-Planetary Species. *New Sp*. 2017;5(2):46-61. doi:10.1089/space.2017.29009.emu

378. Wotring V. Space Pharmacology: How Space Affects Pharmacology. In: *Drug Discovery and Evaluation: Methods in Clinical Pharmacology*. Springer International Publishing; 2018:1-13. doi:10.1007/978-3-319-56637-5_68-1

379. Antonsen E, Bayuse T, Blue R, et al. *Evidence Report: Risk of Adverse Health Outcomes and Decrements in Performance Due to In-Flight Medical Conditions Human Research Program Exploration Medical Capabilities Element Approved for Public Release*. Houston, Texas; 2017.

380. Drake BG, Hoffman SJ, Beaty DW. Human exploration of mars, design reference architecture 5.0. In: *IEEE Aerospace Conference Proceedings*. ; 2010. doi:10.1109/AERO.2010.5446736

381. Rodríguez-Ruiz I, Babenko V, Martínez-Rodríguez S, Gavira JA. Protein separation under a microfluidic regime. *Analyst*. 2018;143(3):606-619. doi:10.1039/c7an01568b

382. Millet LJ, Lucheon JD, Standaert RF, Retterer ST, Doktycz MJ. Modular microfluidics for point-of-care protein purifications. *Lab Chip*. 2015;15(8):1799-1811. doi:10.1039/c5lc00094g

383. Murphy TW, Sheng J, Naler LB, Feng X, Lu C. On-chip manufacturing of synthetic proteins for point-of-care therapeutics. *Microsystems Nanoeng*. 2019;5(1):1-12. doi:10.1038/s41378-019-0051-8

384. Steven Siceloff K. NASA - Recycling Water is not Just for Earth Anymore. https://www.nasa.gov/mission_pages/station/behindscenes/waterrecycler.html. Published 2008. Accessed April 19, 2021.

385. Pathak M, Rathore AS. Mechanistic understanding of fouling of protein A chromatography resin. *J Chromatogr A*. 2016;1459:78-88. doi:10.1016/j.chroma.2016.06.084

386. Shukla AA, Gottschalk U. Single-use disposable technologies for biopharmaceutical manufacturing. *Trends Biotechnol*. 2013;31(3):147-154. doi:10.1016/j.tibtech.2012.10.004

387. Do S, Owens A, Weck O de. HabNet – An Integrated Habitation and Supportability Architecting and Analysis Environment. In: 45th International Conference on Environmental Systems; 2015. https://ttu-ir.tdl.org/handle/2346/64528. Accessed September 4, 2021.

388. Jones H. How Should Life Support Be Modeled and Simulated? In: 47th International Conference on Environmental Systems; 2017. https://ttu-ir.tdl.org/handle/2346/72914. Accessed September 4, 2021.

389. Hardy JM, Kusuma P, Bugbee B, Wheeler R, Ewert M. *Providing Photons for Food in*

Regenerative Life Support: A Comparative Analysis of Solar Fiber Optic and Electric Light Systems. 2020 International Conference on Environmental Systems; 2020. https://ttu-ir.tdl.org/handle/2346/86378. Accessed August 28, 2020.

390. Levri JA, Vaccari DA, Drysdale AE. Theory and application of the equivalent system mass metric. In: *SAE Technical Papers*. SAE International; 2000. doi:10.4271/2000-01-2395

391. Wen AM, Steinmetz NF. Design of virus-based nanomaterials for medicine, biotechnology, and energy. *Chem Soc Rev*. 2016;45(15):4074-4126. doi:10.1039/C5CS00287G

392. Nikitin NA, Trifonova EA, Karpova O V., Atabekov JG. Biosafety of plant viruses for human and animals. *Moscow Univ Biol Sci Bull*. 2016;71(3):128-134. doi:10.3103/S0096392516030081

393. Hefferon K. Plant virus expression vectors: A powerhouse for global health. *Biomedicines*. 2017;5(3). doi:10.3390/biomedicines5030044

394. Ibrahim A, Odon V, Kormelink R. Plant viruses in plant molecular pharming: Toward the use of enveloped viruses. *Front Plant Sci*. 2019;10:803. doi:10.3389/fpls.2019.00803

395. Azizgolshani O, Garmann RF, Cadena-Nava R, Knobler CM, Gelbart WM. Reconstituted plant viral capsids can release genes to mammalian cells. *Virology*. 2013;441(1):12-17. doi:10.1016/j.virol.2013.03.001

396. Czapar AE, Steinmetz NF. Plant viruses and bacteriophages for delivery in medicine and biotechnology. *Curr Opin Chem Biol*. 2017;38:108-116. doi:10.1016/j.cbpa.2017.03.013

397. Canizares MC, Nicholson L, Lomonossoff GP. Use of viral vectors for vaccine production in plants. *Immunol Cell Biol*. 2005;83(3):263-270. doi:10.1111/j.1440-1711.2005.01339.x

398. Balke I, Zeltins A. Use of plant viruses and virus-like particles for the creation of novel vaccines. *Adv Drug Deliv Rev*. 2019;145:119-129. doi:10.1016/j.addr.2018.08.007

399. Shukla S, Steinmetz NF. Virus-based nanomaterials as positron emission tomography and magnetic resonance contrast agents: From technology development to translational medicine. *Wiley Interdiscip Rev Nanomedicine Nanobiotechnology*. 2015;7(5):708-721. doi:10.1002/wnan.1335

400. Aljabali AAA, Al Zoubi MS, Al-Batanyeh KM, et al. Gold-coated plant virus as computed tomography imaging contrast agent. *Beilstein J Nanotechnol*. 2019;10(1):1983-1993. doi:10.3762/bjnano.10.195

401. Bruckman MA, Czapar AE, Steinmetz NF. Drug-Loaded Plant-Virus Based Nanoparticles for Cancer Drug Delivery. In: *Methods in Molecular Biology*. Vol 1776. Humana Press Inc.; 2018:425-436. doi:10.1007/978-1-4939-7808-3_28

402. Lebel MÈ, Chartrand K, Tarrab E, Savard P, Leclerc D, Lamarre A. Potentiating Cancer Immunotherapy Using Papaya Mosaic Virus-Derived Nanoparticles. *Nano Lett*. 2016;16(3):1826-1832. doi:10.1021/acs.nanolett.5b04877

403. Bäcker M, Koch C, Eiben S, et al. A New Class of Biosensors Based on Tobacco Mosaic Virus and Coat Proteins as Enzyme Nanocarrier. In: *Procedia Engineering*. Vol 168. Elsevier Ltd; 2016:618-621. doi:10.1016/j.proeng.2016.11.228

404. Soto CM, Blum AS, Vora GJ, et al. Fluorescent signal amplification of carbocyanine dyes using engineered viral nanoparticles. *J Am Chem Soc*. 2006;128(15):5184-5189. doi:10.1021/ja058574x

405. Kuo SY, Lin YC, Lai YC, et al. Production of fluorescent antibody-labeling proteins in plants using a viral vector and the application in the detection of Acidovorax citrulli and Bamboo mosaic virus. *PLoS One*. 2018;13(2). doi:10.1371/journal.pone.0192455

406. Yang O, Qadan M, Ierapetritou M. Economic Analysis of Batch and Continuous Biopharmaceutical Antibody Production: a Review. *J Pharm Innov*. 2020;15(1):182-200. doi:10.1007/s12247-018-09370-4

407. Aglietti GS. Current Challenges and Opportunities for Space Technologies. *Front Sp Technol*. 2020;1:1. doi:10.3389/frspt.2020.00001

408. Tiu BDB, Kernan DL, Tiu SB, et al. Electrostatic layer-by-layer construction of fibrous TMV biofilms. *Nanoscale*. 2017;9(4):1580-1590. doi:10.1039/C6NR06266K

409. Shin YC, Lee JH, Jin L, et al. Cell-adhesive RGD peptide-displaying M13 bacteriophage/PLGA nanofiber matrices for growth of fibroblasts. *Biomater Res*. 2014;18(1). doi:10.1186/2055-7124-18-14

410. Zhang Y, Zhou D. Magnetic particle-based ultrasensitive biosensors for diagnostics. *http://dx.doi.org/101586/erm1254*. 2014;12(6):565-571. doi:10.1586/ERM.12.54

411. Schwaminger SP, Fraga-García P, Eigenfeld M, Becker TM, Berensmeier S. Magnetic Separation in Bioprocessing Beyond the Analytical Scale: From Biotechnology to the Food Industry. *Front Bioeng Biotechnol*. 2019;0(SEP):233. doi:10.3389/FBIOE.2019.00233

412. Chan L, Nesbeth D, MacKey T, et al. Conjugation of Lentivirus to Paramagnetic Particles via Nonviral Proteins Allows Efficient Concentration and Infection of Primary Acute Myeloid Leukemia Cells. *J Virol*. 2005;79(20):13190. doi:10.1128/JVI.79.20.13190-13194.2005

413. Majidi S, Sehrig FZ, Samiei M, et al. Magnetic nanoparticles: Applications in gene delivery and gene therapy. *http://dx.doi.org/103109/2169140120151014093*. 2015;44(4):1186-1193. doi:10.3109/21691401.2015.1014093

414. Huang X, Stein BD, Cheng H, et al. Magnetic Virus-like Nanoparticles in N. benthamiana Plants: A New Paradigm for Environmental and Agronomic Biotechnological Research. *ACS Nano*. 2011;5(5):4037-4045. doi:10.1021/NN200629G

415. Shukla S, Steinmetz NF. Virus-based nanomaterials as PET and MR contrast agents: from technology development to translational medicine. *Wiley Interdiscip Rev Nanomed Nanobiotechnol*. 2015;7(5):708. doi:10.1002/WNAN.1335

416. Koch C, Wabbel K, Eber FJ, et al. Modified TMV Particles as Beneficial Scaffolds to

Present Sensor Enzymes. *Front Plant Sci*. 2015;6:1137. doi:10.3389/fpls.2015.01137

417. Sapsford KE, Soto CM, Blum AS, et al. A cowpea mosaic virus nanoscaffold for multiplexed antibody conjugation: Application as an immunoassay tracer. *Biosens Bioelectron*. 2006;21(8):1668-1673. doi:10.1016/J.BIOS.2005.09.003

418. Soto CM, Blaney KM, Dar M, et al. Cowpea mosaic virus nanoscaffold as signal enhancement for DNA microarrays. *Biosens Bioelectron*. 2009;25(1):48-54. doi:10.1016/J.BIOS.2009.06.009

419. Roe S, ed. *Protein Purification Techniques*. 2nd ed. Oxford University Press; 2001. doi:10.1093/oso/9780199636747.001.0001

420. Smith ML, Lindbo JA, Dillard-Telm S, et al. Modified Tobacco mosaic virus particles as scaffolds for display of protein antigens for vaccine applications. *Virology*. 2006;348(2):475-488. doi:10.1016/j.virol.2005.12.039

421. Zeltins A. Construction and characterization of virus-like particles: A review. *Mol Biotechnol*. 2013;53(1):92-107. doi:10.1007/s12033-012-9598-4

422. Marsian J, Lomonossoff GP. Molecular pharming-VLPs made in plants. *Curr Opin Biotechnol*. 2016;37. doi:10.1016/j.copbio.2015.12.007

423. Koudelka KJ, Pitek AS, Manchester M, Steinmetz NF. Virus-Based Nanoparticles as Versatile Nanomachines. *Annu Rev Virol*. 2015;2(1):379-401. doi:10.1146/annurev-virology-100114-055141

424. Mahmoodi S, Pourhassan-Moghaddam M, Wood DW, Majdi H, Zarghami N. Current affinity approaches for purification of recombinant proteins. Hatti Kaul R, ed. *Cogent Biol*. 2019;5(1):1665406. doi:10.1080/23312025.2019.1665406

425. Dias AMGC, Roque ACA. The future of protein scaffolds as affinity reagents for purification. *Biotechnol Bioeng*. 2016;114(3):481-491. doi:10.1002/bit.26090

426. Belfort M, Wood DW, Wu W, Belfort G, Derbyshire V. A genetic system yields self-cleaving inteins for bioseparations. *Nat Biotechnol*. 1999;17(9):889-892. doi:10.1038/12879

427. Shoseyov O, Shani Z, Levy I. Carbohydrate Binding Modules: Biochemical Properties and Novel Applications. *Microbiol Mol Biol Rev*. 2006;70(2):283-295. doi:10.1128/mmbr.00028-05

428. Sheth RD, Bhut B V., Jin M, Li Z, Chen W, Cramer SM. Development of an ELP-Z based mAb affinity precipitation process using scaled-down filtration techniques. *J Biotechnol*. 2014;192(Part A):11-19. doi:10.1016/j.jbiotec.2014.09.020

429. Banki MR, Gerngross TU, Wood DW. Novel and economical purification of recombinant proteins: Intein-mediated protein purification using in vivo polyhydroxybutyrate (PHB) matrix association. *Protein Sci*. 2005;14(6):1387-1395. doi:10.1110/ps.041296305

430. Bhatla SC, Kaushik V, Yadav MK. Use of oil bodies and oleosins in recombinant protein production and other biotechnological applications. *Biotechnol Adv*. 2010;28(3):293-300.

doi:10.1016/j.biotechadv.2010.01.001

431. Dessau M, Goldhill D, McBride RL, Turner PE, Modis Y. Selective Pressure Causes an RNA Virus to Trade Reproductive Fitness for Increased Structural and Thermal Stability of a Viral Enzyme. Malik HS, ed. *PLoS Genet*. 2012;8(11):e1003102. doi:10.1371/journal.pgen.1003102

432. Le Nouën C, McCarty T, Brown M, et al. Genetic stability of genome-scale deoptimized RNA virus vaccine candidates under selective pressure. *Proc Natl Acad Sci U S A*. 2017;114(3):E386-E395. doi:10.1073/pnas.1619242114

433. Hilbrig F, Freitag R. Protein purification by affinity precipitation. *J Chromatogr B Anal Technol Biomed Life Sci*. 2003;790(1-2):79-90. doi:10.1016/S1570-0232(03)00081-3

434. Low D, O'Leary R, Pujar NS. Future of antibody purification. *J Chromatogr B Anal Technol Biomed Life Sci*. 2007;848(1):48-63. doi:10.1016/j.jchromb.2006.10.033

435. Shukla AA, Thömmes J. Recent advances in large-scale production of monoclonal antibodies and related proteins. *Trends Biotechnol*. 2010;28(5):253-261. doi:10.1016/j.tibtech.2010.02.001

436. Mondal K, Roy I, Gupta M. Affinity-based strategies for protein purification. *Anal Chem*. 2006;78(11):3499-3504. doi:10.1021/ac0694066

437. Dixon C, Wilken LR, Woodard SL, Barros GOF. The Impact of Six Critical Impurities on Recombinant Protein Recovery and Purification from Plant Hosts. In: *Molecular Pharming*. Hoboken, NJ, USA: John Wiley & Sons, Inc.; 2018:137-180. doi:10.1002/9781118801512.ch7

438. Buzón P, Maity S, Roos WH. Physical virology: From virus self-assembly to particle mechanics. *Wiley Interdiscip Rev Nanomedicine Nanobiotechnology*. 2020;12(4):e1613. doi:10.1002/wnan.1613

439. Mateu MG. Mechanical properties of viruses analyzed by atomic force microscopy: A virological perspective. *Virus Res*. 2012;168(1-2):1-22. doi:10.1016/j.virusres.2012.06.008

440. Schmatulla A, Maghelli N, Marti O. Micromechanical properties of tobacco mosaic viruses. *J Microsc*. 2007;225:264-268.

441. Falvo MR, Washburn S, Superfine R, et al. Manipulation of individual viruses: Friction and mechanical properties. *Biophys J*. 1997;72(3):1396-1403. doi:10.1016/S0006-3495(97)78786-1

442. Medrano M, Valbuena A, Rodríguez-Huete A, Mateu MG. Structural determinants of mechanical resistance against breakage of a virus-based protein nanoparticle at a resolution of single amino acids. *Nanoscale*. 2019;11(19):9369-9383. doi:10.1039/c9nr01935a

443. Frejd FY, Kim K-T. Affibody molecules as engineered protein drugs. *Exp Mol Med*. 2017;49(3):e306-e306. doi:10.1038/emm.2017.35

444. Lund LN, Gustavsson P-E, Michael R, et al. Novel peptide ligand with high binding capacity for antibody purification. *J Chromatogr A*. 2012;1225:158-167. doi:10.1016/j.chroma.2011.12.074

445. Delahaye M, Lawrence K, Ward SJ, Hoare M. An ultra scale-down analysis of the recovery by dead-end centrifugation of human cells for therapy. *Biotechnol Bioeng*. 2015;112(5):997-1011. doi:10.1002/bit.25519

446. Krajden M, Minor JM, Rifkin O, Comanor L. Effect of multiple freeze-thaw cycles on hepatitis B virus DNA and hepatitis C virus RNA quantification as measured with branched-DNA technology. *J Clin Microbiol*. 1999;37(6):1683-1686. doi:10.1128/jcm.37.6.1683-1686.1999

447. Swartz AR, Xu X, Traylor SJ, Li ZJ, Chen W. One-step affinity capture and precipitation for improved purification of an industrial monoclonal antibody using Z-ELP functionalized nanocages. *Biotechnol Bioeng*. 2018;115(2):423-432. doi:10.1002/BIT.26467

448. McNulty MJ, Berliner AJ, Negulescu PG, et al. Evaluating the Cost of Pharmaceutical Purification for a Long-Duration Space Exploration Medical Foundry. *Front Microbiol*. 2021;0:3056. doi:10.3389/FMICB.2021.700863

449. Saunders K, Lomonossoff GP. In planta synthesis of designer-length tobacco mosaic virus-based nano-rods that can be used to fabricate nano-wires. *Front Plant Sci*. 2017;8. doi:10.3389/fpls.2017.01335

450. Cruz SS, Chapman S, Roberts AG, Roberts IM, Prior DA, Oparka KJ. Assembly and movement of a plant virus carrying a green fluorescent protein overcoat. *Proc Natl Acad Sci*. 1996;93(13):6286-6290. doi:10.1073/PNAS.93.13.6286

451. Nord K, Gunneriusson E, Ringdahl J, Ståhl S, Uhlén M, Nygren P-Å. Binding proteins selected from combinatorial libraries of an α-helical bacterial receptor domain. *Nat Biotechnol 1997 158*. 1997;15(8):772-777. doi:10.1038/nbt0897-772

452. Ståhl S, Gräslund T, Eriksson Karlström A, Frejd FY, Nygren P-Å, Löfblom J. Affibody Molecules in Biotechnological and Medical Applications. *Trends Biotechnol*. 2017;35(8):691-712. doi:10.1016/J.TIBTECH.2017.04.007

453. Xiong Y, Li Q, Kailemia MJ, Lebrilla CB, Nandi S, McDonald KA. Glycoform Modification of Secreted Recombinant Glycoproteins through Kifunensine Addition during Transient Vacuum Agroinfiltration. *Int J Mol Sci*. 2018;19(3). doi:10.3390/IJMS19030890

454. Xiong Y, Karuppanan K, Bernardi A, et al. Effects of N-Glycosylation on the Structure, Function, and Stability of a Plant-Made Fc-Fusion Anthrax Decoy Protein. *Front Plant Sci*. 2019;10:768. doi:10.3389/fpls.2019.00768

455. Giritch A, Marillonnet S, Engler C, et al. Rapid high-yield expression of full-size IgG antibodies in plants coinfected with noncompeting viral vectors. *Proc Natl Acad Sci*. 2006;103(40):14701-14706. doi:10.1073/PNAS.0606631103

456. Bendandi M, Marillonnet S, Kandzia R, et al. Rapid, high-yield production in plants of

individualized idiotype vaccines for non-Hodgkin's lymphoma. *Ann Oncol*. 2010;21(12):2420-2427. doi:10.1093/ANNONC/MDQ256

457. Whaley KJ, Morton J, Hume S, et al. Emerging Antibody-based Products. *Curr Top Microbiol Immunol*. 2012;375:107-126. doi:10.1007/82_2012_240

458. Ortega-Rivera OA, Pokorski JK, Steinmetz NF. A Single-Dose, Implant-Based, Trivalent Virus-like Particle Vaccine against "Cholesterol Checkpoint" Proteins. *Adv Ther*. March 2021:2100014. doi:10.1002/ADTP.202100014

459. Wang J, Yang M, Zhu Y, Wang L, Tomsia AP, Mao C. Phage nanofibers induce vascularized osteogenesis in 3D printed bone scaffolds. *Adv Mater*. 2014;26(29):4961-4966. doi:10.1002/adma.201400154

460. Owens GJ, Singh RK, Foroutan F, et al. Sol–gel based materials for biomedical applications. *Prog Mater Sci*. 2016;77:1-79. doi:10.1016/J.PMATSCI.2015.12.001

461. Livage J, Coradin T. Encapsulation of Enzymes, Antibodies, and Bacteria. *Handb Sol-Gel Sci Technol Process Charact Appl*. July 2018:2909-2931. doi:10.1007/978-3-319-32101-1_23

462. Nassif N, Bouvet O, Noelle Rager M, Roux C, Coradin T, Livage J. Living bacteria in silica gels. *Nat Mater 2002 11*. 2002;1(1):42-44. doi:10.1038/nmat709

463. Reátegui E, Kasinkas L, Kniesz K, Lefebvre MA, Aksan A. Silica–PEG gel immobilization of mammalian cells. *J Mater Chem B*. 2014;2(42):7440-7448. doi:10.1039/C4TB00812J

464. Ponamoreva ON, Kamanina OA, Alferov VA, et al. Yeast-based self-organized hybrid bio-silica sol–gels for the design of biosensors. *Biosens Bioelectron*. 2015;67:321-326. doi:10.1016/J.BIOS.2014.08.045

465. David AE, Yang AJ, Wang NS. Enzyme Stabilization and Immobilization by Sol-Gel Entrapment. *Methods Mol Biol*. 2011;679:49-66. doi:10.1007/978-1-60761-895-9_6

466. Kato K, Lee S, Nagata F. Efficient enzyme encapsulation inside sol-gel silica sheets prepared by poly-L-lysine as a catalyst. *https://doi.org/101080/218707642020174716*7. 2020;8(2):396-406. doi:10.1080/21870764.2020.1747167

467. Crosley MS, Yip WT. Silica Sol–Gel Optical Biosensors: Ultrahigh Enzyme Loading Capacity on Thin Films via Kinetic Doping. *J Phys Chem B*. 2017;121(9):2121-2126. doi:10.1021/ACS.JPCB.6B10949

468. Kangasniemi L, Koskinen M, Jokinen M, et al. Extended release of adenovirus from silica implants in vitro and in vivo. *Gene Ther 2009 161*. 2008;16(1):103-110. doi:10.1038/gt.2008.142

469. Lam P, Gulati NM, Stewart PL, Keri RA, Steinmetz NF. Bioengineering of Tobacco Mosaic Virus to Create a Non-Infectious Positive Control for Ebola Diagnostic Assays. *Sci Reports 2016 61*. 2016;6(1):1-8. doi:10.1038/srep23803

470. Zeno WF, Hilt S, Aravagiri KK, et al. Analysis of lipid phase behavior and protein

conformational changes in nanolipoprotein particles upon entrapment in sol-gel-derived silica. *Langmuir*. 2014;30(32):9780-9788. doi:10.1021/la5025058

471. Bhatia RB, Brinker CJ, Gupta AK, Singh AK. Aqueous sol-gel process for protein encapsulation. *Chem Mater*. 2000;12(8):2434-2441. doi:10.1021/cm000260f

472. OSTER G. THE ISOELECTRIC POINTS OF SOME STRAINS OF TOBACCO MOSAIC VIRUS. *J Biol Chem*. 1951;190(1):55-59. doi:10.1016/S0021-9258(18)56044-0

473. Hodgson RJ, Chen Y, Zhang Z, et al. Protein-doped monolithic silica columns for capillary liquid chromatography prepared by the sol-gel method: Applications to frontal affinity chromatography. *Anal Chem*. 2004;76(10):2780-2790. doi:10.1021/ac0352124

474. Smith AME, Fortuna J, Forsberg EM, Brennan JD. An automated materials screening approach for the development of sol–gel derived monolithic silica enzyme reactor columns. *RSC Adv*. 2014;4(31):15952-15960. doi:10.1039/C4RA00734D

475. Hanke AT, Ottens M. Purifying biopharmaceuticals: knowledge-based chromatographic process development. *Trends Biotechnol*. 2014;32(4):210-220. doi:10.1016/J.TIBTECH.2014.02.001

476. Bolton GR, Mehta KK. The role of more than 40 years of improvement in protein A chromatography in the growth of the therapeutic antibody industry. *Biotechnol Prog*. 2016;32(5):1193-1202. doi:10.1002/btpr.2324

477. Gaughan CL. The present state of the art in expression, production and characterization of monoclonal antibodies. *Mol Divers*. 2016;20(1):255-270. doi:10.1007/s11030-015-9625-z

478. Ghosh R. Membrane chromatography: current applications, future opportunities, and challenges. *Membr Process Dairy Ingred Sep*. July 2015:230-240. doi:10.1002/9781118590331.CH8

479. Barroso T, Hussain A, Roque ACA, Aguiar-Ricardo A. Functional monolithic platforms: Chromatographic tools for antibody purification. *Biotechnol J*. 2013;8(6):671-681. doi:10.1002/biot.201200328

480. Napadensky B, Shinkazh O, Teella A, Zydney AL. Continuous Countercurrent Tangential Chromatography for Monoclonal Antibody Purification. *Sep Sci Technol*. 2013;48(9):1289-1297. doi:10.1080/01496395.2013.767837

481. Dutta AK, Tran T, Napadensky B, et al. Purification of monoclonal antibodies from clarified cell culture fluid using Protein A capture continuous countercurrent tangential chromatography. *J Biotechnol*. 2015;213:54-64. doi:10.1016/j.jbiotec.2015.02.026

482. Shinkazh O, Kanani D, Barth M, Long M, Hussain D, Zydney AL. Countercurrent tangential chromatography for large-scale protein purification. *Biotechnol Bioeng*. 2011;108(3):582-591. doi:10.1002/bit.22960

483. Fedorenko D, Dutta AK, Tan J, et al. Improved protein A resin for antibody capture in a continuous countercurrent tangential chromatography system. *Biotechnol Bioeng*. 2020;117(3):646-653. doi:10.1002/bit.27232

484. Dutta AK, Fedorenko D, Tan J, et al. Continuous countercurrent tangential chromatography for mixed mode post-capture operations in monoclonal antibody purification. *J Chromatogr A*. 2017;1511:37-44. doi:10.1016/j.chroma.2017.06.018

485. Li Z, Gu Q, Coffman JL, Przybycien T, Zydney AL. Continuous precipitation for monoclonal antibody capture using countercurrent washing by microfiltration. *Biotechnol Prog*. 2019;35(6):e2886. doi:10.1002/btpr.2886

486. Burgstaller D, Jungbauer A, Satzer P. Continuous integrated antibody precipitation with two-stage tangential flow microfiltration enables constant mass flow. *Biotechnol Bioeng*. 2019;116(5):1053-1065. doi:10.1002/bit.26922

487. Hung JJ, Borwankar AU, Dear BJ, Truskett TM, Johnston KP. High concentration tangential flow ultrafiltration of stable monoclonal antibody solutions with low viscosities. *J Memb Sci*. 2016;508:113-126. doi:10.1016/J.MEMSCI.2016.02.031

488. Lutz H. Configurations. In: *Ultrafiltration for Bioprocessing: Development and Implementation of Robust Processes*. Woodhead Publishing; 2015:77-94. doi:10.1016/B978-1-907568-46-6.00005-7

489. Kanai S, Liu J, Patapoff TW, Shire SJ. Reversible Self-Association of a Concentrated Monoclonal Antibody Solution Mediated by Fab–Fab Interaction That Impacts Solution Viscosity. *J Pharm Sci*. 2008;97(10):4219-4227. doi:10.1002/JPS.21322

490. Liu J, Nguyen MDH, Andya JD, Shire SJ. Reversible Self-Association Increases the Viscosity of a Concentrated Monoclonal Antibody in Aqueous Solution. *J Pharm Sci*. 2005;94(9):1928-1940. doi:10.1002/JPS.20347

491. Rosenberg E, Hepbildikler S, Kuhne W, Winter G. Ultrafiltration concentration of monoclonal antibody solutions: Development of an optimized method minimizing aggregation. *J Memb Sci*. 2009;342(1-2):50-59. doi:10.1016/J.MEMSCI.2009.06.028

492. Quezada C, Estay H, Cassano A, Troncoso E, Ruby-Figueroa R. Prediction of permeate flux in ultrafiltration processes: A review of modeling approaches. *Membranes (Basel)*. 2021;11(5):368. doi:10.3390/MEMBRANES11050368/S1

493. Dehghani M, Lucas K, Flax J, McGrath J, Gaborski T. Tangential Flow Microfluidics for the Capture and Release of Nanoparticles and Extracellular Vesicles on Conventional and Ultrathin Membranes. *Adv Mater Technol*. 2019;4(11):1900539. doi:10.1002/ADMT.201900539

494. O'Sullivan B, Al-Bahrani H, Lawrence J, et al. Modular microfluidic reactor and inline filtration system for the biocatalytic synthesis of chiral metabolites. *J Mol Catal B Enzym*. 2012;77:1-8. doi:10.1016/J.MOLCATB.2011.12.010

495. Wang Y, Keller K, Cheng X. Tangential Flow Microfiltration for Viral Separation and Concentration. *Micromachines 2019, Vol 10, Page 320*. 2019;10(5):320. doi:10.3390/MI10050320

496. Hajba L, Guttman A. Continuous-flow-based microfluidic systems for therapeutic monoclonal antibody production and organ-on-a-chip drug testing. *J Flow Chem*. 2017;7(3-4):118-123. doi:10.1556/1846.2017.00014

497. Murphy TW, Sheng J, Naler LB, Feng X, Lu C. On-chip manufacturing of synthetic proteins for point-of-care therapeutics. *Microsystems Nanoeng 2019 51*. 2019;5(1):1-12. doi:10.1038/s41378-019-0051-8

498. Bhamla MS, Benson B, Chai C, Katsikis G, Johri A, Prakash M. Hand-powered ultralow-cost paper centrifuge. *Nat Biomed Eng*. 2017;1(1):0009. doi:10.1038/s41551-016-0009

499. Byagathvalli G, Pomerantz A, Sinha S, Standeven J, Bhamla MS. A 3D-printed hand-powered centrifuge for molecular biology. *PLOS Biol*. 2019;17(5):e3000251. doi:10.1371/JOURNAL.PBIO.3000251

500. Sule SS, Petsiuk AL, Pearce JM. Open Source Completely 3-D Printable Centrifuge. *Instruments 2019, Vol 3, Page 30*. 2019;3(2):30. doi:10.3390/INSTRUMENTS3020030

501. Brown J, Theis L, Kerr L, et al. A Hand-Powered, Portable, Low-Cost Centrifuge for Diagnosing Anemia in Low-Resource Settings. *Am J Trop Med Hyg*. 2011;85(2):327. doi:10.4269/AJTMH.2011.10-0399

502. Wong AP, Gupta M, Shevkoplyas SS, Whitesides GM. Egg beater as centrifuge: isolating human blood plasma from whole blood in resource-poor settings. *Lab Chip*. 2008;8(12):2032-2037. doi:10.1039/B809830C

503. WareJoncas Z, Stewart C, Giannini J. An Inexpensive, Open-Source Mini-Centrifuge. *Am Biol Teach*. 2018;80(6):451-456. doi:10.1525/ABT.2018.80.6.451

504. Yoo SY, Lee SJ, Seo JM. Manual centrifuge system: Bearing-based hand spinner made with 3-D printer. *Proc Annu Int Conf IEEE Eng Med Biol Soc EMBS*. September 2017:1603-1606. doi:10.1109/EMBC.2017.8037145

505. Liu C-H, Chen C-A, Chen S-J, et al. Blood Plasma Separation Using a Fidget-Spinner. *Anal Chem*. 2018;91(2):1247-1253. doi:10.1021/ACS.ANALCHEM.8B04860

506. Li E, Larson A, Kothari A, Prakash M. Handyfuge-LAMP: low-cost and electricity-free centrifugation for isothermal SARS-CoV-2 detection in saliva. *medRxiv*. July 2020:2020.06.30.20143255. doi:10.1101/2020.06.30.20143255

507. Rajamanickam V, Herwig C, Spadiut O. Monoliths in Bioprocess Technology. *Chromatogr 2015, Vol 2, Pages 195-212*. 2015;2(2):195-212. doi:10.3390/CHROMATOGRAPHY2020195

508. Burden CS, Jin J, Podgornik A, Bracewell DG. A monolith purification process for virus-like particles from yeast homogenate. *J Chromatogr B*. 2012;880:82-89. doi:10.1016/J.JCHROMB.2011.10.044

509. Zaveckas M, Snipaitis S, Pesliakas H, Nainys J, Gedvilaite A. Purification of recombinant virus-like particles of porcine circovirus type 2 capsid protein using ion-exchange monolith chromatography. *J Chromatogr B*. 2015;991:21-28. doi:10.1016/J.JCHROMB.2015.04.004

510. Steppert P, Burgstaller D, Klausberger M, et al. Purification of HIV-1 gag virus-like particles and separation of other extracellular particles. *J Chromatogr A*. 2016;1455:93-101. doi:10.1016/J.CHROMA.2016.05.053

511. Lucero AT, Mercado SA, Sánchez AC, Contador CA, Andrews BA, Asenjo JA. Purification of adenoviral vector serotype 5 for gene therapy against alcoholism using anion exchange chromatography. *J Chem Technol Biotechnol*. 2017;92(9):2445-2452. doi:10.1002/JCTB.5255

512. Bandeira V, Peixoto C, Rodrigues AF, et al. Downstream Processing of Lentiviral Vectors: Releasing Bottlenecks. *https://home.liebertpub.com/hgtb*. 2012;23(4):255-263. doi:10.1089/HGTB.2012.059

513. Kramberger P, Peterka M, Boben J, Ravnikar M, Štrancar A. Short monolithic columns—A breakthrough in purification and fast quantification of tomato mosaic virus. *J Chromatogr A*. 2007;1144(1):143-149. doi:10.1016/J.CHROMA.2006.10.055

514. Rupar M, Ravnikar M, Tušek-Žnidarič M, Kramberger P, Glais L, Gutiérrez-Aguirre I. Fast purification of the filamentous Potato virus Y using monolithic chromatographic supports. *J Chromatogr A*. 2013;1272:33-40. doi:10.1016/J.CHROMA.2012.11.058

515. Ruščić J, Gutiérrez-Aguirre I, Tušek Žnidarič M, et al. A new application of monolithic supports: The separation of viruses from one another. *J Chromatogr A*. 2015;1388:69-78. doi:10.1016/J.CHROMA.2015.01.097

516. Buyel JF, Twyman RM, Fischer R. Extraction and downstream processing of plant-derived recombinant proteins. *Biotechnol Adv*. 2015. doi:10.1016/j.biotechadv.2015.04.010

517. Buyel JF, Fischer R. Generic chromatography-based purification strategies accelerate the development of downstream processes for biopharmaceutical proteins produced in plants. *Biotechnol J*. 2014;9(4):566-577. doi:10.1002/biot.201300548

518. Sanjuán R, Agudelo-Romero P, Elena SF. Upper-limit mutation rate estimation for a plant RNA virus. *Biol Lett*. 2009;5(3):394-396. doi:10.1098/rsbl.2008.0762

519. Chare ER, Holmes Correspondence EC, Holmes EC. Selection pressures in the capsid genes of plant RNA viruses reflect mode of transmission. *J Gen Virol*. 2004;85:3149-3157. doi:10.1099/vir.0.80134-0

520. Phan SI, Adam CM, Chen Z, et al. Genetic Stability of Parainfluenza Virus 5-Vectored Human Respiratory Syncytial Virus Vaccine Candidates after In Vitro and In Vivo Passage. *J Virol*. 2017;91(19). doi:10.1128/JVI.00559-17

521. Jabara CB, Jones CD, Roach J, Anderson JA, Swanstrom R. Accurate sampling and deep sequencing of the HIV-1 protease gene using a Primer ID. *Proc Natl Acad Sci U S A*. 2011;108(50):20166-20171. doi:10.1073/pnas.1110064108

522. Sena JA, Galotto G, Devitt NP, et al. Unique Molecular Identifiers reveal a novel sequencing artefact with implications for RNA-Seq based gene expression analysis. *Sci Rep*. 2018;8(1):13121. doi:10.1038/s41598-018-31064-7

523. Kou R, Lam H, Duan H, et al. Benefits and Challenges with Applying Unique Molecular Identifiers in Next Generation Sequencing to Detect Low Frequency Mutations. Wang J, ed. *PLoS One*. 2016;11(1):e0146638. doi:10.1371/journal.pone.0146638

524. Gustaw KA, Garrett MR, Lee H, et al. Antigen–antibody dissociation in Alzheimer disease: a novel approach to diagnosis. *J Neurochem*. 2008;106(3):1350-1356. doi:10.1111/J.1471-4159.2008.05477.X

525. Takamatsu N, Watanabe Y, Yanagi H, Meshi T, Shiba T, Okada Y. Production of enkephalin in tobacco protoplasts using tobacco mosaic virus RNA vector. *FEBS Lett*. 1990;269(1):73-76. doi:10.1016/0014-5793(90)81121-4

526. Chen X, Zaro JL, Shen WC. Fusion protein linkers: Property, design and functionality. *Adv Drug Deliv Rev*. 2013;65(10):1357-1369. doi:10.1016/j.addr.2012.09.039

527. Klein JS, Jiang S, Galimidi RP, Keeffe JR, Bjorkman PJ. Design and characterization of structured protein linkers with differing flexibilities. *Protein Eng Des Sel*. 2014;27(10):325-330. doi:10.1093/protein/gzu043

528. Li G, Huang Z, Zhang C, et al. Construction of a linker library with widely controllable flexibility for fusion protein design. *Appl Microbiol Biotechnol*. 2016;100(1):215-225. doi:10.1007/s00253-015-6985-3

529. Ey P, Prowse S, Jenkin C. Isolation of pure IgG1, IgG2a and IgG2b immunoglobulins from mouse serum using protein A-sepharose. *Immunochemistry*. 1978;15(7):429-436. doi:10.1016/0161-5890(78)90070-6

530. Konrad A, Eriksson Karlström A, Hober S. Covalent Immunoglobulin Labeling through a Photoactivable Synthetic Z Domain. *Bioconjug Chem*. 2011;22(12):2395-2403. doi:10.1021/bc200052h

531. Bottomley S, Popplewell A, Scawen M, Wan T, Sutton B, Gore M. The stability and unfolding of an IgG binding protein based upon the B domain of protein A from Staphylococcus aureus probed by tryptophan substitution and fluorescence spectroscopy. *Protein Eng*. 1994;7(12):1463-1470. doi:10.1093/PROTEIN/7.12.1463

532. Sugita T, Katayama M, Okochi M, Kato R, Ichihara T, Honda H. Screening of peptide ligands that bind to the Fc region of IgG using peptide array and its application to affinity purification of antibody. *Biochem Eng J*. 2013;79:33-40. doi:10.1016/j.bej.2013.06.017

533. Gong Y, Zhang L, Li J, Feng S, Deng H. Development of the Double Cyclic Peptide Ligand for Antibody Purification and Protein Detection. *Bioconjug Chem*. 2016;27(7):1569-1573. doi:10.1021/acs.bioconjchem.6b00170

534. Zhao W-W, Liu F-F, Shi Q-H, Dong X-Y, Sun Y. Biomimetic design of affinity peptide ligands for human IgG based on protein A-IgG complex. *Biochem Eng J*. 2014;88:1-11. doi:10.1016/J.BEJ.2014.03.015

535. Högbom M, Eklund M, Nygren P-A, Nordlund P. Structural basis for recognition by an in vitro evolved affibody. *Proc Natl Acad Sci U S A*. 2003;100(6):3191-3196. doi:10.1073/pnas.0436100100

536. Coates JD, Michaelidou U, Bruce RA, O'Connor SM, Crespi JN, Achenbach LA. Ubiquity and diversity of dissimilatory (per)chlorate-reducing bacteria. *Appl Environ Microbiol*. 1999;65(12):5234-5241. http://www.ncbi.nlm.nih.gov/pubmed/10583970. Accessed August 21, 2018.

537. Davila AF, Willson D, Coates JD, McKay CP. Perchlorate on Mars: a chemical hazard and a resource for humans. *Int J Astrobiol*. 2013;12(04):321-325. doi:10.1017/S1473550413000189

538. Ha W, Suarez DL, Lesch SM. Perchlorate Uptake in Spinach As Related to Perchlorate, Nitrate, And Chloride Concentrations in Irrigation Water. *Environ Sci Technol*. 2011;45(21):9363-9371. doi:10.1021/ES2010094

539. Somleva MN, Snell KD, Beaulieu JJ, Peoples OP, Garrison BR, Patterson NA. Production of polyhydroxybutyrate in switchgrass, a value-added co-product in an important lignocellulosic biomass crop. *Plant Biotechnol J*. 2008;6(7):663-678. doi:10.1111/J.1467-7652.2008.00350.X

540. Chow BJ, Chen T, Zhong Y, Qiao Y. Direct Formation of Structural Components Using a Martian Soil Simulant. *Sci Reports 2017 71*. 2017;7(1):1-8. doi:10.1038/s41598-017-01157-w

541. Wheeler RM, Sager JC, Prince RP, et al. Crop Production for Advanced Life Support Systems - Observations From the Kennedy Space Center Breadboard Project. 2003. www.sti. Accessed September 29, 2021.